ISSN 0021-9673

VOL. 522 NOVEMBER 28, 1990

COMPLETE IN ONE ISSUE

JOURNAL OF CHROMATOGRAPHY

INTERNATIONAL JOURNAL ON CHROMATOGRAPHY, ELECTROPHORESIS AND RELATED METHODS

ELSEVIER

JOURNAL OF CHROMATOGRAPHY

Scope. The *Journal of Chromatography* publishes papers on all aspects of chromatography, electrophoresis and related methods. Contributions consist mainly of research papers dealing with chromatographic theory, instrumental development and their applications. The section *Biomedical Applications*, which is under separate editorship, deals with the following aspects: developments in and applications of chromatographic and electrophoretic techniques related to clinical diagnosis or alterations during medical treatment; screening and profiling of body fluids or tissues with special reference to metabolic disorders; results from basic medical research with direct consequences in clinical practice; drug level monitoring and pharmacokinetic studies; clinical toxicology; analytical studies in occupational medicine.

Submission of Papers. Manuscripts (in English; *four* copies are required) should be submitted to: Editorial Office of *Journal of Chromatography*, P.O. Box 681, 1000 AR Amsterdam, The Netherlands, Telefax (+31-20) 5862 304, or to: The Editor of *Journal of Chromatography, Biomedical Applications*, P.O. Box 681, 1000 AR Amsterdam, The Netherlands. Review articles are invited or proposed by letter to the Editors. An outline of the proposed review should first be forwarded to the Editors for preliminary discussion prior to preparation. Submission of an article is understood to imply that the article is original and unpublished and is not being considered for publication elsewhere. For copyright regulations, see below.

Subscription Orders. Subscription orders should be sent to: Elsevier Science Publishers B.V., P.O. Box 211, 1000 AE Amsterdam, The Netherlands, Tel. (+31-20) 5803 911, Telex 18582 ESPA NL, Telefax (+31-20) 5803 598. The *Journal of Chromatography* and the *Biomedical Applications* section can be subscribed to separately.

Publication. The *Journal of Chromatography* (incl. *Biomedical Applications*) has 37 volumes in 1990. The subscription prices for 1990 are:

J. Chromatogr. (incl. *Cum. Indexes, Vols. 451–500*) + *Biomed. Appl.* (Vols. 498–534):
Dfl. 6734.00 plus Dfl. 1036.00 (p.p.h.) (total *ca.* US$ 4365.25)

J. Chromatogr. (incl. *Cum. Indexes, Vols. 451–500*) only (Vols. 498–524):
Dfl. 5616.00 plus Dfl. 756.00 (p.p.h.) (total *ca.* US$ 3579.75)

Biomed. Appl. only (Vols. 525–534):
Dfl. 2080.00 plus Dfl. 280.00 (p.p.h.) (total *ca.* US$ 1325.75).

Our p.p.h. (postage, package and handling) charge includes surface delivery of all issues, except to subscribers in Argentina, Australia, Brasil, Canada, China, Hong Kong, India, Israel, Malaysia, Mexico, New Zealand, Pakistan, Singapore, South Africa, South Korea, Taiwan, Thailand and the U.S.A. who receive all issues by air delivery (S.A.L. — Surface Air Lifted) at no extra cost. For Japan, air delivery requires 50% additional charge; for all other countries airmail and S.A.L. charges are available upon request. Back volumes of the *Journal of Chromatography* (Vols. 1–497) are available at Dfl. 195.00 (plus postage). Claims for missing issues will be honoured, free of charge, within three months after publication of the issue. Customers in the U.S.A. and Canada wishing information on this and other Elsevier journals, please contact Journal Information Center, Elsevier Science Publishing Co. Inc., 655 Avenue of the Americas, New York, NY 10010, U.S.A., Tel. (+1-212) 633 3750, Telefax (+1-212) 633 3990.

Abstracts/Contents Lists published in Analytical Abstracts, Biochemical Abstracts, Biological Abstracts, Chemical Abstracts, Chemical Titles, Chromatography Abstracts, Clinical Chemistry Lookout, Current Contents/Life Sciences, Current Contents/Physical, Chemical & Earth Sciences, Deep-Sea Research/Part B: Oceanographic Literature Review, Excerpta Medica, Index Medicus, Mass Spectrometry Bulletin, PASCAL-CNRS, Pharmaceutical Abstracts, Referativnyi Zhurnal, Research Alert, Science Citation Index and Trends in Biotechnology.

See inside back cover for Publication Schedule, Information for Authors and information on Advertisements.

0021-9673/90/$03.50

This issue is printed on acid-free paper.

Printed in The Netherlands

CONTENTS

(Abstracts/Contents Lists published in Analytical Abstracts, Biochemical Abstracts, Biological Abstracts, Chemical Abstracts, Chemical Titles, Chromatography Abstracts, Current Contents/Life Sciences, Current Contents/Physical, Chemical & Earth Sciences, Deep-Sea Research/Part B: Oceanographic Literature Review, Excerpta Medica, Index Medicus, Mass Spectrometry Bulletin, PASCAL-CNRS, Referativnyi Zhurnal, Research Alert and Science Citation Index)

(Continued overleaf)

In articles with more than one author, the name of the author to whom correspondence should be addressed is indicated in the article heading by a 6-pointed asterisk (*)

Radionuclide X-Ray Fluorescence Analysis with Environmental Application

by **J. Tölgyessy**, *Slovak Technical University, Bratislava, Czechoslovakia,* **E. Havránek** *and* **E. Dejmková**, *Comenius University, Bratislava, Czecholovakia*

(Wilson & Wilson's Comprehensive Analytical Chemistry Vol. XXVI)

G. Svehla *(editor)*

Nuclear analytical methods are being used increasingly for solving analytical problems and, of these methods, radionuclide X-ray fluorescence analysis (radionuclide XRFA) is becoming more important. The purpose of this work is to present a comprehensive, instructive analysis of the basis of radionuclide XRFA, to describe methods of sample preparation for environmental analysis and to make the reader more familiar with the procedures, methods and instrumentation of radionuclide XRFA used in this field. This book discusses the use of radionuclide XRFA for solving analytical problems of the environment and information is presented concerning the current state of research and use of radionuclide XRFA in this significant area. The present volume will serve as a basic source of data and also as a laboratory handbook.

Contents. **1. Nuclear analytical methods and protection of the environment.** The importance of checking the quality of environmental components. Radionuclide X-ray fluorescence analysis (radionuclide XRFA) and the nuclear analytical methods. The origin and development of radionuclide X-ray fluorescence analysis. **2. The physical basis and method of radionuclide X-ray fluorescence analysis.** Physical basis of radionuclide XRFA. The radionuclide X-ray fluorescence analysis methods. **3. Source of environmental pollution.** Sources of atmospheric pollution. Sources of water pollution. Sources of soil pollution. The transport of pollutants from the atmosphere, water and soil into biological materials. The health hazard from the presence of harmful substances in the human environment. **4. Sampling procedures.** Atmospheric sampling. Water sampling. Soil sampling. Sampling of sludges, sediments and solid wastes. Sampling of biological materials. **5. The preparation of samples for the determination of pollutants in components of the environment.** Reference materials and the laboratory preparation of standards. Preparation of samples for determining impurities in the atmosphere. The preparation of samples for determining impurities in water. The preparation of samples of biological materials for analysis. The preparation of samples for the determination of impurities in soil, sludges, sediments and solid wastes. **6. A review of the use of radionuclide X-ray fluorescence analysis of environmental components.** Radionuclide XRFA of air samples. Radionuclide XRFA of air samples. Radionuclide XRFA of water samples. Radionuclide XRFA of soil and sediment samples. Radionuclide XRFA of samples of biological materials. **7. The use of radionuclide X-ray fluorescence analysis in other branches of science and technology.** The mining industry. The production of building materials. Metallurgy. The fuel and petroleum industries. The chemical, photographic and paper industries. Pharmacy. Space Research. Archaeology and art. The measurement of the thickness of thin coating. **8. References.** Subject index.

Distributed in the East European Socialist Countries, Democratic Republic of Vietnam, Mongolian People's Republic, People's Democratic Republic of Korea, People's Republic of China and Republic of Cuba by Alfa, Bratislava, Czechoslovakia

1990 282 pages
Price US$ 120.50 / Dfl. 235.00
Subscr. Price: US$ 107.75 / Dfl. 210.00
ISBN 0-444-98837-8

Elsevier Science Publishers
P.O. Box 211, 1000 AE Amsterdam, The Netherlands
P.O. Box 882, Madison Square Station, New York, NY 10159, USA

Chemometrics Tutorials

Collected from Chemometrics and Intelligent Laboratory Systems - An International Journal, Volumes 1-5

edited by **D.L. Massart,** *Brussels,* **R.G. Brereton,** *University of Bristol, Bristol, UK,* **R.E.Dessy,** *Blacksburg, VA,* **P.K. Hopke,** *Potsdam, NY,* **C.H. Spiegelman,** *College Station, TX,* **W. Wegscheider,** *Graz, Austria*

The journal *Chemometrics and Intelligent Laboratory Systems* has a specific policy of publishing tutorial papers, (i.e. articles aiming to discuss and illustrate the application of chemometric and other techniques) solicited from leading experts in the varied disciplines relating to this subject. This book comprises reprints of tutorials from the first 5 volumes of this journal, covering the period from late 1986 to mid 1989. The authors of the papers include analytical, organic and environmental chemists, statisticians, pharmacologists, geologists, geochemists, computer scientists and biologists, which reflects the strong interdisciplinary communication. The papers have been reorganized into major themes, covering most of the main areas of chemometrics. This book is intended both as a personal reference text and as a useful background for courses in chemometrics and laboratory computing.

1990 viii + 428 pages (Paperback)
Price: US$ 66.75 / Dfl. 130.00
ISBN 0-444-88837-3

Elsevier Science Publishers
P.O. Box 211, 1000 AE Amsterdam, The Netherlands
P.O. Box 882, Madison Square Station, New York, NY 10159, USA

CHEMOMETRICS AND INTELLIGENT LABORATORY SYSTEMS

An International Journal Sponsored by the Chemometrics Society

which includes **"Laboratory Information Management"**

This international journal publishes articles about new developments on laboratory techniques in chemistry and related disciplines which are characterized by the application of statistical and computer methods. Special attention is given to emerging new technologies and techniques for the building of intelligent laboratory systems, i.e. artificial intelligence and robotics. The journal aims to be interdisciplinary; more particularly it intends to bridge the gap between chemists and scientists from related fields, statisticians, and designers of laboratory systems. In order to promote understanding between scientists from different fields the journal features a special section containing tutorial articles.

The journal deals with the following topics: Chemometrics; Computerized acquisition, processing and evaluation of data: Robotics; Developments in statistical theory and mathematics with application to chemistry; Intelligent laboratory systems; Laboratory information management; Application (case studies) of statistical and computational methods; New software; Imaging techniques and graphical software applied in chemistry. The research papers and tutorials are complemented by the **Monitor Section** which contains news, a calendar of forthcoming meetings, reports on meetings, software reviews, book reviews, news on societies and announcements of courses and meetings. This section also contains the "Chemometrics Newsletter", official bulletin of the Chemometrics Society.

Abstracted/Indexed in:

Analytical Abstracts, ASCA, BioSciences Information Service, Cambridge Scientific Abstracts, Chemical Abstracts, Chromatography Abstracts, Current Contents, Current Index to Statistics, Excerpta Medica, INSPEC, SCISEARCH

Subscription Information:

1991: Vols 10-13 (12 issues) US$ 692.00 / Dfl. 1232.00 including postage

ISSN 0169-7439

A free sample copy of the journal is available on request.

Elsevier Science Publishers

P.O. Box 211, 1000 AE Amsterdam, The Netherlands

P.O. Box 882, Madison Square Station, New York, NY 10159, USA

JOURNAL OF CHROMATOGRAPHY

VOL. 522 (1990)

JOURNAL *of* CHROMATOGRAPHY

INTERNATIONAL JOURNAL ON CHROMATOGRAPHY,
ELECTROPHORESIS AND RELATED METHODS

ELSEVIER
AMSTERDAM — OXFORD — NEW YORK — TOKYO

J. Chromatogr., Vol. 522 (1990)

0021-9673/90/$03.50

Printed in The Netherlands

Journal of Chromatography, 522 (1990) 1–21
Elsevier Science Publishers B.V., Amsterdam

CHROM. 22 706

Study of the interaction between two overloaded bands injected successively in non-linear chromatography

M. ZOUBAÏR EL FALLAH and GEORGES GUIOCHON*

**Department of Chemistry, University of Tennessee, Knoxville, TN 37996-1600 and Division of Analytical Chemistry, Oak Ridge National Laboratory, Oak Ridge, TN (U.S.A.)*

(First received March 8th, 1990; revised manuscript received June 25th, 1990)

ABSTRACT

Band interaction in non-linear chromatography was studied using a delayed injection procedure which permits the easy adjustment of the degree of interference regardless of the real selectivity between the two compounds studied. This work represents an investigation of the mechanism of band interference, independent of the separation process. Special attention was given to the converse displacement effect, which corresponds to the displacement of the more strongly retained compound by the less retained one. Experimental evidence of this converse displacement is shown using two different systems. The intensity of this displacement is discussed in relationship to the concentration of the displacer and the waiting time between the two injections. Calculated band profiles, obtained with the semi-ideal model of chromatography and competitive Langmuir isotherms, are compared with experimental profiles. With one system good agreement between experiments and simulations was found whereas the other system studied showed significant deviations from the competitive Langmuir isotherm model.

INTRODUCTION

Non-linear effects have been observed and reported systematically in preparative liquid chromatography when the column is operated under overloaded conditions [1–10]. So far these effects have been noticed mostly when high concentration bands of binary mixtures are introduced into a column, although gradient elution, systems peaks [11,12] and displacement chromatography [13,14] are other non-linear effects. In overloaded elution, the displacement effect [1–5] and the tag-along effect [7,10] are the most important of these non-linear effects. They are both due to the fact that the velocity associated with a certain concentration of a given component depends on the concentration of the other components locally present [6,7].

These non-linear effects occur whenever two or more different species compete for adsorption on the same sites or, more generally, for interaction with the stationary phase. At low coverages of the adsorbent surface (*i.e.*, at low sample sizes), the effects of this competition cannot be observed. At high surface coverages, however, the competition becomes important and strongly affects the propagation of the band system of a mixture. This influence is especially important for the individual elution profiles of incompletely resolved bands.

0021-9673/90/$03.50

As the ability to make accurate predictions of band profiles in overloaded chromatography is critical in any attempt to optimize the operating parameters, a proper understanding of the mechanism of band interactions and especially of the displacement and tag-along effects is very important [15–18]. Theoretical predictions must be compared with experimental results. So far, such comparisons have been performed by injecting high-concentration samples of binary mixtures under conditions where eluted bands are incompletely resolved [4,5]. Then, an accurate determination of the individual band profiles is required. It cannot be made by on-line analysis, which cannot be carried out at a high enough frequency. The best method available involves the collection of *ca.* 100 fractions during the elution of the mixed band and the analysis of these fractions [4,5].

The study of band interactions does not require the simultaneous injection of the two compounds, however. They only need to interact somewhere in the column. This can be achieved very simply by injecting the more strongly adsorbed compound, waiting a certain time and injecting the less retained compound. Depending on the delay between the two successive injections, we have two interesting possibilities: either the faster band of the less retained compound reaches the slower band but does not pass it completely, which leads to the elution of a mixed zone, or the less retained compound passes completely through the more retained one and the resulting chromatogram shows two separated bands. Because of their temporary interaction, however, the profiles of these bands are different from those obtained with the same samples injected in the reverse order. As the bands are resolved, their profiles can be derived simply from the detector signal after proper calibration.

The former situation permits the study of the interaction between a concentration shock layer and a diffuse front, independently of the separation process, under a variety of experimental conditions. The latter situation would be of great potential interest if a large change in the band profiles took place and if either the new band profiles or the change in band profiles due to the band interaction could be related simply to the parameters of the competitive adsorption isotherms of the compounds studied.

Unfortunately, when the faster band has completely passed through the slower one, the band profiles are almost unchanged. Only small shifts in the retention times of their fronts and tails are observed. Of course, these retention-time shifts are related to the band interaction, but it is impossible to extract from these shapes the accurate information needed concerning the nature and the intensity of the interactions, *i.e.* the competitive adsorption isotherms and their parameters.

Obvious changes in the band profiles occur only under conditions where a two-component mixed zone is eluted. This case is discussed in this paper, where the results of theoretical calculations [10,19] are compared with actual profiles. Any pair of compounds can be used, no matter what their actual relative retentions are, to obtain a system of incompletely resolved bands. We may choose these compounds so that one of them can be detected at a wavelength where the other is transparent.

THEORY

The calculations made in this work are based on the use of the semi-ideal model of chromatography and of the calculation programs developed previously in our

laboratory [10,19–21]. All details regarding the theoretical approach and the assumptions made can be found in several recent publications [22,23]. The semi-ideal model assumes that the mass transfers between phases in the column are fast so that the concentrations of any compound in the two phases are never much different from their equilibrium values. The influence of the finite kinetics of mass transfer is accounted for by the use of an apparent coefficient of axial dispersion, which is related to the column efficiency at very low solute concentrations [24–26].

The simulation program used for the calculation of the individual elution band profiles in the case of the delayed injection of two compounds is identical with that used in previous publications to calculate the individual elution bands of the components of a binary mixture [10,20]. In these computations, competitive Langmuir adsorption isotherms were used. The values of the space and time increments were adjusted to account for the finite column efficiency [23,27,28]. Only the injection subprogram had to be changed to provide for the delayed injection of the two solutes. The final program was written in Pascal and run on the VAX 8700 of the Computer Center of the University of Tennessee.

Excellent agreement between the calculated individual band profiles and those determined experimentally has been demonstrated in several previous papers [4,5,29–31]. This agreement has been reported for single- [29,30] and two-component samples [4,5], with a pure mobile phase or a solution of a weak organic solvent (acetonitrile or methanol) in water and also when the mobile phase is a solution of a strong organic modifier in a weak organic solvent [31].

EXPERIMENTAL

Equipment and injection procedure

An HP 1090 liquid chromatograph (Hewlett-Packard, Palo Alto, CA, U.S.A.) equipped with a diode-array detector was used. The mobile phase was used as solvent A. Solutions of sample components in the mobile phase were used as solvents B and C. Injections were carried out by programming step gradients of solvent B or C followed by a return to solvent A in the time-table monitoring the gradient system. These pump injections were reproducible and led to acceptable rectangular injection profiles provided that they lasted long enough (at least 1 min, *i.e.*, more than 1-ml injections at flow-rates above 1 ml/min).

In order to avoid saturation of the UV detector, we made very large-volume injections (not less than 2 ml) and used dilute solutions. For the compounds selected, this led to values of the loading factor which always exceeded 1% (the loading factor is the ratio of the amount of one component injected to the column saturation capacity for this component).

Column and chemicals

A 25 × 0.46 cm I.D. column was packed in the laboratory with YMC-gel 120A, 5-μm particles of octadecyl silica (YMC, Morris Plains, NJ, U.S.A.). The column void volume measured as the retention volume of uracil was 2.66 ml, its porosity, ε, was 0.64 and its phase ratio $[(1 - \varepsilon)/\varepsilon]$ was 0.56. The mobile phase used was acetonitrile (J.T. Baker, Phillipsburg, NJ, U.S.A.)–water (25:75, v/v). All experiments were performed with a mobile phase flow-rate of 1 ml/min. The column was conditioned at 40°C for several hours before use.

In order to simplify the experimental study of overloaded peak interactions, we chose 2,4-dimethylphenol (DMP) (Aldrich, Milwaukee, WI, U.S.A.), which adsorbs at 295 nm, as the slower compound. The faster compound was either 2-phenylethanol (PE) or 2-methylphenethyl alcohol (MPA) (both from Fluka, Ronkonkoma, NY, U.S.A.), which do not show any significant UV absorption at this wavelength.

Isotherm determinations

Single-component isotherms were determined by frontal analysis and retention-time methods. The former method uses the injection of increasing concentration steps and derives isotherm points from the retention times of the breakthrough curves [32]. The latter method, based on the closed-form solution of the ideal model of chromatography [33], derives the two parameters of the best Langmuir isotherm from the retention time of the front of a high-concentration band and the retention time of a very small band, small enough to be eluted under the conditions of linear chromatography [31]. Data were derived from several bands corresponding to different sample sizes.

Data acquisition

The raw data were acquired with the HP 9133 data station. Chromatographic data were then transferred to the VAX 8700 of the University Computer Center for further treatment. Using calibration data acquired from standard solutions, the absorbance profiles were converted into concentration profiles for comparison with calculated profiles.

Separate injections of solutions of each compound were made under the selected experimental conditions. From their retention times, the time between two successive injections or the waiting time needed in order for band interference to occur was obtained. The whole range of waiting times was investigated, from zero (simultaneous injections) to the value for which the front of the first band coelutes with the end of the second band tail. The amount of DMP injected was kept constant throughout the study. A 4-ml pulse of an 11.39 mM solution was pumped into the column. This corresponds to a loading factor of 2.17%.

RESULTS AND DISCUSSION

Results of the calculations

Although we deal in a later section with the comparison between calculated and experimental data, all the input data for the calculations whose results are reported here (*i.e.*, mobile phase flow-rate, phase ratio, column length, isotherm parameters, etc.) were chosen to be as close as possible to the experimental values. Calculations made with our program permit an easy simulation of the different possible degrees of interaction, depending on the value of the injection parameters, *i.e.*, the waiting time, t_w, between the two injections and the concentration of each compound, and a study of the effects of these parameters on the band interference. The waiting time controls the degree of band resolution on elution and the sample sizes the intensity of the non-linear effects.

Bands completely separated

This situation is easily obtained if the two compounds have a large relative retention on the phase system used. It suffices to wait a short period of time between the injection of the slower component and that of the faster one. Fig. 1 compares the band profiles obtained in such a case (solid lines) with those calculated for successive injections of the two components in the reverse order (dashed lines), *i.e.*, when the faster component is injected first. The same profiles in dashed lines would be obtained if we assume no band interaction, *i.e.*, single-component adsorption isotherms, in the simulation whereas the solid line profiles were calculated assuming Langmuir competitive isotherms.

In the calculations for Fig. 1, the concentration of the faster component was ten times higher than that of the slower component and the waiting time was 4 min. The essential effect of the interaction between the two bands seems to be a significant shift

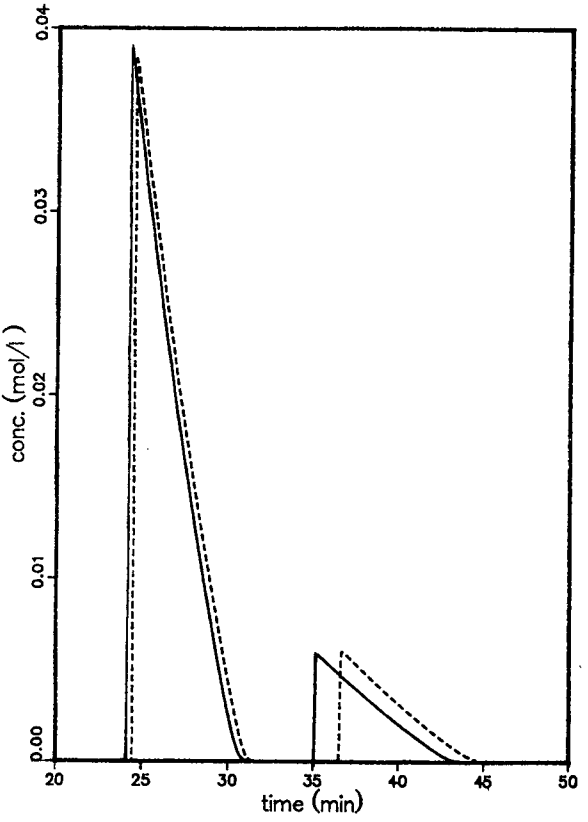

Fig. 1. Interaction between two independent bands. Calculated chromatogram for the successive injection of the slower and the faster moving compounds, with a waiting time t_w = 4 min. Injection characteristics: faster compound, V_1 = 2 ml, c_1 = 113.9 mM; slower compound, V_2 = 1 ml, c_2 = 11.39 mM. Feed composition: $R = c_1/c_2 = 10$. Solid lines: Langmuir competitive isotherms (a_1 = 13.82, a_2 = 26.13, b_1 = 5.26, b_2 = 18.56; a is dimensionless, b in ml/mM). Dashed lines: no competition was assumed (single Langmuir isotherm), or superimposed chromatograms of independent injections. The two bands are completely resolved.

of the whole profile towards shorter retention times. Both bands move faster than when there is no competition. The shift is much larger for the slower than for the faster component.

The waiting time between the two injections was found to have no significant effects on the band profiles over the whole range of waiting times for which band interference has ended before elution of the second band. On the other hand, the amount of one component affects the retention time shift of the band of the other. The profiles obtained for the same amount of the slower component and increasing amounts of the faster component are shown in Fig. 2.

The retention time shift of the band of a constant amount of the slower component increases with increasing amount of the faster component. There is a slight, nearly negligible change in the shape of its tails and the second band becomes slightly shorter (Fig. 2). A similar but much smaller effect is observed for the faster component band profile. Its retention time shift increases at a constant amount of faster component with increasing amount of the slower compound injected.

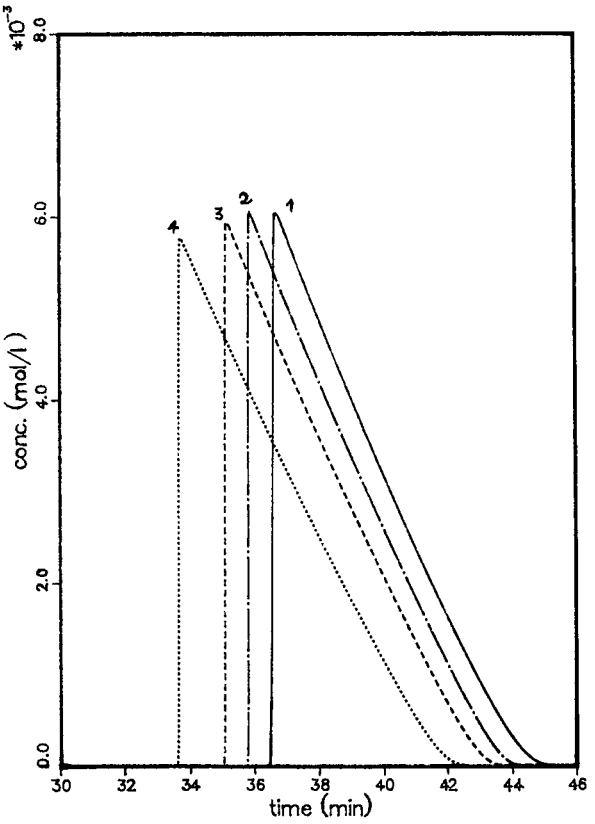

Fig. 2. Influence of the concentration of the faster compound on the elution band profile of the slower one. Same competitive Langmuir isotherm as for Fig. 1. Same injection volumes and waiting time. (1) No faster compound injected; (2) relative concentrations of the two samples = 5; (3) relative concentrations of the two samples = 10; (4) relative concentrations of the two samples = 20.

These phenomena were calculated using the competitive adsorption model. In principle, it would be possible to correlate the retention time shift of one compound band with the loading factor for the other. This could provide a method for the determination of competitive isotherms. The effects calculated are weak, however, and the errors made in the determination of retention data are too large to permit the use of the retention time shift for a study of the possible deviations of the competitive isotherms from the Langmuir model.

Elution of a two-solutes mixed zone

Displacement of the faster solute by the slower one. When the waiting time is chosen so that the front of the faster moving band passes the front of the slower one while the two bands are not fully resolved, the two individual bands profiles are similar to the conventional profiles obtained for the overloaded bands of a binary mixture of closely related compounds, for which the relative retention is not very different from unity [1–5].

Fig. 3 shows the calculated chromatogram obtained in such a case. It is characterized by two concentration shock layers on the faster moving band, one at the front and one at the rear. The latter results from the displacement effect of the slower moving component. As we observed above, the injection procedure provides the possibility of such strong band interaction even if the relative retention is very large. Fig. 3 shows clearly that the displacement effect is due to band interference, to the fact that the velocity associated with a certain concentration of a compound depends (through the competitive isotherm) on the concentration of the other compounds. In other words, a displacement effect of the other components of a system (sample components or mobile phase additives) accompanies a positive concentration shock (or shock layer) of any component. This effect arises because the concentration surge of this component crowds the other ones out of the stationary phase.

As this type of band interaction has already been discussed [8,9], we shall focus on the other case, which has not been reported previously and whose observation would be further proof of the competition between compounds for interaction with the stationary phase.

Displacement of the slower compound by the faster one. When the waiting time is such that the band of the faster compound catches up with the band of the slower one but the front of the slower moving band is still eluted before the front of the faster one, the calculated chromatogram shown in Fig. 4 is typically obtained.

Again, the first-eluted band exhibits two shock layers, the second shock layer marking the beginning of the elution of a mixed zone, but in this instance the chromatogram differs from the previous one (Fig. 3) in two important ways. First, the first eluted band is that of the more strongly retained, slower moving compound (Fig. 4). Hence the second shock layer occurs on the rear of the slower component. Second, this shock layer is positive (Fig. 4), whereas that on the rear of the faster moving band in the previous case was negative (Fig. 3). It produces an increase in the concentration of the slower compound, which physically corresponds to the displacement of the more strongly retained component by the other one.

Such a displacement effect is unlikely to occur in practice in preparative chromatography, but the mutual displacement of solutes is well known in separations and purifications involving adsorption, such as in pressure swing adsorption (PSA)

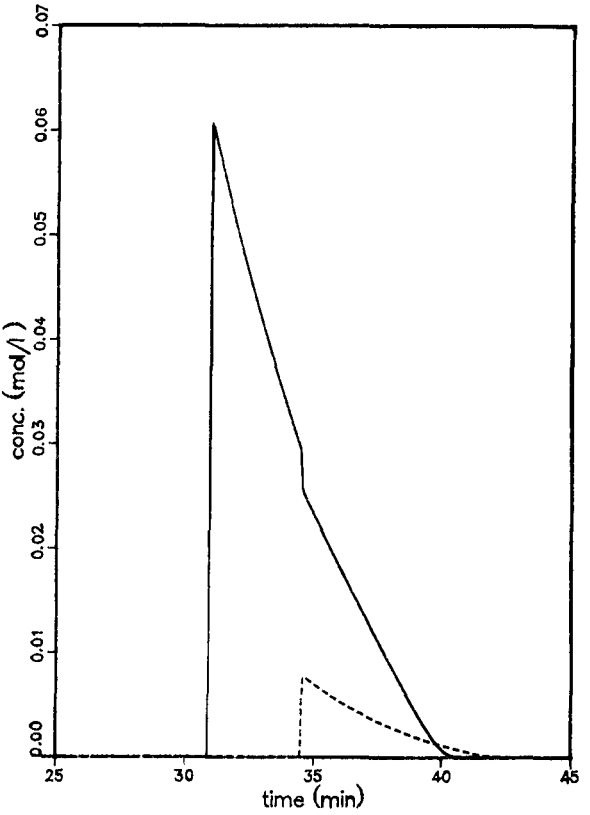

Fig. 3. Influence of the waiting time between the two successive injections on the nature of the displacement effect. Same competitive Langmuir isotherm and concentration as in Fig. 1. Volumes of solution injected: $V_1 = V_2 = 2$ ml. Relative concentrations of the two samples: 10. Waiting time: 12 min. The two bands interact and there is an obvious displacement effect of the faster one by the slower one.

[34,35]. In Fig. 4, all the conditions are identical with those in Fig. 3, except the waiting time. Hence, the displacement of the slower compound by the faster one is part of the interaction pattern involved in the delayed injection experiments as much as the displacement of the faster compound by the slower one. Although in Fig. 3 the only apparent band interaction at the column outlet is the displacement of the faster compound by the slower one, the converse displacement effect has taken place previously, somewhere in the column.

This pattern of interference is general and explains the results shown in Figs. 1 and 2 in the case where the eluted bands are well resolved. The first interaction to take place, the displacement of the slower compound by the faster one, narrows the slower moving band by making its tail move faster than that of a pure compound band. When the faster moving band passes over the slower one, the usual displacement effect takes place and the front of the slower band moves faster. Accordingly, both the front and the rear of the band are accelerated successively, but at different times, by different interaction mechanisms. The result, however, is only a shift of the whole band.

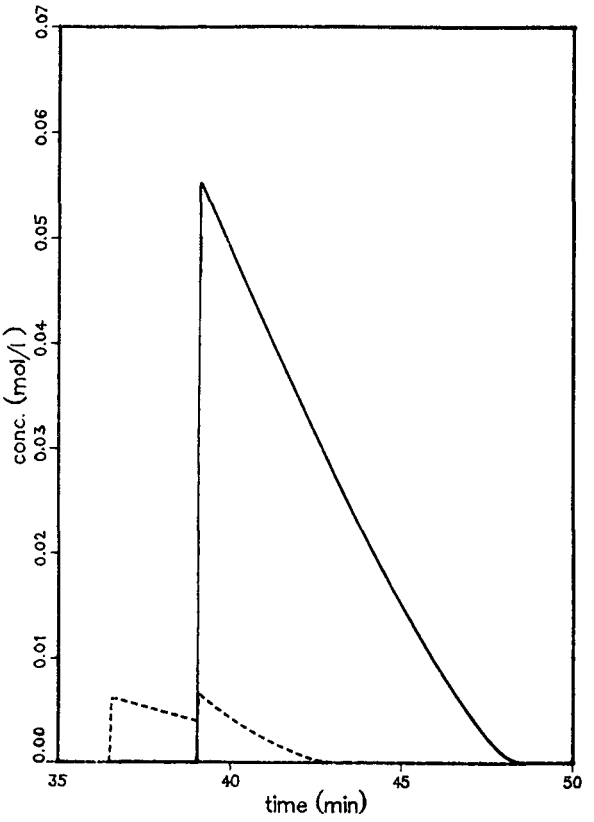

Fig. 4. Same as Fig. 3, except waiting time = 18 min. The two bands interact and there is a converse displacement effect of the slower one by the faster one.

Fig. 5 shows the effect of the waiting time on the intensity of the converse displacement effect when the two sample amounts are kept constant. Fig. 5 shows the profile of the slower band when the concentration of the faster compound is ten times that of the slower one, in order to maximize the effect.

As the waiting time decreases, the faster band reaches the slower one earlier and earlier. Note that the front of the faster band (not shown in Fig. 5) is eluted in the same time as the second shock layer of the slower band (only shown in Fig. 5). When the waiting time, t_w, decreases, the importance of the band interaction increases, the desorption of the slower compound by the faster one occurs earlier and the retention time of its tail decreases, as the interaction lasts longer. We note that when t_w decreases, the ratio of the concentrations of the slower compound just after and before the shock is almost independent of the waiting time. Hence this ratio can be used as a measure of the inverse displacement intensity. A similar ratio has been used to measure the intensity of the normal displacement effect in non-linear chromatography [7,9].

Fig. 6 shows the effect of increasing the amount of faster compound injected at a constant amount of slower compound and constant waiting time.

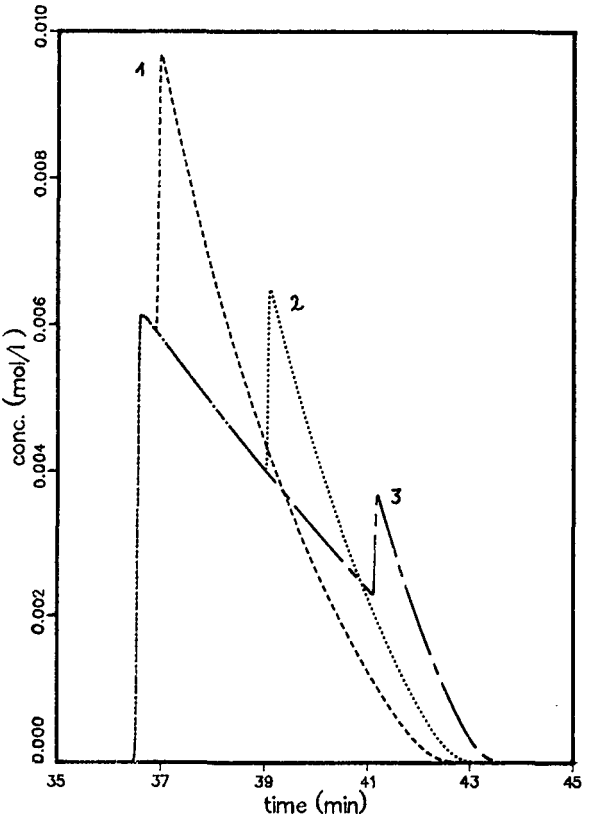

Fig. 5. Influence of the waiting time between the two successive injections on the displacement of the slower compound by the faster one. Same competitive Langmuir isotherm and concentrations as in Fig. 1. $V_1 = V_2 = 2$ ml. Relative concentrations of the two samples: 10. Waiting time: (1) 18 min; (2) 20 min; (3) 22 min.

When the concentration of the faster compound is increased, its band moves faster and, at a constant waiting time, the retention time of its front decreases. At the same time, the relative concentration of the two compounds increases, the ratio of the solute concentrations after and before the shock increases and the intensity of the converse displacement effect increases.

Isotherm determinations

In order to compare quantitatively the results of the calculations with those of experiments, we need to know the adsorption isotherm of each compound used. We selected DMP as the slow-moving compound. Depending on the experiment, either PE or MPA was the fast moving compound. This choice has the advantage that the slower compound can be detected in the presence of the faster one, as DMP absorbs light at 295 nm whereas neither PE nor MPA does.

Two methods were used for the determination of the equilibrium isotherms, frontal analysis (FA) and the retention time method (RTM). FA is a classical method

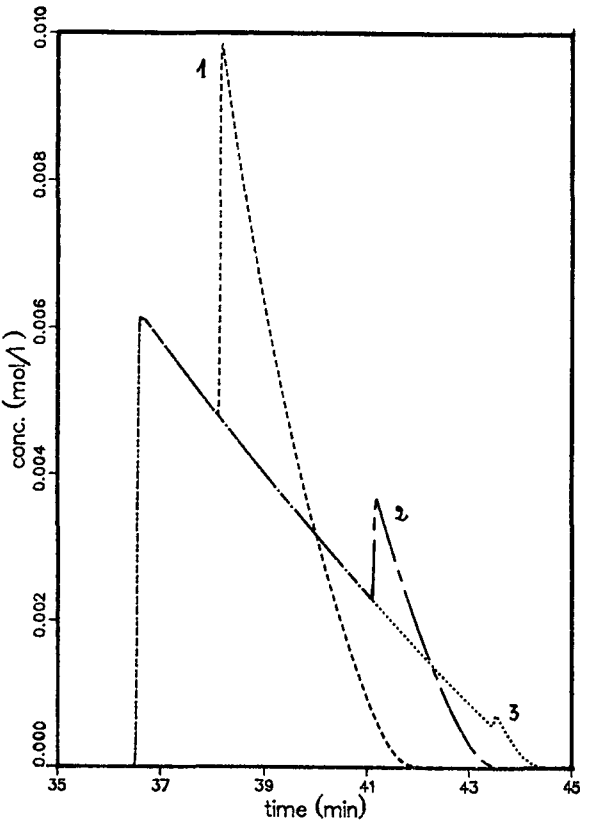

Fig. 6. Influence of the concentration of the faster compound on the elution band profile of the slower one. Conditions as in Fig. 5. Relative concentrations of the two successive samples: (1) 20; (2) 10; (3) 5.

known to be accurate for the measurement of adsorption isotherms in HPLC systems which give convex upwards isotherms [36,37]. RTM [31] is based on the analytical solution of the ideal model of chromatography [33]. It has been shown that when the column efficiency exceeds 5000 plates, the parameters estimated by RTM are in good agreement with those obtained by other methods [31]. The column we used has more than 10 000 theoretical plates, which justifies the use of RTM. This method has the further advantages of being both fast and economical regarding the amount of compound needed to perform a determination.

The FA data were fitted to the Langmuir model [$q = aC/(1 + bC)$ where q and C are concentrations of the compound in the stationary and mobile phase, respectively, and a and b are numerical coefficients]. The values of a obtained by the two methods were found to be in close agreement and slightly different (2%) from the value derived from the capacity factor of small samples ($a = k'/F$, where F is the phase ratio). RTM gave a value of b that was less affected by the concentration range of the data with which the fit was performed than the value given by FA. The value of b given by RTM changed by less than 5% when the amount injected was increased four-fold, whereas decreased by 20% for the FA data. This shows a slight deviation

of the Langmuir model from the exact adsorption behavior of the compounds. The best values of a and b for the three compounds studied in this work are given in Table I.

When using the a and b values obtained from RTM, the simulated individual band profiles for the three compounds were very close to the experimental ones. Fig. 7 compares the band profile recorded for a large amount of DMP with that calculated with the coefficients in Table I. There is excellent agreement. Similar agreement was observed for the other two compounds.

The ratio of the saturation capacities of the two compounds used in this study is markedly different from unity. These ratios are Q_s (MPA)/Q_s (DMP) = 1.86 and Q_s (PE)/Q_s(DMP) = 1.30. The corresponding values of the relative retention are 1.89 and 3.64, respectively.

In order to take into account the competition of the compounds for adsorption, a competitive adsorption model should be adopted. One of the most widely accepted theories of multi-component adsorption is based on the concept of an ideal adsorbed solution (IAS) [38–42]. Its major advantage is that only single-component data are required. Among several IAS competitive adsorption models, the competitive Langmuir isotherm [41] is the simplest and the most popular, although the IAS theory shows that it is thermodynamically consistent only if the two solute saturation capacities are identical [42]. This condition, which is seldom fulfilled in real cases, applies to gas–solid systems. Its extension to liquid–solid adsorption is not straightforward. However, it has been shown that in many instances the competitive adsorption data obtained by frontal analysis of a binary mixture [43] and by the 'simple wave' method [44] were fairly well accounted for by a Langmuir competitive isotherm. Conversely, excellent agreement has been reported between the individual band profiles of the components of binary mixtures measured experimentally and those calculated using the competitive Langmuir isotherm model [4,5]. As the competitive Langmuir isotherm model is also convenient, we have used this model as an approximation to actual isotherms in our calculations.

Experimental results

As experimental proof of the converse displacement effect has never been reported before, in this work we mainly investigated the displacement of the slower compound by the faster one.

TABLE I

VALUES OF THE SINGLE-COMPONENT LANGMUIR ISOTHERM COEFFICIENTS DETERMINED BY RTM

See text for RTM procedure.

Compound	a	b
PE	7.18	3.92
MPA	13.8	5.26
DMP	26.1	18.6

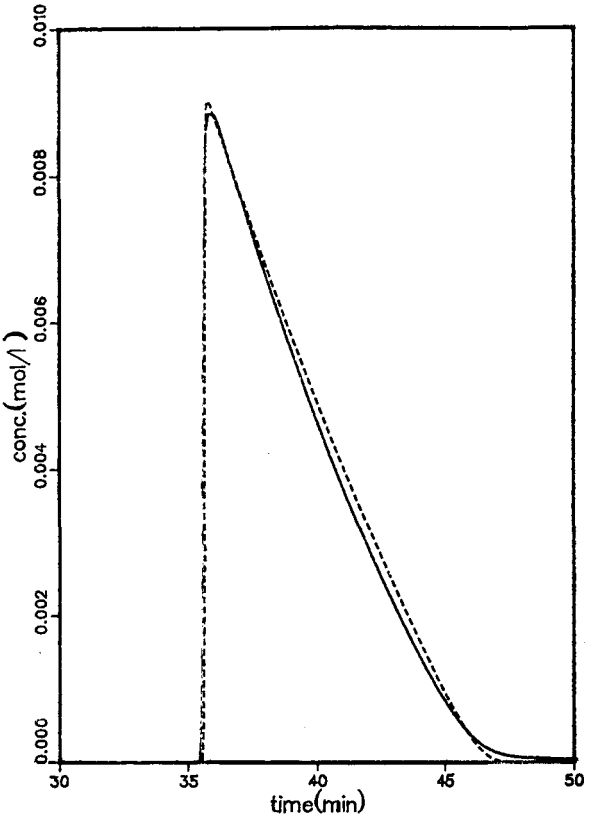

Fig. 7. Comparison between the band profile recorded for a 4-ml sample of an 11.4 m*M* solution of DMP (solid line) and the profile calculated with the isotherm parameters in Table I (dashed line).

Fig. 8 shows a typical chromatogram obtained with the injection procedure described above (see Experimental). A solution of DMP is first injected and after 28 min a solution of PE (see caption) is injected. The chromatogram shown in Fig. 8 was recorded at 240 nm, where both compounds absorb UV radiation.

Fig. 8 shows that there is some interaction between the two bands. The top of the second band profile (faster moving compound) is different from the top of the profile obtained for an unperturbed injection (see Fig. 7). The change in the band profile of DMP is small, however. The dip in its rear profile is due to an impurity in the PE sample.

Effect of the waiting time on the intensity of the displacement effect

Figs. 9 and 10 show the superimposition of the experimental (curve 1) and simulated (curve 2) concentration profile of the elution band of DMP recorded at 295 nm with waiting times of 23 and 18 min, respectively. In both instance the faster moving component was MPA and its concentration was ten times higher than that of the slower moving compound.

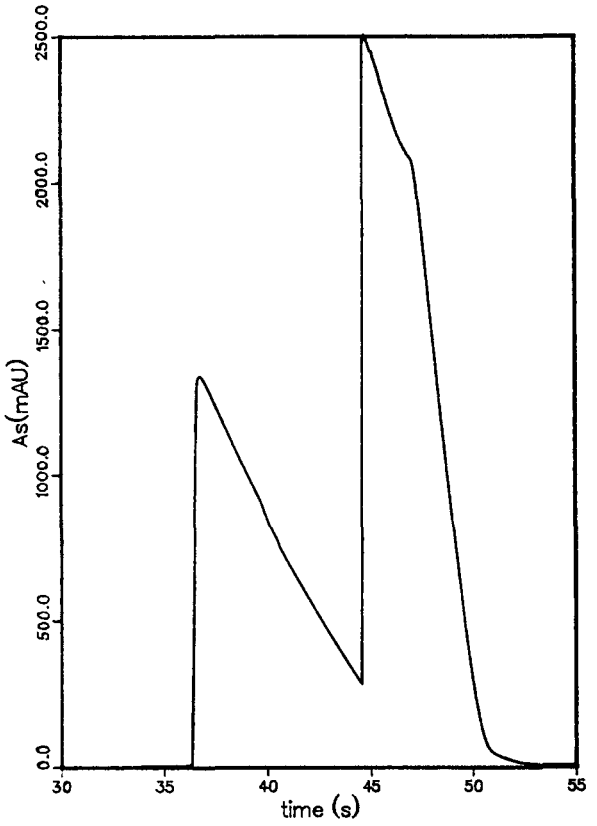

Fig. 8. Experimental chromatogram obtained on injecting first a sample of DMP (V_2 = 4 ml of a solution of DMP in the mobile phase, c_2 = 11.39 mM), then, after a 28-min waiting time, a sample of PE (V_1 = 4 ml of a solution of PE, $c_1 = 6c_2$ = 68.34 mM). UV detection at 240 nm. Flow-rate, 1 ml/min. For other conditions, see text.

In both Figs. 9 and 10 there is excellent general agreement between the behavior of the experimental and calculated band profiles of DMP. The only prominent difference is the small shift in retention time observed. However, this is minor with regard to the total time (less than 1 min in 36 min, *i.e.*, 3% in Fig. 9 and, less than 1% in Fig. 10). Also, the tip of the experimental band is blunter than that of the calculated profile. Except for the top of the two peaks, however, the experimental and calculated profiles are nearly identical. We also note that the only difference in the rear of these profiles is the tailing of the experimental peak, possibly an indication that the adsorbent surface is not completely homogeneous [45].

As we have seen in the numerical study of the displacement effect reported above, when the waiting time decreases, the interaction between the two bands becomes more important. The retention time of the band tail decreases and the concentration at the front shock increases. A quantitative comparison between the profiles in Figs. 9 and 10 shows that the ratios of the concentrations after and before the shock

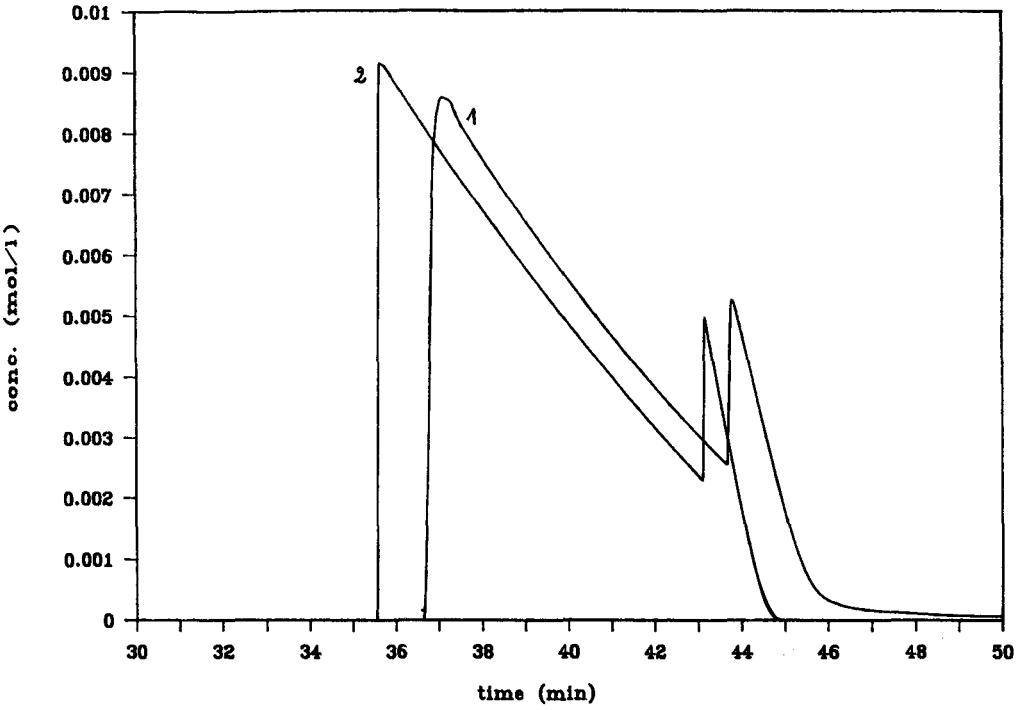

Fig. 9. Comparison between (1) experimental and (2) calculated elution profiles for the slower compound. Experimental conditions: first injection of DMP, V_2 = 4 ml, c_2 = 11.39 mM; waiting time, 23 min; second injection of MPA, V_1 = 6 ml. c_2 = 113.9 mM. Calculated profile with the same Langmuir competitive isotherms as in Fig. 1.

on the two experimental or the two theoretical profiles are equal to within less than 2%. In each figure these ratios differ by less than 7%. This difference between experimental and theoretical results is small, given the several possible sources of error (injection profiles, detector calibration, flow-rate and temperature fluctuations).

Influence of the faster compound concentration on the intensity of the displacement effect

This influence was studied by performing successive experiments using higher and higher concentrations of the faster compound with a constant-volume injection, while keeping constant the amount of the slower compound and the waiting time (Fig. 11). The faster compound is this instance was PE. Its concentration in the feed was increased so that the relative amount of PE injected to that of DMP was 3, 6 and 10 for the three chromatograms.

As expected, when the concentration of the faster compound is increased, the front of its band moves faster and the intensity of the displacement effect increases. Accordingly, the retention time of the slower compound band tail decreases and the ratio of its concentrations on the two sides of the shock increases. Hence the trend predicted in the calculations reported above is well reproduced in the experiments.

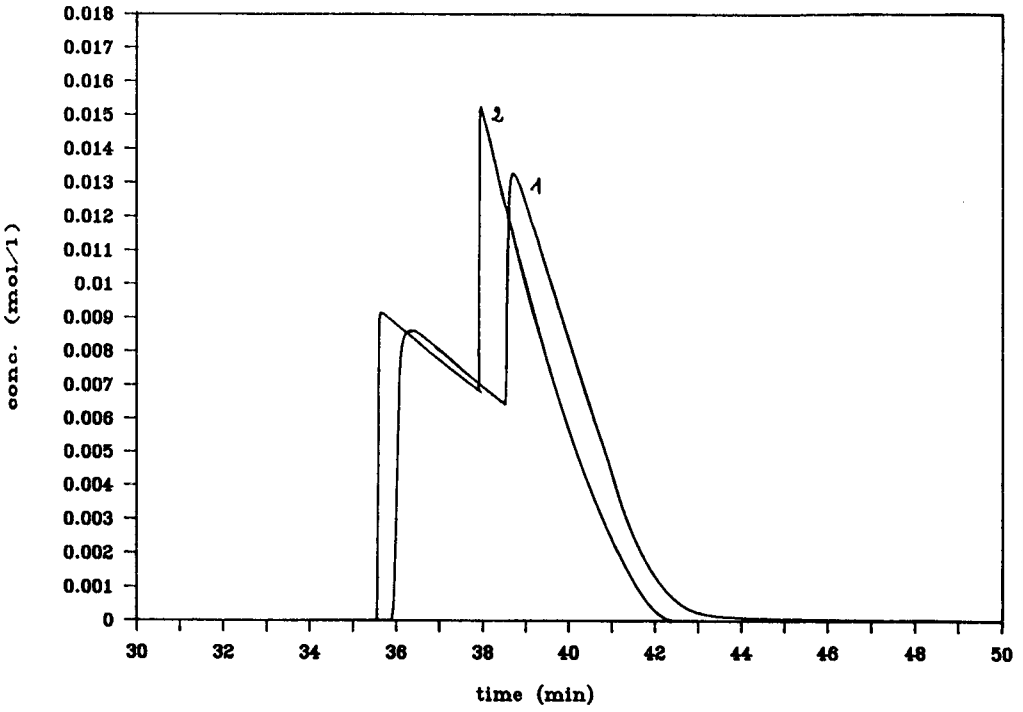

Fig. 10. Same as Fig. 9, except waiting time = 18 min.

For the same concentration, MPA causes a greater displacement effect of DMP than PE. This is demonstrated by the ratio of the slower compound concentrations on the two sides of the shock, *i.e.*, 1.52 and 2.18 for displacement with PE and MPA, respectively. This situation was expected as the relative retention between PE and DMP is almost twice that between MPA and DMP. The intensity of the displacement effect increases with increasing relative retention of the displacer to the displaced compound [8]. This means that the intensity of the converse displacement increases when the two compounds become more closely retained.

The agreement between the experimental and calculated chromatograms is not as good when DMP is displaced by PE than when it is displaced by MPA. As can be seen in Figs. 12 and 13, the calculations predict a much greater displacement effect than that observed experimentally. For example, the calculated ratio of the DMP concentrations on the two sides of the shock differs by more than 10% from the experimental value. The rear profile of the calculated band profile is steeper than that recorded experimentally.

Especially when the band interaction is expected to be important (*e.g.*, in Fig. 13), the faster compound shock appears to move more slowly than predicted by the calculation. On the other hand, there are differences in the degree of disagreement between Fig. 12 and 13. In Fig. 12 we observe that the time shifts of the two shocks are nearly the same, indicating the probably hydrodynamic origin of the band shift.

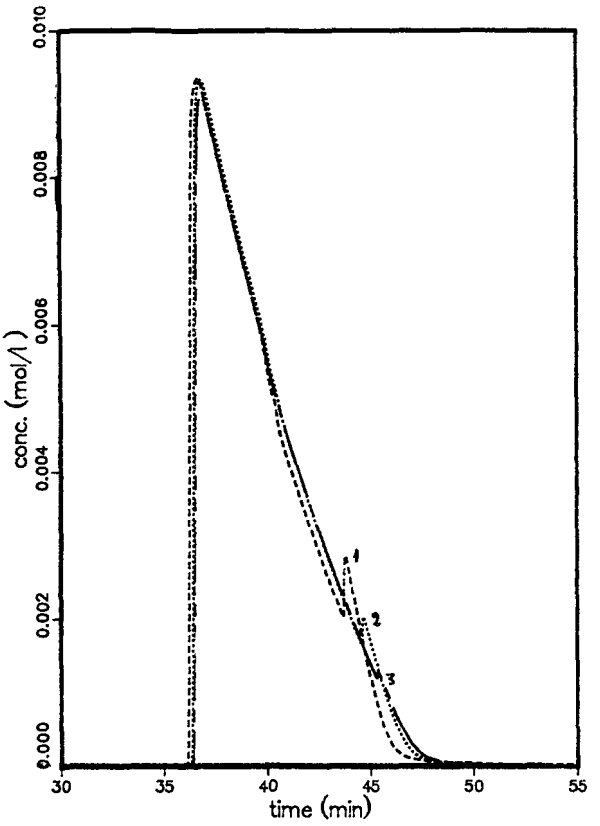

Fig. 11. Influence of the concentration of the faster compound on the intensity of the converse displacement of the slower one. First injection of DMP, V_2 = 4 ml, c_2 = 11.39 mM; waiting time, 28 min; second injection of PE, V_1 = 4 ml. Concentration ratio in the two samples, c_1/c_2: (1) 10; (2) 6; (3) 3.

In Fig. 13, in contrast, there is almost no hydrodynamic band shift, but the front of the faster moving compound has progressed further than predicted. Note the impurity on the front of the experimental band. This is the origin of the slight dip on the rear part of the slower compound band profile seen in Figs. 8 and 11.

Excellent agreement is observed between the calculated and recorded single-component band profiles in this work, as in previous studies [29,30]. The same agreement was also reported for the individual band profiles of optical isomers [5], and good agreement was observed for the bands of 2-phenylethanol and 3-phenylpropanol [4]. Hence the disagreements between calculated and experimental individual band profiles observed here are due to deviations between the true competitive isotherms and the Langmuir model, a topic of intense investigation.

CONCLUSION

Band interaction in non-linear overloaded chromatography is of critical importance as it determines the exact extent of the separation between components of a

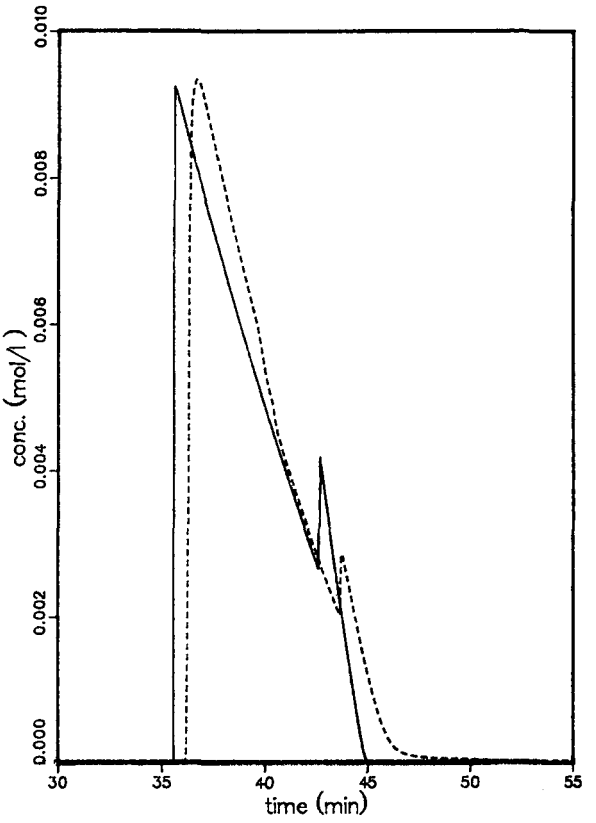

Fig. 12. Comparison between experimental (dashed lines) and calculated (solid lines) elution profiles for the slower compound. First injection of DMP, V_2 = 4 ml, c_2 = 11.39 mM (loading factor for the second component, $L_{f,2}$ = 2.17%); second injection of PE, V_1 = 4 ml, c_2 = 113,9 mM (loading factor for the first component, $L_{f,1}$ = 16.7%); waiting time, 28 min.

mixture and controls the exact values of the production rate and the recovery yield. Selectivity, column saturation capacity and, to a lesser extent, column efficiency control the degree of band interaction. The semi-ideal model of chromatography permits an accurate prediction of the propagation of component bands and of their individual elution profiles, taking the finite column efficiency into account. However, the exact knowledge of the competitive isotherm model is crucial for the exact prediction of the individual elution profiles or at least for an accurate description of the separation between components in non-linear chromatography.

The primary aim of this work was an investigation of the phenomena associated with band interference in chromatography. By studying the interaction between two independent bands in a chromatographic column, we were able to isolate band interference from the separation process itself. The conclusion is that band interaction follows a pattern which has not yet been reported, although it derives directly from the theory of non-linear chromatography. Under the proper set of experimental conditions, the less retained compound can displace the more retained compound, a

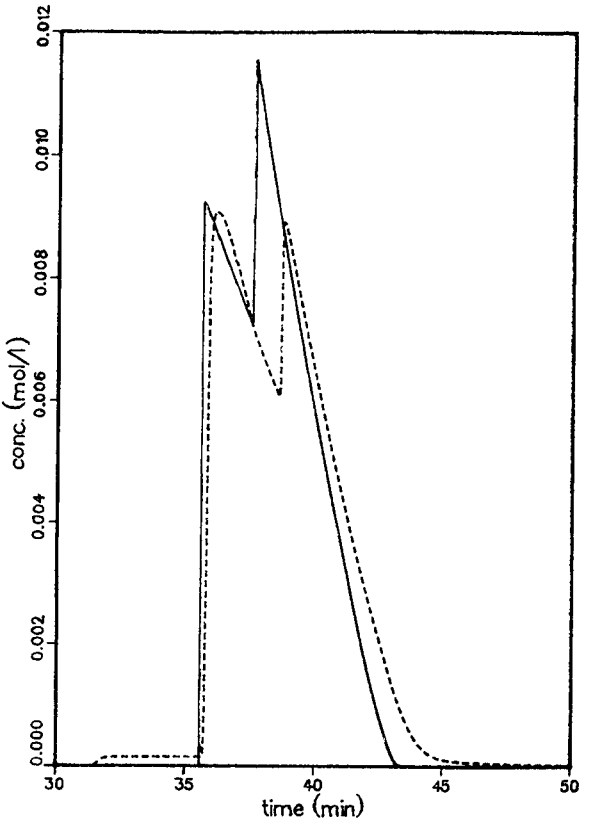

Fig. 13. Same as Fig. 12, except waiting time = 23 min.

phenomenon which cannot take place when the two components are injected together, as usual. This is the paradoxical converse displacement effect. It is due to the decrease in the partition coefficient (ratio of stationary phase and mobile phase concentrations) of the second component which accompanies a surge of the first component concentration at the front of its band. There is a major difference with the classical displacement effect, however. In the classical displacement effect, the concentration of the first component (displaced) behind the front of the second component band (displacer) decreases during the experiment. In contrast, in the converse displacement, the concentration of the second component (now displaced) behind the front of the first component band (now the displacer) increases progressively.

The consequences may be unfavorable in preparative chromatography. A reduction of the cycle time is often attempted by decreasing the time between two successive injections. Then the first eluted component of an injection may interfere with the last eluted component of the previous injection and the phenomenon illustrated in Figs. 8–13 may take place.

A secondary aim of this work was an experimental demonstration of the phenomena associated with band interference in chromatography. The existence of the

converse displacement effect has been demonstrated and its intensity discussed. The injection procedure described in this work makes such investigations easy. Two mixtures were investigated. We found that the experimental data obtained with one of them were well accounted for by a competitive Langmuir model whereas the data obtained with the other mixture were not. In the latter instance, the divergence between the data predicted with the Langmuir competitive model and the experimental data was important. Experimental data of this type must be accumulated until a pattern appears and we understand why the adsorption data for some pairs of compounds are well accounted for by the competitive Langmuir isotherm whereas those for others are not.

REFERENCES

1 J. Perry and T. J. Szczerba, *J. Chromatogr.*, 484 (1989) 267.
2 J. Newburger and G. Guiochon, *J. Chromatogr.*, 484 (1989) 153.
3 G. B. Cox, J. E. Eble and L. R. Snyder, paper presented at the 13th International Symposium on Column Liquid Chromatography, Stockholm, June 1989.
4 A. A. Katti and G. Guiochon, *J. Chromatogr.*, 499 (1990) 5.
5 S. Jacobson, S. Golshan-Shirazi and G. Guiochon, *J. Am. Chem. Soc.*, 112 (1990) 6492.
6 B. Lin, S. Golshan-Shirazi, Z. Ma and G. Guiochon, *Anal. Chem.*, 60 (1988) 2647.
7 S. Golshan-Shirazi and G. Guiochon, *J. Phys. Chem.*, 93(1989) 4143.
8 S. Golshan-Shirazi and G. Guichon, *Anal. Chem.*, 62 (1990) 217.
9 M. Z. El Fallah, S. Golshan-Shirazi and G. Guiochon, *J. Chromatogr.*, 511 (1990) 1
10 G. Guiochon and S. Ghodbane, *J. Phys. Chem.*, 92 (1989) 3682.
11 S. Levin and E. Grushka, *Anal. Chem.*, 58 (1986) 1602.
12 S. Golshan-Shirazi and G. Guiochon, *J. Chromatogr.*, 461 (1988) 19.
13 A. L. Lee, A. Velayudhan and Cs. Horváth, in G. Durand, L. Bobichon and J. Florent (Editors), *8th International Biotechnology Symposium*, Société Française de Microbiologie, Paris, 1989, pp. 593–610.
14 J. Frenz and Cs. Horváth, in Cs. Horváth (Editor), *High-Performance Liquid Chromatography—Advances and Perspectives*, Vol. 5, Academic Press, New York, 1988, pp. 211–314.
15 S. Ghodbane and G. Guiochon, *J. Chromatogr.*, 450 (1988) 27.
16 S. Ghodbane and G. Guiochon, *J. Chromatogr.*, 452 (1988) 209.
17 S. Ghodbane and G. Guiochon, *Chromatographia*, 26 (1987) 53.
18 A. M. Katti and G. Guiochon, *Anal. Chem.*, 61 (1989) 982.
19 S. Ghodbane and G. Guiochon, *Bull. Soc. Chim. Fr.*, (1988) 440.
20 G. Guiochon, S. Golshan-Shirazi and A. Jaulmes, *Anal. Chem.*, 60 (1988) 1856.
21 B. Lin and G. Guichon, *Sep. Sci. Technol.*, 24 (1988) 32.
22 B. Lin, S. Golshan-Shirazi and G. Guiochon, *J. Phys. Chem.*, 93 (1989) 3342.
23 M. Czok and G. Guiochon, *Anal. Chem.*, 62 (1990) 189.
24 G. Houghton, *J. Phys. Chem.*, 67 (1963) 84.
25 A. Jaulmes, C. Vidal-Madjar, A. Ladurelli and G. Guiochon, *J. Phys. Chem.*, 88 (1984) 5379.
26 G. Guiochon and A. M. Katti, *Chromatographia*, 24 (1987) 165.
27 B. Lin, S. Golshan-Shirazi, Z. Ma and G. Guiochon, *J. Chromatogr.*, 500 (1990) 185.
28 B. Lin, Z. Ma and G. Guiochon, *J. Chromatogr.*, 484 (1989) 83.
29 S. Golshan-Shirazi, S. Ghodbane and G. Guiochon, *Anal. Chem.*, 60 (1988) 2630.
30 S. Golshan-Shirazi and G. Guiochon, *Anal. Chem.*, 60 (1988) 2634.
31 S. Golshan-Shirazi and G. Guiochon, *Anal. Chem.*, 61 (1989) 462.
32 J. R. Conder and C. L. Young, *Physicochemical Measurements by Gas Chromatography*, Wiley, New York, 1979, Ch. 9.
33 S. Golshan-Shirazi and G. Guiochon, *Anal. Chem.*, 60 (1988) 2364.
34 D. M. Ruthven, *Principles of Adsorption and Adsorption Processes*, Wiley, New York, 1984, pp. 363–368.
35 D. Basmadjian and P. Coroyannakis, *Chem. Eng. Sci.*, 42 (1987) 1723.
36 A. W. J. de Jong, J. C. Kraak, H. Poppe and F. Nooitgedacht, *J. Chromatogr.*, 193 (1980) 181.

37 J. Jacobson, J. Frenz and Cs. Horváth, *J. Chromatogr.*, 316 (1984) 53.
38 T. L. Hill, *J. Chem. Phys.*, 17 (1949) 520.
39 A. L. Meyers and J. M. Prausnitz, *AIChE J.*, 11 (1965) 121.
40 C. J. Radke and J. M. Prausnitz, *AIChE J.*, 18 (1972) 761.
41 J. A. V. Butler and C. Ockrent, *J. Phys. Chem.*, 34 (1930) 2841.
42 M. D. LeVan and T. Vermeulen, *J. Phys. Chem.*, 85 (1981) 3247.
43 J. M. Jacobson, J. H. Frenz and Cs. Horváth, *Ind. Eng. Chem. Res.*, 26 (1987) 43.
44 Z. Ma, A. M. Katti and G. Guiochon, *J. Phys. Chem.*, 94 (1990) 6911.
45 S. Golshan-Shirazi and G. Guiochon, *J. Phys. Chem.*, 94 (1990) 495.

Journal of Chromatography, 522 (1990) 23–36
Elsevier Science Publishers B.V., Amsterdam

CHROM. 22 707

Measurement of the heats of adsorption of chiral isomers on an enantioselective stationary phase

STEPHEN JACOBSON, SADRODDIN GOLSHAN-SHIRAZI and GEORGES GUIOCHON*
* *Department of Chemistry, University of Tennessee, Knoxville, TN 37996-1600 and Division of Analytical Chemistry, Oak Ridge National Laboratory, Oak Ridge, TN 37831-6120 (U.S.A.)*
(Received May 23rd, 1990)

ABSTRACT

The adsorption isotherms of the N-benzoyl-D- and L-alanine were measured at different temperatures, and the enthalpy of adsorption and the isosteric heat of adsorption were extracted from the data. These thermodynamic functions provide further evidence that a bimodal retention mechanism is present for the separation of enantiomeric pairs on a bovine serum albumin stationary phase. The first mode of interaction is associated with the chiral selective properties of the column whereas the second is associated with the non-chiral selective properties.

INTRODUCTION

The separation of enantiomeric pairs by chromatography has become a topic of substantial interest in the past decade [1,2]. The choice of the proper stationary phase is crucial in order to achieve separation, and currently a number of different types are available. How each stationary phase effects separations has not been fully elucidated for many of them, especially those where a protein is immobilized on the surface of porous silica particles. One such phase is the bovine serum albumin (BSA) immobilized on a solid support, which was developed by Allenmark and co-workers [3–9]. This phase is extremely efficient in resolving the L- and D-isomers of benzoyl derivatives of a number of amino acids.

Much of the previous work has been concerned with the resolution of enantiomers under linear conditions [1–9]. Although the presence of multiple binding sites on the immobilized BSA stationary phase has been recognized [9], little has been done to study the fate of these adsorption sites at high concentrations. Commonly, in linear, reversed-phase chromatography the values of the capacity factor are used to determine the thermodynamic quantities [10–12]. Only the thermodynamic functions at infinite dilution can be determined by this method, however. Under these conditions, it is difficult to separate the contributions of several interaction sites. Most often, the chiral recognition mechanism involves the formation of hydrogen bonds between the enantiomers and the substrate, to stabilize a short-lived but well defined

0021-9673/90/$03.50

complex. This involves interaction (*e.g.*, adsorption) sites on the stationary phase which have a high interaction energy.

Interactions between an immobilized BSA stationary phase and an N-benzoylamino acid involves a large number of possible configurations which can be classified as chiral selective and chiral non-selective. The former include essentially those interactions between an amino acid residue of the protein and the alanine residue of the enantiomeric derivatives in which the relative configuration between the two amino acid residues permits the formation of two hydrogen bonds [1,2]. The column saturation capacity for these sites should be comparable to the number of proteinic amino acid residues fixed in the column, but actually is less because of possible steric hindrance and the inaccessibility of some residues. The latter include all the other interactions, mainly dominated by Van der Waals forces and polar interactions. If we compare these two types of interactions, we can expect the selective type to correspond to a higher energy, hence to vary more rapidly with temperature and to contribute more to the retention under linear conditions, but also to saturate at lower concentrations than the non-selective type.

Thus, a comparison could be drawn between what is called an "active site", which plays an important role in retention in analytical chromatography, and a chiral selective site which is instrumental in the separation of optical isomers. However, the interaction energy with an active site is usually higher than with a chiral selective site. The density of the active sites is usually very low and, consequently, they saturate for small sample sizes, causing peak tailing [13]. It would be more correct to describe the surface of the stationary phase as being covered by two site distributions than by two different but well defined sites, the chiral recognition active site and the non-selective site. The non-selective site should behave identically with both isomers because the two antipodes are chemically identical in an achiral environment. The chiral recogition site should interact strongly, but differently, with the two enantiomers.

Important information regarding these interactions can thus be derived from the determination of the equilibrium isotherms. By measuring the adsorption isotherms at different temperatures, several thermodynamic functions of adsorption can be extracted including the enthalpy of adsorption and the isosteric heat of adsorption. Because of the presence of multiple binding sites on the BSA stationary phase [9], the non-linear effects must be accurately accounted for by the appropriate model. If two site distributions are assumed to exist for the simplest case in a multiple site model and to be non-cooperative, a bi-Langmuir expression is one such avenue [13–15]. This two-site model has been shown to describe precisely both the adsorption isotherms and the band profiles of the enantiomers of N-benzoylalanine [16].

One of the most important applications of phase equilibrium isotherms is in the accurate prediction of individual chromatographic band profiles. The tailing in the elution profile of small or moderate sample sizes attributed to the existence of active (or high-energy) sites is well depicted by the two-term Langmuir isotherm [13]. For preparative work where the recovery of concentrated, pure fractions of optical isomers is desired, the operational concentration range extends into the non-linear region of the adsorption isotherm. One problem with protein-based chiral separations is that the site responsible for the enantiospecific interactions is easily saturated and, as a result, the preparative potential for these stationary phases is limited unless more information about the exact adsorption process is available. If more is known, optimization of the

chiral selectivity of the stationary phase could broaden the preparative applications of these stationary phases.

The purpose of this paper is to investigate further the evidence previously reported [16] that more than one site accounts for the interaction of the optical isomers with the BSA stationary phase, and that a two-site model properly accounts for what can be described as a distribution of selective sites and non-selective sites of adsorption. We studied the influence of temperature on the adsorption isotherms of N-benzoyl-L- and D-alanine on immobilized BSA and determined the thermodynamic functions of the interaction between these compounds and the stationary phase.

THEORY

Adsorption isotherm

If for each of the two isomers the rate of adsorption is proportional to its concentration in the mobile phase and to the number of empty sites available for its adsorption on the stationary phase, and if the rate of desorption is proportional to its concentration in the stationary phase, a first-order Langmuir model can be constructed. While this one-site Langmuir isotherm fails to fit the experimental data accurately, a two-site bi-Langmuir model was found to fit them correctly under the chosen experimental conditions [16].

In the case of the N-benzoyl derivatives of D- and L-alanine, the first site is analogous to the chiral recognition site attributed to the interaction between the alanine residue and the amino acid residues of BSA that is bound to the surface of the silica support. The numerical coefficients for this isotherm were found to differ markedly for the enantiomers [16]. The second of the two sites accounts for the various interaction modes of the solute with a non-chiral selective site, *e.g.*, unreacted silanol groups and peptide bonds, or of the N-benzoyl hydrophobic group with the various residues of the protein. Both isomers adsorb equally to this non-selective site, contributing nothing to the enhancement of the separation between the two isomers [16]. Moreover, the selective site provides a higher energy of adsorption, covers a smaller fraction of the available adsorption surface and, unfortunately, has a much lower saturation capacity than the non-selective site. For the bi-Langmuir adsorption isotherm, the adsorption process for one of the enantiomers at either of the two types of sites must be considered independent, *i.e.*, non-cooperative.

The appropriate kinetic equation for each isomer at each site under these conditions can be described as follows [17,18]:

$$\frac{\partial q_{x,y}}{\partial t} = k_{a,x,y} C_x (q_{s,x,y} - q_{x,y}) - k_{d,x,y} q_{x,y} \tag{1}$$

where q and q_s are the number of adsorption sites occupied and the total number of adsorption sites available (adsorbent saturation capacity), respectively, t is the time, k_a and k_d are the rate constants for the adsorption and for the desorption processes, respectively, C is the concentration of the solute in the mobile phase, x = L or D, corresponding to the L-isomer and D-isomer, respectively, and y = 1 or 2, representing the selective and the non-selective sites of adsorption, respectively.

At equilibrium eqn. 1 is set equal to zero and, following rearrangement, the familiar Langmuir adsorption isotherm equation results [19]:

$$\frac{q_{x,y}}{q_{s,x,y}} = \frac{b_{x,y}C_x}{1+b_{x,y}C_x} \tag{2}$$

where $b_{x,y} = k_{a,x,y}/k_{d,x,y}$.

At high mobile phase concentration, a monolayer coverage of the solute on the stationary phase can be expressed in terms of the Langmuir adsorption isotherm coefficients, $a_{x,y}$ and $b_{x,y}$. The concentration of the solute in the stationary phase approaches a limiting value known as the saturation capacity, which is defined as

$$q_{s,x,y} = \frac{a_{x,y}}{b_{x,y}} \tag{3}$$

Combining eqns. 2 and 3, the Langmuir adsorption isotherm for each of two isomers at each of the two sites can be written as

$$q_{x,y} = \frac{a_{x,y}C_x}{1+b_{x,y}C_x} \tag{4}$$

As the total amount adsorbed, q_{tot}, equals the amount adsorbed on the selective site plus the amount adsorbed on the non-selective site, then

$$q_{tot,x} = q_{x,1} + q_{x,2} \tag{5}$$

Finally, the bi-Langmuir isotherm for the total amount adsorbed for each isomer is accounted for by the following expression [14]:

$$q_{tot,x} = \frac{a_{x,1}C_x}{1+b_{x,1}C_x} + \frac{a_{x,2}C_x}{1+b_{x,2}C_x} \tag{6}$$

Enthalpy of adsorption

As the b coefficients of the bi-Langmuir isotherm are equal to the equilibrium constants of the adsorption processes involving both the selective and non-selective sites, the classical thermodynamic functions of these equilibria can be derived, assuming that the system is in equilibrium. First, the enthalpy of adsorption is ascertained by calculating the slope of a Van 't Hoff plot for a first-order approximation for the selective and non-selective sites. This first-order approximation assumes that the adsorption enthalpy is independent of temperature, *i.e.*, neglects the difference between the heat capacities of the solute in the two phases.

Starting with the Gibbs–Helmholtz equation, which is expressed in terms of the enthalpy, the temperature dependence of the Gibbs function is given by [20]

$$\frac{\partial\left(\frac{\Delta G}{T}\right)}{\partial\left(\frac{1}{T}\right)} = \Delta H \tag{7}$$

where ΔG is the Gibbs free energy at temperature T and ΔH is the enthalpy at T. Again, assuming that the system is in equilibrium, then [21]

$$\Delta G^\circ = -RT \ln K = -RT \ln b \tag{8}$$

where ΔG° is the molar Gibbs free energy at the standard state, R is the gas constant and $K = b = k_a/k_d$ is the thermodynamic equilibrium constant.

Inserting eqn. 8 into eqn. 7, the following expression permits the determination of the molar enthalpy of adsorption at standard state, ΔH_a°, by plotting $\ln b$ against $1/T$:

$$\frac{\partial(\ln b)}{\partial\left(\frac{1}{T}\right)} = -\frac{\Delta H_a^\circ}{R} \tag{9}$$

Having determined both ΔG° and ΔH_a°, the molar entropy of adsorption, ΔS°, is easily calculated by [21]

$$\Delta S^\circ = -\frac{\Delta G^\circ - \Delta H_a^\circ}{T} \tag{10}$$

Isosteric heat of adsorption

Another thermodynamic measure is the heat of adsorption taken for a constant amount of solute adsorbed on the stationary phase. As seen above in eqn. 7, the relationship between the Gibbs free energy and the standard enthalpy at temperature T is the starting point. At equilibrium, the chemical potential of the solute in the liquid phase is equal to the chemical potential in the stationary phase [21]:

$$\mu_s = \mu_l \tag{11}$$

where μ_s and μ_l are the chemical potentials of the solute in the stationary and mobile phase, respectively. These chemical potentials are defined as

$$\mu_l = \mu_l^\circ + RT \ln a_l \tag{12}$$

and

$$\mu_s = \mu_s^\circ + RT \ln a_s \tag{13}$$

where μ_s° and μ_l° are the standard chemical potentials of the solute in the stationary and mobile phase, respectively, and are equal to the molar free energy of the pure solute (*i.e.*, activity equal to unity) in the corresponding phase, and a_l and a_s are the activities of the solute in the mobile and stationary phase, respectively.

Equating eqns. 12 and 13, the expression for ΔG° can be written as

$$\Delta G^\circ = \mu_s^\circ - \mu_l^\circ = RT \ln\left(\frac{a_l}{a_s}\right) \tag{14}$$

Two assumptions are now necessary. First, the activity of the solute on the stationary phase, a_s, remains constant when the temperature changes if the amount adsorbed is kept constant, and second, for a dilute solute concentration in the mobile phase, the activity of the solute is equal to the concentration of the solute in the liquid phase, *i.e.*, $a_l = C$. Following the substitution of eqn. 14 into eqn. 7 and implementing the previous assumptions, the following equation demonstrates a function for the isosteric heat of adsorption [22–24]:

$$\frac{\partial(\ln C)}{\partial\left(\frac{1}{T}\right)} = \frac{\Delta H_{st}^{\circ}}{R} \tag{15}$$

where ΔH_{st}° is the isosteric heat of adsorption.

By plotting ln C *versus* $1/T$ at constant q, the isosteric heat of adsorption for the first-order approximation (*i.e.*, assuming that ΔH_{st}° is independent of the temperature) is extracted from the slope of the best linear fit of the data points.

EXPERIMENTAL

Equipment and materials

The chromatographic experiments were performed on an HP 1090 liquid chromatograph (Hewlett-Packard, Palo Alto, CA, U.S.A.) equipped with a diode-array UV detector, a computer data acquisition system and a multi-solvent delivery system. A Haake (Karlsruhe, F.R.G.) A81 circulating water-bath was used to control the temperature of the column during the entire analysis.

Column. A Resolvosil-BSA-7 column (Alltech, Deerfield, IL, U.S.A.) was used, with dimensions 150 mm × 4 mm I.D.

Chemicals. N-Benzoyl D- and L-alanine (Sigma, St. Louis, MO, U.S.A.) and 1-propanol were used without further purification.

Mobile phase. For all chromatographic runs, the mobile phase was a 0.1 *M* aqueous phosphate buffer solution with a constant concentration of organic modifier, 3% (v/v) 1-propanol, of pH 6.8. The flow-rate of the mobile phase was 1 ml/min.

Procedures

The adsorption isotherm profiles of the two isomers were obtained by frontal analysis [25–27]. Because the HP 1090 chromatograph is not equipped with a large enough sample loop to handle profile measurements by frontal analysis in the standard fashion, the multi-solvent delivery system was modified for the procedure as described in a previous paper [25]. As a broad concentration range was undertaken for the analysis, the adsorption profile for each isomer at each temperature was carefully divided into three smaller concentration ranges. The column was submerged in the circulating water-bath to control the temperature of the column within 0.1°C for the six temperatures measured, 0, 5, 10, 20, 30 and 40°C. Before switching to a new temperature range, the column was cleaned by reversing the direction of flow through the column and by flushing with phosphate buffer containing 10% (v/v) 1-propanol. After subjecting the column to such high concentrations of solute, this procedure was

necessary to obtain accurate retention times at the lower concentrations in the subsequent temperature range. Also, wavelengths from the diode-array detector of 240 and 254 nm were employed, depending on the concentration range under consideration, and the dead time of the column was 92.4 s at a flow-rate of 1 ml/min.

The best-fit bi-Langmuir isotherm parameters were calculated using a simplex algorithm developed in the laboratory. The procedure fitted the q_{tot} *versus* C data weighing each data point equally. Twenty-six points for each profile were fitted with all four parameters being optimized simultaneously, allowing 22 degrees of freedom. Linear regressions were carried out using a standard method.

RESULTS AND DISCUSSION

The temperature range was limited because an aqueous solution was used and, therefore, in spite of the buffer and the organic modifier used, the lower limit could not extend much below 273 K. The upper limit of 313 K was set because a protein is involved and raising the temperature beyond this point might damage the column, resulting in drifting retention times and irreproducible data.

Figs. 1 and 2 show the adsorption isotherm curves for the six temperatures measured in the experiments, for the L- (Fig. 1) and the D- (Fig. 2) isomers, respectively. For both isomers the curve on top represents the data at the lowest temperature measured in the study, and the amount adsorbed at each mobile phase concentration decreases with increasing temperature. The values of the a and b coefficients of the isotherms of the two enantiomers on both types of sites (eqn. 6) are reported in Table

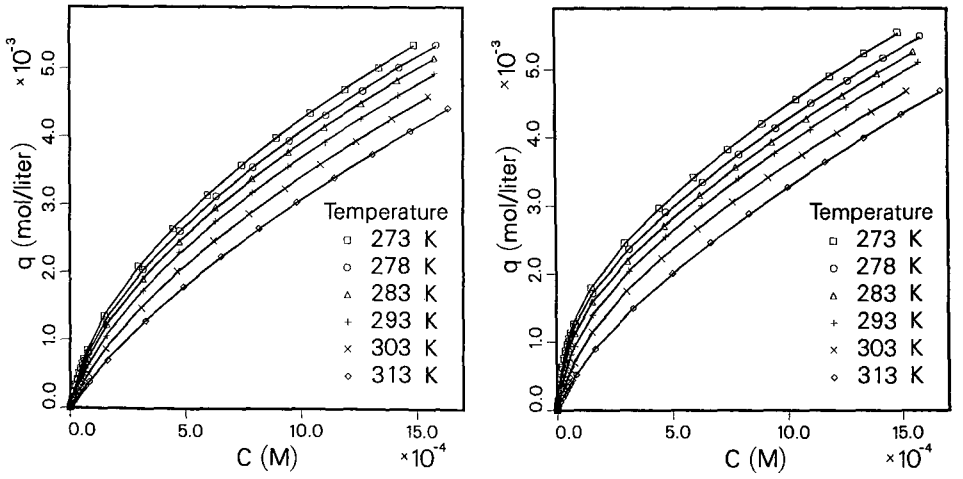

Fig. 1. Adsorption isotherms for N-benzoyl-L-alanine at increasing temperatures. Experimental data (symbols) and best bi-Langmuir isotherms (solid lines). See eqn. 6 for isotherm equation and Table I for isotherm coefficients. Column, 150 mm × 4 mm I.D.; stationary phase, immobilized BSA on silica, mobile phase, 3% (v/v) 1-propanol in 0.1 *M* phosphate buffer (pH 6.8); flow-rate, 1 ml/min.

Fig. 2. Adsorption isotherms for N-benzoyl-D-alanine at increasing temperatures. Experimental data (symbols) and best bi-Langmuir isotherms (solid lines). See eqn. 6 for isotherm equation and Table I for isotherm coefficients. Conditions as in Fig. 1.

I for each temperature, together with the value of the adsorbent saturation capacities. The adsorbent saturation capacity, q_s, and the coefficient b are reported in units of mol/l and l/mol, respectively, owing to the fact that the position of the Gibbs adsorption surface plane is difficult to define.

At low mobile phase concentrations, the disparity in the isotherm coefficients between the isomers at the selective site (Table I) indicates the selectivity of BSA as a chiral recognizer. However, the adsorption isotherms for both isomers are similar for mobile phase concentrations above $2 \cdot 10^{-4}$ M. This is as expected, because the selective sites are easily saturated and the only available sites of adsorption at high concentrations are the non-selective sites [16]. Because the two antipodes behave identically with the non-selective sites, the slopes of the second isotherm components at each temperature should be nearly identical, as previously reported [16]. As seen with the coefficients of the isotherms for the non-selective sites, the a and b parameters (Table I) are almost equal for each of the isomers at each temperature. This maintains the initial understanding that a non-selective site contributes significantly at high concentrations when the chiral selective sites become saturated.

It is remarkable that the saturation capacities of the chiral selective site are nearly the same for both enantiomers at all temperatures (Table I). Only the ratio of the rates of formation and dissociation of the chiral recognition constant is different

TABLE I

ISOTHERM PARAMETERS

Site	Isomer	T (K)	a	b (l/mol)	q_s (mol/l)
Selective	L-	273	13.09	8830	0.00148
		278	11.36	8020	0.00142
		283	9.78	7110	0.00138
		293	7.26	5550	0.00131
		303	4.82	4180	0.00115
		313	2.57	2590	0.00099
	D-	273	36.80	22720	0.00161
		278	33.34	21210	0.00157
		283	27.68	18920	0.00146
		293	17.79	12650	0.00140
		303	10.24	7740	0.00132
		313	5.06	5240	0.00097
Non-selective	L-	273	3.65	249	0.0146
		278	3.46	229	0.0151
		283	3.24	200	0.0161
		293	3.05	181	0.0168
		303	2.85	151	0.0189
		313	2.65	124	0.0213
	D-	273	3.61	248	0.0146
		278	3.39	228	0.0150
		283	3.27	210	0.0155
		293	3.08	187	0.0165
		303	2.83	163	0.0174
		313	2.76	127	0.0218

for the two enantiomers favoring retention of the D-isomer. The saturation capacities for the chiral selective site decrease with increasing temperature, by *ca.* 33% for a 40°C increase in column temperature. On the other hand, the ratio of the saturation capacities of the chiral site for the D- and L-enantiomers seems to decrease only very slowly, if at all, with increasing temperature. If the point at 313 K is eliminated, the average saturation capacity ratio is 1.09 with a standard deviation of only 0.035. At the same time, the selectivity for the D-enantiomer decreases, the ratio $a_{D,1}/a_{L,1}$ decreasing from 2.81 to 1.97. The decrease in saturation capacity with increasing temperature can be attributed to thermal changes in the conformation of the protein, especially in the dimension of the cavity within the structure of the BSA [28], which is in part responsible for the chiral recognition.

The parameters of the non-selective term of the isotherm are the same for the two enantiomers, as expected and as previously reported [16]. The average values of $a_{D,2}/a_{L,2}$ and $b_{D,2}/b_{L,2}$ are 1.003 and 1.029, respectively, with standard deviations of 0.021 and 0.030. This gives the precision of the parameters reported here. The saturation capacity of the non-selective sites increases with increasing temperature, by *ca.* 50% for a temperature increase of 40°C. With the parallel drop of the saturation capacity of the selective sites due to steric changes in the BSA, the non-selective contribution to the retention and column saturation capacity increases. The extent of the increase is sharp considering the relative change in the saturation capacity of the selective site. The saturation capacity of the chiral selective sites falls from 10 to 5% of the total adsorbent saturation capacity when the column temperature increases from 0 to 40°C.

In Fig. 3 the Van 't Hoff plot gives a good estimate of the energies of each of the sites for each compound. By plotting ln *b versus* $1/T$, the energy of adsorption can be determined. The values for the heat of adsorption can be seen in Table II. The top two curves of the plot in Fig. 3 represent the data corresponding to the D- and L-enantiomers at the selective sites, respectively.

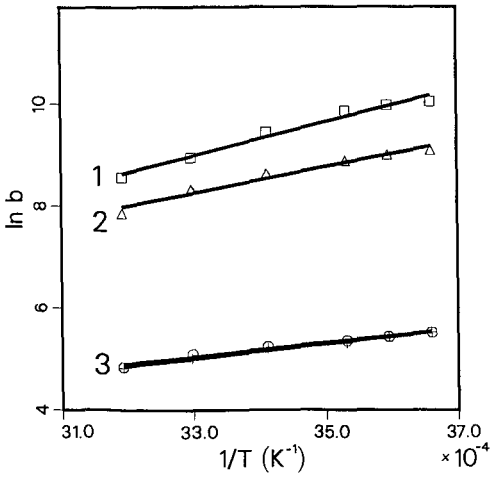

Fig. 3. Van 't Hoff plot for the determination of the enthalpy of adsorption. Calculated values (symbols) and best linear fit (solid lines). (1) D-isomer for the selective site; (2) L-isomer for the selective site; (3) D- and L-isomers for the non-selective site.

TABLE II

THERMODYNAMIC FUNCTIONS OF ADSORPTION

Site	Isomer	T (K)	$\Delta G°$ (kcal/mol)	$\Delta H°_a$ (kcal/mol)	$\Delta S°$ (cal/mol · K)
Selective	L-	273	−4.93	−5.01	−0.30
		278	−4.97	−5.01	−0.16
		283	−4.99	−5.01	−0.09
		293	−5.02	−5.01	0.03
		303	−5.02	−5.01	0.03
		313	−4.89	−5.01	−0.39
	D-	273	−5.44	−6.51	−3.90
		278	−5.51	−6.51	−3.61
		283	−5.54	−6.51	−3.42
		293	−5.50	−6.51	−3.44
		303	−5.39	−6.51	−3.68
		313	−5.33	−6.51	−3.77
Non-selective	L-	273	−2.99	−2.86	0.51
		278	−3.00	−2.86	0.53
		283	−2.98	−2.86	0.45
		293	−3.03	−2.86	0.59
		303	−3.02	−2.86	0.55
		313	−3.00	−2.86	0.47
	D-	273	−2.99	−2.68	1.16
		278	−2.99	−2.68	1.17
		283	−3.01	−2.68	1.18
		293	−3.04	−2.68	1.27
		303	−3.07	−2.68	1.30
		313	−3.01	−2.68	1.08

The more retained compound, the D-isomer, has a higher absolute value of the enthalpy of adsorption than the L-isomer, *i.e.*, 6.5 compared with 5.0 kcal/mol. However, the interaction energy of the less retained L-isomer is still much higher than the average interaction energy of either isomer at the non-selective site, 2.77 kcal/mol. Hence the L-isomer meets some of the requirements for stereoselective interaction with the chiral selective sites, but not all of them as does the D-isomer. The chiral recognition complex appears to form faster and/or dissociate more slowly with the D- than with the L-isomer. Assuming a classical three-point interaction mechanism for chiral recognition, we conclude that the L-isomer can interact with two of the three points, but sterically cannot interact with the third point of the site as well as the D-isomer.

The difference observed between the interaction enthalpies of the two isomers with the non-selective sites (*ca.* 4%) is hardly significant. The value of this enthalpy is reasonable for that kind of reversed-phase system and shows that the interaction of the enantiomers with the non-selective sites is dominated by non-hydrogen bonding contributions. The slight curvature of the plot observed in Fig. 3 is probably a consequence of the wide distribution of interaction configurations, each with its own temperature dependence, and of possible changes in the degree of solvation of the protein residues and of the solutes. A more precise fit of the enthalpy of adsorption could not be obtained utilizing the classical temperature dependence of the enthalpy

due to the difference between the molar heat capacities of the solute in the two phases. The curvature is too strong and the numbers obtained had no physical meaning, showing that another effect is responsible for this curvature.

In Table II, the thermodynamic functions of adsorption are calculated for both isomers at each of the sites for all of the temperatures. The Gibbs free energy for each of the groups of data are essentially constant and are within experimental error. The values for the D-isomer at the selective sites should and are the lowest numbers generated, guaranteeing that the most energetically favorable interactions occur there, as expected. The adsorption entropies calculated from these previous values also explain why the D-isomer is the more retained enantiomer, because the formation of the corresponding complex increases the degree of order the most in comparison with the other three groups of data. The set of numbers with the second greatest order corresponds to the L-isomer at the selective site. This implies that these molecules undergo more ordering than when interacting with the low-energy non-selective sites, but not as much as the D-isomer at the selective sites.

Figs. 4 and 5 depict the determination of the isosteric heats of adsorption for the two isomers at both sites. To determine the isosteric heat of adsorption, the amount adsorbed must be held constant, and the corresponding value C of the mobile phase concentration is determined for each temperature. Then $\ln C$ is plotted against $1/T$ and the slope is proportional to the isosteric heat of adsorption. For both of these plots the greatest amounts adsorbed are the lines at the top (line 1) and the least amounts adsorbed are the lines at the bottom (line 4). In Fig. 4 (selective sites) the data points for the L-isomer are higher than those for the D-isomer, for an identical amount adsorbed. To adsorb the same amount of D- or L-isomer, a lower concentration of the more retained D-isomer in the mobile phase is needed. In Fig. 5 the lines for the two isomers coincide, providing further evidence that no special consideration is given to either

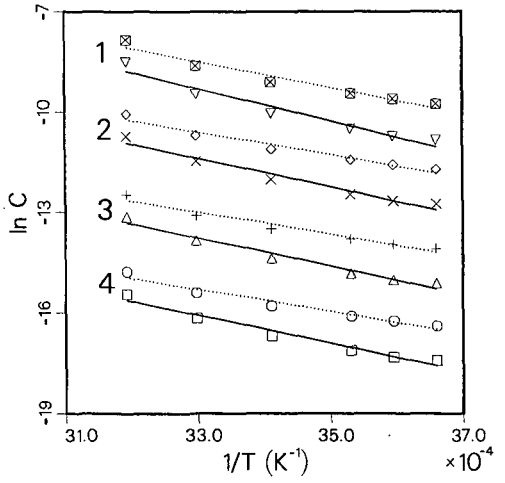

Fig. 4. Plots for the determination of the isosteric heat of adsorption for the selective site. Calculated values (symbols), best linear fits for the L-isomer (dotted lines) and best linear fits for the D-isomer (solid lines). Constant amounts adsorbed: (1) q = 0.00025 mol/l (loading factor, 19%); (2) q = 0.0001 mol/l (loading factor, 8%); (3) q = 0.00001 mol/l (loading factor, 0.8%); (4) q = 0.000001 mol/l (loading factor, 0.08%).

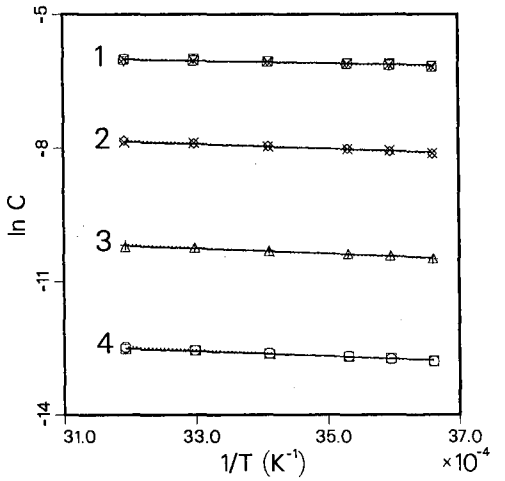

Fig. 5. Plot for the determination of the isosteric heat of adsorption for the non-selective site. Calculated values (symbols), best linear fits for the L-isomer (dotted lines) and best linear fits for the D-isomer (solid lines). Constant amounts adsorbed: (1) $q = 0.003$ mol/l (loading factor, 17%); (2) $q = 0.001$ mol/l (loading factor, 6%); (3) $q = 0.0001$ mol/l (loading factor, 0.6%); (4) $q = 0.00001$ mol/l (loading factor, 0.06%).

isomer. The energies differ slightly owing to experimental error in determining the adsorption isotherms, as reported and discussed above. As the constant surface concentration at which the determination is made decreases, the isosteric heat approaches a limiting value which is recorded for each isomer at each site in Table III.

In Fig. 6 the isosteric heat of adsorption is plotted against the percentage loading of the column in an attempt to normalize the isosteric heat of adsorption between the selective and non-selective sites. The percentage loading is the fraction of the amount injected divided by the saturation capacity of the adsorption site. Here, the saturation capacities of the selective sites are averaged, and a value of 0.00131 mol/l is used as the mean for this site for both the L- and D-isomers. Also, the saturation capacities of the non-selective sites were averaged to obtain a value of 0.0174 mol/l. The average saturation capacity of the non-selective site is *ca.* thirteen times that of the selective site.

For the selective site a slight decrease in the isosteric heat of adsorption is seen as the percent loading increases, and conversely, for the non-selective site a slight increase

TABLE III

ISOSTERIC HEATS OF ADSORPTION

$q = 10^{-7}$ mol/l.

Site	Isomer	ΔH°_{st} (kcal/mol)
Selective	L-	−6.63
	D-	−8.40
Non-selective	L-	−1.31
	D-	−1.14

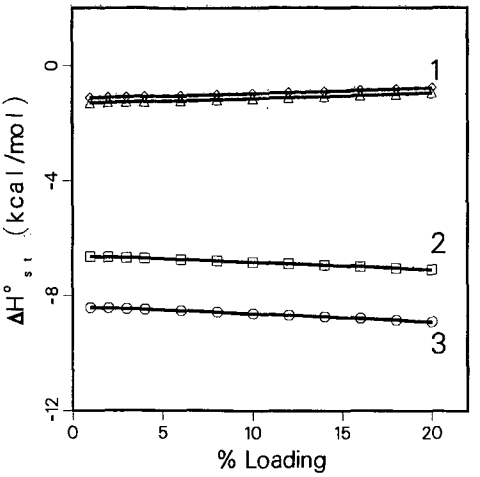

Fig. 6. Plot of the isosteric heat of adsorption for increasing loading factor (%). Calculated values (symbols). (1) D- and L-isomers for the non-selective site; (2) L-isomer for the selective site; (3) D-isomer for the selective site.

is seen as the temperature increases. The value calculated for the isosteric heat is different from the value of the enthalpy of adsorption. This occurs because the isosteric heat not only reflects the enthalpy of adsorption but also several other factors such as the energy associated with rearrangement of adsorbed molecules which are not directly attached to the surface and the heat of adsorption of the solvent. Unlike the enthalpy of adsorption, the isosteric heat can increase or decrease with a change in the surface coverage due to these factors.

However, the data in Fig. 6 do not give the exact value of the isosteric heat, as two other errors are introduced because of the assumptions made in order to extract the isosteric heat. The first assumption is that the solute is present in a low concentration in the mobile phase and the activity is proportional to the concentration. The second is that the activity of the solute on the stationary phase is independent of the temperature. Both of these assumptions are no longer valid once the mobile phase concentration is increased above linear chromatographic conditions, *e.g.*, for loading factors above 0.1%. As the concentration of the amount adsorbed increases, the activity of the solute changes because interactions between adjacent solute molecules must be included.

CONCLUSION

The results of this work verify the assumption that at least two types of sites exist when considering the separation of chiral isomers on an immobilized protein and probably on a number of other chiral selective phases. For the sake of simplicity, the type of sites were broken down into two groups: chiral selective sites and achiral, non-selective sites. The former sites have a higher interaction energy and lower saturation capacity than the latter. This result was established by considering the values of the enthalpy of adsorption and the isosteric heat of adsorption whereby the energies were calculated for each type of site.

ACKNOWLEDGEMENTS

We thank Irving W. Wainer (St. Jude's Medical Center, Memphis, TN, U.S.A.) for useful discussions. The gift of the Resolvosil-BSA-7 column by Alltech (Deerfield, IL, U.S.A.) is gratefully appreciated. We acknowledge the continuous support of our computational effort by the University of Tennessee Computing Center. This work was supported in part by grant CHE-8901382 from the National Science Foundation and by the cooperative agreement between the University of Tennessee and the Oak Ridge National Laboratory.

REFERENCES

1 D. W. Armstrong and S. M. Han, *CRC Crit. Rev. Anal. Chem.*, 19 (1988) 175.
2 W. H. Pirkle and T. C. Pochapsky, *Chem. Rev.*, 89 (1989) 347.
3 S. Allenmark, B. Bomgren and H. Boren, *J. Chromatogr.*, 237 (1982) 473.
4 S. Allenmark and B. Bomgren, *J. Chromatogr.*, 252 (1982) 297.
5 S. Allenmark, B. Bomgren and H. Boren, *J. Chromatogr.*, 264 (1983) 63.
6 S. Allenmark, B. Bomgren and H. Boren, *J. Chromatogr.*, 316 (1984) 617.
7 S. Allenmark and S. Andersson, *J. Chromatogr.*, 351 (1986) 231.
8 S. Allenmark, S. Andersson and J. Bojarski, *J. Chromatogr.*, 436 (1988) 479.
9 S. Allenmark, *Chem. Scr.*, 20 (1982) 5.
10 H. Colin, J. C. Diez-Masa, G. Guiochon, T. Czajkowska and I. Miedziak, *J. Chromatogr.*, 167 (1978) 41.
11 W. Melander, D. E. Campbell and Cs. Horváth, *J. Chromatogr.*, 185 (1976) 153.
12 J. H. Knox and G. Vasvari, *J. Chromatogr.*, 83 (1973) 181.
13 S. Golshan-Shirazi and G. Guiochon, *J. Phys. Chem.*, 94 (1990) 495.
14 D. Graham, *J. Phys. Chem.*, 57 (1953) 665.
15 R J. Laub, *ACS Symp. Ser.*, 297 (1986) 1.
16 S. Jacobson, S. Golshan-Shirazi and G. Guiochon, *J. Am. Chem. Soc.*, 112 (1990) 6492.
17 G. B. Whitham, *Linear and Non-linear Waves,* Wiley, New York, 1974.
18 B. C. Lin, Z. Ma, S. Golshan-Shirazi and G. Guiochon, *J. Chromatogr.*, 475 (1989) 1.
19 I. Langmuir, *J. Am. Chem. Soc.*, 38 (1916) 2221.
20 P. W. Atkins, *Physical Chemistry,* Freeman, New York, 1986.
21 B. Karger, L. Snyder and C. Horvath, *An Introduction to Separation Science*, Wiley, New York, 1973.
22 S. Ross, J. D. Saelens and J. P. Olivier, *J. Phys. Chem.*, 66 (1962) 696.
23 R. L. Gale and R. A. Beebe, *J. Phys. Chem.*, 68 (1964) 555.
24 P. A. Elkington and G. Curthoys, *J. Phys. Chem.*, 73 (1969) 2321.
25 S. Golshan-Shirazi, S. Ghodbane and G. Guiochon, *Anal. Chem.*, 60 (1988) 2630.
26 D. H. James and C. S. G. Phillips, *J. Chem. Soc.*, (1954) 1066.
27 G. Schay and G. Szekely, *Acta Chim. Hung.*, 5 (1954) 167.
28 Th. Peters, Jr., in F. W. Putnam (Editor), *The Plasma Proteins,* Vol. 1, Academic Press, New York, 1975, p. 133.

Journal of Chromatography, 522 (1990) 37–48
Elsevier Science Publishers B.V., Amsterdam

CHROM. 22 672

Linear solvation energy relationships in the study of the solvatochromic properties and liquid chromatographic retention behaviour of benzodiazepines

M. C. PIETROGRANDE* and C. BIGHI
Department of Chemistry, Analytical Chemical Laboratory, University of Ferrara, Via L. Borsari 46, 44100 Ferrara (Italy)
P. A. BOREA
Pharmacology Institute, University of Ferrara, Ferrara (Italy)
and
F. DONDI
Department of Chemistry, Analytical Chemical Laboratory, University of Ferrara, Via L. Borsari 46, 44100 Ferrara (Italy)
(First received November 21st, 1989; revised manuscript received June 1st, 1990)

ABSTRACT

The solvatochromic behaviour of a series of benzodiazepines was studied in order to characterize their molecular properties [polarity/polarizability and hydrogen bonding (HB) acidity and basicity]. Such experimental parameters, compared with those calculated according to Kamlet and co-workers, were employed in the study of the chromatographic retention behaviour by means of linear solvation energy relationships. Various high-performance liquid and thin-layer chromatographic systems were analysed for testing the confidence of this methodology in the study of different retentions in reversed-phase (RP) and normal-phase (NP) chromatographic systems. The most important parameters influencing benzodiazepine retention were established as size and HB basicity for RP retention and polarity and HB acidity or basicity for NP retention. For this series of solutes the present method also appears suitable for predicting retention in the studied systems and for selecting the optimum chromatographic conditions for analytical purposes.

INTRODUCTION

Solvent effects are often small and not easily measured accurately, as they are commonly the resultant of several individual effects which sometime reinforce one another and sometimes cancel each other out. Over the past decade, Kamlet and co-workers have developed a methodology for quantifying such interactions and the influence of bulk solvents on a wide variety of solution-phase processes [1,2]. They made use of the phenomenon of solvatochromism [3,4] (*i.e.*, the effect of a solvent on a spectroscopic property) to establish three carefully constructed scales representing solvent dipolarity (π^*) and hydrogen bond (HB) acidity (α) and basicity (β). Based on these parameters, linear solvation energy relationships (LSERs) have been widely

0021-9673/90/$03.50

used to deconvolve, evaluate and rationalize the multiple interaction effects that influence various solubility properties (SPs) [5,6]. The general LSER form is

$$SP = SP_0 + mV/100 + s\pi^* + a\alpha + b\beta \quad (1)$$

and includes (i) a cavity term ($mV/100$) to measure the endoergic process of separating the solvent molecules to provide a suitably sized enclosure for the solute (V being the molecular volume), (ii) a dipolarity/polarizability term ($s\pi^*$) to measure the exoergic effects of solute–solvent dipole–dipole and dipole–induced dipole dielectric interactions and (iii) hydrogen bonding terms to measure the exoergic effects of HBs involving the solute as an HB donor (HBD) acid ($a\alpha$) and as an HB acceptor (HBA) base ($b\beta$). V, π^*, α and β are parameters characteristic of a solute and are measures of differences in ground- and excited-state properties. The regression coefficients, m, s, a and b, represent how sensitive the solubility properties are to the characteristics of each solute. A large number of physico-chemical processes in condensed phases can be discussed in terms of LSERs, particularly liquid chromatographic capacity factors [7–10].

In this work, the solvatochromic behaviour of selected benzodiazepines (BDZs) was studied in different solvents to test if a reliable indication of their properties (*i.e.*, dipolarity, HBD acidity and HBA basicity) as a function of their molecular structure can be obtained. Through the use of LSERs these solvatochromic parameters were used to study the effects of BDZ molecular structure on retention in different chromatographic systems and to establish the solute properties that determine retention. For pharmacologically active compounds, such as BDZs, a comparison with the molecular properties determining their binding to the receptor, and therefore essential for their pharmacological activity, may be useful. Moreover, taking into account all the complex interactions that affect the retention, this method makes it possible to select the best solvent conditions for BDZ separation and analysis.

EXPERIMENTAL

High-performance liquid chromatographic (HPLC) measurements were performed with a Waters Assoc. Model 600 multi-solvent delivery system with a Waters Assoc. Model 990 photodiode-array detector. The column was μBondapak C_{18} (30 cm × 3.9 mm I.D.) from Waters Assoc. Different mixtures of methanol–water, acetonitrile–water and tetrahydrofuran–water were used as mobile phases. For the solvatochromic measurements the following solvents were used: *n*-hexane, cyclohexane, *n*-heptane, ethyl acetate, dioxane, tetrahydrofuran (THF), acetonitrile (ACN), dichloromethane, chloroform, 2-propanol and methanol (CH_3OH), all of HPLC grade from Carlo Erba. The standard BDZ compounds (whose molecular structures are reported in Table I) were analysed as 1 mM methanol solutions. The previously reported thin-layer chromatographic (TLC) retention data set was completed with measurements carried out under the same experimental conditions [11].

RESULTS AND DISCUSSION

Solvatochromic measurements

The solvent effects on the electronic spectra of selected BDZs were studied.

TABLE I

MOLECULAR STRUCTURES OF THE STUDIED BENZODIAZEPINES

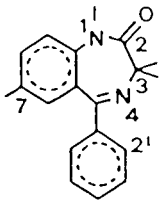

No.	Compound	Substituents			
		1[a]	3	2′	7
1	Diazepam	Me	H	H	Cl
2	Demethyldiazepam	H	H	H	Cl
3	Nitrazepam	H	H	H	NO_2
4	Flunitrazepam	Me	H	F	NO_2
5	Medazepam	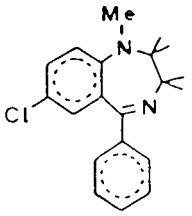			
6	Chlordiazepoxide	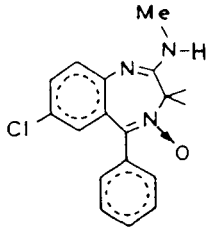			
7	Oxazepam	H	OH	H	Cl
8	Lorazepam	H	OH	Cl	Cl

[a] Me = methyl.

Solvent-induced frequency shifts have been interpreted in terms of specific solute–solvent interactions by means of the solvatochromic equation

$$\nu_{max} = \nu_0 + s\pi^* + a\alpha + b\beta \quad (2)$$

which correlates solvatochromic effects on electronic spectral transitions, $\nu_{max} - \nu_0$, with solvent properties, defined as the parameters π^*, α and β. The BDZ solvatochromic behaviour was studied in twelve selected solvents with different π^*, α and β values, as reported in Table II. As both solvents and solutes are HB donors and acceptors, a stepwise version of the solvatochromic comparison method was chosen in order to reveal and quantify the multiple effects of solvent properties on the UV–VIS spectra of BDZs [15]. Table III reports all the coefficients s_{ex}, a_{ex} and b_{ex} for the three variable regressions (eqn. 2) of each studied BDZ.

TABLE II

π^*, α AND β PARAMETER VALUES OF THE SOLVENTS USED IN THE SOLVATOCHROMIC MEASUREMENTS

Solvent	V_x	π^*	α	β
n-Hexane	220.24	−0.08	0	0
n-Heptane	253.81	−0.08	0	0
Cyclohexane	202.62	0	0	0
Dioxane	159.94	0.55	0.37	0
Ethyl acetate	143.59	0.55	0.45	0
Tetrahydrofuran	147.5	0.58	0.55	0
Chloroform	87.91	0.58	0	0.44
Dichloromethane	66.96	0.82	0	0.30
2-Propanol	131.16	0.48	0.95	0.76
Methanol	63.62	0.60	0.62	0.93
Acetonitrile	73.22	0.75	0.31	0.19
Water	29.85	1.09	0.18	1.17

The interpretation of the solvatochromic frequency shift is difficult for HB donor-acceptor solutes, such as BDZs, because the polarity–polarizability effect is obscured by interference from hydrogen bonding. A multiple regression must be calculated to fit the data for the twelve solvents and some doubts may exist owing to the small data set used for evaluating each parameter. The present results show a very high correlation ($P < 0.005$) between ν_{max} and π^*, indicating the predominant role that polarity/polarizability forces play in determining solvent–solute interactions. The statistical procedure based on Student's *t*-test demonstrates that inclusion of the α variable is statistically justified in most instances ($P < 0.05$), except for diazepam and demethyldiazepam. Only for oxazepam and lorazepam is the statistical goodness of fit increased by introduction of the variable β. The negative value of s_{ex} shows a bathochromic shift with increased solvent polarity. The maximum in the absorption spectrum of the BDZ molecule is to be ascribed to a $\pi^* \leftarrow \pi$ transition involving the conjugated system. The red shift is consistent with an increase in the dipole moment and/or in the HB ability of the excited form compared with the ground state: the more polar solvent increases the solvation energy of the excited state [1,2,12].

It should be noted that the *s*, *a* and *b* coefficients are not directly affected by overall electronic molecular properties, but more properly they are thermodynamic measures of differences in ground- and excited-state properties of the solute [2,13–15]. Moreover, they may be regarded as good indicators of the chemical properties of the solute, mainly when the molecules considered belong to the same family, as was recently demonstrated [16]. The coefficients of the LSERs have been shown to be a linear combination of solute and solvent properties [17]. With the above-mentioned hypotheses, s_{ex}, a_{ex} and b_{ex} estimated from the multiple regression may be considered to be reliable indicators of the BDZ polarity/polarizability, basicity and acidity, respectively [16,18]. The s_{ex} terms in Table III show a reasonable trend with systematic variations in the BDZ structure: the higher the number of substituents able to donate or accept HBs with the solvent, the larger is *s*. Replacement of a Cl atom with an NO_2 group in position 7 [compounds 3 and 4 *vs.* 1 and 2 (Table I)] markedly increases the

TABLE III

COEFFICIENTS AND STATISTICAL PARAMETERS OF THE EQUATION $\nu_{max} = \nu_0 + s\pi^*_{ex} + a_{ex}\alpha + b_{ex}\beta$ CALCULATED FOR THE STUDIED BDZs

No.	Compound	s_{ex}	a_{ex}	b_{ex}	r	S.D.[a]
1	Diazepam	−1.91	0.56	0.13	0.972	0.283
		±0.19	±0.48	±0.16		
2	Demethyldiazepam	−1.88	0.74	−0.08	0.974	0.284
		±0.19	±0.58	±0.29		
3	Nitrazepam	−3.05	−0.08	0.5	0.989	0.152
		±0.41	±0.04	±0.29		
4	Flunitrazepam	−2.54	−0.08	0.07	0.990	0.140
		±0.25	±0.04	±0.05		
5	Medazepam	−0.91	−0.05	0.10	0.989	0.126
		±0.12	±0.03	±0.10		
6	Chlordiazepoxide	−3.06	−0.77	0.43	0.989	0.161
		±0.38	±0.38	±0.34		
7	Oxazepam	−3.13	−0.61	0.34	0.995	0.085
		±0.19	±0.19	±0.17		
8	Lorazepam	−3.07	−0.42	0.17	0.996	0.071
		±0.18	±0.18	±0.11		

[a] $n = 12$.

values of s. In fact, a quantum-mechanical approach to BDZs shows that the more electron-withdrawing the substituent in this position is, thus lowering the frontier orbital (HOMO and LUMO) energies, the stronger the electrostatic interactions of the negatively charged atoms of the molecule will be [19,20]. The negative values of a_{ex} (Table III) mean that an increase in HBD solvent acidity further increases the solvation energy: the BDZ molecule interacts with solvent mainly as an HBA base, probably with negatively charged O-2 and N-4 atoms via HBs accepted from the solvent. In the medazepam molecule, only the N-4 group may interact with the solvent, as confirmed by the low value of s_{ex}, whereas in chlordiazepoxide the O atom in position 4 is the HBA centre. The positive values of a_{ex} for diazepam and demethyldiazepam are contrary to the above. On the other hand, for these compounds, the α term was not statistically significant in eqn. 2. The improvement in the statistical significance of eqn. 2 obtained when the β term is added for oxazepam and lorazepam demonstrates that the presence of an OH group in the BDZ molecule increases its ability to interact as an HBD acid.

Calculated solvatochromic parameters

In order to check the reliability of s_{ex}, a_{ex} and b_{ex} coefficients as indicators of solute properties, their values were correlated with the calculated BDZ π^*, α and β values. Parameter estimation rules were used by Kamlet *et al.* [6,8,16] to arrive at π^*, α and β values for solid compounds when these were not otherwise available. These estimated parameters were validated by correlations of octanol–water partition coefficients, aqueous solubilities, solvent–water partition coefficients and HPLC capacity factors involving large numbers of solutes and stationary and mobile phases [6,21]. For complex solutes, containing more dipolar substituents, the assumption was made

TABLE IV

CALCULATED SOLVATOCHROMIC PARAMETERS OF THE STUDIED BDZs

No.	Compound	$V_x/100$	π^*	β	α
1	Diazepam	2.09	0.96	0.74	0
2	Demethyldiazepam	1.95	1.00	0.73	0
3	Nitrazepam	2.01	1.30	0.96	0
4	Flunitrazepam	2.23	1.29	0.94	0
5	Medazepam	2.06	0.38	0.93	0
6	Chlordiazepoxide	2.17	1.42	1.52	0
7	Oxazepam	2.01	1.40	1.18	0.33
8	Lorazepam	2.14	1.52	1.15	0.33

that polar and HB effects at the multiple sites are additive (*i.e.*, $\Sigma\pi_i$, $\Sigma\alpha_i$ and $\Sigma\beta_i$ for each substituent i were calculated). The values obtained are reported in Table IV. For the BDZs studied a good correlation exists between experimental s_{ex} and a_{ex} valves and calculated π^* and β values, respectively ($r = 0.971$ and $r = 0.945$, excluding compounds 1 and 2). This relationship is reliable evidence that this method is valid for obtaining good indicators of the solute polarity and basicity. The relationship between b_{ex} and α is not informative ($r = 0.148$), as only two solutes (7 and 8) have appreciable HB acidity.

The cavity term, $V/100$, was also calculated for the studied BDZs (Table IV). McGowan's characteristic volume V_x was used [22]. This value, which can easily be calculated, has proved to be entirely equivalent to the Leahry computer-calculated intrinsic volume and therefore appropriate as a cavity term in LSERs [23].

LSER in RP-HPLC systems

The solvatochromic parameters and LSERs were used to test the ability of this methodology to evaluate the multiple interaction effects that influence RP-HPLC capacity factors. Retention values in various RP chromatographic systems were studied by means of solvatochromic LSERs. The experimental s_{ex}, a_{ex}, b_{ex} values were used, together with the characteristic volume V_x in a stepwise LSER method involving subsequent single-parameter correlations. Table V reports the coefficients and the statistical parameters of the final calculated multiple linear regressions. Different mobile phases were used on a C_{18} column to analyse the effects of the organic modifier (CH_3OH, ACN and THF) and the mobile phase composition on BDZ retention. Some measurements on C_{18} TLC plates were also studied to compare corresponding HPLC and TLC systems. When methanol is the strong solvent, in both HPLC and TLC systems, the leading term in the correlation equations is the measure of the cavity formation ($V_x/100$): this term alone can explain more than 99% of the total variance of retention times, the other terms being, in most instances, nearly zero and not statistically significant at the 95% confidence level. Also, the term relating to solute HB basicity is statistically significant at the 99% confidence level in those equations where ACN and THF are the organic modifiers. The statistical goodness of the calculated equations also demonstrates that experimental solvatochromic parameters are highly suitable for prediction purposes.

TABLE V

COEFFICIENTS AND STATISTICAL PARAMETERS OF THE LSER EQUATION LOG $k' = SP_0 + mV_x/100 + ss_{ex} + ba_{ex} + ab_{ex}$ CALCULATED FOR LOG k' VALUES IN DIFFERENT RP CHROMATOGRAPHIC SYSTEMS

SP_0	m	s	b	a	r	S.D.[d]	Modifier
1.04	1.22	0.01	−0.01	−0.01	0.997	0.009	40% CH_3OH[b]
±0.14	±0.07[a]	±0.01	±0.01	±0.01			
−1.60	1.13	−0.01	−0.01	−0.01	1	0.002	50% CH_3OH[b]
±0.02	±0.01[a]	±0.01	±0.01	±0.01			
−1.82	1.12	0.01	0.02	0.01	0.996	0.010	60% CH_3OH[b]
±0.09	±0.04[a]	±0.01	±0.04	±0.01			
−2.08	1.10	−0.01	0.03	0.01	0.997	0.009	70% CH_3OH[b]
±0.08	±0.04[a]	±0.01	±0.04	±0.01			
−1.34	1.26	0.01	−0.03	−0.01	1	0.004	30% ACN[b]
±0.04	±0.02[a]	±0.01	±0.01[a]	±0.01			
−1.37	1.08	−0.01	0.04	0.01	1	0.003	40% ACN[b]
±0.03	±0.01[a]	±0.01	±0.01[a]	±0.01			
−1.55	0.97	−0.01	−0.03	0.01	0.999	0.005	50% ACN[b]
±0.04	±0.02[a]	±0.01	±0.01[a]	±0.01			
−1.37	0.77	−0.01	−0.10	−0.03	0.997	0.009	60% ACN[b]
±0.25	±0.12[a]	±0.01	±0.03[a]	±0.07			
−0.70	0.77	−0.01	−0.02	0.01	0.999	0.002	20% THF[b]
±0.02	±0.01[a]	±0.01	±0.01[a]	±0.01			
−0.83	0.71	−0.02	−0.02	−0.01	0.998	0.005	30% THF[b]
±0.02	±0.01[a]	±0.01	±0.01[a]	±0.01			
−0.90	0.66	−0.01	−0.02	0.01	0.998	0.004	40% THF[b]
±0.03	±0.02[a]	±0.02	±0.01[a]	±0.01			
−1.13	0.62	0.01	−0.02	−0.01	0.996	0.005	50% THF[b]
±0.05	±0.02[a]	±0.01	±0.01[a]	±0.02			
−1.69	1.03	+0.01	−0.01	0.01	0.993	0.012	60% CH_3OH[c]
±0.12	±0.06[a]	±0.01	±0.04	±0.01			
−1.75	0.92	+0.01	0.05	0.01	0.998	0.005	70% CH_3OH[c]
±0.05	±0.02[a]	±0.01	±0.02	±0.01			

[a] $p < 0.01$.
[b] HPLC.
[c] TLC.
[d] $n = 8$.

Table V also shows the following:

(i) In all instances m values increase in the order THF < ACN < CH_3OH. This reflects the order of solvent cohesiveness, as measured by the cohesive energy δ_H^2: in fact, the Hildebrand solubility parameter (δ_H) is 14.4, 11.8 and 9.1 for CH_3OH, ACN and THF, respectively [9]. The dependence of solute retention on the solvent solubility parameter is well established in LC [24].

(ii) For each solvent, the m term increases regularly with increasing water content in the mobile phase. This is an expected result, as δ_H, the solvent parameter influencing the cavity term, would also be expected to increase regularly with increase in water content [7].

(iii) When the retention in the corresponding TLC and HPLC systems was considered, the resulting equations were very similar. This result is further evidence

TABLE VI

COEFFICIENTS AND STATISTICAL PARAMETERS OF THE EQUATION LOG $k'_w = SP_0 + mV_x/100 + ss_{ex} + ab_{ex} + ba_{ex}$ FOR LOG k' VALUES EXTRAPOLATED TO PURE WATER

SP_0	m	s	a	b	r	S.D.[b]	Column
2.93	1.42	−1.02	0.18	−0.61	0.997	0.058	C_{18}
±0.59	±0.28[a]	±0.04[a]	±0.11	±0.07[a]			
1.40	1.54	−0.71	−0.04	−0.32	0.997	0.037	Phenyl
±0.38	±0.18[a]	±0.02[a]	±0.11	±0.04[a]			
2.44	0.18	−0.42	0.06	−0.22	0.973	0.099	Cyano
±0.47	±0.08[a]	±0.03[a]	±0.14	±0.05[a]			

[a] $P < 0.01$.
[b] $n = 8$.

that the chromatographic behaviour of corresponding HPLC and TLC systems is nearly the same [25].

In order to study the behaviour of different stationary phases, the retention values, extrapolated to pure water, were employed in LSERs. Table VI reports the coefficients and the statistical parameters of the final multiple linear regressions. The major factors influencing HPLC properties are the cavity ($mV_x/100$), dipolar ($s\pi^*$) and hydrogen bonding ($b\beta$) terms. The HBA basicity of BDZs contributes significantly to changes in retention, while the dependence on HBD acidity is not statistically significant at the $P < 0.01$ level. This result confirms, as reported above, that the BDZ molecules mainly act as HBA bases. The signs of the terms in the equation were as expected: (i) increasing solute size (V) causes an increase in retention, *i.e.*, free energy concepts favour solute transfer from the more cohesive mobile phase to the less cohesive stationary phase; (ii) increases in solute dipolarity (π^*) and HB basicity (β) lead to lower log k' values because the solutes have increased affinities for the more dipolar and HB-donating aqueous mobile phase.

The value of the m term reflects the endoergity of cavity formation in the elution process. The very similar values for C_{18}- and phenyl-bonded stationary phases (m = 1.42 and 1.54, respectively) may be interpreted in terms of the similar hydrophobicities of the two phases, whereas the lower m value for the cyano-bonded phase (m = 0.18) may be ascribed to the higher polarity of this column.

LSER in NP-HPLC systems

The solvatochromic parameters were also used to study the retention behaviour of BDZs in NP systems, reported previously [26]. LSERs were built up in a stepwise fashion in order to relate log k' values (as intercepts of the Soczewinski–Snyder equations) to solute molecular properties, as described by the parameters V_x, s_{ex}, a_{ex} and b_{ex} (Table VII). The statistical parameters of the calculated equations show that for the present compounds the solvatochromic values are sufficiently unbiased to describe the retention behaviour in NP-LC systems.

For each stationary phase, a close similarity is noted in the equations describing retention with ethyl acetate and 2-propanol as polar solvents. Unlike RP-LC, here the dominant solute properties are dipole–dipole interactions and HB formation when

TABLE VII

COEFFICIENTS AND STATISTICAL PARAMETERS OF THE LSER EQUATION LOG $k' = SP_0 + mV_x/100 + ss_{ex} + ab_{ex} + ba_{ex}$ CALCULATED FOR THE INTERCEPT (LOG k') OF THE SOK-ZEWINSKI–SNYDER EQUATIONS (LOG k' *VS.* LOG X_s)

Strong solvent	SP_0	m	s	a	b	r	S.D.[b]	Column
Ethyl acetate	−0.61	−0.40	0.73	3.31	−0.65	0.999	0.026	Amino
	±0.19	±0.09[a]	±0.01[a]	±0.09[a]	±0.03[a]			
2-Propanol	−2.55	−0.32	0.73	2.64	−0.44	0.916	0.238	Amino
	±0.23	±0.11[a]	±0.16[a]	±1.07[a]	±0.26[a]			
Ethyl acetate	−1.44	−0.13	0.37	0.47	0.16	0.988	0.037	Cyano
	±0.34	±0.16	±0.02[a]	±0.16[a]	±0.06[a]			
2-Propanol	−0.89	−0.37	0.35	0.75	0.05	0.993	0.027	Cyano
	±0.25	±0.11[a]	±0.02[a]	±0.12[a]	±0.04			
Ethyl acetate	1.04	−1.51	0.20	0.22	0.10	0.960	0.058	Silica
	±0.55	±0.26[a]	±0.04[a]	±0.27	±0.09			
2-Propanol	1.73	−1.35	0.17	0.53	0.19	0.921	0.080	Silica
	±0.75	±0.36[a]	±0.05[a]	±0.36	±0.12			

[a] $P < 0.01$.
[b] $n = 8$.

the solute acts as an HB acid. The signs of these coefficients are all positive: an increase in dipole–dipole and dipole–induced dipole interactions increases retention, whereas more HBD acidic and HBA basic solutes give stronger HBs with the stationary phase, thus increasing retention. The only exception is the amino-bonded phase, where the negative sign of the solute basicity term indicates the basic properties of this stationary phase. The study of solute acidity and basicity coefficients in the equation given in Table VII makes it possible to examine the relative HB acidities and basicities of the different stationary phases. The amino-bonded phase is markedly more basic than the silica and cyano-bonded phases (higher dependence on α values), whereas the cyano-bonded and silica phases are definitely more acidic than the amino-bonded phase (positive dependence on β values), exhibiting a similar behaviour [27–31]. In

TABLE VIII

COEFFICIENTS AND STATISTICAL PARAMETERS OF THE EQUATION LOG $k' = SP_0 + mV_x/100 + ss_{ex} + ab_{ex} + ba_{ex}$ CALCULATED FOR ISOCRATIC LOG k' VALUES IN DIFFERENT NP CHROMATOGRAPHIC SYSTEMS

Column	SP_0	m	s	a	b	r	S.D.[b]	X_s (ethyl acetate)
Amino	−0.90	−0.79	0.43	0.31	−0.17	0.961	0.226	−0.1
	±0.46	±0.13[a]	±0.16[a]	±0.20[a]	±0.13			
Cyano	−1.08	−1.07	0.45	0.32	−0.03	0.995	0.096	−0.3
	±0.26	±0.09[a]	±0.07[a]	±0.18[a]	±0.10			
Silica	0.34	−0.50	0.25	0.74	0.37	0.945	0.124	−0.2
	±0.16	±0.12[a]	±0.09[a]	±0.38[a]	±0.12[a]			

[a] $P < 0.01$.
[b] $n = 8$.

comparison with RP retention studies, the influence of the V_x term is much less important and not always statistically significant at the 99% confidence level. Even if the displacement model of NP chromatography neglects mobile phase solute–solvent interactions at the first level of analysis [27–29], the V_x term accounts for the cavity formation energy in the solvent.

The ability of the present methodology to predict NP retention of BDZs was investigated with an LSER study of the log k' values at a fixed composition of ethyl acetate in the mobile phase on amino, cyano and silica columns. Table VIII reports the coefficients and the statistical parameters of LSERs calculated with V_x, s_{ex}, a_{ex} and b_{ex} values. The chief factors controlling NP retention are solute size, polarity and HBD acidity, solute HBA basicity being, in this instance, a less important factor. The predictive power is good for these systems, particularly for the cyano phase.

Analytical application

When similar solutes belonging to the same family are studied, the shift of the UV–VIS adsorption spectrum maxima with various solvents as a function of solvent–solute interactions and of the differences in solute ground- and excited-state properties may give information regarding solute molecular structure. In this case, with a photodiode-array detector, it is possible to measure both the chromatographic and the spectroscopic data fundamental to solute characterization.

When the solvatochromic parameters of the solutes are known (both calculated or experimentally determined), the correct solvent for optimizing elution can be chosen on the basis of its solvatochromic properties. Methanol is a strong HBA base and an intermediate acid and polar solvent; ACN is mostly a polar solvent, as it is only a weak HB base and acid; THF has, above all, a high molecular volume (see Table II). Therefore, CH_3OH would exhibit a specific selectivity towards polar, HBD acid solutes, and THF towards large apolar molecules.

The effects that different solvents have on the group increment to retention were

TABLE IX

EFFECT OF DIFFERENT SOLVENTS (CH_3OH, ACN AND THF) ON THE GROUP INCREMENT TO THE RETENTION OF SOME SUBSTITUENT GROUPS OF THE BDZ MOLECULE

Group	BDZs	V_x	π^*	β	α	ΔLog k'[a]		
						CH_3OH	ACN	THF
OH	7 – 2	0.06	0.44	0.41	0.33	−0.17 (±0.03)	−0.07 (±0.01)	−0.05 (±0.01)
NO_2	4 – 2	0.06	0.30	0.23	0	−0.14 (±0.02)	−0.06 (±0.01)	−0.04 (±0.01)
CH_3	1 – 2	0.14	−0.04	−0.03	0	0.08 (±0.02)	0.08 (±0.02)	0.15 (±0.03)
Cl	8 – 7	0.13	0.12	0.03	0	0.09 (±0.02)	0.10 (±0.02)	0.16 (±0.03)
F	4 – 8	0.22	−0.01	0	0	0.05 (±0.01)	0.06 (±0.01)	0.18 (±0.03)

[a] Mean data over four solvent compositions with their standard deviations. CH_3OH concentration range, 40–70%; ACN concentration range, 30–60%; THF concentration range, 20–50%.

studied for some substituents of the BDZ molecule (Table IX). The $\Delta\log k'$ values, a function of free energy changes involved in the retention process, are related to the solvatochromic parameters of the solvent. The reported $\Delta\log k'$ values are mean data over four solvent compositions (Table IX). For each solvent studied the group contributions are constant and independent of the organic modifier concentration. In the BDZ skeleton, the OH and NO_2 groups, mainly affecting solute polarity and HB acidity and basicity, are best separated by CH_3OH, whereas the effects of ACN and THF are low. The selectivity of THF for CH_3, Cl and F substituents is high. In fact, these groups mainly give rise to variations in molecular volume. The selectivity of ACN and CH_3OH is low owing to the low variation in the molecular polarity.

To confirm these effects and to analyse how these results are affected by the molecular environment, an attempt was made to compare the present results with the literature. However, as only a few, heterogeneous data concerning the simpler benzene nucleus were available [9,32], it was impossible to obtain unequivocal, reliable information. If the solvatochromic comparison method were applied to a wider homogeneous series of compounds, this might help in identifying and evaluating the individual solute–solvent interactions contributing to retention selectivity.

CONCLUSION

The results showed that solvatochromic studies are suitable for examining the chemical and physical solute characteristics when a set of similar compounds, such as BDZs, are analysed. Moreover, for these solutes LSERs may be applied to recognize molecular properties governing retention and to predict retention behaviour by means of solute solvatochromic parameters. For the studied BDZs the solvatochromic method has identified the same solute properties (polarity and HB acidity and basicity) as essential to their pharmacological activity [19,20]. More complex mathematical methods, *e.g.*, partial least squares in latent variables (PLS) or principal component regression (PCR) may also be appropriate models of multi-component statistical analysis to be applied to these studies.

ACKNOWLEDGEMENTS

This work was supported by the Italian Ministry of Public Education (MPI) and the National Research Council of Italy (CNR).

REFERENCES

1 M. J. Kamlet, J. L. Abboud and R. W. Taft, *J. Am. Chem. Soc.*, 99 (1977) 6027.
2 M. J. Kamlet, T. N. Hall, J. Boykin and R. W. Taft, *J. Org. Chem.*, 44 (1979) 2599.
3 H. H. Jaffé and M. Orghin, *Theory and Applications of Ultraviolet Spectroscopy*, Wiley, New York, 1966.
4 G. J. Braeley and M. Kaska, *J. Am. Chem. Soc.*, 77 (1955) 4462.
5 M. J. Kamlet, J. L. Abboud, M. H. Abraham and R. W. Taft, *J. Org. Chem.*, 48 (1983) 2877.
6 M. J. Kamlet, R. M. Doherty, M. H. Abraham, Y. Marcus and R. M. Taft, *J. Phys. Chem.*, 92 (1988) 5244.
7 P. C. Sadek, P. W. Carr, R. M. Doherty, M. J. Kamlet, R. W. Taft and M. H. Abraham, *Anal. Chem.*, 57 (1985) 2971.
8 P. W. Carr, R. M. Doherty, M. J. Kamlet, R. M. Taft, W. Melander and C. Horvath, *Anal. Chem.*, 58 (1986) 2674.

9 J. H. Park, P. W. Carr, M. H. Abraham, R. W. Taft, R. M. Doherty and M. J. Kamlet, *Chromatographia,* 58 (1986) 373.
10 J. H. Park and P. W. Carr, *J. Chromatogr.,* 465 (1989) 123.
11 M. C. Pietrogrande, P. A. Borea and G. L. Biagi, *J. Chromatogr.,* 447 (1988) 404.
12 N. S. Bayliss and E. G. McRae, *J. Am. Chem. Soc.,* 58 (1954) 404.
13 J. E. Brady and P. W. Carr, *J. Phys. Chem.,* 86 (1982) 1003.
14 T. Yokoyama, I. Hamazome, M. Mishima, M. J. Kamlet and R. W. Taft, *J. Org. Chem.,* 52 (1987) 163.
15 W. Liptay, *Angew. Chem., Int. Ed. Engl.,* 8 (1969) 177.
16 S. C. Rutan, P. W. Carr and R. W. Taft, *J. Phys. Chem.,* 93 (1989) 4292.
17 M. J. Kamlet, M. H. Abraham, R. M. Doherty and R. W. Taft, *J. Am. Chem. Soc.,* 106 (1984) 464.
18 R. Fuchs and K. Stephenson, *J. Am. Chem. Soc.,* 105 (1983) 5159.
19 G. Gilli, P. A. Borea, V. Bertolasi and M. Sacerdoti, in J. F. Griffin and W. L. Duax (Editors), *Molecular Structure and Biological Activity,* Elsevier, Amsterdam, 1982, p. 253.
20 P. A. Borea, G. Gilli, V. Bertolasi and M. Sacerdoti, *Biochem. Pharmacol.,* 31 (1982) 889.
21 M. J. Kamlet, R. M. Doherty, M. H. Abraham, P. W. Carr, R. F. Doherty and R. W. Taft, *J. Phys. Chem.,* 91 (1987) 1996.
22 M. H. Abraham and J. C. McGowan, *Chromatographia,* 23 (1987) 243.
23 D. E. Leahry, P. W. Carr, R. S. Pearlam, R. W. Taft and M. J. Kamlet, *Chromatographia,* 21 (1986) 473.
24 J. H. Knox (Editor), *High Performance Liquid Chromatography,* Edinburgh University Press, Edinburgh, 1980.
25 F. Dondi, G. Grassini-Strazza, Y. D. Kaie, G. Lodi, M. C. Pietrogrande, P. Reschiglian and C. Bighi, *J. Chromatogr.,* 462 (1989) 205.
26 M. C. Pietrogrande, F. Dondi, G. Blo, P. A. Borea and C. Bighi, *J. Liq. Chromatogr.,* 11 (1988) 1313.
27 E. Soczewinski, *Anal. Chem.,* 41 (1969) 179.
28 L. R. Snyder, *Anal. Chem.,* 46 (1974) 1384.
29 W. E. Hammers, M. C. Spanjer and C. L. De Ligny, *J. Chromatogr.,* 174 (1979) 291.
30 E. L. Weiser, A. W. Salotto, S. M. Flach and L. R. Snyder, *J. Chromatogr.,* 303 (1984) 1.
31 M. Verzele and F. Van Damme, *J. Chromatogr.,* 393 (1987) 25.
32 K. Jinno and K. Kawasaki, *J. Chromatogr.,* 116 (1984) 1.

Journal of Chromatography, 522 (1990) 49–55
Elsevier Science Publishers B.V., Amsterdam

CHROM. 22 673

Quantitative correlation of the parameters log k'_w and $-S$ in the retention equation in reversed-phase high-performance liquid chromatographic and solvatochromic parameters

HANFA ZOU*, YUKUI ZHANG and PEICHANG LU

Dalian Chromatographic R & D Centre of China, Dalian Institute of Chemical Physics, Academia Sinica, Dalian (China)

(First received October 23rd, 1989; revised manuscript received May 29th, 1990)

ABSTRACT

Multi-variable regression analysis between log k'_w and $-S$ in the retention equation $\log k' = \log k'_w - S\varphi$ and solvatochromic parameters was carried out with three kinds of mobile phase and the statistical significance strongly supported the following equations:

$$\log k'_w = p_1 + p_2 (V_w/100) + p_3\pi^* + p_4\beta_m + p_5\alpha_m$$
$$-S = q_1 + q_2 (V_w/100) + q_3\pi^* + q_4\beta_m + q_5\alpha_m$$

These equations indicate that the forces involved in the separation mechanism in reversed-phase liquid chromatography have a mutual nature.

INTRODUCTION

In high-performance liquid chromatography (HPLC), quantitative correlations between molecular structure parameters and retention values are important because they can (i) predict chromatographic retention behaviour, (ii) measure physicochemical parameters and (iii) lead to an understanding of the retention mechanism. Various methods have been used to correlate quantitatively the logarithm of the capacity factor with the molecular structure parameters such as the molecular connectivity index [1,2], hydrophobic parameter [3,4], Van der Waals volume [5] and solvatochromic parameters [6] in reversed-phase (RP) HPLC. It is unfortunate that almost all of these investigations were carried out with isocratic elution, as it is very difficult to extrapolate the results to a wide range of mobile phase compositions.

We consider that it is better to correlate quantitatively the parameters log k'_w and $-S$ in the retention equation $\log k' = \log k'_w - S\varphi$ in reversed-phase high-performance liquid chromatography with the molecular structure parameters of the solutes, which make it possible to predict the retention values for a fairly wide range of mobile phase compositions and to recommend separation modes in HPLC [7]. In this paper, we consider the quantitative correlation of log k'_w and $-S$ in the retention equation with solvatochromic parameters.

0021-9673/90/$03.50

DERIVATION OF THE RELATIONSHIP

According to the solubility parameter concept [8], the relationship between solute retention and the composition of the mobile phase composition can be described by

$$\log k' = \log k'_w + A\varphi^2 - S\varphi \quad (1)$$

where $\log k'_w$ is the capacity factor obtained by extrapolation of retention data from binary eluents to 100% water, A and S are constants for a given solute–eluent combination and φ is the volume fraction of the organic modifier in the aqueous eluent. Snyder *et al.* [9] showed that over a volume fraction range of at most 0.1–0.9, eqn. 1 can be simplified as a good approximation as follows:

$$\log k' = \log k'_w - S\varphi \quad (2)$$

If the linearity prediced by eqn. 2 is actually observed for the series of solutes analysed with a given stationary phase, then one may assume that the constants $\log k'_w$ and $-S$ are functions of the solute molecular structure. Assuming linear free-energy relationships, the molecular properties of the solutes can be expressed as a linear combination of individual structure parameters. According to Park *et al.* [6], the linear free-energy relatonship of the solute can be expressed as

$$X = X_0 + mV_w/100 + s\pi^* + b\beta_m + a\alpha_m \quad (3)$$

where $mV_w/100$ is the cavity term, which measures the endoergic process of separating the solvent molecules to provide a suitably sized enclosure for the solute, $s\pi^*$ measures the exoergic effects of the solute–solvent dipole–dipole and dipole–induced dipole dielectric interactions, $b\beta_m$ and $a\alpha_m$ measure the exoergic effects of hydrogen bonding involving the solvent as an hydrogen bond donor (HBD) acid and solute as an hydrogen bond acceptor (HBA) base and the solvent as an HBA base and solute as an HBD acid, respectively. V_w can be estimated by simple additivity methods such as those of Bondi [10] or Abraham and McGowan [11], π^*, β_m and α_m are solvatochromic parameters that can be found in a paper by Kamlet *et al.* [12] or measured by UV–Visible, IR or NMR methods [13].

Thus, the constants $\log k'_w$ and $-S$ determined for a particular solute would be given by

$$\begin{aligned} \log k'_w &= p_1 + p_2V_w/100 + p_3\pi^* + p_4\beta_m + p_5\alpha_m \\ -S &= q_1 + q_2V_w/100 + q_3\pi^* + q_4\beta_m + q_5\alpha_m \end{aligned} \quad (4)$$

where p_i and q_i ($i=1$–5) are regression coefficients, derived using conventional least-squares methods. Eqn. 4 shows that $\log k'_w$ and $-S$ in the retention equation can be quantitatively correlated with the solvatochromic parameters. On the other hand, if the cavity process is the unique factor in the separation mechanism in RP-HPLC, then eqn. 4 can be expressed as

$$\log k'_w = f_1 + f_2 V_w/100$$
$$-S = g_1 + g_2 V_w/100 \quad (5)$$

In this paper we intend to confirm the validity of eqn. 4 for RP-HPLC and to demonstrate that cavity process, dipole moment and hydrogen bonding interactions can be used in interpreting the separation mechanism by comparing the regression results of eqn. 4 with those of eqn. 5.

EXPERIMENTAL

The experimental results utilized in this work were taken from a paper by Schoenmakers *et al.* [14], which gives an exact description of the analytical conditions employed. In this paper we utilize the capacity factors for thirteen compounds measured in a chromatographic system with Nucleosil 10-RP 18 as stationary phase in a 30 cm × 4.6 mm I.D. and three kinds of binary mobile phases mixed from individually measured volumes of methanol, acetonitrile, tetrahydrofuran and water.

The $\log k'_w$ and $-S$ values for the thirteen solutes in the above chromatographic systems were calculated and taken from a paper by Braumann *et al.* [15].

PRACTICAL VERIFICATION OF THE RELATIONSHIPS

For compounds with single HBA sites that are not capable of self-association, ethe values of $V_w/100$ and the solvatochromic parameters used here were taken from a paper by Park *et al.* [6] and are given in Table I. Table II gives the experimental data for $\log k'_w$ and $-S$ for thirteen substituted aromatic compounds in RP-HPLC with methanol–water as the mobile phase, together with the regression analysis data of $\log k'_w$ and $-S$ according to eqn. 4.

Tables III and IV give the experimental data and regression analysis data for log

TABLE I

SOLVATOCHROMIC PARAMETERS USED IN CORRELATIONS [6]

Solute	$V_w/100$	π^*	β_m	α_m
Aniline	0.562	0.73	0.50	0.16
Acetophenone	0.69	0.90	0.49	0.006
Anisole	0.63	0.73	0.32	0
Benzaldehyde	0.606	0.92	0.44	0
Benzene	0.491	0.59	0.10	0
Benzonitrile	0.59	0.90	0.37	0
Diethyl phthalate	1.153	0.84	0.82	0
Ethylbenzene	0.687	0.53	0.12	0
Methyl benzoate	0.736	0.76	0.39	0
Nitrobenzene	0.631	1.01	0.30	0
p-Nitrophenol	0.676	1.15	0.32	0.93
Phenol	0.536	0.72	0.33	0.61
n-Propylbenzene	0.785	0.51	0.12	0

TABLE II

COMPARISON OF EXPERIMENTAL DATA FOR LOG k'_w AND $-S$ WITH VALUES CALCULATED FROM A CORRELATION EQUATION, WITH METHANOL–WATER AS MOBILE PHASE

The experimental data are from ref. 15.

Solute	Log k'_w			$-S$		
	Exp.	Calc.	Difference	Exp.	Calc.	Difference
Aniline	1.21	1.13	−0.08	−2.73	−2.63	0.10
Acetophenone	1.92	1.80	−0.12	−2.06	−2.09	−0.03
Anisole	2.15	2.13	−0.02	−2.66	−2.81	−0.15
Benzaldehyde	1.80	1.55	−0.25	−2.65	−2.41	0.24
Benzene	2.16	2.23	0.07	−2.63	−2.77	−0.14
Benzonitrile	1.77	1.72	−0.05	−2.63	−2.51	0.12
Diethyl phthalate	2.90	2.98	0.08	−3.70	−3.75	−0.05
Ethylbenzene	3.18	3.16	−0.02	−3.52	−3.53	−0.01
Methyl benzoate	2.28	2.41	0.13	−2.87	−3.07	−0.20
Nitrobenzene	2.03	2.17	0.14	−2.70	−2.82	−0.12
p-Nitrophenol	1.17	1.17	0	−2.79	−2.81	−0.02
Phenol	1.34	1.61	0.27	−2.35	−2.31	0.04
n-Propylbenzene	3.82	3.66	−0.16	−4.15	−3.93	0.22

k'_w and $-S$ for twelve and ten substituted aromatic compounds with acetonitrile–water and tetrahydrofuran–water as mobile phase, respectively.

Table V gives the coefficients p_i and q_i ($i=1$–5) in eqn. 4 when three kinds of mobile phase were used. It can be seen that the regression coefficients in all instances

TABLE III

COMPARISON OF EXPERIMENTAL DATA FOR LOG k'_w AND $-S$ WITH VALUES CALCULATED FROM A CORRELATION EQUATION, WITH ACETONITRILE–WATER AS MOBILE PHASE

The experimental data are from ref. 15.

Solute	Log k'_w			$-S$		
	Exp.	Calc.	Difference	Exp.	Calc.	Difference
Acetophenone	1.42	1.50	0.08	−2.28	−2.40	−0.12
Anisole	1.86	1.76	−0.10	−2.62	−2.55	0.07
Benzaldehyde	1.36	1.34	−0.02	−2.22	−2.24	−0.02
Benzene	1.86	1.88	0.02	−2.57	−2.56	0.01
Benzonitrile	1.54	1.48	−0.06	−2.44	−2.34	0.10
Diethyl phthalate	2.30	2.26	−0.04	−3.22	−3.15	0.07
Ethylbenzene	2.64	2.54	−0.10	−3.37	−3.14	0.23
Methyl benzoate	1.82	1.95	0.13	−2.61	−2.74	−0.13
Nitrobenzene	1.80	1.82	0.02	−2.66	−2.66	0
p-Nitrophenol	1.49	1.47	−0.02	−2.81	−2.79	0.02
Phenol	1.06	1.09	0.03	−2.19	−2.22	−0.03
n-Propylbenzene	2.83	2.90	0.07	−3.27	−3.46	−0.19

TABLE IV

COMPARISON OF EXPERIMENTAL DATA FOR LOG k'_w AND $-S$ WITH VALUES CALCULATED FROM A CORRELATION EQUATION, WITH TETRAHYDROFURAN–WATER AS MOBILE PHASE

The experimental data are from ref. 15.

Solute	Log k'_w			$-S$		
	Exp.	Calc.	Difference	Exp.	Calc.	Difference
Aniline	1.21	1.40	0.19	−2.71	−2.86	−0.15
Acetophenone	1.27	1.14	−0.13	−2.26	−2.30	−0.04
Anisole	1.81	1.70	−0.11	−3.21	−3.01	0.20
Benzaldehyde	1.20	1.31	0.11	−2.62	−2.72	−0.10
Benzene	1.85	1.90	0.05	−3.08	−3.06	0.02
Benzonitrile	1.45	1.44	−0.01	−3.01	−2.87	0.14
Diethyl phthalate	1.80	1.78	−0.02	−3.52	−3.48	0.04
Ethylbenzene	2.33	2.35	0.02	−3.57	−3.68	−0.11
Nitrobenzene	1.80	1.67	−0.13	−3.36	−3.37	−0.01
Phenol	1.50	1.53	0.03	−3.19	−3.18	0.01

were higher than 0.95, and some even higher than 0.98 and 0.99, which strongly supports the relationships shown in eqn. 4.

The regression analysis data according to eqn. 5 are given in Table VI, and the correlation coefficients in all instances are much lower than those in Table V. Hence it can be concluded that forces involved in the separation mechanism in RP-HPLC have a mutual nature, but the cavity process may play the most important role.

For the quantitative correlation between log k'_w and solvatochromic parameters or the Van der Waals volume of a solute, the intercept values p_1 for different mobile phases increase in the order methanol–water < acetonitrile–water < tetrahydrofuran–water, which is the same as that reported by Carr *et al.* [6] when log k' was

TABLE V

PARAMETERS IN EQNS. 4 AND REGRESSION COEFFICIENTS (R) WHEN DIFFERENT KINDS OF MOBILE PHASE ARE USED

Mobile phases: 1 = methanol–water; 2 = acetonitrile–water; 3 = tetrahydrofuran–water.

Mobile phase	p_1	p_2	p_3	p_4	p_5	R
1	0.161	4.829	−0.1192	−0.5440	−3.417	0.983
2	0.3552	3.664	0.0115	−0.4987	−2.841	0.991
3	1.1036	2.428	−0.2731	0.1398	−2.307	0.953
	q_1	q_2	q_3	q_4	q_5	R
1	−1.029	−4.089	0.0859	0.1424	2.324	0.971
2	−1.0596	−3.257	−0.2228	0.0026	2.263	0.962
3	−0.8729	−3.858	−1.0555	−0.9422	3.325	0.962

TABLE VI

PARAMETERS IN EQNS. 5 AND CORRELATION COEFFICIENT (R) WHEN DIFFERENT KINDS OF MOBILE PHASE ARE USED

Mobile phases: 1 = methanol–water; 2 = acetonitrile–water; 3 = tetrahydrofuran–water.

Mobile phase	f_1	f_2	R
1	0.4040	2.5622	0.5434
2	0.7473	1.5847	0.5065
3	1.3286	0.4462	0.2290
	g_1	g_2	R
1	−1.3965	−2.1983	0.6331
2	−1.6726	−1.4845	0.6150
3	−2.5289	−0.7970	0.3540

correlated with solvatochromatic parameters at constant compositions the methanol–water and acetonitrile–water. According to its definition, k'_w is the capacity factor with pure water as the mobile phase and should have the same value when different organic modifiers are used, but in fact different log k'_w values are obtained on extrapolation. A possible explanation may lie in the sorption of organic modifiers in the stationary phase, and extrapolated log k'_w values contain contributions from cavity process and the sorbed organic modifier. The parameter p_2 (or f_2) has a positive sign, which means that the larger the size of the solute molecule the larger is the log k'_w value. We consider that this effect is caused mainly by the cavity process of water. The p_2 values decrease in the order methanol–water > acetonitrile–water > tetrahydrofuran–water, which is the same as their order of Hildebrand solubility parameters [16]. No clearly explicable pattern is seen for the coefficients p_3, p_4 and p_5, which may be caused by the different chemical properties of the stationary phase with sorption of different amounts of the organic modifiers.

For the quantitative correlation between $-S$ and solvatochromic parameters, the coefficients q_1–q_5 cannot be explained clearly, which may be due to the nature of the molecular interactions of the three different organic solvents. Methanol exhibits both hydrogen donor and acceptor abilities and will therefore easily be incorporated into the network of water molecules, whereas acetonitrile and tetrahydrofuran can serve only as hydrogen acceptors and will change the structure of mobile phase more drastically. Hence the solvatochromic parameters for three organic modifiers may be strongly influenced by the surroundings, which will exhibit different interaction behaviours between the solute and mobile phase. On the other hand, the sign of q_1 and q_2 (or g_1 and g_2) is opposite to that of p_1 and p_2 (or f_1 and f_2), which means that the larger the size of a solute molecule, the smaller is the $-S$ value. This effect may be caused mainly by the solute–mobile phase interactions. In order to understand further the retention mechanism in RP-HPLC, more investigations of the influence of the chemical nature of organic solvents on retention are necessary.

REFERENCES

1 M. J. M. Wells, and C. R. Clark, *J. Chromatogr.*, 244 (1982) 231.
2 R. E. Koopmans and R. F. Rekker, *J. Chromatogr.*, 285 (1985) 287.
3 P. J. Schoenmakers, H. A. H. Billiet and L. de Galan, *J. Chromatogr.*, 185 (1979) 179.
4 P. Jandera and J. Churacek, *Adv. Chromatogr.*, 19 (1981) 125.
5 K. Jinno and A. Ishigaki, *J. High Resolut. Chromatogr. Chromatogr. Commun.*, 5 (1982) 668.
6 J. H. Park, P. W. Carr, M. H. Abraham, R. W. Taft, R. M. Doherty and M. J. Kamlet, *Chromatographia*, 25 (1988) 373.
7 H.-F. Zou, Y.-K. Zhang and P.-C. Lu, *Chin. J. Chromatogr.*, 8 (1990) 133.
8 P. J. Schoenmakers, H. A. H. Billiet, R. Tijssen and L. de Galan, *J. Chromatogr.*, 149 (1978) 519.
9 L. R. Snyder, J. W. Dolan and J. R. Gant, *J. Chromatogr.*, 165 (1979) 3.
10 S. Bondi, *J. Phys. Chem.*, 68 (1964) 441.
11 M. H. Abraham and J. C. McGowan, *Chromatographia*, 23 (1987) 243.
12 M. J. Kamlet, J. L. M. Abboud and R. W. Taft, *Prog. Phys. Org. Chem.*, 13 (1981) 485.
13 M. H. Abraham, R. W. Doherty, M. J. Kamlet and R. W. Taft, *Chem. Br.*, 75 (1986) 629.
14 P. J. Schoenmakers, H. A. H. Billiet and L. de Galan, *J. Chromatogr.*, 218 (1981) 261.
15 Th. Braumann, G. Weber and L. H. Grimme, *J. Chromatogr.*, 261 (1983) 329.
16 B. L. Karger, L. R. Snyder and C. Eon, *J. Chromatogr.*, 125 (1976) 71.

Journal of Chromatography, 522 (1990) 57–65
Elsevier Science Publishers B.V., Amsterdam

CHROM. 22 674

Direct deconvolution of Tung's integral equation using a multi-Gaussian function model for instrumental band broadening in gel-permeation chromatography

JING FENG* and XUNPEI FAN

Department of Applied Chemistry, Shanghai Jiao Tong University, 1954 Hua Shan Road, Shanghai 200030 (China)

(First received February 27th, 1990; revised manuscript received May 23rd, 1990)

ABSTRACT

A novel multi-Gaussian function model is reported for deconvoluting directly the Tung equation for instrumental band broadening (column dispersion) in gel-permeation chromatography. Using the Fourier transform technique. Tung's integral equation is reduced to a simple expression for the calculation of the true molecular weight distribution from an experimental chromatogram. An example of numerical calculation with computer simulation and two examples of experimental results for commercial polymers are given.

INTRODUCTION

Since the development of gel-permeation chromatography (GPC) by Moore [1], there has been increasing acceptance and use of this method for determining the molecular weight distributions (MWD) of resins and polymers, and better methods of processing the data and interpreting the results are needed. It has been shown by Tung and co-workers [2–4] and Hess and Kratz [5] that axial dispersion, which results in peak broadening, must be considered and corrected in order to obtain better agreement between calculated and experimental MWD results. For the difficult deconvolution of Tung's proposed equation, mathematical methods proposed by several workers [3–6] lead to some practical difficulties, such as oscillation of the dispersion-corrected results near the beginning and end of the chromatogram [3,4] and computational difficulties [5]. According to Tung's work [4], the Gaussian function is a reasonable approximation for many narrow-distribution chromatograms, and the chromatogram in GPC is considered as a multi-component model in this paper and each component is described by a Gaussian function. Hence the dispersion correction of Tung's equation is transformed into a non-linear regression analysis and a Fourier transform technique. The proposed method describes a polymer as a blend of components, each of them defined by its parameters and weight fraction. It provides the information needed in the development and engineering of a polymerization process and may be related to operating conditions.

0021-9673/90/$03.50

MULTI-COMPONENT MODEL

A chromatogram in this study is assumed to be a blend of several components, each defined by its weight fraction and a set of parameters. A general equation for the normalized experimental chromatogram $f(v)$ is given by

$$f(v) = \sum_{i=1}^{n} C_i U_i(\bar{p}_i, v) \tag{1}$$

and

$$\sum_{i=1}^{n} C_i = 1, C_i > 0, i = 1, 2, \ldots, n \tag{1a}$$

where n represents the number of components in the blend, C_i denotes the weight fraction of the ith component and U_i is the Gaussian equation describing the form of the ith component calculated for an eluent volume v, with parameters given by the vector $\bar{p}$:

$$U_i(\bar{p}_i, v) = \sqrt{h_i/\pi} \cdot \exp[-h_i(v - v_i)^2] \tag{2}$$

and

$$\bar{p}_i = (h_i, v_i), h_i < h, i = 1, 2, \ldots, n \tag{2a}$$

h represents the dispersion factor. Hence $3n - 1$ parameters are needed to characterize a blend and a non-linear optimization procedure is employed.

DETERMINATION OF n, C_i AND VECTOR $\bar{p}_i$

One purpose of this work is to reproduce the whole chromatogram and the objective function of the non-linear regression is to minimize the sum of relative errors:

$$Q_n = \sum_{j=1}^{m} \left[f(v_j) - \sum_{i=1}^{n} C_i U_i(\bar{p}_i, v_j) \right]^2 \tag{3}$$

subject to

$$\sum_{i=1}^{n} C_i = 1, C_i > 0, h_i < h, i = 1, 2, \ldots, n \tag{3a}$$

where m represents the number of experimental points. The unknown parameters n, C_i and $\bar{p}_i$ should be found. The decision-making process involves assigning values to the parameters and we can seek optimum values of the parameters in the least-squares sense, that is, those values for which the sum of squares of the experimental deviations from the theoretical curve is minimized. This procedure is called least-squares fitting

and is a constrained non-linear optimization problem. Determination of the model starts with one component and the number of components is increased until an acceptable fit is obtained between the computed curve and experimental curve. Hence it can be understood that the procedure is binary optimization, one being the optimization of the value of n and the other the optimization of the values of C_i and $\bar{p}_i$ for a given n. A flow chart of the procedure is illustrated in Fig. 1.

FOURIER TRANSFORM TECHNIQUE

The equation for dispersion correction proposed by Tung [2] is

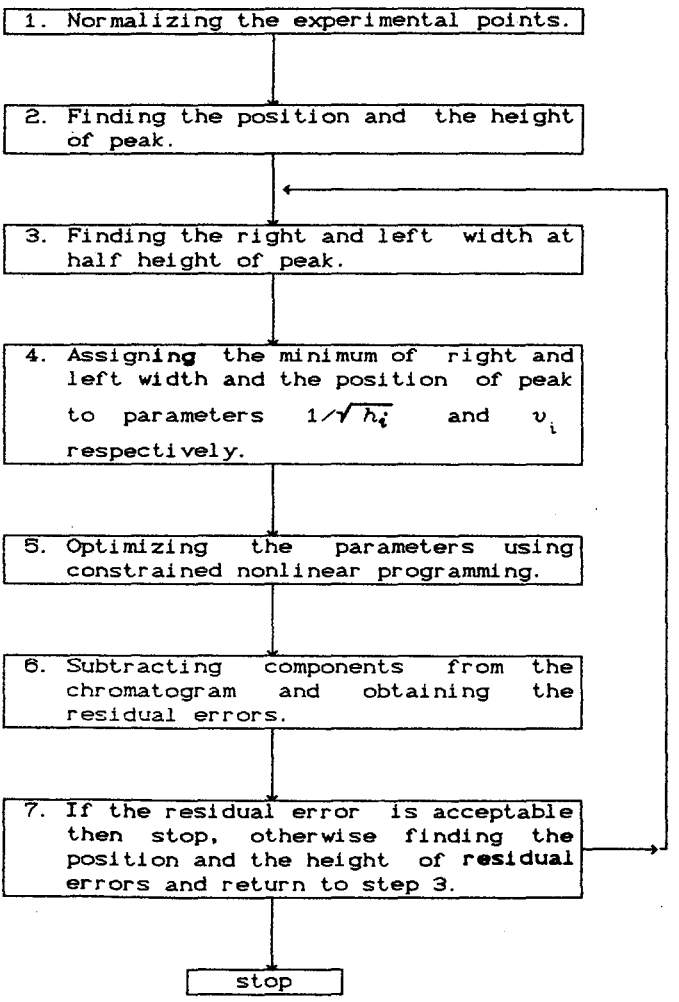

Fig. 1. Flow chart of non-linear regression for optimization of parameters.

$$f(v) = \int_{-\infty}^{+\infty} w(y)g(v - y)\,dy \tag{4}$$

where v and y are used to denote the eluent volume. This equation relates the observed chromatogram $f(v)$ to the distribution function $w(v)$ that would be obtained if axial dispersion effects were absent. The function $g(v - y)$ is the general expression of the dispersion function, which is an approximately Gaussian type [3]:

$$g(v) = \sqrt{h/\pi} \cdot \exp(-hv^2) \tag{5}$$

where h represents the dispersion factor. It is necessary to have some convenient methods of solving Tung's integral equation. The Fourier transform (FT) method [7] can be used to give a formal solution of eqn. 4. We can define the FT of $f(v)$, $w(v)$ and $g(v)$ by

$$F(k) = \frac{1}{\sqrt{2\pi}} \int_{-\infty}^{+\infty} f(v)\exp(ikv)\,dv \tag{6a}$$

$$W(k) = \frac{1}{\sqrt{2\pi}} \int_{-\infty}^{+\infty} w(v)\exp(ikv)\,dv \tag{6b}$$

$$G(k) = \frac{1}{\sqrt{2\pi}} \int_{-\infty}^{+\infty} g(v)\exp(ikv)\,dv \tag{6c}$$

We then take the FT of eqn. 4, applying the Faltung theorem [7] to the integral:

$$F(k) = \sqrt{2\pi}\, W(k)\, G(k) \tag{7a}$$

or

$$W(k) = \frac{F(k)}{\sqrt{2\pi}\, G(k)} \tag{7b}$$

Eqn. 6c can be solved as follows:

$$G(k) = \frac{1}{\sqrt{2\pi}} \int_{-\infty}^{+\infty} \sqrt{h/\pi} \cdot \exp(-hv^2 + ikv)\,dv \tag{8a}$$

Let

$$\xi = \sqrt{h}v - \frac{ik}{2\sqrt{h}} \text{ and } d\xi = \sqrt{h}\,dv$$

then

$$G(k) = \frac{1}{\sqrt{2\pi}}\sqrt{h/\pi} \cdot \exp[-k^2/(4h)] \cdot \frac{1}{\sqrt{h}} \int_{-\infty}^{+\infty} \exp(-\xi^2)\,d\xi$$

$$= \frac{1}{\sqrt{2\pi}} \cdot \exp[-k^2/(4h)] \tag{8b}$$

Solving eqn. 6a for $F(k)$ combined with eqn. 5, by analogy with the method used above, the following expression is derived:

$$F(k) = \frac{1}{\sqrt{2\pi}} \sum_{i=1}^{n} C_i \exp[-k^2/(4h_i) + ikv_i] \tag{9}$$

Combination of eqns. 7b, 8b and 9 gives

$$W(k) = \frac{1}{\sqrt{2\pi}} \sum_{i=1}^{n} C_i \exp[-k^2/(4h_i) + ikv_i + k^2/(4h)] \tag{10}$$

Solving this equation for $W(k)$ and taking the inverse transform of the equation gives

$$W(v) = \frac{1}{\sqrt{2\pi}} \int_{-\infty}^{+\infty} W(k) \exp(-ikv)\,dk$$

$$= \frac{1}{2\pi} \int_{-\infty}^{+\infty} \sum_{i=1}^{n} C_i \exp\{-[1/(4h_i) - 1/(4h)]k^2 - i(v - v_i)k\}\,dk$$

For the validity of the above expression, it is reasonable to ask for h greater than h_i, and putting

$$\xi = \frac{1}{2}\sqrt{1/h_i - 1/h} \cdot k + \frac{i(v - v_i)}{\sqrt{1/h_i - 1/h}}$$

and

$$d\xi = \frac{1}{2}\sqrt{1/h_i - 1/h}\,dk$$

then

$$W(v) = \frac{1}{2\pi}\sum_{i=1}^{n} C_i \exp[-(v - v_i)^2/(1/h_i - 1/h)] \cdot \frac{2}{\sqrt{1/h_i - 1/h}} \int_{-\infty}^{+\infty} \exp(-\xi^2)\,d\xi$$

$$= \sum_{i=1}^{n} C_i \frac{1}{\sqrt{\pi}\sqrt{1/h_i - 1/h}} \cdot \exp[-(v - v_i)^2/(1/h_i - 1/h)]$$

Let

$$\rho_i = 1/(1/h_i - 1/h)$$

then

$$W(v) = \sum_{i=1}^{n} C_i \sqrt{\rho_i/\pi} \cdot \exp[-\rho_i(v - v_i)^2] \tag{11}$$

This simple expression involves the parameter h, which is a function of the set of columns used, and h_i, v_i and C_i, which are related to the ith Gaussian function. The mathematical operations can be performed by using a computer. Several examples are given below.

RESULTS AND DISCUSSION

A numerical example is used to demonstrate the validity of the procedure. We assume that there is a known two-component MWD for $w(v)$, $C_1 = 0.65$, $\bar{p}_1 = (0.5, -1.2)$, $C_2 = 0.35$ and $\bar{p}_2 = (0.45, 1.5)$, and that the value of the dispersion factor h is taken as 0.8 over the entire range. The simulated chromatogram $f(v)$ shown in Fig. 2 (dashed line) is computed by direct integration of eqn. 1. The optimum values of non-linear regression are $C_1 = 0.651$, $\bar{p}_1 = (0.308, -1.19)$, $C_2 = 0.349$ and $\bar{p}_2 = (0.288, 1.50)$. The results of dispersion correction after Fourier transformation are shown in Fig. 2. It is obvious that the procedure works well and effectively.

The dashed line plotted in Fig. 3 represents the chromatogram of commercial polystyrene (PS) with a narrow MWD and the crosses indicate the results of optimization by non-linear regression for which the optimum values are given in Table I. The relative error is $1.89 \cdot 10^{-2}$ for one component and decreases to $1.44 \cdot 10^{-3}$ with two components and to $4.50 \cdot 10^{-4}$ for three components.

The solid line in Fig. 3 illustrates the chromatogram with a set of columns of greater resolving power.

The chromatogram for commercial poly(methyl methacrylate) (PMMA), which has a broader MWD, is shown in Fig. 4 (symbols as in Figs. 2 and 3), and the optimum values of the parameters are given in Table II. The relative error decreases from $4.48 \cdot 10^{-4}$ to $3.10 \cdot 10^{-4}$ when the number of components is increased from one to two. It is apparent that the effect of the dispersion correction for a broader MWD is not as great as that for a narrow MWD, for which the dispersion is important. Satisfactory

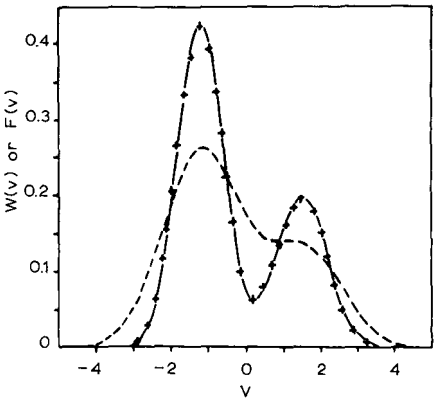

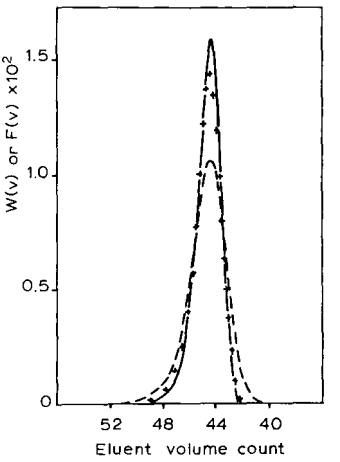

Fig. 2. Uncorrected and corrected chromatograms for a known MWD. Dashed line, uncorrected chromatogram; solid line, known chromatogram, ×, corrected chromatogram.

Fig. 3. Uncorrected and corrected chromatograms for a narrow MWD polystyrene sample. Symbols as in Fig. 2.

TABLE I

OPTIMUM VALUES OF PARAMETERS FOR PS

i	C_i	h_i	v_i	Q_i
1	0.84	0.398	44.08	$1.89 \cdot 10^{-2}$
2	0.12	0.430	46.10	$1.44 \cdot 10^{-3}$
3	0.0399	0.301	47.40	$4.50 \cdot 10^{-4}$

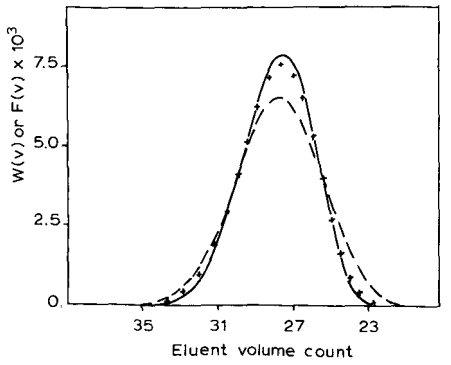

Fig. 4. Uncorrected and corrected chromatograms for a PMMA sample. Symbols as in Fig. 2.

TABLE II

OPTIMUM VALUES OF PARAMETERS FOR PMMA

i	C_i	h_i	v_i	Q_i
1	0.99	0.092	28.25	$4.48 \cdot 10^{-4}$
2	0.01	0.050	31.00	$3.10 \cdot 10^{-4}$

agreement of the dispersion corrections is obviously obtained, but it should be noted that use of dispersion corrections, as shown in Figs. 3 and 4, is not a substitute for use of columns with the highest plate number available.

In the calculation of dispersion corrections for PS and PMMA in Figs. 3 and 4,

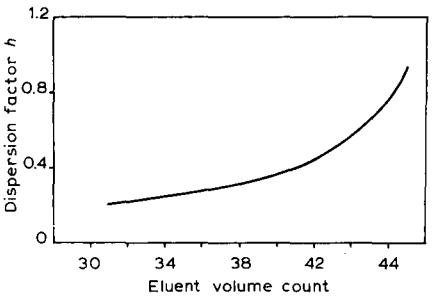

Fig. 5. Relationship between dispersion factor h and eluent volume v.

TABLE III

OPTIMUM VALUES OF PARAMETERS FOR PS

i	C_i	h_i	v_i	Q_i
1	0.85	0.403	44.10	$2.02 \cdot 10^{-2}$
2	0.13	0.410	46.17	$1.14 \cdot 10^{-3}$
3	0.02	0.290	47.45	$6.67 \cdot 10^{-4}$

TABLE IV

OPTIMUM VALUES OF PARAMETERS FOR PMMA

i	C_i	h_i	v_i	Q_i
1	0.98	0.090	28.30	$4.82 \cdot 10^{-4}$
2	0.02	0.052	31.00	$2.28 \cdot 10^{-4}$

a variable value of h was used. The papers by Tung and co-workers [2–4] and Hess and Kratz [5] indicate that h varies, being smaller for smaller eluent volumes. The value of h was determined for monodisperse PS standards by using a Gaussian peak distribution as in eqn. 5. Fig. 5 shows the relationship between h and the eluent volume v.

The two examples shown above were tested in another experiment (chromatograms not shown), and the results of optimum programming are given in Tables III and IV.

We consider that the majority of residual relative errors are produced by the assumption that a Gaussian distribution can be used to determine the dispersion factor h. As mentioned above, the monodisperse PS samples are standard substances for the determination of h but the MWDs of these samples are like the narrow MWD shown in Fig. 3. The assumption leads to the method proposed here, not for total deconvolution. We can deduce from Tables III and IV that the values of the parameters are reproducible experimentally. The uniqueness of the parameters is ensured by the algorithm with optimization theory. Although the parameters may be variable in different optimum algorithms, the final $w(v)$ results are not affected. A more detailed calculation may be needed to test the method described here.

REFERENCES

1 J. C. Moore, *J. Polym. Sci., Part A,* 2 (1964) 835.
2 L. H. Tung, J. C. Moore and G. W. Knight, *J. Appl. Polym. Sci.*, 10 (1966) 917.
3 L. H. Tung, *J. Appl. Polym. Sci.*, 10 (1966) 375.
4 L. H. Tung, *J. Appl. Polym. Sci.*, 10 (1966) 1271.
5 M. Hess and R. F. Kratz, *J. Polym. Sci., Part A-2*, 4 (1966) 731.
6 W. N. Smith, *J. Appl. Polym. Sci.*, 11 (1967) 639.
7 P. M. Morse and H. Feshback, *Methods of Theoretical Physics*, McGraw-Hill, New York, 1953, Part I, Sect. 8.4, p. 464.

Journal of Chromatography, 522 (1990) 67–75
Elsevier Science Publishers B.V., Amsterdam

CHROM. 22 661

Problems in the size-exclusion chromatography of cellulose nitrates: non-exclusion effects and universal calibration

T. E. EREMEEVA*, T. O. BYKOVA and V. S. GROMOV

Cellulose Laboratory, Institute of Wood Chemistry, Latvian AS, 27 Academijas Street, Riga 226006 (U.S.S.R.)

(First received July 17th, 1989; revised manuscript received June 26th, 1990)

ABSTRACT

It is shown that cellulose nitrates (CN) (degree of substitution from 2.1 to 2.97) in pure tetrahydrofuran (THF) during size-exclusion chromatography (SEC) on silanized silica gel exibit polyelectrolytic properties and their behaviour is complicated by several non-exclusion effects. Substitution heterogeneity and ionogenic groups affect the properties of CN solutions and their SEC behaviour. Addition of 0.01 mol/l of acetic acid to the eluent suppresses the non-exclusion effects and leads to validity of a universal calibration between CN and polystyrene. The Mark–Houwink equation parameters for CN in THF–0.01 mol/l acetic acid were calculated to be $\alpha = 0.73$ and $K = 6.44 \cdot 10^{-4}$ dl/g.

INTRODUCTION

Cellulose nitrates (CN) are traditionally used to determine the molecular mass parameters (MMP) and molecular mass distribution (MMD) of cellulose. Although the CN have been the subject of extensive size-exclusion chromatographic (SEC) studies [1–11], a series of problems still remain. It is believed that the separation of CN during SEC occurs by a merely steric mechanism. If the SEC columns are applied with tetrahydrofuran (THF) as the mobile phase, the chromatogram obtained is considered to correspond to the MMD of CN. However, in practice the CN separation is accompanied by several effects.

One of them is the concentration effect, *i.e.*, a change in the retention volume (V_e) with varying polymer concentration. This effect has been observed in the SEC of CN by several workers, using Styragel as the packing material and THF as the eluent [4–7]. Marx-Figini and Soubelet [7] noted this effect for CN in THF with passivated silica gel (LiChrospher CH 8) as the stationary phase. For CN the concentration effect is considerable even with low injected concentrations.

Another effect is partial adsorption of CN on the packing, noted when Styragel, silica gel or porous glass was applied [4,8,9].

Finally, the problem of the validity of the universal calibration concept has not been solved. When the MMP of CN are determined using a universal calibration procedure the results are usually higher then those obtained by absolute methods

0021-9673/90/$03.50

[2,5,6,8]. At the same time, the application of direct calibration with CN fractions provides satisfactory agreement of the MMP values [10,11].

In fact, the universal calibration between CN and other polymers under different experimental conditions is not valid [2,5,7–9]. It is not known whether the failure to obtain a universal calibration is caused by erroneous Mark–Houwink constants or by violation of CN steric separation mechanism. There are no convincing explanations of the concentration effects taking place on different packings. This paper is devoted to the consideration of these problems.

EXPERIMENTAL

Materials

Chemical-grade cotton cellulose was nitrated with the mixture described by Alexander and Mitchell [12] for 0.5, 1, 2 and 4 h at 0°C. Nitrogen contents were determined by the semimicro Kjeldahl technique. Samples with nitrogen contents of 11.7, 12.4, 13.6 and 13.9% were chosen for the investigation of the elution behaviour of CN.

In order to calibrate the chromatographic system for different series of CN fractions, three groups of fractions, with nitrogen contents of 13.3–13.9%, 12.4% and 11.5% in the molecular mass (M_w) range 30 000–300 000, were selected. CN fractions were obtained by the precipitation fractionation technique, using a conventional scheme with acetone–water [13].

Peroxide-free THF, freshly distilled over KOH, was used as solvent and eluent.

Intrinsic viscosity measurements

These were carried out with a Ubbelohde viscometer at 25 ± 0.05°C in THF and in THF–0.01 mol/l acetic acid.

Size-exclusion chromatography

SEC was carried out on a GPC chromatograph (Laboratory Instruments Works, Prague, Czechoslovakia) with a refractometric detector, equipped with a Rheodyne 7125 fixed-loop (20-μl) injector and a set of bimodal Zorbax PSM S 1000 + 60 columns (DuPont) packed with silanized silica gel. The analyses were performed at the room temperature. The analysis time was 20 min at a flow-rate of 0.5 ml/min.

Solutions (0.5–0.05%) of CN samples in THF and in THF–0.01 mol/l acetic acid and 0.05% solutions of CN fractions in THF–0.01 mol/l acetic acid were prepared and shaken overnight. The samples were filtered through a 0.5-μm Millipore filter prior to use.

Polystyrene standards (Waters Assoc., Milford, MA, U.S.A.) and CN fractions with different nitrogen contents characterized according to MMP by ultracentrifugation [14] were used for calibration of the chromatographic system.

RESULTS AND DISCUSSION

Elution behaviour

During SEC, an unchanged elution behaviour of the polymer when its concentration in the injected sample is varied is a chromatographic demonstration of

a pure steric separation mechanism. In this case, the chromatogram is adequate to the differential MMD of the polymer under investigation. An influence of the sample concentration on the elution volume indicates a violation of the steric separation mechanism by some non-exclusion effects.

The elution behaviour of CN with a degree of substitution (*DS*) of 2.05–2.95 (11.7–13.9% N, respectively) in pure THF depends on the CN concentration. Thus, the V_e of the samples decreases with decrease in the injected concentration from 0.5 to 0.05 g/dl (Fig. 1). The fronts of the chromatograms with different concentrations almost coincide, but their ends tend to show a decrease in V_e with decrease in concentration. Such behaviour of the polymer during SEC is typical of polyelectrolytes [15]. Obviously, CN in THF on silanized silica behaves as a polyelectrolyte.

The dependence of V_e on CN concentration is non-linear in the investigated *DS* range (Fig. 2). This indicates that the observed concentration effects have a complex nature and are caused by a sum of phenomena.

The samples elute before the column exclusion limit (V_0), determined by the polystyrene standard with $M_w = 2.7 \cdot 10^6$. Hence the main phenomenon controlling the separation of CN on silanized silica gel in THF is ion exclusion.

CN are never considered as polyelectrolytes. However, cellulose preparations usually contain some amounts of ionogenic carboxyl groups, because cellulose

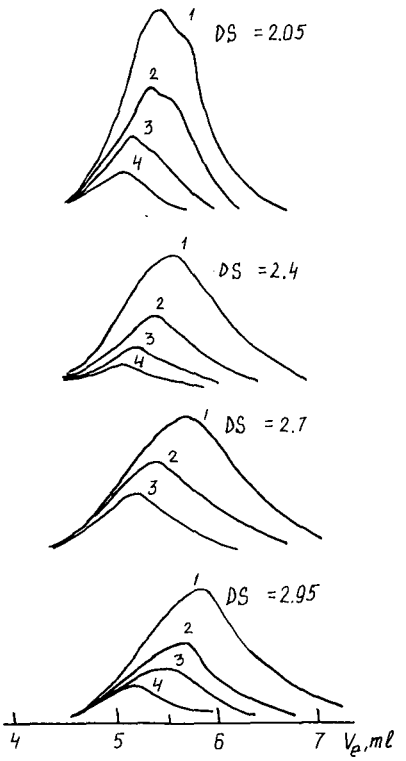

Fig. 1. Experimental chromatograms of CN with different *DS* in pure THF at injected concentrations of (1) 0.5, (2) 0.25, (3) 0.125 and (4) 0.05 g/dl.

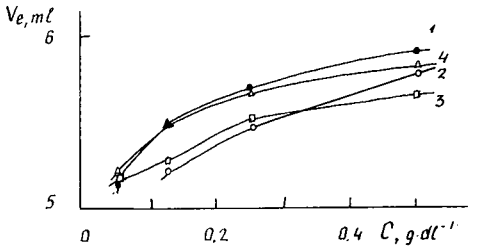

Fig. 2. Retention volume as a function of injected concentration of CN in THF.

undergoes oxidation during processing. Taking into account the fact that the carboxyl groups in THF dissociate [16] and the silica gel in neutral media has a negative charge (owing to dissociation of residual silanol groups), ion exclusion can take place. We assume that the concentration effects observed by other investigators during SEC of CN can be considered to be a consequence of the polyelectrolyte nature of CN solutions.

In this work, the viscometric properties of THF solutions of CN samples were also investigated. The dependence of specific viscosity on concentration, $\eta_{sp}/C = f(C)$, for CN in THF is non-linear (Fig. 3). There is a maximum for the highly substituted samples ($DS \geqslant 2.4$) and η_{sp}/C tends to increase with decrease in the concentration of the sample with $DS = 2.05$.

A similar dependence for highly substituted CN was observed by Siochi and Ward [17], which they explained by the molecular associates present in the solution. Nevertheless, it is known [15] that this non-linear type of dependence is typical of polyelectrolyte solutions with insufficient solvent ionic strength. In our opinion, both the formation of associates and the presence of ionogenic groups in the CN macromolecules can be regarded as a reason for the observed effect.

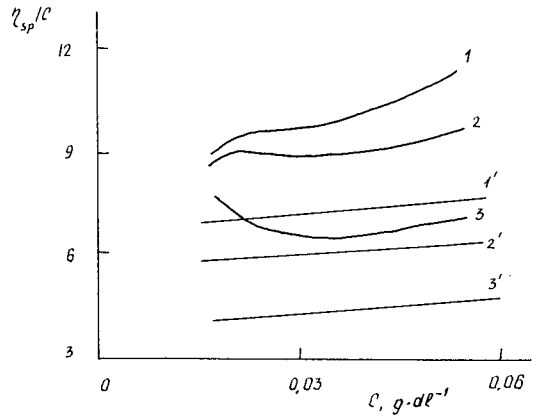

Fig. 3. Viscosity plots for CN with DS = (1) 2.95, (2) 2.4 and (3) 2.05 in THF (1–3) and in THF–0.01 mol/l acetic acid (1′–3′).

Effect of acetic acid

The presence of a charge in the polymer chain causes the coil to expand. A change in the ionic strength and/or pH of the solution results in suppression of the polyelectrolyte effects both in solution and during SEC [15].

In this work, the effect of adding acetic acid to the mobile phase on the elution behaviour of CN was studied.

The addition of acetic acid to the eluent resulted in an increase in the sample V_e irrespective of the *DS* of CN (Fig. 4). No shifts in V_e for the highly substituted CN sample were observed with addition of acetic acid at concentrations exceeding 0.005 mol/l, whereas for the samples with average and low DS 0.01 mol/l acetic acid was required. On adding 0.01 mol/l acetic acid to THF, no concentration dependence was observed.

The addition of acetic acid to CN solutions also influenced the viscosity. The dependence of η_{sp}/C on concentration became linear (Fig. 3), and the $[\eta]$ values tended to decrease. The presence of acid in the solution suppresses the dissociation of ionogenic groups, leading to reduce macromolecule coil dimensions. The reduction of the effective hydrodynamic volume of CN macromolecules results in a corresponding shift in the chromatograms.

Universal calibration

The dependence of log $M[\eta]$ on V_e is nowadays accepted as a universal calibration. It is invariant for a given set of columns and eluent. If the universal calibration between different polymers is valid, it means that only steric exclusion of the polymers under investigation takes place.

In this work, the universal calibration procedure was carried out using CN fractions and polystyrene standards. It is well known that the properties of CN in solution depend on *DS*, and therefore the samples differed in nitrogen content (Table I). Experimental $[\eta]$ values in THF–0.01 mol/l acetic acid were used to determine the CN (log M $[\eta]$).

Fig. 5 demonstrates that the elution behaviour of polystyrenes is not affected by the presence of acid in THF. This means that the hydrodynamic volume of

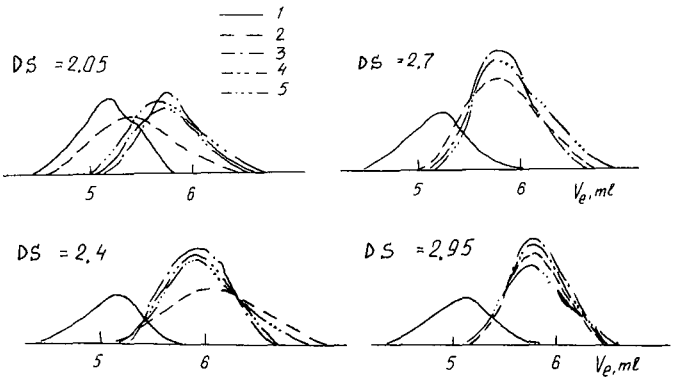

Fig. 4. Effect of acetic acid on CN elution behaviour. (1) Pure THF; (2–5) THF with acetic acid added: (2) 0.005; (3) 0.01; (4) 0.017; (5) 0.05 mol/l.

TABLE I

CHARACTERISTICS OF CN CALIBRATION SAMPLES

No.	N (%)	$M_w \cdot 10^{-3}$	M_w/M_n[c]	$[\eta]$ (dl/g)	Log M $[\eta]$[a]	V_e (ml)
1	14.0	508	1.35	10.27	6.65	5.55
2	13.6	250	1.40	5.94	6.10	6.04
3	13.9	86	1.30	2.62	5.30	6.50
4	13.3	87	1.40	2.65	5.29	6.50
5	13.3	30	1.24	1.23	4.52	7.00
6	13.9	25	1.25	1.00	4.35	7.07
7	12.4	282	1.65	–	6.06[b]	6.02
8	12.4	192	1.25	–	5.87[b]	6.14
9	12.4	172	1.25	–	5.78[b]	6.19
10	12.4	110	1.25	–	5.45[b]	6.40
11	12.4	68	1.25	–	5.08[b]	6.62
12	11.3	316	1.48	7.02	6.26	5.93
13	11.6	187	1.45	5.00	5.89	6.10
14	10.9	147	1.40	3.80	5.67	6.27
15	11.6	77	1.60	2.40	5.16	6.60

[a] Peak molecular mass, calculated as 1/2 ln ($M_w M_n$).
[b] Calculated by $[\eta] = 6.44 \cdot 10^{-4} M_{peak}^{0.73}$.
[c] M_w = mass-average molecular mass. M_n = number-average molecular mass.

polystyrenes remains unchanged. Therefore, the log M $[\eta]$ values for polystyrenes were calculated using the Mark–Houwink constants $K = 13.4 \cdot 10^{-4}$ dl/g and $\alpha = 0.71$, which were established in pure THF [2]. The results obtained are presented in Table II.

As shown in Fig. 6 the universal calibration parameters of CN and polystyrene almost coincide if THF–0.01 mol/l acetic acid is used as the eluent. This means that the universal calibration concept between CN and polystyrene is valid when all non-exclusion effects are eliminated.

Although it was assumed that CN with different *DS* would have different calibrations in terms of log M, we found that the samples with differing nitrogen

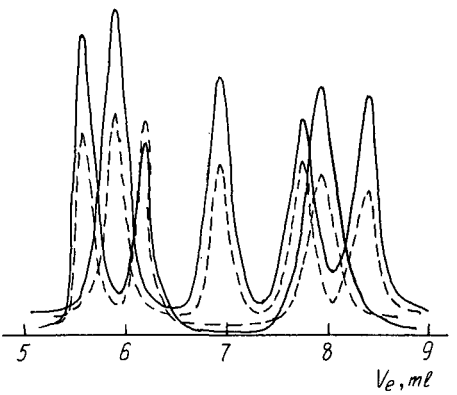

Fig. 5. Experimental chromatograms of polystyrene standards in THF (solid lines) and THF–0.01 mol/l acetic acid (dashed lines).

TABLE II

MMP AND CORRESPONDING RETENTION VOLUMES FOR POLYSTYRENE STANDARDS

M_w	Log M [η]	V_e (ml)
2 700 000	7.13	5.55
867 000	6.29	5.90
470 000	5.83	6.16
111 000	4.57	6.94
20 800	3.52	7.60
15 000	3.28	7.73
10 000	2.97	7.93
4000	2.20	8.40
2100	1.89	8.50

contents and equal molecular masses elute with the same V_e (Fig. 7). The variations in the hydrodynamic properties of this polymer depending on *DS* are connected with the different chain stiffnesses of high- and low-substituted CN [18]. At the same time, it is recognized that the chain stiffness is determined to a marked extent by the hydrogen bond system [19]. The observed levelling of CN in terms of *DS* during SEC in the presence of acid can be explained only if the influence of volume effects on the CN solution properties is taken into account. The added acid destroys the system of bonds formed in pure solvent and changes the nature of the interactions between incompletely substituted CN and THF.

If the size of the CN molecules decreases on adding acetic acid to THF, the Mark–Houwink constants for CN must change. The parameters K and α were

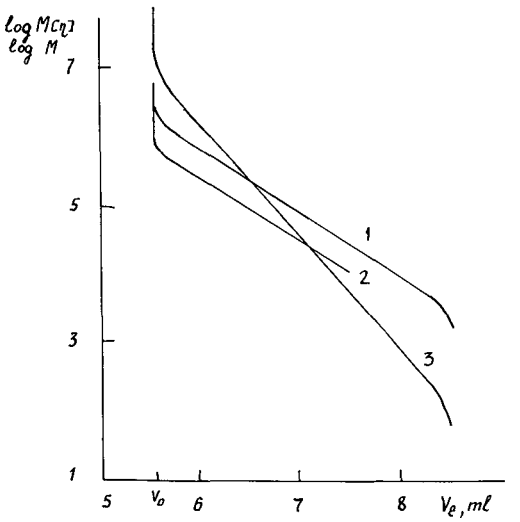

Fig. 6. Calibration graphs, log M = f(V_e), for (1) polystyrene and (2) CN, and (3) universal calibration in THF–0.01 mol/l acetic acid.

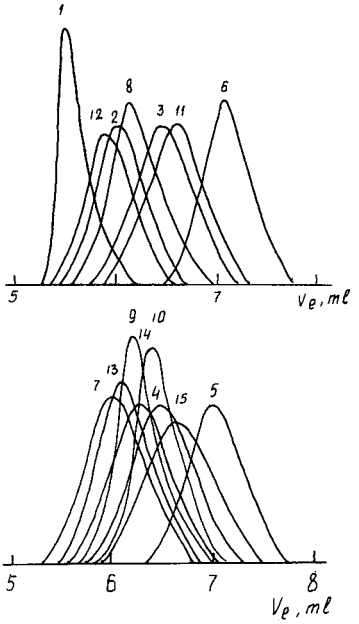

Fig. 7. Normalized chromatograms of CN used for calibration in THF–0.01 mol/l acetic acid. Numbers as in Table I.

established from the combined SEC and viscometric data according to the principle described by Dobbin *et al.* [20]. The Mark-Houwink equation is

$$[\eta] = 6.44 \cdot 10^{-4} M^{0.73} \text{ (dl/g)}$$

The MMP of CN samples caculated using these constants and the universal calibration approach are in good agreement with the values determined by ultracentrifugation and viscometry (Table III).

TABLE III

MOLECULAR MASS PARAMETERS OF CN SAMPLES OBTAINED BY SEDIMENTATION, VISCOMETRY AND SEC

Sedimentation[a]			Viscometry[b]:	SEC			
$M_w \cdot 10^{-3}$	M_w/M_n	M_z/M_w	$M_v \cdot 10^{-3}$	$M_w \cdot 10^{-3}$	$M_v \cdot 10^{-3}$	M_w/M_n	M_z/M_w
282	1.65	–	–	286	–	1.52	1.29
192	1.25	1.15	–	193	–	1.30	1.15
172	1.25	1.20	–	170	–	1.25	1.18
110	1.25	1.25	–	115	–	1.25	1.21
–	–	–	280	295	285	1.65	–
–	–	–	157	160	152	1.45	–
–	–	–	67	70	66	1.74	–

[a] M_z = z-average molecular mass.
[b] M_v = viscosity-average molecular mass.

CONCLUSIONS

It is clear that the separation of CN by SEC is a highly complex process. When determining cellulose MMP via nitrates, the chemical heterogeneity of the latter should be taken into account, as the presence of functional groups differing in polarity, in addition to ionogenic groups, affect the behaviour of CN in the solution. The polyelectrolyte effects on electroneutral packings during SEC may be much less strong, but nevertheless, if they are disregarded, they would lead to incorrect molecular mass data and a distorted molecular mass distribution.

REFERENCES

1 L. Segal, *J. Polym. Sci. Part C*, 21 (1968) 267.
2 L. Segal, J. D. Timpa and J. I. Wadsworth, *J. Polym. Sci., Part A-1*, 8 (1970) 25, 3577.
3 L. Segal, J. I. Wadsworth and J. D. Timpa, *Adv. Chem. Ser.*, 125 (1973) 179.
4 C. Holt, W. Mackie and D. B. Sellen, *Polymer*, 19 (1978) 1421.
5 A. P. Cunningham, C. Heathcote, D. E. Hillman and J. I. Paul, *J. Liq. Chromatogr.*, 12 (1979) 173.
6 L. L. Lloyd, C. A. White, A. P. Brookes, J. E. Kennedy and F. P. Warner, *Br. Polym. J.*, 19 (1987) 313.
7 M. Marx-Figini and O. Soubelet, *Polym. Bull.*, 6 (1982) 501.
8 G. Meyerhoff, *Makromol. Chem.*, 134 (1970) 129.
9 D. M. French and G. W. Nouflett, *J. Liq. Chromatogr.*, 4 (1981) 197.
10 M. Marx-Figini and O. Soubelet, *Polym. Bull.*, 11 (1984) 281.
11 A. Wirsen, *Makromol. Chem.*, 189 (1988) 833.
12 W. J. Alexander and R. L. Mitchell., *Anal. Chem.*, 216 (1949) 1497.
13 C. F. Bennett and T. E. Timell, *Sven. Papperstidn.*, 59 (1956) 73.
14 G. M. Pavlov, P. V. Kozlov, G. N. Marchenko and V. N. Tscvetkov, *Vysokomol. Soedin.*, 24 (1982) 284.
15 H. G. Barth, *J. Chromatogr. Sci.*, 18 (1980) 409.
16 N. Misra and B. M. Mandel, *Makromol. Chem. Rapid Commun.*, 5 (1984) 471.
17 E. J. Siochi and T. C. Ward, *Polym. Prepr., Am. Chem. Soc. Div. Polym. Chem.*, 27 (1986) 133.
18 N. V. Pogodyna, A. B. Melnikova and N. P. Evlampieva, *Khim. Drev.*, 6 (1984) 3.
19 V. N. Tscvetkov, *Rigid-Chain Polymer Molecules*, Nauka, Leningrad, 1986, p. 380.
20 J. B. Dobbin, A. Rudin and M. F. Tchir, *J. Appl. Polym. Sci.*, 27 (1982) 1081.

Journal of Chromatography, 522 (1990) 77–93
Elsevier Science Publishers B.V., Amsterdam

CHROMSYMP. 2009

Adsorption of proteins on porous and non-porous poly(ethyleneimine) and tentacle-type anion exchangers[a]

R. JANZEN and K. K. UNGER*
Institut für Anorganische Chemie und Analytische Chemie, Johannes Gutenberg-Universität, D-6500 Mainz (F.R.G.)
W. MÜLLER
E. Merck, R&D Chromatography, D-6100 Darmstadt (F.R.G.)
and
M. T. W. HEARN
Department of Biochemistry, Monash University, Clayton, Victoria 3168 (Australia)
(First received January 22nd, 1990; revised manuscript received July 7th, 1990)

ABSTRACT

Adsorption isotherms of proteins [bovine serum albumin (BSA), soybean trypsin inhibitor and alcohol dehydrogenase] on anion exchangers were measured by on-line and off-line methods. The poly(ethyleneimine) (PEI) type and the tentacle-type materials exhibited principally different modes of adsorption. On thin layers of PEI, bonded to non-porous silica, BSA adsorption data corresponded to a monolayer of molecules, with 80% adsorbed side-on, with a high affinity constant for binding, and 20% adsorbed more weakly. With porous material, the amount of BSA bound per unit surface with high affinity was smaller.

With tentacle-type anion exchangers, adsorption exceeded a monolayer by far, and data corresponded to a Hill-type isotherm. The Hill coefficients, which were smaller than 1, indicated an approximately Gaussian affinity distribution of the binding sites for the protein. As a consequence, adsorption capacities at elevated ion strength decreased drastically, while the affinity distribution became narrower. Adsorption capacities and binding constants increased with temperature, while Hill coefficients remained unchanged.

INTRODUCTION

The introduction of macroporous ion-exchangers based on surface-modified silicas has substantially improved the analysis and isolation of proteins in terms of resolution, speed and biorecovery [1–3]. A new family of novel macroporous ion-exchangers specially designed for nucleic acid and protein analysis have been recently introduced by E. Merck, Darmstadt, F.R.G. (see ref. 4).

Although the wide-spread applicability of these ion-exchangers has been demonstrated, very few fundamental studies on the kinetics and the equilibria of

[a] Presented at the *9th International Symposium on High-Performance Liquid Chromatography of Proteins, Peptides and Polynucleotides, Philadelphia, PA, November 6–8, 1989*. The majority of the papers presented at this symposium have been published in *J. Chromatogr.*, Vol. 512 (1990).

0021-9673/90/$03.50

proteins on ion-exchangers have been carried out [5–7]. The assessment of isotherms and kinetic data of proteins elucidates the type and strength of interactions and provides valuable hints for the use of ion-exchanger in isolation and purification.

This work examines the effect of the type of surface modification and the pore size of silica support on the adsorption capacity, the adsorption equilibria, the extent of non-specific adsorption and the kinetics of protein adsorption. The results were to be interpreted in the frame of existing models of adsorption. The aim was to contribute to a better understanding of the protein–ion exchanger interactions and to the questions which pore sizes and surface compositions are desirable for ion exchangers.

EXPERIMENTAL

Materials

Silicas (LiChrospher Si 100, 300, 1000 and 4000, with mean pore diameters of 10, 39, 105 and 280 nm, respectively) were obtained from and characterized by E. Merck (Darmstadt, F.R.G.). Non-porous glass beads (type 3000) were provided by Potters-Ballotini (Kirchheimbolanden, F.R.G.). γ-Glycidoxypropyltrimethoxysilane (GLYMO) and polyethyleneimine (PEI-600, mean mol. wt. 600) were purchased from Aldrich (Heidenheim, F.R.G.). Bovine serum albumin (BSA, 67 000 dalton), soybean trypsin inhibitor (STI, 21 500 dalton) and alcohol dehydrogenase from yeast (ADH, 141 000 dalton), all buffer components (reagent grade) and organic solvents (HPLC or reagent grade) were from E. Merck. Water was purified using a Mili-Q system (Millipore, Eschborn, F.R.G.).

Purity of proteins was determined by size-exclusion chromatography on a Zorbax GF-250 column (DuPont, Wilmington, DE, U.S.A.) with UV detection at 278 nm and 0.05 *M* phosphate buffer pH 7.0 containing 0.2 *M* NaCl. The BSA used was 98% pure, the water content was assumed to be 5% according to the data of the manufacturer. The purity of ADH and STI was >99% and 95%, respectively.

PEI modification

Bonded PEI anion exchangers were made using a procedure similar to the one introduced by Chang *et al.* [8]. Silicas were activated overnight at 423 K under vacuum. To 9 g of each material, 60 ml GLYMO were added and heated to 493 K for 2 h under nitrogen. GLYMO-modified silicas were washed with methanol and diethyl ether and dried at 333 K under vacuum. To obtain weak anion exchangers, they were suspended in 100 ml of a 1% PEI solution in methanol and reacted 24 h at 298 K in closed 200-ml erlenmeyer flasks at 140 strokes min^{-1} in a shaking water bath. The materials were collected on a frit, washed with methanol, 0.01 *M* HCl and, finally, water until the filtrate was neutral.

Preparation of the glass beads

The type 3000 glass beads, having a wide size distribution from 0.1 to 40 μm, were fractionated according to size by means of an Alpine 200 zig-zag classifier (Alpine, Augsburg, F.R.G.). A fraction containing particle sizes from 5–10 μm, with a mean value of 8 μm, was treated with an equal volume of *aqua regia* for 2 h at room temperature to remove organic impurities and increase the number of surface silanol groups. Finally, the material was washed to neutrality and dried under vacuum.

Tentacle-type strong anion exchangers

Pretreated glass beads and LiChrospher Si 1000 were subjected to a three-step procedure developed and described by Müller [4,9]. In short, the materials are silanized with GLYMO, the oxirane ring opened by acidic hydrolysis. Then, a radical grafting polymerization of an N-trimethylammoniumethyl(TMAE)–acrylamide salt is initiated by Ce^{4+} ions. The procedure results in individual, linear polyelectrolyte chains chemically bonded to the surface.

The porous (LiChrospher) material is equivalent to the commercial materials of E. Merck, which, according to the manufacturer, have an average chain length of 10 to 50 monomer units. Due to the very low surface area of the non-porous glass beads (the surface area was too low for exact surface determination by nitrogen adsorption, the geometrical surface area is *ca.* 0.3 m^2/g) the polymerization had to be done in the presence of excess monomer, probably resulting in significantly longer polymer chains.

On-line isotherm measurements

These experiments were done using apparatus similar to that previously described by other workers [10–12]. It consisted of a stirred, thermostated glass vessel containing the ion exchanger suspension, a Gelman Science (Ann Arbor, MI, U.S.A.) Acrodisk filter unit (1.2 μm porosity), a total of 40 cm of Tygon tubing with 1.4 mm internal diameter (*ca.* 18 cm^2 internal surface), an IN 4 peristaltic pump (Ismatec, Wertheim-Mondfeld, F.R.G.), a Merck-Hitachi F-1000 fluorescence detector equipped with a 40-μl cell and a Kipp and Zonen (Solingen, F.R.G.) chart recorder. In operation, the flow direction was frequently reversed for a few seconds to resuspend particles accumulating in the filter unit. The fluorescence detector was set to an extinction wavelength of 280 nm and an emission wavelength of 370 nm. To avoid non-specific adsorption of protein to the system components, the whole apparatus was flushed with a 1 mg/ml solution of BSA in 20 m*M* Tris–HCl buffer pH 8.3 for 24 h and subsequently for 8 h with the buffer only. After this procedure, no significant adsorption or desorption of protein to the tubing or glass vessel could be detected.

Isotherms were measured in a cumulative manner. To the stirred suspension of anion exchanger (porous materials: 100 mg in 25 ml, non-porous material: 200 mg in 25 ml), small volumes of BSA solution in buffer were added. After the equilibrium was established (indicated by a constant signal from the fluorescence detector —between 5 min and 2 h), the next portion of protein was added, and so on. Before starting each set of binding measurements the total system was calibrated in absence of ion exchanger, by at least 10 subsequent additions of protein, covering a concentration range from 0.4 μg/ml to 1 mg/ml. In the time scale of these experiments and within the precision limits of the method no proteolytic digestion or denaturation of the BSA was observed. Standards remained almost constant over hours of pumping through the system.

Off-line isotherm measurement

These experiments consisted of three steps.

Step 1. Wet ion exchanger (50–200 mg) was placed into 1.5 ml Eppendorf vials. To achieve conditioning to the buffer composition used in the experiment, vials were several times filled up with buffer, shaken, centrifuged and the supernatant decanted.

Step 2. Buffer and protein solution were added, the vials placed into 100-ml

erlenmeyer flasks filled with 40 ml of water, put into a thermostatted shaking water bath (SW-1P, Julabo, Bernkastel-Kues, F.R.G.). The suspension was shaken overnight (140 strokes per minute, amplitude 15 mm), which prevented particles from settling. Then the suspension was centrifuged in an Eppendorf centrifuge.

Step 3. Variable amounts of the supernatant protein solution were injected into a Merck-Hitachi gradient high-performance liquid chromatography (HPLC) system. The system was equipped with a column 36 × 8 mm, filled with 2.1 nm non-porous, monodisperse, C_{18} modified silica. The injection volume was 100 μl for higher protein concentrations, up to 500 μl for low concentrations. Eluents were: (A) 0.1% trifluoroacetic acid (TFA) in water, (B) 0.1% TFA in acetonitrile–water (80:20, v/v). Elution was performed by the following gradient: 1 min isocratically at 25% B, 5 min linear gradient from 25 to 100% B, 2 min isocratically at 100% B. Quantification was done through UV detection at 220 nm by peak height. Each sample was measured at least twice, with at least one calibration run using a similar BSA solution between the two runs.

To prevent the ion exchangers from drying, the particles were always kept in suspension. The exact weight of the ion exchanger was determined gravimetrically, after completing the measurements, by washing with distilled water and drying overnight at 353 K. Non-specific adsorption to the vials was minimized by preincubation of the vials with 1.5 ml of a 0.1 mg/ml BSA solution in Tris–HCl buffer pH 8.0 overnight and rinsing 3 times for 1 h with 1.5 ml of the buffer used in the particular adsorption experiment.

Desorption experiments

Desorption by dilution was measured using the same off-line system. Adsorption was allowed to take place for 24 h. After centrifugation, the protein solution was decanted and the concentration determined by reversed-phase HPLC as described. Then the vial was weighed, 1.2 ml of fresh buffer were added and the ion exchanger resuspended in the shaking water bath. After each 24 h, the procedure was repeated, finally to give the desorption isotherm, consisting of 4 to 5 points.

Dynamic load capacities

Adsorption capacities of the PEI-bonded silicas were determined by measuring breakthrough curves. HPLC cartridges (E. Merck) 25 × 4 mm I.D. were packed at 250 bar maximum pressure. After conditioning of the column and running a test chromatogram, a 1 mg/ml protein solution in 20 m*M* Tris–HCl buffer pH 8.0 (buffer A) was pumped through the cartridge at a flow-rate of 0.5 ml/min. The effluent concentration was monitored at 278 nm with a UV detector (LKB 2150). The whole area above the recorded curve and below the line representing the final concentration of 1 mg/ml was integrated to give the total adsorption capacity at this BSA concentration.

After loading, the protein was eluted by application of a step gradient: 15 min 0.5 *M* NaCl in buffer A, 15 min 1 *M* NaCl in buffer A, 15 min reconditioning with buffer A, flow-rate 0.5 ml/min.

Adsorption kinetics

The apparatus and method used for on-line isotherm measurements was modified for the adsorption kinetic experiments. The total suspension volume was reduced to 11 ml in a stirred, thermostatted vessel. The concentration was determined by aspiration of adsorbent-free solution through an LKB solvent filter (sinter metal) and the detector (LKB 2150, 278 nm) by means of a peristaltic pump (Ismatec IN 4) and returning it into the adsorption vessel. The total volume of this detection loop was *ca.* 1 ml. The system was filled with 10 ml of protein solution (1 mg/ml in buffer A). A 100-mg amount of ion exchanger was suspended in 1 ml of buffer A and put into an ultrasonic bath for 5 min to break up any agglomerates. The suspension was added to the vigorously stirred protein solution by means of a 5-ml syringe (the addition took not more than 1 s), while the peristaltic pump worked at a flow-rate of 2 ml/min.

RESULTS AND DISCUSSION

Dynamic load capacities of ion exchangers

The load capacities measured varied significantly with the pore size of the material, with the size of the protein (Table I), and with the number of repetitive loadings onto the same column (Table II). Especially the last finding, namely a successive decrease in loading capacity after every loading/elution cycle, made it impossible to use the same packed cartridge for a series of experiments. Such a series would, for example, be required for an isotherm calculated from breakthrough experiments. The full adsorption capacity could not be reestablished even by an extensive washing cycle, including overnight washing with 1 *M* NaCl in buffer A and a gradient from 0–80% isopropanol in 0.1% aqueous TFA. It seems unlikely that this fouling process is caused by a significant decomposition of the anion-exchange

TABLE I

DYNAMIC LOAD CAPACITY OF PEI-BONDED ION EXCHANGERS FOR SELECTED PROTEINS

Pore diameter and surface area as reported by supplier, E. Merck. Buffer 1: 20 m*M* Tris–HCl, pH 8.0; buffer 2, 50 m*M* NaCl in buffer 1.

Support material	Pore diameter (nm)	Surface area (m^2/g)	Load capacity (mg/ml; in parentheses: mg/m^2)			
			Buffer 1			Buffer 2
			ADH	STI	BSA	BSA
LiChrospher Si 100	10	370	21.9 (0.08)	64.3 (0.24)	17.3 (0.07)	11.8 (0.04)
LiChrospher Si 300	39	58	41.0 (0.9)	126.1 (2.8)	70.9 (1.6)	51.1 (1.1)
LiChrospher Si 1000	105	25	84.8 (4.4)	53.1 (2.8)	43.3 (2.2)	28.3 (1.5)
LiChrospher Si 4000	280	9	41.8 (5.8)	18.5 (2.6)	19.5 (2.7)	13.0 (1.8)
Non-porous silica	–	1.8	13.1 (5.4)	6.1 (2.5)	6.5 (2.7)	5.5 (2.3)

TABLE II

DECREASE IN DYNAMIC BSA LOAD CAPACITY ON POROUS AND NON-POROUS PEI-BONDED ION EXCHANGERS AFTER SIX CONSECUTIVE FRONTAL LOADINGS

For buffers, see Table I.

Support material	% decrease in BSA load capacity	
	Buffer 1	Buffer 2
LiChrospher Si 100	29	32
LiChrospher Si 300	33	37
LiChrospher Si 1000	30	28
LiChrospher Si 4000	28	27
Non-porous silica	26	17

modification, because (i) several empty cycles, *i.e.* pumping of loading and elution buffers in the absence of protein did not cause a further decrease of the adsorption capacity, (ii) the "fouling rate" was slightly dependent on the pore size (Table I), and (iii) the non-porous surface, which should be most exposed to hydrolytic or other degrading mechanisms, showed the smallest decrease in adsorption capacity; the "fouling rate" was highly dependent on the protein. With ADH, capacities dropped, in some cases, more than 50% between the first and the second cycle.

The dependence of the absolute load capacities (Table I) on the pore size is consistent with the findings of other authors [13,14]. The calculation of the load capacity per unit surface (Table 1) allows more insight into the surface accessibility of materials with different pore sizes. The results suggest that the surface of the 39-nm material and, in the case of ADH, even the 105-nm material can not adsorb protein at the same density as a non-porous or 280 nm porous anion exchanger. It needs to be mentioned that dynamically measured load capacities are not identical with the equilibrium adsorption capacities q_m obtained from batch experiments [14]. Adsorption kinetic experiments in suspension with the same PEI-bonded materials used in this study [15] showed that for the 105- and 280-nm porous materials adsorption of proteins (initial concentration *ca.* 1 mg/ml) is more than 90% complete after 1 min. For the 39- and 10-nm porous ion exchangers, 90% saturation required between 10 min and several hours, depending on the protein and the specific material. The differences between dynamic and equilibrium load capacity are, therefore, larger for the materials with smaller pores than for the macroporous and non-porous materials. However, they are not large enough to explain the drastic decline of load capacity per unit surface with increasing protein size and decreasing pore diameter. This appears to be more of a steric rather than a kinetic effect.

Adsorption isotherms

All isotherms measured by each method were of type 1 [16]. This means that they were singlestep, hyperbolic isotherms with a relatively well-defined saturation value.

Adsorption isotherms for BSA on PEI-bonded weak anion exchangers

These isotherms are illustrated in Fig. 1a. For better comparison, the data for

bound BSA (concentration on adsorbent), q^*, in Fig. 1a were reduced to relative saturation data, θ ($\theta = q^*/q_{max}$). In view of the non-linearity of the Scatchard and Hill plots the q_{max} values used were determined by extrapolation from a double reciprocal plot. The Scatchard and Hill plots (Fig. 1b and c) show clearly that the overall adsorption behavior does not fit a simple Langmuir isotherm.

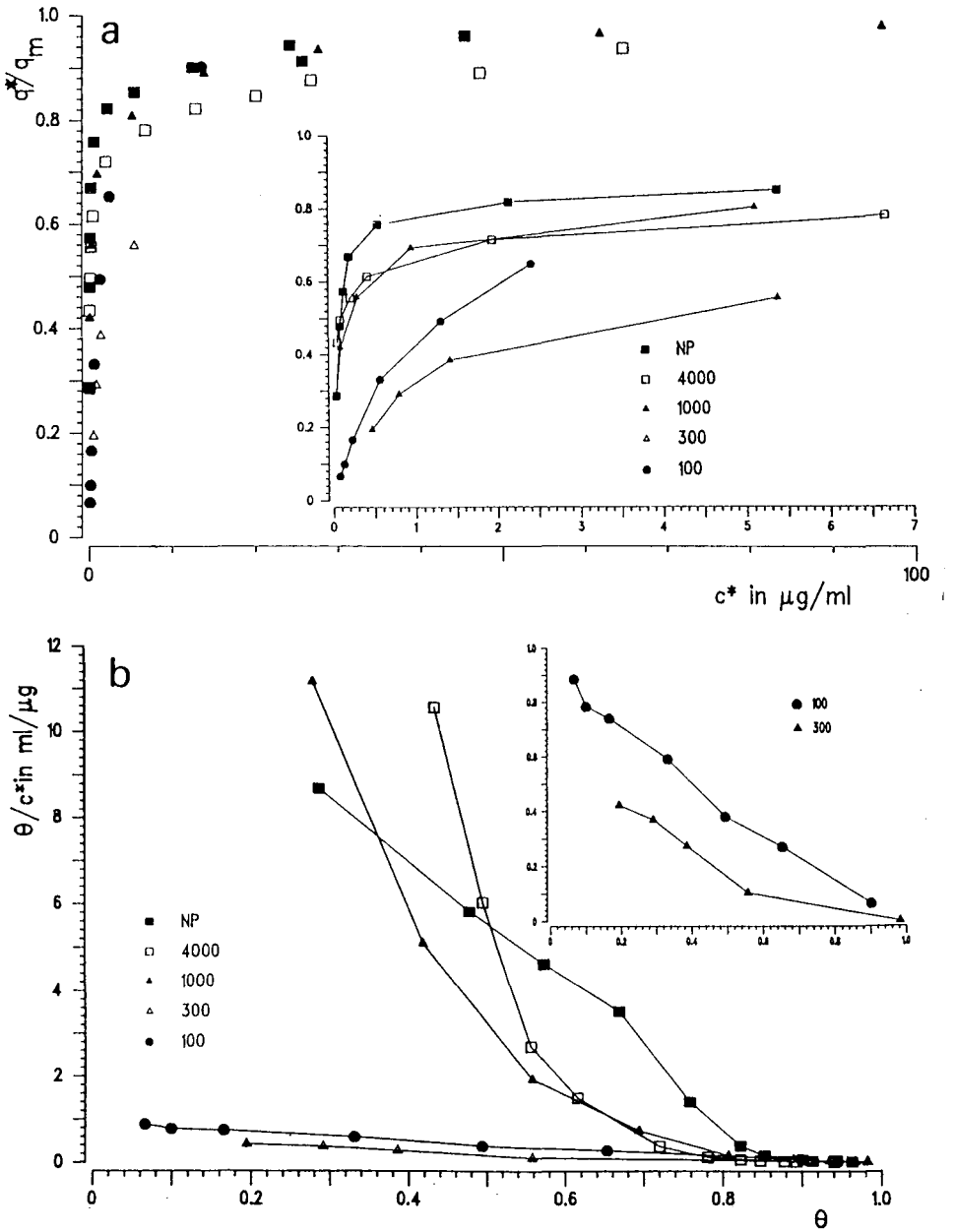

Fig. 1.

(Continued on p. 84)

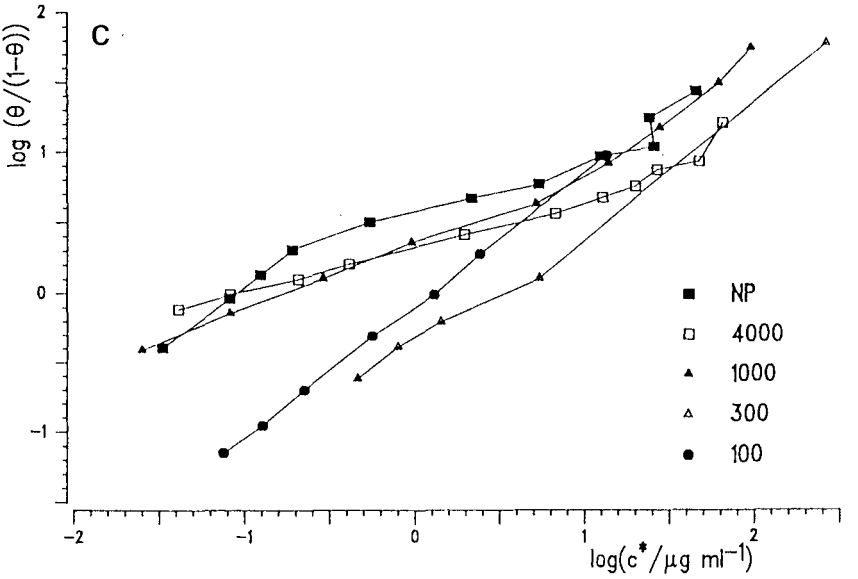

Fig. 1. Adsorption isotherms for BSA on PEI-bonded silicas of varying pore diameter (for conditions see Experimental). (a) Isotherm plot; (b) Scatchard plot; (c) Hill plot. Abbreviations: NP = non-porous silica, PEI coated; 4000 = LiChrospher Si 4000, PEI coated; 1000 = LiChrospher Si 1000, PEI coated; 300 = LiChrospher Si 300, PEI coated; 100 = LiChrospher Si 100, PEI coated. c* = Equilibrium concentration of BSA in solution.

The data for 39- and 10-nm silicas indicate a much lower binding constant compared to the macroporous and non-porous materials. However, in the case of LiChrospher Si 300, this lower association constant does not correspond with the chromatographic data (not shown), where this 39-nm material exhibited the strongest retention of all PEI-bonded ion exchangers. Because the adsorption time for every point in the isotherm was limited, it is likely that the data for LiChrospher Si 300 (and Si 100) do not represent a real equilibrium. This is further supported by kinetic data [15].

The non-porous material behaves ideally up to a saturation of *ca.* 80% of the total capacity, as can be seen from the low concentration part of the Scatchard plot. With LiChrospher Si 4000 and especially with Si 1000, this tendency is weaker, meaning that a Langmuir-like adsorption occurs only at lower degrees of saturation, if at all. Nevertheless, all materials exhibit a final load capacity that is higher than predictable through linear extrapolation of the data at low saturation, which indicates a change in adsorption mechanism. The Hill plots obtained from the data are S-shaped.

Data of Reynaud *et al.* [17] on the adsorption of BSA to graphite powder show an adsorption density of 2 mg/m^2. This was interpreted as a monolayer adsorption of the ellipsoidal BSA molecule in side-on position and further confirmed by voltammetric data. At higher BSA concentration an additional adsorption step of *ca.* 0.5 mg/m^2 occurred. The authors also found that in the adsorbed state the protein layer was only 2.4 nm thick, compared to a minimum of 38 nm as expected from

crystallographic data. This implies a strong conformational change or denaturation of BSA in the adsorbed state. On the chromatographic ion exchangers used in the present study the conformation is not expected to change so much, and the molecule should

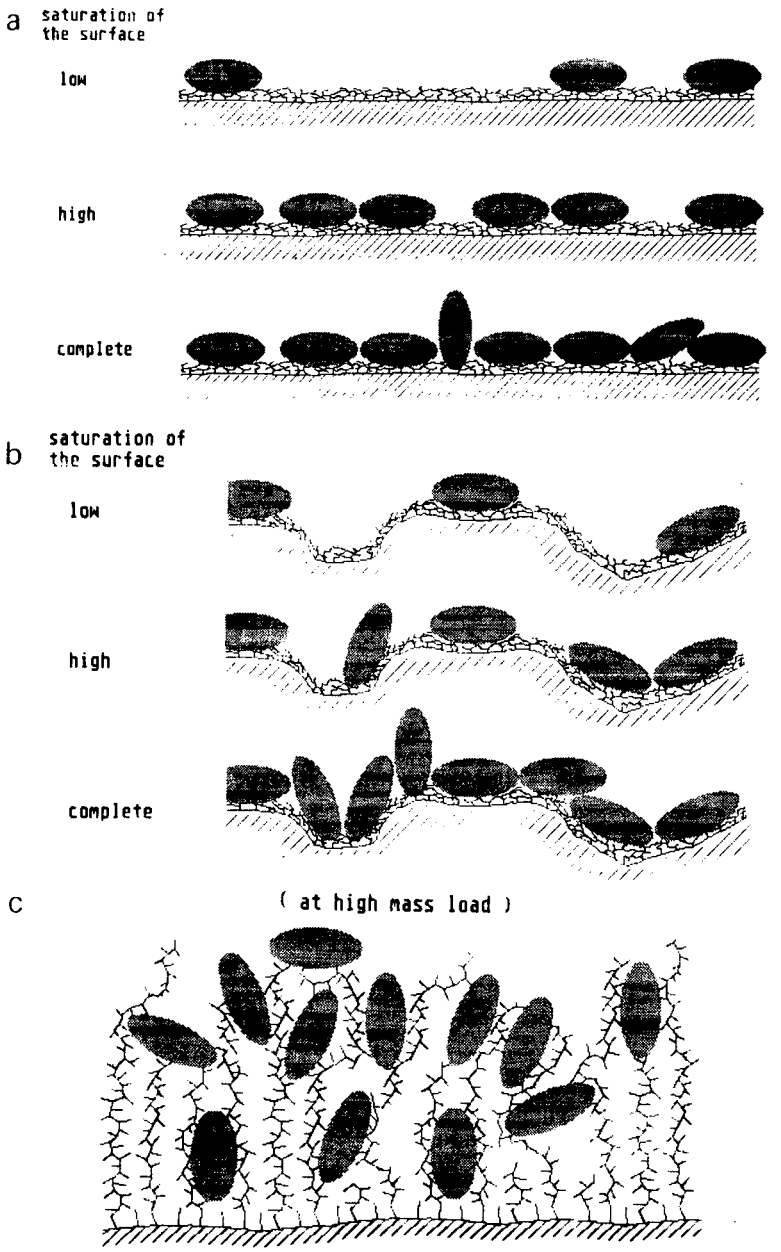

Fig. 2. Illustration of the adsorption of BSA molecules on the surface of different types of anion exchangers, (a) Non-porous PEI-bonded silica; (b) porous PEI-bonded silica; (c) silica or glass with "tentacle"-type modification.

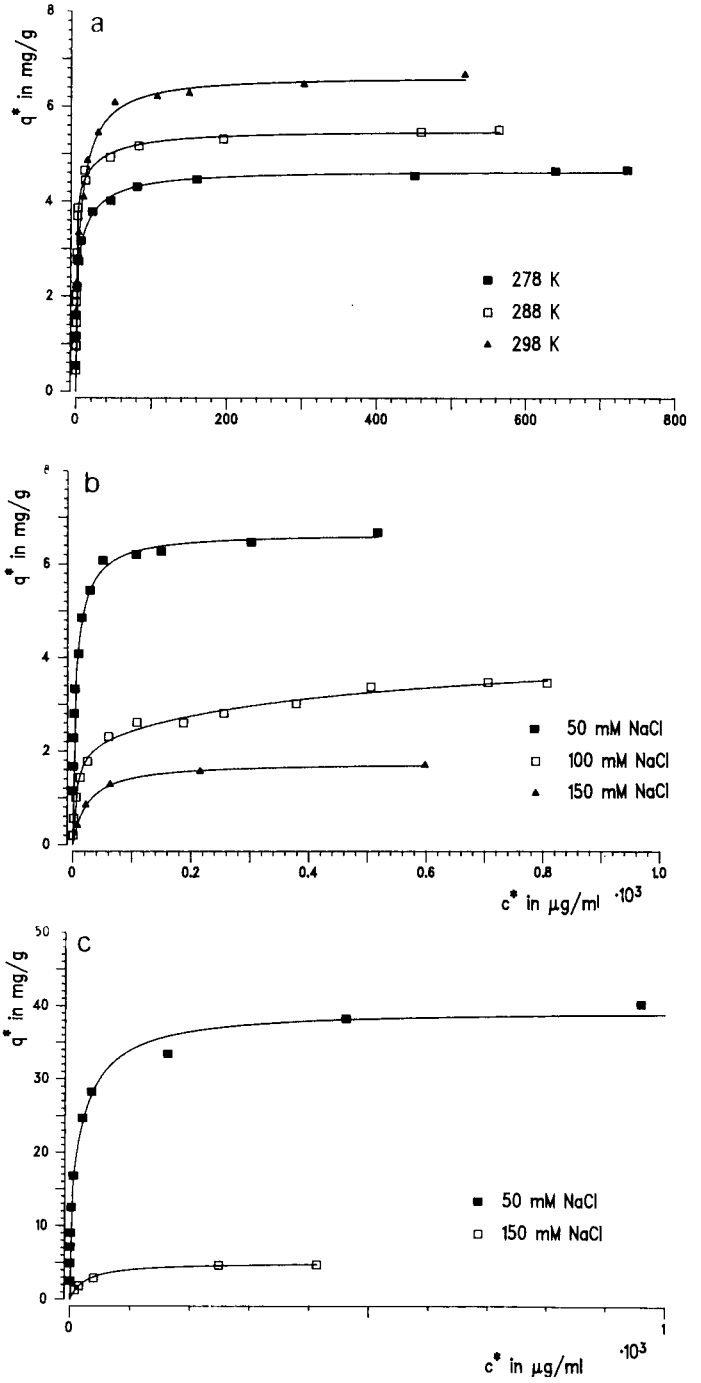

Fig. 3. Adsorption isotherms for BSA on TMAE "tentacle"-type anion-exchanger. (a) Non-porous support material, 50 m*M* NaCl, variation of temperature; (b) non-porous support material, 298 K, variation of NaCl concentration; (c) 105-nm porous support material, 298 K, variation of NaCl concentration. c* = Equilibrium concentration of BSA in solution.

occupy less space. The values obtained in the present study are 2.3 ± 0.1 mg/m^2 for the Langmuir-type adsorption limit and 2.8 ± 0.05 mg/m^2 for the total adsorption capacity (non-porous material). They may therefore very well reflect the capacity for side-on adsorption and the filling of remaining binding sites by molecules adsorbed in less favorable positions (Fig. 2a). The values are also consistent with data from other recent studies of methacrylate-based anion exchange packings [12].

Porous silicas are built up from primary particles in the diameter range of 2–10 nm [18], depending on the specific production process. Thus their pores can not have smooth walls and an ideally cylindrical shape. Hydrothermal processes used to convert mesoporous into macroporous materials are likely to smooth minor irregularities without producing a really flat surface. The non-porous silica wich is produced by a continuous process without or with extremely small ($\leqslant$1 nm) primary particles, shows no surface irregularities in a range observable by electron microscopy [19]. A thin, tightly bound modification applied to porous and non-porous silicas should retain these characteristics. The smoother, more homogeneous surface offers more adsorption sites with identical environment per unit surface (as illustrated in Fig. 2a and b). This can explain the greater extent of linearity in the Scatchard plots for the non-porous ion exchanger compared with the 280- and 105-nm porous materials.

Adsorption isotherms on tentacle-type ion exchangers

These results are given in Figs. 3a–c and 4a–c and Tables III–V. All isotherms on both tentacle-type materials fit the Hill isotherm quite well. According to Sips [20], this can be interpreted as a Gaussian-like distribution of binding sites, *e.g.* the Sips coefficient, r, approaches a value of 1.

The Hill coefficients at a sodium chloride concentration lower than 150 mM were substantially smaller than unity (see Fig. 3) which always corresponds to concave Scatchard plots (not shown). This type of behavior is often interpreted as a sign for negative cooperativity between the binding sites.

From the data shown in Figs. 3 and 4 an increase of adsorption capacity with temperature is obvious. Also the dissociation constant at lower saturation, as indicated by the distribution constant (K_d) (2-site Langmuir fit) is dependent on the temperature. In accordance with published chromatographic data on PEI-coated ion exchangers [21], the binding strength increases with temperature (Table III, Fig. 4a). The calculated Hill coefficients are all in the same range.

TABLE III

CHARACTERISTIC PARAMETERS OF BSA ADSORPTION ON NON-POROUS TMAE "TENTACLE"-TYPE ION EXCHANGER AT DIFFERENT TEMPERATURES (ALL AT 50 mM NaCl)

q_m extrapolated from double reciprocal plot; q_{m1}, q_{m2}, K_{d1} and K_{d2} values derived from two-center Langmuir isotherm (simplex fit).

Temperature (K)	q_m (mg/g)	Hill coefficient (n)	Hill constant (K)	q_{m1} (mg/g)	q_{m2} (mg/g)	K_{d1} (μg/ml)	K_{d2} (μg/ml)
278	4.9	0.53 ± 2%	0.61 ± 10%	2.8	2.0	0.4	20
288	5.8	0.52 ± 5%	0.89 ± 11%	4.2	1.4	0.3	28
298	7.1	0.56 ± 3%	0.49 ± 8%	2.4	4.3	0.2	12

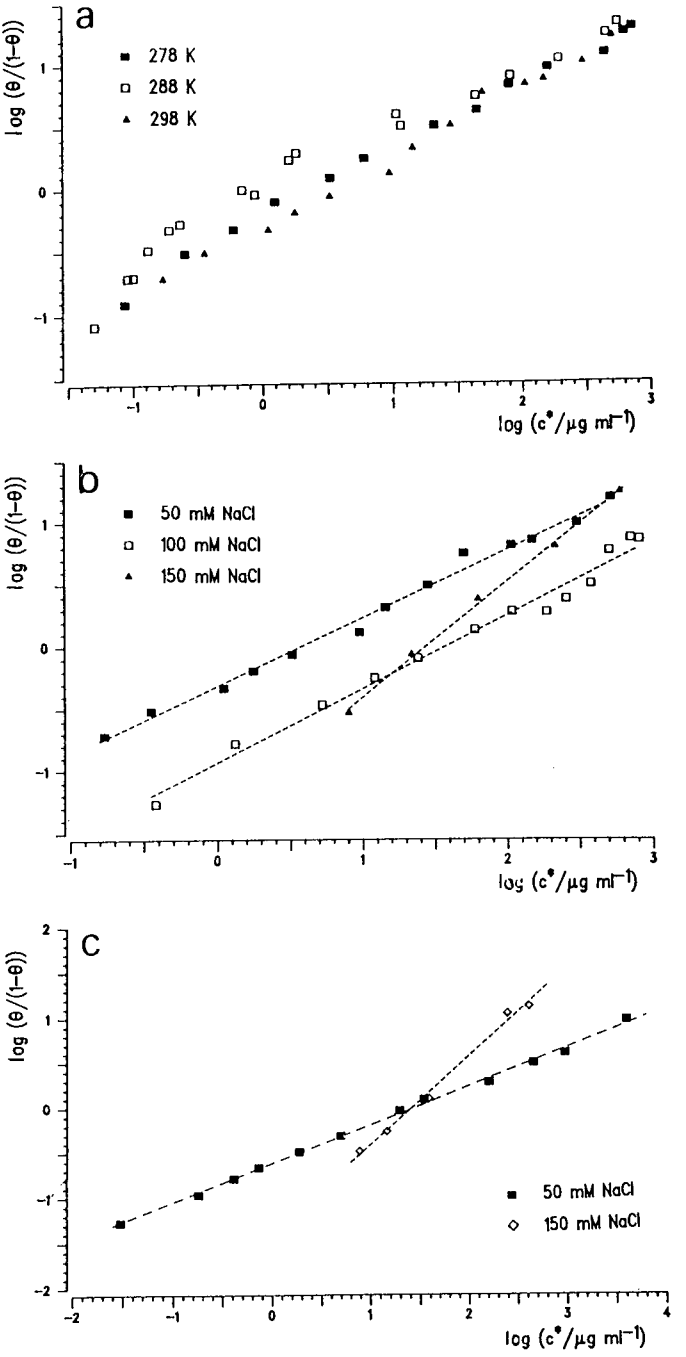

Fig. 4. Hill plots of the data in Fig. 3. (a) Non-porous support material, 50 m*M* NaCl, variation of temperature; (b) non-porous support material, 298 K, variation of NaCl concentration; (c) 105-nm porous support material, 298 K, variation of NaCl concentration.

TABLE IV

CHARACTERISTIC PARAMETERS OF BSA ADSORPTION ON NON-POROUS TMAE "TENTACLE"-TYPE ION EXCHANGER AT DIFFERENT NaCl CONCENTRATIONS (ALL AT 298 K)

For q_m, q_{m1}, q_{m2}, K_{d1} and K_{d2} see Table III.

Concentration (mol/l)	q_m (mg/g)	Hill coefficient (n)	Hill constant (K)	q_{m1} (mg/g)	q_{m2} (mg/g)	K_{d1} (μg/ml)	K_{d2} (μg/ml)
0.05	7.1	0.56 ± 3%	0.49 ± 8%	2.4	4.3	0.2	12
0.10	3.9	0.61 ± 4%	0.11 ± 5%	2.2	2.2	6.0	500
0.15	1.8	0.95 ± 3%	0.05 ± 12%	1.8		25	
0.4	0	–	–	–		–	

Increased salt concentrations lead to lower binding strength (higher K_d) and lower binding capacity. The first observation could be foreseen from the theory of ion exchange and the practice of ion exchange chromatography. However, the decrease in binding capacity is not to be expected in the case of Langmuir-type adsorption, but is a natural consequence, when the linear Hill plots are interpreted as a distribution of binding affinities. The sites with low affinity will only bind at low ionic strength. The decrease is more drastic with the porous material than with the non-porous beads. With increasing ionic strength and decreasing binding capacity, the slope of the Hill plots gets steeper. At 150 mM NaCl content, both materials exhibit a Hill coefficient close to one, indicating a Langmuir-type behavior. This adsorption behavior has been documented for biomimetic affinity chromatography of proteins [12]. These data indicate that at last two interaction modes occur at low salt concentrations.

The differences betweeen the PEI-bonded weak anion exchangers and the tentacle-type quaternary anion exchangers involve not only the form of the isotherm but also the adsorption capacity. With the latter materials, the apparent surface coverages exceed the expected monolayer density of side-on adsorbed molecules. On the 105-nm tentacle-type material, the capacity is 2 mg/m^2 at 50 mM NaCl in the buffer (nearly 3 mg/m^2 without NaCl, not shown) compared to 1.5 mg/m^2 (50 mM NaCl) and

TABLE V

CHARACTERISTIC PARAMETERS OF BSA ADSORPTION ON POROUS TMAE "TENTACLE"-TYPE ION EXCHANGER AT DIFFERENT NaCl CONCENTRATIONS (TEMPERATURE 298 K)

For q_m, q_{m1}, q_{m2}, K_{d1} and K_{d2} see Table III.

Concentration (mol/l)	q_m (mg/g)	Hill coefficient (n)	Hill constant (K)	q_{m1} (mg/g)	q_{m2} (mg/g)	K_{d1} (μg/ml)	K_{d2} (μg/ml)
0.05	50	0.43 ± 2%	0.25 ± 3%	23	22	1.3	163
0.15	5.0	1.0 ± 5%	0.04 ± 20%	5		26	
0.4	<0.1	–	–	–		–	

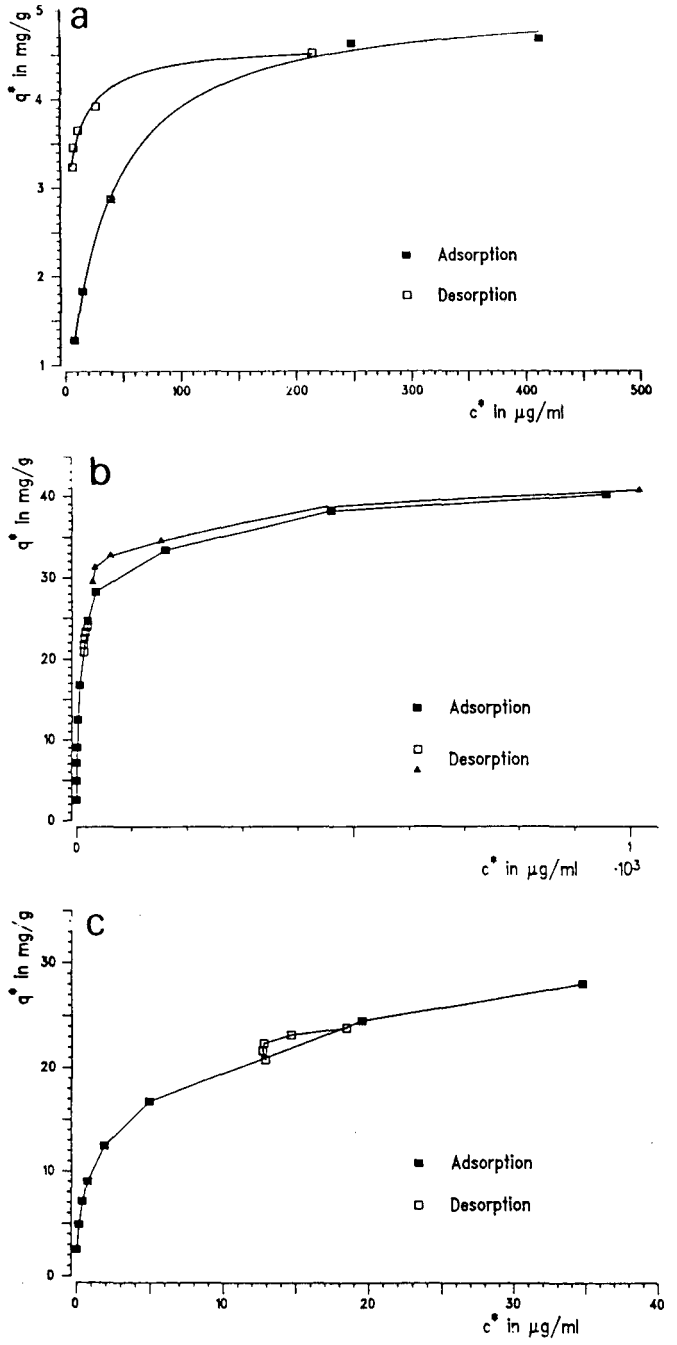
a
q* in mg/g
c* in µg/ml
Adsorption
Desorption
b
q* in mg/g
c* in µg/ml
·10³
Adsorption
Desorption
c
q* in mg/g
c* in µg/ml
Adsorption
Desorption

Fig. 5.

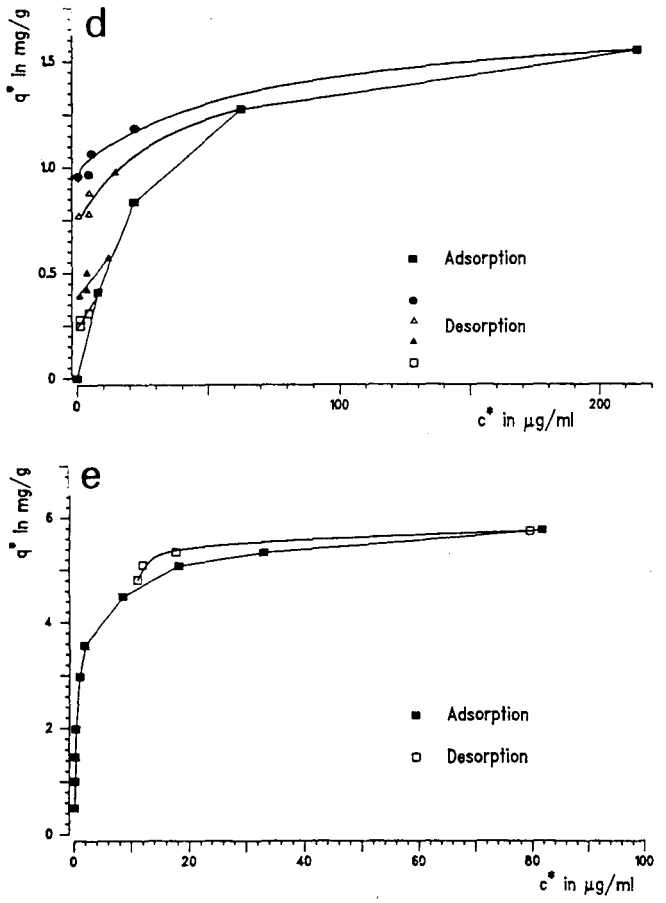

Fig. 5. Desorption of BSA from "tentacle"-type anion exchangers by dilution of the protein solution. Samples were taken 24 h after dilution (for other conditions see Experimental). (a) 105-nm porous material, 150 m*M* NaCl; (b) 105-nm porous material, full concentration range 50 m*M* NaCl; (c) 105-nm porous material, low concentration range 50 m*M* NaCl; (d) non-porous material, 150 m*M* NaCl; (e) non-porous material, 50 m*M* NaCl.

2.2 mg/m^2 (without NaCl) on the PEI-bonded material. The non-porous tentacle-type material exhibited an extremely high load capacity. Based on the estimate of 0.3 m^2/g specific surface area, the measured value of 7.1 mg/g gives a specific load capacity of 23.7 mg/m^2. This value exceeds the monolayer density in any orientation of the BSA molecules by far. Hence the protein must be adsorbed in multilayers or "dissolved" in the polymer layer (as illustrated in Fig. 2c).

The reason why all these isotherms on the tentacle-type adsorbents fit the Hill equation is not clear. An actual Gaussian-like distribution of discrete binding sites is not probable in this highly flexible polymer layer. Due to the dynamic character of the stationary phase it appears much more likely that the actual sites of binding form during the interaction with the protein, and their shape is largely determined by the properties of the protein. Negative binding cooperativity is a better explanation for the

isotherm shape. Thus, a BSA molecule adsorbed into the layer decreases the affinity for the uptake of more molecules in its immediate surrounding, *e.g.* by occupying the charged groups or changing the conformational structure of the "tentacle" layer. At higher salt content and therefore, weaker interaction, the adsorbed BSA molecules would be more isolated, not influence each other very much, but only permit a relatively low density of adsorption.

Desorption measurements

Desorption "isotherms" were done with the 105-nm porous and the non-porous tentacle-type ion exchanger, at two different ionic strengths and starting from different points in the adsorption isotherm. In all cases, significant adsorption hysteresis was observed (Fig. 5a–e) characteristic of extremely slow desorption phenomena. If the isotherms represent a real equilibrium state, this is impossible [10]. The reason for the behaviour must therefore be sought in kinetics.

Considering the fast uptake rates (adsorption kinetics), with an equilibrium constant of 26.3 mg/ml (porous material, 150 m*M* NaCl), the desorption rate equals the adsorption rate at a solution concentration of 26.3 mg/ml. Control experiments showed that the protein adsorption from 40 μg/ml initial concentration was very probably diffusion controlled and equilibrium was virtually established within 2 min. The actual surface interaction step is probably even faster. The desorption from the surface should, according to these facts, only take minutes till equilibrium is reached. The extremely slow desorption leading to the hysteresis must therefore be due to secondary equilibria, as other authors have proposed [22].

CONCLUSIONS

The experimental data obtained in this study strongly suggest that the manner of protein adsorption to anion exchangers can be different with different kinds of surface properties and chemical modifications of the support material. At moderate and high values of relative saturation, low surface area materials with thin layers of modification exhibit less negative cooperativity than those with either higher surface area or thick layers of modification. At high relative saturation the amount of protein adsorbed can range from less-than-monolayer (thin modification layer, rough surface) over monolayer density (thin modification layer, smooth surface) to far more than monolayer density (thick tentacle-type modification layer). Both the thin layer and the tentacle-type of anion exchangers seem to be principally useful for the preparative separation of proteins. Hill plots and especially the Hill coefficient n obtained from the measurement of adsorption isotherms can in either case be useful. They allow to estimate how much of the total load capacity is actually available for interaction in both isocratic and gradient separations. Similar criteria have been documented for immunoaffinity chromatography of proteins [23].

REFERENCES

1 K. K. Unger, *Chromatographia*, 24 (1987) 144.
2 K. K. Unger, B. Anspach, R. Janzen, G. Jilge and K. D. Lork, in Cs. Horváth (Editor), *High-Performance Liquid Chromatography —Advances and Perspectives*, Vol 5, Academic Press, New York, 1988, pp. 2–87.

3 F. Regnier, *Chromatographia,* 24 (1987) 241.
4 W. Müller, *8th International Symposium on HPLC of Proteins, Peptides and Polynucleotides, Copenhagen, Oct. 31–Nov. 2, 1988*, poster No. 121.
5 J. X. Huang and Cs. Horváth, *J. Chromatogr.*, 406 (1987) 285.
6 E. E. Graham and C. F. Fook, *AIChE J.*, 28 (1982) 245.
7 H. Pedersen, L. Furler, K. Venkatasubramanian, J. Prenosil and E. Stuker, *Biotechnol. Bioeng.*, 27 (1985) 96.
8 S. H. Chang, K. M Gooding and F. E. Regnier, *J. Chromatogr.*, 120 (1976) 321.
9 W. Müller, *Eur. J. Biochem.*, 155 (1986) 203.
10 H. A. Chase, *J. Chromatogr.*, 297 (1984) 179.
11 F. B. Anspach, A. Johnston, H. J. Wirth, K. K. Unger and M. T. W. Hearn, *J. Chromatogr.*, 476 (1989) 205.
12 B. Anspach, A. Johnston, K. K. Unger and M. T. W. Hearn, *J. Chromatogr.*, 499 (1990) 103.
13 M. A. Rounds, W. Kopaciewicz and F. E. Regnier, *J. Chromatogr.*, 362 (1986) 187.
14 W. Kopaciewicz, S. Fulton and S. Y. Lee, *J. Chromatogr.*, 409 (1987) 111.
15 R. Janzen, K. K. Unger and W. Müller, *9th International Symposium on HPLC of Proteins, Peptides and Polynucleotides, Philadelphia, PA, Nov. 6–8, 1989*, poster No. 109.
16 S. J. Gregg and K. S. W. Sing, *Adsorption, Surface Area and Porosity*, Academic Press, London, 1982.
17 J. A. Reynaud, J. Tavernier, L. T. Yu and J. M. Cochet, *Bioelectrochem. Bioenerg.*, 15 (1986) 103.
18 N. Tanaka, K. Hashidzume, M. Araki, H. Tsuchiya, A. Okuno, K. Iwaguchi, S. Ohniski and N. Takai, *J. Chromatogr.*, 389 (1987) 115.
19 K. K. Unger, G. Jilge, R. Janzen, H. Giesche and J. Kinkel, *Chromatographia,* 22 (1986) 379.
20 R. Sips, *J. Chem. Phys.*, 16 (1948) 490.
21 G. Jilge, K. K. Unger, U. Esser, H. J. Schäfer, G. Rathgeber and W. Müller, *J. Chromatogr.*, 476 (1989) 37.
22 H. P. Jennissen, *J. Colloid Interface Sci.*, 111 (1986) 570.
23 J. D. Davies and M. T. W. Hearn, *J. Chromatogr.*, in press.

Journal of Chromatography, 522 (1990) 95–105
Elsevier Science Publishers B.V., Amsterdam

CHROM. 22 776

Chemically modified polymeric resins for high-performance liquid chromatography

JEFFREY J. SUN and JAMES S. FRITZ*

Ames Laboratory–U.S. Department of Energy and Department of Chemistry, Iowa State University, Ames, IA 50011 (U.S.A.)

(First received March 5th, 1990; revised manuscript received August 24th, 1990)

ABSTRACT

Chemical reactions were used to attach various hydrophilic functional groups and one hydrophobic group to cross-linked polystyrene resins. Those with hydrophilic groups had much better wettability by water. The capacity factors of a number of test compounds were compared on columns packed with derivatized and underivatized polymeric resins. The capacity factor of most test compounds were distinctly different on columns packed with the derivatized resins. In some cases the elution order of test compounds was different on the derivatized resin columns. The modified resins offer an additional selectivity parameter for liquid chromatographic separations.

INTRODUCTION

Reversed-phase liquid chromatography is generally performed on columns packed with C_{18}- or C_8-bonded phase silica [1]. Although such columns are very efficient, they do have several drawbacks. The most serious of these is the instability of silica in alkaline solutions or in highly acidic solutions. Silica also has residual silanol groups that can cause peak broadening or tailing by interaction with polar compounds such as amines and alcohols. After a gradient elution, silica-based columns may require some time to re-establish equilibrium for the next run [2].

In recent years there has been a growing interest in polymeric materials for use in reversed-phase high-performance liquid chromatography (HPLC). In particular, resins based on poly(styrene–divinylbenzene) (PS–DVB) are stable with eluents from pH 1–14 and give excellent separations [3–6]. Some difficulties have been associated with polymeric resins, such as swelling in the presence of organic solvents, which can be especially troublesome when solvent gradients are used [7]. However, rapid improvements are being made in stability and performance so that polymeric resins can now be considered to be very attractive for HPLC.

A considerable variety of polymeric resins have been prepared and used for HPLC [8–13]. There has been a remarkable tendency to bond C_{18}-hydrocarbon groups to the surface so that the retention behavior of the polymeric resins will closely approximate that of the popular C_{18} silica materials [11,13,14]. In fact, silica resins with a C_{18}- or C_8-bonded phase dominate the field of reversed-phase liquid

0021-9673/90/$03.50

chromatography. Using these resin columns, necessary changes in selectivity are brought about by varying the solvents that make up the mobile phase. However, several investigators have used silica columns with more polar bonded phases to provide an additional parameter for varying selectivity in liquid chromatography [15–17].

In the present work cross-linked polystyrene resins have been modified by introduction of any of several hydrophilic functional groups, and in one case by introduction of a more hydrophobic group. The modified resins are easily prepared by the Friedel–Crafts reaction with the benzene ring of the polymer. It is shown that the derivatized resins can be used for practical liquid chromatographic separations and that the type of functional group incorporated in the resin has a major effect on the retention behavior of various analytes.

EXPERIMENTAL

Apparatus

A Gilson 302 HPLC system equipped with a microprocessor controller (Gilson Medical, Middleton, WI, U.S.A.), a 7125 Rheodyne injector (Rheodyne, Berkeley, CA, U.S.A.) equipped with a 20-μl loop, a Spectroflow 783 Kratos variable-wavelength UV–VIS detector (Kratos, Ramsey, NJ, U.S.A.), a Fisher Recordall series 5000 recorder (Fisher Scientific/Instrument Lab., Itasca, IL, U.S.A.) and a Hitachi D-2000 intergrator (EM Science, Cherry Hill, NJ, U.S.A.), were used for HPLC. A Shandon HPLC packing pump (Shandon Southern, Sewichley, PA, U.S.A.) was used for column packing. A Bruker FT-IR 98 instrument (USA Bruker Instruments, San Jose, CA, U.S.A.) was used for structure determination.

Reagents and chemicals

Two kinds of PS–DVB resins were used in this experiment; non-spherical XAD-4 resin (Rohm & Haas, Philadelphia, PA, U.S.A.) of 45–58 μm particle size, 50 Å pore size and 784 m^2/g surface area, and 10-μm spherical resin (Sarasep, Santa Clara, CA, U.S.A.) of 80 Å pore size and 415 m^2/g surface area. The XAD-4 resin was ground and then sieved with a Model L3P sonic sifter (Allen-Bradley, Milwaukee, WI, U.S.A.). The particles of size 45–58 μm (*ca.* 250–325 mesh) were chosen for derivatization. The ground resin was washed with water and acetonitrile, Soxhlet-extracted overnight with methanol, ether and acetonitrile, and then dried. The 10-μm spherical resin was cleaned by the same way.

The reagents and solvents used for the derivatization reactions were reagent grade and were dried by molecular sieves. Reagent grade test compounds were used for the HPLC experiments. HPLC-grade acetonitrile was used, and laboratory distilled water was further deionized by a Barnstead Nanopure II system (Sybron Barnstead, Boston, MA, U.S.A.).

Synthetic procedures

Different functional groups were introduced into the benzene ring of PS–DVB resins by the following procedures:

(1) $-CH_2OH$ derivative. Add 1.2 g of paraformaldehyde, 16 ml of acetic acid and 4 ml of acetic anhydride to 5.2 g of PS–DVB resin. Stir for a few minutes, then add 6.0

g of anhydrous zinc chloride and keep at 60°C overnight. Filter the resin, rinse with methanol, then heat with a solution of methanol–conc. HCl (90:10) for 1 h. Wash the final product with methanol and dry. The concentration of $-CH_2OH$ on the resin was 1.3 mmol/g. This was determined by a standard acetylation procedure using acetic anhydride in pyridine as the reagent.

(2) $-COCH_2CH_2CO_2H$ derivative. Mix 2.5 g of resin with 3.6 g of succinic anhydride, 30 ml of tetrachloroethane and 15 ml or nitrobenzene. Stir for a few minutes, then add 10.7 g of anhydrous aluminum chloride and keep at 45°C for 24 h. Pour the product into ice water. Isolate the resin, wash with acetone, methanol and water, then dry. The amount of derivatization was found to be 1.1 mmol/g by acid-base titration of the carboxylic acid.

(3) $-COCH_3$ derivative. To 5.1 g of resin add 30 ml of carbon disulfide, 9.5 g of anhydrous aluminum chloride, add 5.5 g of acetyl chloride, added dropwise. Keep at 50°C for 24 h. Pour the product into ice water. Isolate the resin, wash with acetone, methanol and water, then dry. The presence of a carbonyl group was proved by a good band at 1690 cm^{-1} on the spectrum obtained by Fourier transform infrared spectrometry (FT-IR). The concentration of $-COCH_3$ on the resin was determined as 1.2 mmol/g by derivatization of –CO– group.

(4) $-C(CH_3)_3$ derivative. Mix 4.6 g of resin, 60 ml of nitromethane, 8.0 g of *tert.*-butylchloride and 8.0 g of $AlCl_3$. Keep at 60°C for 24 h. Pour into ice water, wash with acetone, methanol and water then dry. The capacity of the *tert.*-butyl group is difficult to determine because of lack of suitable methods, though the chromatographic behavior is greatly different from that of the underivatized resin.

(5) $-CH_2CN$ derivative. To 5.4 g of resin add 30 ml of tetrachloroethane and 20 ml of chloroacetonitrile. Keep at 85°C for 24 h. Pour the product into ice water, then wash and dry as above. The concentration of $-CH_2CN$ on the resin was 0.9 mmol/g, determined by nitrogen analysis.

RESULT AND DISCUSSION

XAD-4 resin derivatives

Ground up and sieved XAD-4 resin was chosen for the first experiments because it is highly cross-linked and has a very high surface area (784 m^2/g), which makes for easy preparation of various derivatives. XAD-4 resins were prepared containing each of the following functional groups attached to the benzene ring: $-C(CH_3)_3$, $-CH_2OH$, $-COCH_3$, $-COCH_2CH_2CO_2H$ and $-CH_2CN$.

The parent XAD-4 resin and its derivatives were packed into 250 × 2.1 mm columns and the retention times of various organic compounds were measured by the UV-VIS detector at wavelength 270 nm, using acetonitrile–water (50:50) as the eluent. Capacity factors (k') of the analytes on the various resins are given in Table I. The results show some interesting trends:

(1) The less-polar analytes all have lower capacity factors on the resins containing polar functional groups than on the parent XAD-4 resin (R is the ratio of k' values of derivatized:parent resin). The opposite is true for the polar analytes; these have larger k' values on the polar derivatized resins.

(2) On the *tert.*-butyl resin the less polar analytes have significantly larger k' values than on the parent XAD-4 resin. However, the polar analytes are less attracted to the *tert.*-butyl resin and have lower k' values.

TABLE I

CAPACITY FACTORS (k') OF TEST COMPOUNDS ON XAD-4 RESIN AND ITS DERIVATIVES

R is the ratio of k' on the derivatized resin to k' on the XAD-4 resin. Chromatographic conditions: 250 × 2.1 mm column; acetonitrile–water (50:50) eluent, adjusted to pH 1.7 with HCl.

Compounds	XAD-4, k'	Derivatives of XAD-4 resin									
		$-C(CH_3)_3$		$-CH_2OH$		$-COCH_3$		$-COCH_2-CH_2COOH$		$-CH_2CN$	
		k'	R	k'	R	k'	R	k'	R	k'	R
Cumene	19.3	23.2	1.20	18.4	0.80	14.2	0.74	17.7	0.92	15.6	0.81
o-Dichlorobenzene	18.7	22.0	1.18	17.0	0.91	16.9	0.91	18.7	1.00	17.1	0.91
Toluene	9.83	11.5	1.17	8.83	0.90	8.50	0.86	8.83	0.90	8.78	0.89
Anisol	6.53	7.33	1.12	5.81	0.89	6.22	0.95	5.83	0.89	5.67	0.87
Diethylphthalate	6.25	7.30	1.19	4.83	0.77	4.58	0.73	5.17	0.83	3.89	0.78
Methylbenzoate	5.25	5.83	1.11	4.84	0.92	4.61	0.88	4.15	0.90	4.78	0.91
2,4-Dinitrofluorobenzene	4.92	4.41	0.89	4.50	0.92	4.28	0.87	4.83	0.98	4.08	0.83
Acetophenone	3.17	3.25	1.03	3.17	1.00	3.00	0.95	3.00	0.95	3.00	0.95
p-Cresol	2.17	1.92	0.88	2.25	1.04	2.69	1.24	2.08	0.96	2.11	0.97
Phenol	1.50	1.42	0.94	1.67	1.11	1.94	1.30	1.67	1.11	1.61	1.07

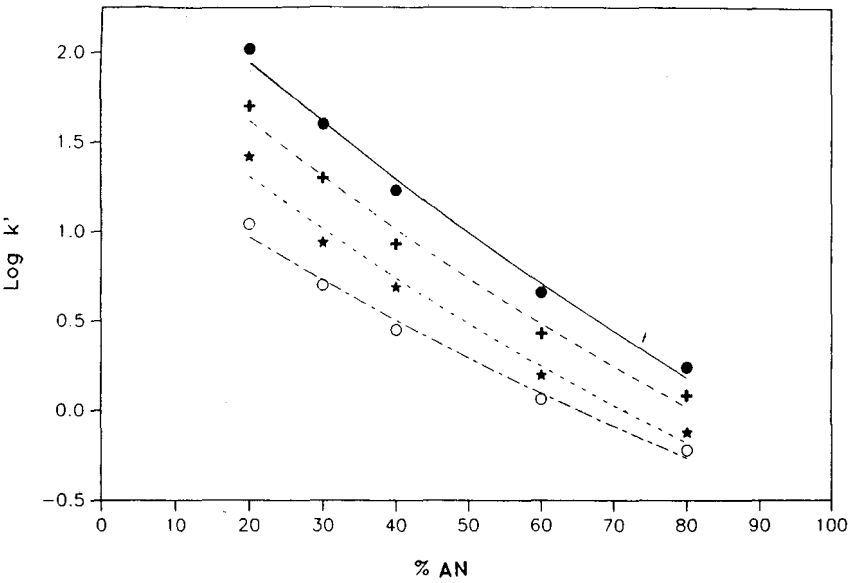

Fig. 1. Log k' on XAD-CH_2OH resin column as a function of the percentage of acetonitrile (AN) in the eluent. ● = Toluene; + = methylbenzoate; ★ = *p*-cresol; ○ = phenol.

Capacity factors for some of the analytes were measured as a function of the percentage acetonitrile in the eluent. Fig. 1 was typical of the results that were obtained. The plots are not quite linear and show better separation factors at lower concentrations of acetonitrile in the eluent.

Derivatives of small, spherical PS–DVB resins

The fairly large and somewhat irregular particle size of the XAD-4 resin limited their separation ability. For this reason a spherical polymeric resin of small, uniform particle size was sought. The material used was a spherical PS–DVB resin of 10 μm average diameter and a surface area of 415 m^2/g [18]. The coverage of the functional group was calculated to be 3.1 $\mu mole/m^2$ for the hydroxymethyl resin, which is similar to the coverage of typical silica resins reported by Antle *et al.* [16]. Portions of this resin were derivatized as before, packed into columns, and the k' values of several analytes measured using acetonitrile-water eluents.

Several test compounds were separated on each of the columns using a very fast chart speed so that column efficiency and peak shape could be observed. The theoretical plate numbers of the polymeric resin columns were rather low (*ca.* 10 000 plates/m), but this would be expected because the average resin diameter was around 10 μm. Peak asymmetry factors [19] for the four test compounds are given in Table II for the three polymeric resin columns and for a commercial 5-μm silica C_{18} column. The *tert.*-butyl column shows the most tailing. The parent polymeric resin column shows essentially no tailing for three of the four test compounds. The acetyl column also compares favorably with the silica column.

In Table III the k' values for 20 aromatic compounds are compared to the k'

TABLE II

PEAK ASYMMETRY FACTORS OF FOUR TEST COMPOUNDS ON DIFFERENT RESIN COLUMNS

Resin	Peak asymmetry factor			
	Toluene	Anisol	Acetophenone	4-Nitrophenol
PS-$C(CH_3)_3$	1.97	1.43	1.67	1.86
PS	0.96	0.95	0.96	1.33
PS-$COCH_3$	1.46	1.48	1.44	1.50
Silica C_{18}	1.38	1.50	1.53	1.77

value of benzene on each of the three polymeric columns. In this way the effect of a single aromatic substituent can be measured.

The k' values relative to benzene in Table III are listed in decreasing order. Compared to the underivatized resin the relative k' values on the *tert.*-butyl resin are higher for the more hydrophobic test compounds and lower for the polar compounds.

TABLE III

CAPACITY FACTORS (k') AND CAPACITY FACTORS RELATIVE TO k' (BENZENE) FOR BENZENE DERIVATIVES ON THREE POLYMERIC RESIN COLUMNS

R is the ratio of k' on the derivatized resin compared to the underivatized resin. The eluent was acetonitrile–water (50:50), acidified with HCl. k'_x is the capacity factor of a benzene derivative.

Compounds	PS–DVB		PS–DVB–$COCH_3$			PS–DVB–$C(CH_3)_3$		
	k'	$k'_x/k'_{benzene}$	k'	$k'_x/k'_{benzene}$	R	k'	$k'_x/k'_{benzene}$	R
Benzene	6.59		4.82			7.21		
Biphenyl	41.28	6.27	28.46	5.90	0.69	50.63	7.02	1.23
Cumene	22.98	3.49	11.25	2.33	0.49	28.71	3.98	1.25
o-Dichlorobenzene	19.18	2.91	12.38	2.57	0.65	24.29	3.37	1.27
Iodobenzene	17.89	2.71	13.83	2.87	0.77	23.19	3.22	1.30
Bromobenzene	15.53	2.36	12.93	2.68	0.83	19.78	2.74	1.27
Chlorobenzene	11.98	1.82	10.18	2.11	0.85	15.05	2.09	1.26
Toluene	10.83	1.64	6.61	1.37	0.61	12.84	1.78	1.19
Anisol	6.93	1.05	4.50	0.93	0.65	7.73	1.07	1.12
Diethylphthalate	6.33	0.96	2.97	0.62	0.47	6.72	0.94	1.06
Fluorobenzene	5.99	0.91	5.17	1.07	0.86	6.85	0.95	1.14
Methylbenzoate	5.48	0.79	3.57	0.74	0.65	6.12	0.85	1.12
Nitrobenzene	5.24	0.80	4.70	0.98	0.90	5.99	0.83	1.14
2,4-Dinitrofluorobenzene	4.56	0.69	4.08	0.85	0.89	4.29	0.60	0.94
Acetophenone	3.06	0.46	2.05	0.43	0.67	3.25	0.45	1.06
p-Cresol	1.70	0.26	1.96	0.41	1.15	1.65	0.23	0.97
3-Nitrophenol	1.59	0.24	2.07	0.43	1.30	1.50	0.21	0.94
4-Nitrophenol	1.43	0.22	1.97	0.41	1.38	1.27	0.18	0.89
Phenol	1.23	0.19	1.42	0.29	1.15	1.11	0.15	0.90
Benzoic acid	0.78	0.12	2.55	0.53	3.27	0.75	0.10	0.96
Benzyl alcohol	0.76	0.12	0.93	0.19	1.22	0.71	0.10	0.93

However, the *order* of the relative k' values is the same for the *tert.*-butyl and the underivatized resin, with the minor exception of diethylbenzene and fluorobenzene.

The relative k' values of non-polar test compounds are lower on the resin derivatized with a polar acetyl group than on the underivatized resin. Exactly the opposite is true for the polar test compounds. More significantly, there are numerous changes in the elution *order* of the various test compounds on the acetyl resin.

It is interesting to compare the relative k' values for the halogenated benzenes on the three resin columns (Table IV). The relative k' values of the four simple halobenzenes are higher on both the butyl and acetyl columns than on the underivatized resin column. However, the ratio of relative k' (butyl) to relative k' (unsubstituted) increases in the order F, Cl, Br, I. The ratio of relative k' (acetyl) to relative k' (unsubstituted) decreases in the same order.

TABLE IV

RELATIVE k' VALUES ($k'_x/k'_{benzene}$) FOR HALOGENATED BENZENES (C_6H_5X) ON THREE RESIN COLUMNS

X	Relative k'			k' (*tert.*-butyl)	k' ($COCH_3$)
	tert.-Butyl	Unsubstituted	$-COCH_3$	k' (unsubstituted)	k' (unsubstituted)
I	3.22	2.71	2.87	1.19	1.06
Br	2.74	2.36	2.68	1.16	1.14
Cl	2.09	1.82	2.11	1.15	1.16
F	0.95	0.91	1.07	1.04	1.18

Following the treatment of Sadek and Carr [15], log k' was plotted against the number of carbon atoms in the side chain of alkyl benzenes and of alkyl phenols. Excellent linear plots were obtained for both classes of compounds (Fig. 2 and Table V). The slopes show the effect of a single $-CH_2$ group on the increased retention of a test compound. The higher slopes on the butyl resin indicate a greater affinity for a $-CH_2$ group than on the underivatized phenyl resin. The lower slopes on the more polar acetyl resin indicates a lower affinity for a $-CH_2$ group. The slopes of each of the three resins were higher for the alkyl benzenes than for the alkyl phenols.

The intercepts for the alkyl benzenes (Table V) are in the order of decreasing polarity of the resins acetyl < underivatized < *tert.*-butyl. The intercepts of the more polar alkyl phenols are in exactly the opposite order: *tert.*-butyl < underivatized < acetyl.

The capacity factors of several test compounds were measured on a column packed with polymer resin derivatized with $-CH_2CN$ groups. In Table V, the results are compared with values obtained under identical conditions using underivatized resin. Polar test compounds are retained a little longer and non-polar compounds are less retained on the cyanomethyl column, although the differences are generally less than those between underivatized and acetyl resin columns.

It is interesting to compare the effects of introducing a cyanomethyl group into

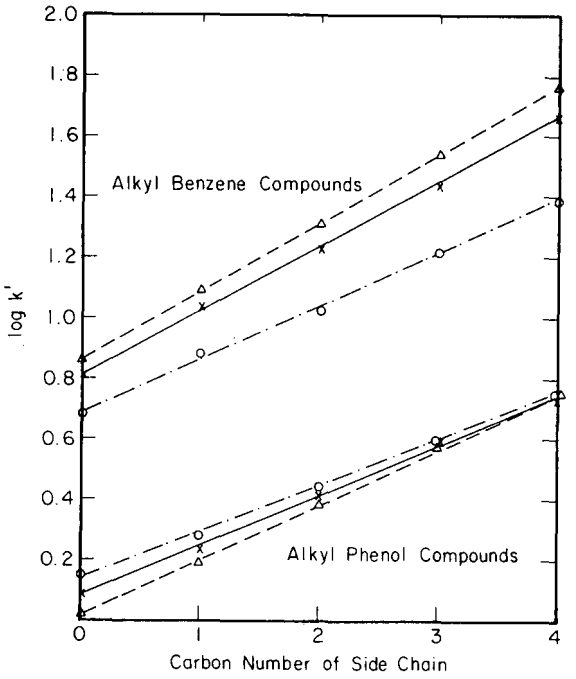

Fig. 2. Plot of log k' *vs.* carbon number of side chain of alkyl benzene and aklyl phenol compounds on diferent polystyrene resins. Chromatographic conditions as in Table I. △---△ = PS–DVB–$C(CH_3)_3$; ×—× = PS–DVB; ○–·–·–○ = PS-DVB–$COCH_3$.

TABLE V

LINEAR REGRESSION DATA FOR PLOTS OF LOG k' AGAINST THE NUMBER OF CARBON ATOMS IN THE R GROUP FOR C_6H_5R AND FOR HOC_6H_4R

Resin	Slope	y-intercept	Correlation coefficient
For C_6H_5R, where R = 0, 1, 2, 3, 4			
PS–$C(CH_3)_3$	0.23	0.86	0.9997
PS	0.21	0.81	0.9995
PS–$COCH_3$	0.18	0.69	0.9995
For HOC_6H_5R, where R = 0, 1, 2, 3, 4			
PS–$C(CH_3)_3$	0.185	0.016	0.9996
PS	0.165	0.081	0.9995
PS–$COCH_3$	0.15	0.140	0.9992

a polystyrene resin with changing from a C_{18}- to cyanoalkyl bonded-phase silica resin column. The results in Table VI show a much lower retention for cumene and *o*-dichlorobenzene on cyano silica than on C_{18} silica. Polar test compounds are more strongly retained on the cyano silica column, but the overall range of k' values is much less on the cyano silica than on the C_{18} silica. It is probably for this reason that cyano silica columns have generally been less used for reversed-phase LC than for normal-phase chromatography.

It is logical to expect a large change in capacity factors with cyanoalkyl silica column compared to an alkyl silica column because of the drastic difference in polarity of the bonded groups. The difference in polarity between a phenyl group and a cyanomethyl phenyl group in polystyrene resins is less drastic. Accordingly, smaller differences in capacity factors of test compounds would be expected.

Separations of mixtures by 10-μm spherical PS–DVB resins. Separations of several mixtures were compared on a parent 10 μm spherical resin and an acetyl-derivatized one. The column was 100 mm × 4.6 mm I.D. for practical applications. While columns packed with 10-μm resins are no longer state-of-the-art, the separations are still good enough to be of practical value and to show clearly the effects of derivatization.

Examination of the data in Table III shows several pairs of analytes for which the separation factor ($\alpha = k'_2/k'_1$) is larger on the acetyl resin. For several pairs of analytes the separation factors on the acetyl resin and the un-derivatized resin are as follows: anisol and diethylphthalate α = 1.52 and 1.09, 3-nitrophenol and phenol α = 1.47 and 1.29, 4-nitrophenol and phenol α = 1.40 and 1.16. Figs. 3 and 4 show that better separations are indeed obtained on the acetyl resin under the same experimental conditions.

Several actual separations were performed to confirm the differences in elution orders predicted by the data in Table II. For example methyl benzoate elutes before diethyl phthalate on a column of underivatized resin, but the elution order is reversed on the acetyl resin column.

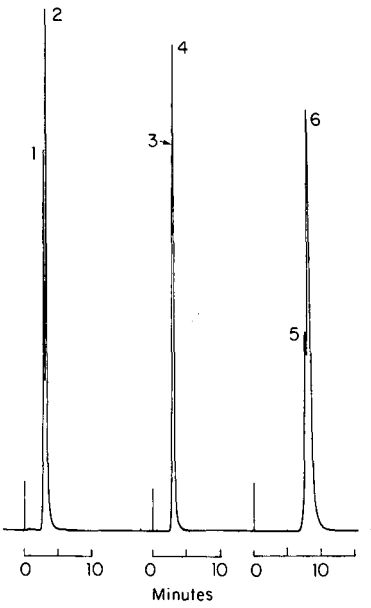

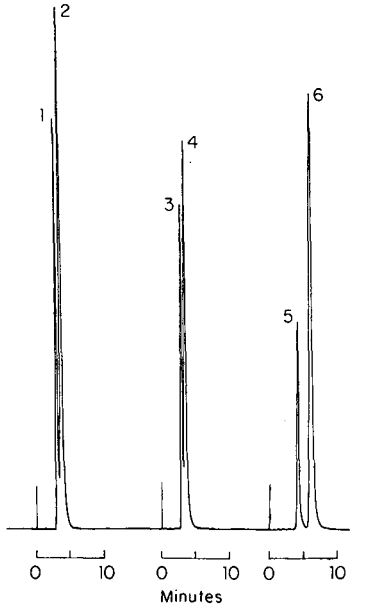

Fig. 3. Chromatographic separations on PS–DVB resin column (100 × 4.6 mm), using 60% aqueous acetonitrile (pH 1.7) eluent. Peaks: 1 = phenol; 2 = 3-nitrophenol; 3 = phenol; 4 = 4-nitrophenol; 5 = diethylphthalate; 6 = anisol.

Fig. 4. Chromatographic separations on an acetyl derivatized PS–DVB column. Conditions as in Fig. 3.

TABLE VI

COMPARISON OF CAPACITY FACTORS (k') ON CYANO SILICA TO C_{18} SILICA AND OF CYANOMETHYL POLYMERIC TO POLYMERIC RESIN

The eluent was acetonitrile–water (50:50), adjusted to an apparent pH of 1.7 with HCl.

Compound	Silica columns			Polystyrene columns		
	$k'(C_{18})$	k'(CN)	$\frac{k'(CN)}{k'(C_{18})}$	k'(PS)	k'(CN)	$\frac{k'(CN)}{k'(PS)}$
Cumene	3.51	1.33	0.38	23.0	20.6	0.90
o-Dichlorobenzene	2.40	1.17	0.49	19.2	16.4	0.85
Toluene	1.57	0.97	0.62	10.8	10.5	0.97
Anisol	0.92	0.80	0.87	6.93	6.32	0.91
Diethylphthalate	1.13	0.89	0.79	6.33	5.08	0.80
Methylbenzoate	0.82	0.75	0.91	5.48	4.79	0.87
2,4-Dinitrofluorobenzene	0.69	0.90	1.30	4.56	4.41	0.97
Acetophenone	0.53	0.64	1.21	3.06	3.08	1.01
p-Cresol	0.40	0.56	1.40	1.70	1.74	1.02
Phenol	0.29	0.49	1.69	1.23	1.35	1.10

CONCLUSION

Even with the limited number of test compounds studied, it is apparent that functional groups introduced into PS–DVB resins have an appreciable effect on the retention times and k' values obtained in reversed-phase liquid chromatography. The retention times of all compounds are distinctly different on the derivatized columns, and in several cases the relative capacity factors (R) of many of the test compounds are significantly different on the derivatized columns. Therefore, derivatized polymeric columns offer an additional selectivity parameter (*e.g.* interaction of analyte with the resin) over reversed-phase chromatography with C_{18}- or C_8-silica-bonded resin in which the selctivity effects are determined primarily by interaction between the analytes and the solvents in the mobile phase.

ACKNOWLEDGEMENTS

We thank John Naples of Rohm and Haas Co. and D. T. Gjerde of Sarasep, Inc. for the gifts of the resin beads used in this research.

Ames Laboratory is operated for the U.S. Department of Energy under Contract W-7405-Eng-82. This work was supported by the Director of Energy Research, Office of Basic Energy Sciences.

REFERENCES

1 A. M. Krstulovic and P. R. Brown, *Reversed-Phase High-Performance Liquid Chromatogrqphy*, Wiley-Interscience, New York, 1982.
2 L. A. Cole and J. G. Dorsey, *Anal. Chem.*, 62 (1990) 16.
3 D. P. Lee, *J. Chromatogr. Sci.*, 20 (1982) 203.

4 R. L. Smith and D. J. Pietrzyk, *J. Chromatogr. Sci.*, 21 (1983) 282.
5 J. V. Dawkins, L. L. Lloyd and F. P. Warner, *J. Chromatogr.*, 352 (1986) 157.
6 H. A. McLeod and G. Laver, *J. Chromatogr.*, 244 (1982) 385.
7 F. Nevejans and M. Verzele, *J. Chromatogr.*, 350 (1985) 145.
8 Y. B. Yang and M. Verzele, *J. Chromatogr.*, 387 (1987) 197.
9 Y. Tanaka, H. Sato, K. Miyazaki and Y. Yamada, *J. Chromatogr.*, 407 (1987) 197.
10 K. Yasukawa, Y. Tamura and T. Uchida, *J. Chromatogr.*, 410 (1987) 129.
11 J. V. Dawkins, N. P. Gabbott, L.L. Lloyd, J. A. McConville and F. P. Warner, *J. Chromatogr.*, 452 (1988) 145.
12 G. Schomburg, *LC·GC*, 6 (1988) 36.
13 K. Yanagihara, K. Yasukawa, U. Tamara, T. Uchida and K. Noguchi, *Chromatographia*, 24 (1987) 701.
14 J. R. Benson and A. Woo, *J. Chromatogr. Sci.*, 22 (1984) 386.
15 P. C. Sadek and P. W. Carr, *J. Chromatogr.*, 288 (1984) 25.
16 P. E. Antle, A. P. Goldberg and L. R. Snyder, *J. Chromatogr.*, 321 (1985) 1.
17 J. L. Glajch, J. C. Gluckman, J. G. Charikofsky, J. M. Minor and J. J. Kirkland, *J. Chromatogr.*, 318 (1985) 23.
18 D. T. Gjerde, personal communication, 1989.
19 L. R. Snyder, J. L. Glajch and J. J. Kirkland, *Practical HPLC Method Development*, Wiley, 1989, p. 69.

Journal of Chromatography, 522 (1990) 107–116
Elsevier Science Publishers B.V., Amsterdam

CHROM. 22 666

Reversed-phase liquid chromatography of polar benzene derivatives on poly(vinylbenzo-18-crown-6)-immobilized silica as a stationary phase

HIROYA HARINO*
Osaka City Institute of Public Health and Environmental Science, 8–34 Tojo-cho, Tennoji-ku, Osaka 543 (Japan)
and
KEIICHI KIMURA, MINORU TANAKA and TOSHIYUKI SHONO
Department of Applied Chemistry, Faculty of Engineering, Osaka University, Yamada-oka, Suita, Osaka 565 (Japan)
(First received July 4th, 1989; revised manuscript received June 26th, 1990)

ABSTRACT

A packing in which poly(vinylbenzo-18-crown-6) is immobilized covalently to silica was tested for its usefulness as a stationary phase in the reversed-phase liquid chromatography of polar disubstituted benzene derivatives. Both electrostatic and hydrophobic interactions contribute considerably to the chromatographic separation. When potassium cations, which are complexed by the crown ether moiety on the stationary phase, are added to the mobile phase during chromatography using the poly(crown ether)-immobilized silica, positive charges are generated on the surface of the stationary phase and some electrostatic interaction occurs between polar disubstituted benzene derivatives and the stationary phase. Hence the retention behaviour of polar organic compound can be controlled easily by adding metal cations to the mobile phase. This type of reversed-phase chromatography using poly(crown ether)-immobilized silica is useful for separating positional isomers of various disubstituted benzene derivatives.

INTRODUCTION

Various crown ether-immobilized silicas have been synthesized [1–5], and were designed as stationary phases for the high-performance liquid chromatographic (HPLC) separation of cations, particularly alkali and alkaline earth metal cations. Poly(crown ether)-immobilized silicas can be synthesized easily by copolymerization between vinyl-modified silica and crown ether vinyl monomers [6]. The ion chromatographic behaviour of poly(crown ether)-immobilized silica reflects the cation-complexing abilities of the corresponding poly(crown ether)s. The poly(crown ether)-immobilized silicas turned out to be promising stationary phases for ion chromatography [7–9]. Poly(crown ether)-immobilized silicas generally contain both hydrophobic and hydrophilic moieties. There is, therefore, a possibility of applying poly(crown ether)-immobilized silica to stationary phases in reversed-phase liquid

0021-9673/90/$03.50

chromatography [10]. In conventional reversed-phase liquid chromatography using octadecylsilanized silica as the stationary phase, the interaction between the solute and the stationary phase is based mainly on hydrophobic interactions. On the other hand, in reversed-phase liquid chromatography on poly(crown ether)-immobilized silica, both electrostatic and hydrophobic interactions are expected to play an important role in the separation. In this paper, we report on the chromatographic retention behaviour of poly(benzo-18-crown-6)-immobilized silica in the reversed-phase liquid chromatography of disubstituted benzene derivatives, which are difficult to separate by conventional reversed-phase liquid chromatography. The effect of the addition of metal salts and the effect of the pH of the mobile phase in this reversed-phase liquid chromatography is also described. The chromatographic behaviour was compared with that for poly(benzoglyme-6)- and polystyrene-immobilized silica.

EXPERIMENTAL

Synthesis of poly(vinylbenzo-18-crown-6)-immobilized silica

Silica gel for HPLC (10 μm, spherical, Wako LC-10) was activated in concentrated hydrochloric acid. To this activated silica, a toluene solution of 3-(methacryloyloxy)propyltrimethoxysilane was added and the mixture was refluxed. The resulted vinyl-modified silica was washed successively with toluene, chloroform and methanol and then dried overnight under vacuum at 80°C. A glass tube containing a mixture of vinyl-modified silica and vinylbenzo-18-crown-6 [11–13] and α,α′-azobisisobutyronitrile dissolved in toluene was degassed by the freeze–thaw method and sealed. The polymerization was carried out by shaking the sealed tube in an incubator at 80°C for 21 h. After the polymerization, the modified silica was washed successively with toluene, chloroform and methanol and then dried overnight under vacuum at 80°C. The crown ether content of the poly(vinylbenzo-18-crown-6)-immobilized silica, which was calculated from the weight increase and carbon elemental analysis, was 0.57 mmol/g.

Synthesis of poly(vinylbenzoglyme-6)- and polystyrene-immobilized silica

Vinylbenzoglyme-6 or styrene, instead of vinylbenzo-18-crown-6, was employed for copolymerization with the vinyl-modified silica. The polymerization was carried out in a similar manner to that for the vinylbenzo-18-crown-6 system. The glyme content of poly(vinylbenzoglyme-6)-immobilized silica was 0.37 mmol/g and the styrene content of polystyrene-immobilized silica was 1.19 mmol/g.

Chromatography

The HPLC system consisted of a pumping system (Waters Assoc. Model 6000A), a sample injector (Waters Assoc. Model U6K) and a UV detector (Oyo-Bunko Uvilog-7). The stainless-steel columns (150 mm × 4 mm I.D.) were packed with the modified silicas 1, 2 and 3 in Scheme 1 using the balanced-density slurry technique. The mobile phases were generally methanol–water mixtures and the aqueous components were adjusted to pH 5 [acetic acid–lithium acetate (0.2 *M*)] or pH 8 [0.1 *M* tris(hydroxymethyl)aminomethane–HCl]. Chromatography was performed at a flow-rate of 1.0 ml min^{-1}. The organic compounds used as the solutes were phenol, benzene and the *ortho*, *meta* and *para* isomers of nitrophenol, aminobenzoic acid, nitrobenzoic

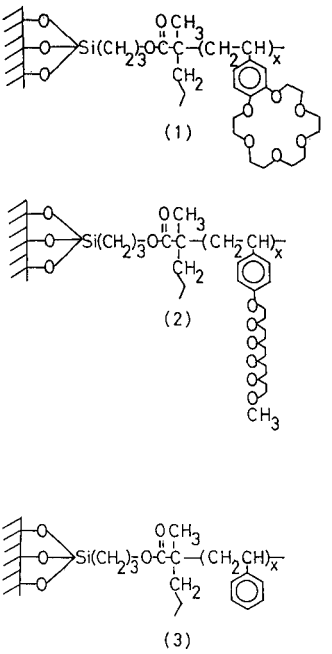

Scheme 1.

acid, iodoaniline, toluidine and nitroaniline. The sample concentration and volume injected were 0.2 mM and 5 μl, respectively, in each instance.

RESULTS AND DISCUSSION

Interaction between poly(vinylbenzo-18-crown-6)-immobilized silica and solutes

Liquid chromatography of the *ortho*, *meta* and *para* isomers of disubstituted benzene derivatives was carried out by using poly(vinylbenzo-18-crown-6)-immobilized silica as the stationary phase and methanol–water mixtures as the mobile phase. The dependence of the retention of the nitrophenol isomers on the mobile phase composition is shown in Fig. 1. The retention of nitrophenol was generally diminished by increasing the methanol fraction of the mobile phase at pH 5 or pH 8. This phenomenon was also observed in the chromatography of other disubstituted benzene derivatives such as iodoaniline and toluidine. It is suggested from this result that the chromatographic retention of the solutes on the stationary phase is derived basically from hydrophobic interactions. There might be some other interaction such as hydrogen bonding between the ring oxygen of the crown ether moiety on the stationary phase and the polar group of the solutes. However, the contribution of the hydrogen bonding to the retention is possibly small under the mobile phase conditions involving highly polar solvents such as methanol–water mixtures.

On the column of poly(vinylbenzo-18-crown-6)-immobilized silica, the three isomers of nitrophenol were eluted in the order *ortho* < *meta* < *para* at pH 5. The same

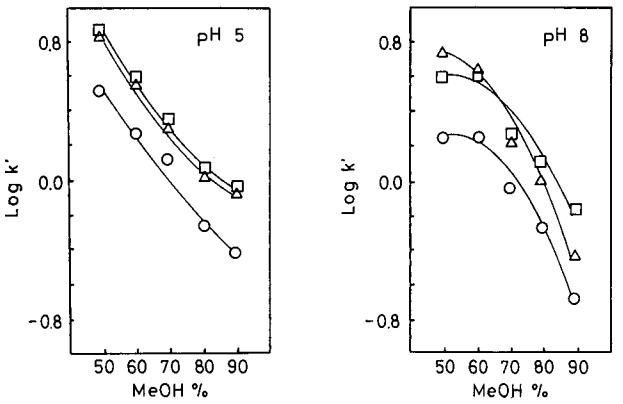

Fig. 1. Dependence of retention of nitrophenol isomers (○ = *ortho*; △ = *meta*; □ = *para*) on the methanol (MeOH) content in the mobile phases on poly(vinylbenzo-18-crown-6)-immobilized silica. For experimental conditions, see text.

elution order holds for polystyrene-immobilized silica, which does not contain any crown ether moiety. A reversal of the retention order of the *para* and *meta* isomers was observed at an eluent pH of 8 with methanol concentrations less than 60%. Moreover, the shapes of the retention curves at pH 5 and 8 are different, especially for the *ortho* and *para* isomers.

We speculate the cause as follows. From a rough calculation, the proportion of the anionic form of *m*-nitrophenol is 28% in water at pH 8, compared with 86 and 92% for *o*- and *p*-nitrophenol, respectively. It is reasonable that the hydrophobic interaction with the stationary phase is weaker for the anionic than for the neutral forms. Also, the electrostatic repulsive interaction with the crown units is stronger for the anionic forms. The dissociation of the solutes is considered to reduce as the methanol concentration increases. Consequently, the *ortho* and *para* isomers are less retained than the *meta* isomer at pH 8, especially in the lower methanol concentration range, because of their greater dissociation. At pH 5, on the other hand, the three isomers are hardly dissociated ($< 1\%$). This supposedly gives rise to the above-mentioned reversal of the elution order and difference in the shapes of the retention curves. It is therefore suggested that the hydrogen bonding between the crown ether moiety and the hydroxy group of nitrophenol is not very important.

Effect of addition of metal salts to the mobile phase

We previously carried out ion chromatography of alkali metal cations by using poly(vinylbenzo-18-crown-6)-immobilized silica as the stationary phase [8]. It became apparent that K^+ is retained strongly on the crown ether stationary phase, because the benzo-18-crown-6 moiety on the stationary phase forms a stable complex with K^+. We attempted to improve the separation of the *ortho*, *meta* and *para* isomers of disubstituted benzene derivatives by reversed-phase liquid chromatography by taking advantage of the cation-complexing ability of the stationary phase. The effect of the addition of crown ether-complexing cations to the mobile phase was therefore

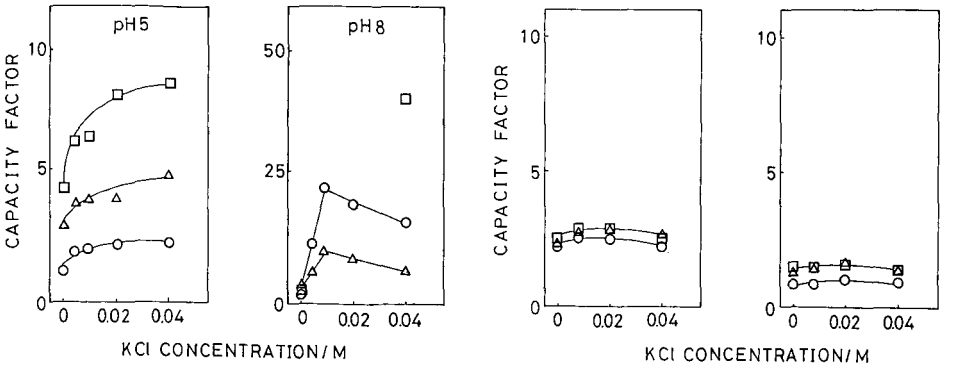

Fig. 2. Dependence of retention of nitrophenol isomers (○ = *ortho*; △ = *meta*; □ = *para*) on KCl concentration in methanol–water (60:40, v/v) on poly(vinylbenzo-18-crown-6)-immobilized silica.

Fig. 3. Dependence of retention of nitrophenol isomers (○ = *ortho*; △ = *meta*; □ = *para*) on KCl concentration in methanol–water (pH 5) (60:40, v/v) on poly(vinylbenzoglyme-6)-immobilized silica (right) and polystyrene-immobilized silica (left).

examined in the chromatography of anionic solutes such as nitrophenol and aminobenzoic acid isomers on the poly(crown ether)-immobilized silica.

The dependence of the retention times of nitrophenol in the potassium chloride concentration in the methanol–water (60:40) mobile phase is depicted in Fig. 2. On adding a small amount of potassium chloride to the aqueous component of the mobile phase at pH 5 or 8, the retention of nitrophenol isomers was increased substantially, especially at pH 8. However, when polystyrene- or poly(vinylbenzoglyme-6)-immobilized silica was used instead of the poly(crown ether)-immobilized silica, such a marked change in the retention behaviour was not observed (Fig. 3).

The retention enhancement may be explained as illustrated in Scheme 2. K^+ in the mobile phase is complexed strongly by the benzo-18-crown-6 moiety on the stationary phase in poly(vinylbenzo-18-crown-6)-immobilized silica, which is thus positively charged. Therefore, an electrostatic attractive force between the positive charge and the polar group (OH) of nitrophenol is generated, which in turn enhances the retention of each isomer. In spite of the addition of potassium chloride to the mobile phase, the retention behaviour was not changed with either poly(vinylbenzo-

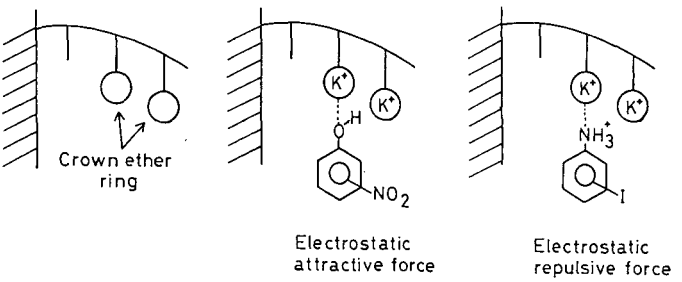

Scheme 2.

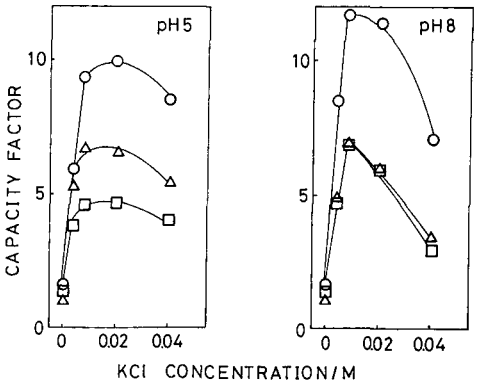

Fig. 4. Dependence of retention of aminobenzoic acid isomers on KCl concentration. Details as in Fig. 2.

glyme-6)- or polystyrene-immobilized silica. As neither the benzoglyme-6 nor the styrene moiety on the stationary phase can form stable complexes with K^+, the stationary phases do not acquire positive charges on addition of potassium chloride to the mobile phase. Therefore, electrostatic interactions do not seem to occur between the solutes and the poly(vinylbenzoglyme-6)- and polystyrene-immobilized silica stationary phases. As described above, most of the *ortho* and *para* isomers are dissociated at pH 8. It is reasonable that the anionic forms are retained much more strongly than the neutral forms by the positively charged stationary phase. The *ortho* isomer is, therefore, retained more strongly than the less dissociated *meta* isomer.

Similar phenomena were observed for aminobenzoic and nitrobenzoic acid isomers. Fig. 4 shows the considerable retention enhancement for the former acid on addition of potassium chloride. In contrast with nitrophenol, the increased retentions at pH 5 and 8 are similar in this instance. This is ascribed to the much smaller pK_a values of the aminobenzoic acid isomers than those of the nitrophenol isomers, *i.e.*, each acid isomer is dissociated more than 50% even at pH 5 and almost quantitatively at pH 8. This may result in comparable interactions with the stationary phase at both pH values.

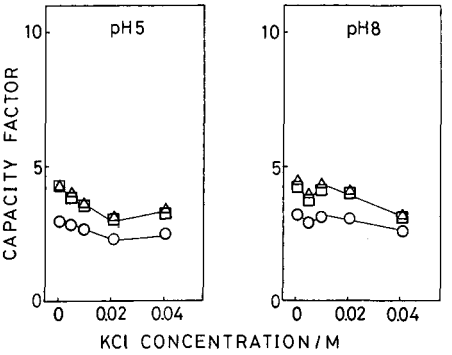

Fig. 5. Dependence of retention of iodoanilines on the KCl concentration. Details as in Fig. 2.

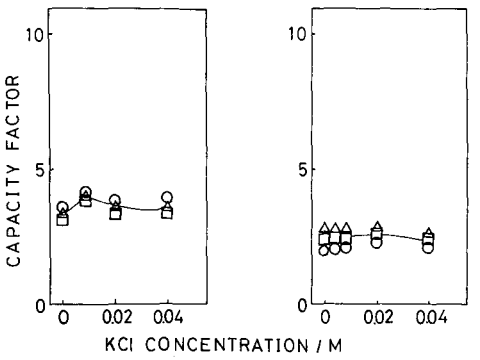

Fig. 6. Dependence of retention of iodoaniline isomers on KCl concentration on poly(vinylbenzoglyme-6)-immobilized silica (right) and polystyrene-immobilized silica (left). Details as in Fig. 3.

Figs. 5 and 6 show the retention dependence of iodoaniline on the potassium chloride concentration in the mobile phase. When poly(vinylbenzo-18-crown-6)-immobilized silica was used as the stationary phase, the retention of iodoaniline was decreased on adding 0.04 *M* potassium chloride to the mobile phases, although the change in the retention was not as drastic as that for the anionic solutes. However, as shown in Fig. 6, on poly(vinylbenzoglyme-6)- or polystyrene-immobilized silica the addition of potassium chloride to the mobile phase hardly afforded any change in the retention times, as was the case with the anionic solutes. With the mobile phase at pH 5, the polar group (amino) of iodonaniline is easily protonated, thus being positively charged. The electrostatic repulsive force between the positive charges of the cationic solutes and the crown-complexed cation on the stationary phase decreases their retention (Fig. 5).

On the poly(vinylbenzo-18-crown-6)-immobilized silica, the change in the retention for the cationic solutes was not greater than that for the anionic solutes. The reason may be explained as follows. The 18-crown-6 moiety may form complexes with the anilinium ion of the cationic solutes in addition to K^+. The complex formation between the 18-crown-6 moiety and the anilinium ions would enhance the chromatographic retention of the cationic solutes. Probably, K^+ competes with the anilinium

TABLE I

DEGREE OF RETENTION ENHANCEMENT ON ADDITION OF POTASSIUM CHLORIDE TO THE MOBILE PHASE ON POLY(VINYLBENZO-18-CROWN-6)-IMMOBILIZED SILICA

Mobile phase: methanol–water (60:40, v/v) containing 2 m*M* KCl.

pH	Aminobenzoic acid			Nitrophenol			Nitroaniline		
	o-	*m*-	*p*-	*o*-	*m*-	*p*-	*o*-	*m*-	*p*-
5	4.23	4.96	2.41	1.24	1.21	1.67	0.90	0.85	0.85
8	6.10	4.49	4.11	4.50	1.52	—[a]	0.97	0.92	0.97

[a] Not eluted within 60 min.

ions on complex formation with the 18-crown-6 moiety on the stationary phase. Thus, the electrostatic repulsion is alleviated by the binding of the anilinium ion to the crown ether moiety of the stationary phase. In contrast, on poly(vinylbenzoglyme-6)- or polystyrene-immobilized silica, the addition of potassium chloride to the mobile phase hardly affects the retention behaviour of the cationic solutes. This is again explained by the fact that the benzoglyme-6 and styrene moieties do not form stable complexes with K^+ (Scheme 2).

Table I summarizes the degree of retention enhancement by adding potassium chloride (2 m*M*) to the methanol–water (60:40) mobile phase, that is, t'_{R_1}/t'_{R_2}, where t'_{R_1} and t'_{R_2} are the adjusted retention times with and without the salt added to the mobile phase, respectively, on poly(vinylbenzo-18-crown-6)-immobilized silica.

The dependence of the retention times of phenol and benzene, which are difficult to or are not able to proton-dissociate at pH 5, on the potassium chloride concentration in the mobile phase was examined. Even in the chromatography on poly(vinylbenzo-18-crown-6)-immobilized silica, the addition of potassium chloride to the mobile phase did not give any change in the retention as expected. As phenol and benzene are hardly charged, there is very little electrostatic interaction between the solutes and the stationary phase.

When potassium chloride was added to the mobile phase, the retention of aminobenzoic acid increased as described above. However, when lithium chloride was added to the mobile phase, the retention of aminobenzoic acid hardly changed. This is probably due to the fact that the 18-crown-6 moiety cannot form a stable complex with Li^+. Hence the addition of lithium chloride instead of potassium chloride to the mobile phase hardly affects the chromatographic retention of the polar organic compounds on poly(vinylbenzo-18-crown-6)-immobilized silica.

Separation of isomers of polar organic compounds by reversed-phase liquid chromatography on poly(vinylbenzo-18-crown-6)-immobilized silica

The isomers of aminobenzoic acid and nitrophenol were separated successfully by reversed-phase liquid chromatography on poly(vinylbenzo-18-crown-6)-immo-

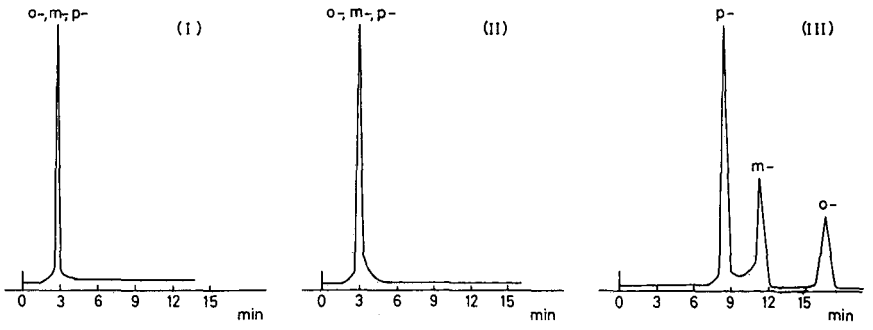

Fig. 7. Comparison of separation of aminobenzoic acid isomers (I) on ODS in methanol–water (pH 5) containing 20 m*M* KCl (60:40, v/v), (II) on poly(vinylbenzo-18-crown-6)-immobilized silica in methanol–water (pH 5) (60:40, v/v) and (III) on poly(vinylbenzo-18-crown-6)-immobilized silica in methanol–water (pH 5) containing 20 m*M* KCl (60:40, v/v).

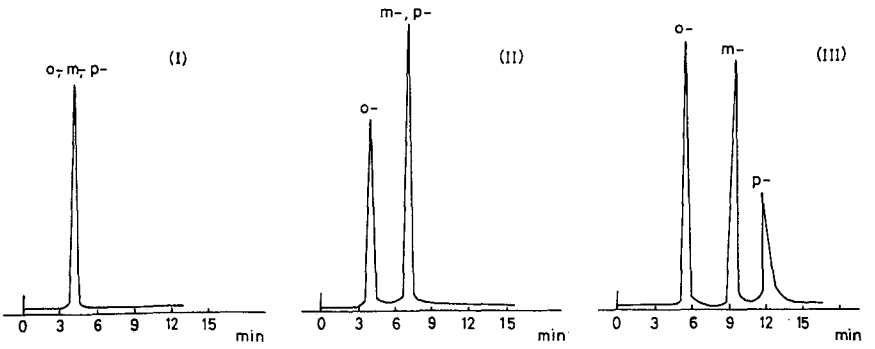

Fig. 8. Comparison of separation of nitrophenol isomers. Details as in Fig. 7.

bilized silica. In conventional reversed-phase liquid chromatography on octadecylsilanized (ODS) silica using methanol–water (pH 5) (60:40) as the mobile phase, the *o*-, *m*- and *p*-aminobenzoic acid isomers were not separated at all. Even on poly(vinylbenzo-18-crown-6)-immobilized silica, the aminobenzoic acid isomers were not separated without the addition of potassium chloride to the mobile phase. However, the addition of 20 m*M* potassium chloride to the mobile phase improved the chromatographic separation of the aminobenzoic acid isomers drastically, affording a baseline separation, as illustrated in Fig. 7.

In the case of the nitrophenol isomers, chromatography on ODS with methanol–water (pH 5) (60:40) could not separate *o*-, *m*- and *p*-nitrophenol at all (Fig. 8). When poly(vinylbenzo-18-crown-6)-immobilized silica was used as the stationary phase, *o*-nitrophenol could be separated from *p*- and *m*-nitrophenol, but the latter two were still difficult to separate. On addition of 20 m*M* potassium chloride to the mobile phase, however, *p*-nitrophenol was retained strongly on poly(vinylbenzo-18-crown-6)-immobilized silica. Consequently, the *ortho*, *meta* and *para* isomers were separated successfully, being eluted in the order *ortho* < *meta* < *para*. It is interesting and of great value to compare the poly(crown ether) phase with the well known β-cyclodextrin for the separation of isomers. On the cyclodextrin phase, the isomers of both nitrophenol and aminobenzoic acid are eluted in the order *meta* < *ortho* < *para*. The retention of nitrophenol increases with increasing pH, whereas that of aminobenzoic acid decreases [14]. Therefore, it is apparent that the retention mechanisms of the two stationary phases are different.

Accordingly, poly(crown ether)-immobilized silica is promising as a stationary phase for the reversed-phase liquid chromatography of polar organic compounds, and the chromatographic behaviour can be modified by adjusting not only the composition of the organic–aqueous mobile phase but also the pH and the concentration of K^+, which forms a stable complex with the crown ether moiety in the stationary phase. This type of chromatography is different from conventional reversed-phase liquid chromatography in that the crown-complexing cation affects the chromatographic separation considerably. The poly(crown ether)-immobilized silica seems to be useful for the separation of other polar organic compounds and might be also applied as a stationary phase for protein separations without denaturation by applying salt concentration gradient elution.

REFERENCES

1 E. Blasius, K.-P. Janzen, M. Keller, H. Lander, T. Nguyen-Tien and G. Scholten, *Talanta*, 27 (1980) 107.
2 E. Blasius, K.-P. Janzen, W. Adrian, H. Klotz, H. Luxenburger, E. Mernke, V. B. Nguyen, T. Nguyen-Tien, R. Rausch, J. Stockemer and A. Toussaint, *Talanta*, 27 (1980) 127.
3 E. Blasius, K.-P. Janzen, W. Klein, V. B. Nguyen, T. Nguyen-Tien, R. Pfeiffer, G. Scholten, H. Simon, H. Stockemer and A. Toussaint, *J. Chromatogr.*, 20 (1980) 147.
4 P. Gramain and Y. Frere, *Ind. Eng. Chem., Prod. Res. Dev.*, 20 (1980) 524.
5 M. Igawa, I. Ito and M. Tanaka, *Bunseki Kagaku*, 29 (1980) 580.
6 K. Kimura, M. Nakajima and T. Shono, *Anal. Lett.*, 13 (1980) 741.
7 M. Nakajima, K. Kimura and T. Shono, *Anal. Chem.*, 55 (1983) 463.
8 M. Nakajima, K. Kimura and T. Shono, *Bull. Chem. Soc. Jpn.*, 56 (1983) 3052.
9 M. Nakajima, K. Kimura, E. Hayata and T. Shono, *J. Liq. Chromatogr.*, 7 (1984) 2115.
10 K. Kimura, H. Harino, M. Nakajima and T. Shono, *Chem. Lett.*, (1985) 747.
11 S. Kopolow, T. H. Hogen Esch and J. Smid, *Macromolecules*, 6 (1973) 133.
12 R. Sinta and J. Smid, *Macromolecules*, 13 (1980) 339.
13 D. N. Reinhoudt, F. de Jong and H. P. M. Tomasson, *Tetrahedron Lett.*, 22 (1979) 2067.
14 Y. Kawaguchi, M. Tanaka, M. Nakae, K. Funazo and T. Shono, *Anal. Chem.*, 55 (1983) 1852.

Journal of Chromatography, 522 (1990) 117–129
Elsevier Science Publishers B.V., Amsterdam

CHROM. 22 736

Quantitative comparisons of reaction products using liquid chromatography with dual-label radioactivity measurements

LAWRENCE C. THOMAS* and CHRISTI L. WOOD
Department of Chemistry, Seattle University, Seattle, WA 98122 (U.S.A.)
(Received June 12th, 1990)

ABSTRACT

Dual-label methods for radiometric measurements with liquid chromatography are evaluated. The procedures show marked improvements in data quality for comparisons of product formations and relative product abundances in multiple-pathway reaction systems. The results from these procedures are shown to be relatively unaffected by large variations in uncertainties in pretreatment steps and volume measurements. Moreover, these methods yield much better quantitative results than do commonly used corresponding conventional comparisons.

These quantitative comparisons use reference substances generated by a reference reaction system as internal standards. A suite of reaction products is compared via the internal standards for components common to both reference and sample reaction systems. The dual-label methods are especially suitable for toxicologic metabolism comparisons, but could easily be adapted to other reaction systems such as syntheses or degradations. Moreover, the dual-label procedures should be amenable to non-radioactive measurements with isotope-selective methods such as mass fragmentometry, emission spectrometry or resonance methods.

INTRODUCTION

Radioactivity measurements for chromatography are especially helpful in experiments involving multiple reaction pathways, partly because radiochemical detection can provide good selectivity and high sensitivity. Resulting low limits of detection and freedom from many interferences can make radiometric procedures powerful quantitative methods. Recent work with chromatographic applications of radiometric detection has been reviewed [1] including commercial instruments available for flow-through measurements of radioactive eluates.

Several factors plague radiometric procedures for reaction product evaluations and can cause large uncertainties in resulting data and comparisons [2–4]. Variations in extraction efficiencies and variable losses during volume reductions can be partially compensated by traditional internal-standard techniques using differently labeled compounds which are otherwise identical to the target eluates. However, those procedures require both availability and careful characterization of appropriate reference materials for *every* measured component. Unfortunately, for complex systems such as metabolism studies, several reaction product analytes may be measured for each sample, which exacerbates difficulties associated with use of internal-standard meth-

0021-9673/90/$03.50

ods; moreover, identities of the products are not always known, which precludes use of conventional internal- or external-standard methods.

In previous work [2–4], compounds labeled with two different radioactive isotopes were used with high-performance liquid chromatography (HPLC) for special dual-label procedures which mimic internal-standard methods. In those studies biologically generated radiolabeled reference solutions were used and their components separated along with differently labeled respective coeluting metabolites from samples from biological experiments.

Two methods were described, each exploiting radioactivity detection of two labeled forms of each individual reaction product. One method employs a homogeneous reference solution of radiolabeled metabolites as a mixed internal-standard reference solution [2,4]. A known amount of the reference solution is added to each differently labeled experimental sample before sample preparation, but after biological reactions have taken place. This procedure may be used to quantitatively compare metabolism profiles and to test for differences between control *vs.* test groups in metabolic efficacy.

The second method uses a combined solution of differently labeled forms of the same compound with concurrent exposure of the two forms into a biological system via addition of an aliquant of the mixed dosage solution [2,3]. They are thereby concurrently metabolized under identical conditions. The respective metabolites then serve as mutual internal standards for quantitative comparisons to evalute: (a) effects of impurities on metabolism experiments, (b) effects of isotope exchange upon experiments and (c) effects of kinetic differences between the forms which may be caused by their different respective masses.

Those dual-label methods allow for compensation for variations in extraction efficiencies, variable losses during concentration of extracts, imprecisions of volume measurements and uncertainties in specific activities of dosage compounds and metabolism products. Moreover, the procedures greatly obviate difficulties caused by unavailability of pure reference compounds.

Improvements from the dual-label methods upon quantitative biological experiments have been estimated for a few selected circumstances [2], but no detailed evaluations of data-quality enhancements offered by the dual-label techniques had been done. In this study, detailed evaluations of improvements provided by use of the dual-label procedures are reported.

THEORY

A main advantage of the dual-label procedures discussed above is that several special ratios yield well-defined, theoretically predictable results which may be tested statistically [2,3]. Two of those special ratios are evaluated in this work.

Dual-label reaction-product determinations

In the absence of pure standards, a fixed known volume, V_a, of a homogeneous internal-standard solution generated by a reference reaction system which contains several radioactive reference compounds can be used in place of a conventional standard solution made by mixing known quantities of pure radiolabeled substances [2,3]. One may add these X-labeled reference compounds to subsamples of mixtures of

Y-labeled compounds of unknown concentrations which have been generated from reactions being investigated. By judicious selection, some of the *X*-labeled components will be chemically identical to the *Y*-labeled components, except for their respective radioactivities. Hence, pretreatments of the mixtures can yield equivalent extraction/concentration/dilution efficiences, E_i, for the two extractable forms of each common component. Thus, if V_t is the volume of the prepared subsample, and V_{ss} is the volume of the prepared subsample used for chromatographic separation, then $E_{Y,i} = A_{X,i}V_tA_{s,X,i}^{-1}V_{ss}^{-1} = E_{X,i}$, where $A_{X,i}$ and $A_{s,X,i}$ are corrected measured radioactivities for the *X*-labeled component *i* in the volumes V_{ss} and V_a, respectively. This equivalence is a reasonable assumption when isotope exchange is negligible, and the two forms are chemically alike and are not entrapped or bound in tissue or precipitates [2,3].

This method is similar to use of several radiolabeled internal standards using conventional radiochemical calculations and counting procedures. Consequently, the mass of each *Y*-labeled component from the sample can be determined by using that component's subsample activity data from the dual-label chromatogram, $A_{X,i}$ and $A_{Y,i}$, the total *X*-label activity in volume V_a for the reference solution, $A_{s,X,i}$, and the analyte specific activity, S_Y; $M_{Y,i} = A_{Y,i}A_{s,X,i}\,S_Y^{-1}$. This approach can be useful but is subject to several uncertainties which are avoided by use of the *R*- and *U*-ratio methods discussed below.

Single-component comparisons using the R ratio

In many experiments the absolute masses of analytes are often less important than their relative concentrations between experiments, *e.g.* in comparisons of metabolism in control *vs.* test organisms [5,6]. Such comparisons are suitable for use of multiple internal standards generated by a reference reaction system and the dual-label procedures described herein.

One may expose two sets of reactions, 1 *vs.* 2, to the same homogeneous dosage of *Y*-labeled compound, add volume V_a of *X*-labeled reference solution to each resulting sample, and then pretreat and separate each by liquid chromatography. Of course, $S_{Y,1} = S_{Y,2}$, as the dosage specific activities must be identical, and if $V_{a,1} = V_{a,2}$, then $A_{s,X,1} = A_{s,X,2}$. Moreover, if $V_{t,1} = V_{t,2}$ and $V_{ss,1} = V_{ss,2}$ by design,

$$R_{12} = (M_1/M_2) = (A_{Y,1}A_{X,2})\,(A_{Y,2}A_{X,1})^{-1} \tag{1}$$

for the component of interest, and this *R* ratio is calculated from counting data only.

If reaction efficacy is hypothesized to be not different between two groups, *e.g.*, control *vs.* test groups, then $R_{12} = 1$ if this null hypothesis is valid and R_{12} can be tested statistically to ascertain if it is different than unity for the specified component of interest, *e.g.*, if the compound reacts differently in the two systems.

Multiple-component comparisons using the U ratio

If the procedure used for the *R* ratio above is extended to several reaction products, then the resulting multiparametric method can be used to characterize several reaction pathways. Thus, relative magnitudes of several intrasample parameters may be tested and yield results which are more important than their absolute magnitudes or individual single-component comparisons between groups. For this,

an extension of the dual-label coelution method can be formulated for groups 1 *vs.* 2 and components *i vs. j* such that

$$U_{12} = (R_{12,i}/R_{12,j}) = A_{Y,i,1}A_{X,j,1}A_{Y,j,2}A_{X,i,2}A^{-1}_{Y,j,1}A^{-1}_{X,i,1}A^{-1}_{Y,i,2}A^{-1}_{X,j,2} \quad (2)$$

where X and Y represent the measured radioactive forms, subscripts i and j indicate the two components of interest, the subscripts 1 and 2 indicate samples from which the components were isolated and A indicates corrected measured radioactivities. If that reaction product profile for both groups is the same, then $U_{12} = 1$. This U ratio may be tested statistically, and the null hypothesis of identical relative reaction rates for those components may be assumed unless U_{12} is shown to be significantly different than unity.

Of course, by comparing several components, *i, j, k, l...*, one may evaluate reaction product profiles representing several modes *e.g.*, several metabolism pathways.

EXPERIMENTAL

Reagents

All organic solvents used were Mallinckrodt ChomAR. Radiolabeled compounds were purchased from Amersham. Water used was distilled in all-glass apparatus and other chemicals were reagent-grade quality.

Apparatus

HPLC. An Altex HPLC system with two Model 110 pumps, a Model 420 control module and a Beckman Model 171 dual-channel flow-through radioactivity counter interfaced to an Equity I+ computer and an Epson Model 810 printer was used. Separations were done on an Altex 25 cm × 4 mm I.D. stainless-steel column packed with 5-μm octadecylsilyl reversed-phase column material. Eluted fractions were collected in scintillation vials by a Pharmacia FRAC-100 fraction collector after automatic mixing with Beckman Ready-Flow II scintillation cocktail in the Model 171. Collected fractions were counted on a Beckman Model 5000 liquid scintillation counter and corrected for energy overlaps according to conventional procedures. Labware used was treated with dimethyldichlorosilane in hexane, and washed with water and acetone prior to use.

Computer simulations. An Epson Equity II+ computer with EGA graphics, a 20-Mbyte hard disk, an Intel 80287 supplemental mathematics coprocessor and an Epson 286e printer were used for mathematical modeling of dual-label chromatography separations and measurements. Computer programs were written in Microsoft's Quickbasic 4.0 (listings available from author upon request).

Chromatograms from the simulations were generated for specified enzymatic reaction rates of aryl hydrocarbon hydroxylases (AHHs), using relative metabolite concentrations from others' data compilations [7]. For rats metabolizing benzo[*a*]pyrene (B*a*P) relative concentrations in Table I were used, with other minor metabolic products ignored.

Efficiencies of component recoveries from extractions, reduction of extract volumes and dilutions to appropriate volume were taken from other work using reason-

TABLE I

METABOLITE RETENTIONS, PERCENTAGE OF METABOLITES AND UNCERTAINTIES DUE TO PRETREATMENTS

Metabolite	Retention time (min)	Met (%)[a]	E/C/D Eff[b] ± S.D. (%; n = 1,2 or 3)
9,10-B*a*P-dihydrodiol	16	8	0.4 ± 0.05 n
7,8-B*a*P-dihydrodiol	24	6	0.4 ± 0.05 n
1,6-B*a*P-dione	31	7	0.5 ± 0.05 n
3,6-B*a*P-dione	34	8	0.5 ± 0.10 n
6,12-B*a*P-dione	38	7	0.8 ± 0.10 n
9-OH-B*a*P	45	11	0.8 ± 0.10 n
3-OH-B*a*P	54	40	0.9 ± 0.05 n
B*a*P	65		0.9 ± 0.05 n

[a] Percentage of metabolites; assumed same for both reference metabolism and sample metabolism.
[b] Extraction/concentration/dilution efficiency for specified metabolite.

able standard deviations [2,7] (see Table I). No differences in these efficiencies were assumed for the differently labeled forms, consistent with their nearly identical chemical properties [2,3]. Random variations in these efficiencies were generated by an accepted procedure [8]. Variations in volume measurements for the diluted extract, the added reference solution and the subsample taken for HPLC were generated using reasonable standard deviations for volume measurements [9] and random Gaussian deviations [8].

Masses for each respective metabolite in subsamples taken for HPLC were calculated from assumed but varied AHH activities in the respective reaction systems, uncertainties in pretreatment recoveries, uncertainties in volumes and the volumes used. Mass *vs.* time relations for components separated by HPLC were calculated from respective injected masses, assumed HPLC peak widths at half-maximum of 1.0 min and presumed Gaussian peak shapes. The activities of the two labeled forms eluting from the column over all 1-s intervals throughout the separation duration were calculated. These interval activities were then summed into consecutive intervals of 6-, 15-, 30-, 60-, 90- or 120-s durations to simulate contents of collected fractions of corresponding times (see Fig. 1). Radioactivities were assumed to be ^{3}H and ^{14}C for these calculations. The measured activity for each fraction was calculated from the contained masses, specific activities, appropriate counting efficiencies for the relative concentrations of solvents and mixed scintillation cocktail, and imposed random variations in counting according to accepted procedures and appropriate compensation for energy overlaps [8,10].

Histograms simulating counted elution fractions were generated and total measured activities for each respective metabolite and labeled form were calculated by conventional methods [10]. Those data were saved for later computations and statistical analyses.

Fifteen replicates were done for each variation in combinations of: (a) four values for AHH reaction rates (10^{0}, 10^{-1}, 10^{-2} and 10^{-3} I.U./dl) (I.U. = 10^{-6} mol/min) for the reference solution, *i.e.*, yielding reference metabolite radioactivities; (b) 20 values for AHH reaction rates for the sample solution (10^{-3}–$2 \cdot 10^{-7}$ I.U./dl),

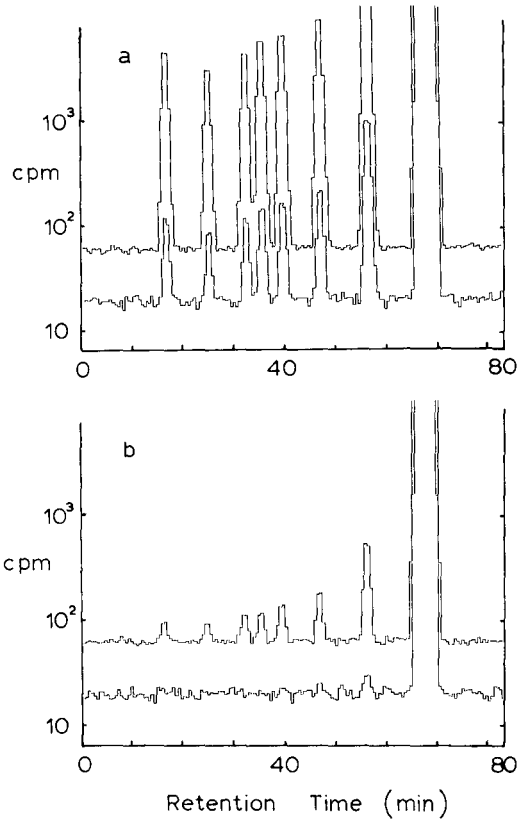

Fig. 1. Histograms of measured activity *vs.* time for 30 s eluted fractions. Upper chromatograms with approximately 49 cpm background are for ^{3}H from reference-solution eluates and lower chromatograms with approximately 16 cpm background represent ^{14}C components from samples. AHH enzymatic rates for the reference and sample incubations: (a) 10^{-1} I.U./dl for [^{3}H]B*a*P and 10^{-5} I.U./dl for [^{14}C]B*a*P, and (b) 10^{-3} I.U./dl for [^{3}H]B*a*P and 10^{-7} I.U./dl for [^{14}C]B*a*P.

i.e., yielding sample metabolite radioactivities; (c) three values for uncertainties in extraction/concentration/dilution efficiencies (1, 2 and 3 × S.D.; see Table I for values) and (d) six values for fraction-collection duration (6, 15, 30, 60, 90 and 120 s). Other values were held constant: (a) 10-min counting times were used; (b) 60-min enzymatic incubations were assumed for both reference and sample solutions; (c) specific activities of 500 and 325 mCi/mmol for ^{3}H-labeled and ^{14}C-labeled B*a*P, respectively; (d) 0.01 mol [^{3}H]B*a*P and 0.0001 mol [^{14}C]B*a*P added to reference and sample incubation solutions, respectively; (e) volumes of 25 ml for the total reference solution, 0.100 ml for reference solution added to sample prior to pretreatment, 100 ml for the sample incubation volume, 1.00 ml for the combined ^{3}H and ^{14}C mixture's resulting concentrate and 0.100 ml used for separation by HPLC, and (f) background count rates of 49 cpm for ^{3}H and 16 cpm for ^{14}C.

Measured radioactivities for each labeled form of each metabolite were saved and those data later were used to calculate *R* ratios within each replicate set for every metabolite-label pair and calculation of *U* ratios for all metabolites within each repli-

cate set relative to their respective 3-OH-B*a*P activities. Means (x) and standard deviations (S.D.) were computed and data quality was estimated as x/S.D. for each set of replicates. Confidence ranges ($x \pm$ S.D.) were calculated for *R*- and *U*-ratio results for the various replicate sets and plotted *vs.* AHH activities for sample solutions done under otherwise identical conditions.

Test organisms. Microsomes were prepared from tissue or isolated cells via homogenization in 1% KCl and centrifugation at 60 000 *g* for 60 min of the 20-min 20 000 *g* supernatant. Livers were excised from Sprague-Dawley rats (approximately 200 g) and treated immediately.

Procedures. Microsomes were incubated with reduced nicotinamide-adenine dinucleotide phosphate (NADPH), glucose-6-phosphate and glucose-6-phosphate dehydrogenase in oxygen-saturated 0.1 *M* PO_4^{3-} buffer at pH 7.5 with nicotinamide and B*a*P dosage compound at 37.5°C for rat-liver microsomes. After 2-h incubations, the metabolism was halted by additions of acetone. The incubates were then saturated with $NaCl_{(s)}$ and extracted four times with ethyl acetate. Descriptions of reagent volumes and concentrations may be found elsewhere [2,3]. The extracts were evaporated to dryness at 25°C under a stream of nitrogen and the residue partially dissolved into 1.0 ml of methanol. Aliquants (50 μl) of the methanolic concentrate were then separated by HPLC with the effluent being mixed with scintillation cocktail just prior to flow-through counting. The outflow from the Model 171 counter was collected as 1-min fractions in glass scintillation vials and each was counted for 20 min each on a multichannel liquid scintillation counter.

Data were plotted as histograms and net activities calculated for the eluted components. Eluate activities were then used for computations using eqns. 1 and 2, and for statistical calculations.

RESULTS AND DISCUSSION

Dual-label chromatograms from simulations were developed and histograms representing collected fraction radioactivities *vs.* time for those dual-label chromatograms (Fig. 1) were like results expected from corresponding biological experiments [2,7]. The histograms spanned a wide range of variations including those for which all metabolite-peaks' radioactivities were easily calculated (Fig. 1a) and others for which many eluates were below the limits of reliable measurement (Fig. 1b), with some circumstances allowing easy measurement of one labeled form but difficult to unfeasible measurements for the other.

Precisions were generally better for individual conventional calculations involving simple ratios for ^{14}C-labeled components between chromatograms, as compared to corresponding *R*- or *U*-ratio comparisons. This is consistent with the increased imprecision expected due to inclusion of additional radioactivity data in the calculations, *e.g.*, (A_{c1}/A_{c2}) has less uncertainty than $(A_{c1}/A_{H1}) / (A_{c2}/A_{H2})$. However, these simple one-label ratios are much less useful (see Fig. 2) than the corresponding *R* and *U* ratios as they yield no theoretically valid result unless volume and efficiency uncertainties are eliminated experimentally, which is typically unfeasible.

R and *U* ratios, as predicted by theory, yield unity for metabolism via the same pathways and metabolic systems (Figs. 2 and 3), even if experimental variations fluctuate dramatically. This powerful predictive factor was confirmed in all our theo-

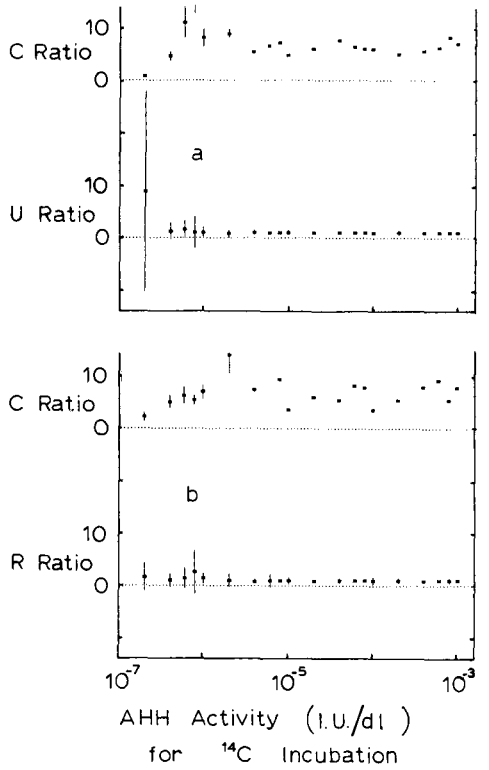

Fig. 2. Sample enzymatic rate (I.U./dl) *vs.* *U* ratios or corresponding ratios using only the C-label data: *U* ratio lower in each. These figures show results for two levels of extraction/concentration/dilution uncertainties: (a) ± 10% (R.S.D.); (b) ± 30% (R.S.D.). These data were attained using a reference solution for which AHH activity was 0.1 I.U./dl during incubation, *R* ratios for 6,12-B*a*P-dione and via *U* ratio comparisons between 6,12-B*a*P-dione and 3-OH-B*a*P.

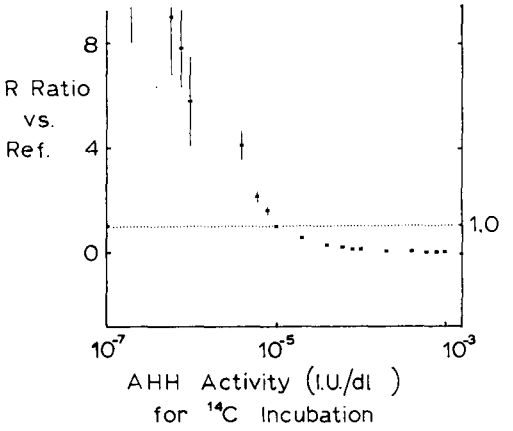

Fig. 3. *R* ratio *vs.* sample enzymatic rate (I.U./dl) for comparisons to metabolites from incubations with 10^{-5} I.U./dl AHHs in referenced sample incubation (Ref.) and 0.01 I.U./dl in the reference ^{3}H incubation. These data are for comparisons of 9,10-B*a*P-dihydrodiol between groups.

retical results, with typical standard deviations within replicate sets of only about ± 2–5% (R.S.D.), *e.g.*, 1.00 ± 0.03 with $n = 15$. Means of different replicate sets for U ratios varied little for similar reaction conditions and sample AHH values above 10^{-6} I.U./dl, with variations approximating 3–8% (R.S.D.), *e.g.*, 1.00 ± 0.05. R ratios showed somewhat better predictability than the U ratios, with values for $R = 1$ varying with about 3–5% (R.S.D.). Consequently, ratios for circumstances for which $R \neq 1$ or $U \neq 1$ are easily distinguished from those for which $R = 1$ or $U = 1$. Corresponding conventional one-label ratios varied greatly despite use of many replicates, typically with means of different replicate sets varying about ± 50–100% (R.S.D.), *e.g.*, 2.5 ± 2.0 (Fig. 2). This imprecision is due primarily to their lack of compensation for experimental variations. The advantages of the highly predictable, low-uncertainty U and R ratios are very important in regard to statistical hypothesis testing.

The magnitudes of measured radioactivities for reference-solution metabolites affects data quality for the corresponding R and U ratios. As expected, higher reference-component activities reduce the relative uncertainties in total-peak-activity calculations and thereby improve R- and U-ratio results. Of course, sufficient activity is necessary to ensure reasonable data quality (Fig. 1a *vs.* Fig. 1b), but very high activities provide only marginal improvements after reasonably good data quality is achieved (Fig. 4).

Interestingly, data quality for fairly long fraction-collection durations, *e.g.*, 60 s, was often better than that for shorter durations (6, 15 and 30 s) and was usually somewhat superior to that achieved for longer durations (90 and 120 s) (see Fig. 5). This observation is consistent with reduced ability to distinguish peaks when fewer data, *i.e.*, fractions, are used such as herein where the peak widths at half maximum are 1 min; that allows only several fractions to be used to characterize each peak. Conversely, using too many fractions detracts from the integrating ability of longer fractions, and can result in worse precision resulting from the diminished total counts for each fraction.

As extraction/concentration/dilution uncertainties increase greatly, corresponding R and U ratios become a little less precise. Moreover, the predictability, *i.e.*, the uncertainty for unity in the null hypothesis, changes only slightly due to those somewhat larger standard deviations in the R or U ratios (see Fig. 2). Thus, use of these ratios substantially reduces difficulties encountered due to large variations in recovery efficiencies and other pretreatment variables.

Increased numbers of replicates enhance data quality for the R and U ratios (see Fig. 6). As expected, improvements are significant for low numbers of replications, *e.g.*, 2 *vs.* 3, but the added relative advantage for high numbers is only slight. Thus, one may select a number of replicates which allows for appropriate statistical comparisons, *e.g.*, 3–5, and save the expense of using many repetitions of the corresponding experiments; when using conventional single-label comparisons, even very high numbers of replications do not result in the excellent predictability offered by only a few replicates with the R or U ratios.

Use of the dual-label procedures discussed above has the potential for dramatically improving statistical comparisons between reaction product profiles in experiments. This is mainly due to the theoretically valid predictability for the R and U ratios, *i.e.*, $R = 1$ or $U = 1$ for the null hypothesis. Also, because the added reference

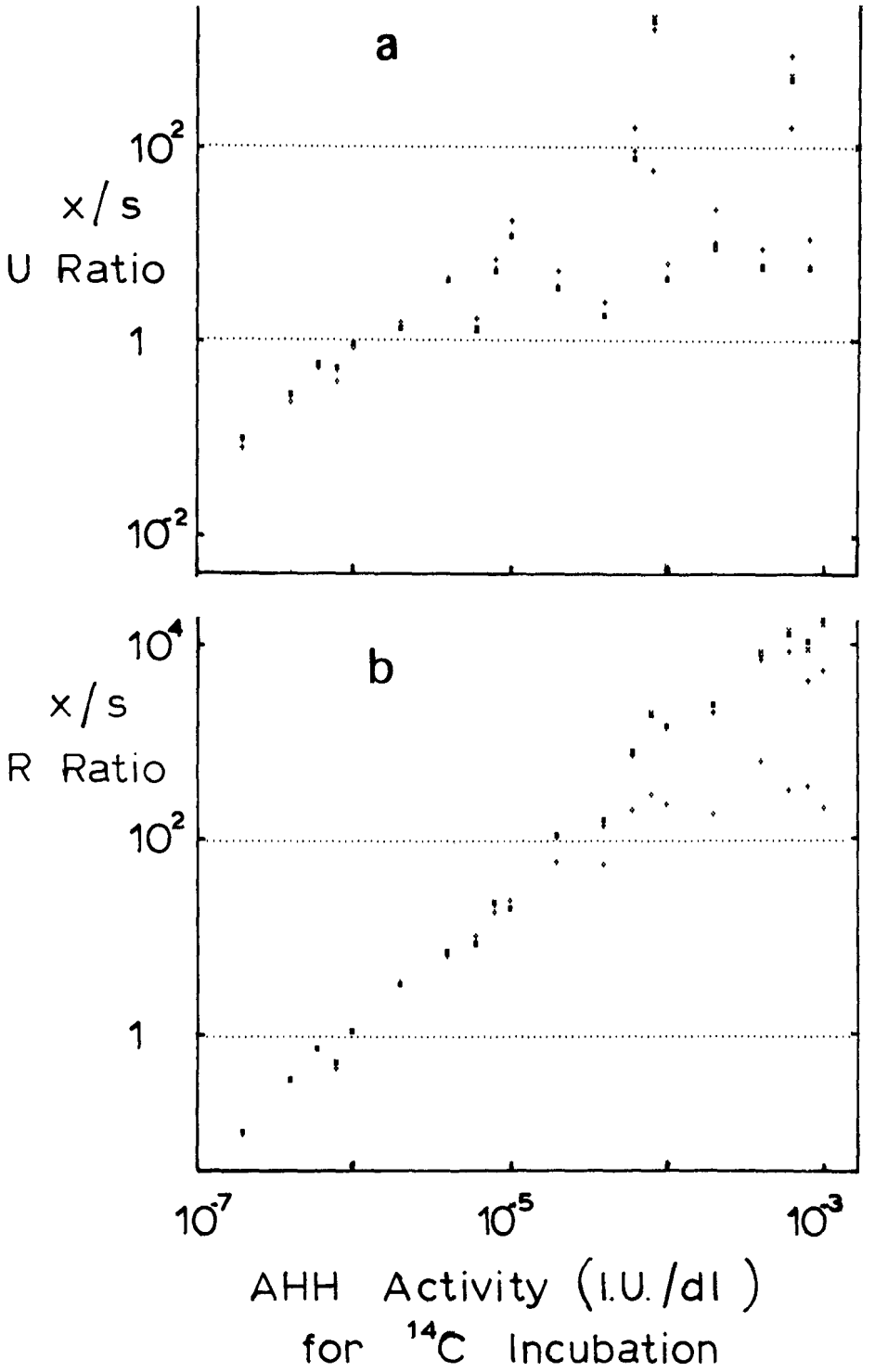

Fig. 4. (x/S.D.) for 3,6-BaP-dione with four AHH enzymatic rates in reference ^3H incubation, with 10% uncertainty in extraction/concentration/dilution efficiency; (a) for U ratios compared to 3-OH-BaP *vs.* sample AHH rates, and (b) for R ratios *vs.* sample AHH rates. ■ = 10^0 I.U./dl; × = 10^{-1} I.U./dl; + = 10^{-2} I.U./dl; ◇ = 10^{-3} I.U./dl. s = Standard deviation.

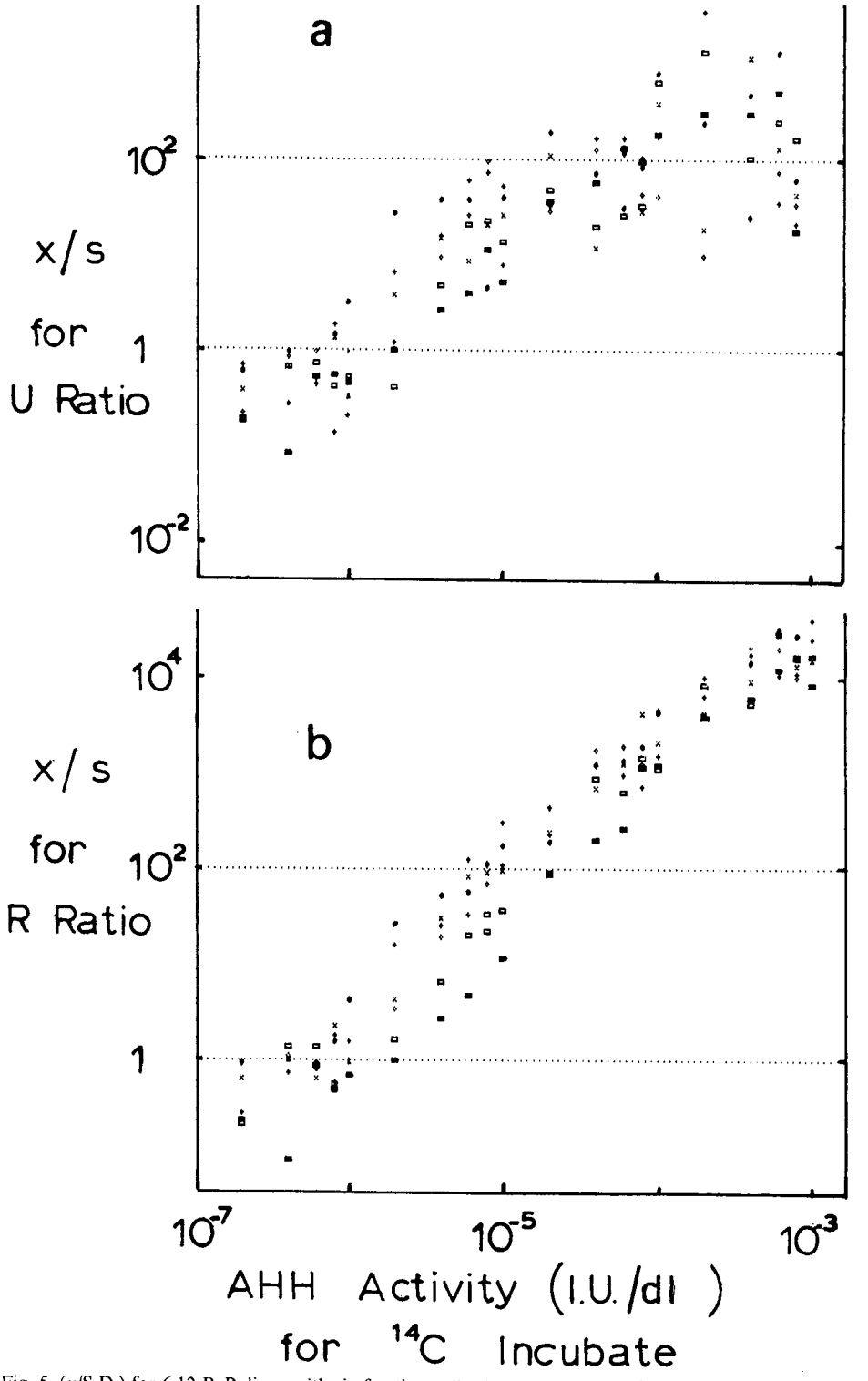

Fig. 5. (x/S.D.) for 6,12-B*a*P-dione with six fraction-collection durations, 10^{-1} I.U./dl in [^{3}H]B*a*P reference incubation and 10% extraction/concentration/dilution uncertainty. (a) for U ratios compared to 3-OH-B*a*P *vs.* AHH rates and (b) for R ratios *vs.* sample AHH rates. ● = 6 s; □ = 15 s; ◆ = 30 s; x = 60 s; + = 90 s; ■ = 120 s. s (In figure) = standard deviation.

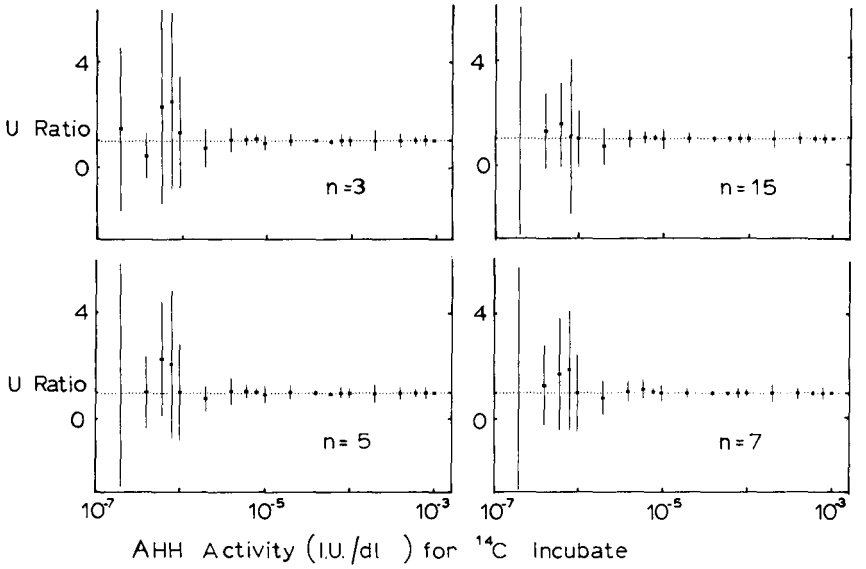

Fig. 6. *U* ratios *vs.* AHH rates (I.U./dl) for four variations in the number of replicates used for comparisons; these results are for 6,12-B*a*P-dione, with 10^{-1} I.U./dl AHH rate in the [^{3}H]B*a*P reference incubation and 10% uncertainty in extraction/concentration/dilution efficiency.

components are properly used as internal standards, the contributions due to uncertainties in recoveries, volume measurements, etc. are reduced appreciably, resulting in small standard deviations for corresponding *R* and *U* ratios. Moreover, because of the mathematical form of these ratios, needs for carefully defining specific activities and some other variables are obviated.

Results of laboratory tests are consistent with the theoretical results discussed above. For replicates which were split after mixing of the reference solution and sample, *R* ratios were typically 1.0 ± 0.06 (R.S.D., $n = 5$) and *U* ratios were typically 1.0 ± 0.10 (R.S.D., $n = 5$) for comparisons relative to 3-OH-B*a*P. Corresponding values for conventional ratios based only upon ^{14}C varied dramatically with R.S.D. values between 50–300%. All these results were somewhat worse than predicted by theory, perhaps due to interferences from other components and drifting chromatogram baselines. However, the marked advantages for the *R* and *U* ratio were corroborated by the empirical results.

These dual-label techniques are powerful for comparing reaction efficacies and should be adaptable to isotope-selective measurements such as emission spectrometry, mass fragmentometry and resonance spectroscopic methods, which would allow for use of non-radioactive compounds. Additionally, they could be easily used for non-biological reaction systems such as synthesis reactions and decompositions.

REFERENCES

1 H. C. Barth, W. E. Barber, C. H. Lochmuller, R. E. Majors and F. E. Regnier, *Anal. Chem.*, 60 (1988) 387R.

2 L. C. Thomas and T. L. Ramus, *Anal. Chim. Acta*, 154 (1983) 143.
3 L. C. Thomas and T. L. Ramus, *Anal. Lett.*, 17 (1984) 2001.
4 L. C. Thomas, W. D. MacLeod, Jr. and D. C. Malins, *Special Publication No. 519*, National Bureau of Standards, Gaithersburg, MD, 1979, pp. 79–84.
5 T. A. Loomis, *Essentials of Toxicology*, Lea and Febiger, Philadelphia, PA, 1978.
6 J. R. Bend and M. O. James, in *Biochemical and Biophysical Perspectives in Marine Biology*, Vol. 4, Academic Press, New York, 1978, pp. 125–188.
7 R. I. Freudenthal, S. G. Hundley and S. M. Cattaneo, in P. W. Jones and R. I. Freudenthal (Editors), *Carcinogenesis, Vol. 3, Polynuclear Aromatic Hydrocarbons*, Raven Press, New York, 1978, pp. 313–323.
8 P. R. Bevington, *Data Reduction and Error Analysis for the Physical Sciences*, McGraw-Hill, New York, 1969.
9 G. D. Christian, in *Analytical Chemistry*, Wiley, New York, 1986, 4th ed.
10 T. R. Roberts, *Radiochromatography*, Elsevier, Amsterdam, 1978.

Journal of Chromatography, 522 (1990) 131–141
Elsevier Science Publishers B.V., Amsterdam

CHROM. 22 682

Étude par chromatographie liquide haute performance des antioxydants phénoliques présents dans les matériaux plastiques

Comparaison de trois méthodes de détection: spectrophotométrique dans l'ultra-violet, electrochimique, et évaporative à diffusion de la lumière

NAJET YAGOUBI*, ARLETTE E. BAILLET, FERNAND PELLERIN et DANIELLE BAYLOCQ
Centre d'Études Pharmaceutiques, Laboratoire de Chimie Analytique, Rue J.B. Clément, F-92290 Chatenay-Malabry (France)
(Reçu le 20 février 1990; manuscrit modifié reçu le 9 juillet 1990)

ABSTRACT

Comparison of three detection systems for reversed-phase high-performance liquid chromatography of traces of antioxidants in plastics: UV spectroscopy, electrochemical detection and light-scattering diffusion.

National and international regulations require the identification of penolic antioxydants in plastic materials used for the packaging of pharmaceuticals, food and cosmetics, and the detection of their possible migration into the contents. The objective of this paper is to propose a method for the identification of these compounds by high-performance liquid chromatography and to determine their limit of sensitivity by UV spectrophotometry, electrochemistry and light scattering diffusion. The results are discussed for four phenolic antioxidants generally used in plastic materials.

INTRODUCTION

Les impératifs technologiques et économiques des industries pharmaceutiques et alimentaires ont développé considérablement l'emploi d'agents antioxydants [1]. Un certain nombre de ces molécules sont présentes dans les matières plastiques pour protéger le polymère au cours de sa transformation. Leur utilisation est impérative lorsque la température nécessaire à la polymérisation totale du matériau est élevée.

Plusieurs méthodes d'analyse des antioxydants phénoliques ont déja été proposées dans la littérature. Nous rappelons les méthodes colorimétriques [2], les méthodes chromatographiques: chromatographie sur couche mince [3,4], chromatographie gaz–liquide [5], chromatographie liquide haute performance (CLHP) à polarité de phases inversée [6,7], phase normale [8] et perméation de gel [9].

La complexité de la structure des matériaux plastiques a posé le problème des

0021-9673/90/$03.50

incompatibilités et des interactions des substances à leur contact. Des études d'interactions contenant–contenu ont été éffectuées et se sont traduites par des modifications diverses [10]. Elles sont dues à une solubilité réciproque entre récipient et forme pharmaceutique ou alimentaire. Les migrations des antioxydants étant très faibles il nous a semblé judicieux de mettre au point une méthode d'analyse par

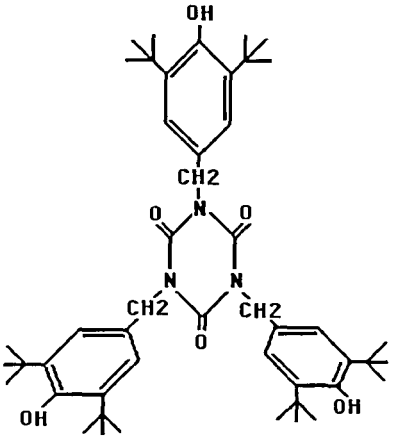

GOODRITE 3114

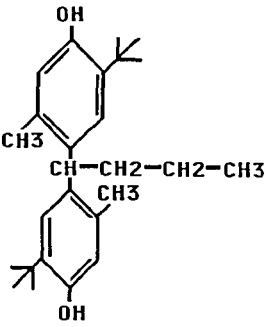

SANTOWHITE

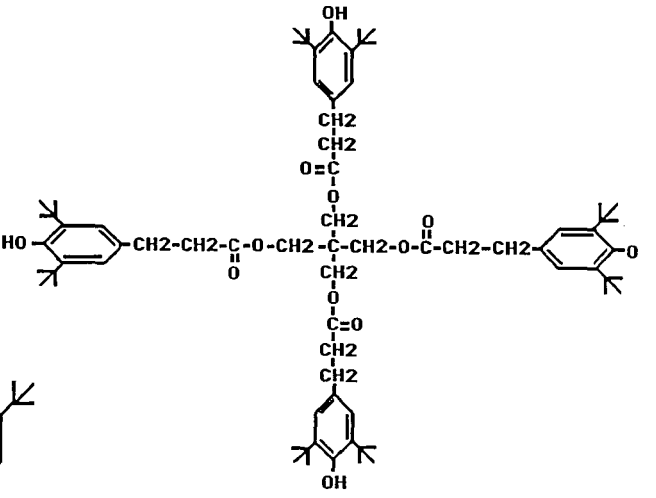

IRGANOX 1010

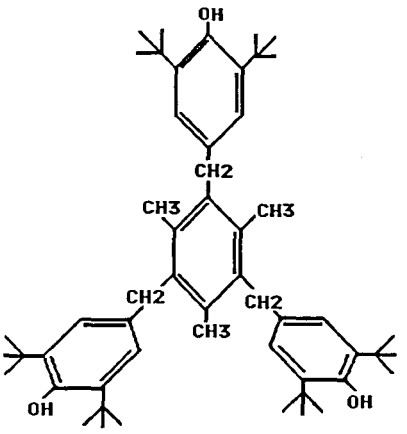

IRGANOX 1330

CLHP avec trois modes de détection afin de pouvoir quantifier ces échanges éventuels.

Les techniques ont été validées par des critères statistiques qui ont permis de confirmer les performances des méthodes de détection choisies pour le dosage des traces.

Nous avons appliqué notre étude à quatre antioxydants phénoliques rencontrés habituellement dans les matériaux plastiques, seuls, ou le plus souvent en mélange: Santowhite [bis(methyl-3-*tert.*-butyl-6-phenol)-4,4′-butyldene], Irganox 3114 [tris(di-*tert.*-butyl-3,5-hydroxy-4-benzyl)isocyanurate], Irganox 1010 {pentaerythrityl-tetrakis[3-(3,5-di-*tert.*-butyl-4-hydroxyphenyl)-propionate]} et Irganox 1330 [trimethyl-1,3,5-tris(di-*tert.*-3′,5′-hydroxy-4′-benzyl)-2,4,6-benzene].

PARTIE EXPÉRIMENTALE

Appareillage

L'appareil utilisé est un chromatographe en phase liquide equipé d'une pompe Chromatem 800 (Touzart et Matignon, Vitry sur Seine, France) muni d'un programmateur Altex 420 et d'une vanne Rhéodyne à boucle de 20 μl. La séparation des quatre molécules a été effectuée avec une colonne de silice greffée C_{18} Spherisorb ODS2, 5 μm, 250 × 4.6 mm D.I. (S.F.C.C., Neuilly Plaisance, France). L'analyse a été réalisée en mode isocratique avec un éluant composé d'acétonitrile pur. Pour la détection électrochimique un électrolyte indifférent le perchlorate de lithium sera ajouté à raison de 5 g/l.

Les différents modes de détection ont été réalisés suivant les cas à l'aide d'un détecteur par spectrophotométrie dans l'ultraviolet SPD 2A Shimadzu (Touzart et Matignon) à longueurs d'ondes variables, d'un détecteur à diffusion de la lumière DDL 11 (Cunow, Cergy Saint Christophe, France) (gaz nébuliseur: azote) et d'un détecteur ampérométrique (Metrohm Roucaire, Velizy Villacoublay, France) constitué de deux unités: une cellule électrochimique type 656 constituée d'une électrode indicatrice en carbone vitreux, une électrode de référence Ag (AgCl), KCl 3 *M* et une électrode auxiliaire constituée d'un disque de platine; une unité ampérométrique type 641 VA. La mesure du signal est réalisée sur un intégrateur type SP 4270 (Spectra-Physics, De Courtabuef, France).

Réactifs

Quatre antioxydants témoins ont été analysés: Santowhite, Irganox 3114, Irganox 1010 et Irganox 1330 (Ciba-Geigy, Rueil, France). Ils ont été dissous dans l'acétonitrile (Carlo Erba, Milan, Italie). Le perchlorate de lithium est utilisé comme électrolyte indifférent (Merck, Nogent sur Marne, France).

Choix des conditions opératoires

Pour chaque type de détection un certain nombre de paramètres ont été étudiés afin d'optimiser les conditions opératoires.

Détection par spectrophotométrie dans l'ultra-violet (UV). Pour chaque molécule un spectre d'absorption dans l'UV a été réalisé et la longueur d'onde de 280 nm commune aux quatre composés a été retenue comme longueur d'onde de détection.

Détection ampérométrique. Des voltampérogrammes pour les quatre antioxy-

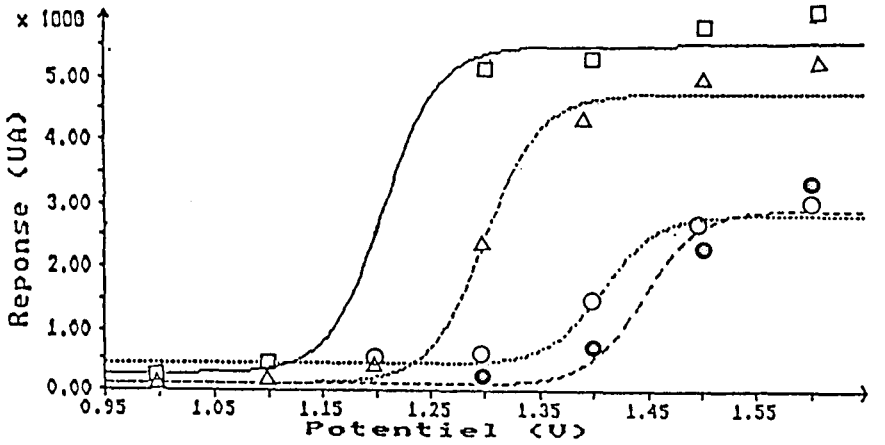

Fig. 1. Voltampérogramme hydrodynamique, □ = Santowhite; ● = Irganox 3114; ○ = Irganox 1010; △ = Irganox 1330.

dants ont été préalablement tracés et ont permis de démonter leur électroactivité et donc la possibilité d'une étude par CLHP couplée à une détection ampérométrique directe. Ces courbes ont été obtenues en opérant dans l'acétonitrile en présence de perchlorate de lithium (5 g/l). En outre les courbes voltampérometriques hydrodynamiques ont été obtenues par injection de 20 µl d'une solution à 5 µg/ml de chaque composé, à des potentiels allant de 1,0 V, 1,2 V, 1,3 V, 1,4 V, 1,5 V et 1,6 V. (Fig. 1) et ont conduit à fixer le potentiel de détection à 1,6 V.

Détection à diffusion de la lumière. De nombreux auteurs ont établi des correlations entre les valeurs théoriques et expérimentales obtenues avec ce système de détection [11] et les effets de la nature du solvant et des solutés sur la réponse du détecteur [12]. Nous avons optimisé l'analyse par l'étude de deux paramètres déterminants sur la réponse du détecteur: la température du tube de diffusion et la pression de gaz de nébulisation. L'intensité de la réponse en fonction de l'accroissement de la température du tube de diffusion évolue de manière identique pour les quatre molécules (Fig. 2A). L'augmentation de la pression de gaz de nébulisation donne une réponse hétérogène. La pression optimale varie légèrement en fonction des molécules étudiées (Fig. 2B). Cependant elle reste supérieure ou égale à 2 bar. Une température de 30°C et une pression de 2 bar ont été retenues comme conditions optimales.

RÉSULTATS ET DISCUSSION

L'objectif de l'étude a été d'une part de détecter et de doser des antioxydants présents dans les polyoléfines et d'autre part de quantifier leur migration éventuelle dans des formulations pharmaceutiques; en effet les concentrations autorisées pour la conservation des matériaux peuvent être aisément dosées par les méthodes déja citées. La sensibilité des trois systèmes de détection utilisés a été comparée et il a été possible de justifier leur utilisation pour le dosage de traces.

Cette étude a été menée à l'aide des critères suivants. Analyse qualitative: seuil de détection. Analyse quantitative: regression linéaire, domaine de linéarité et seuil de quantification. Les résultats sont rassemblés (Tableau I).

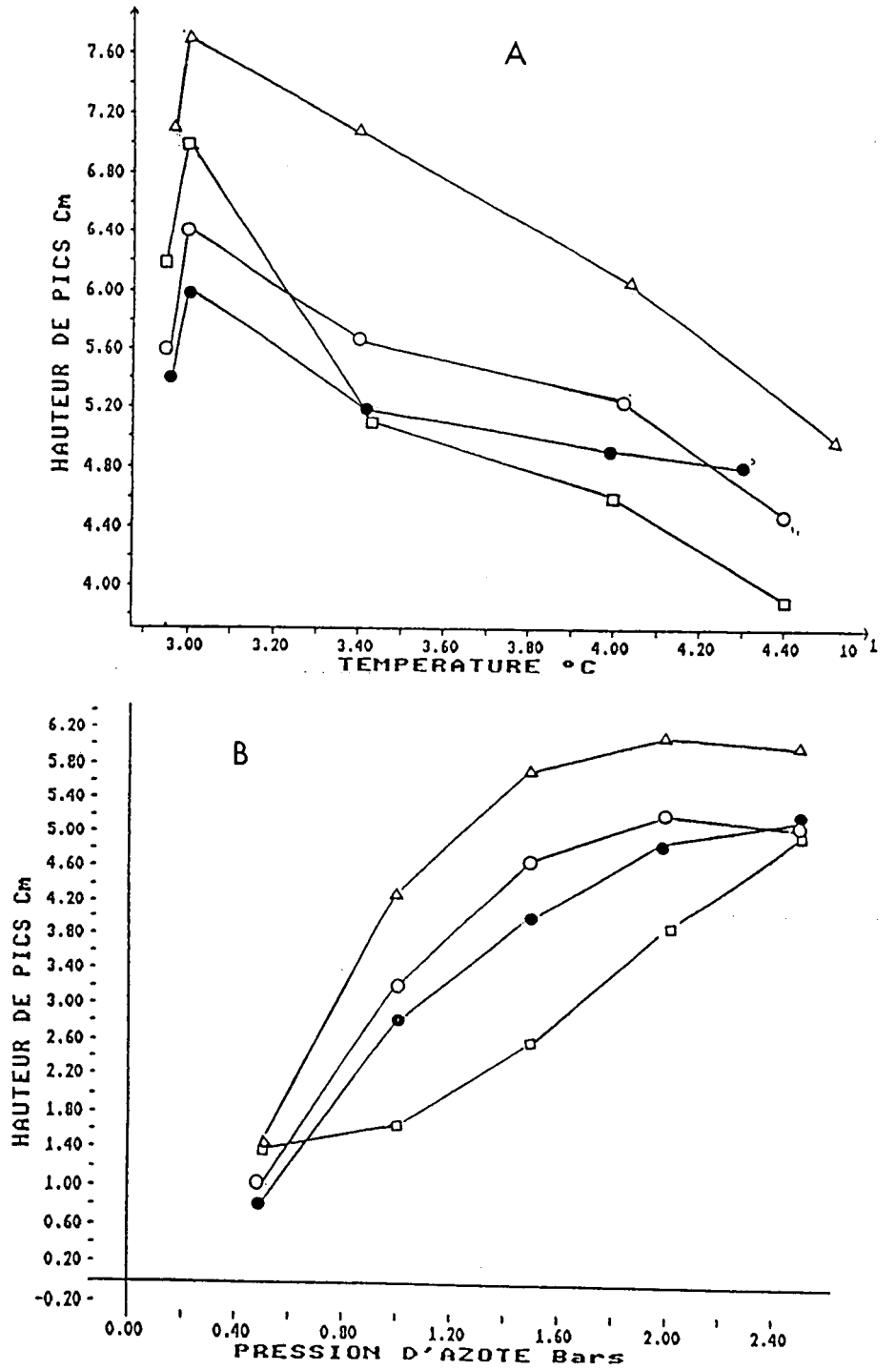

Fig. 2. Optimisation de deux paramètres de la détection à diffusion de lumière. □ = Santowhite; ● = Irganox 3114; ○ = Irganox 1010; △ = Irganox 1330. (A) Hauteur en fonction de l'augmentation de la température de nébulisation; (B) Hauteur en fonction de l'augmentation de la pression d'azote.

TABLEAU I

VALIDATION QUANTITATIVE ET LIMITE DE DÉTECTION

● = UV: relation réponse–quantité injectée. ■ = détection ampérométrique: relation réponse–quantité injectée. ▲ = détection à diffusion de lumière: relation réponse–quantité injectée en coordonnées logarithmiques.

Antioxydants	Domaine de linéarité (μmol)	Droite de regression		Coefficient de variation (% sur le facteur de réponse)	Seuil de quantification		Limite de détection (pmol)[a]
		Pente	Ordonnée a l'origine		μmol	C.V. (%)	
Santowhite	3.3–0.40 ●	20.1	−4.81	2.07	0.40	0.44	1.6
	1.8–0.24 ■	11.3	+6.64	3.70	0.24	2.13	0.3
	1.4–0.50 ▲	1.40	+1.07	6.01	0.50	0.87	69
Irganox 3114	2.5–0.32 ●	7.66	+5.30	3.18	0.32	1.44	2.4
	2.3–0.15 ■	4.70	−1.66	3.20	0.15	2.34	1.8
	0.7–0.23 ▲	1.36	+1.01	6.07	0.23	0.40	28
Irganox 1010	2.0–0.24 ●	9.11	−1.80	2.36	0.24	0.77	1.7
	3.0–0.30 ■	3.67	−1.65	2.97	0.30	1.00	1.7
	0.5–0.16 ▲	1.38	+0.89	4.91	0.16	0.94	43
Irganox 1330	4.0–0.20 ●	13.2	+22.4	3.44	0.20	1.02	2
	2.0–0.20 ■	7.80	−7.42	3.20	0.20	0.57	2
	1.0–0.30 ▲	1.42	+0.95	4.25	0.30	0.76	46

[a] Test de student, 5% de risque.

Seuil de détection

La limite de détection est la plus faible valeur de la grandeur mesurée dont la méthode permet d'affirmer qu'elle n'est pas nulle [13]. Elle est estimée *à priori* par la valeur du rapport signal sur bruit égal à trois. Nous l'avons complétée par un test statistique qui consiste à comparer les résultats obtenus pour une valeur vraie faible mais différente de zéro avec ceux correspondant à une valeur vraie nulle (blanc) [14].

A partir des résultats obtenus les remarques suivantes peuvent être formulées:

– la détection à diffusion de lumière est la méthode la moins sensible du fait de son caractère non spécifique;

– la détection ampérométrique et l'UV donnent des résultats similaires et selon l'encombrement stérique des molécules l'une ou l'autre méthode sera choisie.

Il faut noter que la détection ampérométrique a été menée à un potentiel élevé, c'est à dire dans des conditions opératoires limites du détecteur utilisé, de ce fait le maximum de sensibilité de l'appareillage n'a pas été atteint. Toutefois ces deux systèmes de détection (ampérométrique et UV) se révèlent performants pour le dosage de traces.

Régression linéaire

L'étude de la régression nous a amené à vérifier si la relation entre les quantités injectées et les réponses observées peut être assimilée à une droite. Les équations ont été calculées par la méthode des moindres carrés. Pour les systèmes de détection ampérométrique et UV cette relation est linéaire (Fig. 3). Cependant il est à noter que dans le cas de la détection à diffusion de lumière cette relation n'est pas linéaire. L'allure de la courbe est celle d'une sigmoïde (Fig. 4A), sur laquelle une faible zone de linéarité a été déterminée allant de 0,5 a 0,3 μmol. Par conséquent cette courbe a été tracée en coordonnées logarithmiques (Fig. 4B). Des résultats similaires ont été publiés sur d'autre types de molécules par d'autres auteurs [15].

Le domaine de linéarité a été déterminé à l'aide du coefficient de corrélation. Ce calcul n'est pas suffisant pour verifier si la représentation concentration–réponse est bien linéaire. Une autre approche, plus précise, consiste à calculer le coefficient de variation du facteur de réponse de la droite de regression. Le facteur de réponse est le rapport réponse–concentration.

Si cette relation est une droite dans une zone déterminée, ce facteur sera constant qu'elles que soient les valeurs des couples (concentration–réponse) [16]. Les concentrations étudiées satisfont l'analyse de traces avec un domaine de linéarité comparable pour les systèmes de détection ampérométrique et UV, mais reste relativement limité dans le cas de détection à diffusion de lumière.

Seuil de quantification

La limite de détection est une valeur imprécise pour effectuer des dosages quantitatifs. Nous avons utilisé le seuil de quantification défini par le Comité des Spécialités Pharmaceutiques concernant la validation analytique des dosages dans les milieux biologiques [17]. C'est la plus petite quantité d'une substance à examiner dans un échantillon pouvant être dosée dans les conditions expérimentales décrites avec un coefficient de variation du facteur de réponse acceptable.

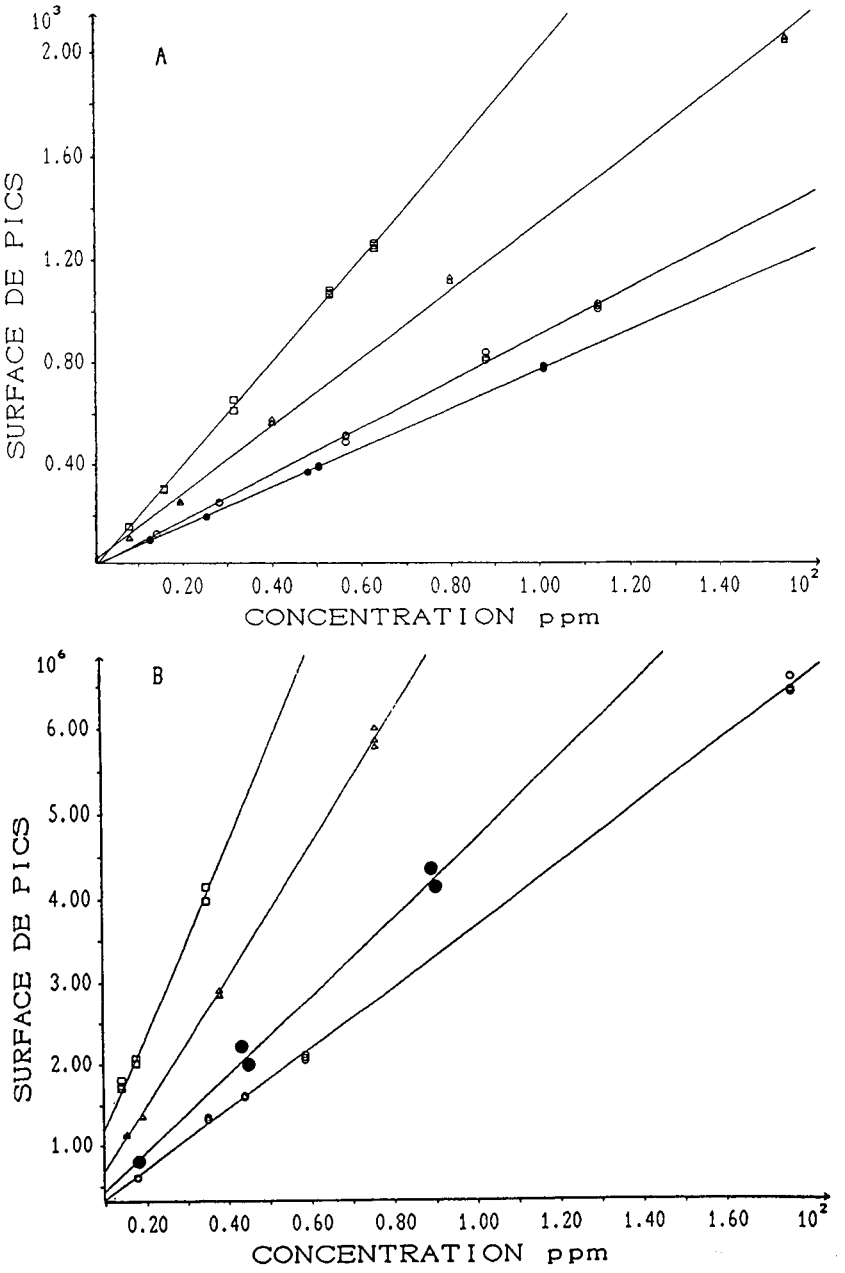

Fig. 3. Représentation graphique de la relation réponse–quantité injectée. □ = Santowhite; ● = Irganox 3114; ○ = Irganox 1010; △ = Irganox 1330. (A) UV; (B) détection ampérométrique.

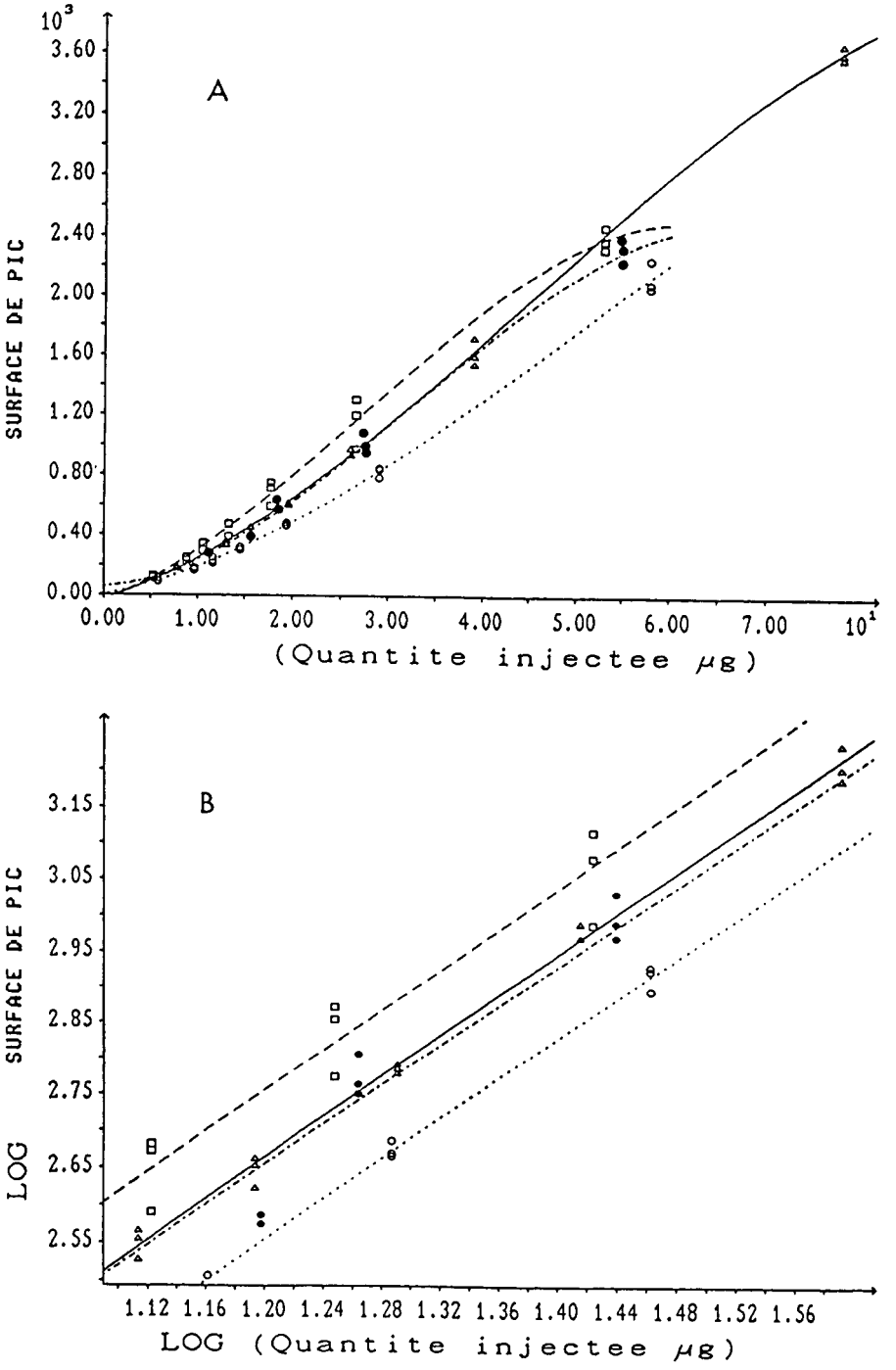

Fig. 4. Représentation graphique de la relation réponse du DDL–quantité injectée. □ = Santowhite; ● = Irganox 3114; ○ = Irganox 1010; △ = Irganox 1330. (A) Relation sigmoïdale en coordonnées directes; (B) relation linéaire en coordonnées logarithmiques.

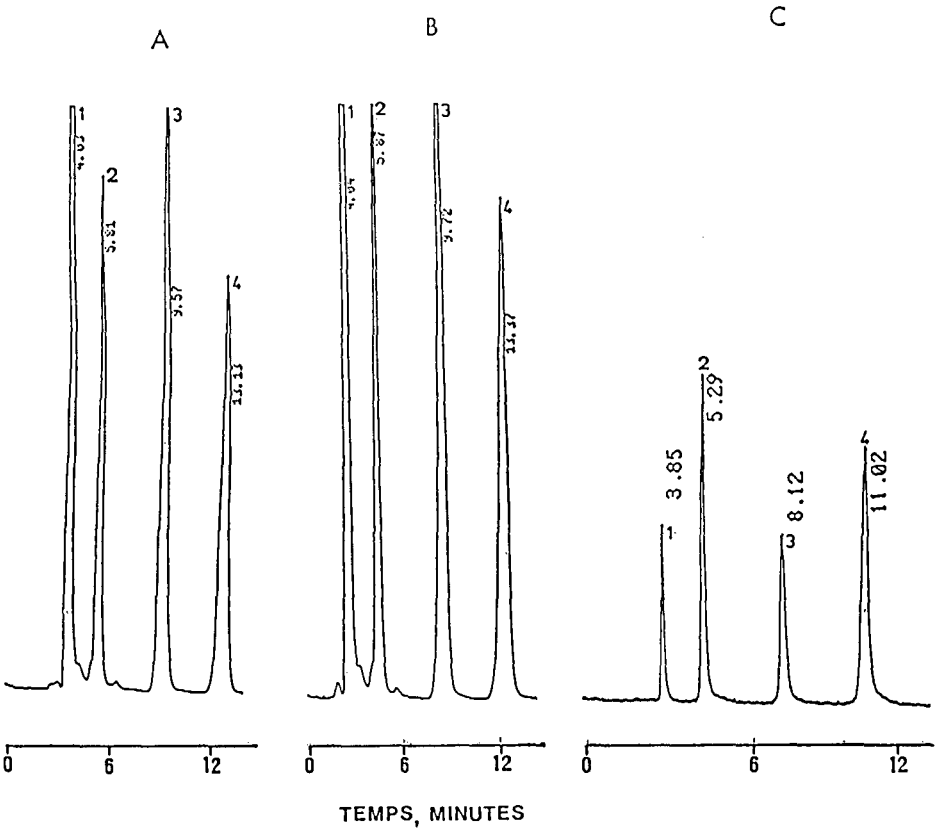

Fig. 5. Chromatogramme d'une solution étalon d'antioxydants de concentration voisine de 5 μg/ml. Conditions: colonne, C_{18} Spherisorb ODS2, 5 μm, 250 × 4,6 mm D.I.; phase mobile, acétonitrile; 20 μl de quantité injectée. Pics: 1 = Santowhite; 2 = Irganox 3114; 3 = Irganox 1010; 4 = Irganox 1330. (A) UV; (B) détection ampérométrique (1 ml/min); (C) détection à diffusion de lumière (1,2 ml/min).

CONCLUSION

Les antioxydants phénoliques contenus dans les matériaux plastiques sont susceptibles de migrer à l'état de traces dans les médicaments, les aliments ou les cosmétiques. Les analyses obtenues avec trois systèmes de détection couplés à la CLHP (Fig. 5) ont été comparées et les résultats validés par des critères statistiques.

Les détections ampérométrique et spectrophotométrique dans l'ultraviolet se sont révélées très performantes. La détection par diffusion de la lumière est moins sensible mais reste exploitable dans ce domaine d'étude. Une mise au point est actuellement en cours pour la détermination des produits de dégradations des antioxydants phénoliques aprés stérilisation par les radiations ionisantes à l'aide d'un détecteur à barette de diodes.

RÉSUMÉ

Les réglementations Européenne et Internationnale exigent une identification des antioxydants contenus dans les articles en matières plastiques destinés à être mis en contact avec les produits pharmaceutiques, les aliments et les produits cosmétiques.

L'objectif de cette étude est de proposer une méthode d'identification et de dosage de quatre antioxydants phénoliques communément utilisés dans les matériaux plastiques (Santowhite, Irganox 3114, Irganox 1010, Irganox 1330).

BIBLIOGRAPHIE

1 J. Alary et C. Grosset, *Bull. Trav. Soc. Pharm. Lyon*, 26 (1982) 80.
2 C. S. Prakasa Sastry, K. Ekambareswara Rao et U. V. Prasad, *Talanta*, 29 (1982) 917.
3 Ch. B. Airaudo, A. Gayte-Sorbier, P. Laurent et R. Creusevau, *J. Chromatogr.*, 314 (1984) 349.
4 Ch. B. Airaudo, A. Gayte-Sorbier et P. Creusevau, *J. Chromatogr.*, 392 (1987) 407.
5 J. A. Denning et J. A. Marshall, *Analyst.*, 97 (1972) 710.
6 D. Baylocq, C. Majcherczyk et F. Pellerin, *Ann. Pharm. Fr.*, 43 (1985) 329.
7 S. Yamamoto, M. Kanda, M. Yokouchi et S. Tahara, *J. Chromatogr.*, 370 (1986) 179.
8 H. Indyk et D. C. Woollard, *J. Chromatogr.*, 356 (1986) 401.
9 A. M. Wims et S. J. Swarin, *J. Appl. Polym. Sci.*, 19 (1975) 1243.
10 F. Pellerin, D. Baylocq, D. André, C. Majcherczyk et N. Al Laham, *Ann. Pharm. Fr.*, 42 (1984) 15.
11 A. Stolyhwo, H. Collin et G. Guiochon, *J. Chromatogr.*, 265 (1983) 1.
12 M. Righezza et G. Guiochon, *J. Liq. Chromatogr.*, 11 (1988) 1967.
13 Union Internationale de Chimie Pure et Appliquée, *Compendium de la Nomenclature en Chimie Analytique, Règle de définition de 1977*, Société Chimique de France, Paris, 1977.
14 Commission d'etablissement des methodes d'analyses du Commissariat á l'energie atomique, *Statistiques Appliquées à l;Exploitation des Mesures*, Edition Masson, Paris, 1986.
15 J. M. Charlesworth, *Anal. Chem.*, 50 (1978) 1414.
16 D. Lecompte, *S.T.P. Pharma*, 2 (No. hors série) (1986) 843.
17 *Comite des spécialistes Pharmaceutiques, Groupe de Travail; "Qualité des Medicaments", octobre (1988), circulaire No. 13375*. Office des Publications Officielles des Communautées Européennes Luxembourg, 1988.

Journal of Chromatography, 522 (1990) 143–152
Elsevier Science Publishers B.V., Amsterdam

CHROM. 22 740

Effects of mobile phase composition on the reversed-phase separation of dipeptides and tripeptides with cyclodextrin-bonded-phase columns[a]

C. ALLEN CHANG*[,b], HONG JI and GWOCHUNG LIN
Department of Chemistry, University of Texas at El Paso, El Paso, TX 79968-0513 (U.S.A.)
(First received May 4th, 1990; revised manuscript received July 31st, 1990)

ABSTRACT

The effects of mobile phase composition on the reversed-phase separation of several dipeptides and tripeptides with a γ-cyclodextrin-bonded-phase column have been studied. The addition of organic modifier (*i.e.* methanol) into the aqueous buffer (pH 4.65) mobile phase causes a minimum capacity factor value to be observed for each peptide. This is interpreted to result from two retention mechanisms involved in the separation. The adsorption process causes the retention time to decrease as the water content in the mobile phase is increased. The inclusion process acts in the opposite fashion. The presence of Cu(II) salt in the mobile phase allows further modifications of separation selectivity. This is because the peptide conformation changes upon Cu(II) complexation which in turn alter the hydrophobicity and/or inclusion stability of the peptide. The effects of mobile phase pH (3.6–5.6) and ionic strength (0.001–0.06) were not significant in the present application. Studies with a β-cyclodextrin column show similar results.

INTRODUCTION

Stable cyclodextrin (CD)-bonded phases were recently developed to be used in a traditional reversed-phase mode for the separation of enantiomers [1–8]. Examples of compounds resolved include dansyl and naphthyl amino acids, several aromatic drugs, steroids, alkaloids, metallocenes, binaphthyl crown ethers, aromatic acids, aromatic amines and aromatic sulfoxides. It seems that aromatic groups are necessary for effective enantioselective separations by an inclusion process on cyclodextrin columns. The degree of inclusion determines retention and resolution, which in turn can be controlled by altering the amount of organic modifiers (*e.g.*, methanol, 2-propanol and acetonitrile) in the mobile phase. However, aromatic groups are not necessary for inclusion complex formation or extensive retention. Alkanes and

[a] Part of this paper was presented at the *11th International Symposium on Column Liquid Chromatography, Amsterdam, June 1987.*

[b] Present address: Contrast Media Department, Bristol-Myers Squibb Pharmaceutical Research Institute, New Brunswick, NJ 08903-0191, U.S.A.

0021-9673/90/$03.50

hydrocarbons all bind tightly to cyclodextrins but are probably too flexible to show enantioselectivity.

In addition to chiral separations, CD-bonded phases have been used as conventional column packings for the separation of organometallic compounds, polynuclear aromatic hydrocarbons, substituted phenols, benzoic acids, and anilines, and styrene polymers, in both normal- and reversed-phase modes [9–15]. The use of a β-CD-bonded column for the separation of a selected group of dipeptides was explored [16]; however, detailed study was lacking.

To further test the versatility of CD-bonded phases as "universal" packings, we have performed their separations of dipeptides and tripeptides under various mobile phase conditions. In particular, a study is performed with the presence of copper(II) ions in the mobile phase which allows further modifications of retention behaviors. The results are reported in this paper.

EXPERIMENTAL

A Beckman Model 332 gradient liquid chromatographic system was used for the CD-bonded column separation. This system was equipped with two Model 110A pumps, a Model 210 sample injector valve and a Model 420 system controller. A Waters Model 440 absorption detector (254 nm) and an Omniscribe Model D5000 recorder were also applied.

The CD-bonded-phase columns (both β-CD and γ-CD) were obtained from Advanced Separation Technologies. The peptide analytes were obtained from Sigma and used without further purification. HPLC-grade solvents were obtained from Fisher Chemical. A total of 18 dipeptides and tripeptides were selected for this study. All have aromatic ring(s) which can form inclusion complexes with the cyclodextrin and can be easily detected at 254 nm. Cu(II) acetate (Aldrich) was used to prepare mobile phase solutions. The mobile phase was prepared using aqueous buffer and HPLC-grade methanol. Aqueous buffer solutions were prepared using acetic acid and ammonium acetate. Ionic strength was 0.01 *M* for most mobile phases unless otherwise stated. Before the separation experiments, the columns were pre-equilibrated for about 3 h using the mobile phase. After equilibrium was achieved, a flow-rate of 1 ml/min was used in the chromatographic process. For each separation, the peptides (0.1 m*M*) were dissolved in a solution containing the mobile phase. A back pressure of about 2000 p.s.i. was usually observed. All data points were collected by averaging more than three reproducible separations.

RESULTS AND DISCUSSION

Effects of organic modifier on peptide retention

Table I lists the values of capacity factors (k') of the dipeptides and tripeptides at various binary (methanol–aqueous buffer, pH 4.65) mobile phase compositions using a γ-CD column. It is seen that for each peptide there is a solvent composition that gives the lowest k' value, *i.e.*, the plot of k' *vs.* increasing organic modifier concentration is parabolic in shape which is in contrast to the linear relationship (plotted on a logarithmic scale) for non-cyclodextrin type columns [17]. This solvent composition is, in most cases, methanol–buffer (20:80). These minimum k' values increase when the

TABLE I

DEPENDENCE OF k' ON MOBILE PHASE COMPOSITION FOR DI- AND TRIPEPTIDES USING A γ-CD COLUMN

An asterisk indicates where the lowest k' value is observed.

Peptide	k'							
	Aqueous buffer–methanol							
	20:80	30:70	40:60	50:50	60:40	80:20	95:5	100:0
L-Trp–L-Phe	1.937		1.689		1.254*	1.305	2.365	3.698
L-Phe–L-Ala	1.273		1.216		0.749	0.444*	0.511	0.810
L-Ala–L-Trp	0.937		0.486		0.413	0.378*	0.533	0.765
L-Ala–L-Tyr	0.832		0.349		0.216	0.105*	0.105	0.133
L-Val–L-Trp	1.387		0.762		0.663	0.571*	0.917	1.429
L-Val–L-Phe	1.241		0.603		0.537	0.387*	0.578	0.968
Gly–L-Phe	0.873		0.387		0.356	0.219*	0.287	0.419
Gly–D-Phe	0.873		0.375		0.355	0.167*	0.268	0.397
Gly–L-Tyr	0.759		0.260		0.257	0.095	0.079*	0.105
L-Val–L-Tyr	1.241		0.556		0.454	0.206*	0.210	0.295
Gly–L-Trp	1.010		0.492		0.476	0.365*	0.476	0.683
Gly–L-Phe–L-Phe	0.686	0.508		0.371	0.369*	0.483	1.397	2.365
DL-Leu–Gly–DL-Phe	0.667	0.476		0.289*	0.308	0.365	1.11, 1.15	2.02, 2.16
L-Tyr–Gly–Gly	1.476	1.086		0.581	0.546	0.460	0.415*	0.765
L-Val–L-Tyr–L-Val	0.863	0.670		0.365	0.327	0.257*	0.400	0.635
L-Trp–Gly–Gly	1.762	1.210		0.508	0.470	0.283	0.206*	0.222
Gly–Gly–L-Phe	1.254	0.711		0.340	0.289	0.229*	0.292	0.429
Gly–L-Phe–L-Ala	0.829	0.505		0.317	0.244	0.210*	0.343*	0.552

methanol content in the mobile phase is either increased or decreased. Similar phenomena were also observed when substituted phenols and anilines were separated using CD colunns except that the solvent composition provided the lowest k' values contained more organic modifier, *i.e.*, 2-propanol–water (80:20) [13].

A tentative rationalization of this observation can be provided if it is assumed that at least two mechanisms are involved in the retention of solutes. The first retention mechanism is the adsorption process which occurs between the peptides and the polar groups at the surface of the stationary phase. The major interactions of the adsorption process are the hydrogen bonding and ion–dipole interactions. These interactions gradually diminish as the water content in the mobile phase is increased. This also causes a concomitant decrease of peptide k' values.

Another retention mechanism is the inclusion of the peptides into bonded cyclodextrins. The degree of inclusion can be mediated by the amount of organic modifier. In general, inclusion is favored if the mobile phase is more hydrophilic. Thus, the peptides are held more tightly when the water content in the mobile phase is higher, *i.e.*, greater k' values.

It is believed that when the methanol content is high, the adsorption process is dominant, which causes the peptide k' value to decrease with increasing water content in the mobile phase. This decrease in k' value is stopped when a lowest k' value is reached. Upon further increase of water content in the mobile phase, the inclusion process prevails and the k' value increases.

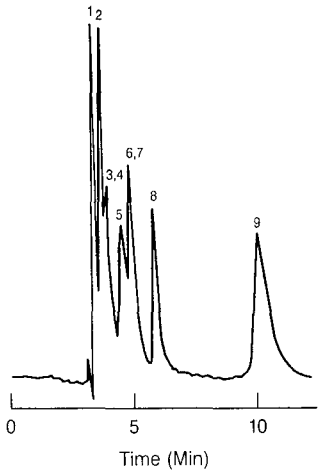

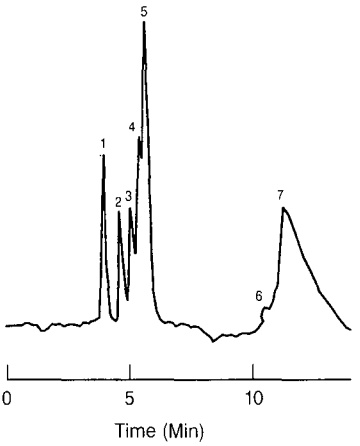

Fig. 1. Chromatogram for the separation of several dipeptides, γ-CD column, methanol–aqueous buffer (5:95), pH 4.65, flow-rate 1 ml/min. Peaks: 1 = Gly–L-Tyr; 2 = L-Val–L-Tyr; 3 = Gly–L-Phe; 4 = Gly–D-Phe; 5 = L-Phe–L-Ala; 6 = L-Ala–L-Trp; 7 = L-Val–L-Phe; 8 = L-Val–L-Trp; 9 = L-Trp–L-Phe.

Fig. 2. Chromatogram for the separation of several tripeptides, γ-CD column, 100% aqueous buffer, pH 4.65, flow-rate 1 ml/min. Peaks: 1 = L-Trp–Gly–Gly; 2 = Gly–Gly–L-Phe; 3 = Gly–L-Phe–L-Ala; 4 = L-Val–L-Tyr–L-Val; 5 = L-Tyr–Gly–Gly; 6 = DL-Leu–Gly–DL-Phe; 7 = Gly–L-Phe–L-Phe.

The presence of the inclusion process can be further substantiated when a peptide contains more hydrophobic functional groups, *e.g.*, Gly–L-Phe–L-Phe and DL-Leu–Gly–DL-Phe. A much greater increase of k' value (as compared to those peptides with less hydrophobic functional groups) is observed when the water content is increased in the mobile phase. This is evident particularly when the water content is high, *e.g.*, 80%.

Figs. 1 and 2 show the chromatograms of several dipeptides and tripeptides at mobile phase compositions of 5% methanol in aqueous buffer and 100% aqueous buffer (pH 4.65), respectively. In the two cases, the organic modifier content is low to take advantage of substrate inclusion for chromatographic resolution. However, it is also possible to apply greater amount of organic modifier to diminish the inclusion and to increase the adsorption process for substrate resolution. For example, Fig. 3 shows the separation of a mixture of selected dipeptides and tripeptides using methanol–aqueous buffer (50:50) as the mobile phase.

Effects of mobile phase pH and ionic strength on peptide retention

The effect of mobile phase pH on peptide retention is examined with acetic acid–ammonium acetate buffer solutions at pH 5.6, 4.6 and 3.6 with an ionic strength of 0.01 *M*. The results shown in Table II indicate that the variation of mobile phase pH does not drastically affect the peptide retention. This is probably because the peptides in their zwitter ionic form are the dominant species in this pH range. A mobile phase pH 4.65 is chosen for further testing of the mobile phase ionic strength effect on peptide retention.

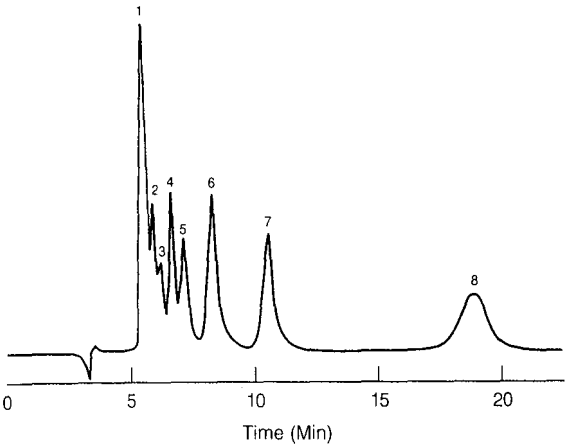

Fig. 3. Chromatogram for the separation of several dipeptides and tripeptides, γ-CD column, methanol–aqueous buffer (50:50), pH 4.65, flow-rate 1 ml/min. Peaks: 1 = Gly–L-Tyr; 2 = Gly–D-Phe; 3 = Gly–L-Tyr–L-Ala; 4 = Gly–L-Phe–L-Ala; 5 = Gly–L-Phe–L-Leu; 6 = Gly–L-Phe–L-Phe; 7 = L-Phe–Gly; 8 = L-Phe–L-Tyr.

Table II also shows the retention data of peptides obtained at three different mobile phase ionic strength, *i.e.*, 0.06, 0.01 and 0.001 *M*. It turns out that the mobile phase ionic strength is not very significant in changing the peptide retention times. However, for practical applications, ionic strength cannot be too high in order to avoid precipitation of the buffer salt in the column. Neither can it be very low in order to

TABLE II

RETENTION TIMES OF A SERIES OF PEPTIDES WITH pH AND IONIC STRENGTH USING A γ-CD COLUMN

Peptide	Retention time (min)					
	pH dependent: total ionic strength of buffer 0.01 *M*			Ionic strength dependent: pH 4.65		
	pH			Concentration of buffer (*M*)		
	5.55	4.65	3.65	0.06	0.01	0.001
Gly–D-Phe	4.42	4.43	4.15	4.43	4.28	4.12
Gly–L-Phe	4.47	4.53	4.12	4.53	4.32	3.98
L-Phe–L-Ala	4.55	4.77	4.35	4.77	4.57	4.70
Gly–L-Tyr	3.63	3.65	3.60	3.65	3.33	3.53
L-Val–L-Trp	6.33	6.58	5.40	6.58	6.17	6.43
L-Ala–L-Tyr	3.73	3.73	3.62	3.73	3.43	3.62
L-Trp–L-Phe	12.97	12.67	12.50	12.67	10.33	10.67
Gly–L-Phe–L-Ala	4.57	4.45	4.42	4.45	4.05	4.17
Gly–Gly–L-Phe	4.38	4.42	4.32	4.42	4.02	4.37
L-Trp–Gly–Gly	4.45	4.67	4.58	4.67	4.45	4.75
L-Tyr–Gly–Gly	3.32	3.38	3.63	3.38	3.38	3.58

avoid the decrease of buffer capacity. A mobile phase with an ionic strength of 0.01–0.05 *M* is recommended for general applications.

Effect of Cu(II) ion on peptide retention

The use of metal ions and their complexes in modern liquid chromatography has been demonstrated to be a powerful technique to achieve unique separation selectivities. In general, metal ions and their complexes can be classified into two categories: substitution inert and substitution labile, based on their kinetics of ligand displacement reactions [18]. For example, copper(II) ion and its complexes are considered to be substitution labile when chromatography time scale is concerned. Depending on whether the metal ion or complex is fixed on the stationary phase or when it is moved along the column in the mobile phase, one can distinguish two types of chromatography: (1) the chromatography of ligands in which the metal ion is held by the stationary phase via strong complex formation or adsorption [19,20]; (2) the chromatography of complexes in which the metal ion is bound more strongly towards the ligands in the mobile phase [21,22]. Both approaches have been applied in the novel separation of enantiomers, *e.g.*, amino acids.

In the present study, copper(II) ions can form complexes with peptide ligands in the mobile phase. The Cu(II) ion complex formation can change the peptide conformation and therefore, their retention behavior. In Table III are listed the k' values of several peptides in the absence and presence of various concentrations of copper(II) ion in the mobile phase using a γ-CD column (pH 4.65). At the present experimental condition, a Cu(II) concentration of $1.25 \cdot 10^{-3}$ *M* or higher is required for significantly different separation selectivity. A separate spectrophotometric experiment also confirmed the presence of Cu(II)–peptide complex formation when

TABLE III

PEPTIDE RETENTION TIME AS A FUNCTION OF MOBILE PHASE COMPOSITION WITH A γ-CYCLODEXTRIN-BONDED-PHASE COLUMN

Group	Peptide	Retention time (min)				
		Mobile phase: aqueous buffer[a]–methanol				
		100:0	100:0 with $1.25 \cdot 10^3$ *M* Cu(II)	80:20 with $1.25 \cdot 10^3$ *M* Cu(II)	60:40 with $1.25 \cdot 10^3$ *M* Cu(II)	40:60 with $1.25 \cdot 10^3$ *M* Cu(II)
I	Gly–D-Phe	4.43	6.00	5.03	5.03	6.08
	Gly–L-Phe	4.53	5.88	5.27	4.97	6.13
	L-Val–L-Trp	6.58	7.20	6.33	5.87	6.58
	L-Ala–L-Tyr	3.73	9.30	7.00	5.78	6.10
	L-Trp–Gly–Gly	4.67	5.87	5.17	7.00	10.00
	L-Tyr–Gly–Gly	3.38	4.60	4.23	5.27	8.33
II	L-Phe–L-Ala	4.77	3.92	5.10	3.50	4.42
	Gly–L-Tyr	3.65	3.17	5.55	3.58	4.63
	L-Trp–L-Phe	12.67	7.67	5.27	5.25	6.00
	Gly–L-Phe–L-Ala	4.45	3.92	5.33	3.63	4.23
	Gly–Gly–L-Phe	4.42	4.10	5.13	5.03	6.83

[a] pH 4.65 acetic acid–acetate buffer, ionic strength 0.01 *M*; 25°C.

Cu(II) concentration is greater than $1.25 \cdot 10^{-3}$ *M* since the complex has a characteristic UV absorption band at 230 nm.

A careful examination of the peptide retention data using aqueous buffer in the absence and presence of $1.25 \cdot 10^{-3}$ *M* Cu(II) ion shows that the retention times increase for some peptides (group I) and decrease for others (group II), upon complexation with Cu(II) ion. It is still reasonable to assume that when an aqueous buffer solution is used as the mobile phase without the organic modifier, the contribution to retention by inclusion of Cu(II)–peptide complex is the greatest, as compared to those mobile phases containing some amount of organic modifier. Thus, the group I peptides which result in longer retention times upon Cu(II) ion complexation may either form stronger cyclodextrin inclusion complexes due to favorable conformational change, or be less hydrophilic than the corresponding uncomplexed ones, or be both. On the other hand, the group II complexed peptides with shorter retention times (than the uncomplexed ones) should be more hydrophilic or less readily to form cyclodextrin inclusion complexes or both, upon Cu(II) ion complexation.

Further testing of the above hypothesis can be performed by adding methanol to the mobile phase. The addition of methanol to the mobile phase should decrease the retention time for those group I peptides which are more hydrophobic and/or form stronger inclusion complex upon complexation because methanol can compete for inclusion with the cyclodextrin and also make the mobile phase more hydrophobic. This is observed as expected, as shown in Table III. The group II peptides which give shorter retention times upon Cu(II) ion complexation can be held either longer or shorter, depending on the prevailing retention mechanism in the CD column, when methanol is introduced into the mobile phase. If the shortening of retention time is due to unfavorable inclusion and increased hydrophilicity (less adsorption), the increase of methanol content in the mobile phase would make it more hydrophobic, thus results in more substrate adsorption and increased retention. It would also further reduce the inclusion, thus results in decreased retention. The net effect would be determined by the extent of contribution to retention by the two mechanisms. A quantitative prediction of retention contribution by the two proposed mechanisms is not possible at this moment. However, the experimental results indicate that four out of five peptides tested have increased retention upon addition of methanol (Table III). One peptide, L-Trp–L-Phe, shows further decrease in retention time. Tests with other peptides such as Gly–L-Phe–L-Leu and Gly–L-Phe–L-Phe also show similar decrease in retention time.

Both groups of complexed peptides eventually show increased retention times after minimum k' values are achieved, as explained previously (Table III). Fig. 4 is the chromatogram for the separation of several dipeptides and tripeptides using a γ-CD column with $1.25 \cdot 10^{-3}$ *M* Cu(II) ion in the mobile phase. It is observed that the retention orders of these peptides are indeed different from that without the presence of Cu(II) ion in the mobile phase. For example, the retention order of Gly–L-Phe–L-Leu and Gly–L-Phe–L-Ala in Fig. 4 is reversed in Fig. 3. On the other hand, the peptide peaks in the chromatogram are in general broader than those without Cu(II) ion. This indicates that the Cu(II) ion complexation equilibrium may have caused additional zone broadening in the present case.

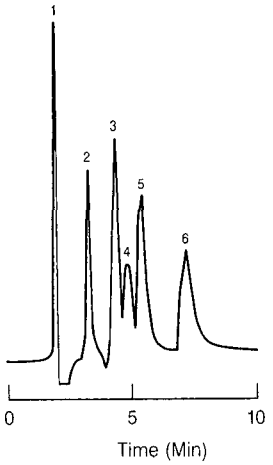

Fig. 4. Chromatogram for the separation of several dipeptides and tripeptides, γ-CD column, ammonium acetate–acetic acid buffer, [Cu(II)] = $1.25 \cdot 10^{-3}$ *M*, pH 4.65, flow-rate 1 ml/min. Peaks: 1 = system peak; 2 = Gly–L-Tyr; 3 = Gly–L-Phe–L-Leu; 4 = Gly–L-Phe–L-Ala; 5 = L-Val–L-Tyr; 6 = L-Phe–Gly.

Comparison of β-CD and γ-CD columns

Tables IV and V list the retention times of some selected peptides in the absence and presence of $1.25 \cdot 10^{-3}$ *M* Cu(II) ion in the mobile phase buffer solutions, respectively. The general observations for the separations using the γ-CD column are also observed for the β-CD column, *i.e.*, minimum k' values and selectivity change upon Cu(II) ion complexation. The mobile phase composition to observe minimum k' values now shifts to methanol–aqueous buffer (40:60) indicating that β-CD columns afford stronger inclusion complex formation with the peptides. This is consistent with the general notion that the binding of aromatic substrates with β-cyclodextrin is stronger than that with γ-cyclodextrin presumably because of a better cavity size fit [14]. Further comparisons are difficult because the cyclodextrin columns have different

TABLE IV

DEPENDENCE OF RETENTION TIME ON MOBILE PHASE COMPOSITION FOR SOME PEPTIDES USING A β-CD COLUMN

Peptide	Retention time (min)			
	Methanol–aqueous buffer[a]			
	0:100	20:80	40:60	60:40
L-Phe–L-Ala	4.76	4.30	5.60	7.32
L-Ala–L-Tyr	4.18	3.91	4.00	4.40
L-Val–L-Trp	6.10	5.05	5.25	5.45
Gly–L-Phe–L-Ala	4.49	4.09	4.20	4.80
L-Val–L-Tyr–L-Val	4.95	4.26	4.50	5.48
DL-Leu–Gly–DL-Phe	6.90	4.67	4.52	5.00

[a] pH 4.65 acetic acid–ammonium acetate buffer, ionic strength 0.01 *M*.

TABLE V

DEPENDENCE OF RETENTION TIME ON MOBILE PHASE COMPOSITION FOR SOME PEPTIDES USING A β-CD COLUMN

[Cu(II)] = $1.25 \cdot 10^{-3}$ *M*; ammonium acetate–acetic acid buffer (0.01 *M*), pH 4.65.

Peptide	Retention time (min)			
	Methanol–aqueous buffer			
	0:100	20:80	40:60	60:40
L-Phe–L-Ala	6.20	5.78	4.73	7.31
L-Ala–L-Tyr	6.25	5.30	4.95	6.25
L-Val–L-Trp	8.97	5.80	5.20	7.91
Gly–L-Phe–L-Ala	3.82	4.89	4.80	11.20
L-Val–L-Tyr–L-Val	7.53	3.93	3.83	7.34
DL-Leu–Gly–DL-Phe	9.78	4.60	4.20	8.33

degree of mixed surface coverage of functional groups (*i.e.*, cyclodextrin, alkyldiol and silanol groups), partly because of the difficulty of controlling the extent of surface derivatization reaction [23].

ACKNOWLEDGEMENTS

This work was supported in part by grants from the NIH-MBRS program and the Robert A. Welch Foundation of Houston, TX, U.S.A.

REFERENCES

1 D. W. Armstrong, *Anal. Chem.*, 59 (1987) 84A.
2 D. W. Armstrong, T. J. Ward, R. D. Armstrong and T. E. Beesley, *Science (Washington, D.C.)*, 232 (1986) 1132–1135.
3 D. W. Armstrong, *J. Liq. Chromatogr.*, 7 (1984) 353.
4 D. W. Armstrong and W. DeMond, *J. Chromatogr. Sci.*, 22 (1984) 411.
5 D. W. Armstrong, W. DeMond and B. P. Czech, *Anal. Chem.*, 57 (1985) 481.
6 D. W. Armstrong, T. J. Ward, A. Czech, B. P. Czech and R. A. Bartsch, *J. Org. Chem.*, 50 (1985) 5556.
7 D. W. Armstrong, W. DeMond, A. Alak, W. L. Hinze, T. E. Riehl and K. H. Bui, *Anal. Chem.*, 57 (1985) 234.
8 W. L. Hinze, T. E. Riehl, D. W. Armstrong, W. DeMond, A. Alak and T. Ward, *Anal. Chem.*, 57 (1985) 237.
9 C. A. Chang, H. Abdel-Aziz, N. Melchor, Q. Wu, K. H. Pannell and D. W. Armstrong, *J. Chromatogr.*, 347 (1985) 51–60.
10 C. A. Chang, Q. Wu and D. W. Armstrong, *J. Chromatogr.*, 25 (1986) 454–458.
11 C. A. Chang, Q. Wu and L. Tan, *J. Chromatogr.*, 361 (1986) 199–207.
12 C. A. Chang and Q. Wu, *Anal. Chim. Acta*, 189 (1986) 293–299.
13 C. A. Chang, Q. Wu and M. P. Eastman, *J. Chromatogr.*, 371 (1986) 269–282.
14 C. A. Chang and Q. Wu, *J. Liq. Chromatogr.*, 59 (1987) 1359–1368.
15 C. A. Chang, H. Ji, Q. Wu and M. P. Eastman, *Anal. Chim. Acta*, 194 (1987) 287–292.
16 H. J. Issaq, *J. Liq. Chromatogr.*, 9 (1986) 229–233.
17 W. R. Melander and Cs. Horváth, in Cs. Horváth (Editor), *High-Performance Liquid Chromatography —Advances and Perspectives*, Vol. 2, Academic Press, New York, 1980, p. 176.
18 C. A. Chang, C.-S. Huang and C.-F. Tu, *Anal. Chem.*, 55 (1983) 1390–1396.

19 J. D. Navratil, E. Murgia and H. F. Walton, *Anal. Chem.*, 47 (1975) 122–125.
20 V. A. Davavkov, S. V. Rogozhin, A. V. Senenchkin and T. P. Sachkova, *J. Chromatogr.*, 82 (1973) 359–365.
21 W. Lindner, J. N. LePage, G. Davies, D. E. Seitz and B. L. Karger, *J. Chromatogr.*, 185 (1979) 323–344.
22 E. Grushka and F. K. Chow, *J. Chromatogr.*, 199 (1980) 283–293.
23 D. W. Armstrong, *U.S. Pat.*, 4 539 399 (Sept. 1985).

Journal of Chromatography, 522 (1990) 153–162
Elsevier Science Publishers B.V., Amsterdam

CHROM. 22 732

Effect of feed flow-rate, antigen concentration and antibody density on immunoaffinity purification of coagulation factor IX

JOHN P. THARAKAN*
Department of Chemical Engineering, Howard University, 2300 6th Street NW, Washington, DC 20059 (U.S.A.)
and
DAVID B. CLARK and WILLIAM N. DROHAN
American Red Cross, Rockville, MD 20855 (U.S.A.)
(First received January 30th, 1990; revised manuscript received July 3rd, 1990)

ABSTRACT

A simple physical model of immunoaffinity chromatography (IAC) demonstrates that immobilized monoclonal antibody (MAb) capacity in IAC purification will be a function of many parameters, including feed flow-rate and antigen concentration, and MAb density (mg MAb immobilized/ml resin). We studied IAC of factor IX, and examined the effect of parameter variation on MAb capacity. MAb capacity (1) was not affected by feed flow-rate or antigen concentration, and (2) decreased as MAb density increased. (1) Suggested that diffusion of factor IX into the resin bead was not limiting. Characteristic diffusion, convection and reaction times were calculated and used in dimensional analysis to compare their relative magnitudes. If MAb was assumed to be localized to the outer 10% of the bead volume, this analysis concluded that diffusion was not limiting, consistent with the suggestions of our experimental data. (2) Suggests that high MAb densities make MAb less accessible.

INTRODUCTION

The isolation and purification of proteins from complex mixtures is a current focus in bioprocessing research. Proteins may be purified by several methods such as liquid chromatography [1,2], gel electrophoresis [3], fractional precipitation and liquid–liquid extraction [4]. One method for isolating a protein to near 100% homogeneity is immunoaffinity chromatography (IAC) using monoclonal antibodies (MAbs) [5] as the affinity ligand. IAC takes advantage of the specific and reversible interaction between the MAb and the desired protein. The MAb is generated following Kohler and Milstein [5], may be produced in large quantities [6], purified [7], and immobilized on a solid support [8] which is then usually packed into a chromatography column [9] for purification of the desired protein.

Factor IX (FIX) deficiency leads to Hemophilia B, a bleeding disorder which is treated by replacement therapy [10]. The American Red Cross has developed an IAC process for purifying FIX [11]. The FIX produced has been shown to be homogeneous [12] and the process has been scaled up to 10-l columns [13].

0021-9673/90/$03.50

In this paper, first, a simple physical model of a resin bead in IAC is developed to show the dependence of MAb capacity (mg antigen/mg immobilized MAb, or, more specifically, units FIX/mg MAb) for FIX on feed flow-rate and FIX concentration, and on MAb density. Second, we use simple dimensionless analysis [14] to develop model equations to compare the relative importance of diffusion, convection and reaction in a packed IAC column. Third, we report results of experiments where the effect of varying feed flow-rate, feed FIX concentration and MAb density on MAb capacity was studied.

We demonstrate that the MAb capacity for FIX is not affected by feed flow-rate or by feed FIX concentration, and show that MAb capacity decreases with increasing MAb density. Possible reasons for these observations are suggested.

MODEL DEVELOPMENT

In IAC, feed containing the protein to be purified is pumped into a packed column containing resin beads on which MAb against the desired protein (or antigen) has been immobilized. The antigen binds to the MAb while contaminating proteins are washed through. Column conditions are subsequently altered permitting the MAb to release the antigen, yielding a homogeneous protein product.

Studying an individual resin bead, as shown in Fig. 1, several variable groups that mediate MAb capacity for antigen, are evident. These are: (1) the bead, (2) the MAb, (3) the antigen (FIX, in this instance), and (4) kinetics, and are described in detail below.

(1) Bead: the radius of the particle has been used as a measure of a characteristic diffusion distance [14]. Bead porosity affects the movement of protein in the bead, but is not considered explicitly because it is fixed upon choice of a particular commercial resin.

(2) MAb (or other ligand): Eveleigh and Levy [15] have shown that decreasing ligand density increases the efficiency of antigen capture. With immobilized MAb (IMAb), orientation also affects the efficiency of antigen capture. Typically, a MAb is represented as a Y-shaped structure, with the two "arms" of the Y having the antigen-binding sites (the Fab regions) while the third "leg" is called the constant region (Fc) [16]. If the Fc portion of the molecule is bound to the bead, the MAb will, potentially, be 100% active. If the Fab regions attach to the bead, the MAb may be less active. In all our experiments the method of coupling was the same and thus orientation of MAb is not considered as an independent variable.

The depth and homogeneity of MAb coupling may also affect the efficiency of antigen capture. Lasch *et al.* [17] concluded that radial gradients of ligand are present which are symmetric around the center of the bead. Carleysmith *et al.* [18] found that the depth of immobilized protein penetration depended on initial protein concentration in the immobilization mixture as well as the contact time between the resin bead and the protein. At a bulk protein concentration of 2 mg/ml, they found that only 13% of the outer radial depth of the bead had been penetrated at saturation. This has implications for the assumed diffusion distances used in modelling. If the IMAb does not penetrate homogeneously throughout the bead, the actual diffusion distance may be the MAb penetration depth, which may be estimated if the immobilization conditions are known and following the empirical correlations that can be deduced

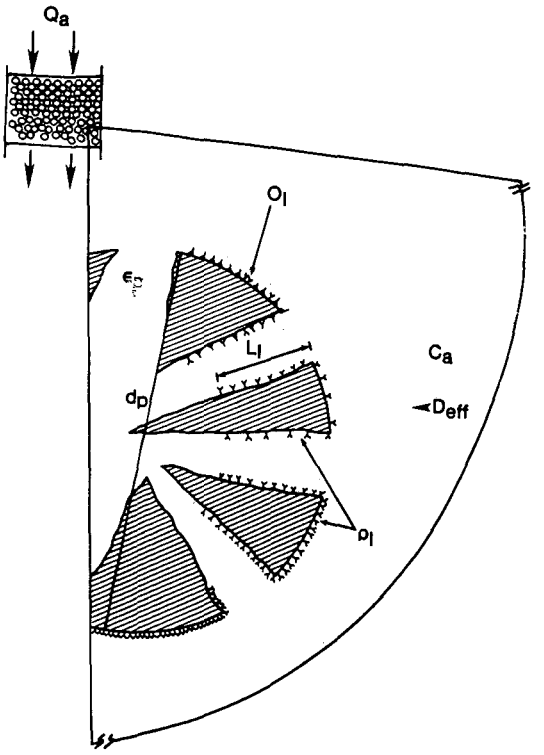

Fig. 1. Expanded view of a bead within an affinity column. C_a is the bulk concentration of FIX which flows past the beads at a flow-rate Q_a. The beads are of porosity ε_p, of diameter d_p (radius r_p), and have MAb (represented here as Y's) immobilized on them. The MAb is immobilized at a certain density, ρ_l, depth, L_l, and orientation, O_l.

from Carleysmith *et al.* [18]. In this work MAb penetration depth was not measured.

(3) FIX (or other antigen): FIX concentration and effective diffusion coefficient will affect the penetration of FIX into the bead. The diffusion coefficient will be fixed for a particular solute under set conditions and so $D_{eff,a}$ is not considered as a variable. Increasing the bulk FIX concentration may, however, enhance FIX flux into the bead. Also, slower bulk FIX feed flow-rates may offer longer times for antigen binding to MAb, which may be important if the kinetics of antigen–MAb binding are slow.

(4) Kinetics: the rate of FIX–MAb coupling in solution is the intrinsic association rate and will be a constant, as for any specific MAb–antigen pair at defined conditions. Upon immobilization, the rate of association is modified due to conformational changes in the IMAb as well as steric hindrances. Consequently, an adsorption rate constant must be measured with IMAb as was done here (see Table I). This parameter will be fixed for this MAb–FIX pair, and thus k_{ads} is considered constant in the equations.

Other factors may be involved such as the kinetics of cross reaction of the MAb with non-specific proteins. However, these interactions have been shown to be unimportant in this system [12] and have been excluded from the model development.

TABLE I

VARIABLES USED IN ANALYSIS

Parameter group	Parameter	Symbol	Value	Reference
Bead	Radius	r_p (= $d_p/2$)	80 μm	27
Ligand	Density	ρ_l	0.5–10 mg MAb/ml resin	12[a]
	Depth of penetration	L_l	8–80 μm	18
	Orientation	O_l[b]	–	–
Antigen (FIX)	Bulk concentration	C_a	7–115 units/ml	12[a]
	Effective diffusion coefficient	$D_{eff,a}$	$6 \cdot 10^{-7}$ cm^2/s	26
	Flow-rate	Q_a	0.003–0.02 cm^3/s	12[a]
Kinetics	Adsorption constant	k_{ads}	2 units FIX/(ml $\cdot$ s^{-1})	[c]

[a] Value from this study.

[b] A numerical value for O_l is difficult to establish. It may, for example, range from 0.0, completely inactive MAb, to 1.0, where the MAb may be coupled to the resin by the Fc region and be 100% active; the symbol is provided to show that this is a parameter that may affect MAb capacity.

[c] Calculated from a batch kinetic experiment: MAb resin was mixed in a plastic beaker with feed material. Samples were removed at short time intervals through a syringe filter and the FIX activity was assayed. Plotting the decrease in supernatant FIX concentration as a function of time yielded a preliminary value for an adsorption rate constant. On desorption, the FIX eluted at an equal rate; data not shown.

Table I lists the variables. Defining the capacity of the MAb as moles of FIX bound per mole of MAb, the following functional relationship may be written:

$$\begin{aligned} \text{Capacity} &= (\text{moles FIX/mole MAb or units of FIX/mg MAb}) \\ &= f(r_p, \rho_l, L_l, C_a, Q_a, D_{eff,a}, k_{ads}, \ldots) \end{aligned} \tag{1}$$

Eqn. 1 may be simplified by eliminating the parameters considered as fixed. It then becomes:

$$\text{Capacity} = f(\rho_l, C_a, Q_a) \tag{2}$$

Following this equation, we designed our experiments to examine the effect on MAb capacity of variation of feed flow-rate and FIX concentration, and the MAb density.

It is also useful to estimate the relative importance of convection, diffusion and reaction. We may use the parameters enumerated above to estimate relative diffusion, convection and reaction times. We can utilize C_a, Q_a, $D_{eff,a}$ and r_p to define a Peclet and a Damkohler number [19]:

$$\text{Peclet number} = Pe = \frac{\text{Characteristic diffusion time}}{\text{Characteristic convection time}} \tag{3a}$$

$$= \frac{[(r_p)^2]/D_{eff,a}}{(V_o/Q_a)} \tag{3b}$$

and

$$\text{Damkohler number} = Da = \frac{\text{Characteristic diffusion time}}{\text{Characteristic reaction time}} \quad (4a)$$

$$= \frac{[(r_p)^2]/D_{\text{eff,a}}}{(C_{\text{o.a}}/k_{\text{ads}})} \quad (4b)$$

Using typical values for the parameters as shown in Table I, *Pe* and *Da* for each experiment may be calculated. If a system is not limited by diffusion, *Pe* should be much less than one [14]. A large *Da* would imply that the diffusion time is very large or the antibody–antigen kinetics are slow. Slow binding kinetics may be possible for ligands other than MAbs. *Da* should be less than or equal to one, which implies that the rate of antigen binding to the IMAb is equal to or greater than the rate of antigen diffusion to the IMAb.

MATERIALS AND METHODS

Monoclonal antibody and resins

A monoclonal antibody to FIX that binds FIX in the presence of divalent cations was obtained from ascites fluid [20], purified [12], and coupled at a resin–MAb density of 1.6 mg MAb/ml resin to cyanogen bromide-activated Sepharose CL2B (Pharmacia) following the protocol of March *et al.* [21]. In this method, purified MAb solution was mixed with cyanogen bromide-activated Sepharose CL2B resin beads overnite in the cold. The resin was then washed to remove all non- or loosely bound MAb and then blocked. The amount of IMAb was determined by measuring the total protein remaining in the supernatant of the coupling mixture after MAb immobilization, as well as the protein in the resin washes, and then subtracting this sum from the total protein that was in the initial coupling mixture. Dividing this by the total volume of resin provided the amount of MAb immobilized per unit volume of resin. The amount of MAb on the resin bead was also varied to yield IAC resins with MAb densities of 0.5, 1.0, 2.96, 8.12 and 9.67 mg MAb/ml resin, respectively.

Experimental protocol for purification of FIX

The coupled resin was packed in an Amicon G10X150 Column, forming a bed of volume 7.5 cm^3. The column was equilibrated with five column-volumes of 10 m*M* magnesium chloride, 100 m*M* sodium chloride, 20 m*M* Tris, pH 6.8 buffer at a flow-rate of 1.5 ml/min. The FIX source to be used as the load material was an eluate from DEAE Sephadex adsorption of cryo-poor plasma [22]. Magnesium chloride at 1 *M* was added to this material to bring the final magnesium ion concentration to 40 m*M*. The load material was then pumped onto the column. Subsequently, the column was washed with 10 m*M* magnesium chloride, 1 *M* sodium chloride, 20 m*M* Tris, pH 6.8 buffer until the absorbance at 280 nm was below 0.09. At this point the buffer was changed to 20 m*M* sodium citrate, 110 m*M* sodium chloride, pH 6.8 which yielded one eluate peak. Column effluent pools of load, unadsorbed, wash and eluate were assayed for protein and FIX clotting activity. The affinity columns were regenerated by washing with 2 *M* sodium chloride and were re-used a minimum of ten

times during the course of this study and process development (over a year) with no noticeable decrease in either purity of the FIX obtained or in MAb capacity. All chemicals were reagent grade from Sigma.

In the first series of experiments the column volume was kept at 7.5 cm^3 and the flow-rates were varied from 0.19 to 1.4 ml/min. The MAb density was 1.6 mg MAb/ml resin and inlet FIX concentration was 50 units/ml for all the experiments. These flow-rates gave mean residence times in the column of 5.4, 12.5, 21 and 39 min, respectively.

Second, the inlet FIX concentration was varied from 7 to 115 units/ml. The flow-rate was kept constant at 0.6 ml/min and the column volume was 7.5 cm^3. The experiments were performed with resin that had a MAb density of 1.6 mg MAb/ml resin.

In the third series of experiments, MAb density was varied. MAb densities of 0.5, 1.0, 1.6, 2.96, 8.12 and 9.67 mg MAb/ml resin were obtained by using different initial concentrations of MAb in the immobilization mixture. The feed FIX concentration was 50 units/ml, mean residence time was 5 min, and the column volume was 7.5 cm^3.

The columns used in all experiments were identical. In all experiments, the amount of FIX activity bound was determined by subtracting the unadsorbed FIX activity from the total FIX activity loaded. A constant ratio of total FIX loaded per mg coupled MAb was maintained for all experiments. The experiments were repeated a minimum of three times and the data is presented as the mean $\pm$ one standard deviation.

Protein assays

Absorbance at 280 nm was used to measure protein content. Protein mass was estimated using a FIX extinction coefficient of 13.3 [23] for a 1% solution.

Coagulation assays

FIX activity was measured by a standard one-stage coagulation assay as described by Biggs [24] using FIX-deficient plasma (George King). Samples were pre-diluted in a buffer containing bovine albumin and Tween 20, as described by Miekka [25], to approximately one unit FIX/ml. Pooled fresh frozen plasma was used as the standard. The FIX activities were calculated from a semi-log plot. Further details of the assay method are given in Tharakan *et al.* [12].

RESULTS AND DISCUSSION

Fig. 2 shows the capacity of MAb for FIX at varying feed FIX concentrations. The MAb capacity remained similar when the bulk FIX concentration was changed from 7 to 115 units/ml. FIX diffusive flux into the bead is proportional to its bulk phase concentration. The relative invariance of MAb capacity with FIX concentration suggests that FIX diffusion into the bead is not limiting in this concentration range. Since the capacity of the MAb does not increase with increasing bulk phase concentration, and thus probable increasing penetration of FIX into the bead, there may not be MAb molecules immobilized deeper in the resin bead; instead, MAb may be localized near the surface of the bead. In this event, diffusion distances cannot be assumed to be the radius of the bead but are probably smaller and of the order of the depth of penetration of the MAb into the bead.

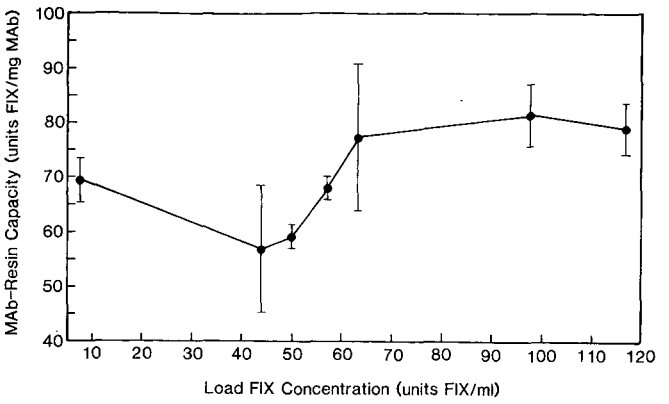

Fig. 2. Effect of feed factor IX concentration on the capacity of the MAb.

The effect of varying mean residence time on MAb capacity is shown in Fig. 3. Although the mean residence time was varied from 5 to 39 min, MAb capacity remained similar. In a diffusion limited system, increasing the mean residence time should increase the capacity of the MAb as the antigen has more time to diffuse into the bead and bind to any MAb that may be immobilized deeper in the bead. The lack of significant variation in MAb capacity with mean residence time suggests that the system is not diffusion limited. If the antibody were localized to the outer bead radius, the diffusion distances would be small, and increasing the contact time between FIX and the bead would not increase access to the MAb.

Fig. 4 compares the capacity of the MAb for different MAb densities and shows that the capacity of the IMAb increases as the MAb density decreases. For a density of 1.6 mg MAb/ml resin, the average capacity was 80 units of FIX/mg of MAb. If one assumes a molar ratio of 2:1 for FIX–MAb coupling, and a molecular weight ratio of 1:3 for FIX:MAb [10,13], the theoretical upper MAb capacity limit would be

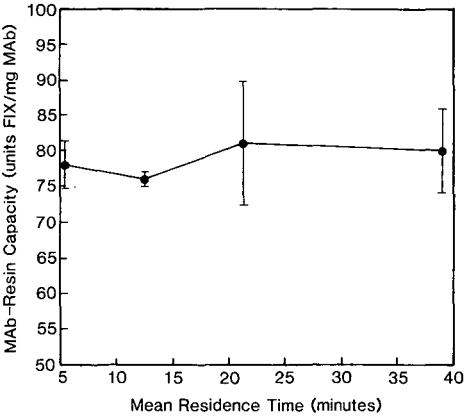

Fig. 3. Effect of mean residence time (column volume divided by bulk antigen flow-rate) on the capacity of the MAb.

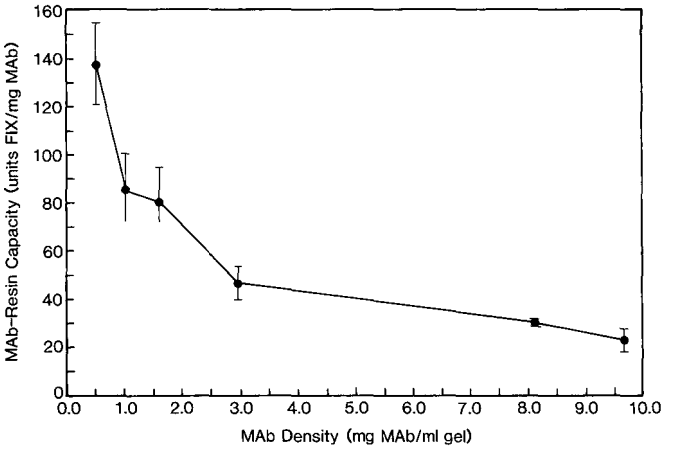

Fig. 4. Effect of resin MAb density on the capacity of the MAb.

133.3 units FIX per mg MAb, assuming a specific activity for FIX of 200 units/mg [20]. With this theoretical maximum, at 1.6 mg MAb/ml resin, 61% of MAb is active in binding FIX, while only 17% of MAb is active with resin at 9.67 mg MAb/ml resin.

Eveleigh and Levy [15] observed that increasing antibody density on an affinity resin decreases the capacity of the antibody for antigen. They noted that although a low antibody density yielded a matrix with low binding capacity per unit volume, binding capacity per unit of antibody was high. Chase [9] concluded that low binding per unit volume of resin was desirable for efficient adsorption operations. These observations and our results suggest that optimum MAb use will obtain at lower resin MAb densities. This has important implications for IAC process development, since MAb cost is a crucial process viability determinant.

Brandt *et al.* [14] analysed resin and membrane based IAC and suggested that $Pe \ll 1$ (of order 0.001) for non-diffusion limited IAC. They based their analysis on the assumption that a characteristic diffusion distance was bead radius. The range of *Pe* (eqn. 3b) in our experiments where the flow-rates were varied is 0.04 to 0.33, consistent with apparent diffusion limitation. Additionally, if the reaction time is equal to or smaller than the diffusion time, FIX will bind as soon as it diffuses to the immobilized MAb. For the experiments where the inlet concentration of FIX was varied, *Da* (eqn. 4b) ranges from 2 to 31, which is also suggestive of diffusion limitation. The IAC of FIX appears, however, to be non-diffusion limited within the parameter ranges of concentration and flow examined here.

This apparent contradiction may result from the assumption that MAb is homogeneously distributed throughout the bead. Lasch *et al.* [17] have shown that this is usually not the case. Also, following Carleysmith *et al.* [18], protein immobilized on a resin bead only penetrates a certain radial depth into the bead, depending on protein concentration in the initial immobilization mixture and the length of immobilization. Considering the conditions of immobilization employed here and generalizing the results of Carleysmith to our MAb, the MAb may only be immobilized to the outer 10% of the bead. If this is the case, we may consider the actual diffusion distance to be

10% of r_p or about 8 μm. Recalculating *Pe* (eqn. 3b) and *Da* (eqn. 4b) with $r_p = 8$ μm, the ranges of *Pe* and *Da* are $0.0004 < Pe < 0.0033$ and $0.2 < Da < 3$, respectively. These values suggest the system is not diffusion limited and are consistent with the suggestions of the data.

CONCLUSION

The use of immunoaffinity chromatography as a tool for generating very pure preparations of a single protein is becoming increasingly common in the biotechnology industry. Understanding the fundamental transport and kinetic phenomena that occur is essential for efficient process design and optimum operation. This paper provides an empirical approach to understanding the role that the various transport and kinetic phenomena play in the affinity chromatographic purification of Factor IX. Utilizing the methods in this study, a simple set of experiments that evaluates the effects of feed antigen concentration, mean antigen residence time and support matrix MAb density can be performed to provide information that will help optimize IAC process design.

SYMBOLS

C_a	Antigen (FIX) concentration, units/ml
C_o	Feed antigen concentration, units/ml
$D_{eff,a}$	Effective antigen diffusion coefficient, cm^2/s
Da	Damkohler number, eqn. 4
d_p	Resin bead diameter, cm
k_{ads}	Antigen adsorption rate constant, units FIX/ml $\cdot$ s^{-1}
L_l	Depth of penetration, μm
O_l	MAb orientation
Pe	Peclet number, eqn. 3
Q_a	Antigen flow-rate, cm^3/s
r_p $(= d_p/2)$	Resin bead radius, μm
V_o	Column volume, cm^3
ε_p	Resin bead porosity
ρ_l	IMAb density, mg MAb/ml resin

REFERENCES

1 R. W. Yost, L. S. Ettre and R. D. Conlon, *Practical Liquid Chromatography*, Perkin-Elmer, Norwalk, CT, 1980.
2 V. K. Garg, M. A. Costello and B. A. Czuba, in R. Seetharam, S. K. Sharma and C. McGregor (Editors), *Purification and Analysis of Recombinant Proteins*, Marcel Dekker, New York, 1990, pp. 29–54.
3 B. D. Hames and D. Rickwood (Editors), *Gel Electrophoresis of Proteins —A Practical Approach*, IRL Press, Washington, DC, 1987.
4 T. Becker, J. R. Ogez and S. E. Builder, *Biotechnol. Adv.*, 1 (1983) 247–261.
5 G. Kohler and C. Milstein, *Nature (London)*, 256 (1975) 495–497.
6 J. Feder and W. R. Tolbert (Editors), *Large-Scale Mammalian Cell Culture*, Academic Press, Orlando, FL, 1985.
7 V. K. Garg, R. Tyle and B. P. Ram (Editors), *Targeted Diagnosis and Therapy, Vol. III, Targeted Therapeutic Systems*, Marcel Dekker, New York, 1990, pp. 45–73.
8 J. S. Garvey, N. E. Cremer and D. H. Sussdorf, *Methods in Immunology*, WA Benjamin, Reading, MA, 3rd ed., 1977, pp. 245–255.

9 A. H. Chase, *Chem. Eng. Sci.*, 39 (1984) 1099–1125.
10 C. Michalski, F. Bal, T. Burnouf and M. Goudemand, *Vox Sang.*, 55 (1988) 202.
11 W. H. Velander, C. L. Orthner, J. P. Tharakan, R. D. Madurawe, A. H. Ralston, D. K. Strickland and W. N. Drohan, *Biotechnol. Prog.*, 5 (1989) 119.
12 J. Tharakan, D. Strickland, W. Burgess, W. N. Drohan and D. Clark, *Vox Sang.*, 58(1) (1990) 21.
13 J. P. Tharakan, S. I. Miekka, H. E. Behre, B. D. Kolen, D. M. Gee, W. N. Drohan and D. B. Clark, *Thromb. Haemostas.*, 62 (1989) 56.
14 S. Brandt, R. A. Goffe, S. B. Kessler, J. L. O'Connor and S. E. Zale, *Bio/Technology*, 6 (1988) 779.
15 J. W. Eveleigh and D. E. Levy, *J. Solid-Phase Biochem.*, 2(1) (1977) 45.
16 L. M. Amzel and R. J. Poljak, *Ann. Rev. Biochem.*, 48 (1979) 961.
17 J. Lasch, R. Koelsch, S. Weigel, K. Blaha and J. Turkova, in T. C. J. Gribnau, J. Visser and R. J. F. Nivard (Editors), *Affinity Chromatography and Related Techniques*, Elsevier, Amsterdam, 1982, p. 245.
18 S. W. Carleysmith, M. B. L. Eames and M. D. Lilly, *Biotechnol. Bioeng.*, 22 (1980) 957–967.
19 J. Carberry, *Chemical and Catalytic Reaction Engineering*, McGraw-Hill, New York, 1976.
20 H. L. Wang, J. Steiner, F. Battey and D. Strickland, *Fed. Proc.*, 46 (1987) 2119.
21 S. C. March, I. Parikh and P. Cuatrecasas, *Anal. Biochem.*, 60 (1974) 149–152.
22 D. Menache, H. E. Behre, C. L. Orthner, H. Nunez, H. D. Andersen, D. C. Triantaphyllopoulos and D. P. Kosow, *Blood*, 64 (1984) 1220.
23 H. A. Liebman, S. A. Limentani, B. C. Furie and B. Furie, *Proc. Natl. Acad. Sci. U.S.A.*, 82 (1985) 3879.
24 R. Biggs (Editor), *Human Blood Coagulation Haemostasis and Thrombosis*, Blackwell Scientific, Oxford, 1st ed., 1972, p. 614.
25 S. I. Miekka, *Thromb. Haem.*, 58 (1987) 349.
26 J. Wei and M. B. Russ, *J. Theor. Biol.*, 66 (1977) 775.
27 *Data Sheet: Sepharose and Sepharose CL Gel Filtration Media*, Pharmacia, Uppsala, 1985.

Journal of Chromatography, 522 (1990) 163–170
Elsevier Science Publishers B.V., Amsterdam

CHROM. 22 761

Reversed-phase chromatography of *Escherichia coli* ribosomal proteins

Correlation of retention time with chain length and hydrophobicity

W. SCOTT CHAMPNEY
Department of Biochemistry, College of Medicine, East Tennessee State University, Johnson City, TN 37614 (U.S.A.)
(First received February 28th, 1990; revised manuscript received July 24th, 1990)

ABSTRACT

The elution times of 52 bacterial ribosomal proteins from a C_4 reversed-phase column have been predicted. The prediction is based upon the use of the hydrophobicity coefficients for the protein amino acid content as defined by Guo *et al.* [*J. Chromatogr.*, 359 (1986) 499–518]. A strong positive correlation was observed when the difference between predicted and observed protein retention time was plotted against the product of net hydrophobicity and natural log of protein chain length. Observations with this class of related proteins strengthens and extends the observations of Mant *et al.* [*J. Chromatogr.*, 476 (1989) 363–375]. Observed deviations from predicted chromatographic behavior can be explained for several proteins which elute as dimers or which have modified amino acid residues.

INTRODUCTION

Reversed-phase high-performance liquid chromatography has been demonstrated by several groups to be an effective and efficient method for the separation of the complex mixture of proteins found as a part of the bacterial ribosome structure [1–3]. Proteins from both subunits of the bacterial ribosome have been separated and identified by this method, using a variety of similar chromatographic techniques. Both analytical and preparative separations have been performed. The analysis has recently been extended to examine questions related to the function of particular proteins in the process of translation [4,5].

The sequences of all of these proteins are known [6]. Information about the amino acid composition has permitted a calculation of the coefficient of hydrophobicity for each protein, using the values derived by Guo *et al.* [7]. Protein hydrophobicity and chain length can be used to accurately predict the retention time for a number of unrelated proteins under several conditions of reversed-phase chromatography [8].

In this work we show the application of this method to the elution behavior of 52 bacterial ribosomal proteins, as mixtures derived from the two ribosomal subunits.

0021-9673/90/$03.50

A very strong correlation between predicted and expected elution time was found. In addition, certain predictions about protein structure and protein-protein interactions were confirmed.

EXPERIMENTAL

Materials

Acetonitrile and trifluoroacetic acid (TFA) were purchased from Pierce, as were the C_4 cartridge (BU-300, 100 × 4.6 mm I.D.) and guard columns. Ribosomal proteins were prepared from the subunits of *Escherichia coli* strain SK901 as previously described [9]. The dried proteins were dissolved in 100 μl of 66% aqueous acetic acid prior to injection.

Reversed-phase high-performance liquid chromatography

The Waters HPLC system consisted of a pair of Model 510 pumps, a U6K injector, a Model 680 gradient controller, a Model 481 Lambda Max detector and a Model 730 data module. A C_4 (butyl) cartridge and guard column were used for all separations. Gradients were run at 0.25 ml/min using 0.1% TFA in Milli-Q water (pH 2.0) as the stationary phase and 0.1% TFA in acetonitrile as the mobile phase. The detector was set at 215 nm. Samples of 400 μg of 30S proteins and 600 μg of 50S proteins were injected in 100 μl of 66% acetic acid. The proteins were eluted with a linear gradient of 30% to 50% acetonitrile for 155 min followed by a second linear gradient of 50% to 60% for 30 min. Retention times and peak areas were determined by the data module for each run. Column fractions (0.5 ml) were freeze-dried and examined for protein content by one and two dimensional gel electrophoresis as described previously [9–11].

RESULTS AND DISCUSSION

As others have shown previously, reversed-phase HPLC is an excellent method for resolving the complex mixture of similar proteins from the bacterial ribosome [1–3]. Fig. 1 shows the separation of the 30S subunit proteins of *Escherichia coli* on a C_4 column using a linear gradient for elution. The 21 proteins were resolved into 17 peaks. Identification of the proteins was carried out by one- and two-dimensional gel electrophoresis of the column fractions. The separation of the 50S subunit proteins under the same conditions is shown in Fig. 2. The 32 proteins in this mixture were resolved into 25 peaks as shown.

It has been demonstrated by Mant *et al.* [8] that the elution of different proteins from reversed-phase columns can be predicted based on the total hydrophobicity and chain length of the protein. They derived the following relationship: $\Sigma R_c - t_R = A(\Sigma R_c \ln N) + C$; where ΣR_c = the summed hydrophobicity coefficients of the protein amino acids (after Guo and co-workers [7,12]), t_R = the observed protein retention time and $\ln N$ = the natural log of the number of amino acids in the protein. A plot of this linear relationship gives a line with a slope of A and a y-intercept of C.

We have applied this method to predict the elution times of the individual 30S and 50S subunit proteins from the C_4 column. Using the data of Giri *et al.* [6] for the

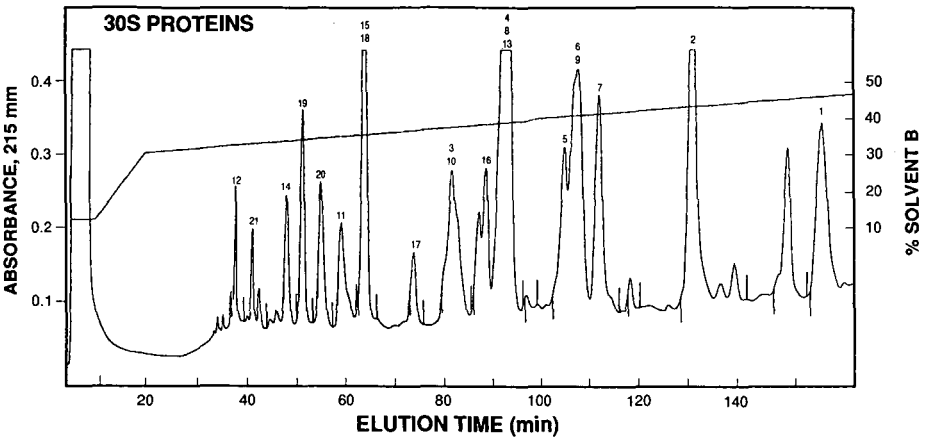

Fig. 1. C_4 reversed-phase HPLC elution profile of 30S subunit proteins. The separation of 400 μg of proteins with a linear gradient of acetonitrile (solvent B) was conducted as described in Experimental. The protein identification and gradient slope are indicated on the tracing.

amino acid composition and chain length of each protein, we have calculated the total hydrophobicity for each protein. Minor corrections in the amino acid composition of proteins S4, S9, S15, S18, L9 and L10 were made based on the DNA sequences of the genes [13–17]. The relevant values for the 30S subunit ribosomal proteins are shown in Table I. The 50S subunit protein values are compiled in Table II.

Mant *et al.* [8] have shown that the difference between predicted (ΣR_c) and observed (t_R) retention times for 23 distinct proteins is a linear function of $\Sigma R_c \cdot \ln N$, the protein hydrophobicity and chain length. This strong correlation is also true for the separated ribosomal proteins as Figs. 3 and 4 indicate. A correlation of 0.996 for the predicted and expected elution of the 30S subunit proteins was found. For the 50S proteins the correlation was 0.964. For these 52 related proteins the product $\Sigma R_c \cdot \ln N$ was a very accurate predictor of retention time.

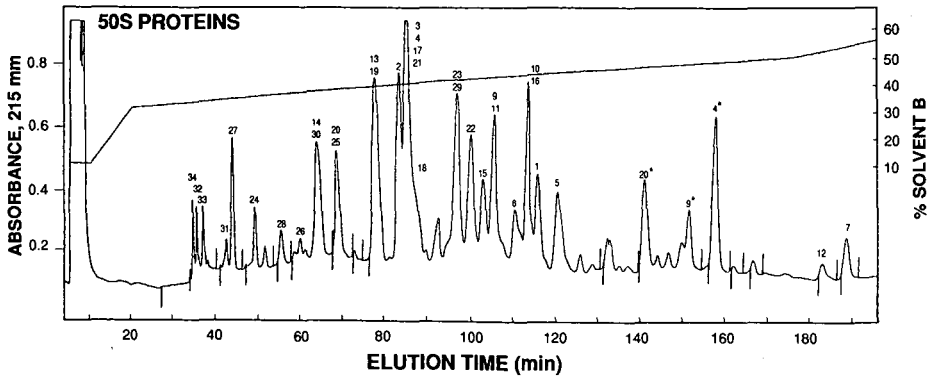

Fig. 2. C_4 reversed-phase HPLC elution profile of 50S subunit proteins. The separation of 600 μg of proteins with a linear gradient of acetonitrile (solvent B) was conducted as described in Experimental. The protein identification and gradient slope are indicated on the tracing. 4*, 9* and 20* indicate the second, later eluting positions for these proteins.

TABLE I

30S SUBUNIT PROTEIN HYDROPHOBICITY COEFFICIENTS AND RETENTION TIMES

Protein	N^a	$\Sigma R_c{}^b$	$\Sigma R_c \cdot \ln N$	$t_R{}^c$	$\Sigma R_c - t_R{}^d$
S1	557	1230.4	7779.3	158.0(0.51)	1072.4
S2	240	544.4	2983.7	129.4(0.65)	415.0
S3	232	471.4	2567.6	92.5(0.66)	378.9
S4	205	398.3	2120.2	93.0(0.66)	305.3
S5	166	331.0	1692.1	105.9(0.51)	225.1
S6	135	261.9	1284.7	106.1(0.34)	155.8
S7	177	358.7	1856.7	111.4(0.76)	247.3
S8	129	285.1	1385.5	93.0(0.66)	192.1
S9	129	238.1	1157.1	104.2(0.54)	133.9
S10	103	231.2	1071.5	87.3(0.82)	143.9
S11	128	217.3	1054.4	59.7(0.55)	157.6
S12	123	183.6	883.5	38.6(0.42)	145.0
S13	117	218.1	1038.6	92.5(0.66)	125.6
S14	98	161.5	740.5	48.8(0.29)	112.7
S15	88	158.4	709.2	63.5(0.62)	94.9
S16	82	169.3	746.1	80.7(0.88)	88.6
S17	83	170.6	753.9	73.0(0.57)	97.6
S18	74	156.7	675.3	63.5(0.62)	93.2
S19	91	157.7	711.4	52.2(0.40)	105.5
S20	86	115.8	515.8	56.2(0.39)	59.6
S21	70	101.6	431.7	41.8(0.35)	59.8

[a] Number of amino acid residues from Giri *et al.* [6].
[b] Sum of retention coefficients calculated from values of Guo *et al.* [7].
[c] Mean of observed retention times ($n = 6$) with standard error in parentheses.
[d] Difference between predicted and observed retention times.

Post translational modifications in the form of methyl and acetyl group additions are found for several of the ribosomal proteins [6]. Corrections for the presence of these groups and their influence on the ΣR_c for the affected proteins have been calculated (Table III). The presence of a methyl group was predicted to increase the ΣR_c by $+1.8$, the difference in R_c between glycine and alanine [7]. For example, protein L11 contains 9 methyl groups. The difference in predicted retention times for the unmodified and modified forms of L11 are indicated in Table III and in Fig. 4. The method is sensitive enough to reveal differences in elution time as a consequence of these modifications. Corrections have also been made for the N-terminal acetylation of proteins S5, S18 and L7 which increases the ΣR_c by a value of $+6.9$ [7]. Proteins S12 and L16 each contain an additional modified amino acid [6]. Corrections have not been made for these changes since the nature of the alteration and the contribution to the protein hydrophobicity are not known.

Ribosomal protein L7 is the N-terminal acetylated form of protein L12. This alteration is responsible for the slight difference in retention time for these two proteins. Both of these proteins exist in the ribosomal particle as dimers, unlike any of the other ribosomal proteins [18]. It is obvious from the observed retention times for these two proteins that they eluted from the C_4 column as dimers and not in the position expected for the monomeric form of each protein (Fig. 4). For the L7 dimer

TABLE II

50S RIBOSOMAL PROTEIN HYDROPHOBICITY COEFFICIENTS AND RETENTION TIMES

Protein	N^a	$\Sigma R_c{}^b$	$\Sigma R_c \cdot \ln N$	$t_R{}^c$	$\Sigma R_c - t_R{}^d$
L1	233	466.1	2540.7	113.0(0.91)	353.1
L2	272	426.8	2392.6	78.8(0.62)	348.0
L3	209	400.7	2140.5	81.4(0.66)	319.3
L4	201	432.0	2291.0	81.4(0.66)	350.6
L5	178	421.1	2182.0	117.8(1.05)	303.3
L6	176	341.9	1767.8	108.6(1.2)	233.3
L7	120	272.2	1303.0	187.0(0.98)	85.2
L7(d)[e]	240	272.2	2981.0	187.0(0.98)	352.0
L9	148	334.6	1675.3	93.2(0.55)	241.6
L10	165	377.2	1926.2	109.9(0.91)	267.8
L11	141	299.2	1480.7	104.4(0.93)	194.8
L12	120	265.3	1270.1	181.3(0.89)	84.0
L12(d)[e]	240	265.3	2906.0	181.3(0.89)	346.0
L13	142	286.4	1419.4	73.0(0.65)	213.4
L14	123	266.9	1284.4	66.3(1.0)	200.6
L15	144	263.9	1311.5	104.4(0.93)	159.5
L16	136	290.1	1425.2	110.6(1.16)	179.5
L17	127	245.3	1188.3	81.4(0.66)	163.9
L18	117	210.3	1001.5	81.4(0.66)	128.9
L19	114	215.6	1021.1	73.0(0.66)	142.6
L20	117	238.9	1144.3	70.1(1.58)	170.2
L21	103	199.4	924.2	81.4(0.66)	118.0
L22	110	201.9	949.0	99.0(0.77)	102.9
L23	99	183.4	842.7	96.6(0.77)	86.8
L24	103	176.9	819.9	46.9(1.2)	130.0
L25	94	190.7	866.4	66.3(1.0)	124.4
L26[f]	86	115.8	515.8	56.0(0.39)	59.8
L27	84	107.6	476.8	42.9(0.27)	64.7
L28	77	131.2	569.9	54.6(0.84)	76.6
L29	63	128.0	530.3	93.2(0.55)	34.8
L30	58	118.2	479.9	60.3(0.67)	57.9
L31	62	92.5	381.8	42.8(0.26)	49.7
L32	56	55.0	221.4	35.8(0.19)	19.2
L33	54	78.0	311.1	36.7(0.24)	41.3
L34	46	50.4	192.9	34.7(0.17)	15.7

[a] Number of amino acid residues from Giri *et al.* [6].
[b] Sum of retention coefficients calculated from values of Guo *et al.* [7].
[c] Mean of observed retention times ($n = 9$) with standard error in parentheses.
[d] Difference between predicted and observed retention times.
[e] Proteins L7 and L12 as dimers (d).
[f] Protein L26 is the same as protein S20 [6].

the product $\Sigma R_c \cdot \ln N$ increases from 1302 to 2981 and for the L12 dimer the value changes from 1270 to 2906. Protein L7 recovered after the HPLC separation was found to elute from a calibrated gel filtration column at the position expected for a protein of 24 000 dalton, the size of the L7 dimer (unpublished observations).

A similiar explanation may apply to the observed elution of 50S proteins L4, L9 and L20. These three proteins have each been found to elute in two distinct locations

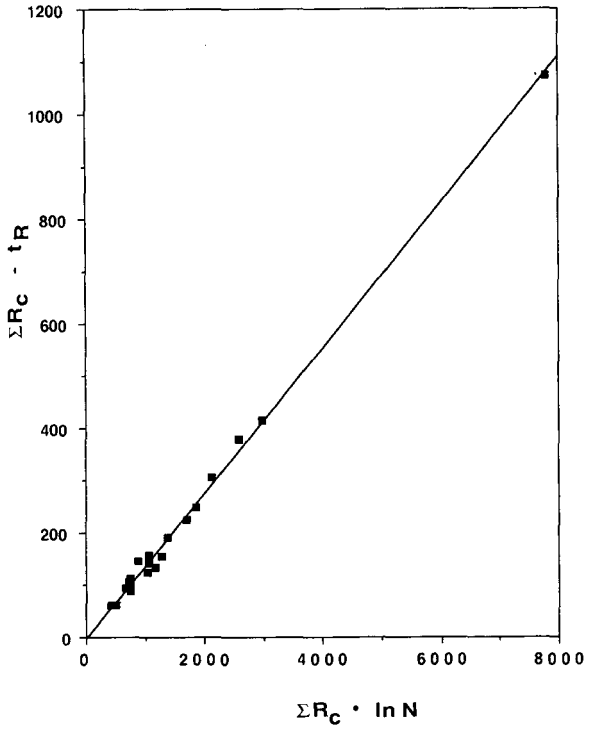

Fig. 3. Correlation of 30S protein retention times with polypeptide chain length and hydrophobicity. Predicted *minus* observed retention time $\Sigma R_c - t_R$ *versus* $\Sigma R_c \cdot \ln N$. The slope of this line is defined by $y = 0.1389\ x - 2.766$ ($r = 0.996$).

from the column, as Fig. 2 indicates. The later elution position of each is consistent with the expected location of each as a protein dimer. There is no indication that any of these function as dimers in the 50S subunit [6]. Alternatively, the later elution positions may reflect interactions between these and other proteins which are only disrupted by the increased acetonitrile concentration during the chromatography. The anomalous elution of protein L9 has been noted previously [4].

Finally, we have investigated the elution profiles of 50S proteins from a pair of temperature-sensitive mutants of *E. coli* with independent alterations in protein L22 [9]. Both mutant proteins are less basic than the normal protein as revealed by their mobility in two-dimensional gel electrophoresis. Both altered proteins eluted as less hydrophobic species under these chromatography conditions, with retention times decreased by 1 and 2 min, respectively. A single amino acid change in each protein was sufficient to promote this difference in elution time, indicating the specificity and sensitivity of this separation method.

The excellent agreement found between the expected and predicted elution behavior of these 52 proteins supports the suggestions of Mant *et al.* [8] that protein hydrophobicity and chain length are the primary determinants of chromatographic properties under these conditions. In 0.1% TFA at pH 2, these proteins should be fully denatured and thus allow maximal interaction between the amino acid sequences and the hydrophobic column matrix. The use of a linear gradient under the same

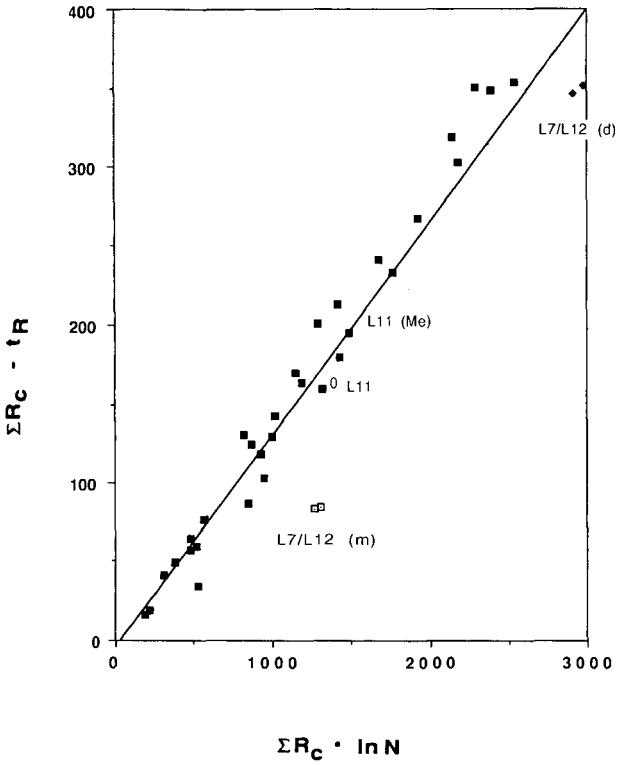

Fig. 4. Correlation of 50S protein retention times with polypeptide chain length and hydrophobicity. Predicted *minus* observed retention time $\Sigma R_c - t_R$ *versus* $\Sigma R_c \cdot \ln N$. The expected locations of the L7/L12 monomer (m) and dimers (d) are indicated as are the positions for the unmodified (0) and methylated (Me) forms of L11. The slope of this line is defined by $y = 0.1368\ x - 3.678$ ($r = 0.964$).

TABLE III

RIBOSOMAL PROTEIN MODIFICATION AND EFFECTS ON ΣR_c

Protein	Modification	ΣR_c	
		Unmodified	Modified[a]
S5	N-Acetyl-Ala	324.1	331.0
S11	N-Me-Ala	208.6	217.3
S18	N-Acetyl-Ala	149.8	156.7
L3	N-Me-Gln	398.9	400.7
L7	N-Acetyl-Ser		
	N-Me-Lys	263.5	272.2
L12	N-Me-Lys	263.5	265.3
L11	N-Me_3-Ala		
	$(N\text{-}Me_3\text{-}Lys)_2$	283.0	299.2
L16	N-Me-Met	288.3	290.1
L33	N-Me-Ala	76.2	78.0

[a] A value of +1.8 was added for each methyl group (Me) and a value of +6.9 was added for each blocked N-terminal amino acid.

solvent conditions as Guo and co-workers [7,12] and Mant and co-workers [8,19] allowed a direct correlation of these protein hydrophobicity values with their predicted hydrophobicity coefficients.

We have also used this method to compare the elution pattern of the ribosomal proteins published by Kerlavage *et al.* [1], using their α values to compute retention times. Although they used hyperbolic gradients for elution of the proteins from a C_{18} column, a good correlation was found between the observed and expected elution of the 30S proteins under their conditions (data not shown). The relationship for the expected elution of the 50S proteins was not as good as observed in the present work. Other workers [2,3] have used more complex gradient procedures to optimize ribosomal protein separation, making a direct comparison with the present results difficult.

We have extended the work of Mant *et al.* [8] to a complex group of related proteins. We have shown that their rules for predicting protein retention time apply to the ribosomal proteins separated under the conditions described. Their methods also allow predictions about protein–protein interactions (as dimers), about post translational modifications and about the elution of mutationally altered protein molecules. This method should have wide application for predicting the separation of other well characterized protein complexes, for identifying the principles underlying separations on reversed-phase columns and for analyzing modified forms of similiar protein molecules.

ACKNOWLEDGEMENTS

The excellent technical assistance of Kiersten Hutchinson is gratefully acknowledged. This work was supported by NIH grant GM 38492.

REFERENCES

1 A. R. Kerlavage, T. Hasan and B. S. Cooperman, *J. Biol. Chem.*, 258 (1983) 6313–6318.
2 R. M. Kamp, A. Bosserhoff, D. Kamp and B. Wittmann-Liebold, *J. Chromatogr.*, 317 (1984) 181–192.
3 R. J. Ferris, C. A. Cowgill and R. R. Traut, *Biochemistry*, 23 (1984) 3434–3442.
4 B. S. Cooperman, C. J. Weitzmann and M. A. Buck, *Methods Enzymol.*, Vol. 164, 1988, pp. 523–532.
5 A. R. Kerlavage, C. Weitzmann, M. Cannon, T. Hasan, K. M. Giangiacomo, J. Smith and B. S. Cooperman, *BioTechniques*, Jan./Feb. (1985) 26–36.
6 L. Giri, W. E. Hill, H. G. Wittmann and B. Wittmann-Liebold, in C. B. Anfinsen, J. T. Edsall and F. M. Richards (Editors), *Advances in Protein Chemistry*, Academic Press, New York, 1984, pp. 1–78.
7 D. Guo, C. T. Mant, A. K. Taneja, J. M. R. Parker and R. S. Hodges, *J. Chromatogr.*, 359 (1986) 499–518.
8 C. T. Mant, N. E. Zhou and R. S. Hodges, *J. Chromatogr.*, 476 (1989) 363–375.
9 W. S. Champney, *Biochim. Biophys. Acta*, 609 (1980) 464–474.
10 G. A. Howard and R. R. Traut, *FEBS Lett.*, 29 (1973) 177–180.
11 D. B. Datta, L.-M. Changchien, C. R. Nierras, W. A. Strycharz and G. R. Craven, *Anal. Biochem.*, 173 (1988) 241–245.
12 D. Guo, C. T. Mant, A. K. Taneja and R. S. Hodges, *J. Chromatogr.*, 359 (1986) 519–532.
13 D. Bedwell, G. Davis, M. Gosink, L. Post, M. Nomura, H. Kestler, J. M. Zengel and L. Lindahl, *Nucl. Acids Res.*, 13 (1985) 3891–3903.
14 S. Isono, S. Thamm, M. Kitakawa and K. Isono, *Molec. Gen. Genet.*, 198 (1985) 279–282.
15 L. E. Post, G. D. Strycharz, M. Nomura, H. Lewis and P. P. Dennis, *Proc. Natl. Acad. Sci. U.S.A.*, 76 (1979) 1697–1701.
16 J. Schnier, M. Kitakawa and K. Isono, *Molec. Gen. Genet.*, 204 (1986) 126–132.
17 R. Takata, T. Mukai, M. Aoyagi and K. Hori, *Molec. Gen. Genet.*, 197 (1984) 225–229.
18 W. Moller and J. A. Maassen, in B. Hardesty and G. Kramer (Editors), *Structure, Function and Genetics of Ribosomes*, Springer, New York, 1986, pp. 309–325.
19 C. T. Mant, T. W. L. Burke, J. A. Black and R. S. Hodges, *J. Chromatogr.*, 458 (1988) 193–205.

Journal of Chromatography, 522 (1990) 171–177
Elsevier Science Publishers B.V., Amsterdam

CHROM. 22 694

Use of metal chelate affinity chromatography for removal of zinc ions from alkaline phosphatase from *Escherichia coli*

VIOLETTA K. LUBIŃSKA and GRAŻYNA MUSZYŃSKA*
Institute of Biochemistry and Biophysics, Polish Academy of Sciences, 36 Rakowiecka St., 02-532 Warsaw (Poland)
(First received February 6th, 1990; revised manuscript received July 10th, 1990)

ABSTRACT

Alkaline phosphatase from *Escherichia coli* (APEC) is not retained at 4°C on a metal-free tris(carboxymethyl)ethylenediamine (TED) column, but at 15°C the metalloenzyme becomes bound to the gel. Chromatography of phosphatase on metal-free TED gel indicates a decline in its enzymic activity and zinc content to about 26% and 40%, respectively. The activity of chromatographed APEC can be partially restored by addition of zinc ions, indicating that metal-free TED gel is capable of removing zinc ions from alkaline phosphatase.

INTRODUCTION

Immobilized metal affinity chromatography (IMAC) is commonly used not only for protein purification, but also for the topography of reactive residues on the surface of proteins (for reviews see refs. 1–3). In "regular" IMAC the metal, mostly chelated by iminodiacetate (IDA) to the gel, interacts with amino acid residues of the protein. In "reversed" IMAC the metal, a structural component of the protein, interacts with an immobilized chelator. This type of chromatography has not been exploited very extensively. In "reversed" IMA adsorption a long spacer arm is probably essential for the chelating group to reach the metal located internally in the metalloprotein [4].

Porath and Olin [5] described the synthesis of tris(carboxymethyl)ethylenediamine (TED)–agarose. Compared with IDA–agarose, the TED gel is characterized by longer spacer arms and makes stabler complexes with metal ions. Passage of carboxypeptidase A (Zn^{2+}–CPD) through metal-free TED gel abolished the peptidase activity of the enzyme. The activity can be fully restored by adding zinc ions [6]. The results strongly suggested that TED–agarose exhibits a strong affinity to metal ions, and therefore could be used for removing the metal from some proteins. In this work, to confirm this suggestion, attempts to remove zinc ions from another metalloprotein, alkaline phosphatase from *Escherichia coli* (APEC), were made. The chromatography of APEC on metal-free TED gel was followed by determination of its zinc content and enzymatic activity.

0021-9673/90/$03.50

EXPERIMENTAL

Materials

MES, Trizma Base (analytical-reagent grade), *p*-nitrophenyl phosphate (pNPP), alkaline phosphatase from *E. coli* (APEC) and EDTA were obtained from Sigma. Tris(carboxymethyl)ethylenediamine–Sepharose 6B (TED gel) was a kind gift from Professor J. Porath (Uppsala University). PD-10 columns were obtained from Pharmacia and the protein assay dye solution from Bio-Rad Labs. All other reagents were of analytical-reagent grade.

Methods

Preparation of columns. The chromatographic adsorbent (TED–Sepharose 6B) was packed into the columns (3.3 × 1.0 cm I.D., $V_t = 2.8$ ml) in distilled water and equilibrated with 50 m*M* MES (pH 5.5), then 1 mg of the enzyme in 1.2 ml of equilibration buffer was applied to the column. The column was washed with 0.5 ml of the same buffer and allowed to stand for 1 h. Washing with the same buffer was then continued until all of the non-adsorbed material was eluted from the column; at a flow-rate 6 ml/h, fractions of 0.5 or 1 ml were collected. In the case of protein binding on the gel, sodium chloride was included for the elution.

Dialysis of alkaline phosphatase (APEC) against EDTA. Treatment of EDTA (by dialysis) was performed under the described conditions [7], with slight modification. Holoenzyme dissolved in 50 m*M* MES (pH 6.0) up to a protein concentration of 0.5 mg/ml was dialysed at 25°C against a 400-fold volume excess of 10 m*M* Tris–HCl (pH 8) containing 10 m*M* EDTA. After dialysis the protein was filtered on PD-10 columns previously equilibrated with 10 m*M* Tris–HCl (pH 8).

Removing of metal contamination. Adventitious metal ions, especially zinc, present in trace amounts in water, buffers and eluents were eliminated by passing all these solutions through metal-free TED gel (22 × 1.3 cm I.D. column), at a flow-rate of 18 ml/h at room temperature. To metal-free TED gel, 3 m*M* substrate solution (pNPP) was added. The suspension was kept in the dark for 16 h at 4°C, with occasional shaking, then the gel was removed by centrifugation. For storage of protein fractions and determination of enzymatic activity all tubes, pipette tips, cuvettes and vessels were made of plastic and before use were thoroughly washed with 10 m*M* EDTA, water, 10 m*M* sulphuric acid and finally metal-free water.

Determination of activity of alkaline phosphatase from E. coli (APEC). To 0.9 ml of 1 *M* Tris–HCl buffer (pH 8), 0.1 ml of enzyme solution (containing 1–6 μg of protein) and 0.5 ml of substrate were added. Each sample was incubated for 10 min at 37°C, cooled in an ice-bath and the amount of product formed was measured directly at 410 nm. To parallel samples a 5-molar excess of zinc sulphate (calculated on the phosphatase concentration) was added. Phosphatase activity is expressed in units (U), where 1 U is that activity liberating 1 μmol of *p*-nitrophenol per minute in 0.6 *M* Tris–HCl (pH 8)–1 m*M* pNPP at 37°C.

Protein determination. Protein was determined according to Bradford [8] with bovine serum albumin as a standard.

Zinc determination. Zinc was determined, after wet combustion, in a Perkin-Elmer 300 atomic absorption spectrometer. The zinc content was calculated based on the molecular weight of a subunit (43 000).

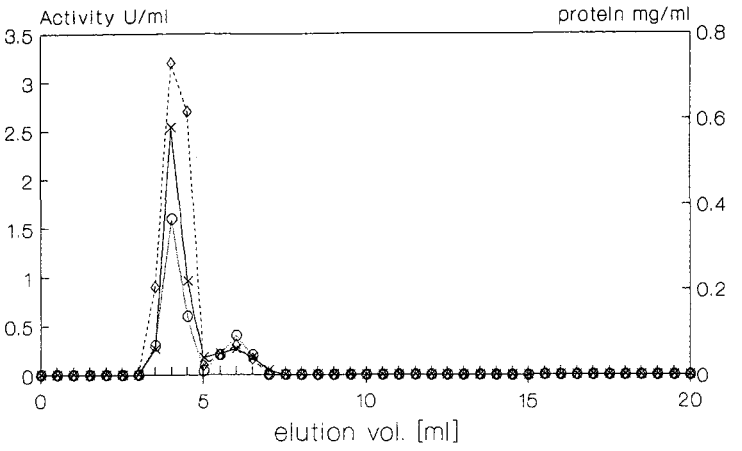

Fig. 1. Chromatography of alkaline phosphatase on metal-free TED gel at 4°C. The column was washed with 0.05 *M* MES (pH 5.5). X = Protein; enzyme activity (○) in the absence and (◇) in the presence of zinc ions.

RESULTS

Commercial APEC did not bind to metal-free TED gel at 4°C and enzymatic protein was eluted in the equilibration buffer [0.05 *M* MES (pH 5.5)] (Fig. 1). However, when the chromatography was performed at elevated temperature (15°C) the enzyme was retained on the column and its elution was possible by inclusion of sodium chloride (Fig. 2a). Using a linear gradient of the salt APEC emerged from the chelated column at a 0.2 *M* concentration of sodium chloride (Fig. 2b).

Passage of APEC through the metal-free TED gel reduced its enzymatic activity to about 26% or 10% of the initial value in chromatography at 4 and 15°C, respectively. Also, the zinc content of the enzyme decreased markedly, from *ca.* 3 mol per enzyme subunit initially to 1.1–1.2 mol after chromatography on the metal-free gel (Table I).

The chromatographed enzyme was partially reactivated, to 50–60% of its initial level, by addition of Zn^{2+} to the incubation sample. "Short" dialysis (90 min) against soluble chelating agent did not decrease the zinc content of the chromatographed enzyme (data not shown), whereas "prolonged" dialysis (12 h) of native enzyme reduced its zinc content to about 0.5 mol per monomer of enzyme (Table I).

DISCUSSION

APEC is a dimeric metalloenzyme with two reactive centres. The reactive centre per monomer of the enzyme contains three metal sites; two metal sites are occupied by zinc and the third by magnesium or, in the absence of magnesium, by zinc [9]. These results are consistent with our data. As can be seen from the present results, the native form of APEC contains about three metal ion per monomer of the enzyme. Passage of the enzyme through a metal-free TED column reduces the amount of the metal to about one atom with a simultaneous decrease in phosphatase activity. Earlier studies

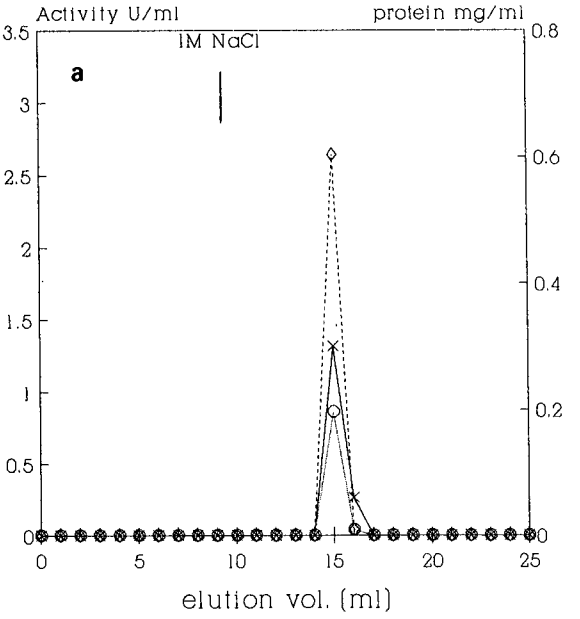

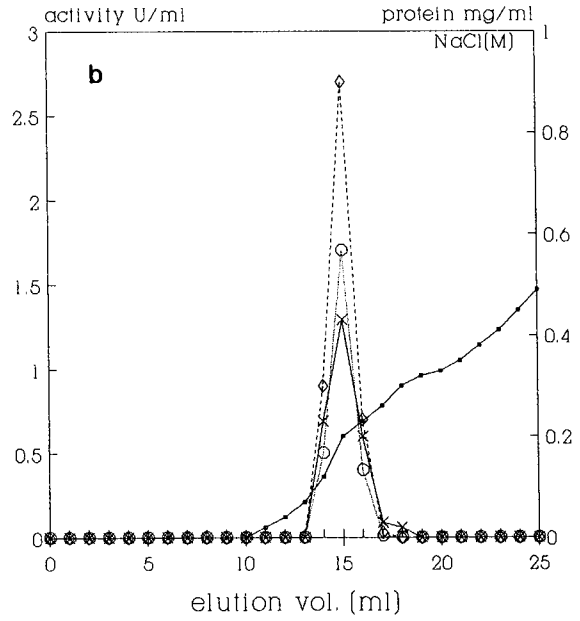

Fig. 2. Chromatography of alkaline phosphatase on metal-free TED gel at 15°C. For the enzyme elution, (a) a step gradient or (b) a linear (0–0.5 *M*) gradient of sodium chloride in 0.05 *M* MES (pH 5.5) was applied. X = Protein; enzyme activity (○) in the absence and (◇) in the presence of zinc ions.

TABLE I

EFFECT OF CHROMATOGRAPHY ON A METAL-FREE TED–SEPHAROSE COLUMN ON THE ZINC CONTENT AND ACTIVITY OF APEC

Each value is the average from 3–5 separate chromatographic experiments.

Chromatographic conditions for the enzyme elution	Moles of Zn^{2+} per monomer of enzyme	Activity		
		U/mg protein	%	% after incubation with Zn^{2+}
Control:				
Native enzyme	2.9	31.0	100	102.6
Enzyme after dialysis for 12 h against EDTA	0.5	6.1	19.6	63.7
Isocratic elution at 4°C	1.2	8.0	25.9	62.2
Elution by step gradient of NaCl at 15°C	1.2	3.7	12.1	46.0
Elution by linear gradient (0–0.5 *M*) NaCl at 15°C	1.1	3.3	8.1	19.6

of the properties of immobilized subunits of APEC showed that the catalytically inactive monomer of the enzyme binds tightly one zinc atom [10].

When APEC is chromatographed at 4°C, the enzyme does not bind to the gel. However, during chromatography at higher temperatures from 15 to 23°C (data for 23°C are not shown), APEC acquires the ability to bind with metal-free TED gel. The binding at higher temperature might be caused by an increase in binding energy, probably from electrostatic interactions of the gel itself or conformational changes of the enzyme. Alkaline phosphatase, as an oligomeric enzyme with an α/β topology of subunits, could undergo of molecular movements. Analysis of the topology indicated that binding crevices occur in the region where the strand order switches and that they are located at the carboxyl end of the strands. It was reported previously [11] that when the temperature is raised from 4°C to $\geqslant$20°C conformational changes of the enzyme are observed; for example, approximately four tyrosine residues per monomer are replaced on going from an aqueous to a hydrophobic environment. Therefore, the increase in accessibility of APEC binding to the metal-free chelated gel at higher temperature observed here, probably through zinc ions is not excluded.

Fig. 3 compares the effects of the chromatography on the activity of APEC and carboxypeptidase A (CPD). Passage of metalloenzymes through the metal-free TED gel reduces their catalytic activity. The decrease in activity is greatest when the eluting CPD has remained for some time (*ca.* 1 h) on a TED column. The delayed desorption phenomenon was first observed by Porath and Belew [4]. A new peak appeared when the elution of human serum from a Zn–TED–Sepharose 6B column was interrupted for 1 h or even for a shorter time. The desorbed peak differed substantially from the previously displaced proteins. Delayed desorption is not a phenomenon restricted to IMA gel but seems to reflect a property shared by all kinds of agarose gels and possibly cross-linked dextran and polyacrylamide gels [4].

The catalytic activity of chromatographed CPD is fully restored by the addition of Zn^{2+} ions, whereas the activity of APEC is restored to 75% of the initial activity

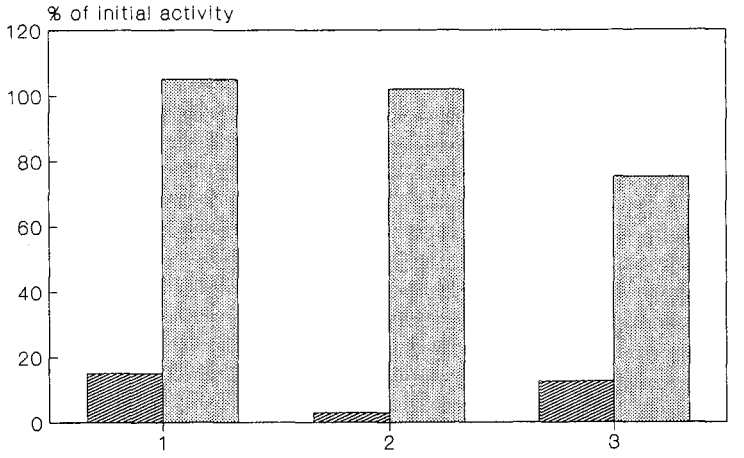

Fig. 3. Activities of metalloenzymes after elution from metal-free TED gel. Chromatography was performed at 4°C: (1) directly (carboxypeptidase); (2) with 1 h delayed desorption (carboxypeptidase); (3) with 1 h delayed desorption (alkaline phosphatase). Enzyme activity (hatched) without and (dotted) in the presence of zinc ions.

(Fig. 3). Similar results for APEC were obtained by using the solute chelating agent. Simpson and Vallee [12] found that when alkaline phosphatase was exposed to 8-hydroxyquinoline-5-sulphonic acid, two zinc atoms were rapidly removed and the enzyme was inactivated to *ca.* 10% of the initial level. When zinc was added to apoenzyme the activity was restored to 85% of the initial level. The differences in the restoration of the activity of the two enzymes might be a consequence of the different stabilities of the enzymes. Chromatography of the enzyme at higher temperature and dilution of the enzyme (*e.g.*, after elution caused by a linear gradient of salt, see Fig. 2b) have greater effects on the activity. In such a case reactivation of APEC by zinc ions might be less effective (Table I).

There is still some uncertainty concerning the role of zinc in the phosphatase activity [13]. The rate of inactivation of enzyme by EDTA (in the solution) seems to be biphasic, corresponding to different zinc binding sites associated with phosphatase [7]. Lazdunski *et al.* [7] found that after 50 min of EDTA treatment of alkaline phosphatase, zinc was partially removed from the enzyme, and prolonged exposure (12 h) of the enzyme to the chelator was able to remove essentially all of the metal from the protein. Their findings are consistent with our results. Short dialysis against EDTA (data not shown) does not have a further effect on the chromatographed enzyme, whereas prolonged dialysis causes a considerable decrease in zinc content. Prolonged dialysis is more effective than chromatography for removing the zinc from alkaline phosphatase.

Carboxypeptidase A is a much more stable enzyme than APEC. Carboxypeptidase A is a monomeric enzyme with one binding site for zinc ions; zinc ions are thought not to play a critical role in maintaining the overall three-dimensional structure of the enzyme. The metal was only essential for the catalytic activity of carboxypeptidase [14]. Although it has been shown that removing Zn^{2+} ions from APEC did not cause the dissociation of the dimer, the role of metal is probably more complex and cooperative.

Metalloenzymes offer unusual opportunities in the study of the mechanism of enzyme action. The physical and chemical properties of metal ions are readily differentiated from those of the amino acid side-chains of proteins, and thus become valuable probes of the active site. Therefore, the important task is the removal of metal ions from the proteins. For a long time chelating agents in solution have served this purpose. However, apart from the removal of the metal, free chelating agents may inhibit the enzymatic activity through the formation of mixed complexes. Also, the preparation of any apoenzyme in such a fashion includes a long procedure, mostly extensive dialysis, first against the chelator and second against buffer to remove the agent. The drawbacks to such an approach might be inactivation of the enzyme during prolonged dialysis and unpredictable effects of traces of chelating agents still present in the solution.

Therefore, the application of immobilized chelating agent for removing metal ions from proteins was highly desirable. Treatment of alkaline phosphatase with Chelex 100 resulted in a loss of the activity; the enzyme was reactivated by addition of zinc ions [15]. However, lack of data concerning the metal content of the enzyme without and after treatment with Chelex made the direct determination of the efficiency of the applied gel impossible.

Based on the determination of the catalytic activity, the effect of zinc on the reactivation and the measurement of metal content, we have now demonstrated the usefulness of metal-free TED gel for removing metal ions from proteins. However, it should be mentioned that the metal ion, which is very tightly bound, was not removed from proteins by this technique. Being conscious of some limitations, in our opinion the use of "reversed" IMAC, where the chelating agent is immobilized on the insoluble support, offers new possibilities for the characterization of metalloproteins and the preparation of their metal-free forms.

REFERENCES

1 E. Sulkowski, *Trends Biotechnol.*, 3 (1985) 1.
2 A. J. Fatiadi, *CRC Crit. Rev. Anal. Chem.*, 18 (1987) 1.
3 G. Muszynska, in T. W. Hutchens (Editor), *Protein Recognition of Immobilized Ligands*, Alan R. Liss, New York, 1989, p. 279.
4 J. Porath and M. Belew, in I. M. Chaiken, M. Wilchek and I. Parikh (Editors), *Affinity Chromatography and Biological Recognition*. Academic Press, New York, 1983, p. 173.
5 J. Porath and B. Olin, *Biochemistry*, 22 (1983) 1621.
6 G. Muszynska, Y.-J. Zhao and J. Porath, *J. Inorg. Biochem.*, 26 (1986) 127.
7 C. Lazdunski, C. Petitclerc and M. Lazdunski, *Eur. J. Biochem.*, 8 (1969) 510.
8 M. M. Bradford, *Anal. Biochem.*, 72 (1976) 248.
9 J. M. Sowadski, M. D. Handschumacher, K. H. M. Murthy, B. A. Foster and H. W. Wyckoff, *J. Mol. Biol.*, 186 (1985) 417.
10 S. McCracken and E. Meighen, *J. Biol. Chem.*, 255 (1980) 2396.
11 J. A. Reynolds and M. J. Schlesinger, *Biochemistry*, 6 (1967) 3552.
12 R. T. Simpson and B. L. Vallee, *Biochemistry*, 7 (1968) 4343.
13 T. W. Reid and I. B. Wilson, in P. D. Boyer (Editor), *The Enzymes*, 4 (1971) 373.
14 F. A. Quiocho and W. N. Lipscomb, *Adv. Protein Chem.*, 25 (1971) 1.
15 H. Csopak, *Eur. J. Biochem.*, 7 (1969) 186.

Journal of Chromatography, 522 (1990) 179–194
Elsevier Science Publishers B.V., Amsterdam

CHROM. 22 710

Liquid chromatography–thermospray mass spectrometric study of N-acylamino dilactones and 4-butyrolactones derived from antimycin A

S. L. ABIDI*,[a] and S. C. HA
U.S. Fish and Wildlife Service, National Fishery Research Center, P.O. Box 818, La Crosse, WI 54602-0818 (U.S.A.)
and
R. T. ROSEN
Center for Advanced Food Technology, Rutgers University, New Brunswick, NJ 08903 (U.S.A.)
(First received October 17th, 1989; revised manuscript received June 24th, 1990)

ABSTRACT

Reversed-phase high-performance liquid chromatography–thermospray mass spectrometric (HPLC–MS) characteristics of four sets of lactonic complexes (one 4-butyrolactones and three dilactone complexes) derived from antimycin A were investigated. Three types of 8-hydroxy analogues were also included in the study. Pairs of a–b structures isomeric at the 8-acyloxy ester side-chains were best separated with a high-efficiency octadecylsilica column prior to analysis by HPLC–MS. Mass spectra of the a–b pairs each with identical molecular weights exhibited virtually indistinguishable fragmentation patterns, although their relative intensities were not superimposable. In some cases, HPLC–MS of the title compounds yielded mass chromatograms showing the minor components more easily recognizable than the HPLC–UV counter parts because of the apparent higher ionization efficiency of the minor isomers and increased resolution of subcomponents in the MS system. Under the mobile phase conditions employed, analyte ionization occurred with variable degrees of gas phase ammonolysis depending upon the ammonia concentration of the buffer. Potential applicability of the on-line HPLC–MS technique for the characterization of components in mixtures of antimycin analogues and isomers is demonstrated.

INTRODUCTION

Antimycin A (an effective fish toxicant) is a mixture of closely related antibiotic substances produced by streptomyces fermentation [1]. This cluster of dilactonic compounds consists of at least ten components [2]. Of these, the five major homologues (a-isomers) and five minor homologues (b-isomers) are designated as a-subcomponents and b-subcomponents, respectively (Fig. 1). The presence of

[a] Present address: U.S. Department of Agriculture, Northern Regional Research Center, 1815 North University Street, Peoria, IL 61604, U.S.A.

0021-9673/90/$03.50

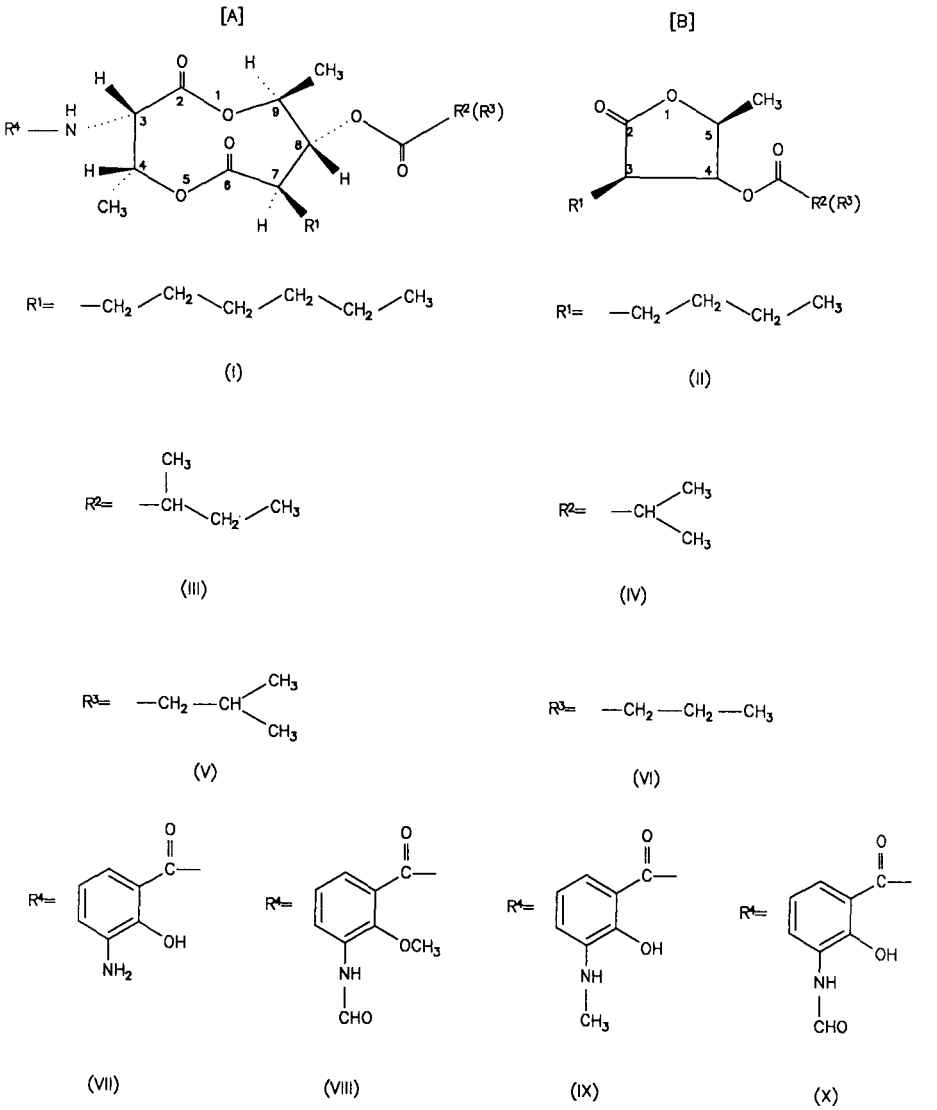

Fig. 1. Structures of (A) N-acylamino dilactones and (B) 4-butyrolactones (antimycin lactones). Subcomponents: 1a, $R^1 = I$, $R^2 = III$; 1b, $R^1 = I$, $R^3 = V$; 2a, $R^1 = I$, $R^2 = IV$; 2b, $R^1 = I$, $R^3 = VI$; 3a, $R^1 = II$, $R^2 = III$; 3b, $R^1 = II$, $R^3 = V$; 4a, $R^1 = II$, $R^2 = IV$; 4b, $R^1 = II$, $R^3 = VI$. Antimycins (AT): $R^4 = X$; methylated antimycins (AT-OMe): $R^4 = VIII$; deformylated antimycins (AT-DF): $R^4 = VII$; 3′-N-methylantimycins (AT-NMe): $R^4 = IX$; debenzoylated antimycins (AT-DB): $R^4 = H$.

structurally isomeric R^2 and R^3 alkyls of the acyloxy side chains in the structures is responsible for the existence of the a–b forms of antimycins. Most recent nuclear magnetic resonance (NMR) studies [3,4] revealed that structures of each of the corresponding a–b subcomponent pairs A_{1a}–A_{1b}, A_{2a}–A_{2b}, A_{3a}–A_{3b}, and A_{4a}–A_{4b} are isomers of the same molecular weight (Fig. 1).

Preparative-scale separations and isolations of antimycin have been cumbersome, lengthy, and laborious [5]. A pure material of antimycin A_1, A_2 A_3, or A_4 containing an inherent pair of a–b subcomponents has recently been marketed in the form of individual antimycin homologues [6], but these individually isolated compounds are too expensive to purchase in quantity for practical largescale applications. None of the antimycin subcomponents A_{1a}, A_{1b}, A_{2a}, A_{2b}, A_{3a}, A_{3b}, A_{4a} and A_{4b} has been separated nor been isolated on a commercial scale. If available, the isomerically homogeneous materials would be costlier than the four antimycin homologues A_1, A_2, A_3 and A_4. In the premise of severe supply shortage of single-component antibiotics, relatively more affordable mixtures of antimycin A complex have frequently been used at our laboratories in a number of organic preparations and biological investigations. Furthermore in fishery management, field workers in practice have routinely employed the toxicant formulations solely prepared from mixtures of antimycin A complex. In consequence, for studying the biological and environmental fates of antimycins, it is necessary that analytical efforts should be directed toward mixture analysis in lieu of single-component analysis.

There are several reactive sites in the antimycin molecule (Fig. 1). Metal hydride reduction of antimycin A complex yields a host of heterogeneous mixtures in the products whose compositions vary depending on reaction parameters. Unless the acyloxy side chains have not been cleaved, the products are typical mixtures of homologous complexes each of which should have the same number of subcomponents as in antimycins (Fig. 1). In a few of our earlier studies [2,7] involving the precursor antimycin A complex, it was found that diagnostic and qualitative product analyses of both known and unknown mixtures of products were most conveniently and effectively carried out by using a combined high-performance liquid chromatography–thermospray mass spectrometry (HPLC–MS) technique [8]. Direct probe chemical ionization (CI) and electron impact (EI) MS techniques [9] proved to be useful for antimycin mixture analysis. However, the direct probe methods suffer from certain limitations that require the use of strictly pure compounds of known structures. Due to thermal instability, the title dilactonic compounds are not amenable to gas chromatographic (GC) analysis. Analysis of unusually complicated samples containing multiple sets of complexes must be accomplished by HPLC–MS. This paper reports the HPLC–MS results of N-acylamino dilactonic compounds and 4-butyrolactones derived from antimycin A.

EXPERIMENTAL

Chemicals and reagents

Crude antimycin A was a gift from Aquabiotics (Bainbridge Island, WA, U.S.A.). Pure analytical standards of antimycin A were obtained from Sigma (St. Louis, MO, U.S.A.) or prepared from the crude materials following a published method [6]. For preparation of methylated antimycin (AT-OMe) having the methoxy group at the 2′-position, a previously described procedure [2] was modified for improving yields and product purity. Thus, a solution of antimycins in diethyl ether was stirred with an equivalent amount of diazomethane at 35°C for 30 min. Another equal portion of diazomethane was added to the reaction mixture. The mixture was stirred at 35°C for additional 30 min and left standing at room temperature overnight.

Mixtures of deformylated antimycins, 3'-aminoantimycins (AT-DF), were prepared by treating antimycins with either hot hydrochloric acid [1] or diisobutylaluminum hydride. The 3'-N-methyl analogues (AT-NMe) were prepared from antimycins by reaction with diborane. Detailed procedures for the above hydride reductions are described in a separated paper [10]. The 4-butyrolactone complex (AT-LCT) was readily prepared by mild alkaline hydrolysis of antimycins at room temperature [11].

Adequately clean samples of individual dilactone mixtures were often desirable for use as reference standards. In such cases, the crude reaction products were purified by thin-layer chromatography (TLC). According to sample sizes, the TLC experiments were performed on analytical or preparative silica gel plates (Analtech, Newark, DE, U.S.A.) using solvent systems as described previously [2,12].

All organic reagents were obtained from Aldrich (Milwaukee, WI, U.S.A.). Chromatography-grade buffer salts and solvents were the products of J. T. Baker (Phillipsburg, NJ, U.S.A.).

High-performance liquid chromatography–thermospray mass spectrometry

A Waters liquid chromatograph equipped with a Model 600 multi-solvent delivery system and a Model 490-MS detector was used. For obtaining optimal separation of components within reasonable retention times, mobile phases were prepared from variable proportions of methanol and buffered water (0.1 *M* ammonium acetate). The buffer solutions were adjusted to pH 5 with acetic acid. Depending on the type of compounds analyzed, HPLC eluents were pumped isocratically at a flow-rate of 0.5–2 ml/min or with gradient elution [2]. All samples were frozen in dry state prior to analysis. Analytical samples were dissolved in methanol and aliquots (50–150 μg) were injected into a HPLC column via a Waters U6K injector. Analyte components were first separated with a Hibar Superspher RP-18e column (25 cm $\times$ 4 mm, 3 μm, EM Science) or an Altex Ultrasphere ODS column (25 cm $\times$ 4.6 mm, 5 μm) and then analyzed with an on-line HPLC–thermospray mass spectrometer.

The chromatograph was coupled via a Vestec Model 45 (for analyis of AT-OMe) or Model 701C [for analysis of AT-DF and 8-hydroxy-AT-DF (AT-DF-80H)] thermospray interface to a Finnigan Model 4600 triple-stage quadrupole mass spectrometer. The models 45 and 701C HPLC–MS systems were operated in the positive ion mode with the "filament off" and "filament on", respectively. For the analysis of compounds in the other series, a Vestec Model 201 thermospray mass spectrometer was used and all spectra were obtained in the positive ion discharge mode. The MS temperatures were adjusted to optimum conditions suitable for different compound types: temperature ranges used for the probe tip, the vaporizer, and the ion block were 178–236, 238–269, and 268–300°C, respectively. The mass spectrometers were scanned from m/z 150-700 in 2 s.

RESULTS AND DISCUSSION

The investigated N-acylamino dilactone- and 4-butyrolactone complexes (Fig. 1) include AT-OMe, AT-DF, AT-NMe, AT-LCT, 8-hydroxy-N-methyl antimycin (AT-NMe-8OH), AT-DF-8OH and 8-hydroxydebenzoyl antimycin (AT-DB-8OH). As mentioned earlier, mixtures of closely related compounds were invariably obtained whenever the antimycin A complex was used as the starting material in organic

preparations. Most of the nine-membered dilactone compounds under study were found to be fairly short-lived reaction intermediates, especially in solution. In our experience, a solution of a given sample in methanol gradually decomposed within a few days at room temperature. Isolation of individual components from each complex would be extremely tedious and particularly impractical in view of the lability of the nine-membered dilactone structures. The compounds isolated could be the decomposition products, which would lead to misinterpretation of results. Therefore, direct and timely analysis of the dilactonic compounds by on-line HPLC–MS provided the most effective means not only for accurate assessment of various reaction courses dealing with unstable compounds, but also for structural confirmation and identification of products. In consideration of the potential application of the analytical data in biochemical and fishery research, HPLC–MS approaches to mixture analysis of antimycin degradation products are of biochemical and environmental significance.

Table I shows HPLC–MS data for the ten methylated antimycin components, AT-OMe ([A] in Fig. 1). After on-line HPLC separation, mass spectra of individual AT-OMe components in all cases exhibited protonated molecules along with fragment ions characteristic of the homologous series. Structures of some of the observed ions are given in Fig. 2 which generally depicts the four major fragment ions commonly

TABLE I

HPLC–MS DATA FOR METHYLATED ANTIMYCIN A COMPLEX (AT-OMe)

Component[a]	*m/z* Value of observed ion and its relative abundance in parenthesis[b]									
	[E]	[F]−$R^{2(3)}$CO	[D]−CO_2	[C]	[D]	[F]−NH_3	[F]	M−CO	M+1	M+NH_4
(AT-OMe)$_{1a}$	195	218	235	261	279	285	302	535	563	580
	(2.0)	(8.0)	(22)	(100)	(60)	(14)	(14)	(6.5)	(54)	(16)
(AT-OMe)$_{1b}$	195	218	235	261	279	285	302	535	563	580
	(8.7)	(10)	(24)	(100)	(71)	(19)	(22)	(15)	(75)	(20)
(AT-OMe)$_{2a}$	195	218	235	261	279	271	288	521	549	566
	(2.0)	(7.0)	(22)	(100)	(47)	(9.9)	(12)	(5.2)	(40)	(12)
(AT-OMe)$_{2b}$	195	218	235	261	279	271	288	521	549	566
	(6.5)	(6.2)	(20)	(100)	(60)	(13)	(19)	(11)	(59)	(14)
(AT-OMe)$_{3a}$	195	190	235	261	279	257	274	507	535	552
	(2.3)	(9.9)	(29)	(100)	(32)	(14)	(17)	(2.0)	(41)	(14)
(AT-OMe)$_{3b}$	195	190	235	261	279	257	274	507	535	552
	(11)	(3.7)	(26)	(100)	(84)	(16)	(26)	(4.7)	(92)	(28)
(AT-OMe)$_{4a}$	195	190	235	261	279	243	260	493	521	538
	(1.6)	(8.4)	(20)	(100)	(53)	(13)	(15)	(16)	(80)	(34)
(AT-OMe)$_{4b}$	195	190	235	261	279	243	260	493	521	538
	(5.1)	(8.0)	(19)	(100)	(59)	(13)	(23)	(19)	(71)	(28)
(AT-OMe)$_{5a}$	195	190	235	261	279	229	246	479	507	524
	(1.6)	(5.8)	(34)	(100)	(59)	(13)	(30)	(13)	(57)	(25)
(AT-OMe)$_{5b}$	195	190	235	261	279	229	246	479	507	524
	(0.9)	(2.1)	(10)	(39)	(51)	(8.6)	(13)	(25)	(100)	(40)

[a] For compound abbreviations, see Results and Discussion.

[b] For ion identification, see Figs. 1 and 2.

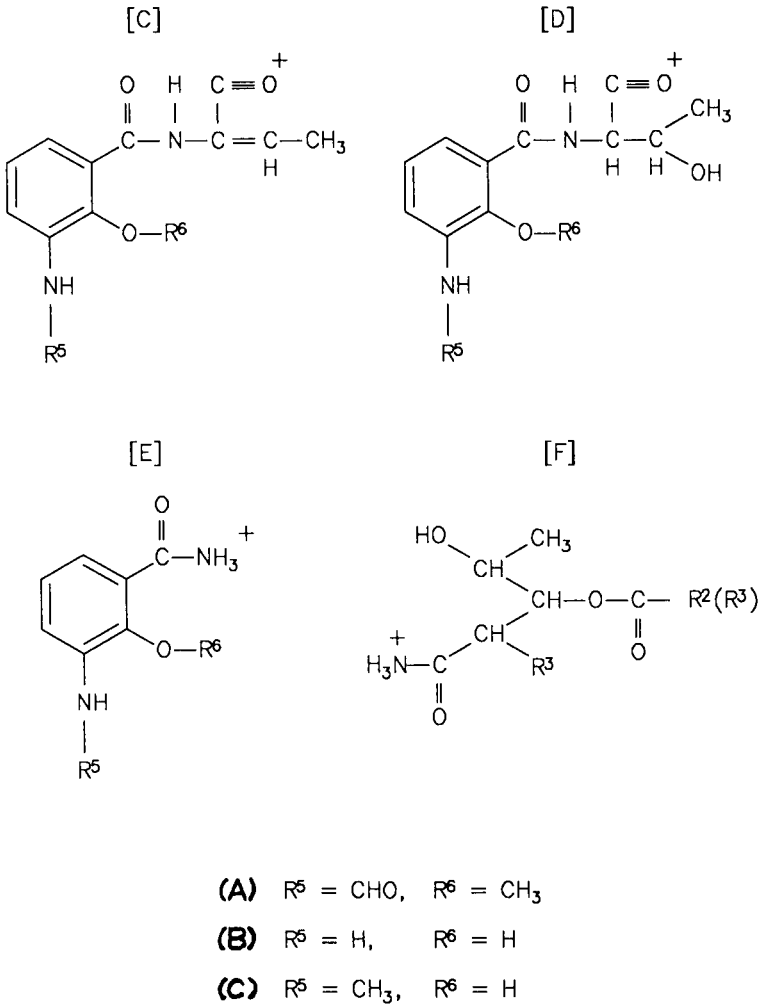

Fig. 2. Significant fragments observed in HPLC–MS of the N-acylamino dilactones: (A) methylated antimycins (AT-OMe), (B) deformylated antimycins (AT-DF), and (C) 3′-N-methylantimycins (AT-NMe).

observed in the mass spectra of the dilactonic compounds related to antimycin. With the exception of $(AT\text{-}OMe)_{5b}$, each homologue gave rise to a base peak at *m/z* 261 attributable to fragment [C] presumably produced by a concerted rearrangement leading to cleavage at the 1–2 and 5–6 bonds (Fig. 1) with hydrogen transfer to the esterified oxygen to yield initially ion [D], followed by the loss of water [9]. Other less abundant ions at *m/z* 279, *m/z* 235 ($[D]-CO_2$), and *m/z* 195 [E] were universally present in the spectra. It should be noted that these fragments devoid of R^1 and $R^{2(3)}$ groups have no bearing on the distinction of isomers of interest. In the spectra of the homologous series, there were six additional weaker, but diagnostically significant, peaks. These were attributed to $(M+NH_4)^+$, $(M+1)^+$, $(M-CO)^+$, $[F]^+$,

$([F]-NH_3)^+$, and $([F]-R^{2(3)}CO)^+$. All but the last of these ions contain the R^1 and $R^{2(3)}$ groups contributing to the observation of homologous mass ions. Analysis of the five sets of fragmentation data (Table I) confirmed the homologous relationships among the AT-OMe components. Because ammonium acetate was used in the HPLC mobile phase system, occurrence of gas phase ammonolysis [9] during positive ion reversed-phase HPLC–MS of methylated antimycins was evident. Fig. 2 shows possible structures of some adduct ions.

Comparisons of the HPLC–MS results (Table I) between a-components and b-components of AT-OMe indicated that mass spectra of these structural isomers with identical molecular weights exhibited virtually indistinguishable fragmentation patterns except for notable differences in their relative intensities of the corresponding ions. In general, HPLC–MS of the minor $(AT\text{-}OMe)_b$ compounds tended to give more abundant ions (including the protonated molecules) than the corresponding major a-isomers, $(AT\text{-}OMe)_a$ (Table I). Fig. 3 presents a typical reconstructed total ion current chromatogram and a mass chromatogram showing separation of a pair of a–b subcomponents.

The HPLC–MS results for the deformylated antimycin A complex, AT-DF([A] in Fig. 1), are summarized in Table II. The most abundant base peak was located at *m/z* 237 ([D], Fig. 2) in every spectrum of the ten components in the series. Besides the protonated molecule $(M+1)^+$ and the $([F]-NH_3)^+$ fragment, the two non-isomer-specific peaks at *m/z* 219 and 193 correspond respectively to [C] and $[D]-CO_2$ (Fig. 2). Also, several ammonia adducts [F], $[F]-R^{2(3)}CO$, $[F]-R^{2(3)}CO-H_2O$, and [E] were present in the spectra. The detection of ammonia adducts of moderate intensity is indicative of some degree of gas phase ammonolysis of the ions. Examples of reconstructed mass chromatograms of the a–b subcomponents $(AT\text{-}DF)_{1a}$ and $(AT\text{-}DF)_{1b}$ are shown in Fig. 4. Although the a–b subcomponents in the series showed partial resolution in HPLC–UV (not shown here), superior separations of the two subcomponents of identical mass were clearly demonstrated in analysis by HPLC–MS and reconstruction of appropriate mass chromatograms.

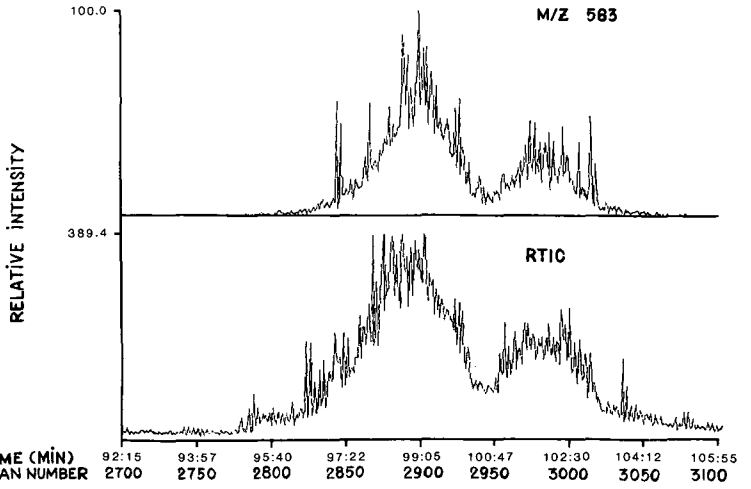

Fig. 3. HPLC–MS chromatograms of a selected pair of methylated antimycin subcomponents: $(AT\text{-}OMe)_{1a}$, left; $(AT\text{-}OMe)_{1b}$, right. RTIC = Reconstructed total ion current chromatogram. Sample injected: 10 μg.

TABLE II

HPLC–MS DATA FOR THE DEFORMYLATED ANTIMYCIN A COMPLEX (AT-DF)

Component[a]	*m/z* Value of observed ion and its relative abundance in parenthesis[b]								
	[E]	[D]$-CO_2$	[F]$-R^{2(3)}CO-H_2O$	[F]$-R^{2(3)}CO+1$	[C]	[D]	[F]$-NH_3$	[F]	M+1
$(AT\text{-}DF)_{1a}$	153	193	200	218	219	237	285	302	521
	(34)	(26)	(9.8)	(12)	(72)	(100)	(21)	(55)	(49)
$(AT\text{-}DF)_{1b}$	153	193	200	218	219	237	285	302	521
	(47)	(36)	(12)	(10)	(94)	(100)	(24)	(64)	(50)
$(AT\text{-}DF)_{2a}$	153	193	200	218	219	237	271	288	507
	(23)	(20)	(6.6)	(9.7)	(59)	(100)	(19)	(41)	(45)
$(AT\text{-}DF)_{2b}$	153	193	200	218	219	237	271	288	507
	(35)	(29)	(8.9)	(14)	(63)	(100)	(20)	(50)	
$(AT\text{-}DF)_{3a}$	153	193	172	190	219	237	257	274	493
	(39)	(28)	(13)	(16)	(75)	(100)	(23)	(58)	(52)
$(AT\text{-}DF)_{3b}$	153	193	172	190	219	237	257	274	493
	(41)	(26)	(18)	(15)	(76)	(100)	(29)	(60)	(68)
$(AT\text{-}DF)_{4a}$	153	193	172	190	219	237	243	260	479
	(19)	(25)	(10)	(11)	(60)	(100)	(20)	(50)	(45)
$(AT\text{-}DF)_{4b}$	153	193	172	190	219	237	243	260	479
	(26)	(26)	(13)	(12)	(67)	(100)	(21)	(55)	(50)
$(AT\text{-}DF)_{5a}$	153	193	172	190	219	237	229	246	465
	(20)	(29)	(8.3)	(9.3)	(65)	(100)	(23)	(48)	(49)
$(AT\text{-}DF)_{5b}$	153	193	172	190	219	237	229	246	465
	(35)	(25)	(8.9)	(10)	(71)	(100)	(26)	(53)	(55)

[a] For compound abbreviations, see Results and Discussion.

[b] For ion identification, see Figs. 1 and 2.

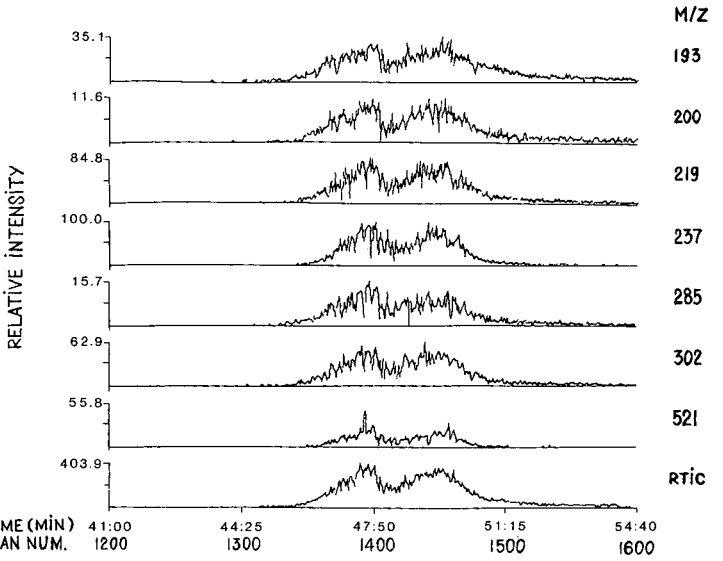

Fig. 4. HPLC–MS chromatograms of a selected pair of deformylated antimycin subcomponents: $(AT\text{-}DF)_{1a}$ (left) and $(AT\text{-}DF)_{1b}$ (right). Sample injected: 10 μg.

TABLE III

HPLC–MS DATA FOR THE N-METHYLATED ANTIMYCIN A COMPLEX (AT-NMe)

Component[a]	*m/z* Value of observed ion and its relative abundance in parenthesis[b]							
	[E]−CH_3	[E]	[D]−CO_2	[C]	[D]	[F]−NH_3	[F]	M+1
$(AT\text{-}NMe)_{1a}$	153	167	207	233	251	285	302	535
	(16)	(81)	(18)	(75)	(95)	(69)	(97)	(100)
$(AT\text{-}NMe)_{1b}$	153	167	207	233	251	285	302	535
	(18)	(90)	(19)	(77)	(97)	(74)	(95)	(100)
$(AT\text{-}NMe)_{2a}$	153	167	207	233	251	271	288	521
	(21)	(98)	(13)	(63)	(93)	(76)	(68)	(100)
$(AT\text{-}NMe)_{2b}$	153	167	207	233	251	271	288	521
	(25)	(98)	(15)	(66)	(93)	(80)	(73)	(100)
$(AT\text{-}NMe)_{3a}$	153	167	207	233	251	257	274	507
	(12)	(58)	(15)	(60)	(97)	(78)	(45)	(100)
$(AT\text{-}NMe)_{3b}$	153	167	207	233	251	257	274	507
	(15)	(62)	(16)	(69)	(96)	(79)	(53)	(100)
$(AT\text{-}NMe)_{4a}$	153	167	207	233	251	243	260	493
	(36)	(94)	(15)	(80)	(93)	(35)	(20)	(100)
$(AT\text{-}NMe)_{4b}$	153	167	207	233	251	243	260	493
	(23)	(89)	(19)	(77)	(95)	(58)	(53)	(100)
$(AT\text{-}NMe)_{5a}$	153	167	207	233	251	229	246	479
	(23)	(58)	(12)	(58)	(83)	(98)	(14)	(100)
$(AT\text{-}NMe)_{5b}$	153	167	207	233	251	229	246	479
	(10)	(83)	(13)	(71)	(90)	(87)	(33)	(100)

[a] For compound abbreviations, see Results and Discussion.

[b] For ion identification, see Figs. 1 and 2.

TABLE IV

HPLC–MS DATA FOR THE ANTIMYCIN LACTONE COMPLEX [4-ACYLOXY-3-ALKYL-5-METHYL-γ-BUTYROLACTONE (AT-LCT)]

Component[a]	*m/z* Value of observed ion and its relative abundance in parenthesis[b]				
	$M-R^{2(3)}CO+1$	$M+1$	$M+NH_4-1$	$M+NH_4$	$M+NH_4+1$
$(AT\text{-}LCT)_{1a}$	200 (20)	285 (38)	301 (23)	302 (100)	303 (15)
$(AT\text{-}LCT)_{1b}$	200 (22)	285 (49)	301 (21)	302 (100)	303 (17)
$(AT\text{-}LCT)_{2a}$	200 (16)	271 (32)	287 (25)	288 (100)	289 (16)
$(AT\text{-}LCT)_{2b}$	200 (20)	271 (33)	287 (27)	288 (100)	289 (16)
$(AT\text{-}LCT)_{3a}$	172 (25)	257 (61)	273 (35)	274 (100)	275 (22)
$(AT\text{-}LCT)_{3b}$	172 (26)	257 (69)	273 (40)	274 (100)	275 (20)
$(AT\text{-}LCT)_{4a}$	172 (13)	243 (40)	259 (29)	260 (100)	261 (17)
$(AT\text{-}LCT)_{4b}$	172 (14)	243 (45)	259 (30)	260 (100)	261 (19)

[a] For compound abbreviations, see Results and Discussion.
[b] For ion identification, see Figs. 1 and 2.

Table III shows the HPLC–MS data for the 3′-N-methyl-analogues of antimycin A complex, AT-NMe ([A] in Fig. 1). In the spectra of the homologous series, the most intense ion was the protonated molecule $(M+1)^+$ under the HPLC–MS conditions employed. It was noteworthy that no detectible ions were produced by deacylation. This mode of fragmentation was significant in the case of the deformylated compounds (described in the preceding paragraph) differing merely at the 3′-N-substituents from the compounds in the present case. By careful examination of fragmentation patterns and protonated molecules, we were able to determine for the first time structures of the hitherto unknown AT-NMe compounds present in the crude reaction products. The structures were later confirmed by ^1H and ^{13}C NMR spectrometry [10].

4-Butyrolactone complex ([B] in Fig. 1), known as antimycin lactone (AT-LCT), is a mixture of the primary degradation products of antimycin A in mildly alkaline media. Since the acyloxy side-chains of the lactone products have been established to be identical with those of parent antimycins [10], it was deemed logical to include these environmentally important lactones in this study. The HPLC–MS results for the compounds in this series are presented in Table IV. Interestingly, the base peaks were the ammonia adducts of the intact molecules, $(M+NH_4)^+$, which is illustrative of the molecular stability of the five-membered ring systems in 4-butyrolactones under the ionization conditions. In contrast, the base peaks in the spectra of the dilactones were ascribed to various ions other than the ammonia adducts of the intact molecules. As

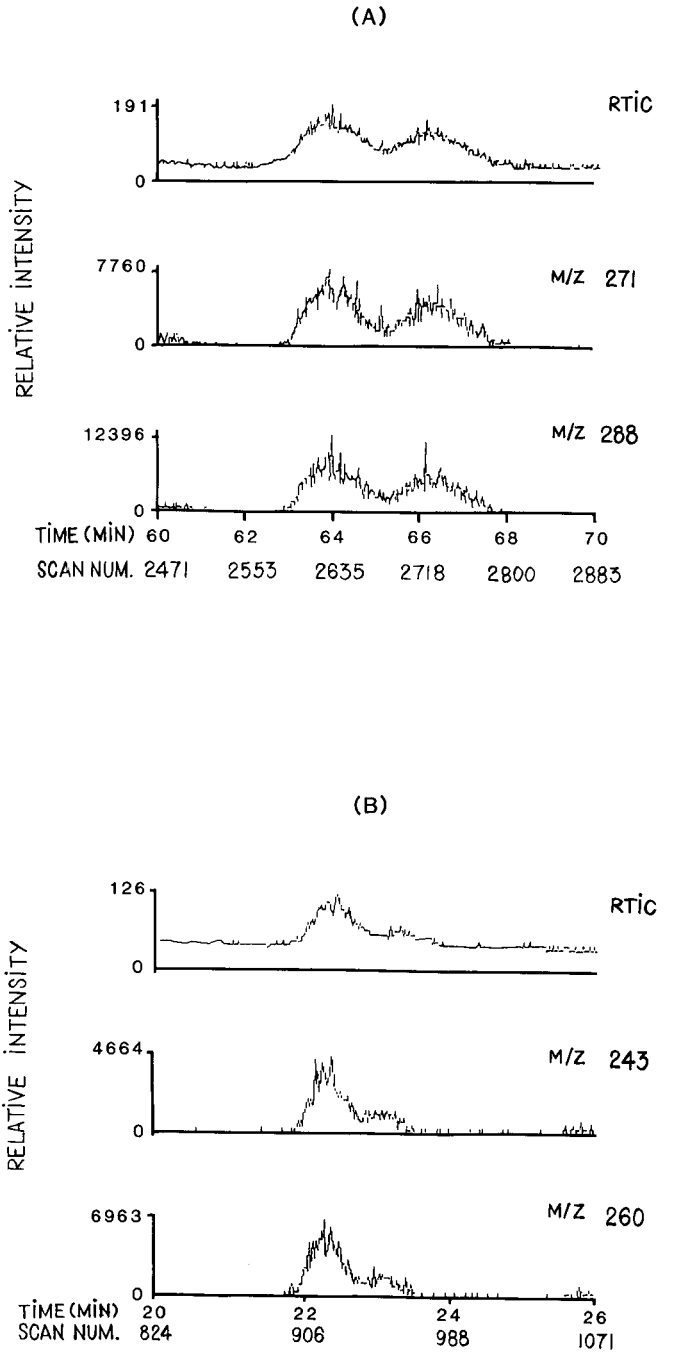

Fig. 5. HPLC–MS chromatograms of minor antimycin lactone homologues $(AT\text{-}LCT)_2$ and $(AT\text{-}LCT)_4$ with subcomponents: (A) $(AT\text{-}LCT)_{2a}$ (left) and $(AT\text{-}LCT)_{2b}$ (right), sample injected: 10 μg, and (B) $(AT\text{-}LCT)_{4a}$ (left) and $(AT\text{-}LCT)_{4b}$ (right). These subcomponents correspond to the 2a, 2b, 4a, and 4b peaks in Fig. 6. Each sample injected: 10 μg.

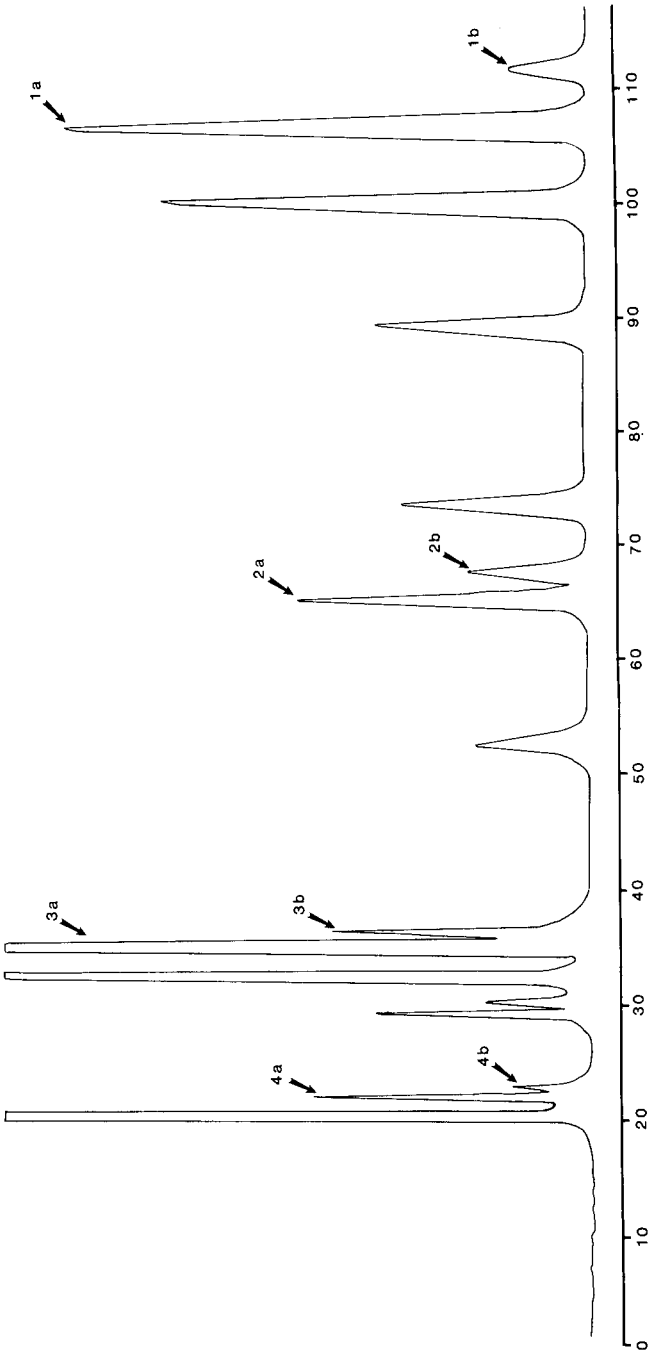

Fig. 6. HPLC–UV chromatogram of a crude sample of antimycin lactones. Sample injected: 80 μg. The chromatogram was obtained under HPLC conditions identical with those in Fig. 5.

compared with the spectral data for the dilactones described in the foregoing paragraphs fewer ions were generated by HPLC–MS of homologues in the 4-butyrolactone series. Nonetheless, the specific spectral features for the latter lactones were informative and sufficed for structure identification. In the absence of other detectible ions, the major fragmentation pathway for AT-LCT compounds seemed to proceed via a deacylation process leading to the $(M-R^{2(3)}CO+1)^+$ ion. However, under the experimental conditions employed, there were no fragments formed by alkyl scissions normally observed for some simple lactones [13–16]. Nearly identical spectra were obtained with thermospray MS in the "filament on" mode or in the "discharge" mode as the mechanisms of ion production are identical. Fig. 5 presents HPLC–MS chromatography tracings showing separations of a–b subcomponents in minor homologues $(AT\text{-}LCT)_2$ and $(AT\text{-}LCT)_4$. Without mass spectral data, it was very difficult, if not impossible, to identify these components in the crude degradation products by HPLC–UV (Fig. 6). The latter technique lacks the auxiliary spectral information as provided by HPLC–MS. It is postulated that the vacuum system from the mass spectrometer causes a pressure drop at the end of the LC column resulting in increased resolution. This phenomenon is very observable in GC–MS where the end of the capillary GC column is at the entrance of the ion source, and a larger pressure drop occurs than when the end of the GC column is at ambient pressure. This phenomenon could also occur in HPLC–MS. This may explain why the a–b subcomponents were somewhat better resolved in HPLC–MS than in HPLC–UV. In addition, it was apparent that the minor b-isomers in some cases showed more intense chromatographic peaks in HPLC–MS than HPLC–UV because of the apparent high ionization efficiency of the minor isomers in the former system.

The HPLC–MS data for three different types of 8-hydroxy homologues are shown in Table V. The mixture in each type consists of two homologues that differ in molecular weight by 28 u due to the difference in *n*-butyl and *n*-hexyl of the 7-R^1 alkyl group. Fragmentation of $(AT\text{-}NMe\text{-}8OH)_{1,2}$ under the HPLC–MS conditions employed, yielded a base peak at *m/z* 302 $[(M-ArCO+1)^+$, Fig. 1], whereas under identical conditions the most intense peak for the 7-butyl analogue, $(AT\text{-}NMe\text{-}8OH)_{3,4}$, was found at *m/z* 172 ($[F]-R^{2(3)}CO-H_2O+1$, Fig. 2). While spectral characteristics of homologues in other series were alike and the observed most abundant ions corresponded to the same fragment or $(M+1)^+$ ions in the homologous series, it is unclear why HPLC–MS of the two homologues of AT-NMe-8OH led to base peaks of different fragments shown above. The HPLC–MS spectra of deformyldeacylantimycins, AT-DF-8OH, exhibited fragmentation patterns similar to those of the corresponding N-methyl analogues, except that the dearylcarbonylation process was apparently unimportant in the ionization of the AT-DF-8OH compounds. The $(M+1)^+$ ions of both $(AT\text{-}DF\text{-}8OH)_{1,2}$ and $(AT\text{-}DF\text{-}8OH)_{3,4}$ were responsible for the base peaks observed. Fig. 7 shows a reconstructed total ion current chromatogram and mass chromatograms from the analysis of $(AT\text{-}DF\text{-}8OH)_{1,2}$ which was one of the many ill-resolved, early eluting (first 5 min) components in the crude samples. For unsubstituted aminodilactones (Fig. 1), $(AT\text{-}DB\text{-}8OH)_{1,2}$ and $(AT\text{-}DB\text{-}8OH)_{3,4}$, thermospray ionization of these 3-amino-dilactones afforded the base peaks at $(M+1)^+$ attributable to the protonated molecules. As seen in Table V, relatively simple spectral data for the debenzoylated compounds (AT-DB-8OH) were obtained under the conditions used, though these compounds are the least stable compounds of all types investigated.

TABLE V

HPLC–MS DATA DESACYLATED ANTIMYCIN COMPOUNDS AT-NMe-8OH, AT-DF-8OH AND AT-DB-8OH

Component[a]	*m/z* Value of observed ion and its relative abundance in parenthesis[b]				
	[E]	[D]−ArCO	[F]−$R^{2(3)}CO-H_2O+1$	[D]−CO_2	[F]−$R^{2(3)}CO+1-NH_3$
$(AT\text{-}NMe\text{-}8OH)_{1,2}$	167		200	207	
	(66)		(72)	(72)	
$(AT\text{-}NMe\text{-}8OH)_{3,4}$	167		172	207	
	(82)		(100)	(48)	
$(AT\text{-}DF\text{-}8OH)_{1,2}$	153		200	193	
	(16)		(21)	(16)	
$(AT\text{-}DF\text{-}8OH)_{3,4}$	153		172	193	
	(25)		(45)	(10)	
$(AT\text{-}DB\text{-}8OH)_{1,2}$		102			201
		(19)			(8.6)
$(AT\text{-}DB\text{-}8OH)_{3,4}$		102			173
		(18)			(11)

[a] For compound abbreviations, see Results and Discussion.
[b] For ion identification, see Figs. 1 and 2. Ar = aryl group.

In general, reversed-phase HPLC–MS results of the title dilactones can be interpreted partly based on gas phase ammonolysis [9] as corroborated by the observation of ammonia-containing fragments [E] and [F] in all cases (Fig. 2), and the adduct $[M+NH_4]^+$ in some cases. The occurrence of equimass subcomponents in

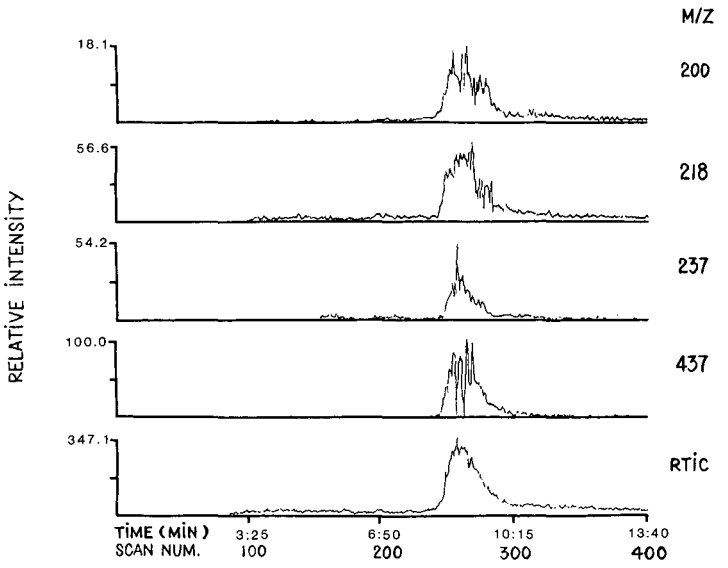

Fig. 7. HPLC–MS chromatograms of deformyldeacylantimycin $(AT\text{-}DF\text{-}8OH)_{1,2}$. Sample injected: 10 μg.

[F]−$R^{2(3)}$CO+1	[C]	[D]	M−ArCO−NH_3+1	M−ArCO+1	M+1
218	233	251	285	302	451
(43)	15)	(12)	(79)	(100)	(13)
190	233	251	257	274	423
(74)	(33)	(25)	(19)	(34)	(27)
218	219	237			437
(77)	(33)	(28)			(100)
190	219	237			409
(80)	(43)	(33)			(100)
218					302
(13)					(100)
190					274
(16)					(100)

lactones having 8-acyloxy side-chains has been unequivocally established and the results were consistent with those reported by NMR assignments [3,4]. The potential analytical utility of the HPLC–MS technique for qualitative analysis of the complex lactone mixtures is demonstrated notwithstanding the noise spikes observed in many cases (Figs. 3, 4, 5 and 7) presumably caused by the unavoidable fluctuation in HPLC pumping systems [17]. This technique is not appropriate for trace analysis due to low sensitivity. The method may be applicable to the quantification of mixtures of antimycin conjugates at sufficient concentrations in biochemical systems. The on-line HPLC–MS technique provides a unique means to direct mixture analysis of enriched samples from tissues and environmental waters treated with antimycin A complex. Logarithmic peak pattern recognition of HPLC chromatograms combined with the mass spectral information facilitate analysis of antimycin residues and identification of complex degradation products. The method reported here has proven to be the sole instrumental technique for the characterization of new dilactonic products obtained from reaction of antimycin A complex with various reagents. Further, diagnostic product analysis of mixtures of unknown derivatives of antimycin A complex can be carried most effectively by HPLC–MS.

ACKNOWLEDGEMENT

The authors wish to acknowledge The Center for Advanced Food Technology (CAFT), a New Jersey Commission on Science and Technology Center.

REFERENCES

1 E. E. Van Tamelen, J. P. Dickie, M. E. Loumans, R. S. Dewey and F. M. Strong, *J. Am. Chem. Soc.*, 83 (1961) 1639; and references cited therein.
2 S. L. Abidi, *J. Chromatogr.*, 447 (1988) 595.
3 S. L. Abidi and B. R. Adams, *Magnet. Reson. Chem.*, 25 (1988) 1078.

4 S. L. Abidi, T. K. Ha and C. L. Wilkins, *Anal. Chem.*, 61 (1989) 404.
5 S. L. Abidi and G. Mack, presented at the *39th Pittsburgh Conference and Analytical Chemistry and Applied Spectroscopy, New Orleans, LA, February 22–27, 1987.*
6 S. L. Abidi, *J. Chromatogr.*, 234 (1982) 187.
7 S. L. Abidi and S. Callister, unpublished results.
8 M. L. Vestal, *Science (Washington, D.C.)*, 226 (1984) 275.
9 K. D. Haegele and D. M. Desiderio, Jr., *J. Org. Chem.*, 39 (1974) 1078; and references cited therein.
10 S. L. Abidi and R. T. Rosen, *J. Org. Chem.*, submitted for publication.
11 G. M. Tener, F. M. Bumpus, B. R. Dunshee and F. M. Strong, *J. Am. Chem. Soc.*, 75 (1953) 1100.
12 S. L. Abidi, *J. Chromatogr.*, 464 (1989) 453.
13 L. Friedman and F. L. Long, *J. Am. Chem. Soc.*, 75 (1953) 2832.
14 W. H. McFadden, E. A. Day and M. J. Diamond, *Anal. Chem.*, 37 (1965) 89.
15 E. Honkanen, T. Moisio and P. Karvonen, *Acta Chem. Scand.*, 19 (1965) 370.
16 B. J. Millard, *Org. Mass. Spectrom.*, 1 (1968) 279.
17 M. L. Vestal, Vestec Corp., Houston, TX, personal communication.

Journal of Chromatography, 522 (1990) 195–203
Elsevier Science Publishers B.V., Amsterdam

CHROM. 22 715

Study of the stereochemistry of ethambutol using chiral liquid chromatography and synthesis

B. BLESSINGTON* and A. BEIRAGHI
Bradford University, Pharmacy Department, Pharmaceutical Chemistry, Bradford BD7 1DP (U.K.)
(First received February 27th, 1990; revised manuscript received July 30th, 1990)

ABSTRACT

Ethambutol [N,N-ethylenebis(2-aminobutan-1-ol)dihydrochloride] is shown to have *S,S* absolute stereochemistry by unambiguous synthesis of each of its possible stereomers and chiral chromatography, using Pirkle π interaction chiral stationary phases. Separation of the *R,R*; *S,S* and *R,S* stereomers together with separation of the entantiomers of 2-aminobutan-1-ol, as their perbenzoyl derivatives, is described. The method is used to study therapeutic tablets. Spectroscopic data is used to characterise these derivatives.

INTRODUCTION

Ethambutol is the approved name [1] for the (+)isomer of N,N-ethylenebis(2-aminobutan-1-ol) dihydrochloride (hereafter referred to as the diamine I). It is an important drug [2] used in the treatment of tuberculosis and was introduced by Lederle and marketed under their trade name of Myambutol.

Examination of the structure of the diamine I shows that three stereomers (I_a–I_c) are possible depending on the absolute stereochemistry of the two chiral (*) centres. I_a and I_b are "enantiomers" whilst the third isomer is an optically inactive *"meso"* form.

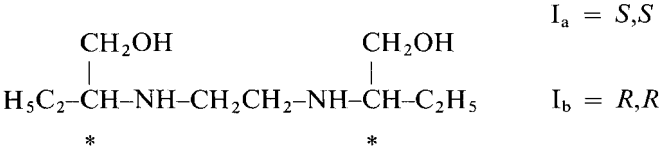

Diamine I

I_a = *S,S*

I_b = *R,R*

I_c = *R,S*

Ethambutol must be prescribed with care [3,4] because of its known visual-disturbance side effects, which may progress to irreversible optic nerve damage. These side effects are associated, to an equal extent, with each of the stereomers (I_{a-c}) [5].

However, the beneficial antibacterial activity [6,7] is markedly dependent upon the stereomer used. The (−)isomer is virtually inactive whilst the (+)isomer is 12 times

0021-9673/90/$03.50

more active than the *meso* isomer. For this reason one "pure" enantiomer (+) is used therapeutically and its specific rotation $[\alpha]_D$ has been specified in official monographs [8–10]. [British Pharmacopoeia (BP), United States Pharmacopoeia (USP), European Pharmacopoeia (EP).]

Early monographs (*e.g.*, BP 1973) only specified the optical activity of ethambutol but this was changed in the 1980 BP to define the absolute stereochemistry of (+)ethambutol as *R,R*. Similar changes took place in the USP and the EP. In contrast, the stereochemistry of (+)ethambutol is shown as *S,S* in Klyne's Atlas [11].

However,the USP XXI (1985) changed the stereochemical designation to *S*-(*R**,*R**) and the BP (1988, amendment No. 3) changed the stereochemistry to *S,S*.

The EP (1987) defined the stereochemistry of ethambutol as *R,R* and also introduced an assay based on the optical rotation of a copper complex, measured at the mercury wavelength 436 nm. This was quite different from the polarimetry studies of the sodium D wavelength 589 nm, used in BP and USP monographs. Clearly there has been serious confusion concerning ethambutol.

We now report studies of the diamine I, using chiral chromatography and synthesis, which permit independent analysis of the three stereomers and confirm the *S,S* absolute stereochemistry of the therapeutic stereomer, (+)ethambutol.

EXPERIMENTAL

Material

Ethambutol hydrochloride was purchased from Sigma (Poole, U.K.). Ethambutol tablets (400 mg) were obtained from the Pharmacy dispensary, Barnsley District General Hospital, Barnsley, U.K. *R*-(−)-2-Aminobutan-1-ol (97%) was purchased from Fluka. *S*-(+)-2-aminobutan-1-ol (98%), racemic 2-aminobutan-1-ol (97%), benzoyl chloride (99%) and 1,2-dibromoethane (99%) were purchased from Aldrich (Gillingham, U.K.). All solvents used were HPLC grade, other materials were of laboratory grade and used as purchased.

Equipment

The high-performance liquid chromatographic (HPLC) system used contained an LKB (Bromma, Sweden) 2150 pump and a Rheodyne (Berkeley, CA, U.S.A.) injection valve (Model 7125) with a 20-μl loop. Two chiral columns were used, a (25 cm × 4.9 mm I.D., 5 μm particle size) Pirkle covalent bonded N-3,5-dinitrobenzoyl derivative of D-phenylglycine (Regis, Morton Grove, IL, U.S.A.) and a (25 cm × 4 mm I.D.) Nucleosil Chiral-2 (Macherey-Nagel, Düren, F.R.G.). A variable-wavelength UV detector (DuPont, Stevenage, U.K.) set at 230 nm and a Hewlett-Packard 3388A integrator–printer/plotter were employed. The mobile phase flow-rate was set at 1 ml/min in all studies but two different phase compositions were used, as indicated in the text. Mobile phases were prepared by premixing the required proportions of solvents, by volume, and were used without further degassing or filtration. An in-line filter (2 μm) was fitted between the solvent reservoir and the pump.

IR spectra were run on a Perkin-Elmer 297 instrument. Electron impact mass spectrometry (EI-MS) was carried out on an AEI MS902 instrument, using a direct-insertion probe and electron-impact source (250°C; 70 eV ionising energy), equipped with a Mass Spectrometry Services data system.

Synthesis of the three diamine stereomers of ethambutol

R-(−)-2-Aminobutan-1-ol was reacted with 1,2-dibromoethane, converted to the hydrochloride salt of *R,R*-ethambutol and crystallised from ethanol as outlined [7]. An analogous reaction was carried out using *S*-(+)-2-aminobutan-1-ol to yield the *S,S*-ethambutol isomer.

When the same reaction was carried out using racemic 2-aminobutan-1-ol, a mixture of products was obtained from which the *meso* (*R,S*) isomer of ethambutol selectively precipitated as its free base, as outlined [7]. The contents of the mother liquors were converted to a crystalline hydrochloride salt which was examined by chiral HPLC.

Preparation of perbenzoyl derivatives of individual ethambutol stereomers, micro-derivatisation (general method)

The required diamine (1–2 mg) as its free base or hydrochloride salt was weighed into a quickfit centrifuge tube and sodium hydroxide (2 *M*, 3 ml) was added followed by benzoyl chloride (0.1 ml). The tube was stoppered and swirled for at least 8 min. More benzoyl chloride (0.025 ml) was added and the stoppered tube was shaken for a further 7 min. The mixture was then extracted with dichloromethane (3 × 3 ml) and the pooled extracts were dried over sodium sulphate, filtered and reduced to dryness using a rotary evaporator. The residue was dissolved in hexane–propan-2-ol (10 ml, 75:25, v/v) and examined by chiral HPLC.

This method was used to perbenzoylate ethambutol (Sigma) and ethambutol extracted from a tablet with dichloromethane. Synthetic samples of *S,S*-diamine, *R,R*-diamine, *R,S*-diamine (*meso*) and racemic diamine (*R,R*/*S,S* equal mixture) were also individually derivatised and examined by chiral HPLC.

Subsequent scale up produced sufficient perbenzoylated product for each isomer to permit examination by MS and IR spectroscopy. None of the derivatives could be obtained in crystalline form.

Preparation of the dibenzoyl derivative of R-(−)-2-aminobutan-1-ol (AMB), micro reaction

R-(−)-2-Aminobutan-1-ol (0.04 ml) was pipetted into a volumetric flask (100 ml), dissolved and adjusted to volume with dichloromethane. A sample (1 ml) was transferred to a quickfit centrifuge tube and reduced to dryness with a stream of dry nitrogen. Sodium hydroxide (2.5 *M*, 1 ml) was added to the tube, followed by benzoyl chloride (0.025 ml) and the tube was stoppered and swirled for at least 10 min. The mixture was then extracted with dichloromethane (3 × 3 ml) and the pooled organic layers were dried over sodium sulphate, filtered and reduced to dryness under reduced pressure. The residue was dissolved in hexane–propan-2-ol (12 ml, 9:1, v/v) and examined by chiral HPLC.

Preparation of the dibenzoyl derivatives of S-(+) and racemic AMB

Each sample of AMB was, in turn, derivatised using the micro reaction described for *R*-(−)-AMB above. The derivatives produced were examined by chiral HPLC.

These reactions were scaled up to produce sufficient material from each isomer to enable mass spectrometry and infra red characterisation. Each product was obtained in crystalline form.

RESULTS AND DISCUSSION

Many methods of chiral HPLC analysis have been reported and recently reviewed [12] but few permit the separation of purely aliphatic enantiomers. Usually at least one aromatic ring is required to give the necessary "3-point interaction". In contrast, aliphatic amino acids have been separated by chiral gas chromatography (GC) [13,14].

Our initial approach was to examine ethambutol, its stereomers and its synthetic precursor AMB as both their free bases and as their trifluoroacetyl derivatives [15,16] using a XE-60–*S*-valine-*S*-α-phenylethylamide chiral capillary GC column (Chrompack). The trifluoroacetylation procedure and the free base extraction methods used were as reported [16] in the literature. The chiral column was tested using racemic N-trifluoroacetyl amino acid-*n*-butyl esters [17].

Achiral GC, using both packed and capillary columns, was used to monitor the extraction and derivatisation stages, prior to examination of the free bases and their trifluoroacetyl derivatives on the chiral GC column.

Chiral GC results were, in our hands, disappointing because we could not detect any separation of racemic AMB, either as its free base or its trifluoroacetyl derivative. The chiral column was shown to be in working order as it gave baseline separation for each derivatised racemic amino acid (Ala, Val, Leu). With ethambutol no peak could be eluted, either as free base or trifluoroacetyl derivative, because of the low thermal stability of the chiral column (maximum operating temperature 190°C).

Our next approach was to study chiral HPLC. We initially chose Pirkle-type columns since they are some of the less expensive chiral columns, were in use already in our laboratory and are relatively robust. A prerequisite of such studies was derivatisation. Perbenzoyl derivatives were made since they contained both an aromatic ring chromophore to enable UV detection and amide/ester groups capable of dipole stacking and so producing strong, enantioselective column interactions. These derivatives were only examined on two different π-interation chiral stationary phases (CSPs) because of cost limitations. Preliminary results were encouraging so reference compounds were synthesised and examined.

Synthetic procedures

Individual isomers (*S,S* and *R,R*) of the diamine were prepared by reacting *S*-(+)-AMB or *R*-(−)-AMB respectively with 1,2-dibromoethane, as outlined by Wilkinson *et al.* [7].

The absolute stereochemistry of each AMB isomer was specified in the supplier's catalogue and we assumed they correspond to the chemical transformation reactions from *S*-(−)-methionine outlined in Klynes and Buckingham's work [11].

An analogous reaction was carried out using racemic AMB. Part of the yield crystallised first as a relatively insoluble free-base, corresponding to the *R,S-"meso"*-diamine isomer as reported by Wilkinson and co-workers [6,7]. The remainder of the yield was subsequently obtained as a crystalline hydrochloride. This was essentially a racemic mixture (equal *R,R* and *S,S* isomers) contaminated with a variable amount of *"meso"* isomer.

Derivatisation procedure

The same general reaction (Schotten Baumann) was used to perbenzoylate each of the above synthetic diamines and mixtures of diamine stereomers, as well as starting AMB stereomers and commercial ethambutol.

The nitrogen base or its hydrochloride was dissolved in aqueous alkali and then swirled with excess benzoyl chloride at room temperature. If the benzoyl derivatives were in sufficient quantity and crystalline they were collected by filtration. If not, they were extracted into dichloromethane. The organic solvent was dried, removed under reduced pressure and the residue was dissolved in appropriate mobile phase prior to HPLC.

Spectroscopic characterisation of perbenzoyl derivatives

The perbenzoyl derivative of racemic AMB was obtained as a crystalline product (m.p. 102–104°C). Its IR spectrum (KBr disc) showed two carbonyl absorbances at wavenumbers 1630 cm^{-1} (amide group) and 1710 cm^{-1} (ester) together with a singlet N–H absorbance at 3300 cm^{-1}.

Its low-resolution EI-MS showed a weak (M^+) molecular peak at *m/z* 297.

These data are consistent with the dibenzoylation reaction shown below.

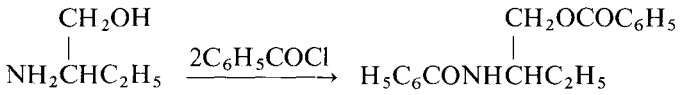

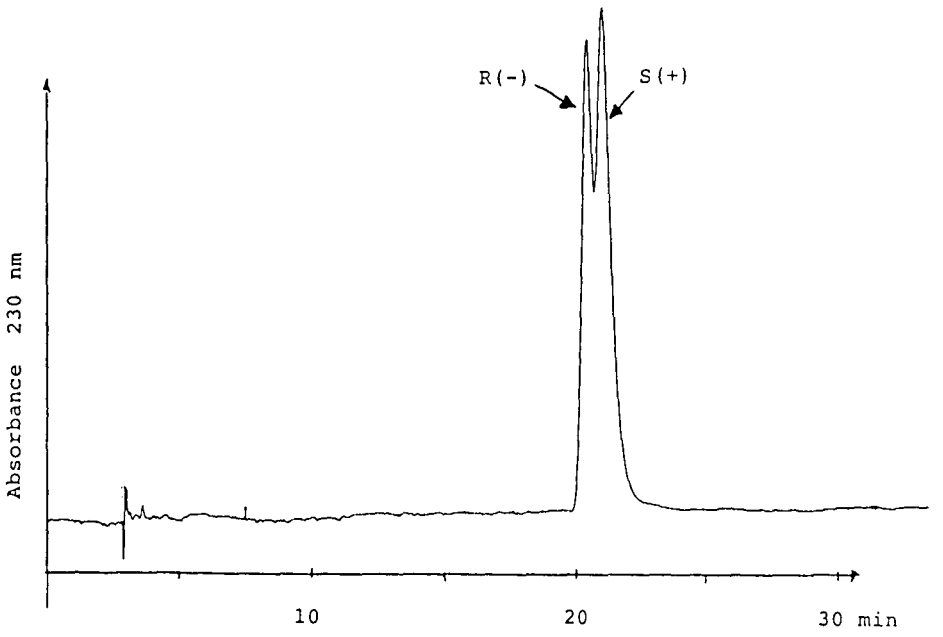

Fig. 1. Separation of enantiomers of 2-aminobutan-1-ol, as perbenzoyl derivatives on a Pirkle D-phenylglycine column. Mobile phase, hexane–propan-2-ol (9:1, v/v). Flow-rate, 1 ml/min. Equivalent to 5 μg of free base "on column".

A similar crystalline product (m.p. 112–113°C) was obtained when *R*-(−)-AMB was similarly treated. Its IR and MS spectra were almost identical to those of the racemic derivative. However, both these dibenzoyl derivatives could be clearly distinguished when studied by chiral chromatography (see Figs. 1 and 2).

When ethambutol dihydrochloride (Sigma) was perbenzoylated in a similar manner a non-crystalline product was obtained. Its IR spectrum (chloroform solution) showed two carbonyl absorbances at wavenumbers 1720 cm^{-1} (ester) and 1630 cm^{-1} (amide). No N–H band at 3300 cm^{-1} was observed.

Its low-resolution EI-MS was not definitive because a very weak and hard-to-measure molecular peak was observed at *m/z* 619. However, significant fragment peaks were observed at *m/z* 591 ($M - C_2H_5$), 515 ($M - C_6H_5CO$) and 485 ($M - CH_2OCOC_6H_5$). Work using NMR and milder ionisation methods (chemical ionization, fast atom bombardment) is in hand to rigorously establish the structure of this derivative.

The above spectroscopic data are consistent with the tetrabenzoylation reaction shown below.

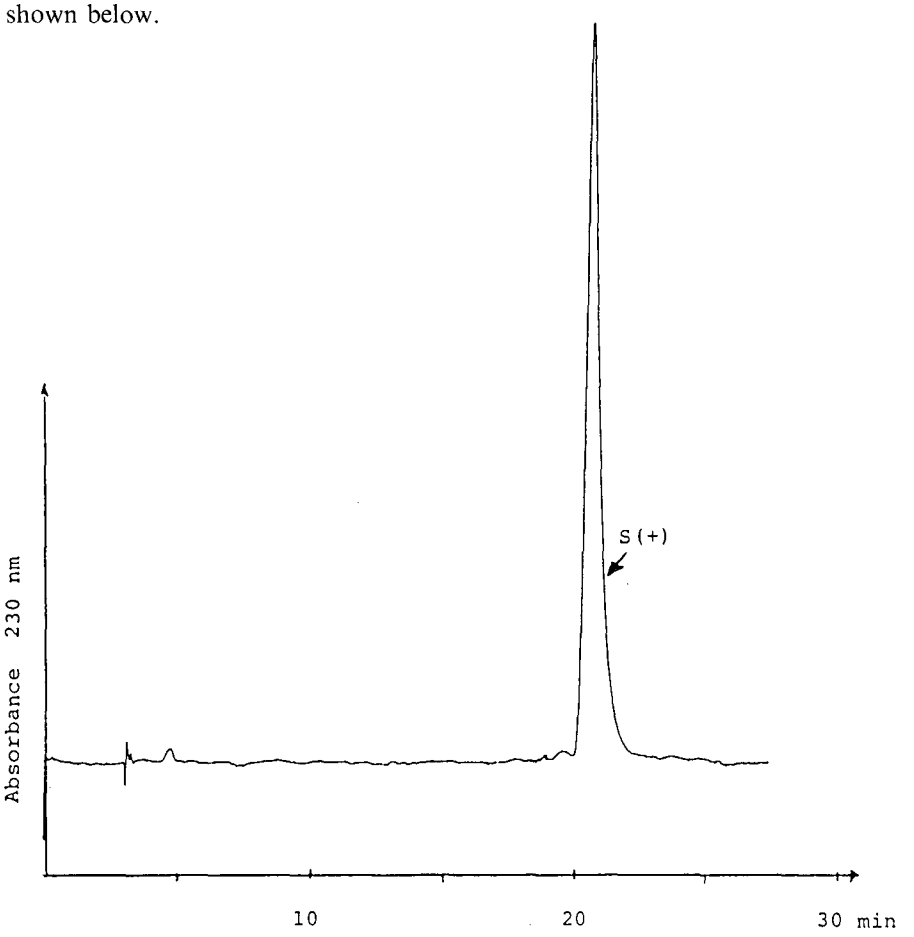

Fig. 2. Commercial sample of *S*-(+)-2-aminobutan-1-ol, as its perbenzoyl derivative on a Pirkle D-phenylglycine column. Mobile phase, hexane–propan-2-ol (9:1, v/v). Flow-rate, 1 ml/min. Equivalent to 5 μg of free base "on column".

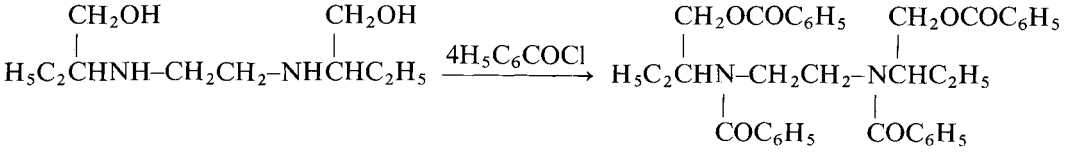

Similar perbenzoylation reactions were carried out starting with our synthetic samples of *S,S*-; *R,R*-; *R,S*-(*meso*)- and racemic (*S,S*/*R,R*)-diamines. All these derivatives were obtained in non-crystalline form and their MS were very similar.

However, all stereomers could be distinguished when examined by chiral HPLC (see Figs. 3 and 4).

Micro derivatisation

To facilitate chromatographic studies and as a preliminary to developing a usable assay, a simplified microderivatisation procedure, involving no crystallisation stages, was developed. This was applied to each of the commercial or synthetic materials discussed above as well as being used to study ethambutol in tablets. In this way samples (*ca.* 1 mg) of AMB or diamine isomers could be rapidly examined.

Chiral chromatography

Two commercial chiral columns were used in isocratic mode (hexane–propan-2-ol, 75:25, v/v). The first was a Pirkle column containing covalently bound, 3,5-dinitrobenzoyl-D-phenylglycine (Regis). The second was a Machery-Nagel column, Nucleosil Chiral 2 but the manufacturers regard this as proprietary and supply no

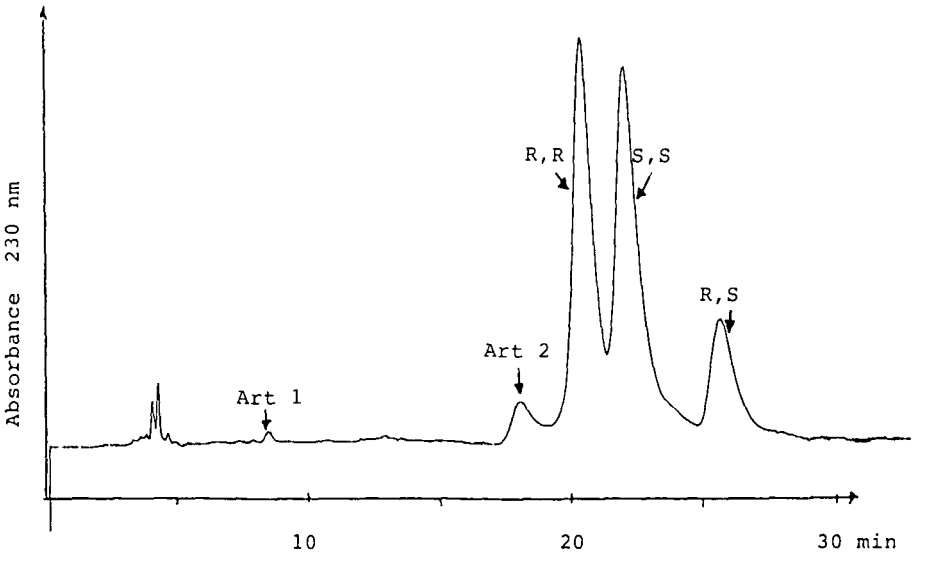

Fig. 3. Separation of a mixture of N,N-ethylenebis(2-aminobutan-1-ol) stereomers and reaction artefacts, as perbenzoyl derivatives on a Pirkle D-phenylglycine column. Mobile phase, hexane–propan-2-ol (75:25, v/v). Flow-rate, 1 ml/min. Equivalent to 1–3 μg of free base "on column".

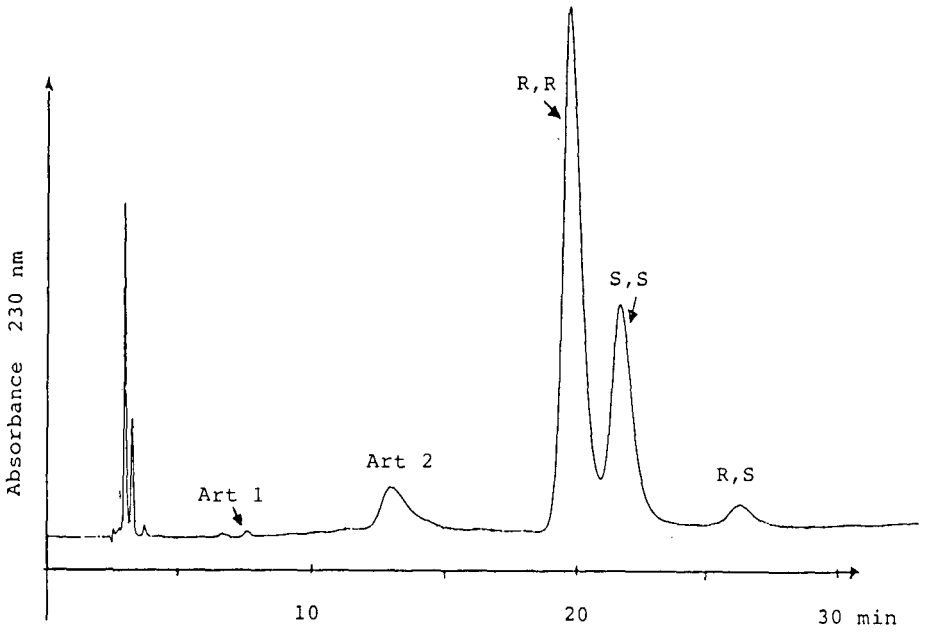

Fig. 4. Separation of a mixture of N-ethylenebis(2-aminobutan-1-ol) stereomers and reaction artefacts, as perbenzoyl derivatives on a Macherey-Nagel Nucleosil Chiral 2 column. Mobile phase, hexane–propan-2-ol (75:25, v/v). Flow-rate, 1 ml/min. Equivalent to 1–3 μg of free base "on column". For peaks Art 1 and Art 2, see text.

details of its chiral ligands or preparation. In previous studies of herbicides we had found this column to behave similar to the Pirkle column.

Both these columns behaved similarly towards the derivatised diamine stereomers (but not amino butanols, see later) and gave separation of all three isomers (see Figs. 3 and 4). By using individual stereomers it was possible to assign the absolute configuration to each elution peak and show that the *R,R*-isomer eluted first, the *S,S*-isomer next and the *R,S-meso*-isomer last. This elution order was the same on both columns.

Samples of ethambutol (Sigma) and ethambutol extracted from a medicinal tablet were microderivatised separately and then shown to correspond to the *S,S*-isomer. In both cases minor impurity peaks could be detected corresponding to the *R,S-meso*-isomer, but no peak corresponding to the *R,R*-isomer was detected. It was noticed during some micro derivatisation runs that two groups of minor peaks sometimes eluted before the diamine derivatives. One (Art 1) appears to arise from AMB contaminating the diamine, particularly some of our synthetic samples. This peak was identified by spiking samples with dibenzoyl AMB. The other (Art 2) peak probably arises from incomplete perbenzoylation since its appearance depends upon the time allowed for derivatisation. The approximate retention time for these artefacts is indicated on the chromatograms (Figs. 3 and 4).

Under the isocratic conditions described for diamine HPLC analysis no separation of the dibenzoyl derivative (Art 1) of racemic AMB was observed.

However, when the mobile phase was changed to hexane–propan-2-ol (90:10, v/v) partial resolution of this dibenzoyl derivative was found using the Pirkle column (see Figs. 1 and 2). The elution order was checked using authentic samples of *R*-(−)-AMB and *S*-(+)-AMB. The derivatised *R*-(−)-isomer eluted first. Surprisingly no resolution on the Nucleosil Chiral 2 column could be obtained. Unless Macherey-Nagel supply further details of its mode of action this column can only be used in an empirical manner.

Both columns gave reproducible separations and were used over several months without obvious deterioration in performance.

CONCLUSION

Unambiguous characterisation of the three stereomers of N,N-ethylenebis(2-aminobutan-1-ol) can be accomplished by perbenzoylation and chiral chromatography, using a covalent Pirkle column. More work is required to validate the method before it can be used for stereochemical and chemical assay of ethambutol.

REFERENCES

1 *British Pharmacopoeia*, Vol. I, HMSO, London, 1980, p. 178.
2 C. S. Lee, L. Z. Benet and K. Florey (Editors), *Analytical Profiles of Drug Substances*, Vol. 7, Academic Press, London, 1978, pp. 231–249.
3 K. Farrar, *Pharm. J.*, 240 (1988) 149–151.
4 L. Dodds, *Pharm. J.*, 240 (1988) 182–183.
5 J. P. Thomas, C. Baughn, R. G. Wilkinson and R. G. Shepherd, *Am. Rev. Respir. Dis.*, 83 (1961) 891.
6 R. G. Wilkinson, R. G. Shepherd, J. P. Thomas and C. Baughn, *J. Am. Chem. Soc.*, 83 (1961) 2212–2213.
7 R. G. Wilkinson, M. B. Cantrall and R. G. Shepherd, *J. Med. Pharm. Chem.*, 5 (1962) 835–845.
8 *British Pharmacopoeia*, Vol. I (Amendment No. 3), HMSO, London, 1988, p. 2.
9 *United States Pharmacopoeia*, Revision XXI, USP Convention, Rockville, 1985, p. 408.
10 *European Pharmacopoeia*, Part II-11, Maisonneuve SA, St. Ruffine, 2nd ed., 1987, p. 553.
11 W. Klyne and J. Buckingham, *Atlas of Stereochemistry*, Chapman & Hall, London, 1974, p. 12.
12 I. W. Wainer, *A Practical Guide to the Selection and Use of HPLC Chiral Stationary Phases*, J. T. Baker, Phillipsburg, NJ, 1988.
13 H. Frank, G. J. Nicholson and E. Bayer, *J. Chromatogr. Sci.*, 15 (1977) 174.
14 W. A. Konig, I. Benecke and S. Sievers, *J. Chromatogr.*, 217 (1981) 71–79.
15 C. S. Lee and L. H. Wang, *J. Pharm. Sci.*, 69 (1980) 362–363.
16 M. R. Holdiness, Z. H. Israili and J. B. Justice, *J. Chromatogr.*, 224 (1981) 415–422.
17 W. A. Konig and S. Sievers, *J. Chromatogr.*, 200 (1980) 189–194.

Journal of Chromatography, 522 (1990) 205–211
Elsevier Science Publishers B.V., Amsterdam

CHROM. 22 653

On-line precolumn photochemical generation of pH gradient: micro-high-performance liquid chromatography of methotrexate and its impurities

JAROSLAV ŠALAMOUN* and KAREL ŠLAIS
Institute of Analytical Chemistry, Kounicova 82, 611 42 Brno (Czechoslovakia)
(First received March 23rd, 1990; revised manuscript received June 26th, 1990)

ABSTRACT

On-line UV irradiation of a flowing mobile phase that contains formate buffer and hydrogen peroxide results in a significant increase in pH owing to the chain reaction to carbonic acid. This reaction was used for pH gradient formation in micro-high-performance liquid chromatography. The gradient was started by switching on a photoreactor which was inserted in front of the injection valve. The shape of the pH gradient was affected by covering part of the PTFE capillary from UV light. The range between the initial and final pH values corresponds to the range of pK_a values of formic and carbonic acid. The use of photochemical pH control for the separation of methotrexate and its impurities without buffer mixing is illustrated. The reproducibility of retention times was better than 1% and of peak heights better than 25%. The detection limit for methotrexate was 5 pmol at 315 nm.

INTRODUCTION

The popularity of microcolumn high-performance liquid chromatography (HPLC) has increased in recent years [1,2]. However, special requirements are placed on the miniaturization and optimization of the instrumentation.

Generally, the analytical sensitivity and selectivity can be improved by the use of a continuous gradient of the mobile phase composition which leads to a continuous decrease in solute retention on the separation column [3]. The retention of ionizable solutes can be controlled by adjusting the mobile phase pH, ionic strength and concentrations of organic solvents and ion-interacting compounds. In micro-HPLC tubular mixers [4,5], which can generate a gradient of variable profile for microcolumns of 1 mm I.D., splitters [6] with a conventional low-pressure gradient system and small-volume mixing vessel and magnetic stirrer [7,8] have been suggested.

An example of a pH gradient elution programme based on trichloroacetate reduction generated in a coulometric cell by the control of the electrolysis current without buffer mixing was demonstrated by Wright and Evilia [9]. This gradient programme was used for the separation of amino acids in preparative chromatography.

0021-9673/90/$03.50

Baxendale and Wilson [10] described the chain reaction of formic acid with hydrogen peroxide when irradiated by UV light:

$$H_2O_2 \rightarrow HO^{\cdot} + HO^{\cdot}$$
$$HO^{\cdot} + HCO_2H \rightarrow H_2O + {}^{\cdot}CO_2H$$
$${}^{\cdot}CO_2H + H_2O_2 \rightarrow CO_2 + H_2O + HO^{\cdot}$$
$$HO^{\cdot} + {}^{\cdot}CO_2H \rightarrow CO_2 + H_2O$$

Formic acid of pK_a 3.75 is converted into carbon dioxide or at higher pressures, into carbonic acid of pK_a 6.35.

Recently, hydrogen peroxide was used as a mobile phase additive for the post-column on-line photo-oxidative conversion of the cytostatic drug methotrexate to highly fluorescent products [11,12]. These reactions significantly improved sensitivity and selectivity of HPLC determinations in complex biological matrices. On the other hand, such a small amount of hydrogen peroxide in the mobile phase did not affect the retention and stability of solutes.

Methotrexate (MTX, 4-amino-N^{10}-methylpteroylglutamic acid) is an antifolate that has significant antitumour activity in various neoplastic diseases. The parent compound may contain up to 1% of impurities and/or degradation products which can cause febrile reaction after administration. There is a great need for a selective and sensitive determination of aminopterine (AMTP, 25 times more toxic than MTX) and methopterine (METP, degradation product) in MTX (*e.g.*, [13]). A review [14] that included HPLC methods for the determination of methotrexate has been published. The effect of pH on the retention behaviour of pteroylglutamates has also been reported [13].

In this paper, the photoreaction of formate buffer and hydrogen peroxide for pH gradient formation in micro-HPLC is suggested. An example of the separation of methotrexate from its impurities is demonstrated.

EXPERIMENTAL

Methotrexate (99.5% purity by HPLC), aminopterine (95%) and methopterine (93%) were prepared in the Research Institute of Pure Chemicals (Lachema, Brno, Czechoslovakia). Acetonitrile (LiChrosolv grade) was obtained from Merck (Darmstadt, F.R.G.). All other chemicals were of analytical-reagent grade.

Chromatographic separations were performed on a Spectra-Physics (Darmstadt, F.R.G.) Model SP 8700 liquid chromatograph equipped with Rheodyne Model 7125 six-port valve fitted with a 60-μl external loop. A Model SF 769Z UV detector (Kratos, Ramsey, NJ, U.S.A.) was equipped with a 0.5-μl flow cell and set at 315 nm. An OP 208/1 pH meter (Radelkis, Budapest, Hungary) equipped with a 100-μl flow electrode was connected to the outlet of detector to monitor the pH of the column effluent. Chromatograms were recorded on a TZ 4200 dual recorder (Laboratory Instruments, Prague, Czechoslovakia). A CGC 150 mm × 1 mm I.D. glass microcolumn (Laboratory Instruments) was packed with Silasorb SPH C_{18} (d_p = 7.5 μm) (Lachema).

The photo-oxidation was accomplished in a PTFE capillary (0.35 mm I.D., 1.59 mm O.D.) which was coiled around the moving quartz tube inside which was placed a

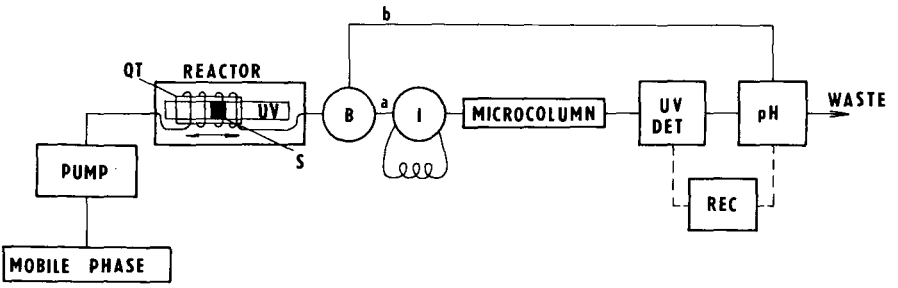

Fig. 1. Schematic diagram of the chromatographic apparatus. Solid lines, liquid connections, dashed lines, electrical connections. I = injection valve; B = bypass-valve; UV DET = UV detector; UV = UV lamp; pH = pH detector; S = strip of black paper; QT = quartz tube.

tubular 8-W low-pressure mercury lamp (GTE, Sylvania G8T5); the length of the irradiated capillary was 500 cm, representing a volume of 480 μl. A strip of black paper served to shield the central part of the capillary from UV illumination. A schematic diagram of the apparatus is shown in Fig. 1.

The mobile phase for the separation of methotrexate and its derivatives was 0.05 *M* formate buffer (initial pH 3.8)–acetonitrile–30% hydrogen peroxide (90:10:0.5, v/v/v) at a flow-rate of 50 μl/min.

RESULTS AND DISCUSSION

Formation of gradient

The typical course of the photoreaction which takes place in the stream of the mobile phase as detected by a pH meter is shown in Fig. 2, which also illustrates the dependence of pH on the irradiation time and shows that the photoreaction is completed in 120 s.

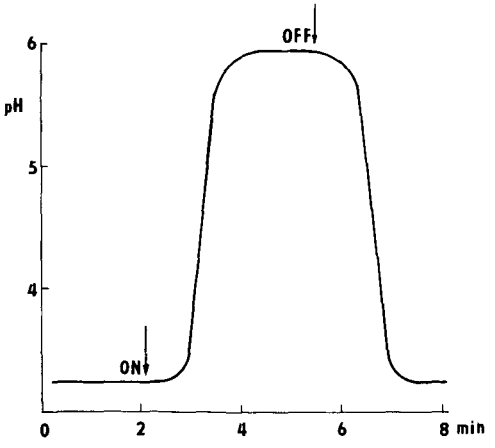

Fig. 2. Time dependence of the pH of the mobile phase after switching on the UV lamp. Configuration of the apparatus as in Fig. 1 (bypass in position b). Mobile phase, 0.05 *M* formate buffer (pH 3.3) with 0.5% of 30% hydrogen peroxide; volume of the PTFE capillary, 480 μl; flow-rate, 200 μl/min.

In order to create different gradient profiles, part of the PTFE capillary was shielded from UV light as shown in Fig. 1. An example of such a profiled gradient is shown in Fig. 3. The part of the curve preceding point 0 has a constant pH determined by the pumped mobile phase. The UV lamp is switched on at time 0 and the gradient is started. The section a represents the volume of the mobile phase, which is illuminated from time 0 to t_1 and the first part of the gradient takes place; t_1 is the time period which the mobile phase needs to pass from the shielded part through the illuminated part of the capillary a (100 μl) to the end of the capillary. In the next segment, b, the mobile phase is irradiated for a time period t_1 and an isocratic part corresponding to the volume of the shielded part of the capillary b (225 μl) is obtained. Part c corresponds to the mobile phase volume illuminated for a time period of t_1 up to time t_2, where a further pH change occurs; t_2 is the time period which the mobile phase needs to pass from entering the irradiated part of the capillary to its shielded part, *i.e.*, 80 μl. The last section, d is where the mobile phase is irradiated for a time $t_1 + t_2$; the photo-oxidation is completed and the pH value remains constant. After the lamp has been switched off, the curve slopes down in two steps. The first one is longer than c and its length is in accord with the larger volume of the first part of the capillary. The middle section, f, is the isocratic part of the previously irradiated part as in b. Broadening of the last section, g, is caused by the dispersion of the corresponding pH gradient band in the capillary. In this a way a variable gradient profile can be formed. Bubbles arising at a formate buffer concentration higher than 0.1 *M* (see below) indicated that some additional reactions can occur. Anyway, the initial gradient shape is rather distorted by mixing in the analytical column, so that a nearly exponential shape is characteristic.

Effect of various parameters on photoreaction

Photochemical reactions are functions of many variables and experimental approaches, and all these variables should be considered whenever one wishes to utilize photochemical reactions in HPLC.

Even the addition of small amounts of methanol limited the photoreaction. On the other hand, acetonitrile did not seriously affect the pH jump, but it was slightly

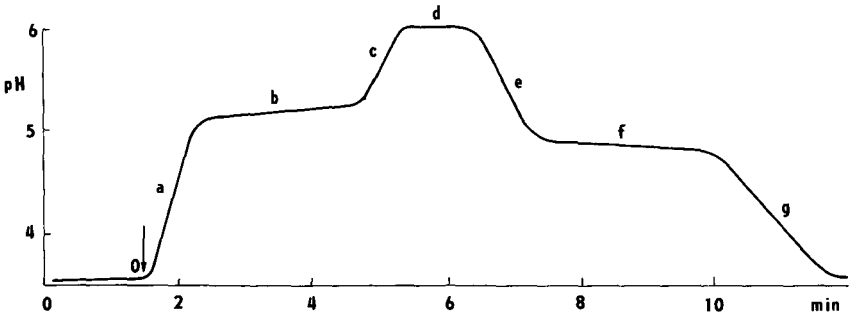

Fig. 3. Formation of the profiled gradient with the aid of a strip of paper shielding part of the PTFE capillary. Configuration of the apparatus as in Fig. 1 (bypass in position b). Mobile phase, 0.05 *M* formate buffer (pH 3.6) with 0.5% of 30% hydrogen peroxide; volume of the PTFE capillary, 480 μl; flow-rate, 100 μl/min; volumes of the parts of the PTFE capillary, a = 100 μl, b = 225 μl, c = 80 μl.

lower. An additional amount of hydrogen peroxide suppressed this decrease. The small concentration of acetonitrile present in the mobile phase did not cause any damage to the PTFE capillary wall or any cracking even at a pressure of 40 bar. The possibility of using small amounts of acetonitrile is also supported by other workers [15,16].

As stated by Baxendale and Wilson [10], in the presence of air the rate of hydrogen peroxide decomposition in the presence of formic acid decreased considerably. However, neither the formate decomposition not the pH change was significantly dependent on the presence of air.

One problem associated with this method of pH variation is the formation of bubbles at formate concentrations higher than 0.1 *M*. This drawback was eliminated at concentrations below than 0.1 *M* and by using a back-pressure source, *e.g.*, a bent PTFE capillary inserted behind the UV detector.

Measurements of the stability of the pH of the mobile phase showed that the pH increased by not more the 0.1 after 24 h.

The pH change is dependent on the initial pH of the formate buffer. At pH $\leq$ 3.0 the pH jump decreased considerably. The negligible change in the presence of an excess of formic acid occurs because only a small amount of formate is present. The formic acid is thus converted into carbonic acid without a significant pH change. A similar effect takes place at high pH values. The optimum region of the initial pH of the formate buffer is 3.0–4.5. However, the method is applicable with pH varying over the range 3–7.5, which covers the range of pH used with modified silica packings in practical HPLC.

Application

In order to demonstrate the utilization of this method, methotrexate and its impurities were separated. The effect of the pH gradient applied in micro-HPLC is shown in Figs. 4 and 5. The sample was first chromatographed isocratically at the initial pH of the formate buffer (Fig. 4a). Only AMPT was eluted, after 16 min; MTX

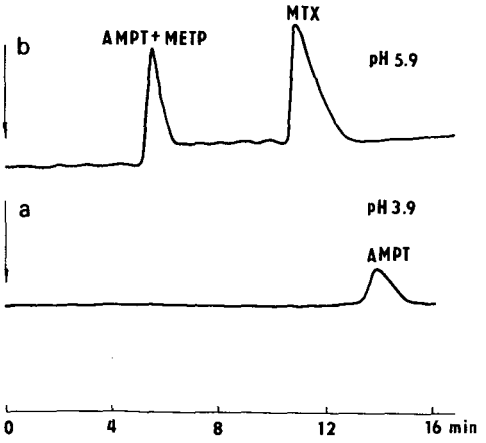

Fig. 4. Chromatograms of a mixture of MTX and its impurities separated with the UV lamp (a) switched off (pH 3.9) or (b) switched on (pH = 5.9). For other conditions, see Experimental.

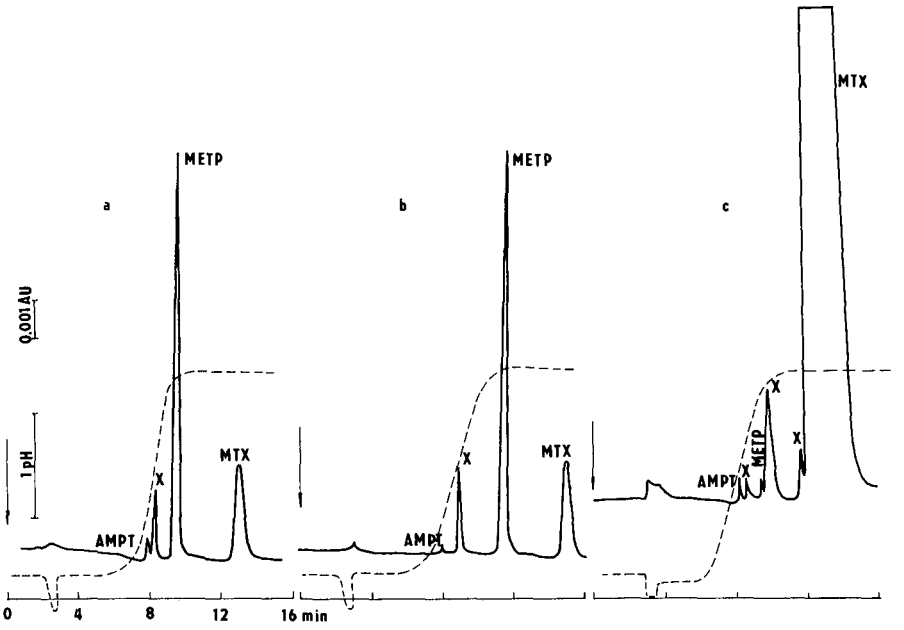

Fig. 5. Chromatograms of MTX and its impurities at (a) the unshielded and (b) and (c) the shielded part (150 μl) of the PTFE capillary. Samples: (a) and (b) mixture of standards; (c) real sample of MTX containing 0.2% of AMPT and 0.15% of METP. X = unknown impurities. For other conditions, see Experimental.

and METP were strongly adsorbed on the reversed-phase material and did not appear even after elution for 35 min. With the lamp switched on at the final pH value, AMPT and METP were coeluted as a broad peak (Fig. 4b). The retention order of compounds is in accord with the results reported by Feyns *et al.* [13].

The influence of the slope of the pH gradient on retention or resolution of solutes is shown in Fig. 5a and b. The unsatisfactory separation of AMPT and an unknown impurity is observed when the pH gradient is too sharp (Fig. 5a). Fig. 5b shows the separation of the same mixture with part of the PTFE capillary shielded from UV light. The resolution of all the peaks in this model mixture was good. Compounds in real MTX sample were also sufficiently separated (Fig. 5c). In addition to the three known compounds, other unidentified peaks were present. The 150-μl volume of the shielded part of the capillary should result in a gradient that is 3 min longer and should also involve two steps. It is possible to explain this smooth gradient by the buffering capacity of silanol groups on Silasorb C_{18} [17].

The jump height decreased to 2 pH units owing to the presence of acetonitrile, as discussed above. The reproducibility of retention times was better than 1% and of peak heights better than 2.5%, as calculated of four injections. The detection limit (signal-to-noise ratio = 3) for MTX was 5 pmol at 315 nm.

CONCLUSIONS

The purpose of these experiments was to demonstrate the feasibility of using a photochemically generated reagent for elution gradient programming. Formation of the gradient during on-line pre-column photo-oxidative reactions is a novel technique in HPLC. It permits variable gradient formation in both directions, *i.e.*, to an upper pH value and also in the opposite direction. The gradient is independent of the injection of the sample and can be started when needed. The method can be applied in micro-HPLC.

ACKNOWLEDGEMENTS

We thank Dr. S. Luňák and Dr. P. Sedlák of the Institute of Inorganic Chemistry of the Czechoslovak Academy of Sciences for advice concerning photochemical reactions.

REFERENCES

1 P. Kucera, *Microcolumn High-Performance Liquid Chromatography*, Elsevier, Amsterdam, 1984.
2 M. Novotný and D. Ishii, *Microcolumn Separations: Columns, Instrumentation, and Ancillary Techniques*, Elsevier, Amsterdam, 1985.
3 P. Jandera and J. Churáček, *Gradient Elution in Column Liquid Chromatography*, Elsevier, Amsterdam, 1985.
4 K. Šlais and V. Preussler, *J. High Resolut. Chromatogr. Chromatogr. Commun.*, 10 (1987) 82.
5 K. Šlais and R. W. Frei, *Anal Chem.*, 59 (1987) 376.
6 Sj. van der Wal and F. J. Yang, *J. High Resolut Chromatogr. Chromatogr. Commun.*, 10 (1987) 82.
7 T. Takeuchi and D. Ishii, *J. Chromatogr.*, 253 (1982) 41.
8 T. Takeuchi and D. Ishii, *J. Chromatogr.*, 279 (1983) 439.
9 J. C. Wright and R. F. Evilia, *J. Liq. Chromatogr.*, 2 (1979) 719.
10 J. H. Baxendale and J. A. Wilson, *Trans. Faraday Soc. Soc.*, 53 (1957) 344.
11 J. Šalamoun and J. František, *J. Chromatogr.*, 378 (1986) 173.
12 J. Šalamoun, M. Smrž, F. Kiss and A. Šalamounová, *J. Chromatogr.* 419 (1987) 213.
13 L. V. Feyns, K. D. Thakker, V. D. Reif and L. T., Grady, *J. Pharm. Sci.*, 71 (1982) 1242.
14 S. Eksborg and H. Ehrsson, *J. Chromatogr.*, 340 (1985) 31.
15 H. Engelhardt and U. D. Neue, *Chromatographia*, 15 (1982) 403.
16 R. W. Schmid and C. Wolf, *J. Chromatogr.*, 478 (1989) 369.
17 S. G. Weber and W. G. Tramposch, *Anal. Chem.*, 55 (1983) 1771.

Journal of Chromatography, 522 (1990) 213–226
Elsevier Science Publishers B.V., Amsterdam

CHROM. 22 762

Use of a short analytical column for the isolation and identification of degradation products of ICI 200 880, a peptidic elastase inhibitor

JOHN C. MEYER*

Analytical New Drug Evaluation Section, Analytical Development and Automation Department, ICI Pharmaceuticals Group, ICI Americas Inc., Wilmington, DE 19897 (U.S.A.)

and

RUSSELL C. SPREEN and JAMES E. HALL

Structural Chemistry Section, Medicinal Chemistry Department, ICI Pharmaceuticals Group, ICI Americas Inc., Wilmington, DE 19897 (U.S.A.)

(Received July 5th, 1990)

ABSTRACT

This paper describes a new approach to maximize sample throughput in an analytical column for the isolation of dilute peptidic compounds. This approach exploits the chromatographic behavior of peptidic compounds which is a large change in retention relative to the change in mobile phase strength. A a result, a small decrease in solvent strength gives added retention without the loss of solubility of the sample. This same behavior also allows the use of an injection solvent which is only slightly weaker than the mobile phase to concentrate the peaks at the head of the column in a solvent overload mode. A short column allows the use of large capacity factors while maintaining reasonable elution times. In addition, cleanup of the column can be accomplished by a single injection of strong solvent in the large loop. This approach was applied to the isolation and identification of degradation products of a peptidic elastase inhibitor, ICI 200 880.

INTRODUCTION

The identification of synthetic impurities and degradation products is part of the characterization of drug substances. These compounds may be present in the drug substance or product at levels under 1%. Some techniques may enhance the concentration of the impurities and degradation products. However, usually these compounds remain as relatively dilute components of the sample. In order to ensure identification and structural verification, sufficient quantities of each unknown must be isolated. This could be as much as 1 mg [1]. In order to obtain these quantities, a preparative strategy to maximize sample throughput is needed.

One approach which has been reported is to use preparative or semi-preparative columns [2]. While a linear relationship exists between sample size and the size of the column with good column technology, scale-up from analytical methods directly has limitations [3]. In addition, preparative chromatography is operated in an over-

0021-9673/90/$03.50

load condition further limiting scale-up. As a result, this approach requires additional development work.

An alternative preparative approach which utilizes an analytical column is displacement chromatography [4,5]. Displacement chromatography involves concentration of the sample on the column using a weak solvent. The components of the sample are displaced from the column using a displacer added to the mobile phase. This approach also requires additional development and column regeneration.

A separation based on the analytical method would be ideal. In order for this to be practical, the loading onto an analytical column would have to be increased and the regeneration between runs minimized. The loading on the column could be optimized by either sample (concentration) overload or volume (solvent) overload conditions [6]. However, both conditions are limited by the resolution between peaks. For reversed-phase separations, the solubility of the analytes usually limits concentration overloading. Since the analytes to be isolated are dilute, optimizing solvent overload conditions offers the best opportunity to maximize throughout. Utilizing a weak injection solvent, the analytes would concentrate at the head of the column similar to displacement chromatography. The limit on the weakness of the solvent is the solubility of the sample.

Peptides have a unique retention characteristic under reversed phase conditions. Namely, there is a large change in retention time with only small changes in organic modifier concentration under isocratic conditions [7]. One approach to control this phenomenon in analytical methods is to use short columns in the gradient mode [8]. However, this characteristic provides the opportunity to increase volume overload without a significant loss of solubility. By operating at high capacity factors (>20), it should be possible to load large volumes of sample onto the column with the sample in the mobile phase. With these high capacity factors, the effect is preconcentration of the band at the head of the column. By reducing the length of the column to a minimum, total run times would be reduced to practical limits.

Another increase in throughput can be realized as a result of the short column. With a reduced void volume and the use of a large loop, a step change gradient of the mobile phase can be utilized to facilitate cleanup using a strong solvent injection. The column should rapidly equilibrate after the injection.

This paper reports the successful application of the use of a short column, operated at large capacity factors, to the isolation and identification of degradation products of ICI 200 880, a peptidic neutrophil elastase inhibitor.

EXPERIMENTAL

Reagents

Acetonitrile was HPLC grade, and acetic acid, acetone, ethyl acetate, glycerol, hydrochloric acid, methanol, phosphoric acid and sodium phosphate were reagent grade from J. T. Baker (Phillipsburg, NJ, U.S.A.). Deuterated dimethylsulphoxide (DMSO-d_6) was 99.9% atom% ^2H from MSD Isotopes (Montreal, Canada). Deionized water was prepared using a Millipore (Bedford, MA, U.S.A.) Milli-Q cartridge deionizer system. ICI 200 880 and synthetic samples of products I and III (see Fig. 1) were provided by Medicinal Chemistry Department, ICI Americas (Wilmington, DE, U.S.A.). Product II was not synthesized.

Chromatographic instrumentation

All chromatographic analyses and isolation procedures were performed on a modular chromatographic system consisting of a Spectra-Physics (San Jose, CA, U.S.A.) Model 8800 pump, a Rheodyne (Cotati, CA, U.S.A.) Model 7010 Injector and a Kratos (Ramsey, NJ, U.S.A.) Model 773 variable-wavelength detector. The loop size on the injector was either 50 μl (analytical mode) or 5 ml (preparative mode). Injections were performed using a Hamilton (Reno, NV, U.S.A.) Model 1005TEFLL 5-ml gas-tight syringe. Analog data from the variable-wavelength detector were converted to digital data and processed using a VG Laboratory Systems (Altrincham, UK) Multichrom chromatographic data acquisition system on a Digital Equipment Corporation (Maynard, MA, U.S.A.) MicroVAX II processor.

The column was a 3.3 cm × 0.46 cm I.D. column packed with 3-μm Supelcosil LC-8 DB from Supelco (Bellefonte, PA, U.S.A.). The mobile phase for the isolation of the preparative separations was acetonitrile–0.1 *M* acetic acid (20:80). The flow-rate was 2.0 ml/min. The back pressure was about 90 bar.

Chromatographic retention studies

The mobile phase was a solution of 0.1 *M* acetic acid and acetonitrile. The concentration of acetonitrile was varied from 18 to 30% (v/v). Analytical samples (1 mg/ml) of ICI 200 880 and products I and III were prepared and injected.

Diluted samples (10 μg/ml) of products I and III were prepared over the range of 10 to 22% acetonitrile in 0.1 *M* acetic acid. Large volumes (5 ml) were injected in the acetonitrile–0.1 *M* acetic acid (20:80) mobile phase to determine the extent of concentration of these analytes at the head of the column.

Degradation products and isolation procedures

Solid-state degradation was produced by heating ICI 200 880 drug substance (80 and 90°C) for three months. Solution degradation products were produced in a 10 mg/ml solution of ICI 200 880 in a 50 m*M* sodium phosphate buffer at pH 7 heated at 80 or 90°C for two to four days.

The degraded solid-state sample was dissolved in acetonitrile and diluted with 0.1 *M* acetic acid to a final concentration of 15% acetonitrile. The solution degradation products were isolated by acidification with phosphoric acid and extraction with ethyl acetate. The ethyl acetate layer was evaporated to dryness at 40°C with a nitrogen stream using an Organomation Associates (New Berlin, MA, U.S.A.) Model 111 N-Evap. The residue was dissolved in acetonitrile and diluted with 0.1 *M* acetic acid to a final concentration of 15% acetonitrile for injection.

After injection, the analytes were collected (rejecting the beginning and end tails of each peak) as each analyte eluted from the column. After the last peak to be collected had eluted, 5 ml of acetonitrile–water (45:55) was injected to elute the remaining peaks (including ICI 200 880) in the sample. The collected portions of each degradation product were pooled and the mobile phase was reduced by evaporation. The residue solution was acidified with phosphoric acid and extracted with ethyl acetate. After evaporation of the ethyl acetate, the residue for each degradation product was dissolved in acetonitrile, diluted with 0.1 *M* acetic acid and reinjected for final purification. The collected portions were concentrated, acidified and extracted with ethyl acetate as above. The ethyl acetate layers were evaporated and transferred to sample vials with acetone.

Mass spectral analysis

Positive ion liquid secondary ion mass spectra (+L-SIMS spectra) were measured using a VG Analytical (Manchester, UK) Model 70-250/SEQ double focusing tandem hybrid mass spectrometer equipped with a standard VG cesium ion gun. The cesium ion gun was operated at 35 kV with an anode emission current of approximately 2 μA. Samples were first dissolved in methanol and then mixed with approximately 1 μl of glycerol (doped with 0.1 *M* HCl) on the surface of the L-SIMS target. The mass spectrum was scanned at a rate of 3 s/decade from *m/z* 950 to 100. Data were collected by multichannel averaging and subsequently mass assigned using a VG OPUS data system.

NMR analysis

The proton NMR spectra were obtained at 400 MHz on a Bruker (Rheinstetten, West Germany) Model AM-400 spectrometer. The samples were dissolved in 0.5

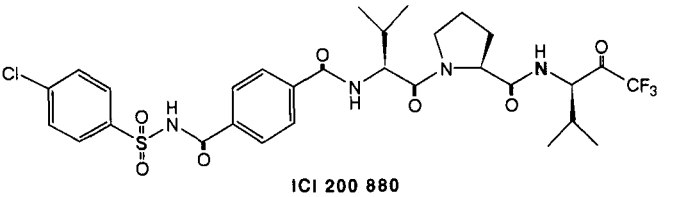

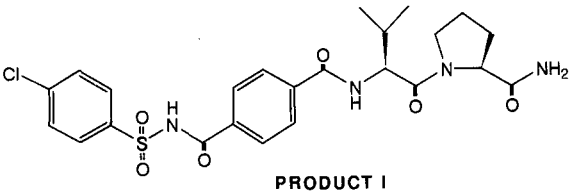

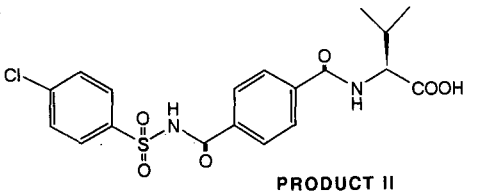

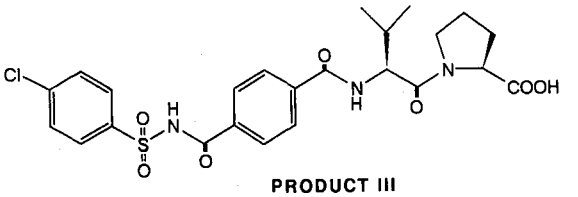

Fig. 1. Structure of ICI 200 880 and its degradation products (isomeric designations in parentheses).

ml DMSO-d_6. The spectra were run in a 5-mm diameter NMR tube at 25°C with a spectral width of 7046 Hz and memory size of 32K words, resulting in a digital resolution of 0.43 Hz/pt.

RESULTS AND DISCUSSION

Chromatographic behavior of components

The peptidic drug substance, ICI 200 880 (Fig. 1) exists as a pair of interconverting diastereoisomers. The SSS isomer is designated as isomer 1 and the SSR isomer is designated as isomer 2. The two isomers are well separated chromatographically, but elute as broad peaks with apparent separation efficiencies on the order of one tenth of that of test solutes on the column. At least two secondary equilibria appear to be the cause of this loss of efficiency. The first is slow positional isomerization around the proline ring [9,10]. The second is the hydration and dehydration of the carbonyl group during the separation process between the hydrophobic stationary phase and the hydrophilic mobile phase.

The drug substance has a large change in capacity factor with relatively small

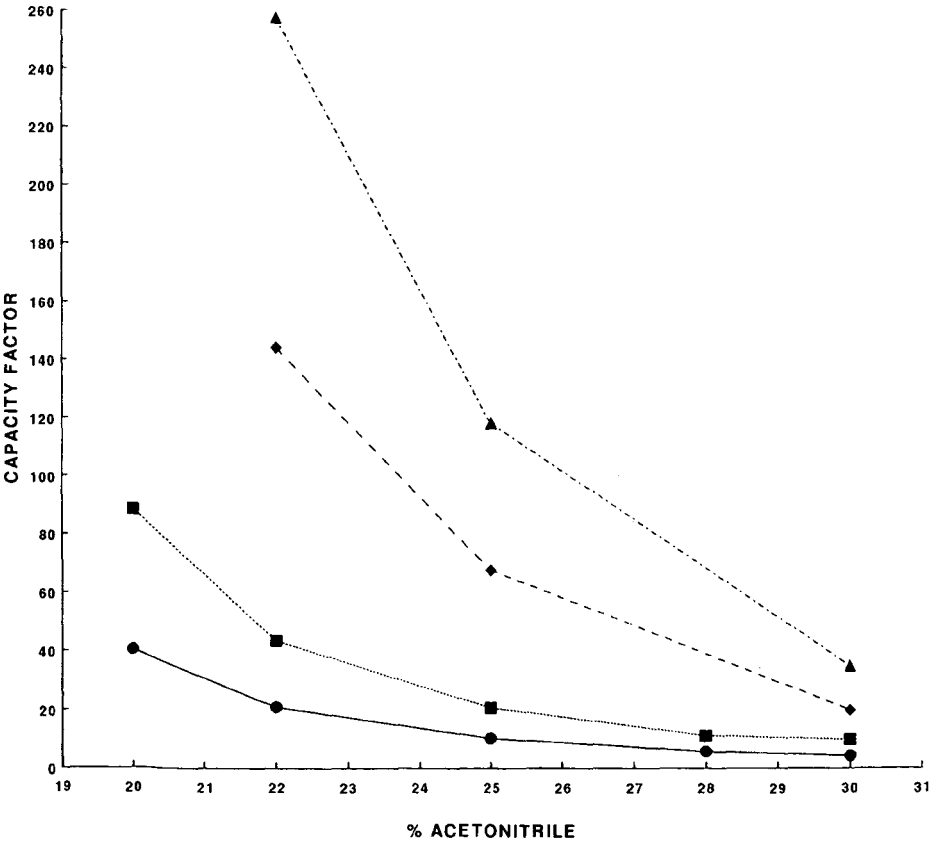

Fig. 2. Effect of solvent strength on the retention of ICI 200 880 isomers and its degradation products on the column. ● = Product I; ■ = product III; ◆ = isomer 1; ▲ = isomer 2.

changes in acetonitrile concentration in the mobile phase. This is shown in Fig. 2. Even at 30% acetonitrile, the capacity factors for the two isomers are large. With a standard 25-cm column, with a void volume of about 2.5 ml, it would take over 40 min for the second isomer to elute with a flow-rate of 2 ml/min. Using a 3.3-cm column, isomer 2 eluted in less than 10 minutes.

The elution behavior of the degradation products was observed to parallel that of ICI 200 880 as seen in Fig. 2, although the large changes were at lower concentrations of acetonitrile. As a result, at concentrations of 20% acetonitrile, all components had capacity factors greater than 40 and the drug substance is essentially retained on the column while the degradation products elute.

In a solvent overload condition, the injection solvent can have a dramatic effect on peak width. The peak width would be equal to the peak width of the analytical peak (normal band spreading) plus the width caused by the large injection volume [6]. For a 5-ml injection, this would be an additional 5 ml of width or 2.5 min at 2 ml/min flow-rate. For the 3.3-cm column, this is over 10 column volumes. By reducing the

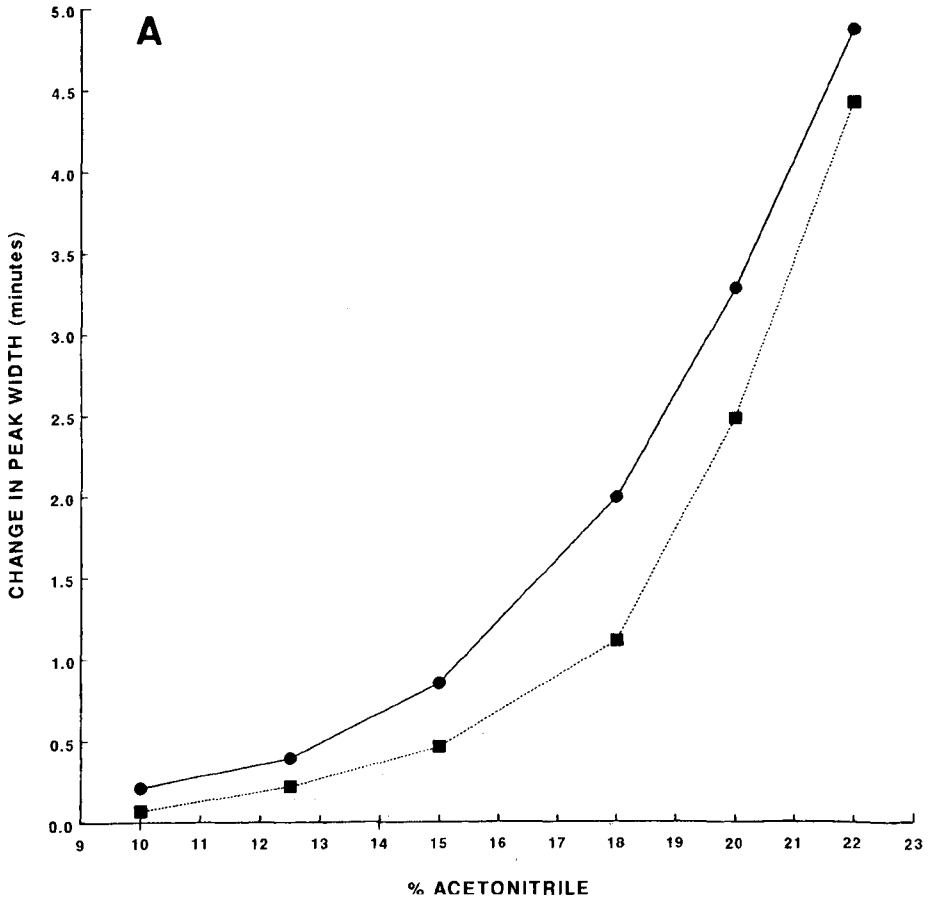

Fig. 3.

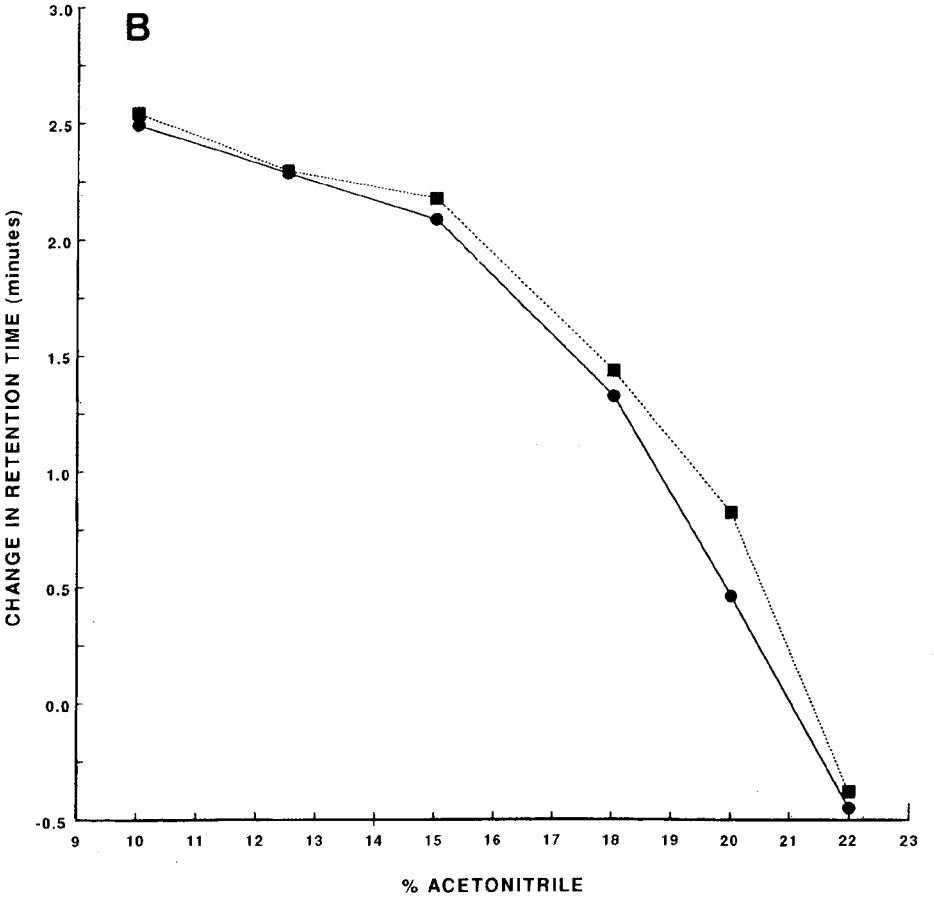

Fig. 3. Effect of injection solvent on sample concentration on column. (A) Effect on peak width. (B) Effect on retention time. ● = Product I; ■ = product III.

solvent strength of the injection solvent, a concentrating effect can be observed.

Fig. 3A shows this concentrating effect on peak width for products I and III (Fig. 1). As the solvent strength of the injection solvent increases from 10 to 22%, the peak widths increase. At 15% acetonitrile, the peak width is only 0.85 min (1.7 ml) more than the analytical peak for product I and only 0.41 min (0.92 ml) more for product III. This is only 34 and 18% of the 5 ml volume injected, for products I and III, respectively. It can be seen that at the longer retention of product III, there is a larger concentrating effect. Even when the injection solvent approaches the mobile phase at 20% acetonitrile, some concentrating effect is realized at high capacity factors. However, at slightly higher acetonitrile concentrations, the peaks broaden even more than the 5-ml volume, with the resultant loss of resolution.

The concentrating effect was also demonstrated by the retention time shifts of the components. In solvent overload conditions, the retention time (center of the band) will be equal to the retention time of the analytical separation plus one half the injection volume divided by the flow-rate. This is 1.25 min for a 5-ml injection. If the analyte is completely retained at the head of the column prior to elution, the retention

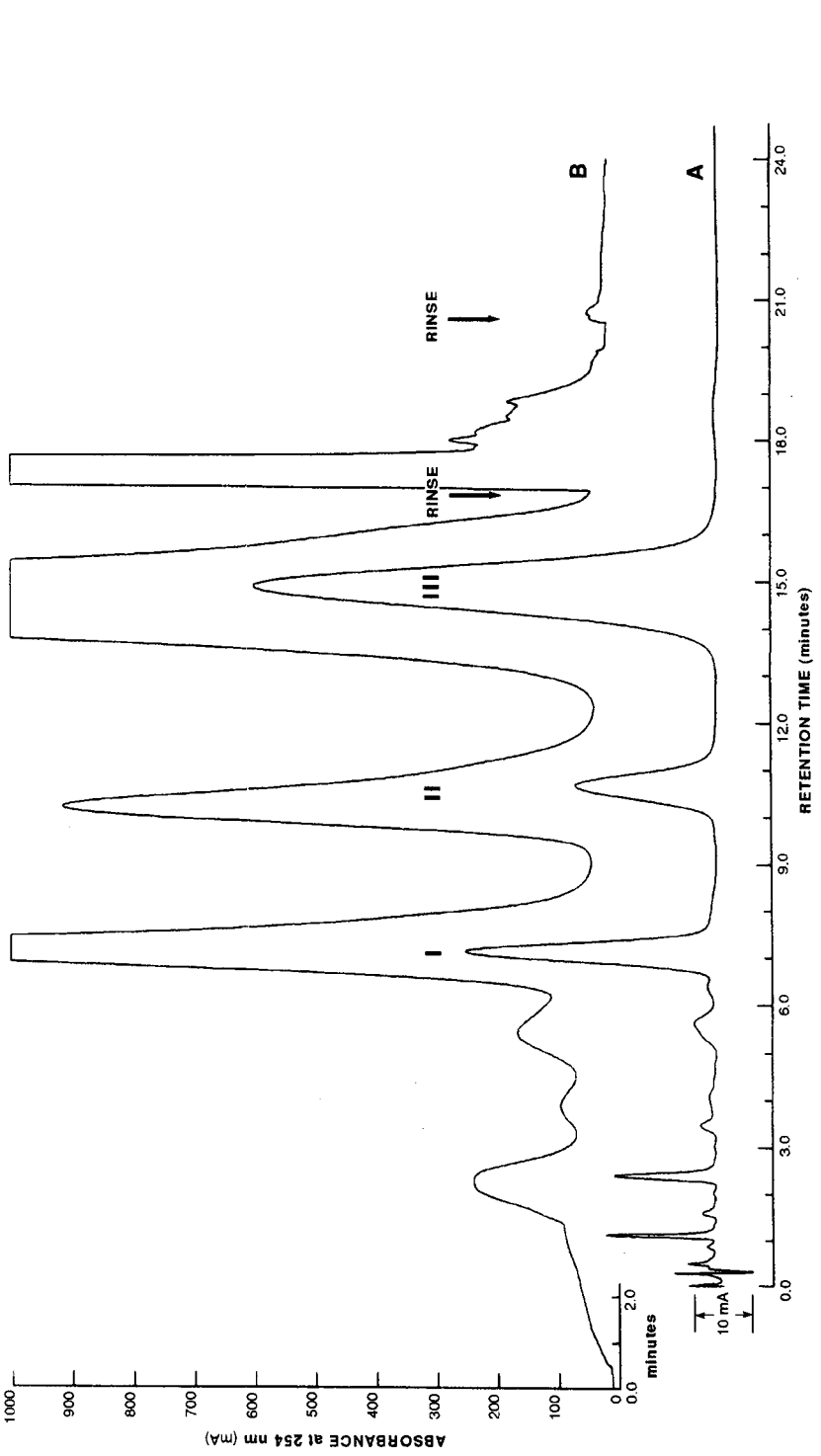

Fig. 4. Chromatograms of ICI 200 880 solid-state degradation products. (a) Analytical separation. (B) Preparative separation. Note the 2-min delay for the preparative separation. Rinse injections shown by arrows. See text for conditions. mA = 10^{-3} absorbance units.

time would increase to the limit of the time for the total injection volume to elute. This would be 2.5 min for a 5-ml injection (at 2 ml/min flow-rate). Fig. 3B shows the shift in retention times of product I and III with acetonitrile concentration in the injection solvent. The trend is according to the prediction. The retention times were shifted a maximum of 2.5 min at 10% acetonitrile. At 15% acetonitrile, the retention times were 2.1 and 2.2 min longer for products I and III, respectively. This is still over 80% of the maximum shift. The use of 15% acetonitrile in the injection solvent was a compromise between the concentrating effect and sample solubility.

Degradation products and isolation procedure

Three degradation products were observed in both solid-state and solution degraded samples (products I, II, and III). The retention times of the three products were similar from both the solid-state and solution studies, suggesting that the degradation products were the same.

In solution, a significant amount of degradation was observed. After four days at 80°C, only 25% of the compound remained. A single peak (product III) accounted for 70% of the 75% loss. Two other minor peaks (products I and II) were about 2 and 1% of the sample, respectively. While all three products were observed in the solid-state samples, much less degradation was observed. Products I, II and III were about 2, 1 and 8% of the sample, respectively.

The chromatograms in Fig. 4 illustrate an analytical and a 5-ml injection of the solid-state degraded samples. In the analytical separation, the peak widths were 1.3, 1.9 and 3.1 min for products I, II and III, respectively. The peak widths for the same components in the 5-ml injection were 2.05, 2.8 and 4.3 min, respectively. These values indicate that a 50 to 75% concentrating effect was realized for a 5-ml injection.

The increases in retention times observed between the analytical and large-volume injection in Fig. 4 were 2.2, 1.7 and 1.9 min for products I, II and III, respectively. These values are close to the predicted value of 2.5 min for complete concentration at the head of the column. Note the 2-min offset of the time axis between the analytical and preparative chromatograms in the figure to account for the delay.

Fig. 5 illustrates similar behavior for the solution sample. The peak widths in the analytical separation were 1.3, 1.8 and 3.5 min for products I, II and III, respectively. The peak volumes for the 5-ml injection were 2.9, 2.75 and 6.2 min, respectively. These results indicate a 40 and 60% concentrating effect for products I and II. It appears that some concentration overload was observed for product III. Retention time increases for the products in the solution sample were also similar to those in the solid-state sample.

Since the 5-ml loop is over 10 column volumes (void volume was 0.4 ml), an injection of a strong solvent is an efficient way of cleanup of late eluting components. After the last peak of interest eluted, the column was rinsed by injection of 5 ml of acetonitrile–water (45:55). Figs. 4 and 5 demonstrate the effectiveness of this technique. The rinse was injected at 19 min (17 min on the analytical chromatogram time axis). An additional 5 ml were also injected at 23 min (21 min on the analytical time axis). Note a minimum of response after the second injection verifying the rinse was complete.

With a target of 1 mg for each component, it was necessary to inject and collect

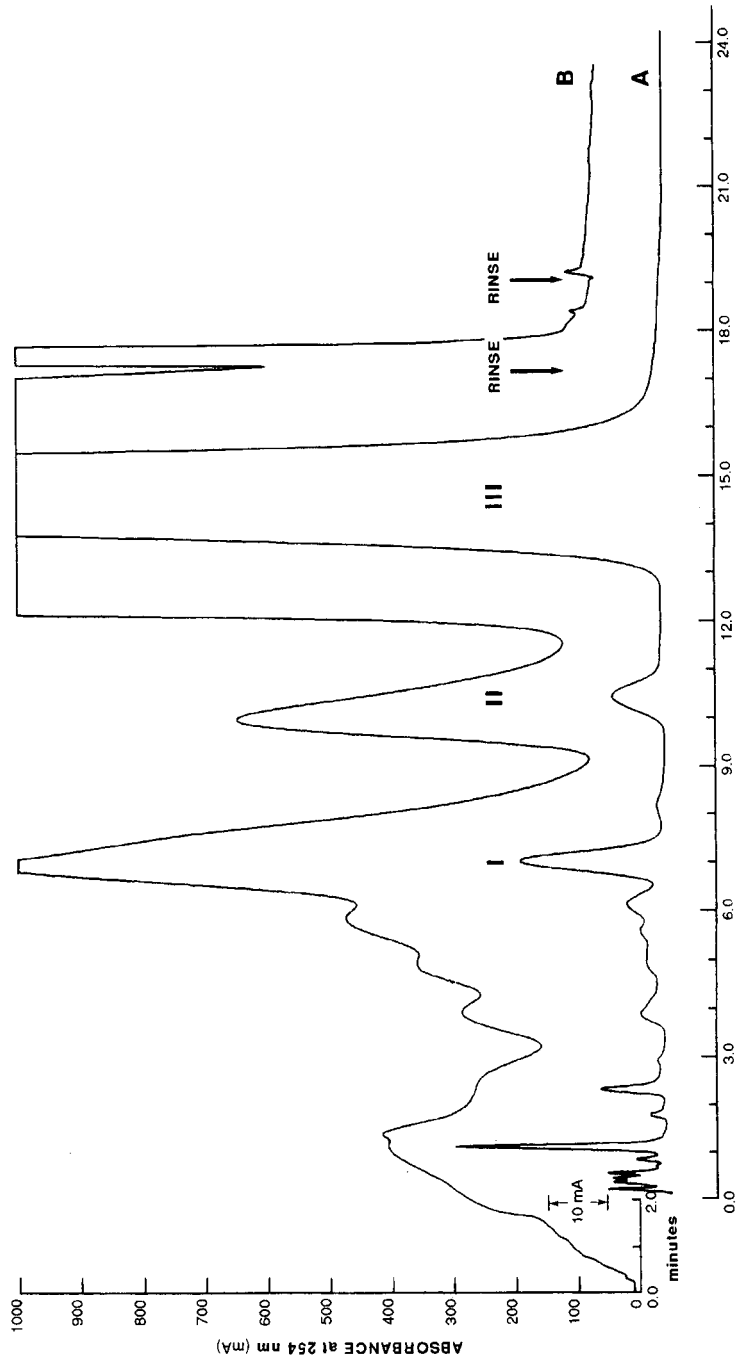

Fig. 5. Chromatograms of ICI 200 880 solution degradation products. (A) Analytical separation. (B) Preparative separation. Note the 2-min delay for the preparative separation. Rinse injections shown by arrows. See text for conditions.

20 × 5 ml of a 1 mg/ml solution of the degraded samples, assuming a 1% level for each degradation product. For products I and III, this was easily achieved. Product II was the smallest product and about 500 μg was isolated from both solid-state and solution samples. Since product II has only 65% of the mass of ICI 200 880, the actual recovery is close to 80%. Since product III was a major component of the solution sample and the largest product in the solid-state sample, it was possible to collect enough of that product in fewer injections. For the rest of the injections of that sample, the injection of the strong solvent rinse was made after product II eluted, saving additional time.

Chromatographic analysis of the products indicated that product I isolated from the solid state did not contain any measurable impurities while it contained about 2% impurities when isolated from the solution sample. Product II contained about 0.5% impurities when isolated from either the solid state or solution sample. Product III did not contain any measurable impurities when isolated from either sample.

Spectral identification and confirmation

Mass spectral results. Representative + L-SIMS spectra obtained from the three major degradation products are shown in Fig. 6. The spectra obtained from either the solid-state or solution samples were similar. The major fragmentation pathways are summarized as inserts in each of the spectra. The fragmentations shown are fully consistent with the proposed structures. In addition to the identifications noted, the signal at *m/z* 133 is believed to originate from Cs^+, and the signal at *m/z* 185 corresponds to the protonated dimer of glycerol $(2G+H)^+$. Products I and III yield spectra which match the spectra obtained from corresponding synthetic standards.

NMR results. Fig. 7 shows the proton NMR spectra of products I, II and III. All of the spectra shown were of samples isolated from degraded solutions of ICI 200 880. The spectra obtained from the solid-state samples were similar. It can be seen that all significant signals are related to the samples with the exception of a peak for acetonitrile (2.1 ppm) used in the isolation and the large broad peak for residual water (3.4 ppm) which was in the sample and in the DMSO-d_6 solvent. There are also several small peaks unrelated to the compounds. However, they do not interfere with the identification of the sample and assignment of the spectra.

The identity of products I and III was verified by comparison of the spectra to spectra of authentic samples. The spectrum of the product II is consistent with a structure that results from loss of the proline function from product III. This interpretation is based on integration of the peaks, splitting patterns, and homonuclear decoupling experiments that determined proton–proton connectivities.

Based on the identification of the products and the chemistry that produced them, it is clear that each reaction would produce two products, one containing an ultraviolet chromophore and one which does not. Therefore, it can be inferred that each of the three identified products has another product associated with it. No attempt was made to find these products in this study.

CONCLUSIONS

The results of these studies demonstrate the effectiveness of the use of a short analytical column in the isolation of peptidic compounds for spectral identification.

The procedure is enhanced by the chromatographic behavior of the degradation products. That behavior of relatively large changes in retention with small changes in solvent strength allows solvent overload conditions and concentration at the head of the column. The short column allows for the use of large capacity factors and for a rapid column cleanup between injections.

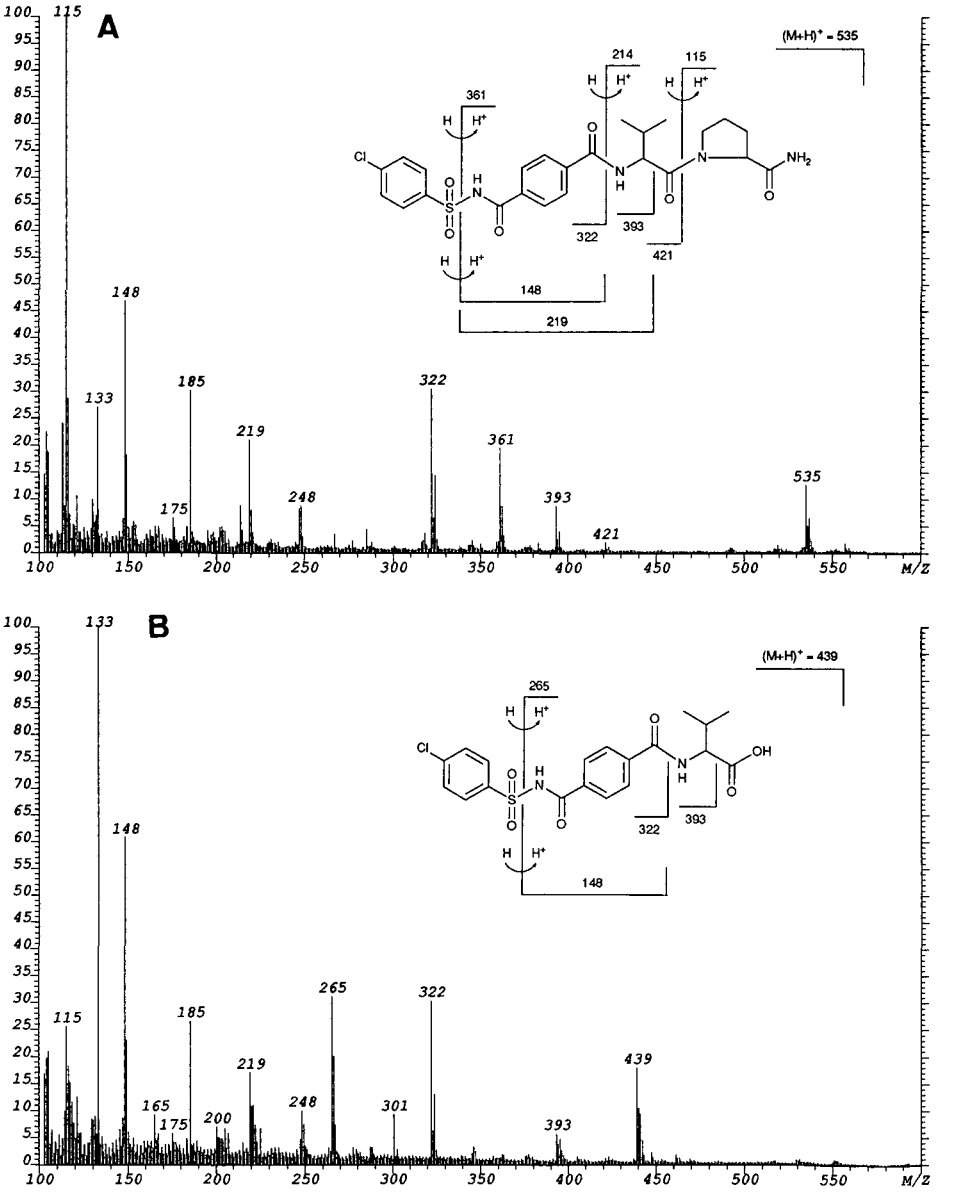

Fig. 6.

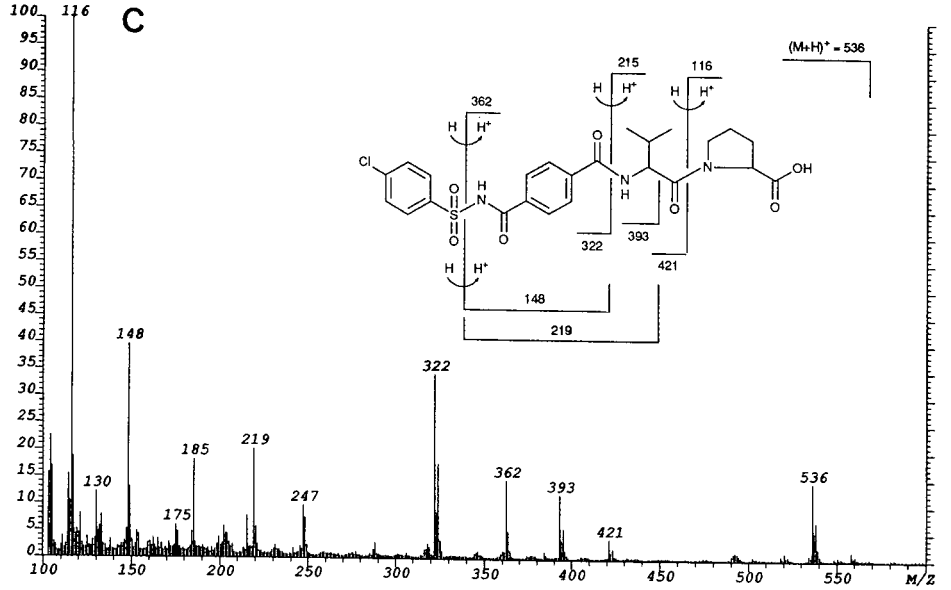

Fig. 6. Positive ion liquid secondary ion mass spectra of the isolated degradation products. (A) Product I; (B) product II; (C) product III.

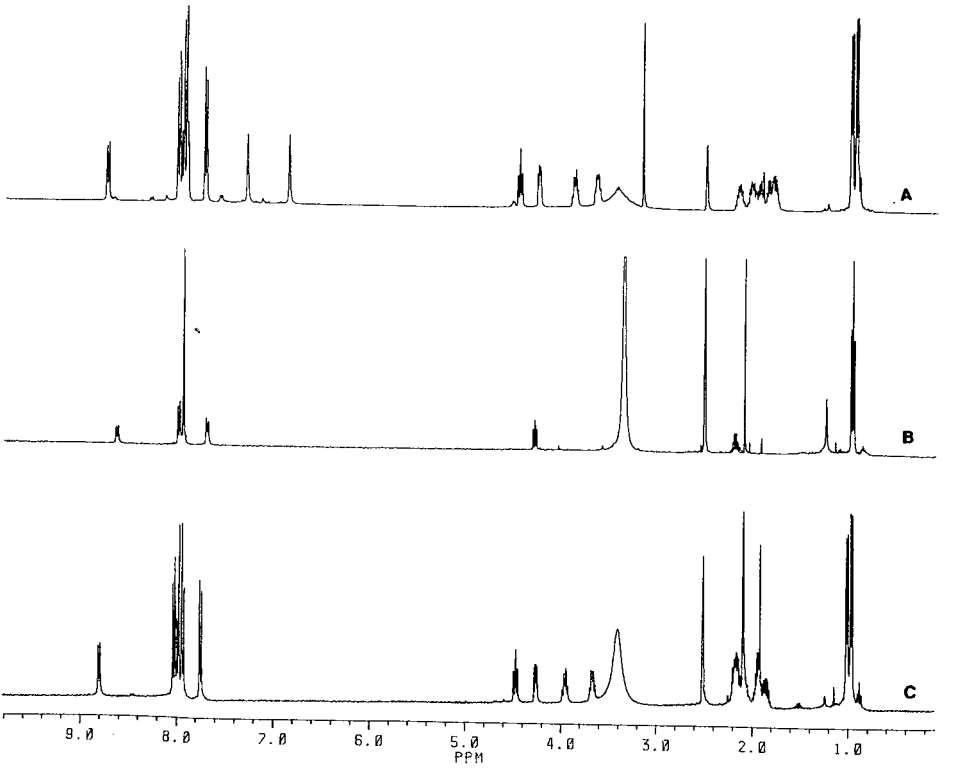

Fig. 7. Proton NMR spectra of degradation products. (A) Product I; (B) product II; (C) product III.

This procedure may also be applicable to the isolation of compounds with more normal chromatographic retention behavior. The extent of the success of this approach would be limited by solubility and any ability to concentrate the sample at the head of the column.

REFERENCES

1 L. R. Snyder and J. J. Kirkland, *Introduction to Modern Liquid Chromatography*, Wiley, New York, 1979, p. 616.
2 R. M. Ladd and A. Taylor, *LC · GC*, 7 (1989) 584.
3 M. Verzele, *Anal. Chem.*, 62 (1990) 265A.
4 J.-X. Huang and G. Guiochon, *J. Chromatogr.*, 492 (1989) 431.
5 R. S. Hodges, T. W. L. Burke and C. T. Mant, *J. Chromatogr.*, 444 (1988) 349.
6 J. H. Knox and H. M. Pyper, *J. Chromatogr.*, 363 (1986) 1.
7 C. L. Mant, T. W. L. Burke and R. S. Hodges, *Chromatographia*, 24 (1987) 565.
8 M. Verzele, Y-B. Tang, C. Dewaele and V. Berry, *Anal. Chem.*, 60 (1988) 1329.
9 W. R. Melander, J. Jacobson and Cs. Horváth, *J. Chromatogr.*, 243 (1982) 269.
10 J. C. Gesquiere, E. Diesis, M. T. Chung and A. Tartar, *J. Chromatogr.*, 478 (1989) 121.

Journal of Chromatography, 522 (1990) 227–234
Elsevier Science Publishers B.V., Amsterdam

CHROM. 22 780

Determination of tretinoin in creams by high-performance liquid chromatography

MICHAEL B. KRIL*, KAREN A. BURKE, JAMES E. DiNUNZIO and R. RAO GADDE
Bristol-Myers Squibb Co., Pharmaceutical Research Institute, 100 Forest Avenue, Buffalo, NY 14213 (U.S.A.)

(First received July 3rd, 1990; revised manuscript received August 30th, 1990)

ABSTRACT

A stability indicating reversed-phase high-performance liquid chromatographic method has been developed to quantify tretinoin (all-*trans*-retinoic acid) in cream formulations. Tretinoin cream samples were dissolved directly in tetrahydrofuran and diluted for injection. Separation was accomplished on a 15 cm Nova-Pak C_{18} column using a tetrahydrofuran–phosphate buffer solvent system (42:58, v/v) and 1.0 ml/min flow-rate. The method is able to separate tretinoin from its degradation products formed under stressing conditions. Excellent precision and accuracy were found for the assay of tretinoin in the cream formulations.

INTRODUCTION

Tretinoin (all-*trans*-retinoic acid) is a compound which is effective for the topical treatment of acne and other skin disorders [1,2]. Tretinoin is also known to be relatively unstable, with the possibility of several types of degradation products being formed [3,4]. Therefore, a stability-indicating high-performance liquid chromatographic (HPLC) method is desired to quantitate tretinoin in cream formulations. The present analytical method in the United States Pharmacopeia (USP) [5] calls for the assay of tretinoin in creams, gels and topical solutions by a ultraviolet spectrophotometry. A normal-phase HPLC method is described for isotretinoin in tretinoin drug substance [5]. Additional HPLC methods for tretinoin and its degradation products/impurities in products and biologiacal samples have been described in the literature [3,6–11]. Although these methods are able to separate tretinoin and its many degradation poducts, none of the methods appeared to be directly applicable to our goal; to develop a quick and simple stability indicating assay for tretinoin in dermatological products. This paper reports a stability-indicating reversed-phase HPLC method for tretinoin which is able to separate the tretinoin and internal standard peaks from the light induced isomers, as well as hydrolysis and oxidation products formed during forced degradation studies. This method has been successfully applied to cream formulations of tretinoin.

EXPERIMENTAL

Materials

Tretinoin and isotretinoin (13-*cis*-retinoic acid) were obtained from BASF (Parsippany, NJ, U.S.A.). The purest lot (compared *vs.* USP standard) of tretinoin raw material was used as a reference standard. Tretinoin creams (0.1%, w/w) and cream placebos used in this study were prepared by our Pharmaceutical Product Development group. HPLC-grade tetrahydrofuran (THF) with and without stabilizer [0.025% butylated hydroxytoluene (BHT)] was obtained from J. T. Baker (Phillipsburg, NJ, U.S.A.). Unless otherwise noted, THF without stabilizer was used. Sodium phosphate monobasic monohydrate, potassium persulfate, sodium hydroxide (Certified, ACS grade), hydrochloric acid (reagent grade) and 85% phosphoric acid (HPLC grade) were obtained from Fisher Scientific (Fair Lawn, NJ, U.S.A.). Anthracene (Gold Label, 99.9%) was obtained from Aldrich (Milwaukee, WI, U.S.A.). Water used was passed through a Millipore Milli-Q Water System (Millipore, Bedford, MA, U.S.A.). Samples and mobile phase were filtered through Millipore type HV filters, 0.45 μm.

Sample preparation precautions

All tretinoin sample and solution preparations were performed under gold lights [12]. Low actinic glassware was used for all preparations unless otherwise noted. Samples for injection were placed in amber vials.

HPLC instrumentation and conditions

Two liquid chromatographic systems were used for the method development: a Hewlett-Packard 1090 system with a 1040 photodiode array detector and Model 85B computer (Hewlett-Packard, Palo Alto, CA, U.S.A.) and a Waters HPLC system comprised of a 6000A solvent delivery system, Model 712 WISP auto injector and Model 441 absorbance detector fixed at 365 nm (all from Waters Assoc., Milford, MA, U.S.A.). The detector sensitivity was set at 0.05 a.u.f.s. for the raw material specificity study and 0.02 a.u.f.s. for the cream analysis study. Detector output was monitored with a Houston Instruments Model D5000 recorder (Houston Instruments, Austin, TX, U.S.A.) set at 10 mV. Data acquisition was accomplished with a Hewlett-Packard 3350 series computer utilizing LAS software (Hewlett-Packard). The computation and plotting of absorbance ratio plots from the photodiode array detector were performed by modified HP 1040A software described earlier [13].

A 150 × 3.9 mm Waters Nova-Pak C_{18} column (4 μm particle size) was used for method related separations in this study. A guard column (Nova-Pak C_{18} Cartridge, Waters Assoc.) was attached prior to the analytical column. Dilute phosphoric acid was prepared by diluting 10 ml of 85% phosphoric acid to 100 ml with water. The mobile phase was prepared by mixing 420 ml of prefiltered THF and 580 ml of prefiltered phosphate buffer. The phosphate buffer was prepared by dissolving 1.38 g of $NaH_2PO_4 \cdot H_2O$ in 1000 ml of water and adjusting to pH 3.0 with dilute phosphoric acid. A mobile phase flow-rate of 1.0 ml/min and injection volume of 25 μl were used for analysis.

Tretinoin degradation (specificity) studies

Tretinoin samples for demonstrating specificity were prepared in the following manner:

Oxidation studies. A 40-mg amount of tretinoin was transferred to a 100-ml volumetric flask along with 10 ml of THF and 10 ml of 0.025 *M* potassium persulfate. The sample was reacted for 12 h, after which it was diluted to volume with stabilized THF and filtered. An aliquot was prepared for analysis by pipetting 5 ml into another 100-ml volumetric flask and diluting with 40 ml of stabilized THF, 0.5 ml of dilute phosphoric acid and water to volume.

Light degradation studies. A 20-ml volume of a 0.40 mg/ml solution of tretinoin in THF was transferred to a 50-ml clear glass screw cap test tube. The sample was irradiated with light (approximately 1000 ft.-candles) for 10 min. A 5.0-ml aliquot of the degraded sample was prepared for analysis as described above (see section *Oxidation studies*).

Heat degradation studies. A 40-mg amount of tretinoin was transferred to a 100-ml volumetric flask and stored in a 50°C constant temperature oven for 47 weeks (the sample was purged with fresh air weekly). It was diluted to volume with THF and a 5.0-ml aliquot of the degraded sample was prepared for analysis as previously described.

Base degradation studies. A 40-mg amount of tretinoin was transferred to a 100-ml volumetric flask along with 20 ml of 0.025 *M* sodium hydroxide. The sample was allowed to react for 12 h after which it was neutralized with 2 ml of 0.25 *M* HCl and diluted to volume with THF. A 5.0-ml aliquot of the degraded sample was prepared for analysis as previously described.

Acid degradation studies. A 40-mg amount of tretinoin was transferred to a 100-ml volumetric flask along with 20 ml of 0.1 *M* HCl. The sample was stored for 47 weeks at room temperature after which it was diluted to volume with THF. A 5.0-ml aliquot of the degraded sample was prepared for analysis as previously described.

Tretinoin cream sample preparation

Internal standard solution. A 100-mg amount of anthracene reference standard was dissolved in 100 ml of THF.

Tretinoin standard solution (0.0040 mg/ml). A 100-mg amount of tretinoin reference standard was accurately weighed into a 250-ml volumetric flask and dissolved in and diluted to volume with stabilized THF. A first dilution was made by pipetting 5 ml of the above solution and 10.0 ml of internal standard solution into a 100-ml volumetric flask and diluting to volume with stabilized THF. A working standard solution was prepared by diluting 5 ml of this solution with 10 ml of stabilized THF, 0.1 ml of dilute phosphoric acid and water to 25.0 ml.

Cream sample preparation. An amount of cream containing 1.0 mg of tretinoin was accurately weighed into a 50-ml volumetric flask. A 5.0-ml aliquot of internal standard solution and 20 ml of stabilized THF were added. The flask was shaken to disperse the cream and the mixture was diluted to volume with stabilized THF. A 5.0-ml volume of this solution was further diluted to 25 ml with 10 ml of stabilized THF, 0.1 ml of dilute phosphoric acid and water to volume. The sample was filtered through a 0.45-μm disposable filter before analysis.

RESULTS AND DISCUSSION

A cream placebo analyzed by the above method exhibited no interfering peaks;

TABLE I

RELATIVE RETENTION TIMES OF MAJOR DEGRADATION PEAKS COMPARED TO TRETINOIN

Relative retention time		
Light	Oxidation	Base
–	0.129	–
–	0.179	0.178
–	0.247	0.246
–	0.318	0.316
–	0.452	–
–	–	0.483
0.785	–	–
0.803	–	–
0.864	–	–
0.946	–	–

therefore removal of the components of the cream formulation was not necessary and the sample could be directly dissolved and diluted for analysis.

The stability-indicating nature of this method was demonstrated by chromatographing the artificially degraded tretinoin solutions previously described and collecting data at multiple wavelengths using photodiode array detection. Table I gives the retention times of the observed degradation products relative to tretinoin. Several peaks were found in each assay (except for the heat-degraded tretinoin sample), with products from light degradation studies eluting generally later than those from

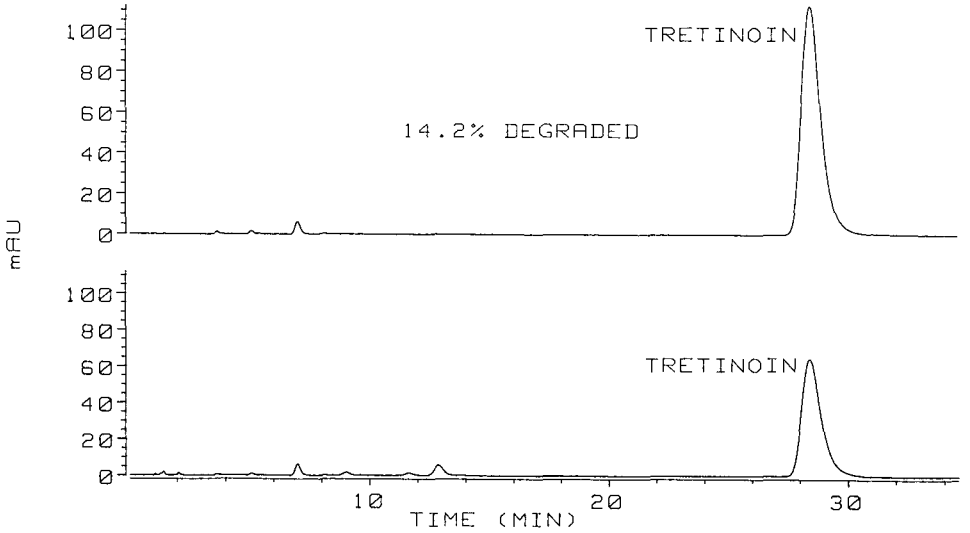

Fig. 1. Chromatograms of tretinoin solution oxidized by potassium persulfate. Injection volume, 25 μl (0.5 μg). Detection wavelengths, (top) 365 nm and (bottom) 320 nm.

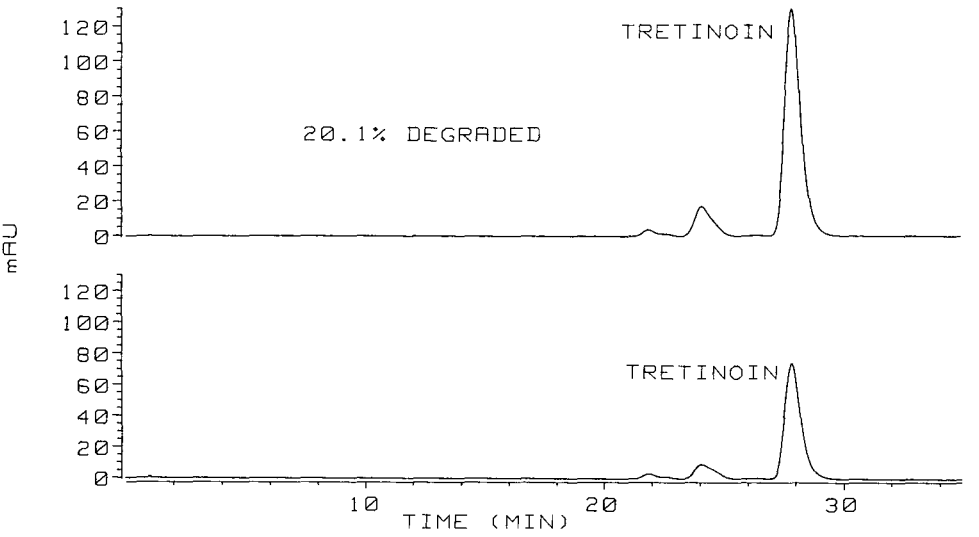

Fig. 2. Chromatograms of light-degraded tretinoin solution. Injection volume, 25 μl (0.5 μg). Detection wavelengths, (top) 365 nm and (bottom) 320 nm.

oxidation and base degradation studies. Although the heat-degraded sample exhibited a lower assay value (27.4% degraded) when compared to a standard, no additional peaks were displayed in the chromatograms at the analytical wavelength. Samples stored in acid showed no degradation after 47 weeks. Sample chromatograms of an oxidized and a light degraded sample are shown in Figs. 1 and 2.

Absorbance ratio plots were computed to determine the absence (or presence) of co-eluting impurities with the tretinoin peak by ratioing the absorbance values of the analytical wavelength against several other wavelengths. A typical absorbance ratio plot of a light degraded sample prepared by comparing 365 nm *vs.* 320 nm is shown in Fig. 3. The linearity of this plot (along with others at different wavelengths, data not shown) for this sample and also of others degraded by oxidation and by base confirms that the method described in this paper is stability-indicating.

Optimization of chromatography: effect of mobile phase concentration

The effects of changes in the mobile phase THF–phosphate buffer concentration ratio on the separation of tretinoin and isotretinoin is shown in Table II (isotretinoin was used because it is an easily formed degradation product of tretinoin). The values shown in Table II were obtained by separating a mixture of 0.02 mg/ml of tretinoin and 0.002 mg/ml isotretinoin over a range of 41–48% THF. For the actual assay method, 42% THF was chosen because it gave the best separation of all isomers/degradation products from tretinoin. Whereas this percentage provides good separation, it also presents a rather long run time of 35 min. This time was found to be necessary to separate a minor light isomerization product which is found directly preceeding the tretinoin peak in Fig. 2. If this product is not present, a substantial reduction in assay time may be accomplished by increasing the THF concentration (*e.g.*, to 46%) without

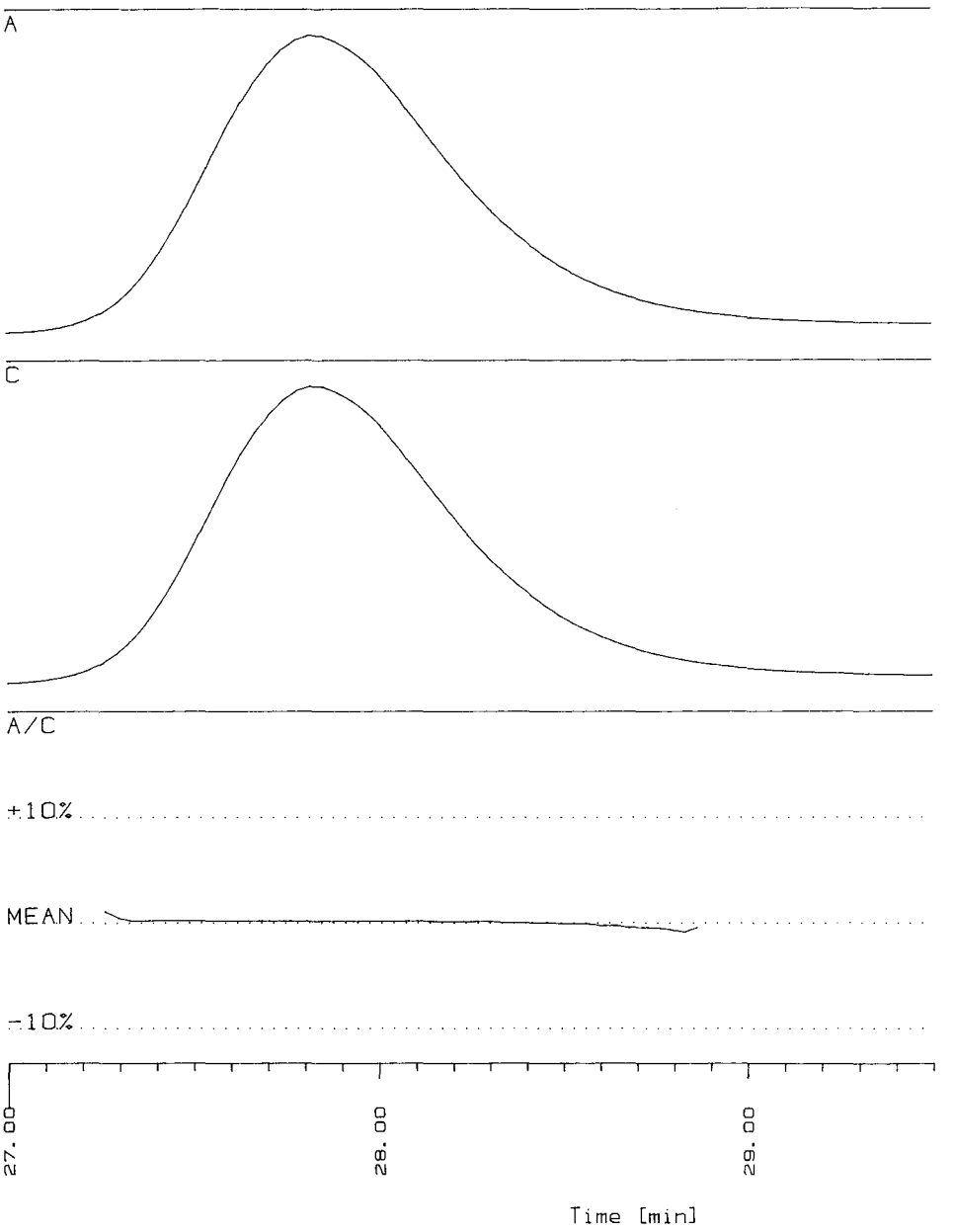

Fig. 3. Absorbance ratio plot of a solution of light-degraded tretinoin sample. Detection wavelengths, 365 nm (A) and 320 nm (C).

sacrificing the separation of tretinoin from all other degradation products as it was found that baseline separation between tretinoin and isotretinoin was achieved even at tretinoin retention times of less than 10 min (see Table II). In typical chromatograms of

TABLE II

EFFECT OF MOBILE PHASE CONCENTRATION ON THE SEPARATION OF ISOTRETINOIN AND TRETINOIN

THF (%)	Retention time (min)		Relative retention time[a]	Chromatographic resolution
	Tretinoin	Isotretinoin		
41	31.5	27.2	0.86	3.1
42	26.1	22.7	0.87	2.9
43	21.5	18.8	0.87	2.4
44	18.0	15.9	0.88	2.5
45	15.2	13.6	0.89	2.4
46	12.9	11.6	0.90	2.3
47	11.0	10.0	0.91	2.3
48	9.5	8.7	0.92	1.9

[a] Retention time of isotretinoin/retention time of tretinoin.

degraded cream sample (storage at 40°C for 16 weeks), the only degradation product found was isotretinoin (Fig. 4). It should also be noted that whereas previous papers described improved separation of light-induced isomers [4,11], the goal of this study was to develop a stability-indicating HPLC assay which would separate any isomers/degradation products formed from tretinoin and internal standard (anthracene). Anthracene was chosen as the internal standard due to its relative inexpensiveness, lack of interference and stability (as opposed to using a retinoid for an internal standard).

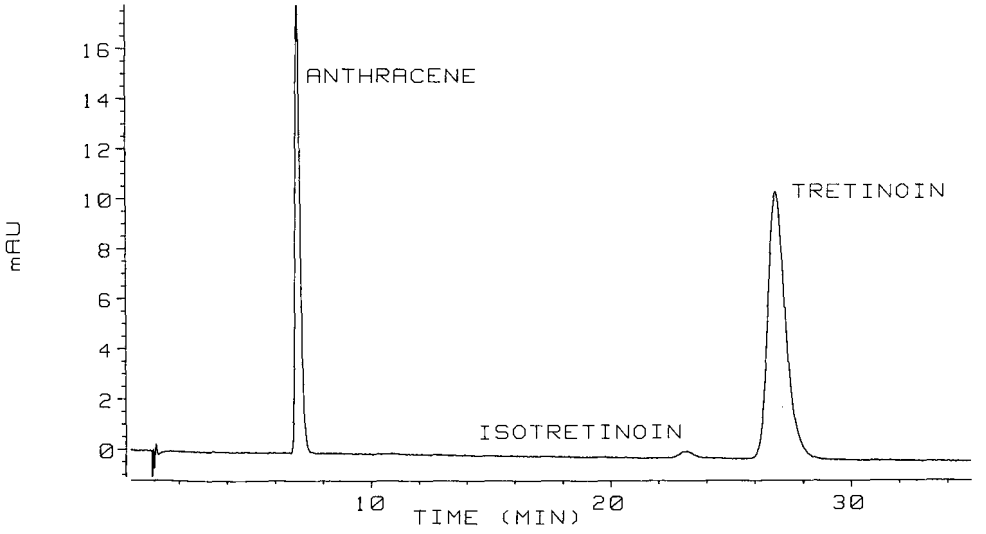

Fig. 4. Chromatogram of a tretinoin cream product stored at 40°C for 16 weeks containing 2.7% isotretinoin. Injection, 25 μl of cream sample preparation (0.106 μg of tretinoin). Detection at 365 nm.

Method validation for creams

The method for determining tretinoin in cream formulations was validated by determining three separate parameters; response linearity, accuracy and precision. Response linearity for tretinoin was determined by analyzing nine standard solutions covering the range of 10 to 300% (0.00040 to 0.012 mg/ml) of the normal sample concentration while keeping internal standard concentration constant. Linear regression analysis of the peak area ratio data gave a correlation coefficient (r) of 0.99997 and a y-intercept of 0.0060 (equivalent to 0.43% of the normal response).

The accuracy of the method was determined by doing standard recovery experiments. These experiments were carried out by spiking cream placebos with tretinoin solutions to simulate samples with tretinoin levels over the range of 50 to 200% of the normal value. The results of this study demonstrate excellent recovery with a mean value of 100.1% and a relative standard deviation of 0.9%. Also, the change in tretinoin level in sample showed no noticeable effect on the % recovery values.

The precision of the method was determined by assaying 0.1% (w/w) tretinoin cream using sample sizes over the range of 50 to 150% of the normal sample preparation weight (1.0 g). The results from these experiments give a mean value of 0.105% tretinoin (w/w) and a relative standard deviation of 1.0%. No effect of change in sample weight for analysis was observed.

CONCLUSIONS

A stability-indicating HPLC method for tretinoin in cream samples is described which is able to separate tretinoin from degradation products formed in both forced degradation studies of raw material and cream samples. The method showed excellent linearity, precision and accuracy for the assay of tretinoin in a cream product. This assay offers a prominent advantage over the current compendial method [5] in that it is able to quantitate both tretinoin and degradation products formed in the cream degradation studies and is thus stability-indicating.

REFERENCES

1 J. R. Thomas and J. A. Doyle, *J. Am. Acad. Dermatol.*, 4 (1981) 505.
2 W. Bollag, in J. H. Saurat (Editor), *Retinoids, New Trends in Research and Therapy*, Karger, Basel, 1984, 274.
3 R. W. Curley and J. W. Fowble, *Photochem. Photobiol.*, 47 (1988) 831.
4 J. P. Boehlert, *Drug. Dev. Ind. Pharm.*, 10 (1984) 1343.
5 *The United States Pharmacopeia*, The United States Pharmacopeia Convention, Rockville, MD, 22nd revision, 1990.
6 C. A. Frolik, T. E. Tavela and M. B. Sporn, *J. Lipid Res.*, 19 (1978) 32.
7 C. K. Mensink, H. L. M. Cox and F. J. van de Vaart, *Pharm. Weekbl.*, 122 (1987) 385.
8 P. V. Bhat and A. Lacroix, *Methods Enzymol.*, 123 (1986) 75.
9 R. Wyss and F. Bucheli, *J. Chromatogr.*, 424 (1988) 303.
10 A. M. McCormick, J. L. Napoli and H. F. Deluca, *Anal. Biochem.*, 86 (1978) 25.
11 M. G. Motto, K. L. Facchine, P. F. Hamburg, D. J. Burinsky, R. Dumphy, A. R. Oyler and M. L. Cotter, *J. Chromatogr.*, 481 (1989) 255.
12 G. M. Landers and J. A. Olson, *J. Assoc. Off. Anal. Chem.*, 69 (1986) 50.
13 H. Cheng and R. R. Gadde, *J. Chromatogr. Sci.*, 23 (1985) 227.

Journal of Chromatography, 522 (1990) 235–243
Elsevier Science Publishers B.V., Amsterdam

CHROM. 22 698

Aqueous two-phase systems with increased density for partition of heavy particles

ANDREAS BLENNOW* and GÖTE JOHANSSON
Department of Biochemistry, Chemical Center, University of Lund, P.O. Box 124, S-221 00 Lund (Sweden)
(First received December 28th, 1989; revised manuscript received June 19th, 1990)

ABSTRACT

The density of aqueous two-phase systems obtained from water, dextran and poly(ethylene glycol) (PEG) was increased by addition of metrizamide, which had a greater affinity for the upper (PEG-rich) phase than for the lower (dextran-rich) phase. The density of both phases could be increased to 1.2 g ml^{-1}. Above certain concentrations of metrizamide the dextran phase became the lighter one. Isopycnic phases were obtained by careful adjustment of the composition of the system, and the effect of metrizamide on phase composition was characterized. The systems were tested by partition of starch grains. Fractionation of mature pollen grains and starch grains was achieved by a counter-current distribution process using these systems.

INTRODUCTION

Fractionation of particles of biological origin can in many instances be achieved by partitioning between the two phases of aqueous two-phase systems [1–3]. Multi-step partition, *e.g.*, counter-current distribution (CCD) according to Craig [4], has been used for high resolution. When large and dense particles are to be studied, sedimentation might interfere with the partition. The possibility of increasing the density of both phases by addition of a "density maker", metrizamide [2-(3-acetamido-5-N-methylacetamido-2,4,6-triiodobenzamido)-2-deoxy-D-glucose], normally used for medical radiology and density gradients [5], was therefore investigated as a means of reducing undesirable sedimentation in dextran–poly(ethylene glycol)–water two-phase systems.

EXPERIMENTAL

Chemicals and materials

Dextran T-500 (MW = 500 000) and Sephacryl-300 were obtained from Pharmacia (Uppsala, Sweden), poly(ethylene glycol) (MW = 3400) from BP Chemicals (Hythe, U.K.) and metrizamide (centrifugation grade) from Nyegaard (Oslo, Norway). ^{32}P-labelled sodium phosphate was obtained from Amersham (Amersham, U.K.).

Mature pollen grains were harvested from *Hordeum vulgare* grown in a green-

0021-9673/90/$03.50

house. Starch grains were prepared from potato tubers by homogenization in 25 m*M* sodium phosphate buffer (pH 7.5) and washing by sedimentation mainly as described by Ohad *et al.* [6].

Density

The densities of the phases were determined by using a 5-ml pycnometer, weighed on an analytical balance.

Sedimentation rate

The relative rate of sedimentation of starch grains in various liquid media was determined by following the change in light scattering with time when the particles were sedimenting in a 3-ml cuvette. The apparent absorbance was followed by using a potentiometric recorder attached to the photometer (Hitachi 100-60). The time for sedimentation was taken from when the content of the cuvette had just been mixed to the inflection point detected by the recorder.

Two-phase systems

Systems with a total weight of 3 g were prepared from concentrated polymer solutions [20% dextran and 40% poly(ethylene glycol) (PEG)]. All systems contained 25% metrizamide. After temperature equilibration the phases were analysed for the content of metrizamide (by absorbance measurements at 240 nm). The concentrations of PEG and dextran in the two phases were determined by gel filtration on a column of Sephacryl-300 (25 × 1.5 cm I.D.) and the eluate was monitored with an Optilab (Vällingby, Sweden) Multiref 902B refractometer. The partition of phosphate was determined by including 0.33 μCi of $^{32}PO_4^{3-}$ per gram of the system. Samples (20 μl) were mixed with 8 ml of scintillation cocktail (Ready Safe; Beckman, Fullerton, CA, U.S.A.) and counted in a Beckman LS1801 scintillator. The concentration of pollen or starch grains in the CCD fractions was determined by measuring the light scattering as the apparent absorbance at 600 nm. Each fraction was diluted with 0.5 ml of water to break the phases and 300-μl (pollen) or 200-μl (starch grains) portions were analysed for the apparent absorbance with an ELISA spectrophotometer.

Two-phase systems with and without metrizamide were used to partition starch grains prepared as described above (5 g kg^{-1} system, dried for 1 min on filter-paper) at various pH values. The systems without metrizamide were composed of 8% dextran, 7% PEG and 0.3 mol kg^{-1} potassium phosphate buffer. The metrizamide-containing systems were composed of 5% dextran, 3% PEG, 25% metrizamide and 0.3 mol kg^{-1} potassium phosphate buffer. Material in the top and bottom phases was determined after 30 min of settling as described above by taking 0.5-ml aliquots from each phase and diluting them with 0.4 ml of water prior to analysis.

Counter-current distribution

The composition of the two-phase systems was either 2.5% dextran, 2.5% PEG, 25% metrizamide and 0.3 mol kg^{-1} K_2HPO_4 (for pollen) or 5% dextran, 3% PEG, 25% metrizamide and 0.3 mol kg^{-1} potassium phosphate buffer (pH 6.8) (for starch grains). The ratio between the volumes of the upper and lower phases was 0.72 at 21 ± 0.5°C (for the pollen experiment) and 0.90 at 23 ± 0.5°C (for the starch grains experiment). Each chamber of the thin-layer CCD apparatus [7] contained 0.90 ml of

bottom phase and 0.65 ml of top phase (pollen) or 0.75 ml of bottom phase and 0.68 ml of top phase (starch grains). A volume of 0.79 ml of the system was stationary and material collecting at the interface including 0.11 ml of bottom phase was therefore transferred together with the upper phase in the case of pollen or stationary in the case of starch grains. Pollen grains (50 mg) or starch grains (100 mg, dried for 1 min on filter-paper) were loaded in the first two chambers (Nos. 0 and 1) and 24 transfers (pollen) or 22 transfers (starch grains) were carried out by mixing for 20 s (pollen) or 1 min (starch) and settling for 8 min (pollen) or 5 min (starch). Theoretical curves and partition ratios, $G = \hat{\imath}/(55 - \hat{\imath})$ where $\hat{\imath}$ is the peak position, were calculated according to Craig [4].

RESULTS AND DISCUSSION

The mean density of the two-phase systems in Table I was increased from 1.03 to 1.20 g ml^{-1} by including metrizamide at up to 25% of the total weight of the system. Higher concentrations gave a strongly viscous dextran phase, making the systems less suitable for extraction. The difference in the densities between the two phases was similar, however, *i.e.*, <0.05 g ml^{-1}, in systems with and without metrizamide.

The phase diagram for a dextran–PEG–metrizamide–K_2HPO_4 system is shown in Fig. 1. The tie-line of one two-phase system is shown where the polymer content of the phases was determined. The inclusion of metrizamide made the PEG-rich phase denser than the dextran-rich phase. This was caused by the higher concentration of metrizamide in the former phase, probably owing to direct PEG–metrizamide interaction. The percentages of metrizamide, dextran and PEG are given in Table I.

Effect of K_2HPO_4 on the phase system

K_2HPO_4 strongly affected the composition of the phases and their volume ratio. Also, the concentration of polymers necessary to produce two phases at a given temperature varied drastically. This can be clearly seen in Table II, which shows

TABLE I

VOLUME RATIOS, DENSITIES OF PHASES AND THE PERCENTAGES OF METRIZAMIDE (MA), DEXTRAN (DX) AND PEG IN THE PHASES OF SYSTEMS WITH DIFFERENT CONCENTRATIONS OF THE TWO POLYMERS

The total concentation of metrizamide was 25% (w/w) in all systems. Temperature, 20°C.

Total composition		Volume ratio (top/bottom)	Density (g ml^{-1})		Phase composition					
					Top phase			Bottom phase		
DX (%)	PEG (%)		Top	Bottom	DX (%)	PEG (%)	MA (%)	DX (%)	PEG (%)	MA (%)
2.0	3.0	0.25	1.16	1.19	N.D.[a]	N.D.	19	N.D.	N.D.	29
3.0	2.5	0.72	1.18	1.23	6.9	0.3	20	<0.1	3.9	32
3.5	3.0	0.58	1.18	1.21	10.8	0.2	17	<0.1	5.0	32
4.5	2.0	1.20	1.20	1.22	9.2	0.2	20	<0.1	4.0	34

[a] N.D.: not determined.

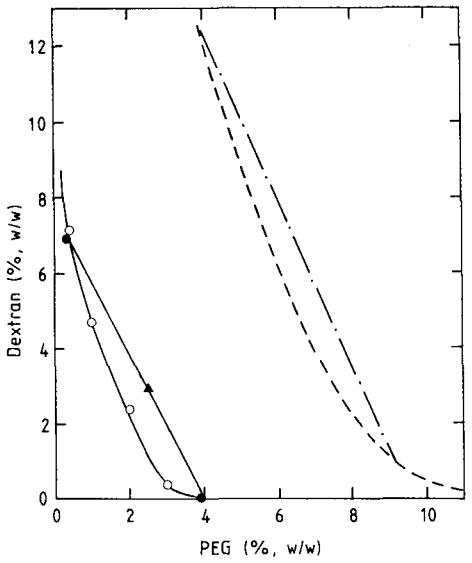

Fig. 1. Phase diagram for a dextran–PEG–metrizamide–K_2HPO_4 system at 20°C. The concentration of metrizamide was 25% (w/w) and that of the phosphate 0.3 mol kg^{-1} of system. ○, Points on the binodial curve obtained by turbidimetric titration. The total composition (▲) and the compositions of the phases (●) of one of the systems in Table I are shown. For comparison, the binodial curve (– – –) for a dextran–PEG system (from ref. 1) at the same temperature is given together with a tie-line (– · –).

the critical temperatures for the phase transition (from two to one phase) of a metrizamide-containing system, depending on the content of phosphate. The critical temperature was increased by as much as 30°C when the phosphate concentration was changed from 0.27 to 0.30 *M*. Also, the volume ratio was strongly dependent on the phosphate concentration and temperature (Table III). Inclusion of 4% (w/w) of sucrose in the system had no effect on either the phase transition or the volume ratio.

TABLE II

EFFECT OF PHOSPHATE ON THE CRITICAL TEMPERATURE OF PHASE TRANSITION (DIM POINT) FOR A SYSTEM CONTAINING 5% DEXTRAN, 2% PEG, 25% METRIZAMIDE AND VARIOUS AMOUNTS OF K_2HPO_4

Content of K_2HPO_4 (mol kg^{-1})	Critical temperature (°C)
0.27	2
0.28	14
0.29	29
0.30	33

TABLE III

EFFECTS OF PHOSPHATE AND TEMPERATURE ON THE VOLUME RATIO

Systems as in Table II.

Content of K_2HPO_4 (mol kg^{-1})	Temperature (°C)	Volume ratio (top/bottom)
0.28	0	1.4
	5	1.8
	10	2.7
	20	One phase
0.29	0	1.2
	5	1.4
	10	1.7
	20	3.0
0.30	0	1.0
	5	1.2
	10	1.4
	20	2.4

Isopycnic phases

A system composed of 7% dextran, 5% PEG, 25% metrizamide and 0.3 mmol kg^{-1} K_2HPO_4 at 20°C was found to have phases with equal densities. On decreasing the temperature to 0°C the dextran-rich phase became the denser one. An increased concentration of the phosphate, on the other hand, caused the PEG-containing phase to be the denser one at room temperature.

Sedimentation of starch grains

The sedimentation rate of dense particles was reduced within the systems containing metrizamide because of the increased density and also owing to a higher viscosity. The sedimentation rate of starch grains from potato tubers (60 μm diameter, 1.4 g ml^{-1}) was reduced by a factor of six when water was replaced with polymers (5% dextran and 2% PEG, which gives one phase at 20°C). When 25% of metrizamide was also included the sedimentation rate was only 2% of that in water. This strong decrease in the rate indicates that there is also an increase in the viscosity.

Partition of starch grains

The pH dependence of the partition of starch grains was studied in two-phase systems with and without metrizamide. Wihout metrizamide the apparent partition was not altered in the pH range 2.3–7.9. All material was found in the lower phase. However, this does not reflect a true solvating-directed partition as the sedimentation rate for the particles through the upper phase is too high. By including metrizamide (25%) and reducing the concentrations of polymer to around half, the starch grains partitioned between the two phases (and the interface) and their distribution could easily be adjusted by changing the pH of the system (Fig. 2). The starch grains partitioned mainly between the interface and one of the phases, which is the usual

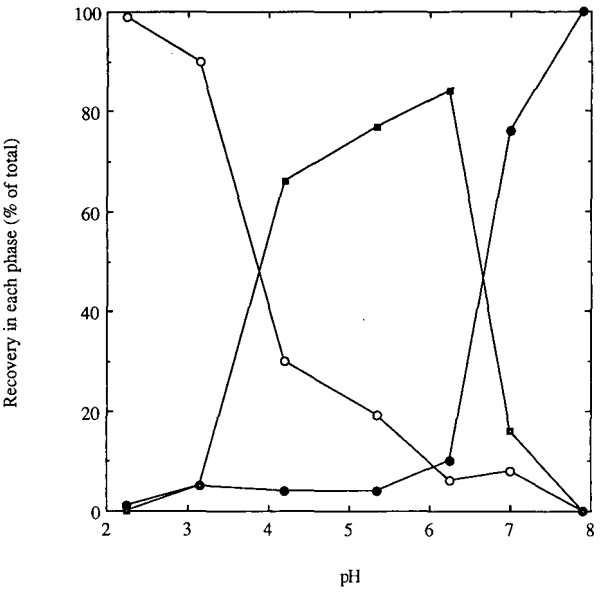

Fig. 2. Starch grains (5 g kg^{-1} of system) partitioned in metrizamide-containing two-phase systems at different pH values at 23°C. The systems were composed of 5% dextran, 3% PEG, 25% metrizamide and 0.3 mol potassium phosphate buffer per kg system. The amount of starch grains in the phases was determined via the apparent light scattering in diluted samples (see Experimental). Percentage of starch grains (●) in top phase, (■) at the interface and (○) in the bottom phase.

partitioning behaviour for particles [1,2]. In the present metrizamide-containing systems the dextran-rich phase was the upper one (checked by using small amounts of dye-labelled dextran and PEG). On increasing the pH the phosphate ion is increasingly charged, and this is known to influence the partition of negatively charged particles and proteins in favour for the PEG-rich upper phase in ordinary dextran-PEG systems [1,8]. However, in the metrizamide-containing systems (Fig. 2), the (negatively charged) starch grains show the opposite behaviour and they are more extracted into the PEG-rich phase with increasing pH.

On increasing the pH the distribution of potassium phosphate showed a small but distinct change in favour of the dextran-rich phase (Table IV). This is similar to what has been observed for the ordinary PEG-dextran systems [8]. The partition

TABLE IV

PARTITION COEFFICIENT, K, OF POTASSIUM PHOSPHATE BUFFER, LABELLED WITH ^{32}P, AT VARIOUS pH VALUES IN THE SAME SYSTEM AS IN FIG. 2 TOGETHER WITH THE VOLUME RATIO BETWEEN THE PHASES (TOP/BOTTOM)

pH	Volume ratio	$K_{phosphate}$
2.25	1.32	1.18
4.20	1.12	1.44
6.25	0.95	1.44
7.90	0.81	1.80

coefficient of the potassium phosphate is the mean of the hypothetical partition coefficients the ions should have had if they could partition independently of the electrostatic forces [9]. The inversion of the "phosphate effect" on the partition of particles indicates that potassium ions have a greater affinity for the dextran phase than the phosphate ions have, thereby reversing (compared with the metrizamide-free systems) the polarity of the electrical double layer at the interface. The change in pH, by varying the relative amounts of primary and secondary phosphate, affected the volume ratio (top/bottom) of the systems containing metrizamide, the volume ratio decreasing with increasing pH (Table IV). This variation shows that a redistribution of the components takes place, making the PEG-rich phase larger but also less attractive for phosphate and especially potassium ions relative to the dextran-rich phase. No variation in the volume ratio (= 1.40) was observed in normal systems.

Counter-current distributions

The metrizamide-containing systems were tested by performing CCDs with pollen grains and starch particles.

Fresh mature pollen grains (diameter 50 μm; density 1.2–1.3 g ml^{-1}) from *Hordeum vulgare* (barley) were showed to be heterogeneous when analysed in a thin-layer CCD apparatus [1,2]. As can be seen in Fig. 3, at least one major and three minor peaks can be fitted to the experimental data. Redistribution of material from fractions 2 and 10–25 (pooled) gave G values of 0.05 and 4, respectively. This

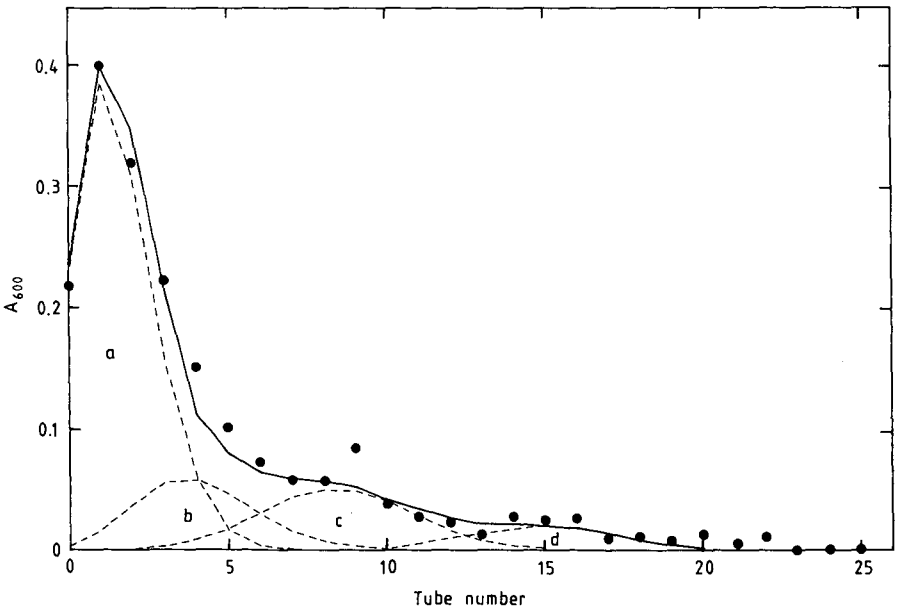

Fig. 3. Thin-layer CCD of mature pollen from *Hordeum vulgare*. The systems were composed of 2.5% dextran, 2.5% PEG, 25% metrizamide and 0.3 mol K_2HPO_4 per kg system. Experimental data are given under Experimental. The interface material was mobile. Theoretical curves for homogeneous substances (– – –) and their sum (———) are fitted to the experimental data (●). The G values for the theoretical curves are (a) 0.07, (b) 0.20, (c) 0.55 and (d) 1.63.

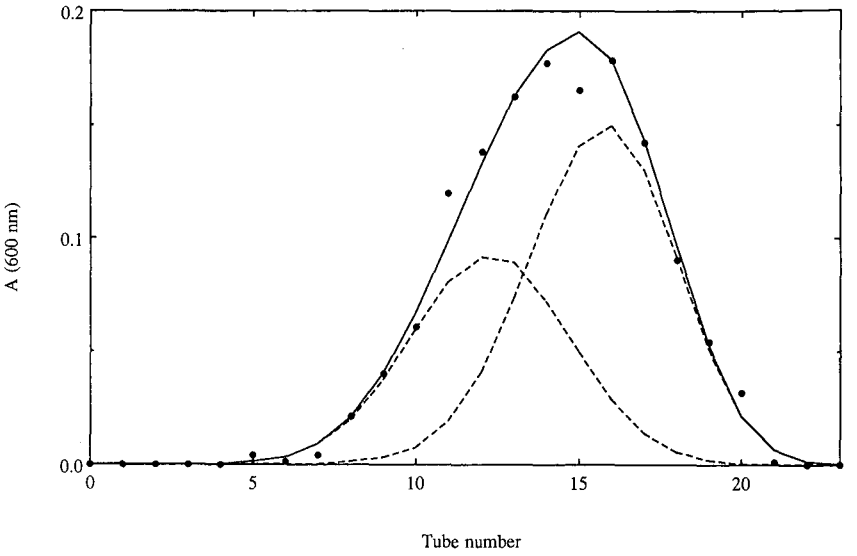

Fig. 4. Thin-layer CCD of starch grains from potatoes at pH 6.8. The composition of the two-phase system was the same as in Fig. 2. The amount of starch grains in the fractions was determined via light scattering measured as the apparent absorbance at 600 nm as described under Experimental. The material at the interface was stationary in this instance. (●) Experimental values; (– – –) theoretical curves for homogeneous substances with G values of 1.15 and 2.20, respectively, and (———) their sum.

demonstrates that the pollen grain population consists of several subfractions differing in the surface properties of the grains. No morphological differences between the fractions could be detected in the light microscope after staining with orcein [10].

Another CCD was performed by using the system described above for the partition of starch grains at pH 6.8 (Fig. 4). Starch grains show a slightly higher density (1.4 g ml^{-1}) than the pollen grains but have approximately the same diameter (60 μm). The starch grains gave rise to a much broader peak than expected for homogeneous particles, which might be due to various charge densities of the negative groups on the surface of the grains. No difference in the size of the starch grains could be observed when the different fractions were studied under the light microscope.

The aqueous two-phase systems with increased density of the two phases will be useful for the partition of various dense hydrophilic particles, both for fractionation and for studies of their surface properties. Examples of particles of interest, in addition to pollen grains and starch, are fish eggs, plant seeds, air-pollutant particles and minerals.

CONCLUSIONS

By addition of metrizamide "density maker", the density (and viscosity) of aqueous dextran–PEG two-phase system can be adjusted so as to reduce strongly the sedimentation of biological particles when they are partitioned between the phases. Metrizamide, however, affects the phase formation, the relative positions of the upper and lower phases and the partition-modifying properties of salts.

ACKNOWLEDGEMENTS

This work was supported by a grant from Svalöf (Svalöv, Sweden). We thank Dr. Eva Thörn for providing the pollen grains and Mrs. Monica Joelsson for the artwork.

REFERENCES

1 P.-Å. Albertsson, *Partition of Cell Particles and Macromolecules*, Wiley, New York, 3rd ed., 1986.
2 H. Walter, D. E. Brooks and D. Fisher, *Partitioning in Aqueous Two-Phase Systems: Theory, Methods, Uses and Applications to Biotechnology*, Academic Press, Orlando, 1985.
3 H. Walter and G. Johansson, *Anal. Biochem.*, 155 (1986) 215.
4 L. C. Craig, in M. Florkin and E. H. Stotz (Editors), *Comprehensive Biochemistry*, Vol. 4, Elsevier, Amsterdam, 1962, p. 1.
5 D. Rickwood, in D. Rickwood (Editor), *Iodinated Density Gradient Media*, IRL Press, Oxford, 1983, p. 1.
6 I. Ohad, I. Friedberg, Z. Ne'eman and M. Schramm, *Plant Physiol.*, 47 (1971) 465.
7 P.-Å. Albertsson, *Anal. Biochem.*, 11 (1965) 121.
8 G. Johansson, *Biochim. Biophys. Acta*, 221 (1970) 387.
9 G. Johansson, *Acta Chem. Scand., Ser. B*, 28 (1974) 873.
10 C. D. Darlington and L. F. La Cour, *The Handling of Chromosomes*, Allen & Unwin, London, 5th ed., 1969, p. 146.

Journal of Chromatography, 522 (1990) 245–253
Elsevier Science Publishers B.V., Amsterdam

CHROM. 22 745

Chromatographic separations of sucrose monostearate structural isomers

M. CECILIA TORRES, MARIA A. DEAN and FRED W. WAGNER*
Department of Biochemistry, University of Nebraska-Lincoln, Lincoln, NE 68583-0718 (U.S.A.)
(First received April 26th, 1990; revised manuscript received July 26th, 1990)

ABSTRACT

High-performance liquid chromatography (HPLC), thin-layer chromatography (TLC) and gas–liquid chromatography (GLC) methods are described for separating sucrose monostearate isomers. The HPLC procedure provides baseline separation of purified monoester isomers into three main peaks at room temperature, and completely separates monoesters with different acyl chain lengths (C_{14}, C_{16}, C_{18}). The TLC method separates up to six of the eight possible positional monostearate isomers, which can be further differentiated by specific color development with a visualizing agent. The GLC technique used resolves monoesters with different acyl chain lengths, and partially separates monostearate isomers. Isomers collected from HPLC were subjected to treatment with invertase, then resolved and detected by TLC to determine fatty acid substitution patterns on the sucrose molecule.

INTRODUCTION

Since sucrose esters of fatty acids were recognized as effective emulsifiers, they have been used in foods, cosmetics and pharmaceuticals [1,2]. The preparation of these compounds by procedures using the transesterification reaction [3] yields a complex mixture of monoesters, diesters and higher esters with fatty acyl groups of various chain lengths. Acylation of sucrose with a single fatty acid can yield 255 different esters, from mono- to octaesters [2]. Several thin-layer (TLC), gas–liquid (GLC) and high-performance liquid chromatographic (HPLC) methods have been developed to separate and identify the different fractions (*e.g.* monoesters, diesters, esters of higher degree of substitution) [4–6], but good separation of the different positional isomers in each fraction has been difficult and an efficient chromatographic system has not been reported. The emulsifying properties of different sucrose monoester preparations depend upon the number and kind of the different isomers [2]. Thus, an effective method for the separation and analysis of sucrose monoesters during synthesis, purification and structural studies is essential. We have developed methods to separate up to six positional isomers of sucrose monostearate. These protocols serve to characterize synthesis of monostearates and other sucrose monoesters and thus meet all requirements of a qualitative analytical procedure.

Invertase catalyses the hydrolysis of sucrose to D-glucose and D-fructose. By combining the separation techniques of HPLC and TLC with the specificity of

0021-9673/90/$03.50

hydrolytic enzymes, we were able to determine whether the fatty acyl residue was located on the glucose or fructose residue of sucrose monoester isomers.

EXPERIMENTAL

Materials

Sucrose monoesters were obtained from Dai-Ichi Kogyo Seiyaku (DKS) (Tokyo, Japan). The sample used (DKS F-160) contained sucrose monomyristates, sucrose monopalmitates and sucrose monostearates [2]. Sucrose monostearates were synthesized in dimethyl sulfoxide (DMSO) using the procedure by Osipow *et al.* [3]. Both monoester samples were purified by chromatography on silica gel 60 (Merck 7734). Samples were dissolved in a minimal volume of chloroform–ethanol (1:1) and monoesters were eluted from the column with hexane–diethyl ether–ethanol (3:1:1).

High-performance liquid chromatography

The Waters Assoc. HPLC system used consisted of a M6000 pump, a U6K injector and a R401 refractive index detector. A Maxima 820 chromatography workstation equipped with an I-200 system interface module (SIM) was used to acquire, save and process data (Waters Assoc.). The column system consisted of a 15 cm × 3.9 mm μBondapak C_{18} (10 μm irregular particle size) stainless-steel column connected to a 15 cm × 3.9 mm Nova-Pak C_{18} (4 μm spherical particle size) stainless-steel column, both of Waters Assoc. Columns were equilibrated and developed isocratically with acetone–water (7:3) at a flow-rate of 0.5 ml/min. HPLC-grade acetone (Aldrich) and water were filtered through a 0.45-μm nylon filter (Millipore) and degassed prior to chromatography. Monoester solutions (2%) in acetone–water (3:1) were passed through a 0.45-μm filter and 10-μl aliquots were used for analysis.

Sucrose monostearate fractions collected from the HPLC effluent were lyophilized after evaporation of the acetone, dissolved in a small amount of chloroform–ethanol (1:1), and subjected to TLC analysis.

Thin-layer chromatography

TLC was performed according to a modified procedure of Lee *et al.* [7]. Separation was achieved on Whatman K5 silica gel plates which had been dipped in 0.2 *M* potassium phosphate buffer and dried at 85°C for 1 h.

The plates were developed for 30 min using ethyl acetate–pyridine–water (80:20:5), then air dried for 15 min; the same procedure was used to redevelop the plates two additional times, for a total of three times. Visualization of sucrose monoesters on the TLC plates was achieved by saturating the dry plates with a solution of 4 g diphenylamine, 4 ml aniline, 30 ml 85% H_3PO_4 and 200 ml acetone [8], and drying them in the hood for 20 min prior to heating at 110°C for 4 min.

Invertase hydrolysis experiments

Approximately 1 mg yeast invertase (β-fructofuranosidase, Sigma) was added to lyophilized isomer fractions collected from HPLC which had been hydrated with 20 m*M* acetate buffer, pH 4.5. The solutions were stirred and heated at 45°C for 24 h and then tested for hydrolysis by TLC analysis.

Gas–liquid chromatography

GLC separations were performed using a 3700 Varian gas chromatograph with a flame ionization detector. The column was a 6 ft. × 1/8 in. O.D. stainless-steel column filled with 3% OV-17 on Chromosorb W-HP, 80–100 mesh. The column temperature was set at 280°C for 12 min, then programmed to increase at 2°C/min to a final temperature of 330°C. The temperature of the injection port was 300°C and the detector temperature was 400°C. The flow-rate of the carrier gas (nitrogen) was 30 ml/min. Samples (2 mg) were silylated with 1 ml TRISIL (Pierce) and heated at 70°C for 30 min prior to analysis. The injection volume was 2 μl.

RESULTS AND CONCLUSIONS

Fig. 1 shows the HPLC separation of the purified DKS F-160 monoester fraction, and standard monostearates. In Fig. 1A, three sets of peaks are completely resolved from each other. The first corresponds to myristoyl monoesters, the second to palmitoyl monoesters and the third to steroyl monoesters. Monostearate peaks were identified based on the chromatographic mobilities of authentic, pure monostearates prepared in our laboratory (Fig. 1B). The assignments of M-I, M-II, P-I, P-II, and P-III (Fig. 1A) are based on their mobilities and their reported composition in DKS F-160 [2]. The three peaks corresponding to the groups of monopalmitates and monostearates, are also well resolved. Others have attempted to separate the monostearate isomers by HPLC, but the limited solubility of sucrose monoesters in the solvents they chose required elevated temperatures and did not provide optimal resolution of positional isomers [9–11]. Cormier *et al.* [9] first reported HPLC analysis of sucrose fatty acid esters, but it is not clear whether they separated positional isomers of both monostearates and distearates, or if they only separated monoesters from diesters and triesters present in their sample. Gupta *et al.* [6] have found HPLC

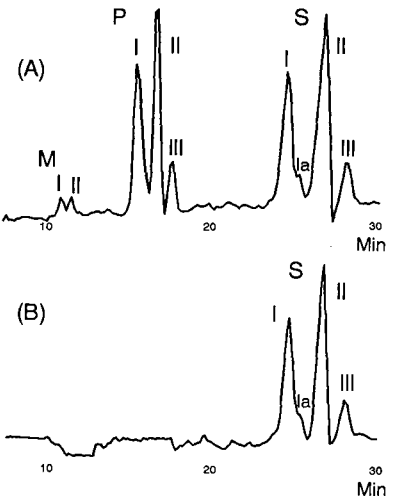

Fig. 1. Reversed-phase HPLC separation of highly purified sucrose monoesters. (A) DKS F-160 monoesters: M-I, M-II = monomyristates; P-I, P-II, P-III = monopalmitates; S-I, S-Ia, S-II, S-III = monostearates. (B) Standard monostearates: S-I, S-Ia, S-II, S-III.

separation of sucrose esters unsatisfactory due to the deleterious effect of potassium soaps and residual sucrose on the separation process. Moreover, they also report that sucrose esters tend to be absorbed strongly on silica gel [6]. More recently Jaspers *et al.* [11] developed a procedure which separated monoesters with different acyl chain lengths. However, their method required an elevated temperature (65°C) and did not separate positional isomers.

Our HPLC procedure has several advantages over previous methods including good sample solubility, chromatography at room temperature, and easy solvent removal from sucrose monoester fractions. In addition, we did not encounter difficulties with sucrose esters absorbing onto C_{18} reversed-phase silica gel. Inasmuch as the three main peaks are effectively resolved, we collected fractions of the different peaks peaks for preliminary structural analysis of the isomers, in combination with TLC techniques.

Although TLC separation of sucrose monostearate isomers has not been reported before, Soljic and Eskinja [12] separated six sucrose monopalmitates on silica gel G plates developed with chloroform–methanol–acetic acid (85:5:10). We were unable to obtain adequate separation of the monostearates by this method probably because silica gel does not give a good separation of sugar compounds unless it is impregnated with inorganic salts (*e.g.* boric acid, mono- and diphosphate, etc.) [13]. Thus, when plates were impregnated with phosphate, sucrose monoesters were effectively separated.

Fig. 2 illustrates the TLC separation of the DKS F-160 monoester fraction, and of pure monostearates. Although the monopalmitates and monostearates from the DKS F-160 sample did not separate from each other, separation of the pure monostearate isomers was good. At least five well resolved components can be seen, which exhibit different colors. The spot labeled 2–3 (Fig. 2) represents two unresolved isomers, which appear pinkish-brown, and are clearly resolved when the initial quantity of sample is lower. Additionally, component 1 appears as a grayish-blue spot, component 4 as a blue spot, and components 5, 6 and 7 as spots of different shades of purple. Component 6 was faint or absent except in heavily spotted samples. Under the conditions of these analyses, sucrose imparts a dark purple color on a TLC plate, fructose a pink color and glucose a blue color [13]. All three sugars are clearly resolved just above the origin. The colors of the different isomers appear to be produced mainly by reaction of the visualizing reagent with the part of the monoester sugar that is not substituted. Thus, sucrose with glucose esterified would most likely appear as a variation of the colors pink or purple and sucrose with fructose esterified would be seen as a variation of the color blue. These observations were confirmed by the experimental results obtained with invertase.

Twelve fractions of the sucrose monostearates were collected from the HPLC effluent (Fig. 3A) and were spotted on silica plates for TLC analysis (Fig. 3B, lanes 1–12). After reaction with the visualizing reagent, each isomer differed in color, intensity and position on the TLC plate. The first five fractions correspond to HPLC peak I and shoulder Ia. In lane 4 of Fig. 3B, the component just under the fastest migrating spot was faint and not always detected in all samples analyzed. Thus, this component may have been an artifact, or an isomer that exists in quantities too small to detect easily. Fractions 6–9 correspond to HPLC peak II (although fraction 6 was contaminated by components present in fraction 5), and fractions 10–12 correspond to

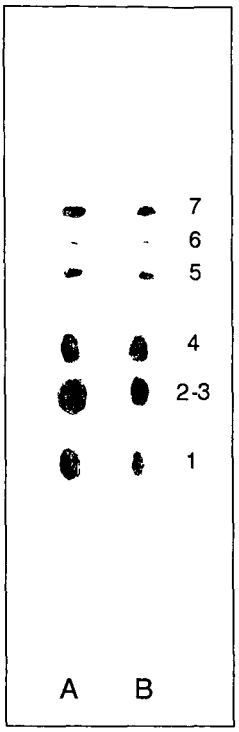

Fig. 2. TLC separation of DKS F-160 monoester samples (lane A) and pure sucrose monostearates (lane B).

HPLC peak III. The colors representing the four isomers in lanes 1–5 in Fig. 3 are predominantly pink or pinkish-purple. From this information we reasoned that the fatty acyl substitution for these fractions is on glucose. The isomers that predominate in lanes 6–12 in Fig. 3 appear as grayish-blue or blue. We interpreted this data to infer that for these fractions, the fructose moiety of sucrose has the fatty acyl substitution. While eight isomers are theoretically possible, only six well defined spots appear in the TLC analysis. There may be an additional isomer in fractions 10–12 that has a similar R_F value as the slowest moving component from fractions 6–9. This would explain the continued appearance of the slowest moving component in fractions 10–12. Another possibility is that the isomer(s) exist in quantities too small to detect.

Invertase catalyses the hydrolysis of sucrose to D-glucose and D-fructose only if the fructose moiety of sucrose is unsubstituted [14]. The specificity of this enzyme provided a convenient test to categorize the monostearate isomers as glucose or fructose substituted. Fig. 4 shows TLC separations for three (fractions 3, 8 and 12) of the twelve isomer fractions collected from HPLC and tested with invertase. Fraction 3 (Fig. 4, lane A) is composed of three isomers represented by three differently colored spots: pinkish-brown (bottom), pinkish purple (middle), light purple (top). When fraction 3 was allowed to react with invertase, hydrolysis of the sucrose monoesters occurred. The three isomer spots were replaced by a glucose monostearate spot near the solvent front at the top of the plate, and a pink spot from fructose above the application point of the TLC plate (Fig. 4, lanes A and B). Fraction 8 appears to be

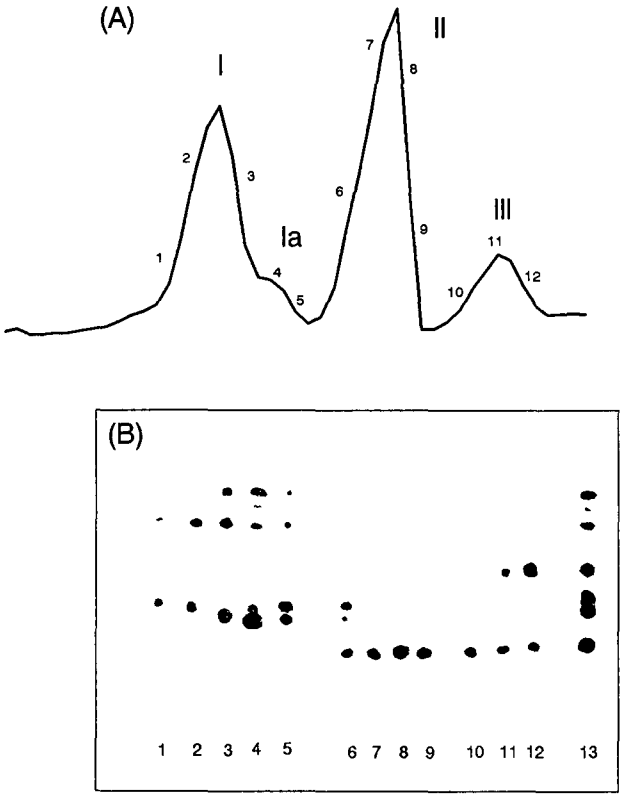

Fig. 3. Correlation of sucrose monostearate HPLC effluent fractions with the corresponding TLC analysis. (A) HPLC separation of monostearate isomers (collected fractions 1–12). (B) TLC of collected HPLC fractions (lanes 1–12) positioned beneath the corresponding HPLC tracing. Lane 13 = purified monostearate isomers sample.

composed of only one isomer (Fig. 4, lane C), represented by a bluish-gray spot, and fraction 12 (Fig. 4, lane E) is composed of two isomers represented by bluish-gray (bottom) and blue (top) spots. Hydrolysis of the sucrose monoester isomers was not detected in either fraction with the addition of invertase, as indicated on the TLC plate by an absence of change in their R_F values (Fig. 4, lanes C–F). A lack of invertase hydrolysis implies that the fatty acid substituent is located on the fructose moiety of the sucrose molecule.

Fractions 1, 2 and 5, like fraction 3, were also hydrolyzed after treatment with invertase. Fraction 4 seemed hydrolyzed; however it was difficult to determine whether the faint spot, appearing second from the top on the TLC plate (Fig. 3), had been hydrolyzed. Fractions 7 and 9, like fraction 8, appeared as a single major component which was not affected by treatment with invertase. Fraction 6 contained the same slow moving component which was not affected by invertase treatment, as well as trace amounts of two components hydrolyzed by invertase that had the same R_F values as the slowest moving components in fraction 5. The results of the hydrolysis experiments indicate that the monostearate isomers eluting in HPLC peaks I and Ia are glucose

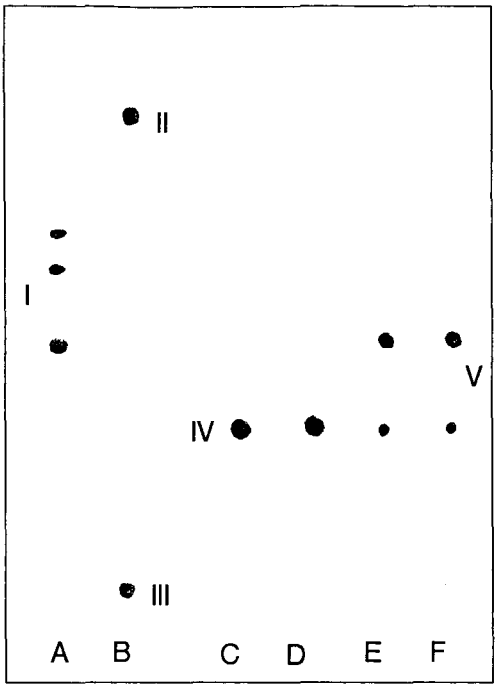

Fig. 4. TLC of invertase experiment samples. Isomer fractions 3, 8 and 12 (Fig. 3) before (lanes A, C and E) and after (lanes B, D and F) the addition of invertase. Lane A (fraction 3): I = monostearate isomers; Lane B (fraction 3, complete hydrolysis): II = glucose monostearates, III = fructose; Lane C (fraction 8): IV = monostearate isomers; Lane D (fraction 8, no hydrolysis detected): IV = monostearate isomers; Lane E (fraction 12): V = monostearate isomers; Lane F (fraction 12, no hydrolysis detected): V = monostearate isomers.

substituted (TLC spot colors are variations of pink and purple), while HPLC peaks II and III represent fructose substituted isomers (TLC spot colors are variations of blue). In every case, except in that of the faint spot in fraction 4, the preliminary visual evaluation of glucose or fructose fatty acyl substitution based on the TLC color given by the isomer was confirmed by enzymatic hydrolysis experiments. Definitive structural assignments will be made based on NMR experiments of the isomer fractions collected from HPLC.

GLC has been used extensively for the quantitative and qualitative analysis of sucrose monoesters and diesters [6]. GLC studies to determine the position of esterification has been done for sucrose monomyristates [15] and sucrose monostearates [16], but only after the isomeric mixtures were methylated, saponified and subjected to methanolysis to yield the methyl glycosides. In an effort to develop a simpler and faster procedure, we separated the monostearate trimethylsilyl derivatives on a 3% OV-17 column (Fig. 5). The DKS F-160 mixture separated into two main isomers and at least five minor ones (Fig. 5A), while the pure monostearate mixture separated into one main isomer and at least three minor ones (Fig. 5B). The individual peaks shown represent more than one isomer.

As an example, the main peak of the group labeled "stearates" in Fig. 5A and

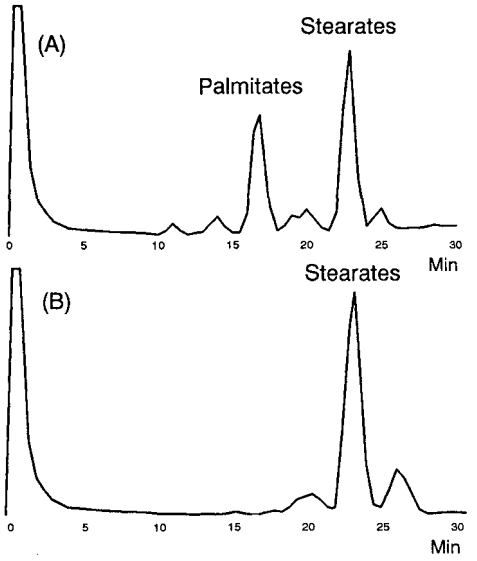

Fig. 5. Computer reconstructed GLC separation of highly purified sucrose monoesters. (A) DKS F-160 monoesters; (B) Standard monoesters.

B contained three components as measured both by HPLC and TLC. Similarly, the leading and following minor peaks in Fig. 5 contained more than one sucrose ester derivative. Thus, we could not assign individual monoesters to GLC peaks. Perhaps the use of capillary GLC would facilitate a sufficient separation for this purpose.

Since we have found that the four isomers corresponding to HPLC peaks I and Ia (Fig. 3) are glucose substituted and the two (possibly three) isomers corresponding to HPLC peaks II and III are fructose substituted, we suspect that substitution of the steroyl group must be predominantly on the fructose moiety of the sucrose molecule. This is contrary to previous findings from studies on the competition of sucrose monostearate isomers [2,16] and sucrose monolaurate isomers [14]. However, the extensive work of Lemieux and McInnes [15] indicated that approximately 60% of the acyl substitution occurs on the fructose moiety of sucrose monomyristate. Clearly, more comprehensive structural studies are needed which will be facilitated by the methods reported here.

We conclude that monostearate isomers can be separated using a combination of HPLC and TLC techniques. Our protocols offer several advantages over previously reported procedures, such as simple and rapid screening of samples for the presence of individual isomers and improved resolution. These uncomplicated techniques can be scaled up to develop preparative methods which can provide adequate quantities of the pure positional monostearate isomers for structural studies.

ACKNOWLEDGEMENTS

The financial support of the Department of Economic Development, State of Nebraska is gratefully acknowledged. A special thanks to Virginia Stryker for her help in the purification of the sucrose monostearates.

This paper was published as Journal Series No. 9189, Agricultural Research Division, University of Nebraska.

REFERENCES

1 G. R. Ames, *Chem. Rev.*, 60 (1960) 541.
2 H. Chung, P. A. Seib, K. F. Finney and C. D. Magoffin, *Cereal Chem.*, 58 (1981) 164.
3 L. Osipow, F. D. Snell, W. C. York and A. Finchler, *Ind. Eng. Chem.*, 48 (1956) 1459.
4 H. Mima and N. Kitamori, *J. Am. Oil Chem. Soc.*, 39 (1962) 546.
5 J. Weiss, M. Brown, H. J. Zeringue and J. R. Feuge, *J. Am. Oil Chem. Soc.*, 48 (1971) 145.
6 R. K. Gupta, K. James and F. J. Smith, *J. Am. Oil Chem. Soc.*, 60 (1983) 1908.
7 K. Y. Lee, D. Nurok and A. Zlatkis, *J. Chromatogr.*, 174 (1979) 187.
8 S. A. Hansen, *J. Chromatogr.*, 105 (1975) 388.
9 R. Cormier, L. H. Mai and P. Pommez, *Proc. Tech. Sess. Can. Sugar Refin. Res.*, (1978) 37.
10 V. R. Kaufman and N. Garti, *J. Liq. Chromatogr.*, 4 (1981) 1195.
11 M. E. A. P. Jaspers, F. F. van Leeuven, H. J. W. Nieuwwenhuis and G. M. Vianen, *J. Am. Oil Chem. Soc.*, 64 (1987) 1020.
12 Z. Soljic and I. Eskinja, *J. Serb. Chem. Soc.*, 52 (1987) 105.
13 M. Ghebregzabher, S. Rufini, B. Monaldi and M. Lato, *J. Chromatogr.*, 127 (1976) 133.
14 W. C. York, A. Finchler, L. Osipow and F. D. Snell, *J. Am. Oil Chem. Co.*, 33 (1956) 424.
15 R. U. Lemieux and A. G. McInnes, *Can. J. Chem.*, 40 (1962) 2394.
16 M. Gee and H. G. Walker, Jr., *Chem. Ind. (London)*, 24 (1961) 829.

Journal of Chromatography, 522 (1990) 255–265
Elsevier Science Publishers B.V., Amsterdam

CHROM. 22 671

Chromatographic separation and partial identification of glycosidically bound volatile components of fruit

CHRISTIAN SALLES, JEAN-CLAUDE JALLAGEAS and JEAN CROUZET*
Centre de Génie et Technologie Alimentaires, Institut des Sciences de l'Ingénieur, Université de Montpellier–Montpellier II, 34095 Montpellier Cedex 05 (France)
(First received April 20th, 1990; revised manuscript received July 3rd, 1990)

ABSTRACT

Synthetic monoterpenic and aromatic β-D-glucosides and β-D-rutinosides were separated by Fractogel TSK HW-40 S chromatography according to their molecular size and interactions occurring between the aglycone moiety and the gel matrix. Under these conditions terpenyl rutinosides were eluted before the homologous glucoside derivatives. In the two classes, monoglucosides and rutinosides, aromatic glycosidically bound components had lower retention times than the corresponding terpenyl components. The use of over-pressure layer chromatography (OPLC) allowed the separation of glucoside and rutinoside derivatives, and in these two classes aromatic and several monoterpene compounds were well separated. Based on these results, the separation of glycosidically bound volatile components isolated from grapes (Muscat of Alexandria) and apricot (Rouge du Roussillon) was undertaken using a three-step process. Silica gel fractionation allowed the separation of mono- and diglycosidic fractions present in apricot. Fifteen peaks were obtained from grape extracts by Fractogel chromatography, and under the same conditions sixteen and eleven peaks were detected in monosaccharidic and disaccharidic fractions, respectively isolated from apricot. The glycosidic fractions isolated by gel chromatography were purified by preparative OPLC, and some of them were sufficiently pure for a subsequent structural analysis. Moreover, partial identification of glycosidically bound volatile components separated by these two methods may be achieved using retention data when standard compounds are available; on the other hand, enzymatic hydrolysis of the isolated pure fractions gives information in the absence of reference compounds.

INTRODUCTION

The presence of glycosidically bounds volatile components such as monoterpenic, aromatic and aliphatic alcohols, phenols, isoprenoids or polyols in plants and more precisely in fruits such as grapes [1–3], papaya [4], passion fruit [5], apricot and mango (6) has been reported. These non-volatile components, which are considered by flavour chemists to be aroma precursors, are present in plants in complex mixtures. Their isolation and their partial separation before analysis are generally performed by selective adsorption either on activated charcoal [7] or on organic hydrophobic adsorbents such as reversed-phase C_{18} or Amberlite XAD-2 [8]. According to Croteau *et al.* [9], a combination of hydrophobic interactions and gel-permeation chromatography on Bio-Gel P-2 provides a selective procedure for the purification of

0021-9673/90/$03.50

monoterpenyl glucosides and galactosides. In some instances pretreatment with insoluble polyvinylpyrrolidone [10] or adsorption chromatography on silica gel [11,12] was used for sample clean-up. More recently, application of droplet countercurrent chromatography to these compounds has allowed the separation and the subsequent analysis of several minor constituents present in grape juice [10].

In our laboratory, the study of glycosidically bound volatile components present in fruits such as grapes, apricot, mango and passion fruit was undertaken using non-destructive methods such as high-performance liquid chromatography (HPLC) and soft ionization modes in mass spectrometry and tandem mass spectrometry [6,13,14]. For these studies further separations of complex mixtures obtained after extraction and prepurification steps were needed.

In this paper, chromatographic separations and partial identifications of glycosidically bound volatile compounds obtained by synthesis or isolated from grape and apricot fruits using gel chromatography on Fractogel TSK HW-40 S and preparative over-pressure layer chromatography (OPLC) are reported.

EXPERIMENTAL

Plant material

Mature, sound grapes (cultivar Muscat of Alexandria) were obtained from experimental vineyards of the Chambre d'Agriculture des Pyrénées Orientales, Rivesaltes, France. Apricots (cultivar Rouge du Rousillon) were gathered in the experimental orchard of the Institut National de la Recherche Agronomique, Manduel, France.

Grape berries and apricot halves were crushed at 5–10°C for 3 min. In order to decrease the viscosity of the apricot purée, the homogenate was treated for 90 min at 25°C with 3.5 g l^{-1} Pectinol D5 S (Röhm, Darmstadt, F.R.G.) and 0.2 g l^{-1} cellulase (Sigma, St. Louis, MO, U.S.A.). The hydrolysis of grape glycosidically bound terpenes present in or added to grape juice was checked under the same conditions. Clear juices were obtained by two successive centrifugations at 2500 *g* for 30 min and 50 000 *g* for 15 min.

Isolation of glycosidic fraction

The glycosidic fraction was obtained according to the procedure described by Williams *et al.* [15] and prepurified by treatment with insoluble polyvinylpyrrolidone, Polyclar AT (Serva, Heidelberg, F.R.G.) [10] A 10-ml volume of the raw glycosidic fraction was poured in a 100 × 10 mm I.D. column filled with Polyclar AT in methanol, elution was performed with 50 ml of methanol and the solution was concentrated to 2 ml under vacuum.

Silica gel chromatography

The concentrate obtained after methanol evaporation of the solution collected from the Polyclar AT column was separated on Chromagel 60 Å C.C. silica gel (230–400 mesh) (Solvants, Documentation, Synthèse, Peypin, France) in a 450 × 15 mm I.D. column. Elution was effected successively with 150 ml of chloroform, 440 ml of chloroform–acetonitrile–32% ammonia (15:85:10, v/v) and 660 ml of the same mixture (12.5:87.5:12.5, v/v). Fractions of 8 ml were collected and the presence of glycosides was checked by thin-layer chromatography (TLC).

Thin-layer chromatography

TLC was performed on 0.2-mm precoated silica plates (Kieselgel 60; Merck, Darmstadt, F.R.G.) with ethyl acetate–isopropanol–water (65:30:15, v/v/v) as eluent. After evaporation of the solvent, mono- and disaccharidic derivatives were revealed using N-(1-naphthyl)ethylenediamine dihydrochloride (Nediac reagent; Merck). Under these conditions monosaccharides were diversely coloured whereas monoglucoside and rutinoside compounds were violet-red and carmine red, respectively.

Fractogel TSK HW-40 S gel chromatography

Fractions isolated by silica gel chromatography and containing heterosidic compounds as indicated by TLC were diluted with distilled water and chromatographied on a Fractogel TSK HW-40 S (0.250–0.040 mm) Superformance column (600 × 26 mm I.D.) (Merck). Elution was performed with distilled water at 8 bar pressure using a Milton-Roy pump at a flow-rate of 3 ml min^{-1}. Eluted compounds were detected at 210 nm using a Varian UV 50 detector, 10-ml fractions being collected. All the fractions corresponding to one peak on the chromatogram were combined and water was eliminated by azeotropic distillation after addition of acetonitrile. The resulting concentrates were dissolved in 2 ml of methanol and stored at 4°C until use.

The column was calibrated using carbohydrates of increasing molecular weight: glucose (180), maltose (342), maltotriose (504) and stachyose (666); in this instance the UV detector was operated at 190 nm.

Over-pressure layer chromatography (OPLC)

A Chrompres 25 apparatus (Radiomatic Instruments et Consommables I) was used. Fractions obtained by gel chromatography, concentrated to 0.05 ml, were spoted on 0.2-mm precoated 20 × 20 cm silica plates (Kieselgel 60; Merck) and eluted with ethyl acetate–*tert.*-amyl alcohol–acetic acid–water (18:1:1:1, v/v) at a flow-rate of 0.75 ml min^{-1}. The elution time was 20 min for monoglucosides and 50 min for disaccharidic derivatives. After evaporation of the solvent, heterosidic compounds were revealed using Nediac reagent.

When OPLC was used in the preparative mode the residue obtained by solvent elimination after the gel chromatographic step was lined in the same plate as that used for the analytical mode, and elution was performed under the same conditions except that the reagent was spread only on the edges of the plates and strips corresponding to glycosidic compounds were scraped off and extracted with methanol.

Gas chromatography (GC)

A Varian 3300 apparatus fitted with a flame ionization detector and a silica capillary column containing CP-Sil 5 CB5 (methylsilicone) (Chrompack, Middelburg, The Netherlands) (50 m × 0.225 mm I.D.) was used. The column was programmed from 70 to 140°C at 2°C min^{-1} then from 140 to 250°C at 10°C min^{-1}; the carrier gas was hydrogen at 1.2 ml min^{-1}. The chromatograph was coupled with a Shimadzu CR 3A integrator. Authentic samples of terpenic alcohols were used for identification purposes.

Mass spectrometry

Desorption chemical ionisation (DCI) spectra in the positive-ion mode were obtained with a ZAB-HF mass spectrometer (Laboratoire d'Analyse du CNRS, Vernaison, France). Ammonia was used for ionization and argon for collision.

Synthesis of reference compounds

The reference compounds geranyl, neryl, α-terpinyl and citronellyl glucosides and rutinosides were obtained by condensation of α-bromoacetylated monosaccharides and alcohols catalysed by silver oxide [16]. Tetraacetylated α-bromoglucose and hexaacetylated α-bromorutinose were obtained according to refs. 17 and 18, respectively. The method of Paulsen *et al.* [19] was used for deacetylation of peracetylated β-D-glucosides.

Peracetylated precurors and monoterpenyl glycosides were purified by silica gel chromatography. For peracetylated compounds the excess of alcohol was eliminated using *n*-hexane–ethyl acetate (80:20, v/v) and the peracetylated compounds were eluted with the same mixture (50:50, v/v). The residue obtained after deacetylation was purified on the same column; dichloromethane–methanol mixtures (first 95:5, v/v, and then 60:40, v/v) were used as eluents; the heterosides were isolated in the second fraction, as indicated by TLC.

Enzymatic hydrolysis

Aspergillus niger pectinase preparation (Sigma) containing β-D-glucosidase, α-L-arabinase and α-L-rhamnosidase activities was partially purified by ultrafiltration (PM 10 Diaflo) and exclusion chromatography on Fractogel TSK HW-55 S before use [20]. A 0.05-ml volume of 0.1 *M* phosphate–citrate buffer (pH 5), 0.02 ml of partially purified pectinase containing 40 g l^{-1} of freeze-dried preparation were added to the residue obtained by elimination of the solvent under a stream of nitrogen from 0.01 ml of a methanolic solution of glycosides. The reaction was performed at 25°C with stirring in a hermetically sealed flask; after 30 min the reaction was stopped by addition of 0.5 ml of dichloromethane and chilling to 0°C. The organic layer was separated, dried over anhydrous sodium sulphate and filtered. The solvent was evaporated under a smooth stream of nitrogen and the concentrate was analysed by gas chromatography.

RESULTS AND DISCUSSION

Separation of synthetic glycosides

Fractogel TSK HW-40S chromatography. Chromatography of thirteen synthetic monoterpenyl and aromatic β-D-glucopyranosides and β-D-rutinosides (MW 270–462) on a Fractogel TSK HW-40 S column previously calibrated with standard carbohydrates (MW 180–660) is shown in Fig. 1. Twelve well resolved peaks, corresponding to thirteen standard glycosidically bound components, are detected; only two compounds, 2-phenylethanol β-D-glucoside and α-terpinyl β-D-rutinoside, lare coeluted. As a rule, monoterpenyl β-D-rutinosides are eluted before monoterpenyl β-D-glucosides according to their respective molecular weights; in these two classes the elution sequence relative to the monoterpenic moiety is linalool, α-terpineol, nerol and geraniol. The more apolar aromatic derivatives, benzyl and 2-phenylethyl glucosides

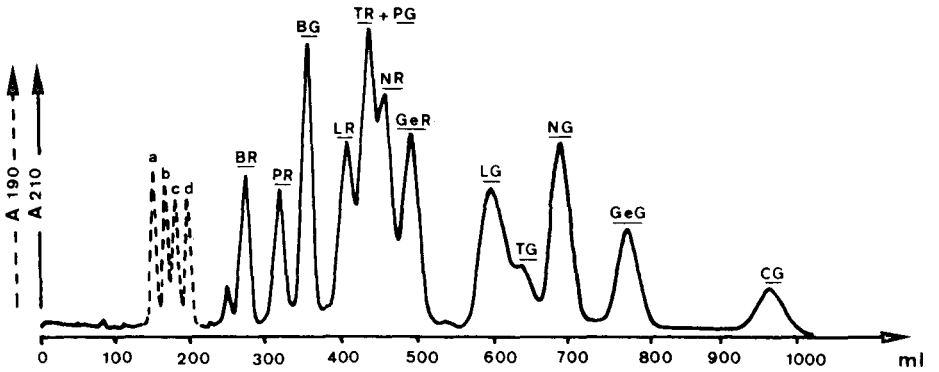

Fig. 1. Fractogel TSK HW-40 S chromatography of a mixture of synthetic glycosidically bound volatile components and of standard carbohydrates. Mobile phase, water at 3 ml min^{-1}; pressure, 8 bar; UV detection at 210 (———) and 190 (·····) nm. a = Stachyose; b = maltotriose; c = maltose; d = glucose; B = benzyl; P = 2-phenylethyl; L = linalyl; T = α-terpinyl; N = neryl; Ge = geranyl; C = citronellyl; R = rutinoside; G = glucoside.

and rutinosides, have lower elution volumes than the corresponding terpenyl compounds.

On the other hand, the elution volumes of glycosides relative to those of carbohydrates with comparable molecular weights show clearly that gel permeation is not the only phenomenon involved in the separation of these compounds. Indeed, the elution volumes of β-D-glucosides differ appreciably from that of maltose whereas the elution volumes of β-D-rutinosides are greater than that of maltotriose. As stated for the purification of monoterpenyl glycosides on Bio-Gel P-2 [9] or of flavonol glycosides [21] and proanthocyanidins [22] on Fractogel TSK HW-40 S, hydrophobic interactions of the aglycone moiety of glycosides with the gel matrix retard selectively the different compounds according to the hydrophobicity of this moiety. Under these conditions the compounds are eluted according to the length of the carbohydrate chain and the hydrophobicity of the aglycone.

Over-pressure layer chromatography. The chromatogram obtained by OPLC for the thirteen standard compounds considered above is given Fig. 2. This technique, previously used for the separation of compounds having related structures [23–26], is more accurate and gives better resolution than TLC. On the one hand it allows a good separation of glucoside and rutinoside derivatives, and on the other, among these two classes, monoterpenyl compounds are well separated from aromatic compounds. More particularly, linalyl derivatives are separated from the other terpenyl compounds present in the mixture.

Fig. 2. OPLC of synthetic glycosidically bound volatile components on 0.2-mm silica gel (Kieselgel 60). Eluent, ethyl acetate–*tert.*-amyl alcohol–acetic acid–water (18:1:1:1, v/v) at a flow-rate of 0.75 ml min^{-1}. Nediac reagent was used for detection. Notation for glycosidically bound components as in Fig. 1.

Separation of fruit glycosidically bound volatile components

Silica gel pre-fractionation. A prefractionation of heterosidic pools obtained from grapes and apricots by adsorption on reversed-phase C_{18} and purified by treatment with Polyclar AT was performed using silicagel chromatography. Two apricot fractions containing essentially monoterpene monoglucosides and diglycosides and one grape fraction containing essentially monoterpene diglycosides, as indicated by TLC, were collected.

Fractogel TSK HW 40-S chromatography. On the Fractogel TSK HW-40 S chromatogram obtained for the fraction isolated from grapes (Fig. 3), fifteen peaks are detected and collected for subsequent OPLC separation. Two of these peaks, 7 and 9, have the same retention times as linalyl and geranyl β-D-rutinosides previously identified among grape glycosidically bound components [3]. In the absence of standard compounds, arabinoglucosides, also present in muscat cultivars [3], were not identified, but the presence of these compounds was suspected in peaks 8 and 10 according to the carmine red colour developed in TLC or OPLC using Nediac reagent. TLC of the different fractions collected showed that some of them are not revealed with this reagent and are not glycosidically bound components. Pyrophosphate [27,28] and other non-sugar derivatives [29,30] have been previously reported in plants.

With apricot the first fraction obtained after silica gel chromatography and containing essentially monosaccharide derivatives gives sixteen peaks (Fig. 4) in Fractogel chromatography; in five of these peaks, linalyl (peak 9), α-terpinyl (peak 10), neryl (peak 11) and geranyl (peak 12) glucosides were tentatively identified on a retention time basis. Benzyl glucoside was present in one another silica gel fraction.

In the fraction containing principally diglycosidic derivatives (Fig. 5) peak 7 has the same elution time as peak 8 detected in grape extract and suspected to be an arabinoglucoside derivative. These results are in good agreement with those previously reported concerning the presence in apricot of monoterpene glucosides in addition to monoterpene diglycosides [6]. The possibility of partial hydrolysis of diglycosides occurring during the juice liquefaction step was discarded on the basis of the low hydrolysis rate of apricot diglycosides by pectinol [6]. On the other hand the fact that rutinosides or arabinoglucosides present in grape juice or added to grape juice are not hydrolyzed under the conditions used for the recovery of apricot glycosidically bound derivatives agrees with this finding.

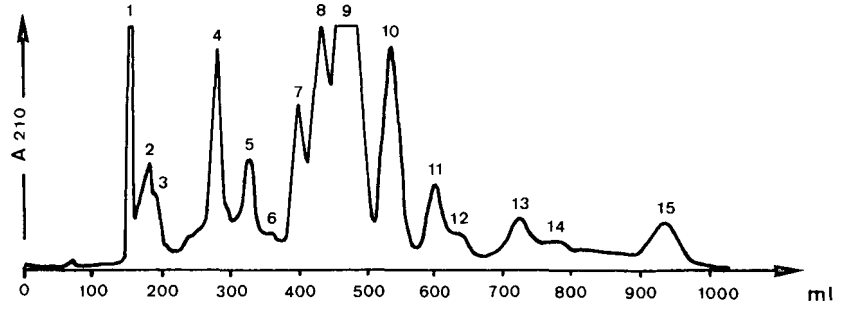

Fig. 3. Fractogel TSK HW-40 S chromatography of grape glycosidically bound fraction obtained after silica gel separation. Mobile phase, water at 3 ml min^{-1}; pressure, 8 bar; UV detection at 210 nm.

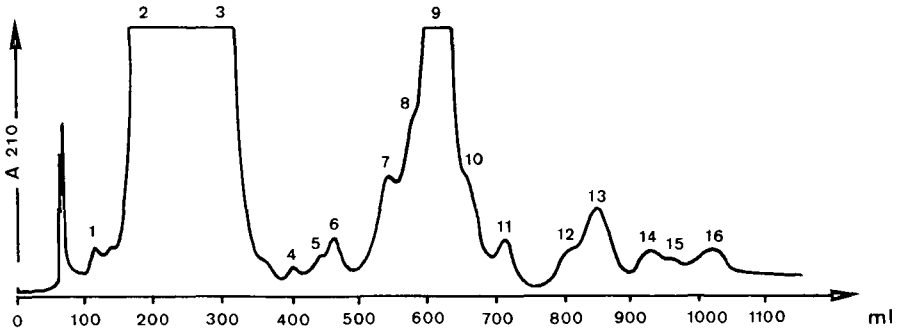

Fig. 4. Fractogel TSK HW-40 S chromatography of apricot monosaccharidic fraction obtained after silica gel separation. Mobile phase, water at 3 ml min^{-1}; pressure, 8 bar; UV detection at 210 nm.

Additionally, the reported data show that chromatography on silica gel is an efficient technique for the separation of glycosidically bound terpenes in two classes, mono- and diglycosidic derivatives.

Over-pressure layer chromatography. The grape heterosidic fractions 7, 8, 9 and 10 isolated by filtration on Fractogel were separated by preparative OPLC. Ninety different fractions were so isolated, but only the quantitatively most important and giving a specific saccharide coloration with Nediac reagent were investigated. The analytical OPLC of these fractions is shown in Fig. 6; linalyl (spot 7-1) and geranyl (spot 9-4) β-D-rutinosides are confirmed as grape juice components. In order to identify the other compounds separated, total enzymatic hydrolysis was applied and the results obtained by GC for the aglycone moiety and by TLC for the saccharidic moiety are reported Table I. The identification of linalool, α-terpineol, nerol and geraniol on the one hand and glucose, arabinose and rhamnose on the other agree with the presence of linaly and geranyl rutinosides or glucorhamnosides and of linalyl, α-terpinyl, neryl and geranyl arabinoglucosides or glucoarabinosides.

A preliminary study using DCI positive-mode mass spectrometry [6] was undertaken in order to obtained information on the sequence of the saccharidic

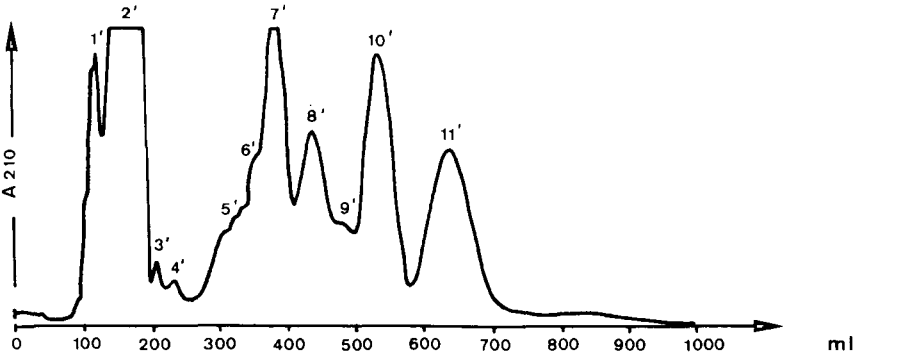

Fig. 5. Fractogel TSK HW-40 S chromatography of apricot disaccharidic fraction obtained after silica gel separation. Mobile phase, water at 3 ml min^{-1}; pressure, 8 bar; UV detection at 210 nm.

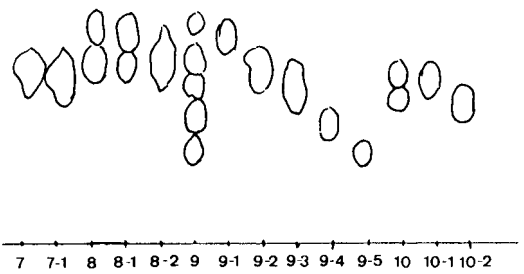

Fig. 6. Analytical OPLC of grape glycosidically bound fractions separated by preparative OPLC on 0.2-mm silica gel (Kieselgel 60). Eluent, ethyl acetate–*tert.*-amyl alcohol–acetic acid–water (18:1:1:1, v/v) at a flow-rate of 0.75 ml min^{-1}. Nediac reagent was used for detection.

moiety. For compounds 7-1 and 9-4 the spectrum obtained (Fig. 7) shows the presence of the molecular ion of m/z 480 $(M + NH_4)^+$ and fragment ions of m/z 334 (OH ~ Glu ~ O~Agl+NH_4)$^+$·[a], 326 (Rut ~ NH_3)$^+$, 180 (Glu ~ NH_3)$^+$ and 164 (Rha ~ NH_3)$^+$. These results are indicative of the sequence rhamnose–glucose–aglycone but no information concerning the nature of the aglycone moiety is available, the fragment ions of m/z 137 and 154 characteristic of this moiety being present in all instances with approximately the same relative abundance.

TABLE I

AGLYCONE AND SACCHARIDIC MOIETIES IDENTIFIED BY GC AND TLC AFTER ENZYMATIC HYDROLYSIS OF GRAPE GLYCOSIDICALLY BOUND COMPOUNDS SEPARATED BY OPLC

Fraction	Aglycone moiety (GC)	Saccharidic moiety (TLC)
7-1	Linalool	Glucose + rhamnose
8-2	Linalool	Glucose + arabinose
9-2	α-Terpineol	Glucose + arabinose
9-3	Nerol	Glucose + arabinose
9-4	Geraniol	Glucose + rhamnose
10-2	Geraniol	Glucose + arabinose

For the other grape heterosidic compounds isolated by OPLC, the following fragments were found in the mass spectra (Fig. 8): m/z 466 $(M + NH_4)^+$, 334 (OH~Glu ~ O~Agl + NH_4)$^+$, 312 (Ara~Glu ~ NH_3)$^+$, 180 (Glu ~ NH_3)$^+$ and 150 (Ara ~ NH_3)$^+$. These fragments are characteristics of the sequence arabinose–glucose–aglycone. As reported by Williams *et al.* [3], the mass spectrometric determinations indicate the presence of rutinosides and arabinoglucosides in grapes.

The analytical OPLC of apricot fractions obtained by preparative OPLC, 9-2, 10-1, 11-1 and 12-1 for glucosidic compounds and 7′-1 for disaccharidic compounds, is shown Fig. 9. The results concerning the relative migration data and the results

[a] ~ = Bond. This symbol is used in order to distinguish between a bond and the sign minus.

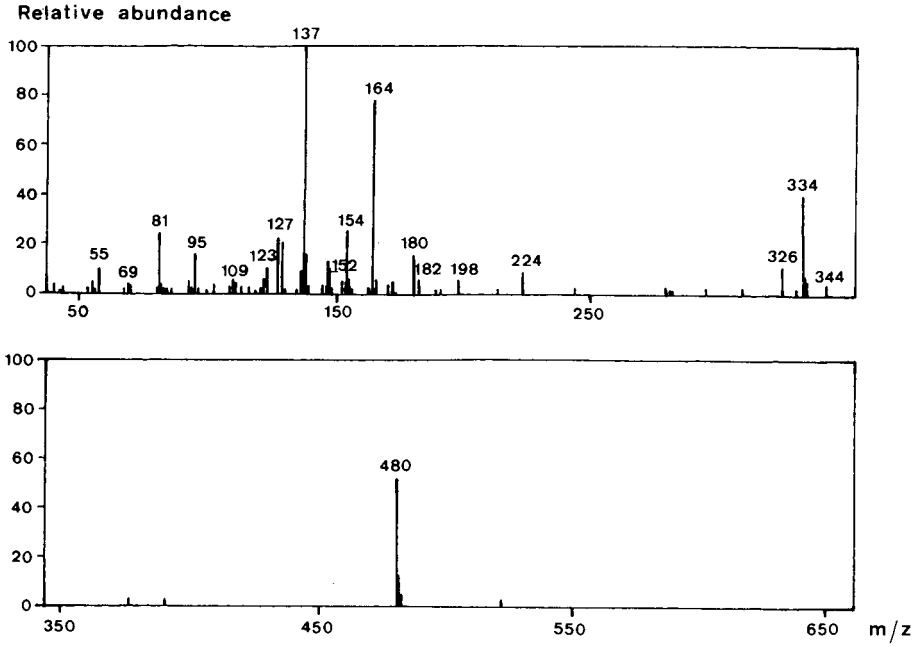

Fig. 7. DCI in positive mode (NH_3/NH_4^+) mass spectrum of OPLC 9-4 grape fraction (geranyl β-D-rutinoside).

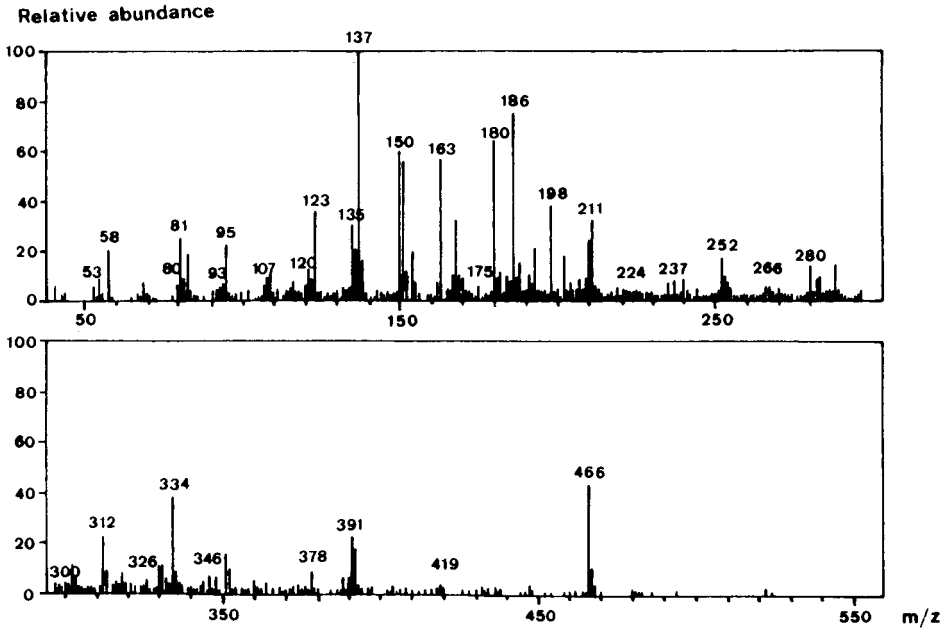

Fig. 8. DCI in positive mode (NH_3/NH_4^+) mass spectrum of OPLC 8-2 grape fraction (linayl arabinoglucoside)

Fig. 9. Analytical OPLC of apricot glycosidically bound fractions obtained after preparative OPLC on 0.2-mm silica gel (Kieselgel 60). Eluent, ethyl acetate–*tert.*-amyl alcohol–acetic acid–water (18:1:1:1, v/v) at a flow-rate of 0.75 ml min^{-1}. Nediac reagent was used for detection.

obtained by GC and TLC after enzymatic hydrolysis confirmed the tentative identification of linaly (9-2), α-terpinyl (10-1), neryl (11-1) and geranyl (12-1) glucosides. The identification of linalool by GC and of arabinose and glucose by TLC after total enzymatic hydrolysis of fraction 7′-1 agrees with the presence of linalyl arabinoglucoside or glucoarabinoside, the former certainly being the actual compound, as indicated by mass spectrometry.

As established from Figs. 6 and 7, the purity of most of the fractions studied was sufficient for subsequent ulterior HPLC or improved mass spectrometric analysis in order to obtain more information on the structure of these compounds and particularly on the nature of the aglycone moiety.

REFERENCES

1 R. Cordonnier and C. Bayonove, *C.R. Acad. Sci.*, 278 (1974) 3387.
2 P. J. Williams, C. R. Strauss and B. Wilson, *Phytochemistry*, 19 (1980) 1137.
3 P. J. Wiliams, C. R. Strauss, B. Wilson and R. A. Massy-Westropp, *Phytochemistry*, 21 (1982) 2013.
4 J. Heidlas, M. Lehr, H. Idstein and P. Schreier, *J. Agric. Food Chem.*, 32 (1984) 1020.
5 K. H. Enge and R. Tressl, *J. Agric. Food Chem.*, 31 (1983) 998.

6 C. Salles, H. Essaied, P. Chalier, J. C. Jallageas and J. Crouzet, in P. Schreier (Editor), *Bioflavor '87*, Walter de Gruyter, Berlin, New York, 1988, p. 145.
7 S. Bitteur, Z. Günata, J. M. Brioullet, C. Bayonove and R. Cordonnier, *J. Sci. Food Agric.*, 47 (1989) 341.
8 Y. Z. Günata, C. L. Bayonove, R. L. Baumes and R. E. Cordonnier, *J. Chromatogr.*, 331 (1985) 83.
9 R. Croteau, S. Al Hundawi and H. El Bialy, *Anal. Biochem.*, 137 (1984) 389.
10 C. R. Strauss, P. R. Gooley, B. Wilson and P. J. Williams, *J. Agric. Food Chem.*, 35 (1987) 519.
11 P. J. O. Francis and C. Allcock, *Phytochemistry*, 8 (1969) 1339.
12 R. Tschesche, F. Ciper and E. Breitmaier, *Chem. Ber*, 110 (1977) 3111.
13 C. Salles, J. C. Jallageas, J. Crouzet, R. Cole and J. C. Tabet, paper presented at the 4th International Symposium on Enology, Bordeaux, 1985.
14 C. Salles, J. C. Jallageas and J. Crouzet, presented at the *198th ACS National Meeting, Miami Beach, FL, 1989.*
15 P. J. Williams, C. R. Strauss, B. Wilson and R. A. Massy-Westropp, *J. Chromatogr.*, 235 (1982) 471.
16 K. E. A. Ishag, H. Jork and M. Zeppezauer, *Fresenius' Z. Anal. Chem.*, 321 (1985) 331.
17 R. U. Lemieux, in R. L. Whistler and M. L. Wolfrom (Editor), *Methods in Carbohydrate Chemistry*, Vol. II, Academic Press, New York, 1963, p. 221.
18 M. K. Shakhova, G. I. Samokhvalov and N. A. Preoluazhensii, *Zh. Obshch. Khim.*, 32 (1962) 390.
19 H. Paulsen, B. Le-Nguyen, V. Sinnwell, V. Heeman and F. Sekofer, *Justus Liebigs Ann. Chem.*, 8 (1985) 1513.
20 V. Reyné, *Diplôme d'Etudes Approfondies*, Montpellier University, Montpellier, 1988.
21 V. K. Dallenbach-Tolke, S. Nyiredy and O. Sticher, *Dtsch. Apoth.-Ztg.*, 127 (1987) 1167.
22 G. Derdelinckx and J. Jerumanis, *J. Chromatogr.*, 285 (1984) 231.
23 Z. Witkiewicz and J. Bladek, *J. Chromatogr.*, 373 (1986) 111.
24 T. Ozawa, *Agric. Biol. Chem.*, 46 (1982) 1079.
25 C. A. J. Erdelmeier, A. Douglas Kinghorn and N. R. Farnsworth, *J. Chromatogr.*, 389 (1987) 345.
26 S. Nyiredy, C. A. J. Erdelmeier, V. K. Dallenback-Tolke, K. Nyiredy-Mikita and O. Sticker, *J. Nat. Prod.*, 49 (1986) 885.
27 S. Nitz, N. Fischer and F. Drawert, *Chem. Mikrobiol. Tech. Lebensm.*, 9 (1985) 87.
28 W. Schwab, C. Mahr and P. Schreier, *J. Agric. Food Chem.*, 37 (1989) 1009.
29 W. Barz and J. Köster, in E. E. Conn (Editor), *The Biochemistry of Plants, Vol. 7, Secondary Plant Products*, Academic Press, London, 1981, p. 35.
30 P. J. Williams, M. A. Sefton, B. Wilson, in R. Teranishi, R. G. Buttery and F. Shahidi (Editors), *Flavor Chemistry —trends and Developments*, American Chemical Society, Washington, DC, 1989, p. 35.

Journal of Chromatography, 522 (1990) 267–275
Elsevier Science Publishers B.V., Amsterdam

CHROM. 22 662

Supercritical fluid chromatography of polychlorinated biphenyls on packed columns

KARL CAMMANN and WOLFGANG KLEIBÖHMER*
Lehrstuhl für Analytische Chemie der Westfälischen Wilhelms-Universität Münster, Wilhelm Klemm Strasse 8, 4400 Münster (F.R.G.)
(First received March 3rd, 1990; revised manuscript received June 28th, 1990)

ABSTRACT

The supercritical fluid chromatographic behaviour of polychlorinated biphenyls using carbon dioxide and nitrous oxide as mobile phases was studied on packed columns. Factors affecting the retention and separation of these compounds were investigated and an application to sediment samples is described.

INTRODUCTION

Mixtures of polychlorinated biphenyls (PCBs) have been produced and used commercially since 1929. PCBs have had multiple uses and from 1929 to 1972 about 500 000 tons of PCBs were manufactured [1]. In recent years, PCBs have become widespread pollutants [2–4].

High-resolution gas chromatography (GC) is the method of choice for the determination of PCBs. Therefore, only a few investigations have been made on the determination of PCBs by high-performance liquid chromatography (HPLC) [5,6] and there appear to be no reports on the determination of PCBs by supercritical fluid chromatography (SFC). The separation of polycylic aromatic hydrocarbons (PAHs) by SFC on different kinds of packed [7,8] and capillary columns [9] is a well investigated and established method. SFC has advantages over HPLC for the analysis of PAHs when the same kind of columns are used. The advantage of SFC is that supercritical fluid possess solvating properties similar to those of a liquid, and the solute diffusion coefficients are more than two orders of magnitude greater than those found in liquids. Therefore, comparable efficiencies to HPLC can be obtained in shorter analysis times [8].

In many complex solid and liquid samples, such as river sediments, fly ashes and waste motor oils, PAHs are accompanied by PCBs and other aromatic compounds. In this work, we investigated the retention characteristics of PCBs on cyanopropyl and octadecylsilane (ODS) columns using carbon dioxide (CO_2) and nitrous oxide (N_2O) as eluents. A very simple, rapid and reproducible method for the determination of PCBs and PAHs in sediments is presented.

0021-9673/90/$03.50

EXPERIMENTAL

A schematic diagram of the chromatographic system is shown in Fig. 1. Liquid CO_2 or N_2O (both from Westfalen, Münster, F.R.G.) is supplied from pressure vessels to an ISCO SFC-500 syringe pump (Colora, Lorch, F.R.G.) through a stainless-steel tube fitted with a 5-μm in-line filter (Valco Instruments, Houston, TX, U.S.A.). It is possible to draw liquid CO_2 from the pressure vessel into the SFC pump by an eductor (siphon) tube, but to obtain liquid N_2O it is necessary to place the N_2O pressure vessel upside down. Cooling the pump head to 0°C enhances the pumping efficiency. The mobile phase (N_2O or CO_2) is delivered from the pump and preheated by passage through a coil placed in the oven, a commercial gas chromatograph (Model 5890, Hewlett-Packard, Ratingen, F.R.G.), in front of the injector. The Valco CI4W injection valve with a 0.5-μl internal sample rotor is mounted on the top of the oven and connected to a microbore SFC column (20 or 25 cm × 1 mm I.D.). The column outlet is connected with a variable-wavelength UV detector (Model LCD 501, Gamma Analysen Technik, Bremerhaven, F.R.G.) via a short piece of 25-μm I.D. fused-silica tubing to minimize the dead volume. The high-pressure microbore flow cell has a path length of 2 mm and a volume of 250 nl. The wavelength of detection was 235 nm. It is possible to optimize the sensitivity by programming the wavelength for each peak, but this is not relevant to this discussion. The outlet of the UV cell is connected to a restrictor to control and maintain supercritical conditions. The restrictors are made from 10-μm I.D. fused-silica tubes and are thermostated.

The chromatographic columns are of 1 mm I.D. and vary in length from 20 cm for columns packed with Deltabond ODS (Raytest, Straubenhardt, F.R.G.) to 25 cm

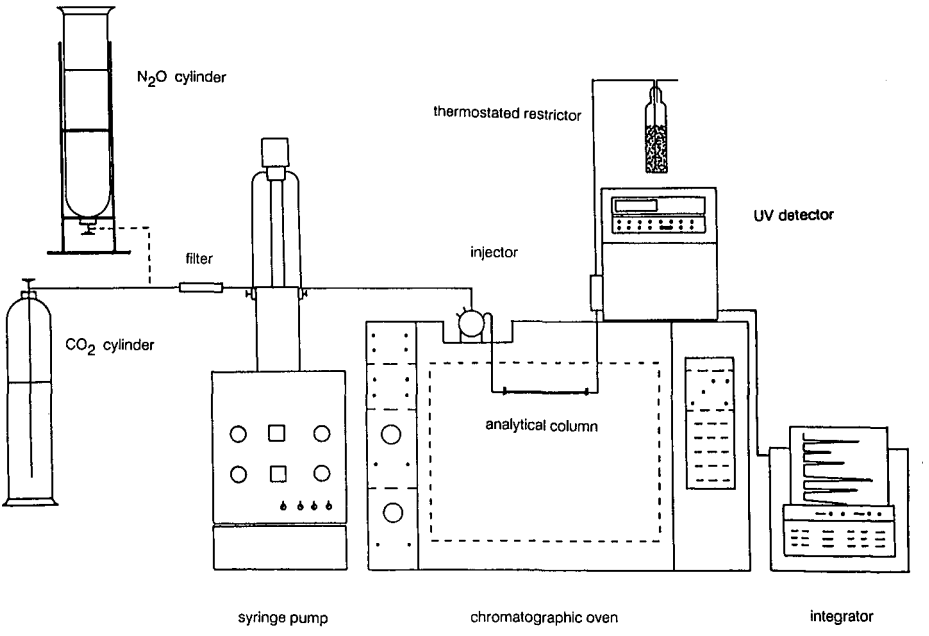

Fig. 1. Schematic diagram of the supercritical fluid chromatograph.

for columns packed with Spheri-5 cyanopropyl (Applied Biosystems, Weiterstadt, F.R.G.).

The reference compounds were obtained from Amchro (Sulzbach, F.R.G.) and Promochem (Wesel, F.R.G.) and named according to Ballschmiter and Zell [10]. The U.S. Environmental Protection Agency (EPA) PCB standard mixture (Amchro) used contained the following: (1) PCB 1, 50 μg/ml; (2) PCB 5, 50 μg/ml; (3) PCB 29, 50 μg/ml; (4) PCB 50, 100 μg/ml; (5) PCB 87, 100 μg/ml; (6) PCB 154, 100 μg/ml; (7) PCB 188, 150 μg/ml; (8) PCB 200, 150 μg/ml; (9) PCB 209, 250 μg/ml. The *ortho*-substituted PCB congeners used were PCB 1, PCB 4, PCB 16, PCB 54, PCB 104, PCB 136, PCB 188, PCB 199 and PCB 209, each at 35 μg/ml, and the non-*ortho*-substituted PCB isomers were PCB 3, PCB 15, PCB 37, PCB 77, PCB 126, PCB 169 (each at 35 μg/ml).

Samples of 5 g of the sediment were extracted with 50 ml of hexane using sonication at 100 W for 30 min. After sonication, the extract was filtered and cleaned using solid-phase extraction tubes filled with silica gel and a strong cation exchanger (both from Baker, Gross-Gerau, F.R.G.). The eluates were evaporated to 1 ml under nitrogen.

RESULTS AND DISCUSSION

Effects of column packing, mobile phase and density on retention

The density of the mobile phase determines retention and resolution in SFC and is therefore the most important parameter for optimizing a separation in SFC. Density programming during an analytical run is similiar to temperature programming in GC or programming of eluent composition in HPLC. At low density, the solubility of a substrate is low, but it increases with increasing density. In the same way the elution power increases and consequently the capacity factor, k', decreases [11].

The influence of density on the retention of decachlorobiphenyl is demonstrated in Fig. 2. The capacity factor of decachlorobiphenyl on two different stationary phases

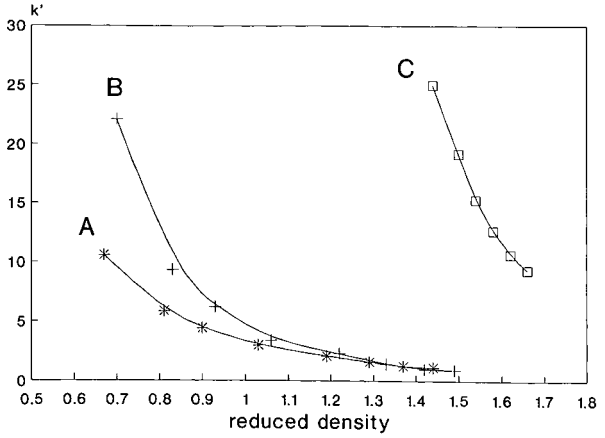

Fig. 2. Capacity factor *vs.* reduced density for decachlorobiphenyl at the same reduced temperature T_R = 1.06. (A) Cyanopropyl column, CO_2; (B) cyanopropyl column, N_2O; (C) ODS column, CO_2.

(ODS and cyanopropyl) is plotted against reduced density, d_R ($d_R = d_E/d_C$, where d_E is the experimental density and d_C the critical density), for a constant reduced temperature, T_R ($T_R = T_E/T_C$, where T_E is the experimental temperature and T_C the critical temperature) and for two different mobile phases (CO_2 and N_2O). The slope of the decrease is not the same for the different mobile and stationary phases. The value of the capacity factor is mainly determined by the interaction between the substrate and the stationary phase. There is no significant difference in elution order between CO_2 and N_2O for a given stationary phase (curves A and B), and the curves coincide at higher densities. On the ODS phase (curve C), the interaction between the stationary phase and the substrate is stronger than that on the cyanopropyl phase, so on ODS phases a higher density is needed to elute the PCBs.

The weight and size of the PCB congeners are the main parameters controlling the elution order in SFC. In addition, the retention is determined by the shape and the electron configuration of the molecule. The two phenyl rings of a biphenyl molecule can rotate freely around their common axis. The conformation with lowest potential energy is a coplanar orientation of the two rings, because the π-electron can delocalize over the two rings. A substituent in a *meta-* or *para*-position or one substituent in an *ortho*-position has no influence on the free rotation about the common axis and the molecule is still coplanar. A further chlorine substituent in an *ortho*-position restricts the coplanar orientation of the rings and according to the number of chlorine atoms in *ortho* positions the degree of out-of-plane orientation increases [1,6].

For these investigations the PCBs were divided into two groups: non-*ortho*-substituted coplanar PCB congeners and *ortho*-substituted PCB congeners. Fig. 3 illustrates the plot of the capacity factor, k', for some PCBs *vs.* the number of chlorine substituents on an ODS column. Curve A represents data for non-*ortho*-substituted PCB congeners (PCBs 3, 15, 37, 77, 126 and 169) and curve B represents data of the maximum *ortho*-substituted PCBs (PCBs 1, 4, 16, 54, 104, 136, 188, 199 and 209) within a group of chloro homologues. All the other PCB congeners within a group of chloro homologues appear between those mentioned above. The coplanar PCB congeners are retained more strongly than the non-planar congeners within a group of

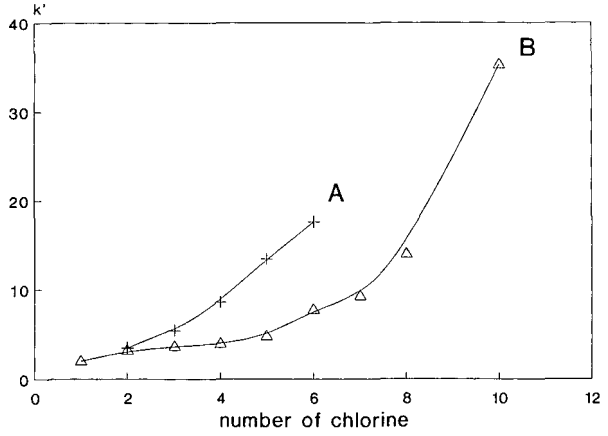

Fig. 3. Capacity factor *vs.* number of chlorine substituents on the ODS column. (A) Non-*ortho*-substituted PCBs; (B) *ortho*-substituted PCBs.

chloro homologues and there is a nearly linear relationship between k' and the number of chlorine substituents for the coplanar PCBs congener (curve A). For the *ortho*-substituted PCB congeners, there is no linear relationship between k' and the number of chlorine substituents (curve B). Both curves coincide for the dichloro homologues.

The difference in retention on an ODS phase between the *ortho*-substituted and non-*ortho*-substituted PCB isomers is caused by an increasing degree of out-of-plane orientation of the *ortho*-substituted PCB isomers and consequently by a weakening of the Van der Waals interaction between the molecule and the C_{18} chains of the stationary phase. This effect is enhanced by a chlorine in a *meta* position. A chlorine atom in a *meta* position pushes the chlorine which is in an *ortho* position towards to the C–C bonding between the two rings and consequently the degree of out-of-plane orientation increases [12].

Similar results were obtained on a cyanopropyl column, as can been seen in Fig. 4. Curve A represents data obtained for the non-*ortho*-substituted PCBs (PCBs 3, 15, 37, 77, 126 and 169) and curve B for the *ortho*-substituted PCBs (PCBs 1, 4, 16, 54, 104, 136, 188, 199 and 209). The cyanopropyl phase is a polar bonded phase and can be used for both normal- and reversed-phase chromatography. In spite of the polar parts of the stationary phase, polar interactions are negligible and the retention can be pictured as a reversible association process between the ligand anchored to the stationary phase and the solute molecule. The coplanar isomers are retained more strongly than *ortho*-substituted isomers because of stronger interactions of the coplanar isomers with the stationary phase. There is a linear relationship between k' and the number of chlorine atoms for the non-*ortho*-substituted isomers. However, for the *ortho*-substituted isomers there is no such linear relationship. The increase in k' for the *ortho*-substituted isomers on a cyanopropyl column is smaller than that on an ODS column, and decachlorobiphenyl is eluted as fast as the coplanar hexachloro isomer (PCB 169). Hence the interactions between solute and stationary phase decrease with increase in the degree of out-of-plane orientation of the isomer. These parameters compensate for the influence of molecular mass on the elution order.

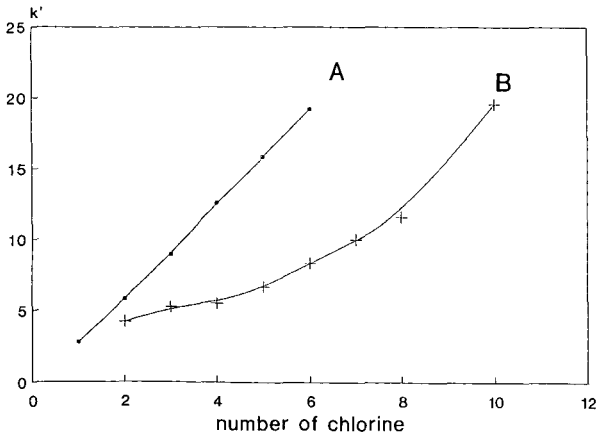

Fig. 4. Capacity factor *vs.* number of chlorine substituents on the cyanopropyl column. (A) Non-*ortho*-substituted PCBs; (B) *ortho*-substituted PCBs.

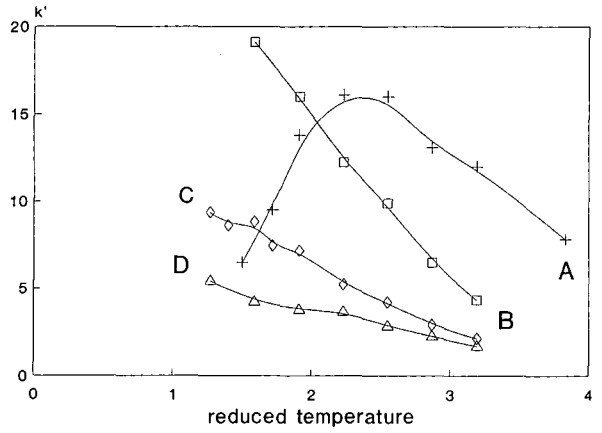

Fig. 5. Capacity factor *s.* reduced temperature on the cyanopropyl column at various densities: (A) 0.369; (B) 0.417; (C) 0.496; (D) 0.580 g/ml.

The results demonstrate that the size and shape of the PCB isomers control retention in SFC. This agrees well with results obtained for HPLC separations by other workers [5,6,12].

Effect of temperature on retention and resolution

The influence of temperature on the capacity factor at constant density can be explained by the Van 't Hoff equation [13,14]. The plots of ln k' *vs.* $1/T$ are straight lines and the enthalpies of substrate transfer from the mobile phase to the stationary phase were determined from these plots [15]. Graphs of k' *vs.* T_R at constant density are shown in Fig. 5 for CO_2 and N_2O as mobile phases and the substrate decachlorobiphenyl. The capacity factor decreases monotonously with increasing temperature above T_C (curves B, C and D). However, for low densities there was first an increase in

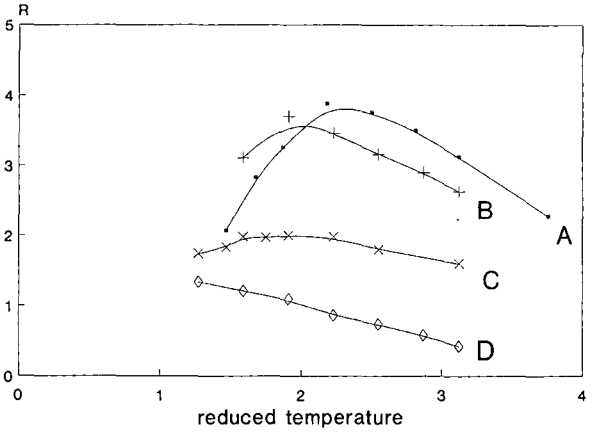

Fig. 6. Mean resolution *vs.* reduced temperature on the cyanopropyl and ODS column at various densities. (A)–(D) as in Fig. 5.

k', decreasing beyond a maximum value for k' (curve A). The shape of the curve is similar to those obtained for k' *vs.* T at constant pressure [15]. Moreover, for the mean resolution, we observed a maximum, illustrated in Fig. 6. The mean resolution, R_m, is

$$R_m = \sum_1^n R/n$$

where n is the number of pairs of neighbouring peaks. R_m was plotted *vs.* T_R at various densities for the PCB congeners of the EPA test mixture. The temperature of the maximum of k' is the same as that for the maximum of R_m. The tendency of R_m to form a maximum, at constant densities, has been reported [13,14], but up to now there has

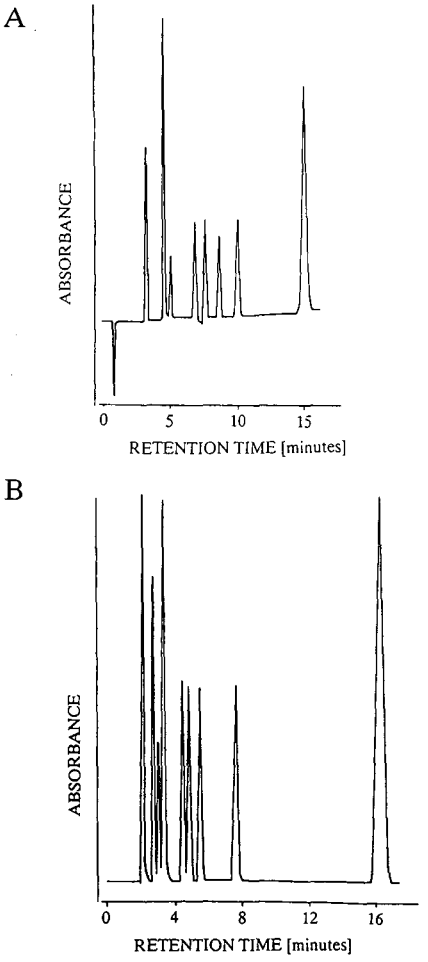

Fig. 7. Separation of EPA PCB mixture with CO_2. (A) On the cyanopropyl column at 0.366 g/ml and 80°C; (B) on the ODS column at 0.744 g/ml and 44°C. Peaks from left to right (order of elution): (A) PCBs 1, 29 + 5, 50, 154, 188, 87, 199, 209; (B) PCBs 1, 29, 5, 50, 154, 188, 87, 199, 209.

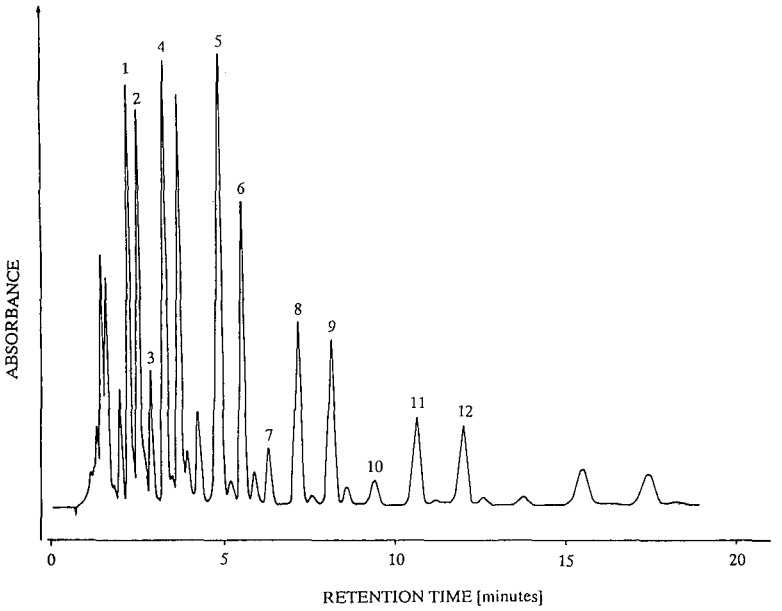

Fig. 8. Chromatogram of a sediment extract obtained on the cyanopropyl column at a CO_2 inlet pressure of 110 bar and 80°C. Peaks: 1 = acenaphtene; 2 = fluorene; 3 = PCB 1; 4 = anthracene; 5 = PCB 28; 6 = PCB 52; 7 = PCB 50; 8 = PCB 154; 9 = PCB 87; 10 = fluoranthene; 11 = PCB 153; 12 = PCB 180.

been no satisfactory explanation. We found that a maximum only appears at densities $d_E < d_C$ (curves A and B), as opposed to densities d_E near d_C, where the curve shows more of a plateau than a maximum (curve C), and for densities $d_E > d_C$ R_m decreases constantly with increasing temperature (curve D).

Fig. 7 compares the best separation of the EPA mixture obtained on an ODS column (B) with the best separation obtained on a cyanopropyl phase; in the latter instance it is not possible to separate PCBs 5 and 29. However, the selectivity of the cyanopropyl column is greater for the higher PCBs and therefore we chose a cyanopropyl column for the rapid analysis of a sediment extract.

Fig. 8 demonstrates the rapid elution and detection within 16 min of PCBs and PAHs in a sediment extract using a cyanopropyl column. The solutes range from acenaphtene eluted at 3 min to PCB 188 at 12 min.

ACKNOWLEDGEMENT

This work was supported by the Bundesministerium für Forschung und Technologie; Förderkennzeichen 01 VQ 89 05.

REFERENCES

1 O. Hutzinger, S. Safe and V. Zitko, *The Chemistry of PCBs*, CRC Press, Cleveland, OH, 1974.
2 A. Jensen, *Sci. Total Environ.*, 64 (1987) 259–293.
3 A. Bryan, P. Olafsson and W. Stone, *Bull. Environ. Contam. Toxicol.*, 38 (1987) 1000–1005.

4 H. Buchert and K. Ballschmiter, *Fresenius Z. Anal. Chem.*, 320 (1985) 707–709.
5 J. J. de Kok, A. de Kok, U. A. Th. Brinkmann and R. M. Kok, *J. Chromatogr.*, 142 (1979) 367–383.
6 W. A. Bruggeman, J. van der Steenand and O. Hutzinger, *J. Chromatogr.*, 238 (1982) 335–340.
7 D. R. Gere, R. Board and D. McManigall, *Anal. Chem.*, 54 (1982) 736–740.
8 I. K. Barker, J. P. Kithji, K. D. Bartle, A. A. Clifford, G. F. Shilstone, P. A. Halford-Maw and M. W. Raynor, *Analyst (London)*, 114 (1989) 41–45.
9 R. D. Smith, H. T. Kalinoski, H. R. Udseth and B. W. Wright, *Anal. Chem.*, 56 (1984) 2476–2480.
10 K. Ballschmiter and M. Zell, *Fresenius Z. Anal. Chem.*, 302 (1980) 20–31.
11 K. Bartle, in R. M. Smith (Editor), *Supercritical Fluid Chromatography*, Royal Society of Chemistry, London, 1989, Ch. 1, pp. 1–28.
12 J. Brodsky, *Ph.D. Thesis*, University of Ulm, Ulm, 1986.
13 C. R. Yonker and R. D. Smith, *J. Chromatogr.*, 351 (1986) 211–216.
14 D. Leyendecker, D. Leyendecker, B. Lorenschat, F. P. Schmitz and E. Klesper, *J. Chromatogr.*, 398 (1987) 89–103.
15 E. Klesper and F. P. Schmitz, *J. Chromatogr.*, 402 (1987) 1–39.

Journal of Chromatography, 522 (1990) 277–284
Elsevier Science Publishers B.V., Amsterdam

CHROM. 22 678

Gas chromatographic methods for the assessment of binary diffusion coefficients for compounds in the gas phase

AGNETA K. BEMGÅRD and ANDERS L. COLMSJÖ*
Department of Analytical Chemistry, National Institute of Occupational Health, S-171 84 Solna (Sweden)
(First received April 9th, 1990; revised manuscript received July 5th, 1990)

ABSTRACT

Binary diffusion coefficients, D_g, were calculated for a number of compounds by using three gas chromatographic methods. All three methods showed good agreement when D_g was extrapolated to zero gas velocity. For the compounds tested, all D_g values were lower than those achieved by using the Fuller–Schettler–Giddings equation.

INTRODUCTION

Diffusion of compounds present in gases or air plays an important role in many chemical and physical processes. Relationships which govern the diffusion have been studied mathematically and empirically over a long period. The diffusion rate is described by individual diffusion coefficients that take into account chemical structure, temperature, viscosity, etc. So far, no method has been described that makes possible the exact calculation of binary diffusion coefficients, although a large number of empirically derived equations based on various methods have been published [1–9]. Thus, diffusion coefficients can be calculated roughly and simply, yielding errors that sometimes exceed 30%. Some equations are better adapted to certain environmental conditions, such as low molecular weight and moderate temperatures, depending on the empirical values available at the time of the formulation of the equation. In 1965, Fuller and Giddings [10] critically reviewed and tested the existing equations. They concluded that the Fuller–Schettler–Giddings (FSG) relationship was so far the best available general equation when utilized for the calculation of diffusion coefficients for a large number of compounds, covering as many applications as possible. Since then, the FSG equation has been commonly used with reference to the original paper [11]. In chromatography, the diffusion coefficients of specific compounds, in particular environments, are of great importance for the chromatographic process. Thus, for the relationship giving the height equivalent to a theoretical plate (HETP or H), diffusion coefficients for a compound in both the mobile and the stationary phase are used. For open-tubular gas chromatography, this relationship is given by [12]

$$H = 2D_{go}f_1/v_o + [C_{go}f_1 + (C_l + C_i)f_2]v_o \quad (1)$$

0021-9673/90/$03.50

where v_o is the carrier gas velocity at the outlet of the tube. The C terms represent the contributions due to resistance to mass transfer in the gas phase (g), liquid phase (l) and the interface (i):

$$C_{go} = \frac{r^2(11k'^2+6k'+1)}{24(1+k')^2 D_{go}} \tag{2}$$

where r is the tube radius, k' the capacity factor and D_{go} is the solute diffusion coefficient in the gas phase at the outlet gas velocity, and

$$C_l + C_i = \frac{2k'd_f}{(1+k')^2}(d_f/3D_l + 1/k_d) \tag{3}$$

where d_f is the film thickness, D_l the diffusion coefficient in the liquid phase and k_d is the desorption rate constant. The C_i term is not regarded as being governed by diffusion. The pressure drop is taken into account by the f factors [13,14]:

$$f_1 = \frac{9(P^4-1)\ (P^2-1)}{8(P^3-1)^2} \tag{4}$$

$$f_2 = \frac{3(P^2-1)}{2(P^3-1)} \tag{5}$$

$$P = p_i/p_o \tag{6}$$

where p_i and p_0 are the column inlet and outlet pressures. Large errors in the D_{go} value (diffusion in the gas phase at the outlet pressure) make all other calculations within the HETP equation erroneous [12].

Some methods for empirically assessing correct D_g values have been described (*e.g.*, refs. 15–17). All such methods are combined with errors, depending on the fact that the instruments used for measuring diffusion themselves add errors owing to their interferences with the diffusion process. Theoretically, it is possible to derive a D_{go} value from eqn. 1 by using a capillary column with no stationary phase present. Ideally, this would give a non-retained peak from which it would be possible to calculate the HETP value. This method was described by several workers in the early 1960s [15,18,19], not taking into account the pressure drop over the column or any other retention mechanisms. If the f factors are included, the calculations still become straightforward. Assuming $k'=0$, $C_l=0$ and $C_i=0$ in eqn. 1 gives:

$$H = 2D_{go}f_1/v_o + C_{go}f_1 v_o \tag{7}$$

where

$$C_{go} = \frac{r^2}{24D_{go}} \tag{8}$$

This yields

$$D_{go} = v_o/4\,[H/f_1 \pm \sqrt{(H/f_1)^2 - r^2/3}] \quad (9)$$

where the positive root is used according to ref. 20. Replacing the outlet velocity in eqn. 9 by the mean velocity or elution time:

$$v_o = v/f_2 = L/(t_r f_2) \quad (10)$$

will give

$$D_{go} = L/(4t_r f_2)\,[H/f_1 + \sqrt{(H/f_1)^2 - r^2/3}] \quad (11)$$

H is determined according to

$$H = L/N = B^2/(8 \ln 2 t_r^2) \quad (12)$$

where L is the tube length, B is the peak width at half-height, N is the number of theoretical plates and t_r is the retention time. This means that it is possible to calculate a D_g value based on a chromatogram of a compound eluted from a column without stationary phase and corrected for the pressure drop over the column (f factors). Measuring diffusion coefficients by gas chromatography was reviewed in 1975 [21].

Unfortunately, the general theory is not as simple as that for determining a correct D_g value. In practice a small compound- and v_o-dependent adsorption/non-laminar flow term exists even when no stationary phase is present. This term will be referred to as C_a. Extra-column contributions will add a v_o^2-dependent term, D, described by Gaspar *et al.* [22]. Eqn. 7 thus becomes

$$H = 2D_{go}f_1/v_o + r^2 f_1 v_o/(24D_{go}) + C_a f_2 v_o + D(f_2 v_o)^2 \quad (13)$$

Solving D_{go} from this equation gives

$$D_{go} = v_o/4(K + \sqrt{K^2 - r^2/3}) \quad (14)$$

where

$$K = [H - C_a f_2 v_o - D(f_2 v_o)^2]/f_1 \quad (15)$$

and v_o can be replaced with v according to eqn. 10.

In this paper, three empirical methods to determine diffusion coefficients are discussed and compared with the FSG method [11].

EXPERIMENTAL

The gas diffusion coefficients were obtained by headspace injections of the solutes into an empty, non-pretreated fused-silica tube of length 100 m and I.D. 0.32 mm (Quarts et Silice, Paris, France). The diffusion tube was installed in a Carlo Erba

(Milan, Italy) 4160 gas chromatograph. Hydrogen was used as the carrier gas and the inlet pressure was measured by a digital pressure gauge (Chrompack, Middelburg, The Netherlands). The inlet pressure ranged from 2.23 to 1.12 atm (outlet pressure = 1 atm), giving outlet velocities from 0.60 to 0.02 m/s.

Headspace samples (7 μl) were injected in the split mode by use of a 10-μl Hamilton syringe equipped with a 7-cm needle. The splitting ratio was maintained at 1:500 and the injector temperature was held at the same temperature as the oven, *i.e.*, 125°C. A flame ionization detector was used.

Four solutes were investigated, *n*-butane, *n*-hexane, *n*-dodecane and toluene. Signal recording and data handling were performed with an ELDS 900 laboratory data system (Chromatography Data Systems, Kungshög, Stenhamra, Sweden). The sampling rate was 18.2 s^{-1}, giving 40–400 data points per peak.

Double or triple injections were performed at each new inlet pressure, giving a total of approximately 80 peaks per compound to be used for further calculations.

RESULTS AND DISCUSSION

If eqn. 7 was true in the case of an open-tubular column with no stationary phase, a plot of D_{go} *versus* v_o according to eqn. 11 should generate a horizontal line. If any other relationship is registered, with a slope differing significantly from zero, this would imply that it was necessary to introduce some other term in eqn. 7. Such a term could be due to retention, caused by the fused-silica surface (*e.g.*, adsorption), to physical retention from gaseous friction on the column wall which could be called interfacial resistance or to extra-column effects (such as peak broadening in the injector or detector and time constants of the electronic recording system).

Indeed, a plot of D_{go}, calculated according to eqn. 11, yields a non-constant value. In Fig. 1 (marked □), D_{go} is plotted *versus* v_o for four compounds. The fact that the diffusion coefficient increases with increasing gas velocity indicates that an additional retention effect (or an extra-column effect) exists. This effect was discussed theoretically by Giddings and Seager in 1962 as "...non-uniform flow velocity existing over the tube crossing", but not applied experimentally [20]. In this work, extra-column effects were minimized by using a 100-m column with an inlet splitting ratio of *ca.* 1:500.

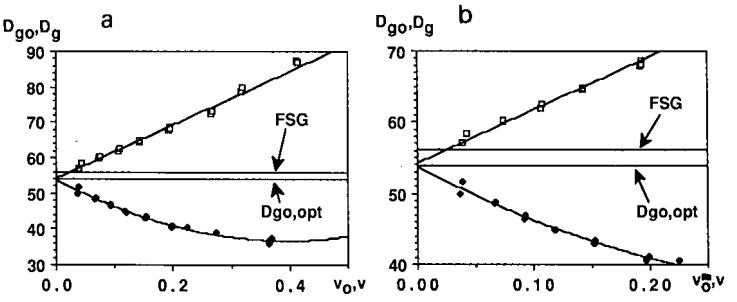

Fig. 1. (a) Diffusion coefficient of toluene at 125°C *versus* gas flow velocity: D_{go} *versus* v_o according to eqn. 11 (□), D_g *versus* v according to eqn. 16 (◆), $D_{go,opt}$ according to eqn. 17 and FSG according to ref. 11. (b) Enlargement of part of (a).

TABLE I

D_{go} VALUES OBTAINED BY DIFFERENT METHODS

Solute	Method[a]	D_{go}	C_a
n-Butane	Opt	63.59	0
	Opt	63.01	78.31
	Extrap1	63.60	–
	Extrap2	62.51	–
	FSG	63.70	–
n-Hexane	Opt	49.25	0
	Opt	49.14	31.13
	Extrap1	48.73	–
	Extrap2	50.16	–
	FSG	52.67	–
n-Dodecane	Opt	29.04	0
	Opt	28.72	87.72
	Extrap1	28.96	–
	Extrap2	27.80	–
	FSG	37.41	–
Toluene	Opt	54.02	0
	Opt	53.85	43.51
	Extrap1	54.23	–
	Extrap2	53.79	–
	FSG	56.05	–

[a] Opt = Optimized according to eqn. 17; Extrap1 = extrapolation to $v_o = 0$ from the plot of eqn. 9; Extrap2 = extrapolation to $v_o = 0$ from the plot of eqn. 16; FSG = calculated according to ref. 11.

The second method applied uses eqn. 11, but not taking into account the pressure drop over the column ($f_1 = 1$ and $f_2 = 1$). This is the method which has been used by many workers (*e.g.*, refs. 20 and 23), preferably with short, wide-bore columns where the *f*-factors practically equal unity. The relationship becomes

$$D_g = L/(4t_r)\,[H + \sqrt{H^2 - (r^2/3)}] \tag{16}$$

where D_g is a mean binary diffusion coefficient and L/t_r equals the mean gas velocity in the column. This plot is also shown in Fig. 1 (marked ◆). All curves tend to show a negative slope whereas earlier reported data on short, wide-bore columns generally yielded positive slopes [23]. Results from these methods are given in Table I.

Third, an optimization program was used by means of a least-squares fit of the measured values (H_i, v_{oi}) to $H = B_o/v_o + Cv_o + Dv_o^2$ according to

$$\min \sum_i [H_i - 2D_{go}f_1/v_{oi} + (r^2 f_1/24D_{go} + C_a f_2)v_{oi}]^2 \tag{17}$$

D was set to zero in eqn. 17 according to the above discussion. D_{go} and C_a were optimized by linear programming, assuming that k' equals zero but taking into account the *f*-factors. The assumption that k' equals zero when a non-negligible C_a term is used is a contradictory but still reasonable simplification. Small k' values

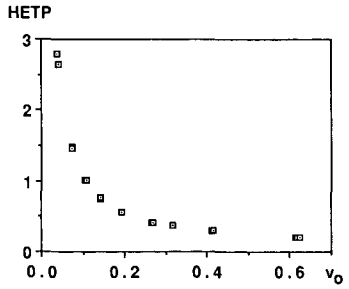

Fig. 2. HETP *versus* v_0 for toluene at 125°C recorded on a non-coated open-tubular column (I.D. 0.32 mm).

(<0.05) are difficult to determine and the error introduced by this assumption is in the range of other errors (HETP calculations, etc.). The fit to the optimum function is given by the square root of the sum given in eqn. 17, divided by the number of observations:

$$\text{Error} = \sqrt{\sum(H_i - H_{\text{calc}})^2/n} \tag{18}$$

In Table I, the calculated values of D_g, obtained using eqn. 17, for a number of compounds are shown. All measured values are on the low velocity side of the optimum v_0 for minimum HETP (see Fig. 2). This also ensures that the correct sign is used in eqn. 9 for all calculations ($v_0 < 4\sqrt{3}\ D_g/r$) [20]. When this extreme side of the HETP plot is used for optimization calculations, variations in the B term will have a very strong influence on the determination of a minimum in eqn. 17, whereas the influence of C_a is much weaker. In practice, an extra-column term, proportional to v_0^2, cannot be derived from these data owing to the small influence of such a term in the low velocity range. Table I also indicates that the existence of a C_a term alters the estimated D_g value by less than 1%.

As the fourth method, the FSG equation is applied to the calculation of D_g values [11]. These values are also listed in Table I.

Obviously, with the two methods where eqns. 11 and 16 are used for determining a D_g value, it is necessary to extrapolate to zero gas velocity in order to exclude all interfering processes. In this case, the f-factors are equal to unity, and D_{go} in eqn. 11 should equal D_g in eqn. 16. The method for making this extrapolation is not straightforward if the curve form is unknown. The deviation from a constant value in the case of eqn. 11 is due to the approximation that $k' = 0$ and $C_a = 0$. Neither of these parameters can easily be determined in these experiments. In Table I, an extrapolation based on a polynomial of the second-order in terms of v_0 has been used. It is possible to show that this is a good assumption for small v_0 values.

As expected, the D_g values calculated with any of the three methods are similar and have a lower limit than the values calculated from the FSG equation (Table I). Most empirical methods can be expected to yield higher values of the diffusion coefficient of a compound because the measurement itself influences (increases) the peak width for the observed compound. In a previous paper [12], especially the D_g values for n-alkanes were found to be significantly lower than the corresponding FSG values. However, the aromatic compound investigated in that study, biphenyl, showed

a much better agreement between observed values and those calculated from the FSG equation.

Table I and Fig. 1 show that the results obtained from the experimental methods are in good agreement, whereas those from the FSG method differ significantly, especially for larger molecules, *e.g.*, the deviation for *n*-butane is negligible, whereas the deviation for *n*-dodecane is as much as 37%. Obviously it is possible to estimate the D_g value by using a capillary column even if the pressure drop over the column is neglected. This can be done as long as an extrapolation back to zero gas velocity is made. When comparing the figures in Table I, it is also important to emphasize that all three experimentally applied methods use the same calculated HETP data, *i.e.*, accurate and carefully made calculations must be used in order not to introduce simultaneously systematic errors in all three methods.

Using this very limited set of data, no general correspondence can easily be observed between the deviation of FSG results from the experimental methods and the boiling points. The deviation for *n*-hexane (b.p. = 68.7°C) is in the same range as that for toluene (b.p. = 110.6°C).

CONCLUSION

All three methods described seem to yield fairly acceptable values for the binary gas diffusion coefficients. The method described by eqn. 16 (marked by ◆ in Fig. 1) is the simplest. This method can be applied accurately to an ordinary gas chromatographic system without the need to measure the pressure drop over the column. Extra-column effects must be minimized by using a long column in conjunction with a high splitting ratio.

The fact that the slope of the plot of D_g *versus* v_o differs significantly from zero cannot easily be attributed to one predominant property such as adsorption or extra-column effects in terms of time constants for the electronic recording system. Extensive calculations within this work have shown that the addition of a single term in the HETP equation, corresponding to adsorption (*i.e.*, proportional to v_o) or corresponding to extra-column effects (*i.e.*, proportional to v_o^2) also yields plots where D_g gives a slope *versus* v_o. Thus, in order to achieve accurate calculations of D_g by using eqn. 11 or 16, an extrapolation to zero gas velocity must be performed.

REFERENCES

1 T. R. Marrero and E. A. Mason, *AIChE J.*, 19 (1973) 498.
2 E. R. Gilliland, *Ind. Eng. Chem.*, 26 (1934) 168.
3 L. Andrussow, *Z. Elektrochem.*, 54 (1950) 566.
4 J. H. Arnold, *Ind. Eng. Chem.*, 22 (1930) 1091.
5 J. O. Hirschfelder, R. B. Bird and E. L. Spotz, *Trans. Am. Soc. Mech. Eng.*, 71 (1949) 921.
6 C. R. Wilke and C. Y. Lee, *Ind. Eng. Chem.*, 47 (1955) 1253.
7 N. H. Chen and D. F. Othmer, *J. Chem. Eng. Data*, 7 (1962) 37.
8 J. C. Slattery and R. B. Bird, *AIChE J.*, 4 (1958) 137.
9 D. F. Othmer and H. T. Chen, *Ind. Eng. Chem., Process Des. Dev.*, 1 (1962) 249.
10 E. N. Fuller and J. C. Giddings, *J. Gas Chromatogr.*, 3 (1965) 222.
11 E. N. Fuller, P. D. Schettler and J. C. Giddings, *Ind. Eng. Chem.*, 58 (1966) 19.
12 A. Bemgård, L. Blomberg and A. Colmsjö, *Anal. Chem.*, 61 (1989) 2165.
13 J. C. Giddings, S. L. Seager, L. R. Stucki and G. H. Stewart, *Anal. Chem.*, 36 (1964) 741.
14 A. T. James and A. J. P. Martin, *Biochem. J.*, 50 (1952) 679.

15 J. C. Giddings and S. L. Seager, *J. Chem. Phys.*, 33 (1960) 1579.
16 N. A. Katsanos and G. Karaiskakis, *J. Chromatogr.*, 237 (1982) 1.
17 J. H. Knox and L. McLaren, *Anal. Chem.*, 36 (1964) 1477.
18 J. Bohemen and J. H. Purnell, *J. Chem. Soc.*, (1961) 360.
19 P. Fejes and L. Czaran, *Hung. Acta Chim.*, 29 (1961) 171.
20 J. C. Giddings and S. L. Seager, *Ind. Eng. Chem., Fundam.*, 1 (1962) 277.
21 V. R. Maynard and E. Grushka, *Adv. Chromatogr.*, 12 (1975) 99.
22 G. Gaspar, R. Annino, C. Vidal-Madjar and G. Guiochon, *Anal. Chem.*, 50 (1978) 1512.
23 T.-C. Huang, S.-J. Sheng and F. J. F. Yang, *J. Chin. Chem. Soc., Ser. 2*, 15 (1968) 127.

Journal of Chromatography, 522 (1990) 285–294
Elsevier Science Publishers B.V., Amsterdam

CHROM. 22 675

Evaluation tests and applications of a double-layer tube-type passive sampler[a]

G. BERTONI*, S. CANEPARI, M. ROTATORI, R. FRATARCANGELI and A. LIBERTI
Istituto sull'Inquinamento Atmosferico del CNR, Area della Ricerca di Roma, Via Salaria Km 29,300, C.P. 10, 00016 Monterotondo Stazione, Rome (Italy)
(First received February 14th, 1990; revised manuscript received July 3rd, 1990)

ABSTRACT

Validation tests on a thermally desorbable tube-type passive sampler filled with two different graphitized carbon blacks were conducted in order to determine the influence of air velocity and direction, concentration and sampling time on sampling rate. A specially made apparatus was used to study the behaviour of the passive sampler in dynamic artificial atmospheres. This apparatus permits the simultaneous sampling of 48 tubes at two different air velocities, minimizing errors due to random variations of the operating conditions during a prolonged sampling time, which allows a better stochastic analysis of data to be performed. The results were in agreement with those obtained by actively sampling the same test-tubes. The results of laboratory and field tests showed that the behaviour of tube-type devices having a small cross-section is independent of the environmental parameters checked over a wide range of operating conditions. The constant sampling rate with these samplers in the range from 30 min up to more than 12 h and the high sensitivity of thermal desorption methods allow the determination of organic species down to the ppb level. A field experiment on the evaluation of the indoor pollution in a domestic environment is also described. The use of a double-layer tube-type passive sampler, with the adsorbent of lower specific surface area positioned at the exposed side of the device, allows a better desorption efficiency.

INTRODUCTION

Diffusive samplers are cheaper, smaller, lighter and more comfortable to wear than active devices. However, a series of drawbacks have been suggested by some workers [1]. Evidence indicates that each device needs a proper study of the accuracy and precision of the method and clear instructions for its use. The sampling validity range in relation to the collected species and to the environmental parameters influencing the properties of the devices [2–8] also needs to be properly evaluated.

Thermal desorption offers the best sensitivity, with respect to solvent extraction, when the whole sample is injected into the chromatographic system [9,10]. However, a disadvantage of this technique is that high-boiling compounds are not quantitatively

[a] Presented in part at the *8th World Clean Air Congress, The Hague, September 11–15, 1989.*

0021-9673/90/$03.50

desorbed at low temperatures, while high temperatures may cause pyrolytic effects with some substances [11].

In this work we performed experimental tests in order to evaluate the desorption efficiency of a double-layer packing in a tube-type sampler. We also carried out a series of tests in order to evaluate the behaviour of this sampler in relation to wind velocity [12] and direction [13], exposure time and sampled species concentration.

THEORY

The passive sampling technique is a practical application of Fick's law regarding the transfer of a gaseous species through a fluid. A suitable expression for this law, valid when the mass transfer through a diffusional path having a constant section is considered, is

$$\frac{dQ_i}{dA\,dT} = -KD_i \cdot \frac{dC_i}{dL} \tag{1}$$

where Q_i (mol) is the amount of species i which passes through a section A (cm^2) during time t (s); this term is proportional to the concentration gradient along the mass transfer direction; D_i (cm^2/s) is the diffusion coefficient of species i in air; C_i (mol/cm^3) is the concentration of species i; L (cm) is the diffusional path length; and K is the mass transfer resistance term; when the diffusional path is "open", it is assumed that $K = 1$, and when a medium (such as a filter or a septum) is placed in the diffusional path before the adsorbent surface, $K < 1$ and its value must be calculated.

By integrating eqn. 1, the following expression is obtained:

$$C_{i,1} - C_{i,0} = \frac{Q_i L}{KAtD_i} \tag{2}$$

where $C_{i,1}$ is the concentration of the species i at the beginning and $C_{i,0}$ is that at the end of the diffusional path.

In the presence of an adsorbing surface, as in a passive sampler, a concentration gradient occurs. If the adsorbent is strong, the vapour tension of the adsorbed molecules on the surface ($C_{i,0}$) is nearly zero, and we may write

$$C_i = \frac{Q_i L}{KAtD_i} \tag{3}$$

This expression permits the caculation of the environmental concentration C_i if the amount Q_i collected on the adsorbent is analytically determined and L, A, K and t are known. The term KD_iA/L is defined as "diffusive uptake rate" for the species i and is the "virtual" flow through a sampler whose diffusional path has a length equal to L and whose section normal to L is A, which corresponds to the geometrical exposed surface of the adsorbent. The diffusive uptake rate is obviously constant only if we can assume that $C_{i,0}$ remains equal to zero during the whole sampling run. When the sampled amount of the species i begins to saturate the adsorbing surface, $C_{i,0}$ increases

and assumes none-negligible values, leading to a non-linear correlation between exposure time and sampled amount.

EXPERIMENTAL

The proposed samplers are made of 10 cm × 6 mm O.D. × 3.9 mm I.D. Pyrex glass tubes. With the aim of ensuring a precise sizing of the device, two porous glass septa with a porosity of 0 (160–250 μm), 2 mm in thickness, are fixed at both ends of the tube by steel springs. A diffusional path of 8 mm at the side used for passive sampling is obtained. The first 5 mm of the tube are filled with Carbopack C (Supelco), a low specific surface (area graphitized carbon black (8–10 m^2/g) with 20–40-mesh particle size, and the next 7 cm with Carbotrap (Supelco), a carbon with an average specific surface area of 80 m^2/g, also 20–40 mesh.

The choice of a 5-mm thickness for the first layer comes from our previous studies [4] in which it was shown that medium- and high-boiling compounds exhibit a low tendency to diffuse in the inner part of the packing, whereas low-boiling species quickly migrate in the back part of the tube. Positioning a reasonable amount of a stronger adsorbent in the second section is also important in order to prevent back-diffusion phenomena.

In order to evaluate the desorption efficiency, two sets of sampling tubes were prepared, the first consisting of fifteen tubes filled with two graphitized carbon blacks as described previously, and the second consisting of fifteen tubes filled with Carbotrap only. All the tubes were sampled by actively collecting a suitable air volume from an artificial atmosphere, generated by bubbling pure air in a very dilute solution of benzene, toluene and ethylbenzene in paraffin oil.

For the analyses we used a two-stage desorption apparatus consisting of a TDAS 5000 sequential desorber connected to an FMA 515 instrument for "focusing" (Carlo Erba, Milan, Italy). The conditions for the primary desorption were 20 ml/min of helium per 30 s after a 30-s pre-heating time, focusing at −150°C; the second stage desorption was carried out at 100°C with a gas flow of 10 ml/min on a Vocol column (60 m × 0.53 mm I.D.) (Supelco, Bellefonte, PA, U.S.A.). An HRGC 5300 MEGA gas chromatograph (Carlo Erba), a flame ionization detector and Hewlett-Packard HP 3396A integrator were also used.

In this trial, five temperatures were employed for the primary desorption, starting from 170 up to 290°C. At each temperature three devices from each kind of packing were used. Results obtained at the higher temperature were selected as a reference standard, by assuming that all the samples were quantitatively desorbed under these conditions.

For the measurements related to the validation of the passive sampling procedure and the evaluation of their behaviour in relation to different environmental conditions, a specially made sampling apparatus was used.

The apparatus used for exposing the samplers to the standard atmospheres (Fig. 1) is made of two coaxially joined tubes, one of diameter 3 cm and the other 9 cm. In each of these tubes there are 24 accesses for the samplers, separated into three groups of eight units, one at a 45° counter flow, one perpendicular to the air flow and one at a 135° angle. The samplers must be fixed at the access point by a series of washers and O-rings to prevent gas leaks. While the tubes are inserted in the apparatus, high-purity

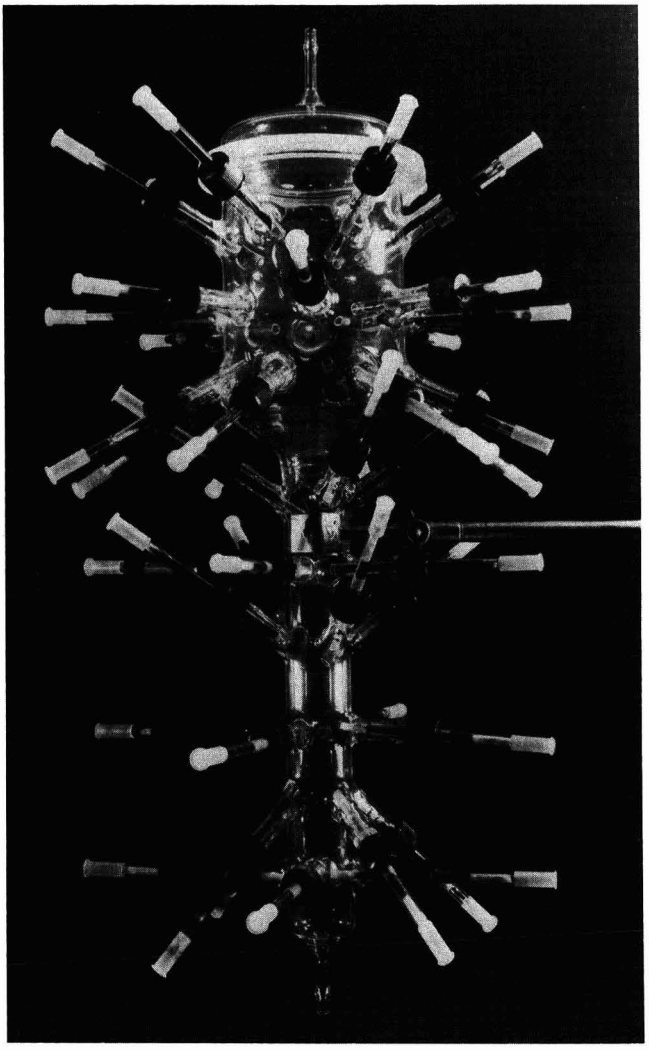

Fig. 1. Apparatus for passive sampling in standard dynamic atmospheres.

artificial air is passed through to ensure that at the beginning of the experiment all the equipment is unpolluted.

To obtain a dynamic atmosphere with the required constant organic contents, a specially prepared pneumatic circuit was constructed. The circuit consisted of three gas lines: the first was used for compressed air, cleaned by means of a active charcoal purifier, the second was connected to an air cylinder certified at a standard content of 100 ± 2 ppm benzene, which also served as a control mixture, and the third was connected to a bubbler filled with a dilute solution of toluene in paraffin with a slow flow of high-purity artificial air passing through. The three lines converged into a tiny mixing chamber. The mixture was then passed into a mechanical volumetric counter, connected to the sampling device by means of a short silicone-rubber tube.

Four devices were actively sampled in each passive sampling trial in order to check the average concentration during passive sampling and to verify if the uptake rate is constant in the experimental conditions selected.

For the analyses we used the previously described apparatus. The conditions employed for primary desorption were 20 ml/min of helium per 30 s with ballistic programming at 300°C, focusing at −150°C; the second-stage desorption was performed at 100°C with a gas flow of 10 ml/min.

A further comparison was carried out by sampling four passive devices and four active devices in the same indoor atmosphere.

RESULTS AND DISCUSSION

Desorption efficiency

In Table I the percentage recoveries of three aromatic compounds obtained with the double-layer samplers are compared with those obtained with samplers filled with Carbotrap only. The values reported for each temperature are the average of three runs for each kind of device. Samplers desorbed at 290°C have were taken as a standard reference, by assuming that at this temperature all the sampled amount is quantitatively desorbed. The results show that the same performance as for the traps filled with Carbotrap only can be achieved by the double-layer traps at a temperature about 50°C lower.

Passive sampling trials

Fig. 2 shows the results obtained for the desorption of passive samplers sampled for different times in a standard atmosphere containing 2 mg/m^3 of benzene. The values, obtained from eighteen samples, lie on straight line with a correlation coefficient of 0.98 and a standard error lower than 7%. The good linearity of the recovered amounts *versus* the exposure time agrees with a constant diffusive uptake rate in the investigated range.

Table II summarizes the conditions of concentration, flow-rate and sampling time for five sets of experiments carried out using the above-described apparatus. Concentration values averaged from the active samplings (not reported in Tables II and III) agree in all instances, witin the standard deviation, with the values obtained by calculations made on passive samplers. Stochastic analysis was performed on the data

TABLE I

RECOVERY OF SAMPLED AMOUNTS ON SINGLE- AND DOUBLE-LAYER SAMPLING DEVICES

Recovery on Carbotrap (%)			Desorption temperature (°C)	Recovery on Carbopack C + Carbotrap (%)		
Benzene	Toluene	Ethylbenzene		Benzene	Toluene	Ethylbenzene
80 ± 6	36 ± 4	17 ± 3	170	100 ± 7	70 ± 6	49 ± 5
100 ± 7	73 ± 7	42 ± 4	200	100 ± 7	100 ± 7	90 ± 6
100 ± 7	95 ± 7	76 ± 6	230	100 ± 7	100 ± 7	100 ± 7
100 ± 7	100 ± 7	100 ± 7	260	100 ± 7	100 ± 7	100 ± 7

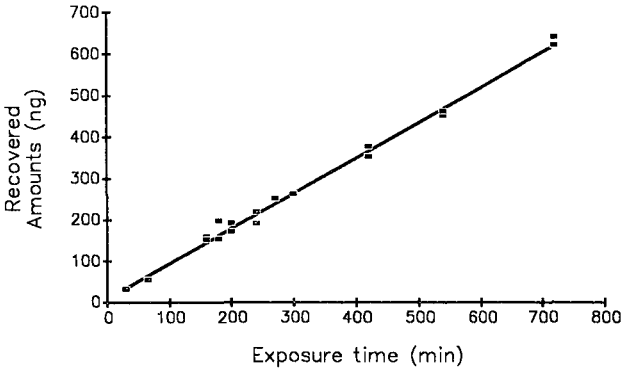

Fig. 2. Recovery of benzene on passive devices at different sampling times.

obtained under various conditions of wind velocity, sampler inclination and analyte concentration.

Table III contains the results obtained in the five tests reported in Table II. The comparison between the samplers kept at 45° and those kept at 135° to the air flow direction demonstrated an average random difference of less than 1%, which is insignificant. All of the values obtained from the angled tubes were therefore grouped and compared with those obtained from the tubes kept perpendicular to the air flow.

According to the literature [9,10], one might have expected a smaller sampling rate from the inclined than from the perpendicular tubes, in proportion to the projection of the orifice diameter on the flow direction and in inverse proportion to the linear velocity. The stochastic analysis of the considered samples, in which two substances were collected together, shows that under the experimental conditions examined there is no variation, as all the values coincide with an insignificant percentage difference. Also, no variation was observed on plotting the uptake rate as a function of the air velocity for values above 0.1 cm/s. Below this value an influence of air speed can be hypothesized, but it is of no interest in practical terms. This observation agrees with experiments already performed [2,3,6] on tube-type samplers characterized by a small sampling surface; this indicates that the influence of air speed decreases with a reduction in diameter.

TABLE II

OPERATING CONDITIONS IN THE SAMPLING RUNS

Test No.	Flow-rate (l/min)	v_1[a] (cm/s)	v_2[b] (cm/s)	Total average benzene concentration (mg/m^3)	Total average toluene concentration (mg/m^3)	Sampling time (min)
1	0.54	0.14	1.27	10.55	1.00	130
2	0.90	0.24	2.12	1.47	0.31	840
3	3.99	1.05	9.41	0.49	0.42	136
4	6.00	1.57	14.1	3.46	2.70	780
5	10.0	2.62	23.58	10.18	4.55	100

[a] Wind velocity through the wide tube of the sampling apparatus.
[b] Wind velocity through the narrow tube of the sampling apparatus.

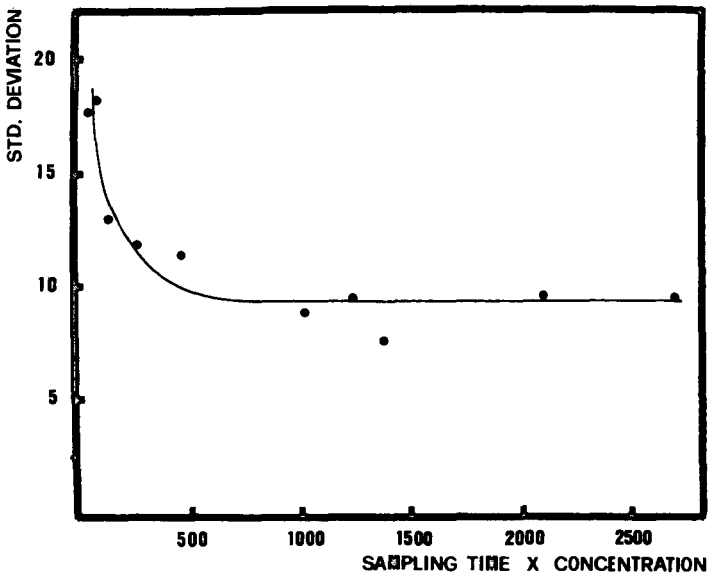

Fig. 3. Plot of percentage standard error *vs.* sampled amounts.

In Fig. 3 the product of time and concentration is plotted *versus* the percentage standard deviation. The measurement error seems to be strictly correlated with the sampled amount, and is probably a pure analytical error. When more than 200 ng are sampled, the total error is lower than 10%, whereas when sampling less than 10 ng there is a tendency toward an error of more than 20%. Evidently, when the trapped amount is below certain values the percentage influence of any type of interference is enhanced: microlosses in the desorption system, solvent residues in the sampler before use and random distribution of high-energy active sites in the trap, in the lines and in the column, which can obstruct the desorption of favour memory effects.

Fig. 4 shows a comparison between two chromatograms obtained by active and passive sampling in indoor trials in which eight samplers were used. All devices were sampled at the same time, starting at 0.8:00 p.m. and ending at 08:30 a.m. the following day, in the living room of a non-smokers' house.

The average concentration of total hydrocarbons calculated from the active samplers was 0.24 mg/m^3 (expressed as benzene) with a multiplicity of about 60 compounds. For the passive samplers, an accurate quantitative calculation of the ambient concentration requires the identification of each species and a knowledge of its diffusion coefficient. In the presence of many unidentified compounds, the uptake rate was calculated by averaging the diffusion coefficients of the identified main components. The approximate calculated value is 0.39 ml/min; a total hydrocarbon concentration of 0.21 mg/m^3 can thus be calculated, which agrees with the results obtained from the active samplers. The same multiplicity is also found.

The use of the porous glass septum for maintaining the adsorbent phase *in situ* provides various advantages: absence of dust particles in the desorption lines, mechanical stability during the sampling and desorption and easy positioning within the Pyrex tube. Disadvantages include the fact that this system constitutes a resistance

TABLE III

INFLUENCE OF WIND VELOCITY AND DEVICE SLOPE ON PASSIVE SAMPLING RATE

Test No.	Benzene concentration (mg/m^3)					Toluene concentration (mg/m^3)				
	v_1[a]	v_2[a]	Average	45° and 135° slope	90° slope	v_1[a]	v_2[a]	Average	45° and 135° slope	90° slope
1	10.36±0.63	10.73±0.75	10.55±0.69	10.52±0.56	10.59±0.86	0.94±0.15	1.06±0.10	1.00±0.13	0.996±0.14	1.00±0.15
2	1.49±0.14	1.46±0.14	1.47±0.14	1.47±0.15	1.47±0.13	0.32±0.04	0.30±0.03	0.31±0.03	0.31±0.03	0.31±0.04
3	0.51±0.08	0.46±0.09	0.49±0.09	0.50±0.08	0.47±0.11	0.46±0.09	0.37±0.05	0.4±0.07	0.44±0.09	0.39±0.07
4	3.42±0.34	3.51±0.33	3.46±0.33	3.46±0.37	3.46±0.25	2.63±0.27	2.78±0.25	2.70±0.26	2.71±0.28	2.68±0.25
5	10.32±0.95	10.03±0.84	10.18±0.90	10.36±0.85	10.03±0.93	4.77±0.59	4.33±0.46	4.55±0.53	4.57±0.46	4.53±0.66

[a] See Table II.

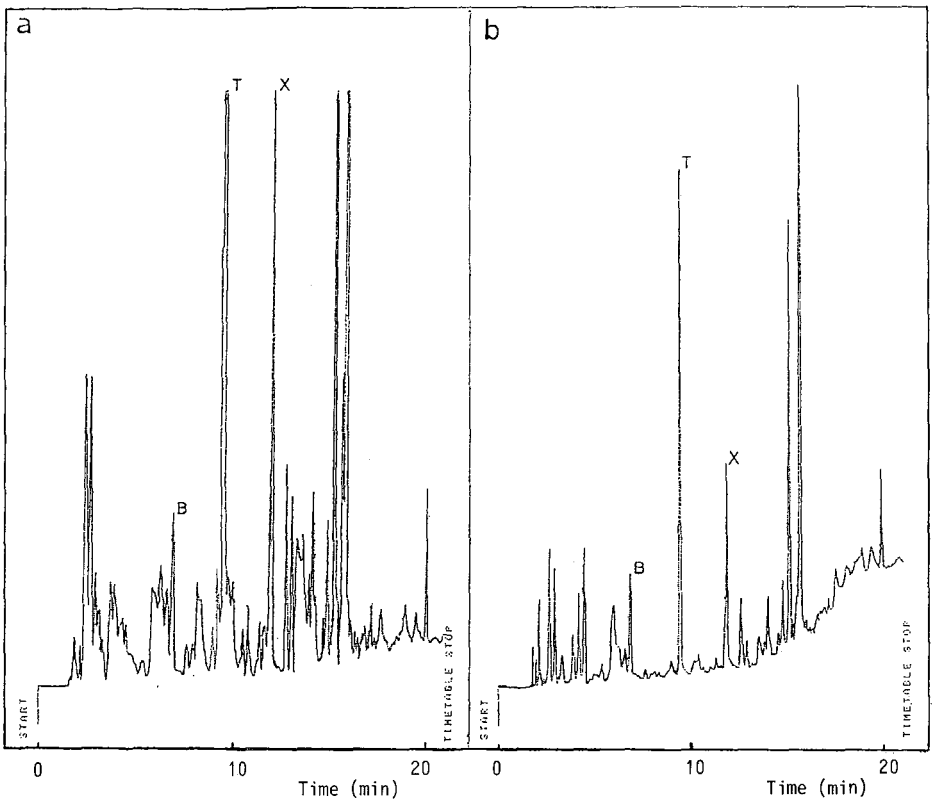

Fig. 4. "Fingerprint" or organics sampled in a domestic living room. (a) Active sampling; (b) passive sampling. B = Benzene; T = toluene; X = xylene.

to the mass transfer. On the basis of the experimental data (see theory) a calculation was made, giving an equivalent sampling rate equal to 0.452 ml/min for benzene, with this value also being confirmed by indoor trial data. Without the septum the theoretical rate should be 0.835 ml/min. The resulting K value is 0.54, which is acceptable because even if the theoretical rate is halved, the order of magnitude of the determinable amounts (about 1 $\mu g/m^3$ in 10 h of sampling) does not substantially change.

CONCLUSIONS

This series of experiments adds to the knowledge already acquired on this subject. The variations proposed in the construction of the sampler facilitate the standardization of the production process and improve the adsorption and desorption characteristics. The tests demonstrated that the devices are versatile, accurate and precise, beyond the levels normally accepted in this types of determination. The large amount of data obtained at low concentration levels indicates that passive sampling can be used efficiently not only at industrial sites but also for the determination of organic vapours in homes, offices, schools and for indoor pollution in general.

REFERENCES

1 D. T. Coker, in *Publication No. 10555 EN of the Commission of the European Communities,* ECSC–EEC–EAEC, Brussels, Luxembourg, 1987, pp. 46–51.
2 G. Moore, in *Publication No. 10555 EN of the Commission of the European Communities,* ECSC–EEC–EAEC, Brussels, Luxembourg, 1987, pp. 1–13.
3 G. Bertoni, C. Perrino and A. Liberti, *Anal. Lett.*, 15(A12) (1982) 1039–1050.
4 G. Bertoni, C. Perrino, R. Fratarcangeli and A. Liberti, *Anal. Lett.*, 18(A4) (1985) 429–438.
5 G. Bertoni, R. Fratarcangeli, A. Liberti and M. Rotatori, in *Publication No. 10555 EN of the Commission of the European Communities*, ECSC–EEC–EAEC, Brussels, Luxembourg, 1987, pp. 63–66.
6 R. H. Brown, R. P. Harvey, C. J. Purnell and K. J. Saunders, *Am. Ind. Hyg. Assoc. J.*, 45, No. 2 (1984) 67–75.
7 J. G. Firth, in *Publication No. 10555 EN of the Commission of the European Communities*, ECSC–EEC–EAEC, Brussels, Luxembourg, 1987, pp. 177–184.
8 R. H. Brown, in *Publication No. 10555 EN of the Commission of the European Communities*, ECSC–EEC–EAEC, Brussels, Luxembourg, 1987, pp. 185–189.
9 P. Ciccioli, G. Bertoni, E. Brancaleoni, R. Fratarcangeli and F. Bruner, *J. Chromatogr.*, 126 (1976) 757–770.
10 G. Bertoni, F. Bruner, A. Liberti and C. Perrino, *J. Chromatogr.*, 203 (1981) 263–270.
11 F. Mangani, A. R. Mastrogiacomo and O. Marras, *Chromatographia,* 15 (1982) 712.
12 R. H. Paunwitz, in *Publication No. 10555 EN of the Commission of the European Communities*, ECSC–EEC–EAEC, Brussels, Luxembourg, 1987, pp. 157–162.
13 M. Zurlo and F. Andreoletti, in *Publication No. 10555 EN of the Commission of the European Communities*, ECSC–EEC–EAEC, Brussels, Luxembourg, 1987, pp. 174–176.

Journal of Chromatography, 522 (1990) 295–302
Elsevier Science Publishers B.V., Amsterdam

CHROM. 22 770

Gas chromatography–mass spectrometry of conjugated dienes by derivatization with 4-methyl-1,2,4-triazoline-3,5-dione

DAVID C. YOUNG and PAUL VOUROS*
Department of Chemistry and Barnett Institute of Chemical Analysis, Northeastern University, Boston, MA 02115 (U.S.A.)
and
MICHAEL F. HOLICK
Vitamin D Laboratory, Boston University School of Medicine, 80 East Concord St., Boston, MA 02118 (U.S.A.)
(First received April 6th, 1990; revised manuscript received August 8th, 1990)

ABSTRACT

The dienophile 4-methyl-1,2,4-triazoline-3,5-dione forms stable adducts with conjugated dienes by generating Diels–Alder cycloaddition products. The reaction is rapid, highly selective for conjugated dienes and the derivatives are suitable for analysis by gas chromatography. Their mass spectra are marked by their simplicity and by the presence of abundant fragment ions diagnostic of the diene position in the parent compound.

INTRODUCTION

A wide variety of naturally occurring organic compounds bearing a long carbon chain contains one or more sites of unsaturation. Definition of the position of unsaturation by mass spectrometry has normally involved a chemical modification of the double bond in order to overcome the problems presented by the randomization of the π-system upon ionization [1]. For example, when using chemical ionization mass spectrometry (CI-MS), the double bond may be localized by reaction with iron ions and the subsequent collisional activation leads to fragment ions diagnostic of the double bond position [2]. Other CI reagents that interact specifically with double bonds include methyl vinyl ether [3], and $Ar–O_3–H_2O$ mixtures [4]. Methods involving electron impact ionization require the formation of derivatives which direct the fragmentation of the molecule about the carbons associated with the original double bond. A classical example is the conversion of the alkene to a glycol followed by formation of a trimethylsilyl ether [5] or isopropylidene [6] derivative.

Conjugated dienes, which are important in certain insects as pheromones, semiochemicals or sex attractants [7–9], require alternative approaches. We recently

0021-9673/90/$03.50

reported on the use of the electrophilic reagent, 4-phenyl-1,2,4-triazoline-3,5-dione (PTAD), as a selective derivatizing reagent for conjugated dienes [10]. The reagent forms Diels–Alder adducts which exhibit prominent molecular ion peaks and characteristic fragment ions which are diagnostic of the position of the conjugated diene on the chain. The PTAD adducts of conjugated dienes were characterized by a high thermal stability. However, their low volatility limits their general applicability for gas chromatography (GC)–MS analysis. We report here on the preparation and utilization of 4-methyl-1,2,4-triazoline-3,5-dione (MTAD), as a derivatizing reagent for conjugated dienes. In addition to displaying structurally informative mass spectra the MTAD adducts appear to be very well suited for analysis by GC–MS as illustrated by their relatively low Kováts indices and good thermal stability.

EXPERIMENTAL

Synthesis of 4-methyl-1,2,4-triazoline-3,5-dione

The procedure for the synthesis of MTAD was based on the method of Cookson et al. [11] for the preparation of PTAD, with the exception that N_2O_4 instead of *tert.*-butyl hypochlorite was used for oxidation of the corresponding urazole. Milligram quantitities of 4-methylurazole (Aldrich, U.S.A.), were placed in the bottom of a Pyrex culture tube, 1.5 ml methylene chloride was then added and the mixture placed in an ice bath. N_2O_4 was gently blown into the tube until the reddish-brown color of NO_2 was seen to fill the tube. The tube was then capped and shaken until the color in the gas phase was observed to go mostly into solution. The red MTAD color develops in minutes and the reaction is complete when all the urazole is seen to go into solution. (A second portion of N_2O_4 may be necessary to effect the dissolution of larger amounts of urazole). After generating the MTAD, the culture tube was transferred to a bath of warm water and the solution evaporated nearly to dryness with a stream of nitrogen in order to eliminate excess N_2O_4.

Preparation of derivatives of conjugated dienes

MTAD adducts of conjugated dienes were prepared as described previously for the PTAD adducts [9]. Quantities in the range of 500 ng to 1 μg were used to generate the data described in this report. The reaction is nearly instantaneous and occurs at room temperature.

Instrumentation

GC–MS analyses were performed on a JEOL DX303HF double-focusing mass spectrometer equipped with a modified Hewlett-Packard gas chromatograph and a JEOL DA5000 data system run by a Digital PDP 11/73 minicomputer. GC injections were made using the split injection mode. The filament and accelerating potential were turned off for 4 min after the injection to protect the mass spectrometer. The injector was set at 300°C and the initial column temperature was 100°C. After 2 min the column was ramped at 15°C/min to 280°C. A 60-m SE-52 capillary column and an alkane mixture of C_{14}, C_{18}, C_{24} and C_{28} were used to assign retention indices.

RESULTS AND DISCUSSION

Fig. 1 shows the Diels–Alder cycloaddition reaction of MTAD with a conjugated diene. Adducts were formed between MTAD and the dienes shown on Table I which summarizes the Kováts retention indices for the test compounds. By comparison to the corresponding PTAD analogues, the MTAD adducts exhibit a dramatic improvement in volatility. For example, the PTAD adducts of 2*E*,4*Z*-hexadiene and of 9*Z*,11*E*-tetradecadienyl acetate were found to have retention indices

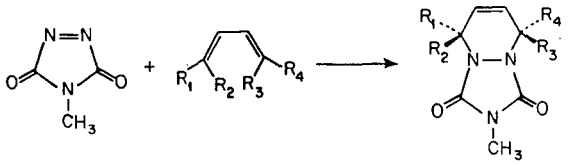

Fig. 1. Cycloaddition reaction of MTAD with a conjugated diene.

of 2210 and 3400, respectively. These compare to values of 1580 and 2750 for the corresponding MTAD derivatives. The chromatographic peak shapes of the MTAD derivatives were comparable to those of the hydrocarbons used for the Kováts index calibrations. Fig. 2A shows a total ion chromatogram of three conjugated diene adducts. An expanded display of the segment encompassing the elution of C_{14} through C_{18} allows a better comparison of the chromatographic behavior of the MTAD adducts with that of the non-polar alkanes.

The MS of the MTAD adducts is fundamentally equivalent to that of the PTAD analogues. The spectra are both simple and easy to interpret. They exhibit well defined molecular ion peaks as well as abundant fragment ions which result from loss of an alkyl side chain and which are diagnostic of the diene position in the hydrocarbon chain. The latter, generally, give rise to the base peak, $[M-R]^+$ and/or $[M-R']^+$, depending on the number of alkyl substituents. This fragmentation is clearly alpha to the nitrogen, typical of the spectra of simple alkyl amines (Fig. 3). A second major fragmentation frequently observed is the loss of methyl isocyanate from the $[M-R]^+$ ions (Fig. 4). This loss is probably favored because of further extension of the

TABLE I

RETENTION INDICES OF THE MTAD DERIVATIVES OF SELECTED CONJUGATED DIENES

Compound		Kováts index
No.	Name	
I	2*E*,4*E*-Hexadiene	1580
II	2*E*,4*Z*-Hexadiene	1580
III	1,3-Hexadiene	1680
IV	7*E*,9*Z*-Dodecadien-1-yl acetate	2530
V	8*E*,10*E*-Dodecadien-1-yl acetate	2560
VI	9*Z*,11*E*-Tetradecadien-1-yl acetate	2750

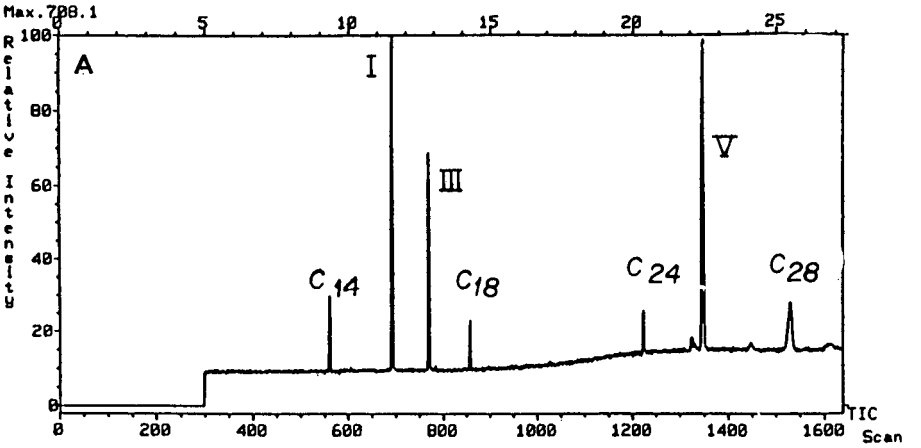

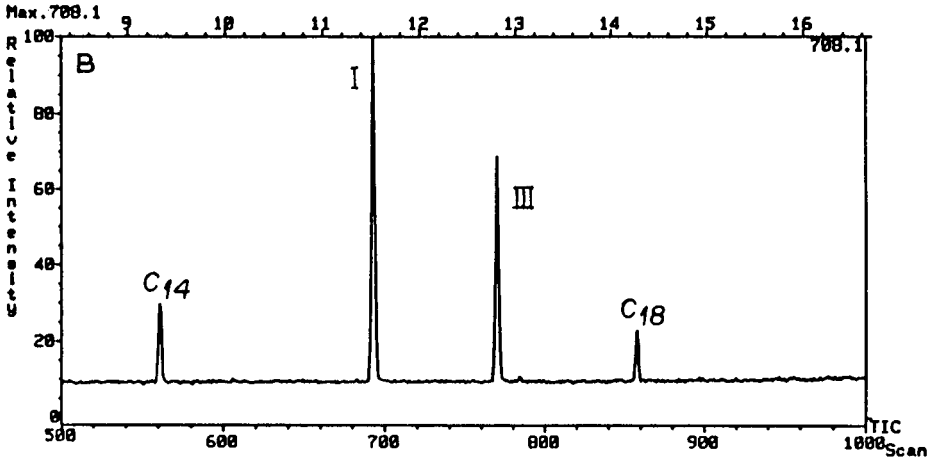

Fig. 2. (A) GC–MS total ion chromatogram of MTAD adducts of 2*E*,4*E*-hexadiene (I), 1,3-hexadiene (III) and 8*E*,10*E*-dodecadien-1-yl-acetate (V), along with indicated alkanes. (b) Expanded segment of C_{14} through C_{18} of Fig. 2A.

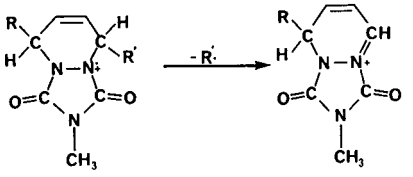

Fig. 3. Probable mechanism for the initial loss of side chain from MTAD–conjugated diene adducts.

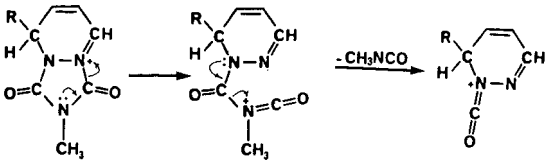

Fig. 4. Mechanism for the loss of methyl isocyanate after formation of the intermediate shown in Fig. 3.

conjugation as well as relief of the potential for instability caused by having the positive iminium center next to a carbonyl carbon in its $[M-R]^+$ precursor.

The mass spectra of three isomeric hexadiene derivatives are compared in Fig. 5. While MTAD adduct formation cannot distinguish between geometric isomers —compare spectra in Figs. 5A and B— positional identification of the conjugated alkenes is readily accomplished, as illustrated from the spectrum in Figs. 5C. The mass spectra of two isomeric dodecadienyl acetates are further compared in Figs. 6A and B. Again, a well defined loss of the side chain in both spectra helps identify the diene positions. The mass spectrum of a tetradecadienyl analogue of the latter two compounds is also shown in Fig. 6, to illustrate the general applicability of the derivatives.

In summary, the mass spectrometry of the MTAD derivatives of conjugated dienes is clearly dominated by the heterocyclic nucleus of the 1,2,4-triazoline-3,5-dione system. The relatively simple spectra resulting from these large, but symmetrical, compounds could probably not be duplicated by another type of derivative and, thus the possibility of error in their structural assignment is minimized. Spectral interpretation is straightforward. All that is necessary is to look for a pair of ions separated by the mass of methyl isocyanate (57 u) and subtract the higher mass ion from the molecular ion in order to determine the mass of one of the groups that was attached to the original conjugated diene. The fact that reaction of MTAD with a conjugated diene results in the formation of only one detectable product in all the cases examined, is ideal behavior for a derivative. Derivatization with 4-methyl-1,2,4-triazoline-3,5-dione should provide a method of choice for the GC–MS analysis of conjugated aliphatic dienes.

ACKNOWLEDGEMENTS

Financial support for this work from the National Science Foundation, Grant No. DCB8545666 (MFH) and the USPHS, Biomedical Support Grant, RR07143 (PV) is gratefully acknowledged. This is contribution No. 428 from the Barnett Institute.

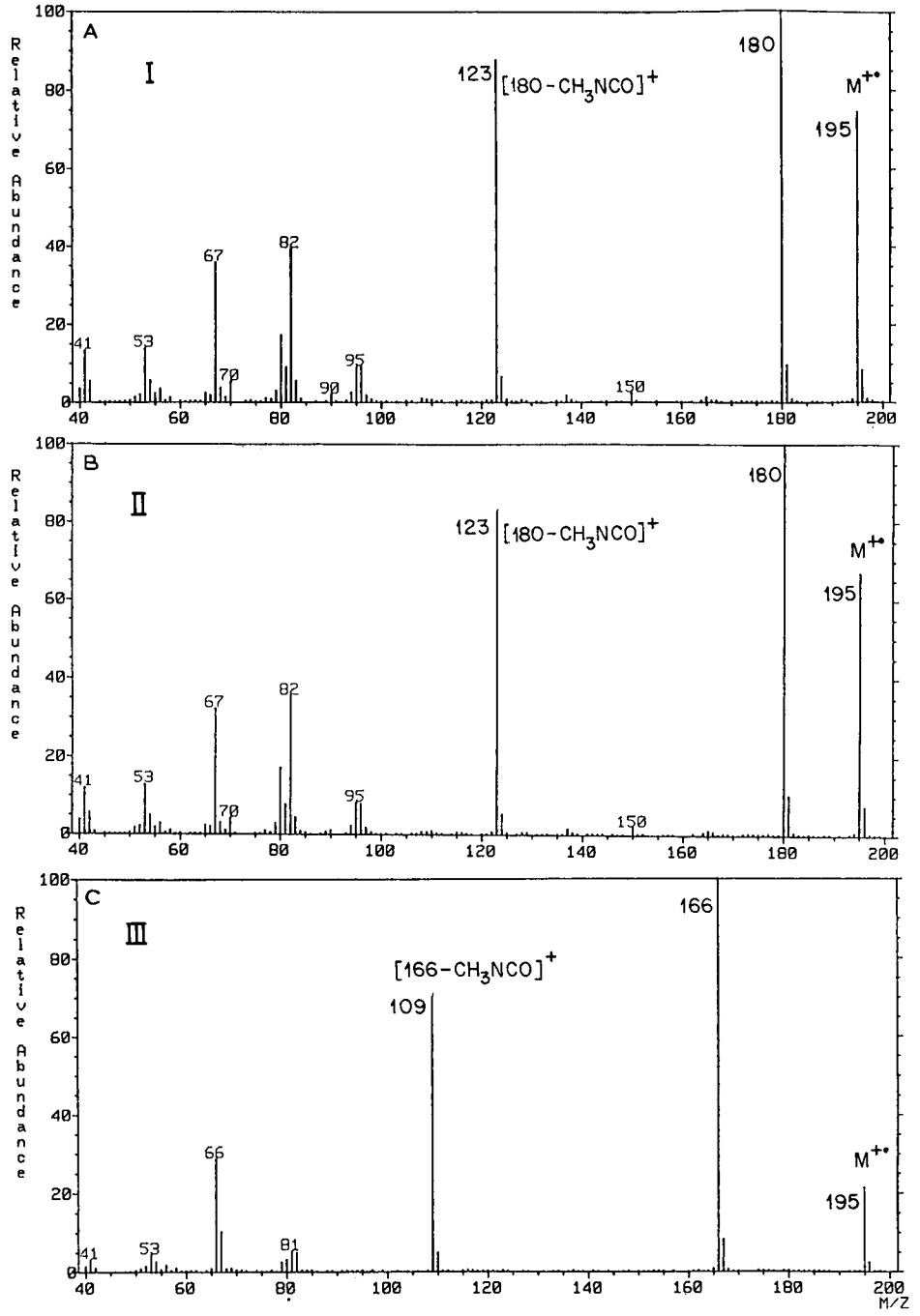

Fig. 5. Electron impact mass spectra of MTAD derivatives of (A) 2*E*,4*E*-hexadiene. (I); (B) 2*E*,4*Z*-hexadiene (II); and (C) 1,3-hexadiene (III).

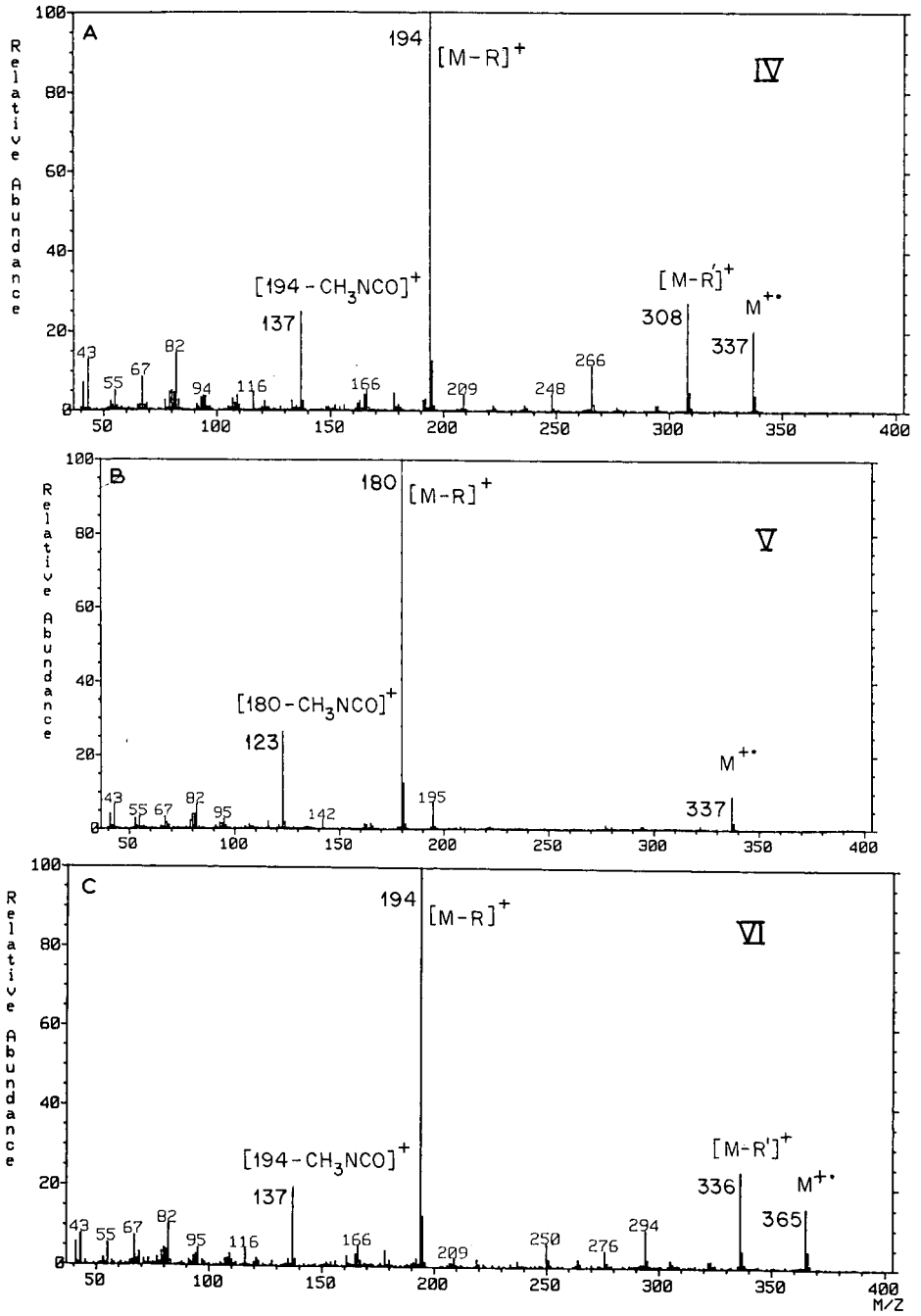

Fig. 6. (A) Electron impact mass spectra of MTAD derivatives of (A) 8*E*,10*E*-dodecadien-1-yl acetate (IV); (B) 7*E*,9*Z*-dodecadien-1-yl acetate (V); and (C) 9*Z*,11*E*-tetradecadien-1-yl acetate. (VI).

REFERENCES

1 K. Biemann, *Mass Spectrometry: Organic Chemical Applications*, McGraw-Hill, New York, 1962, p. 83.
2 D. A. Peake and M. L. Gross, *Anal. Chem.*, 57 (1985) 115–120.
3 R. Chai and A. G. Harisson, *Anal. Chem.*, 53 (1981) 34–37.
4 D. F. Hunt, W. F. Crow and T. M. Harvey, *Proceedings of 23rd Annual Conference on Mass Spectrometry and Allied Topics, Houston, TX, May 25–30, 1975*, ASMS, pp. 568–570.
5 P. Capella and C. M. Zorzut, *Anal. Chem.*, 40 (1968) 1458–1463.
6 R. E. Wolff, G. Wolff and J. A. McCloskey, *Tetrahedron*, 22 (1966) 3093–3101.
7 R. E. Doolittle, W. L. Roelofs, J. D. Solomon, R. T. Carde and M. J. Beroza, *J. Chem. Ecol.*, 2 (1976) 399–410.
8 D. R. Hall, P. S. Beevor, R. Lester and B. F. Nesbitt, *Experientia*, 36 (1980) 152–154.
9 H. G. Davis, L. M. McDonough, A. K. Burditt and B. A. Bieri-Leonhardt, *J. Chem. Ecol.*, 57 (1984) 115–120.
10 D. C. Young, P. Vouros, B. Decosta and M. F. Holick, *Anal. Chem.*, 59 (1987) 1954–1957.
11 R. C. Cookson, S. S. H. Gilani and I. D. R. Stevens, *J. Chem. Soc. C*, (1967) 1906–1909.

Journal of Chromatography, 522 (1990) 303–313
Elsevier Science Publishers B.V., Amsterdam

CHROM. 22 779

Application of multidimensional gas chromatography–mass spectrometry to the determination of glycol ethers in air

EUGENE R. KENNEDY* and PAULA F. O'CONNOR

Inorganic Methods Development Section, Methods Research Branch, Division of Physical Sciences and Engineering, National Institute for Occupational Safety and Health, 4676 Columbia Parkway, Cincinnati, OH 45226 (U.S.A.)

and

ARDITH A. GROTE

Measurements Development Section, Measurements Research Support Branch, Division of Physical Sciences and Engineering, National Institute for Occupational Safety and Health, 4676 Columbia Parkway, Cincinnati, OH 45226 (U.S.A.)

(First received April 25th, 1990; revised manuscript received August 29th, 1990)

ABSTRACT

The applicability of multidimensional gas chromatography–mass spectrometry to the analysis of five glycol ethers in air was demonstrated. Air samples were collected on charcoal tubes and desorbed with 5% methanol in methylene chloride as is described in method 1403 of the National Institute for Occupational Safety and Health Manual of Analytical Methods. The glycol ethers were determined by multidimensional gas chromatography–mass spectrometry. The limit of detection was 5 to 7 μg/sample for each compound.

INTRODUCTION

The analytical technique of multidimensional gas chromatography (MDGC) has been applied successfully to a number of complex analytical separations, such as soil fumigants [1], hydrocarbons and inert gases [2], polynuclear aromatic compounds in crude oil [3], alcohols in gasoline [4] and dibenzodioxins and dibenzofurans [5]. The increased resolving power of this analytical technique over single-column analyses lies in the ability to combine the selectivity of two or more columns with different liquid phases into a unified analysis scheme for improved chromatographic resolution. The inclusion of a mass spectrometer as a chromatographic detector further improves the specificity of the analysis [6].

Because one of the major problems encountered in the chromatographic analysis of industrial hygiene samples is the presence of interfering compounds, additional method development is needed to solve this problem. With the increased resolving power available though the technique of MDGC, the time required to address interference problems is greatly reduced. The overall goal of our research was to apply the analytical technique of MDGC to industrial hygiene sampling and analytical methods for glycol ethers.

The problem addressed in this research was the simultaneous determination of multiple glycol ethers in air samples containing hydrocarbons and other organic compounds. Other researchers have successfully applied the technique of MDGC to the determination of diethylene glycol monoethyl ether [2-(2-ethoxyethoxy)ethanol] in flavor extracts [7].

Concern about occupational exposure to glycol ethers in general has arisen due to reports of adverse reproductive effects [8] of 2-methoxyethanol, 2-ethoxyethanol and related compounds. In light of this concern, industrial hygienists at the National Institute for Occupational Safety and Health (NIOSH) have initiated workplace studies of potential occupational exposure to glycol ethers and related compounds. During one study, air samples were collected on charcoal tubes at a newspaper printing facility in which glycol ether-based fountain and cleaning solutions were used in conjunction with mineral spirits. This report details the method development work and subsequent analysis of these samples for selected glycol ethers using MDGC with mass spectrometric (MS) detection in this sample matrix.

EXPERIMENTAL

Analysis work was performed on a Hewlett-Packard Model 5890 gas chromatograph equipped with two split/splitless capillary injectors, one flame ionization detection (FID) system, a Hewlett-Packard Model 5971 mass selective detector, a Valco 10-port high-temperature (polyimide rotor seal) sampling valve (Hewlett-Packard Part No. 18900C-432) with 1/16-in. fittings (1.6 mm) contained in a separate heated compartment (240°C) above the gas chromatograph column oven, and a Hewlett-Packard Model 7673A autosampler.

Data reduction and system control for MDGC–MS were accomplished with a Hewlett-Packard Model 59970C ChemStation equipped with 2 Mbyte of random access memory, a color video monitor, 40 Mbyte disk drive for on-line storage of data and an additional 80 Mbyte disk drive along with Revision 3.2 mass selective detector operating system (Pascal) software.

A Hewlett-Packard Model 5890 gas chromatograph without multidimensional capability and equipped with a Hewlett-Packard Model 5970 mass selective detector was used for the bulk sample analyses.

The Valco valve actuator in the MDGC system was rewired to allow automated control of the valve from the software in the ChemStation computer. The Valco valve was configurated for "heart-cutting" [9] from the first column onto the second analytical column, as shown in Fig. 1. To facilitate changing the columns, pieces of blank 0.2 mm I.D. fused-silica tubing (Scientific Glass Engineering, Austin, TX, U.S.A.) were routed from the valve ports 1, 2, 3 and 4 into the gas chromatograph oven and column connections were made with 1/16-in. (1.6 mm) zero-dead-volune unions (Supelco, Bellefonte, PA, U.S.A.). The connections of the fused-silica tubing to the valve were made using a fused-silica adapter for 1/16-in fittings (part No. FS1R.5) obtained from Anspec (Ann Arbor, MI, U.S.A.). The blank fused-silica tubing connected to port 4 was inserted into injector "B", which was a source of carrier gas for the second column when the valve was in the "OFF" position. A 1.25-m piece of blank fused-silica tubing connected port 3 (see Fig. 1) to the FID system and acted as a restrictor so the flow in column 2 would not change appreciably during valve

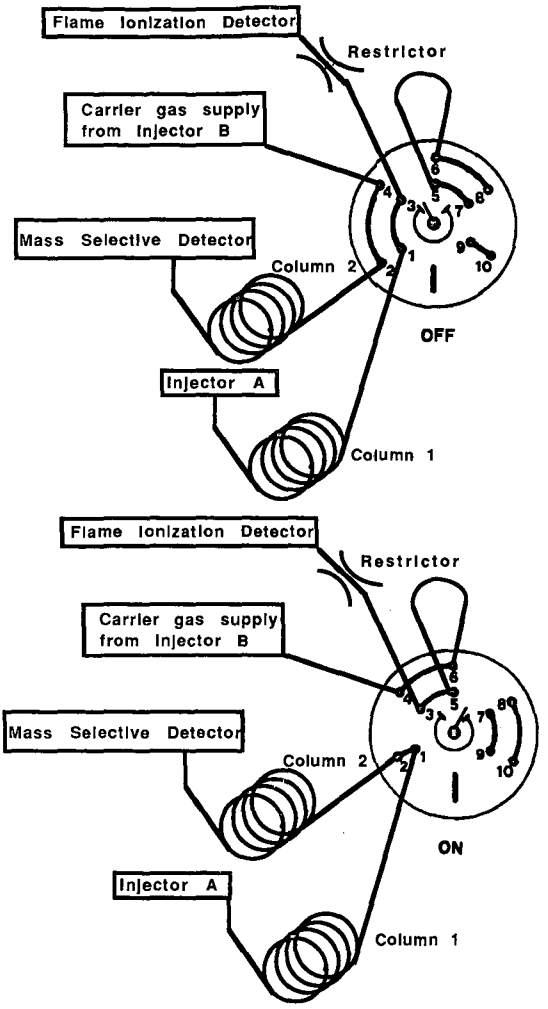

Fig. 1. Schematic diagram of the valve-based multidimensional gas chromatograph–mass spectrometer system used for the analyte of glycol ether-containing samples. (Top) Illustration of the valve in the off position. (Bottom) Illustration of the valve in the on position when a heartcut is being made.

switching operations [10]. Ports 5 and 6 were connected by a short length of 1/16-in. stainless-steel tubing and associated fittings. Ports 7, 8, 9 and 10 were plugged and not used.

The column flow balancing procedure involved opening and closing the Valco valve at 3-min intervals and lowering the head pressure on column 2 (controlled by injector "B" head pressure regulator) by 7 kPa (1 p.s.i.) before each closing. The chromatographic baseline was monitored by the mass selective detector to determine when baseline disturbance was at a minimum during valve switching operations. Optimal column head pressure on column 2 was 35 kPa (5 p.s.i.). Column head pressure on column 1 was maintained at 115 kPa (17 p.s.i.).

During the course of the experimental work, peak tailing of the solvent (5% methanol in methylene chloride) as it passed through the valve was observed with FID. This problem was due primarily to polar solvent (methanol) interaction with the valve assembly as the solvent passed through, since tailing was greatly reduced when solutions containing the glycol ethers in only methylene chloride were analyzed or when column 1 was connected directly to the FID system. To reduce any peak tailing due to interaction with active sites in the valve transfer lines, the blank fused-silica tubing was replaced with lengths of phenyl-methyl silicone deactivated uncoated fused-silica tubing (Anspec).

The chromatographic columns used were as follows: column 1: 30 m × 0.25 mm I.D. fused-silica capillary DB-1, 1.0-μm film (J & W Scientific, Folsom, CA, U.S.A.); column 2: 30 m × 0.25 mm I.D. fused-silica capillary DB-WAX, 0.5-μm film (J & W Scientific). The oven temperature program used for MDGC–MS analysis of the glycol ether samples was 40°C initial temperature, 30°C/min for 1 min, 15°C/min to 180°C, and hold for 16.7 min. The temperature program used for the bulk sample analyses was 35°C for 2 min, 15°C/min to 300°C, and hold for 5.4 min. A 30 m × 0.25 mm I.D. fused-silica capillary DB-1, 1.0-μm film (J & W Scientific) column was also used for the analysis of the bulk sample on the Hewlett-Packard Model 5890 gas chromatograph–Model 5970 mass selective detector.

Toluene, methanol and methylene chloride were obtained from Burdick & Jackson Labs. (Muskegon, MI, U.S.A.). Bulk samples of 1-butoxy-2-propanol and 1-(2-butoxyethoxy)-2-propanol were obtained from Elfco (West Warwick, RI, U.S.A.). 2-Butoxyethanol (butyl cellosolve), dipropylene glycol methyl ether (4 isomers) and 2-(2-butoxyethoxy)ethanol (butyl carbitol) were obtained from Chem Services (West Chester, PA, U.S.A.). Five bulk samples of solutions used at the printing plant were obtained and labeled A–E. Since some of these solutions contained large amounts of water, they were prepared for qualitative analysis by addition of 10 μl of the bulk solution to 1 ml of methylene chloride. The resulting methylene chloride solutions were analyzed by GC–MS to determine composition.

Charcoal tubes (100 mg front section; 50 mg backup section) used for the collection of the glycol ether samples were obtained from SKC (Eighty Four, PA, U.S.A.). Samples for glycol ethers were collected at 50 to 100 ml/min for 4 to 6 h using SKC Model 222 sampling pumps. Front and back sections of the charcoal tube samples were transferred individually to 2-ml vials and desorbed with 1 ml of 5% methanol in methylene chloride for 30 min [11]. Glycol ethers were determined by autosampler injection (1 μl injection, splitless mode) into the MDGC–MS system.

Desorption efficiency of the glycol ethers was determined by fortification of blank charcoal tubes with aliquots of solutions containing the four analytes of interest. The desorption spikes were done using three tubes at three levels. These fortified tubes were analyzed as described above.

RESULTS

Bulk samples

A set of five bulk samples and nine charcoal tube samples collected at a newspaper printing plant was submitted for the determination of glycol ethers during the course of an investigation by NIOSH industrial hygienists. The solutions

comprising the bulk samples were used in the offset printing process and in cleaning the printing plates and contained glycol ethers, kerosene and other organic compounds. GC–MS analysis of bulk sample A identified aliphatic hydrocarbons, pine oil and surfactants. The material safety data sheet indicated that bulk sample B contained only 1-butoxy-2-propanol, but mass spectral analysis also identified 1-(2-butoxyethoxy)-2-propanol, 2-butoxyethanol and other impurities. Bulk sample C was found to contain aliphatic hydrocarbons (a lighter fraction of naphthas than kerosene) and 2-(2-butoxyethoxy)ethanol. Bulk sample D contained dipropylene glycol methyl ether (four isomers). Bulk sample E contained a series of hydrocarbons which was indicative of kerosene. All of the components contained in the bulk samples were present potentially in the air samples. The analysis of the bulk samples also showed that the hydrocarbons would co-elute with glycol ethers using single column analysis, so quantitation of the glycol ethers was attempted by MDGC–MS.

Air samples

This preliminary analysis of these bulk samples indicated that the increased resolution offered by the "heart-cutting" approach would be needed for the analysis of air samples. The identification of compounds present in air samples would be quite difficult due to the large number of compounds present together in each sample, the similarity of mass spectra for glycol ethers and hydrocarbons, and the lack of parent ions for the glycol ethers due to the presence of the hydroxyl group [12]. The possibility also existed that two or more compounds would co-elute at the same retention time on a single analytical column. This possible co-elution of hydrocarbons and glycol ethers in the analysis of air samples was illustrated by the FID chromatograms shown in Fig. 2. The peaks which are due to the glycol ethers are lost in the large number of peaks, primarily due to the hydrocarbons present in the air sample. The technique of MDGC, using "heart-cutting", seemed particularly well suited for the analysis of these air samples, since small segments of the chromatographic effluent of the first column containing the glycol ethers could be directed to a second column of different polarity for further resolution.

For MDGC analysis, the gas chromatograph was configured as shown in Fig. 1, with column 2 connected directly to the mass selective detector. Column 2 was heated to a maximum temperature of 180°C. Above this temperature, there was an excessive amount of column bleed, which had mass spectral fragments similar to the glycol ethers being determined by the mass selective detector. The rationale for the column placement order in the multidimensional analysis system was that the injection onto the non-polar column (column 1, DB-1) would provide an initial separation of polar and non-polar components. Portions of the column 1 effluent containing the glycol ethers could then be directed via the valve to a more polar column (column 2, DB-WAX) which would further resolve the individual glycol ethers. The hydrocarbons which co-eluted with the glycol ethers on the non-polar column were sufficiently separated from the ethers on the polar column to allow baseline resolution in most cases.

Based on the preliminary analysis of the glycol ether standards, two or three "heartcuts" from a sample would be necessary to keep large amounts of the hydrocarbons, present on the air samples, from being "cut" onto the second column. The analysis method was constructed by chromatography of the individual glycol

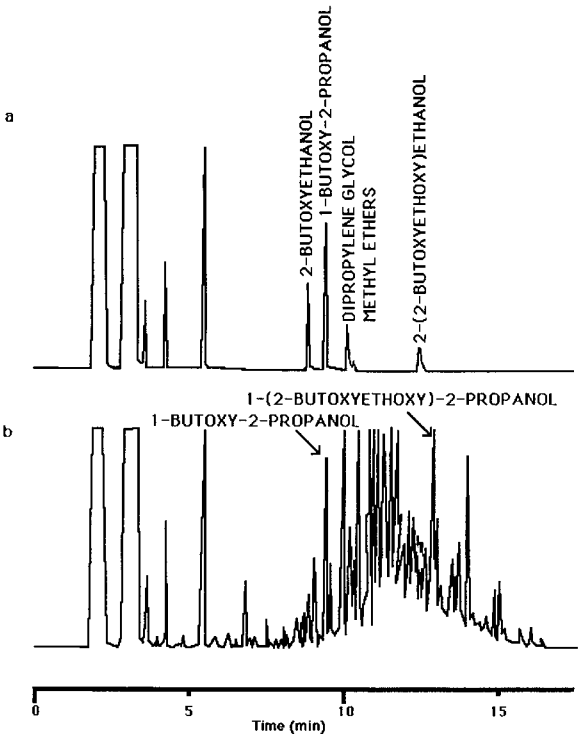

Fig. 2. (a) Single-column GC–FID of glycol ether standard containing 22.5 μg/ml 2-butoxyethanol, 22 μg/ml 1-butoxy-2-propanol, 24 μg/ml dipropylene glycol methyl ether and 24 μg/ml 2-(2-butoxyethoxy)-ethanol. (b) Single-column GC–FID of charcoal tube air sample containing 109 μg 1-butoxy-2-propanol and *ca.* 18 μg 1-(2-butoxyethoxy)-2-propanol (sample G1).

ether standards, in the order of their increasing elution time. Each glycol ether was analyzed without the "heartcut" to determine the approximate time interval for the "heartcut", using the flame ionization detector. The same sample was then analyzed with the "heartcut" to verify that all of the peak was being transferred onto the second analytical column during the "heartcut". During the period which the valve is in the heartcut mode, the flow through column 1 is reduced due to the additional pressure drop caused by column 2 being connected in series with column 1. Because of this, the transfer of the analyte from column 1 to column 2 requires the heartcut time to extend beyond the expected elution time of the analyte from column 1 alone. The determination of the appropriate end time was made on a trial and error basis. After the analytical conditions were established for the first compound, standards of the other glycol ethers identified in the bulk samples were treated in the same fashion, with either the initial heartcut modified or a new heartcut made to include each new compound. Based on this approach, the five glycol ethers under study could be analyzed by using two heartcuts (a cut from 8.1 to 11.5 min and a second cut from 13.55 to 15.1 min). One interesting aspect of the valve arrangement was that when the valve was switched, a small amount of air leaked into the chromatographic tubing. This air

peak was detected with the mass selective detector and provided a reference point for each of the heartcuts.

After the initial analytical method development was completed, a problem with the separation of 1-(2-butoxyethoxy)-2-propanol and 2-(2-butoxyethoxy)ethanol was noted in the analysis of the air samples. Both compounds appeared to be eluting at the same retention time. The initial analytical work on these two compounds indicated that there was a difference of 0.5 min in their respective retention times in the MDGC–MS system. At the time when this problem was found, the samples already had been prepared for analysis, so 1-(2-butoxyethoxy)-2-propanol was not included as a standard because it had not been found in the preliminary analyses of 2 samples. In the sample (G1) where 1-(2-butoxyethoxy)-2-propanol was found, its identity had to be confirmed by examination of the full scan mass spectrum.

The separation of the glycol ethers from the aliphatic compounds using the valve made it possible to identify the five glycol ethers of interest accurately in the air samples. The use of the mass selective detector added to the selectivity of the method, since individual ion chromatograms could be extracted from the total ion chromatogram data. Fig. 3 shows the chromatograms for a standard and one of the samples obtained during a MDGC–MS analysis. The extracted ion chromatograms for ion *m/e* 45 ($C_2H_5O^+$) for both standards and samples were integrated and the results were used for quantitation of the glycol ethers. Calibration results were linear over the range of 5–200 μg/ml for all five glycol ethers using peak area data. For dipropylene glycol methyl ether, the individual peak areas for the two major isomers were summed for data calculations. The limit of detection [13,14] for the five glycol ethers was typically 5–7 μg/sample.

The desorption efficiencies of the glycol ethers were: 2-butoxyethanol 100%, 9–180 μg/sample; 2-(2-butoxyethoxy)ethanol 80%, 9–190 μg/sample; 1-butoxy-2-propanol 94%, 9–180 μg/sample; and dipropylene glycol methyl ether (two major

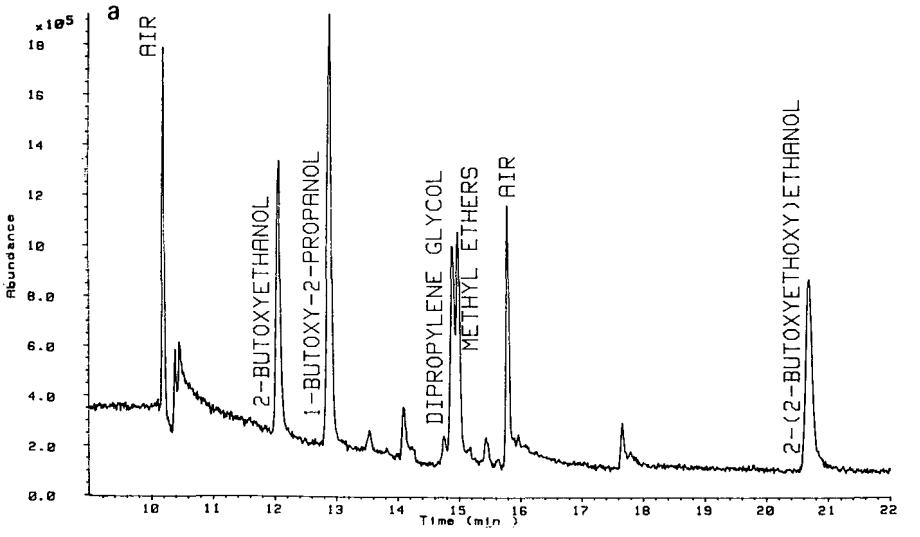

Fig. 3.

(*Continued on p. 310*)

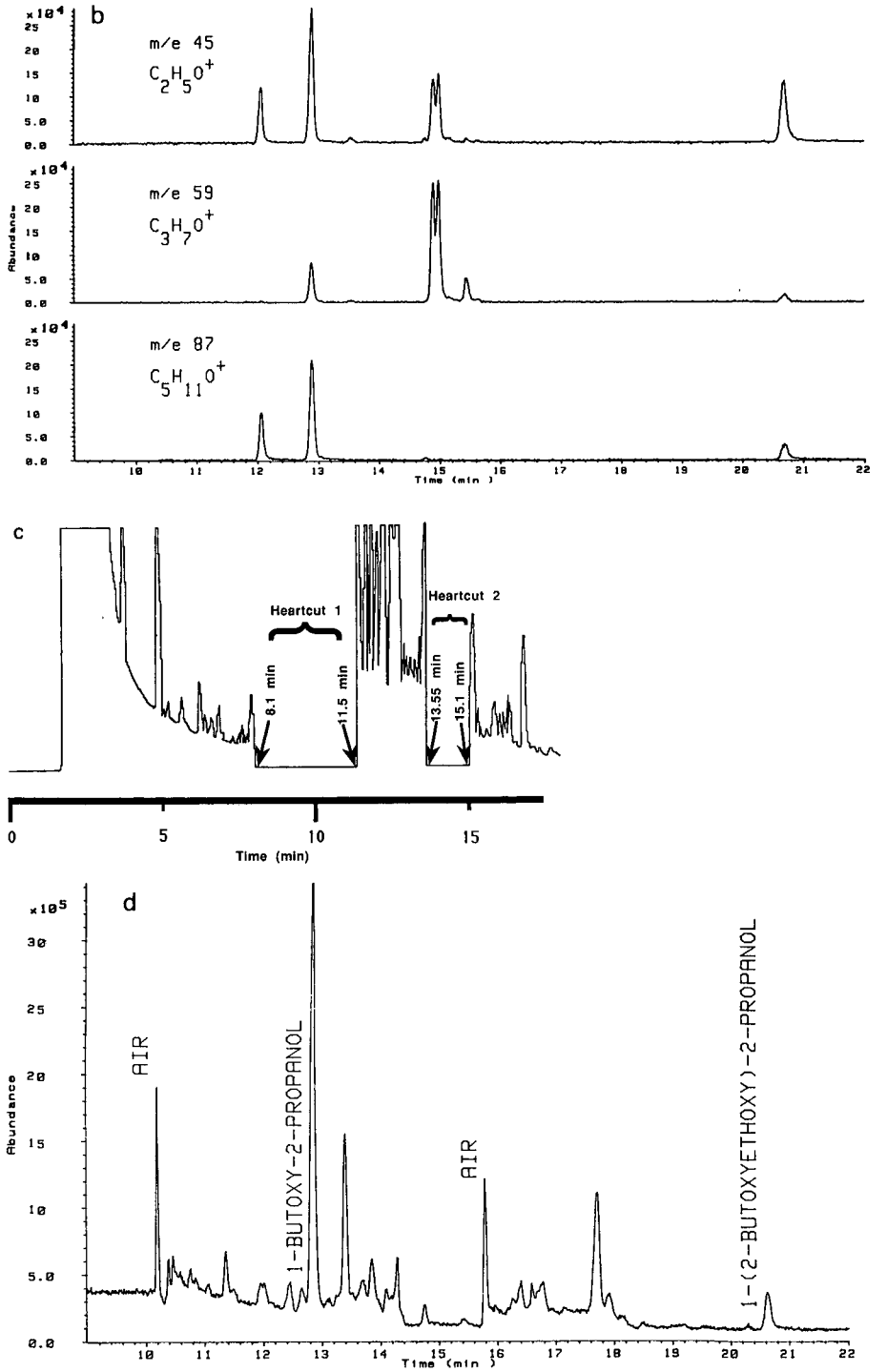
b
m/e 45
$C_2H_5O^+$
m/e 59
$C_3H_7O^+$
m/e 87
$C_5H_{11}O^+$
Abundance
Time (min)
c
Heartcut 1
Heartcut 2
8.1 min
11.5 min
13.55 min
15.1 min
Time (min)
d
AIR
1-BUTOXY-2-PROPANOL
AIR
1-(2-BUTOXYETHOXY)-2-PROPANOL
Abundance
Time (min)

Fig. 3.

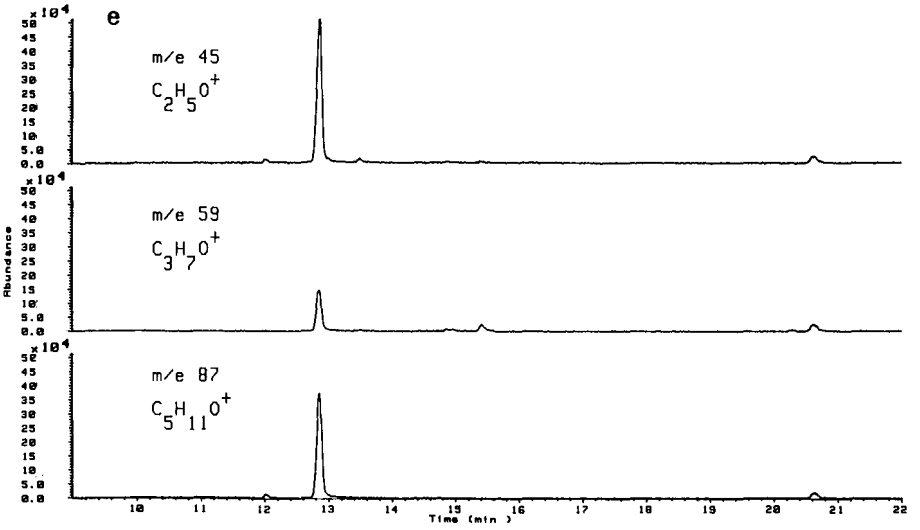

Fig. 3. (a) Total ion and (b) extracted ion chromatograms from multidimensional gas chromatographic analysis of standard containing 22.5 μg/ml 2-butoxyethanol, 22 μg/ml 1-butoxy-2-propanol, 24 μg/ml dipropylene glycol methyl ether and 24 μg/ml 2-(2-butoxyethoxy)ethanol. (c) Flame ionization chromatogram of charcoal tube air sample (sample G1) extract showing regions (8.1–11.5 min and 13.55–15.1 min) which were heartcut onto column 2. (d) Total ion and (e) extracted ion chromatograms of heartcut from charcoal tube air sample containing 109 μg 1-butoxy-2-propanol and *ca.* 18 μg 1-(2-butoxyethoxy)-2-propanol (sample G1).

TABLE I

RESULTS FROM ANALYSES OF AIR SAMPLES FOR GLYCOL ETHERS

ND = Less than limit of detection present (*ca.* 7 μg/sample).

Sample	2-Butoxy-ethanol		1-Butoxy-2-propanol		2-(2-Butoxy-ethoxy)ethanol		1-(2-Butoxy-ethoxy)-2-propanol	
	μg/sample	mg/m^3	μg/sample	mg/m^3	μg/sample	mg/m^3	μg/sample	mg/m^3
G1	ND[a]	–	109	3.6	ND		18[b]	0.6
G2	ND	–	ND[a]	–	9.7	0.4	ND	–
G3	ND	–	ND[a]	–	9.5	0.5	ND	–
G4	ND	–	ND[a]	–	ND[a]	–	ND	–
G5	ND	–	ND	–	35	1.6	ND	–
G6	104	2.6	ND	–	ND[a]	–	ND	–
G7	9.6	0.5	ND	–	ND[a]	–	ND	–
G8	313	13	ND	–	ND[a]	–	ND	–
Blank	ND		ND	–	ND	–	ND	–

[a] Peaks observed at correct retention times for these compounds and mass spectra obtained indicating presence at levels below the limit of detection.

[b] A standard for 1-(2-butoxyethoxy)-2-propanol was not used. Analyte was quantitated using 2-(2-butoxyethoxy)ethanol as standard.

isomers) 83%, 9–190 μg/sample. Only with dipropylene glycol methyl ether was the desorption efficiency observed to change with loading from 74% at 9 μg/sample to 91% at 190 μg/sample.

Four of the eight air samples contained significant amounts of glycol ethers. Table I lists the analysis results of the charcoal tube samples. No dipropylene glycol methyl ether was found in any of the samples. Preliminary analysis of samples G5 and G8 indicated that 1-(2-butoxyethoxy)-2-propanol was not present. Based on this finding and the previously described resolution difficulties with 2-(2-butoxyethoxy)-ethanol, 1-(2-butoxyethoxy)-2-propanol was not included in the standards used for quantitation. However, this compound was identified by mass spectral data interpretation in sample G1 and quantitated based on 2-(2-butoxyethoxy)ethanol calibration data.

The mass spectra of glycol ethers and hydrocarbons present in the samples analyzed in this study have many similar ions, making selected ion monitoring impractical to use alone for compound identification. The use of selected ion monitoring usually offers the advantage of increased sensitivity for a selected compound, particularly if the compound has a very characteristic ion. Unfortunately, the characteristic ions of glycol ethers correspond to the background ions found when using a DB-WAX capillary column. To determine if improvement in sensitivity was possible with selected ion monitoring in this instance, the glycol ether standards used for calibration of the air sample analyses were reanalyzed using this technique. Integration results from the selected ion monitoring chromatograms (ion m/z 45) produced calibration curves that gave slightly lower limits of detection [13,14] than integration data from the extracted ion chromatograms (2-butoxyethanol 2.4 μg/ml; 1-butoxy-2-propanol 1.4 μg/ml; 2-(2-butoxyethoxy)ethanol 4.9 μg/ml; dipropylene glycol methyl ether 2.5 μg/ml using ion m/z 59). The main reason that selected ion monitoring did not give significantly lower limits of detection in this instance was that the baseline noise caused by the column bleed interfered with the integration of the peaks due to the glycol ethers, particularly at low levels.

DISCUSSION

The successful determination of glycol ethers in air samples has shown the multidimensional gas chromatograph to be a useful analytical tool in the analysis of industrial hygiene samples containing low levels of difficult-to-separate components. This system has the resolving power to separate complex mixtures of analytes and may significantly reduce method development time. The selectivity of the mass selective detector enhanced the performance of the system by allowing characteristic ions of the glycol ethers to be monitored.

The use of this detector also aided in the identification of compounds, so that multicomponent standards could be used in the initial method development phases of the research. With a non-specific detection method, such as FID, individual standards and blanks must be prepared and analyzed in order to identify compounds by retention time. The ability to identify individual compounds by mass spectral data is particularly advantageous in a multidimensional gas chromatographic system, where retention times of the analyte of interest may change by alteration of the heartcut time interval.

The valve-based multidimensional gas chromatograph used in this study still has some unresolved problems. Peak tailing due to solvent interaction with the valve assembly was noted in the FID signal. Fortunately, this did not pose a problem with the determination of the glycol ethers. A qualitative test has been proposed by other researchers to evaluate the inertness of such a valve-based multidimensional system [15]. The interaction of the test compounds with the valve components was reported to be reversible when a cryofocusing system at the head of the second column was used. This information indicates that application of MDGC–MS to other samples containing polar, volatile or reactive compounds may require the addition of cryofocusing capability at the head of the analytical column (column 2).

ACKNOWLEDGEMENT

We would like to acknowledge the assistance of Teresa Seitz for the collection of the charcoal tube air samples and bulk liquid samples which provided the basis for the research in this report.

Disclaimer: Mention of company names or products does not constitute endorsement by the National Institute for Occupational Safety and Health.

REFERENCES

1 L. G. M. Th. Tuinstra, W. A. Traag and A. H. Roos, *J. High Resolut. Chromatogr. Chromatogr. Commun.*, 11 (1988) 106.
2 H. Tani and M. Furuno, *J. High Resolut. Chromatogr. Chromatogr. Commun.*, 9 (1986) 712.
3 G. Schomburg, F. Weeke and R. G. Schaefer, *J. High Resolut. Chromatogr. Chromatogr. Commun.*, 8 (1985) 388.
4 N. G. Johansen, *J. High Resolut. Chromatogr. Chromatogr. Commun.*, 7 (1984) 487.
5 G. Schomburg, H. Husmann and E. Hubinger, *J. High Resolut. Chromatogr. Chromatogr. Commun.*, 8 (1985) 395.
6 W. V. Ligon, Jr. and R. J. May, *J. Chromatogr.*, 294 (1984) 77.
7 R. H. M. van Ingen and L. M. Nijssen, *J. High Resolut. Chromatogr. Chromatogr. Commun.*, 12 (1989) 484.
8 *Glycol Ethers—2-Methoxyethanol and 2-Ethoxyethanol, NIOSH Current Intelligence Bulletin 39, DHHS (NIOSH) Publ. No. 83-112*, U.S. Department of Health and Human Services, Cincinnati, OH, 1983,
9 D. R. Deans, *J. Chromatogr.*, 203 (1981) 19.
10 B. M. Gordon, C. E. Rix and M. F. Borgerding, *J. Chrom. Sci.*, 23 (1985) 1.
11 P. M. Eller (Editor), *NIOSH Manual of Analytical Methods, DHHS (NIOSH) Publ. No. 84-100*, National Institute for Occupational Safety and Health, Cincinnati, OH, 3rd ed., 1984, Method 1403 (Alcohols IV).
12 F. W. McLafferty, *Interpretation of Mass Spectra, Third Edition*, University Science Books, Mill Valley, CA (1980) p. 189.
13 A. Hubaux and G. Vos, *Anal. Chem.*, 42 (1970) 849.
14 E. R. Kennedy, Y. T. Gagnon, J. R. Okenfuss and A. W. Teass, *Appl. Ind. Hyg.*, 3 (1988) 274.
15 S. T. Adam, *J. High Resolut. Chromatogr. Chromatogr. Commun.*, 11 (1988) 85.

Journal of Chromatography, 522 (1990) 315–327
Elsevier Science Publishers B.V., Amsterdam

CHROM. 22 769

New sensitive method for the examination of the volatile flavor fraction of cabernet sauvignon wines[a]

JOE O. K. BOISON*
Agriculture Canada, Food Production and Inspection Branch, Health of Animals Laboratory, 116 Veterinary Road, Saskatoon, Saskatchewan S7N 2R3 (Canada)
and
RICHARD H. TOMLINSON
Chemistry Department, McMaster University, Hamilton, Ontario L8S 4M1 (Canada)
(First received January 17th, 1990; revised manuscript received August 15th, 1990)

ABSTRACT

A new design of solvent extractor and a new low-temperature, high vacuum, two stage concentrator apparatus were constructed that enabled the quantitative and qualitative examination of trace level concentrations of the volatile flavor components of *Vitis vinifera* grape musts and wines to be conducted reproducibly. The sensitivity of the new technique, in the ppb range, was demonstrated by the detection and identification of 2-methoxy-3-isobutylpyrazine, an organoleptically significant flavor compound in Cabernet Sauvignon wine for the first time. 2-Hydroxybenzothiazole and ethyl 4-acetyloxybutanoate were also identified for the first time as components in this wine.

INTRODUCTION

It is estimated that the concentrations of volatile flavor compounds in grape musts and wines range between 1 g/l and 1 ng/l [1]. Since the concentrations at which volatile compounds influence the flavor of a given food system are extremely low, sometimes at concentrations well below the detection limits of some of the most sophisticated analytical instruments, it is imperative that the volatile fraction of the grape must or wine be isolated from the bulk of the food sample and concentrated. The extremely low odor threshold values of some of the more significant flavor compounds demand that isolation techniques be aimed at isolating these trace level compounds from other less organoleptically significant components which may be present at concentrations several orders of magnitude higher. Several techniques have been used to achieve this: solvent extraction [2–4]; simple, fractional, steam, atmospheric and vacuum distillation [5,6]; adsorption onto charcoal, Tenax, silica gel, Porapak Q and Chromosorb [7]; and headspace techniques [8]. The isolated extract is usually enriched

[a] A section of this paper was presented at the *69th Canadian Chemical Conference, Saskatoon, June 1–4, 1986.*

0021-9673/90/$03.50

by rotary evaporation, a gentle stream of inert gas, or vacuum techniques to concentrate individual components to within the range of the detectors to be used. Gas chromatographic techniques are employed to separate and identify the components in the volatile extract. Most of these methods can detect only major and minor components but not trace-level components. Very few reports appear in the literature on the simultaneous detection and identification of multiple trace volatile flavor components in wine in the part per billion (ppb) and part per trillion (ppt)[a] concentration range [9,10].

In 1986, Boison *et al.* [11] reported the detection and identification of the organoleptically significant volatile flavor compound, 2-methoxy-3-isobutylpyrazine, as a trace component in Cabernet Sauvignon wine for the first time. Even though this compound, believed to impart a herbaceous aroma to Cabernet Sauvignon grapes and wines, was first identified in the grape in 1966 [12] and confirmed in 1975 [13], its presence in the wine could not be confirmed. Slingsby *et al.* [14] were also unable to establish the presence of this compound in wines they had made from the grapes of the *Vitis vinifera* cultivar Cabernet Sauvignon. Quite recently, however, Harris *et al.* [10] have also reported the identification and quantification of several alkoxypyrazines, including 2-methoxy-3-isobutylpyrazine, in wines and grape juices. This paper decribes in detail the new technique that enabled the detection and identification of 2-methoxy-3-isobutylpyrazine as a trace level component in Cabernet Sauvignon wines.

EXPERIMENTAL

Reagents

All flavor compounds used in this investigation were purchased from one of the following chemical companies: BDH (U.K.), Eastman-Kodak (U.S.A.), Fisher (Canada), Sigma (U.S.A.), Aldrich (U.S.A.), Pyrazine Specialities (U.S.A.) and McArthur (Canada). All compounds were checked for chromatographic purity before use. Freon 11 (Canadian Liquid Air) was purified by vacuum distillation before use. The 1972 red wine bottled by Chateau Pichon Lalande de Pauillac was from the private collection of one of the authors (R.H.T.). The composition of this red wine was approximately 4:1:1 Cabernet Sauvignon, Malbec, and Petit Verdot.

Apparatus

The all-glass solvent extraction apparatus that was used in this analysis is illustrated in Fig. 1. It was operated in the batch mode as follows: The solvent pot, T (onto which an extruding bulb U, with an internal volume of 700 μl and an outer dimension of 2.5 cm $\times$ 0.8 cm O.D., had been blown), initially contained 250.0 ml of freon 11 (b.p. 24.1°C) and a 7 mm $\times$ 12 mm egg-shaped PTFE-coated stirring magnet. The pot, T, sat in a warm water bath held at 35°C by a heater-stirrer which also maintained vigorous stirring in T. The resulting freon vapor condensed into the reflux syphon, D, which provided reflux solvent to the fractionating column, S, (50 cm $\times$ 2.5 cm O.D., packed with 3 mm glass helices) and to the intermittent syphon, F, which provided a critical volume of freon (1.15 ml) sufficient to form a single bead in the

[a] Throughout this article, the American billion (10^9) and trillion (10^{12}) are meant.

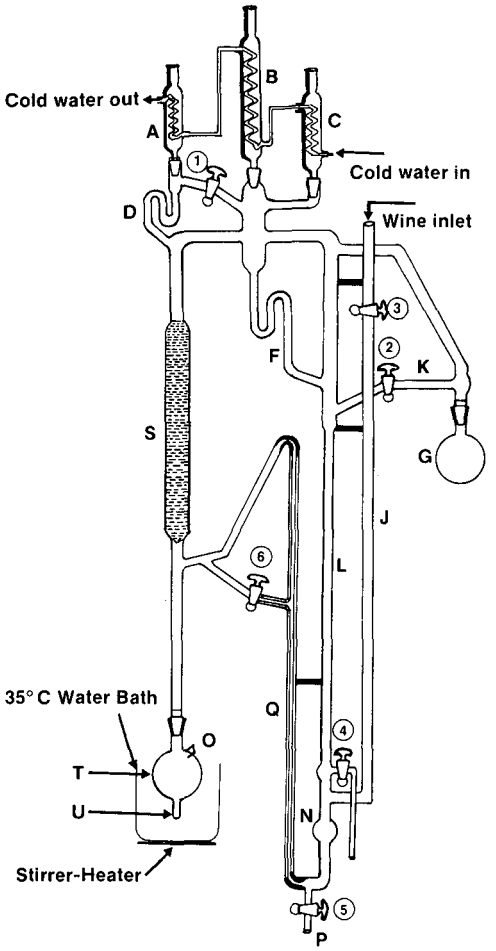

Fig. 1. Solvent extraction apparatus. A, B, C = Condensers; D = reflux syphon; F = intermittent syphon; G = wine/must receiving bulb for continuous extraction; J = inlet tube; K = overflow transfer tube; L = extracting tube; N = collection bulb; O = glass post mounted on the side of the solvent pot for harnessing the horseshoe magnet retriever; P = wine/must outlet tube; Q = capillary tube; S = fractional distillation column; T = solvent pot; U = extruding bulb for handling small sample volumes; 1–6 = taps.

extracting tube, L. L was filled with 95.0 ml of wine through the entry tube, J. The wine was held stationary in L with pressurized, inert gas in the entry tube and with stopcock 3 closed. The freon bead fell through the length of L into the collection bulb, N, at a rate of 4 beads/min. The contents of N could be withdrawn through stopcock 5. As the consecutive freon beads fell, the freon and extracted volatile flavor components flowed into T through the capillary tube, Q. The extracted volatile flavor components collected in T and the warmed, stirred, freon solution in T underwent fractional distillation in S. This enabled purified freon to recycle and reextract the sample in L. After 2.5 h, the 35°C water bath was removed, and T was removed from the extractor and connected, through the transfer tube, K, to the low-temperature, high-vacuum, concentrator (Fig. 2) held under a vacuum of 13–130 mPa. The transfer tube, K, was

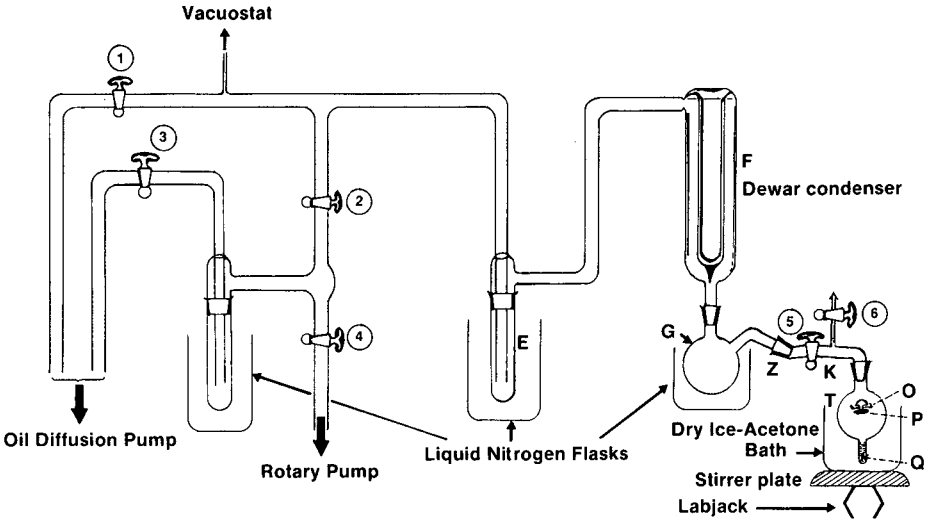

Fig. 2. Low-temperature, high-vacuum, concentrator apparatus used in the first stage of the enrichment procedure. E = Cold trap; F = cold finger of a Dewar condenser; G = distillation bulb; K = transfer tube; O = glass post supporting horseshoe magnet retriever; P = retrieved bar magnet; Q = micro bar magnet for stirring solutions in extruding bulb; T = solvent pot; 1–6 = taps.

designed to provide the desired configuration for performing the necessary distillation procedures. T was held at an initial angle of 45°C to the horizontal. The contents of T were initially frozen in liquid nitrogen and then maintained at −78.1°C by immersion into a dry ice–acetone slush bath. When the contents of T had melted, stopcock 5 was opened with stopcock 6 closed, and liquid nitrogen was poured onto the cold finger, F, and the dewar surrounding the distillation bulb, G, while vigorous stirring was maintained in T. Distillation was continued until visual inspection indicated that the volume of solution left in T was approximately 2 ml, at which time the apparatus was slowly rotated about joint, Z, downward into a vertical position while the adjustable laboratory jack was lowered so that the bulk of the solution in T was slowly transferred into U. The magnetic bar, P, was retrieved with a horseshoe magnet and harnessed in position by O. Vigorous stirring was still maintained in U with the micro magnetic bar, Q, and distillation was continued until the desired volume in U (100 μl) was attained.

The 100 μl concentrated extract in U was transferred into the reservoir bulb, R, (Fig. 3) with a cooled 500-μl syringe. R was cooled in liquid nitrogen in a dewar and connected to the main vacuum line through the adaptor, K, with stopcocks 5, 6 and 7 closed. R was connected to the air-jacketed tube, V (20 cm × 4 mm I.D.) which was maintained at a temperature of 55°C during the distillation, and the sample receiver, Y. With the contents of R still frozen, stopcocks 5, 7, 9 and 10 were opened while stopcocks 6, 11 and 12 were still closed and the system was evacuated. When a suitable vacuum (13–130 mPa) was attained in this system, stopcock 7 was closed and the contents of R were allowed to melt to dislodge any dissolved air. Stopcock 5 was then closed. Then Y was cooled in a liquid nitrogen dewar while the contents of R were allowed to warm up to 40°C (40°C water bath) and stirred vigorously with the

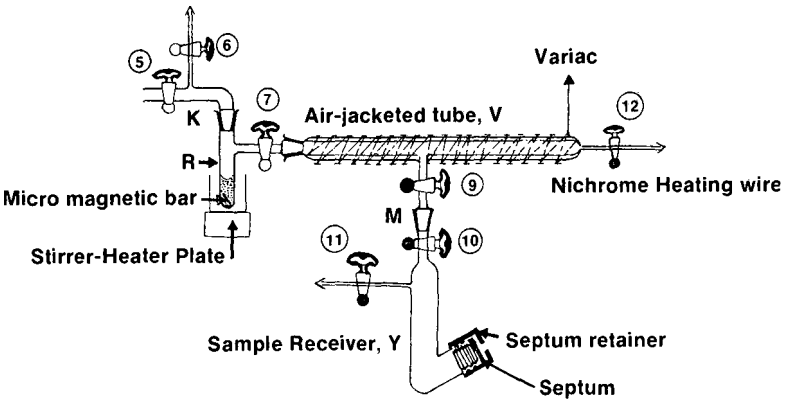

Fig. 3. Low-temperature, high-vacuum, concentrator apparatus used in the final stage of the enrichment procedure. K = Transfer tube; R = reservoir bulb; Y = sample receiver; 5–7, 9–12 = taps.

micromagnetic bar. Forty minutes after the commencement of this process, stopcock 10 was closed, all warming and stirring in R were discontinued. The water bath around R was replaced with liquid nitrogen in a dewar and any uncondensed vapors in V were thus condensed back into R. Stopcock 7 was closed and Y was disconnected from the system by opening stopcock 11. The contents of the reservoir bulb, R (25 μl) and the receiving trap, Y (75 μl) were then ready for analysis by capillary gas chromatography–mass spectrometry (GC–MS).

Wine analysis

A 95.0-ml amount of a 1972 red wine bottled by Chateau Pichon Lalande de Pauillac, France, were extracted in a batch mode for three hours with 250.0 ml of freon 11. The freon extract was enriched 2500-fold to 1000 μl using the low-temperature, high-vacuum concentrator (Fig. 2). The concentrated extract was treated with 100 μl 5% sodium bicarbonate and then 100 μl propylene glycol [14]. The separated freon fraction was concentrated further before analysis by GC–MS (Fig. 3).

Capillary GC analysis

For capillary GC analysis, the isolated and concentrated volatile flavor extract was spiked with a homologous series of *n*-alkanes (concentrations ranging from 1 to 10 ng/μl) and 20 ng/μl of acetophenone as internal standard. Sample sizes of 0.5 to 1.0 μl were injected into a 250°C split/splitless injector of a Varian 3700 GC system which housed either a 50 m × 0.25 mm I.D. fused-silica non-bonded Carbowax 20M (J & W Scientific), or a 30 m × 0.25 mm I.D. fused-silica non-bonded SE-54 capillary column (J & W Scientific), with the split valve closed. After 25 s, the split valve was opened to provide the desired flow of prepurified helium (30 cm/s, linear velocity) through the column while the GC oven was held at 50°C. The GC oven temperature was then programmed to 210°C at 4°C/min for the Carbowax column, 50–280°C for the SE-54 column, and held at the final temperature for 20 min. A microsample splitter, fitted at the end of the capillary column, provided a 1:1 split ratio of the chromatographic effluent to the flame ionization detection (FID) system and thermionic sensitive detection (TSD) system, also known as a nitrogen-specific

detection system, both held at 250°C. When the mass spectrometer (a double-focussing, high-resolution, magnetic sector instrument, MM70-70F, VG Analytical Altrincham, U.K.) served as the detector for the GC effluent, the following operating conditions were used: ion source temperature, 200°C; ionization voltage 70 eV; accelerating voltage, 4 kV; trap current, 100 μA; electron multiplier amplifier gain, 1; sensitivity, 10^{-7} A; response time 0.1 ms. The mass range was scanned repetitively in an exponential downscan mode at 1 s/decade at resolving powers of $\geqslant 1000$ (10% valley) to obtain electron impact (EI) mass spectra. To obtain chemical ionization (CI) mass spectra, the ion source temperature was held at 150°C, the source energy at 500 μA, and the electron energy at 50 eV. Isobutane was used as the reactant gas.

The concentration $C(X)$ of a component X in the aqueous alcoholic or wine solution was estimated from eqn. 1:

$$C(X) = A(X)/A(\mathrm{IS}) \cdot C(\mathrm{IS}) \cdot M(X)/M(\mathrm{IS}) \cdot \frac{1}{RWR} \cdot V(f)/V(i) \qquad (1)$$

where $C(X)$ = concentration of component X in ng/μl of sample
$C(\mathrm{IS})$ = concentration of internal standard in ng/μl (*i.e.* 20 ng/μl)
$M(X)$, $M(\mathrm{IS})$ = molecular weights of component and internal standard
RWR = relative weight response factor
$V(i)$ = initial volume of sample taken for extraction
$V(f)$ = final volume of extract after enrichment
$A(X)$ = area under the selected ion retrieval (SIR) chromatogram for the identifying m/z value for component X
$A(\mathrm{IS})$ = area under the selected ion retrieval (SIR) chromatogram for the identifying m/z value for the internal standard.

RESULTS AND DISCUSSION

The solvent extraction and concentration apparatuses and their constituent

TABLE I

EXTRACTION EFFICIENCY OF THE SOLVENT EXTRACTOR FOR VOLATILE FLAVOR COMPONENTS IN 12% ETHANOL SOLUTION

Compound	Recovery ± S.D. (n=4) (%)		
	2 ppm	0.02 ppm	0.002 ppm
Ethyl hexanoate	99 ± 3	97 ± 3	96 ± 4
Ethyl 3-hydroxybutyrate	98 ± 7	97 ± 5	98 ± 6
Methyl furoate	98 ± 5	99 ± 4	95 ± 5
Diethyl succinate	99 ± 5	99 ± 7	97 ± 5
Hexanoic acid	97 ± 7	96 ± 4	96 ± 4
2-Phenethyl alcohol	100 ± 4	100 ± 6	98 ± 4
Octanoic acid	98 ± 3	99 ± 3	96 ± 4
Diethyl malate	100 ± 4	98 ± 4	98 ± 6
Methyl anthranilate	100 ± 3	99 ± 7	97 ± 4
Decanoic acid	96 ± 7	97 ± 4	97 ± 7

TABLE II

EFFICIENCY OF THE FRACTIONAL DISTILLATION COLUMN, S, IN PURIFYING FREON SOLVENT FOR RE-EXTRACTION

Compound	% (w/w) in distillate[a]
Ethyl hexanoate	0.2
Ethyl 3-hydroxybutyrate	nd[b]
Methyl furoate	nd
Diethyl succinate	0.5
Hexanoic acid	nd
2-Phenethyl alcohol	nd
Octanoic acid	nd
Diethyl malate	nd
Methyl anthranilate	0.8
Decanoic acid	nd

[a] Each component had an approximate concentration of 2 ppm in the solution.
[b] nd = Not detected.

TABLE III

EFFICIENCY OF RECOVERY AND REPRODUCIBILITY OF THE FIRST STAGE OF THE ENRICHMENT PROCEDURE

Compound	Recovery ± S.D. ($n=4$) (%)		
	Approx. concn. of each component		
	2 ppm	0.02 ppm	0.002 ppm
Ethyl hexanoate	98 ± 8	96 ± 7	97 ± 8
Ethyl 3-hydroxybutyrate	99 ± 8	93 ± 7	92 ± 4
Methyl furoate	98 ± 2	98 ± 3	97 ± 5
Diethyl succinate	98 ± 3	96 ± 4	98 ± 6
Hexanoic acid	99 ± 9	98 ± 3	98 ± 4
2-Phenethyl alcohol	100 ± 2	103 ± 5	101 ± 4
Octanoic acid	98 ± 8	96 ± 4	95 ± 5
Diethyl malate	100 ± 3	98 ± 4	97 ± 5
Methyl anthranilate	99 ± 8	99 ± 5	100 ± 6
Decanoic acid	97 ± 8	99 ± 6	93 ± 6

TABLE IV

EFFICIENCY OF THE SODIUM BICARBONATE TREATMENT IN REMOVING ORGANIC ACIDS FROM THE PARTIALLY CONCENTRATED FREON EXTRACT

Compound	Recovery obtained on the freon extract enriched 2500-fold (%)[a]
Ethyl hexanoate	98
Ethyl 3-hydroxybutyrate	96
Methyl furoate	99
Diethyl succinate	97
Hexanoic acid	nd[b]
2-Phenethyl alcohol	96
Octanoic acid	nd
Diethyl malate	97
Methyl anthranilate	98
Decanoic acid	nd

[a] Only 1 analysis was performed.
[b] nd = Not detected.

TABLE V

EFFICIENCY OF THE PROPYLENE GLYCOL TREATMENT IN REMOVING FUSEL ALCOHOLS FROM THE PARTIALLY CONCENTRATED FREON EXTRACT

Compound	Recovery (%)[a]
Ethyl hexanoate	98
1-Pentanol	1
1-Hexanol	1
Isoamyl hexanoate	97
1-Octanol	2
γ-Butyrolactone	95
Diethyl succinate	98
2-Phenethyl alcohol	1
Octanoic acid	96
Methyl anthranilate	98
Decanoic acid	98

[a] Only 1 analysis was performed.

TABLE VI

RECOVERIES AND DISTRIBUTION OF VOLATILE FLAVOR COMPONENTS DISTILLED INTO SAMPLE RECEIVER, Y, IN THE FINAL STAGE OF THE ENRICHMENT PROCEDURE

Compound (Mol. wt.)	B.p. (°C)	Recovery[a] ± S.D. ($n=4$) (%)
Ethyl hexanoate (144)	168	95 ± 4
1-Pentanol (88)	137	97 ± 3
Ethyl 2-hydroxyisopropionate (132)	150	96 ± 4
Amyl butyrate (158)	186	97 ± 6
Ethyl lactate (118)	160	95 ± 3
1-Hexanol (102)	158	93 ± 4
cis-3-Hexen-1-ol (100)	156	97 ± 5
cis-2-Hexen-1-ol (100)	158	93 ± 4
Acetic acid (60)	118	97 ± 6
Ethyl octanoate (172)	208	2.0 ± 0.1
Isoamyl hexanoate (186)	225	3.0 ± 0.4
2-Methylbutanoic acid (102)	176	95 ± 7
Hexanoic acid (130)	223	96 ± 3
Octanoic acid (144)	265	95 ± 4
Decanoic acid (172)	270	95 ± 6

[a] These values have been corrected for the degree of enrichment.

TABLE VII

RECOVERIES AND DISTRIBUTION OF VOLATILE FLAVOR COMPONENTS LEFT BEHIND IN RESERVOIR BULB, R, IN THE FINAL STAGE OF THE ENRICHMENT PROCEDURE

Compound (Mol. wt.)	B.p. (°C)	Recovery ± S.D. (n=4) (%)
Ethyl octanoate (172)	208	96 ± 4
Isoamyl hexanoate (186)	225	96 ± 7
Benzaldehyde (106)	178	89 ± 4
Ethyl 2-hydroxyisopropionate (132)	185	91 ± 5
1-Butyl lactate (146)	200	95 ± 3
1-Octanol (130)	195	89 ± 2
Methyl furoate (126)	181	92 ± 4
Isophorone (138)	215	95 ± 6
γ-Butyrolactone (86)	206	93 ± 4
Ethyl decanoate (200)	241	97 ± 6
Neral (152)	230	91 ± 4
Isoamyl octanoate (214)	270	97 ± 5
Diethyl succinate (174)	217	90 ± 4
Geranial (152)	229	92 ± 7
2-Phenethyl acetate (164)	233	98 ± 1
Ethyl laurate (228)	273	98 ± 6
2-Phenethyl alcohol (122)	219	89 ± 7
trans-Cinnamaldehyde (132)	253	88 ± 3
Diethyl malate (190)	253	91 ± 3
Methyl anthranilate (151)	256	96 ± 4
Ethyl anthranilate (165)	268	97 ± 3
Phthalide (134)	290	98 ± 7

TABLE VIII

ESTIMATION OF THE ACCURACY AND PRECISION OF THE DEVELOPED ANALYTICAL PROCEDURE AT A CONCENTRATION LEVEL OF 2000 ppb

Compound	Concentration of component in model solution (ppb)	Concentration of component found by experiment (mean[a] ± S.D., n=4) (ppb)	Deviation (%)
Ethyl hexanoate	1835	1740 ± 140	5.2
Ethyl 3-hydroxybutyrate	2205	2030 ± 120	7.9
Methyl furoate	2601	2360 ± 220	9.3
Diethyl succinate	2314	2080 ± 220	10.1
Hexanoic acid	2049	1850 ± 60	9.7
2-Phenethyl alcohol	2000	nd[b]	nd
Octanoic acid	1849	1720 ± 160	7.0
Diethyl malate	2517	2260 ± 190	10.2
Methyl athranilate	2594	2340 ± 150	9.8
Decanoic acid	2174	2000 ± 140	8.0

[a] These values refer to the experimentally determined concentrations of volatile flavor components in standard 12% ethanolic solutions following solvent extraction, enrichment and GC–MS analysis after correcting for the degree of enrichment.

[b] nd = Not detected. Alcohols were extracted into propylene glycol but this fraction was not analyzed.

TABLE IX

ESTIMATION OF THE ACCURACY AND PRECISION OF THE DEVELOPED ANALYTICAL PROCEDURE AT A CONCENTRATION LEVEL OF 2 ppb

Compound	Concentration of component in model solution (ppb)	Concentration of component found by experiment (mean ± S.D., $n=4$) (ppb)	Deviation (%)
Ethyl hexanoate	1.8	1.7 ± 0.1	5.6
Ethyl 3-hydroxybutyrate	2.2	2.0 ± 0.1	9.1
Methyl furoate	2.6	2.4 ± 0.3	7.7
Diethyl succinate	2.3	2.1 ± 0.2	8.7
Hexanoic acid	2.1	1.9 ± 0.1	9.5
2-Phenethyl alcohol	2.0	nd	nd
Octanoic acid	1.8	1.7 ± 0.2	5.6
Diethyl malate	2.5	2.3 ± 0.2	8.0
Methyl anthranilate	2.6	2.3 ± 0.2	11.5
Decanoic acid	2.2	2.0 ± 0.1	9.1

parts were evaluated using model solutions of selected wine flavor components in 12% aqueous ethanol. The results of these studies, presented in Tables I–X, demonstrated that this apparatus was highly efficient and reproducible and yields almost 100% recovery of volatiles present in wine at the ppb level. Volatile flavor compounds with boiling points lower than 190°C and the fatty acids generally distilled into the sample receiver, Y, while the higher boiling volatile flavor components were left behind in the reservoir bulb, R (Tables VI and VII). This selective partitioning of flavor components in the final stage of the concentration procedure made it very convenient to carry out GC–MS analysis on essentially two fractions of volatile flavor compounds. Fig. 4 shows a partial total ion chromatogram (TIC) of a 1-μl sample of concentrated and simplified volatile flavor extract (fraction from receiver, R) of the 1972 red wine injected onto a 50 m × 0.25 mm I.D. fused-silica Carbowax 20M capillary column coupled directly to a VG70-70F mass spectrometer source. A total of 260 flavor components were detected in this wine in this analysis, including 16 compounds that still remain to be identified, 15 compounds that have been assigned tentative identities that had not been previously reported as flavor components in this wine [15], and 226 compounds previously reported as flavor components in this wine and confirmed in this analysis. Three new compounds were identified in this wine, namely, ethyl 4-acetyloxybutyrate, 2-hydroxybenzothiazole and 2-methoxy-3-isobutylpyrazine (Table X).

The mass spectrum and retention indices measured on both Carbowax 20M and SE-54 matched those of an authentic sample of this compound obtained from Pyrazine Specialities (U.S.A.). Both Boidron *et al.* [12] and Bayonove *et al.* [13] provided no quantitative data on the amounts present in the grapes. Bayonove *et al.* [13] however predicted that the concentration in the grapes would be about 5 ppb, which is ten times the concentration we found in this wine. The lower concentration may explain why its presence in the wine could not be confirmed by previous investigators.

Subsequent to the publication of a Ph.D. thesis on this work in 1985 by Boison [15], and the presentation of this finding at a scientific meeting in 1986, Harris *et al.* [10]

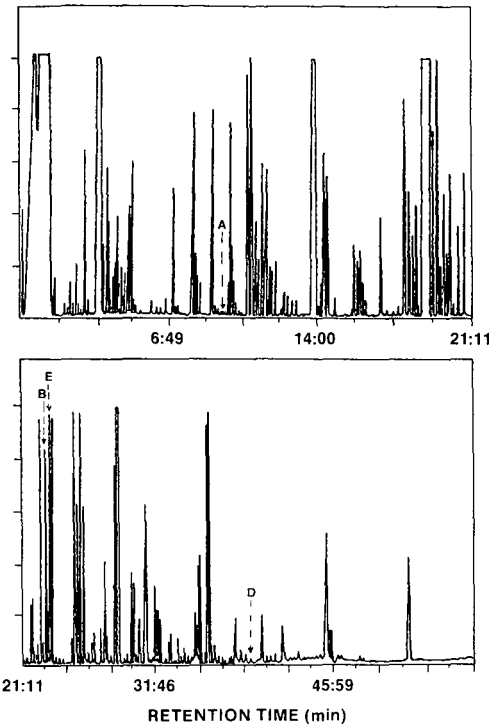

Fig. 4. Partial TIC chromatogram of the volatile flavor extract of Cabernet Sauvignon wine injected onto a 50 m × 0.25 mm I.D. Carbowax 20M fused-silica capillary column coupled directly to a VG70-70F mass spectrometer source. A = 2-Methoxy-3-isobutylpyrazine; B = ethyl 4-acetyloxybutyrate; D = 2-hydroxybenzothiazole; E = ethyl 2-acetyloxy-4-methylpentanoate.

TABLE X

QUANTITATIVE RESULTS AND RETENTION PARAMETERS OF NEW COMPOUNDS IDENTIFIED IN CABERNET SAUVIGNON WINE

	2-Methoxy-3-isobutyl pyrazine	Ethyl 4-acetyl-oxybutyrate	2-Hydroxy-benzothiazole
Mol. wt. confirmed by CI-MS	165	174	151
Odor threshold (ppb)	0.002[a]	–[b]	–[b]
Odor description	Herbaceous/ bell-pepper	Sweet/ mildly fragrant	Smokey/ nutty
Fragment ion monitored by SIR (m/z)	124	87	151
Experimental temperature-programmed retention index on Carbowax 20M	1473	2049	–
Experimental temperature-programmed retention index on SE-54	895	1591	1755
Concentration in wine (ppb) (mean ± S.D., n=4)	0.5 ± 0.07	476 ± 21	7.7 ± 0.6

[a] Ref. 6.

[b] Values not determined or listed in the literature.

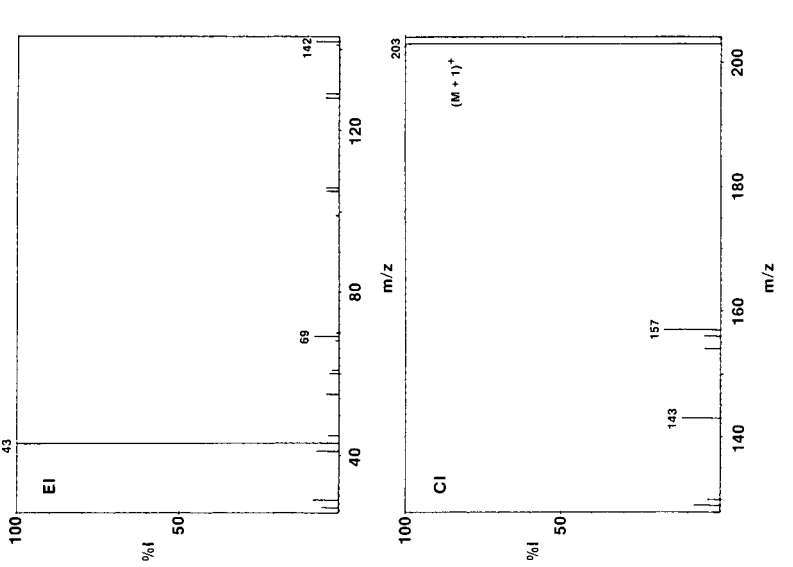

Fig. 5. EI and CI mass spectra of ethyl 4-acetyloxybutyrate. I = Ion intensity.

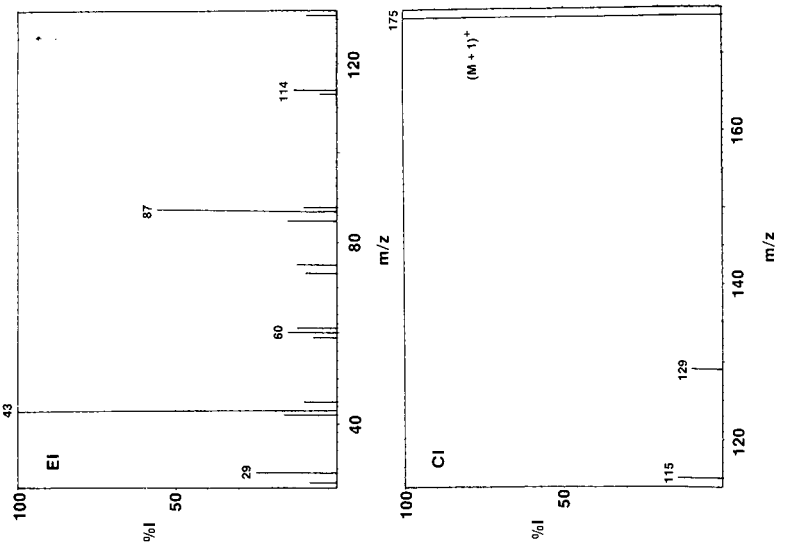

Fig. 6. EI and CI mass spectra of ethyl 2-acetyloxy-4-methylpentanoate.

have published some very interesting findings that have confirmed the finding that the organoleptically significant volatile flavor component, 2-methoxy-3-isobutylpyrazine, is present in Cabernet Sauvignon wines at trace level concentrations.

Fig. 5 shows the EI and CI mass spectra of ethyl 4-acetyloxybutyrate identified in Cabernet Sauvignon wine in this investigation. Retention and mass spectral parameters matched those of an authentic sample of this compound. The presence of another acetyloxy compound, ethyl 2-acetyloxy-4-methylpentanoate (Fig. 6), was established in this wine. There was no indication in the literature that it had been previously reported as a flavor constituent in Cabernet Sauvignon wine. These acetyloxy esters may be considered to be derivatives of the corresponding hydroxy esters arising through fermentation processes. The occurrence of ethyl 2-acetyloxy-4-methylpentanoate in Cabernet Sauvignon wine is of particular interest because it is widely believed that it exhibits a much stronger analgesic effect than acetylsalicylic acid [16]. The anaesthetic effect of the precursor of this ethyl ester, 4-hydroxybutanoic acid has already been discussed by Makoto and Hoshino [17].

REFERENCES

1 A. Rapp, H. Hastrich, L. Engel and W. Knipser, in G. Charalambous and G. E. Inglett (Editors), *Flavor of Foods and Beverages*, Academic Press, New York, 1978, pp. 391–417.
2 K. L. Stevens, J. Bomben and W. H. McFadden, *J. Agric. Food Chem.*, 14 (1966) 249.
3 A. D. Webb, R. E. Kepner and L. Maggiora, *Am. J. Enol. Vitic.*, 20 (1969) 16.
4 P. Schreier, *J. Agric. Food Chem.*, 28 (1980) 926.
5 C. J. Van Wyk, R. E. Kepner and A. D. Webb, *J. Food Sci.*, 32 (1967) 660.
6 R. G. Buttery, R. M. Seiffert, D. G. Guadagni and L. C. Ling, *J. Agric. Food Chem.*, 17 (1969) 1322.
7 A. A. Williams, H. V. May and O. G. Tucknott, *J. Inst. Brew.*, 84 (1978) 97.
8 W. G. Jennings, R. H. Wohleb and M. J. Lewis, *J. Food Sci.*, 37 (1972) 69.
9 P. Schreier, F. Drawert and A. Junker, *Chem. Mikrobiol. Technol. Lebensm.*, 5 (1977) 45.
10 R. L. N. Harris, M. J. Lacey, W. V. Brown and M. S. Allen, *Vitis*, 26 (1987) 201–207.
11 J. O. Boison, R. H. Tomlinson and A. Jackson, *Proceedings of the 69th Canadian Chemical Conference, Saskatoon, June 1–4, 1986*, Chemcan Publishers, Ottawa, 1986, p. 6.
12 J. N. Boidron, *Ph.D. Thesis*, University of Bordeaux, Bordeaux, 1966.
13 C. Bayonove, R. Cordonnier and P. Dubois, *C.R. Hebd. Seances Acad. Sci., Ser D*, 281 (1975) 75.
14 R. W. Slingsby, R. E. Kepner, C. J. Muller and A. D. Webb, *Am. J. Enol Vitic.*, 31 (1980) 360.
15 J. O. K. Boison, *Ph.D. Thesis*, McMaster Univerisity, Hamilton, 1985.
16 J. Nordmann and G. D. Mattioda, *Fr. M. Pat.*, 7593 (1970).
17 M. Makoto and M. Hoshino, *Jekeikai Med. J.*, 23 (1976) 189.

Journal of Chromatography, 522 (1990) 329–343
Elsevier Science Publishers B.V., Amsterdam

CHROM. 22 660

Analysis of haloalkanes on wide-bore capillary columns of different polarity connected in series

G. CASTELLO*, A. TIMOSSI[a] and T. C. GERBINO[a]
Istituto di Chimica Industriale, Università di Genova, Corso Europa 30, 16132 Genova (Italy)
(First received October 7th, 1988; revised manuscript received June 12th, 1990)

ABSTRACT

Thirty chloro-, bromo- and iodo-methanes, -ethanes and -ethenes, with one or more identical or different halogen atoms in the molecule, that can be present as contaminants in polluted surface or underground water were separated by using non-polar (SPB-1) and polar (Supelcowax-10) wide-bore capillary columns connected in series. Retention times and indices were measured at different temperatures and carrier gas flow-rates. The most efficient combination was obtained by connecting the two columns in the order non-polar + polar, which permitted the complete resolution of 26 compounds, while two were partially separated and two were co-eluted. The non-polar column alone co-eluted nine, the polar column eight and the polar + non-polar arrangement four compounds. The polarity of the coupled columns system was evaluated by using Rohrschneider and McReynolds constants with respect to various polarity probes, and by comparison of the slopes and intercept values of the straight lines obtained by plotting the retention values of various homologous series of compounds as a function of the number of carbon atoms in the molecule.

INTRODUCTION

The use of wide-bore capillary columns for the gas chromatographic analysis of halogenated contaminants in environmental samples such as waste water, surface and underground water and contaminated soil, was discussed previously [1] as an improvement of the classical methods that use polar and non-polar packed columns [2–8] after extraction with headspace, purge-and-trap or liquid–liquid partition methods [9,10]. The use of non-polar (SPB-1) and polar (Supelcowax-10) wide-bore columns permitted the separation and identification of 35 different halo-methanes, -ethanes and -ethenes, containing one or more chlorine, bromine or iodine atoms in the molecule. Only nine compounds were not completely resolved on the non-polar and eight on the polar column, compared with 14 and 8, respectively, that gave coincident peaks on packed columns. The simultaneous (parallel) use of two capillary columns of different polarity requires a dual-channel capillary gas chromatograph with two simultaneous injections of the same sample, which can be difficult when the headspace

[a] Present address: CASTALIA, Società Italiana per l'Ambiente SpA, Via dei Pescatori 35, 16129 Genova, Italy.

0021-9673/90/$03.50

method is used for the sample extraction and concentration. In this instance, a unique injection followed by 50:50 splitting of the sample in the two columns installed in the same oven and connected to two identical detectors may be a better choice, but this technique often requires complex changes of the standard pneumatic connections of the instrument (pressure and flow controllers, detector make-up lines) and a precise inter-calibration of the response of the two electron-capture detectors.

Satisfactory results were obtained previously by using mixed polar and non-polar packed columns, obtained by homogeneous mixing of two stationary phases in the same tubing [3] or by a series arrangement of different lengths of polar and non-polar columns [2]. Therefore, the series connection of two wide-bore capillary columns was tested in order to establish whether this technique could permit the complete separation of a very complex mixture of many haloalkanes, similar to the samples that can be found in the polluted environment.

In spite of the better efficiencies and shorter analysis times obtainable with narrow-bore capillary columns, the use of wide-bore columns, whose application is becoming more popular [11], seems to be convenient for the analysis of volatile halocarbons in polluted waters, owing to the possible effect on the quantitative results of the complex procedure of sample extraction and concentration. Some causes of errors were investigated previously: different partition coefficients when liquid–liquid extraction procedures are followed [12]; different polarities, vapour pressures, extraction temperatures, salt concentrations and air/water volume ratios in the headspace methods [2,12]; and different sensitivities and linear dynamic ranges of the electron-capture detector for various compounds whose concentrations in authentic samples may cover a range of several order of magnitude [12].

This means that, when precise quantitative analyses are required, *e.g.*, for official or forensic purposes, a series of calibrations and linearity checks have to be carried out previously: linearity and reproducibility of liquid–liquid or headspace extraction method and linearity and relative response of the electron-capture detector to the various compounds. The use of narrow-bore capillary columns, which requires splitting injectors owing to their reduced sample capacity, may add further uncertainty to the precision of quantitative analysis. The split injection technique is notorious for showing severe discrimination and poor quantitation [13]. First, the linearity of the available splitting systems, which is good enough when mixtures of compounds having similar vapour pressures are injected (methyl and butyl esters, silyl ethers, heptofluorobutyrate derivatives), may be questionable when samples containing compounds whose boiling points range between 30 and 250°C are injected, and would require a further calibration procedure for the determination of correction factors to be applied when different extraction techniques are used.

Experimental tests carried out by using different arrangements of split–splitless systems with narrow-bore columns showed that an relative standard deviation of 5% of the quantitative results is obtained in multiple consecutive samples by skilled operators by using simple splitting systems (manually adjusted at a fixed splitting ratio). This deviation increases to $\pm 10\%$ when manual systems are used by different operators or when they are re-tuned to the same nominal splitting ratio after any change of the column or of the operating conditions, and may be as high as 12% when more complex automatic systems operated by electronic devices (which control system back-pressures following keyboard input of the desired splitting ratio, column parameters, etc.) are used.

These deviations are much greater than other fluctuations due to the sampling procedure (effects on the headspace technique of temperature, partition coefficients, etc.) and are likely to be the main reason for unacceptable quantitative results. Therefore, the direct injection of the whole sample without any splitting or partition, possible with wide-bore columns, will ensure that all of the injected compounds are delivered to the detector.

Moreover, a high sample capacity is sometimes needed in trace analysis, when the compounds of interest are present in very low concentrations in the organic solvent or in the gas sample coming from liquid–liquid or headspace extraction: injections of microlitres of liquid or hundreds of microlitres of gas are common when the detection of compounds in the sub-ppb range is required.

A further advantage of wide-bore over narrow-bore capillary columns is their greater resistance to contamination from unexpected compounds that can be present in environmental samples, in industrial effluents or in landfill sites. Thousands of samples coming from heavily polluted environments or hazardous waste sites were analysed, as received or after simple clean-up, by means of wide-bore columns with a negligible decrease in efficiency, while narrow-bore columns had to be replaced or frequently decontaminated if a complicated clean-up procedure was not carefully followed.

EXPERIMENTAL

The analyses were carried out by using a Varian (Palo Alto, CA, U.S.A.) Model 3700 gas chromatograph equipped with a nickel-63 electron-capture detector, a flame ionization detector, linear temperature programming and a Varian Vista 402 integration and data acquisition system.

Two wide-bore glass capillary columns (60 m × 0.75 mm I.D.) were used: a non-polar dimethylpolysiloxane (SPB-1) and a polar polyethylene glycol (Supelcowax-10) (Supelco, Bellefonte, PA, U.S.A.). The two columns were installed in the instrument oven by using the Supelco conversion kit for direct injection (without initial sample splitting) and a make-up gas detector adapter that supplied the correct amount of carrier gas (nitrogen) to the electron-capture detector. The two columns were connected in series with flexible fused-silica capillary tubing and zero-volume connectors. The carrier gas flow-rate into the columns was set at 4 ml/min, a good compromise between maximum efficiency and suitable analysis speed. The column back-pressure was monitored at the injection port with an accuracy of ± 1 Torr (133 Pa) by using a mercury micromanometer.

Standard solutions of the analysed compounds were prepared at various concentrations (between 10^{-3} and 1 g/l) to take into account the different responses of the electron-capture detector to various halogenated components and obtain peaks of comparable area or height. The shape of the peaks could therefore change slightly when concentrated samples were injected, but the capacity of the columns (about 15 μg per peak) was greater than the maximum amount of a single compound injected (about 0.5 μg) and therefore column saturation phenomena were avoided.

RESULTS AND DISCUSSION

The compounds studied are listed in Table I, and their boiling points, molecular weights, adjusted retention times and retentions relative to 1,1,2-trichloroethylene are

TABLE I

ADJUSTED RETENTION TIMES, t'_R, AND RETENTION RELATIVE TO 1,1,2-TRICHLOROETHYLENE, r, OF HALOGENATED HYDROCARBONS ANALYZED ON SERIES ARRANGEMENTS OF POLAR (P) AND NON-POLAR (NP) WIDE BORE CAPILLARY COLUMNS AT 75°C (BOILING POINTS AND MOLECULAR WEIGHTS ARE ALSO REPORTED)

No.	Compound	B.p. (°C)	Mol.wt.	P + NP		NP + P	
				t'_R (min)	r	t'_R (min)	r
1	1,1,1,2-Tetrabromoethane	112	345.67	10.03	1.10	9.92	1.09
2	1,1,1,2-Tetrachloroethane	130.5	167.85	42.61	4.69	41.40	4.55
3	1,1,2,2-Tetrabromoethane	243.5	345.67	–	–	–	–
4	1,1,2,2-Tetrachloroethane	146.2	167.85	182.27	20.00	171.87	18.90
5	1,1,2-Trichloroethane	113.8	133.41	39.65	4.36	37.80	4.15
6	1,1,2-Trichloroethylene	87	131.39	9.09	1.00	9.10	1.00
7	1,1-Dichloroethane	57.28	98.96	4.12	0.45	4.06	0.45
8	1,1-Dichloroethylene	37	96.94	1.81	0.20	1.86	0.20
9	1,2-Dibromoethane	131.36	187.87	40.24	4.43	38.66	4.25
10	1,2-Dichloroethane	83.74	98.96	11.86	1.30	11.39	1.25
11	1,2-Diiodoethane	200	281.86	–	–	–	–
12	1-Bromo-2-chloroethane	107	143.20	22.01	2.42	21.04	2.31
13	Bromochloromethane	68.11	129.39	10.28	1.13	9.67	1.06
14	Bromoethane	38.4	108.97	2.13	0.23	2.14	0.23
15	Tribromomethane	149.5	252.75	116.37	12.80	110.23	12.10
16	Tetrabromomethane	189	331.65	–	–	–	–
17	Tetrachloromethane	76.54	153.82	5.27	0.58	5.42	0.60
18	*cis*-1,2-Dichloroethylene	60.3	96.94	7.39	0.81	7.05	0.77
19	Trichloromethane	61.7	119.38	8.75	0.96	8.19	0.90
20	Chloroiodomethane	109	176.38	27.14	2.98	25.88	2.84
21	Dibromochloromethane	119	208.29	49.20	5.41	46.87	2.84
22	Dibromomethane	97	173.85	22.01	2.42	21.04	2.31
23	Dichlorobromomethane	90	163.83	20.72	2.28	19.87	2.18
24	Dichloromethane	40	84.93	4.72	0.52	4.55	0.50
25	Diiodomethane	182	267.84	148.83	16.40	140.66	15.46
26	Hexachloroethane	186	236.74	137.30	15.10	136.70	15.02
27	Iodoethane	72.3	155.97	4.56	0.50	4.37	0.48
28	Triiodomethane	218	393.73	–	–	–	–
29	Iodomethane	42.4	141.94	2.66	0.29	2.63	0.29
30	1,1,1-Trichloroethane	74	133.41	5.00	0.55	5.01	0.56
31	Pentachloroethane	162	202.30	119.15	13.10	115.13	12.65
32	Tetrachloroethylene	121	165.83	14.45	1.59	14.98	1.65
33	*trans*-1,2-Dichloroethylene	47.5	96.94	3.53	0.39	3.49	0.38
34	Trichlorobromomethane	104.7	198.28	14.45	1.59	14.42	1.58
35	1-Iodopropane	102.4	169.99	8.75	0.96	8.87	0.97
36	1-Iodobutane	130.5	184.02	16.69	1.84	17.02	1.87
37	1-Iodopentane	157	198.05	32.84	3.61	33.64	3.70
38	1-Iodohexane	181.3	212.08	64.94	7.14	66.79	7.34
39	1-Iodoheptane	204	226.10	129.19	14.20	133.33	14.60

shown for the two series arrangements. Some compounds are listed that were not analysed on the coupled column system, owing to their too long retention times. They were included in Table I in order to maintain the same reference numbers used in a previously published paper on the behaviour of separate columns [1]. Figs. 1 and 2 show the chromatograms obtained by injecting the mixture of compounds.

The P + NP arrangement required about 200 min for the complete analysis, which is much longer than needed with the non-polar column alone (about 50 min) and about 25% greater than that with the polar column alone (150 min), but the resolution of the components increased greatly in comparison with the analyses carried out on separate columns. While nine compounds were not resolved on the non-polar and eight on the polar column [1], with the P + NP arrangement there were only three unresolved peaks, due to simultaneous elution of the compounds: 1-bromo-2-chloroethane and dibromomethane (peaks 12 and 22); tetrachloroethylene and trichlorobromomethane (peaks 32 and 34); and trichloromethane and 1-iodopropane (peaks 19 and 35). Lack of resolution of the last pair of peaks is not important from a practical point of view, because 1-iodopropane is not generally present in environmental samples and was added to the mixture only for the determination of the retention indices of other compounds with respect to the 1-iodoalkane homologous series, I_{ni} [1,14,15].

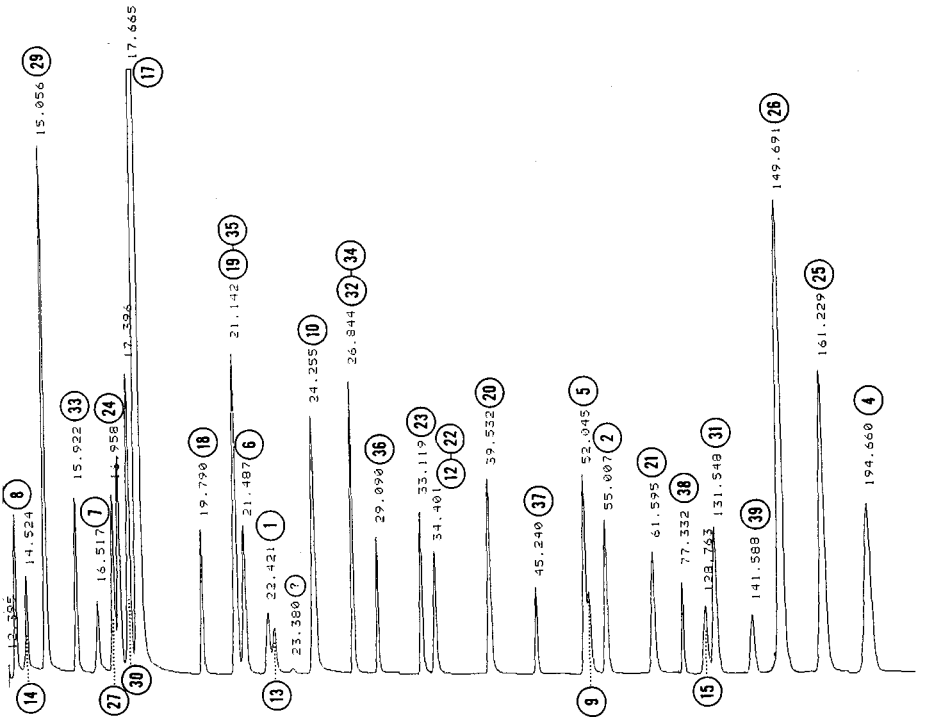

Fig. 1. Chromatogram of the mixture of compounds listed in Table I with a series arrangement of polar (Supelcowax 10) followed by non-polar (SPB-1) wide-bore columns (each 60 m × 0.75 mm I.D.). Temperature, 75°C. Carrier gas (nitrogen) flow-rate, 4 cm^3/min. Variable chart speed: time markers on abscissa represent 1-min intervals; retention times (min) are shown on peak apices.

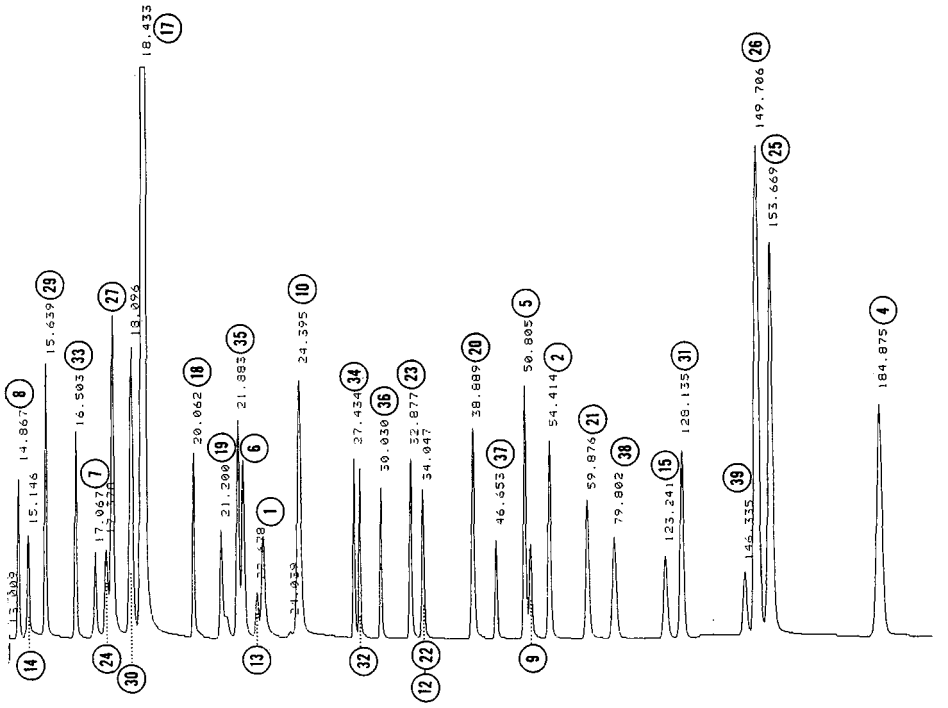

Fig. 2. Chromatogram of the mixture of compounds listed in Table I with a series arrangement of non-polar (SPB-1) followed by polar (Supelcowax 10) wide-bore columns (each 60 m × 0.75 mm I.D.). Temperature, 75°C. Carrier gas (nitrogen) flow-rate, 4 cm^3/min. Variable chart speed: time markers on abscissa represent 1-min intervals; retention times (min) are shown on peak apices.

The NP + P arrangement permitted the resolution of all the compounds, except the pair 1-bromo-2-chloroethane and dibromomethane (peaks 12 and 22), in a time slightly shorter than that needed for complete elution with the P + NP arrangement. This confirms that, for complete resolution of complex mixtures, the selectivity of the column due to slight changes in polarity may be more important than the simple increase in efficiency. In fact, it was observed that the number of theoretical plates, n, was slightly higher in the P + NP arrangement, whereas the separation was better and faster with the reversed column sequence. Moreover, peaks 12 and 22, which were easily resolved on both non-polar and polar individual columns [1], were not separated on coupled columns, showing that the different polarities of the two phases are nearly exactly compensated.

Effect of the polar/non-polar phase ratio

The optimization ("tuning") of the selectivity of coupled columns requires a proper choice of the lengths of the polar and non-polar sections. The optimization of the gas chromatographic separation by using the "window analysis" method was previously suggested for packed columns by Laub and Purnell [16] and further applied by the same group to capillary columns connected in series [17]. More recently, Purnell and Williams [18] published a general theory on the series connection of

chromatographic columns that permits the optimization of the speed of analysis in systems of two columns in series by using the window method and taking into account the pressure gradient.

In this method, the tuning is carried out by optimization of the weight ratio of homogeneously mixed liquid phases or by changing the relative lengths of columns connected in series.

Other selectivity tuning methods have also been suggested that modify the residence times of the carrier gas in the two columns or change the temperature of the column in a different way by using appropriate programming rates [19,20] or installing the column in separate ovens and operating them with different temperature programming [21].

These methods of selectivity tuning of multiple columns in series have also been denoted "multi-chromatography", which should not be confused with the similar term "multi-dimensional chromatography" (MDGC), which indicates a technique in which separate columns are operated in a parallel arrangement and some components that are not well resolved are selectively removed from one column and transferred to the other in order to permit a better resolution of some peak groups.

The aim of this work was to devise a procedure that, by using standard gas chromatographic equipment, without modification of the flow or pressure controls [20] or the need for two separately temperature programmed column ovens [21], would permit the selectivity of the mixed columns to be tuned in order to achieve a satisfactory separation of the compounds present in environmental samples.

This procedure seems rapid enough to be used routinely in control laboratories: the analysis of a standard mixture or of an authentic sample on separate non-polar and polar columns, the tracing of the graphs, the choice of the best arrangement and the connection of two different lengths of columns can permit a column tuned for the required separation to be rapidly obtained. Being a simple system, without a variable initial splitting or separate control of pressure, flow-rates and temperature in the two parts of the column, this series arrangement would behave in an unchanged manner for long periods and does not require frequent calibration and checking of the various parameters.

It should be taken into account, from the practical point of view, that simply by increasing the temperature this column can be used for the analysis of high-boiling samples such as chlorinated pesticides and polychlorinated biphenyls (PCBs), therefore requiring less frequent column changes and reconditioning of the column–electron-capture detector system.

Previous studies on mixed packed columns [2,3] showed that the best resolution of a mixture of compounds similar to that studied in this work can be obtained by using a column made with a 40:60 ratio of polar (SP-1000) and non-polar (OV-1) stationary phases. Further, a nearly linear variation of the resolution of the various compounds with the composition of the mixed phase was found.

The same behaviour was observed with wide-bore capillary columns. Figs. 3–5 show the retention values with respect to trichloroethylene, r, of the compounds listed in Table I, on polar (left) and non-polar (right) columns. The three graphs are shown with different expansions of the vertical axis (where r values are reported), in order to reduce the coincidence of lines for different compounds that eluted close together. On each line the experimental r values with the P + NP arrangement (triangles) and

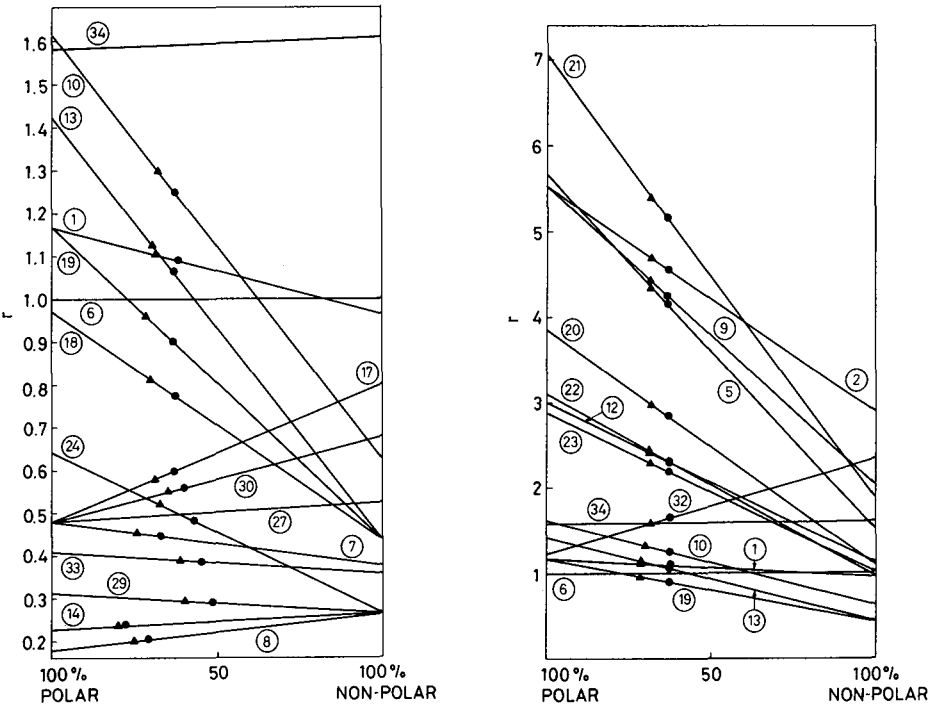

Fig. 3. Retention values with respect to trichloroethylene on polar (Supelcowax 10, left) and non-polar (SPB-1, right) wide-bore columns of compounds listed in Table II. On the connecting lines (theoretical r values on mixed-phase columns) the experimental r values obtained with polar column upstream (▲) and downstream (●) are shown.

Fig. 4. Same as Fig. 3 with a smaller vertical scale in order to show slowly eluted compounds.

NP + P arrangement (circles) are shown, indicating that the behaviour of the series connection of two wide-bore columns having the same length does not correspond to a 50:50 ratio of stationary phases, but is equivalent to a mixed-phase column having a nominal composition with 68–69% of polar phase when the polar column is upstream (directly connected to the injector), and with 63–64% of polar phase when the polar column is downstream (connected to the detector). Some deviations from these values were observed for the fast-eluted compounds, but this is probably due both to errors in the determination of short retention times and to the near-horizontal behaviour of the lines, which causes large variations of the abscissa value with small changes in the r values.

The constant values of the nominal phase composition show that the influence of the polar column is greater than that of the non-polar column, and that this influence increases when the column is connected upstream and thus operates at higher pressure and with a lower linear velocity of the carrier gas. This permits the r value of each compound on mixed columns to be calculated with a good approximation when the r values on each separate column are known and some reference compounds have previously been analysed in order to find their nominal phase ratio. Further, the choice of the abscissa value where the vertical distance between the lines of every pair of

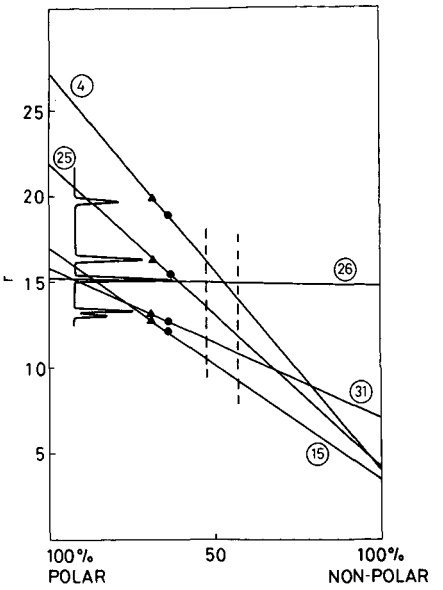

Fig. 5. Same as Figs. 3 and 4 with a smaller vertical scale in order to show the last-eluted compounds. The chromatogram of these compounds at 75°C with the polar column upstream is also shown. Dashed vertical lines show the nominal polar/non-polar ratios where the best resolution of these compounds is expected.

compounds is greatest obtained directly on the graphs in Figs. 3, 4 and 5, or by using the window diagram method [16], permits the preparation of coupled columns with different lengths of non-polar and polar wide-bore capillaries, in order to optimize both resolution and speed of analysis.

As an example, in Fig. 5 the chromatogram of five slow-eluting peaks (Nos. 4, 15, 25, 26 and 31 as listed in Table I) is superimposed on the graph with a scale that shows the correspondence of each peak with r at the nominal composition (68% of polar phase) with the polar column upstream (triangles). The circles on the same graph show that with the polar column downstream the resolution between peaks 25 and 26 decreases, as confirmed by the t'_R values given in Table I. The simple observation of Fig. 5 or the more reliable use of the window diagram method shows that the best separation of the five compounds would be obtained with two different columns having a nominal composition of about 53% or 43% of polar phase (dashed vertical lines in Fig. 5). The better choice (43%) shows an inversion of the elution order between peaks 4 and 26, and gives the shortest analysis time.

The experimental preparation of a P + NP column having the above nominal composition must take into account that a column made by combination of equal lengths of Supelcowax 10 and SPB-1 columns (with the polar column upstream) behaves as a mixed column with 68:32 polar/non-polar ratio. Simple proportion leads to the conclusion that a ratio between polar and non-polar column lengths of 39:61 and 32:68, respectively, would correspond to 53% and 43% nominal concentrations of the polar phase. In practice, the intact non-polar column used in this study (SPB-1, 60 m long) should be connected downstream to a shorter length of polar Supelcowax 10 column, (40 or 28 m, respectively) in order to obtain the separations indicated with

dashed lines in Fig. 5. These length values are valid as a first-degree approximation and for the compounds in Fig. 5 only, and should be recalculated by taking into account all the components of the mixture, which may give interfering peaks, but it is interesting to observe that the 39:61 ratio calculated above is identical with the 40:60 ratio found suitable for the best resolution in mixed-phase packed columns [3].

Effect of temperature

It is known that relative retention values of compounds having different polarities change with column temperature in different ways, mainly on polar columns. The values of r shown on the left-hand ordinate in Figs. 3–5 change slightly with temperature and therefore the intersection points of the lines for different compounds move toward more or less polar compositions of the stationary phase, but it has been found experimentally that temperature changes (in the range 60–115°C) of the two wide-bore columns connected in series (isothermal analysis) do not appreciably change the elution order of peaks. Only a few unresolved peaks show inversion of elution order: peaks 32 and 34 at 70°C and peaks 1 and 13 at 87°C with the P + NP arrangement; peaks 1 and 13 at 63°C on the NP + P column. Of course, higher temperatures often decrease the resolution of partially coincident peaks and lower temperatures lead to very long analysis times.

The greatest influence on the separation was observed when the temperature of the columns was programmed during analysis. Many combinations of the initial isothermal value and programming rate were tested, giving various relative changes of the retentions of many peaks. As commercially available capillary columns (even if from the same producer) may differ in performance, only experimental tests can lead to the correct choice of the best temperature programme for a given separation. A general rule is that temperature increase has a greater effect on the behaviour of slowly eluted compounds, and decreases the influence of the downstream column. In fact, less retained compounds elute when the column temperature is not appreciably changed, while slowly moving peaks are retained at low temperatures in the upstream column and increase their migration speed in the second column at higher temperatures. This effect is more evident with the P + NP arrangement. For example, with the P + NP column connection, an initial isothermal hold at 75°C for times ranging between 15 and 25 min, followed by programming rates of 5–10°C/min up to 120–150°C, produced a separation that, on the basis of the r values, would correspond to a nominal phase composition of about 80% of polar phase, compared with 68% observed with a 75°C isothermal run.

In contrast, with the NP + P arrangement, similar programming rates only gave a change of nominal phase composition from 63 to 60% of polar phase. Temperature programming can therefore be used as a method to change the overall polarity of the coupled columns system slightly, which is obviously more convenient than cutting the column. On the other hand, it was reported above that equal lengths of polar and non-polar columns correspond to a nominal P/NP ratio (P column upstream) of about 70:30. The best choice therefore seems to be to use a coupled column formed with a shorter length of polar column mounted upstream and to change the overall polarity by suitable temperature programming, which can also reduce the total analysis time to below 1 h.

Evaluation of the polarity of coupled columns

The methods of Rohrschneider [22] and McReynolds [23] for the classification of the polarity of stationary phases requires the determination of the retention indices values of various "polarity probes" on squalane and on the stationary phase under study, and the calculation of the ΔI values for each probe. An average polarity value is also obtained by sum of the ΔI values for five probes (benzene, ethanol, methyl ethyl ketone, nitromethane and pyridine in the Rohrschneider method; benzene, 1-butanol, methyl propyl ketone, nitropropane and pyridine in the McReynolds method). These methods are therefore complicated, requiring the analysis of complex mixtures of the probes with *n*-alkanes. For capillary columns, moreover, columns filled with squalane are often unavailable or cannot be used at high temperatures.

By taking into account the low polarity of the non-polar SPB-1 wide-bore column used, filled with polymeric dimethylpolysiloxane, which shows low values of the McReynolds constants, similar to those for OV-1, SE-30, etc., *i.e.*, 16, 55, 44, 65 and 42 for the probes listed above [24], the calculation of the ΔI values with respect to SPB-1 is accurate enough for the comparison of the behaviour of the coupled column with respect of those of the individual non-polar and polar columns.

Table II shows the I, t'_R and ΔI values for P + NP and NP + P arrangements. The average polarity values, *i.e.*, the sum of ΔI values for the Rohrschneider and McReynolds probes, differ slightly and are equal to about half of the sums for the polar column alone. This does not agree with the experimental results discussed above, showing that the polarity of the coupled columns is more similar to that of the polar column (60–70%, depending on the carrier gas flow direction). The use of ΔI values therefore gives information on the physical composition of the column (the same lengths of P and NP sections) but does not permit the prediction of its behaviour in the analysis of halogenated compounds.

The use of CP-index values suggested by ChromPack International [25] for the polarity classification of capillary columns leads to the same results for the simple sum of ΔI values discussed above, because it is also derived from the McReynolds constants. Moreover, it requires a knowledge of the I values for the most polar stationary phase actually known (cyanosilicone OV-275), used as the upper reference term, while squalane is the lower polarity reference, and this further increases the complexity of its determination. The CP-index values calculated for the columns used in this work were 5 for non-polar SPB-1, 52 for polar Supelcowax 10, 27.4 for the P + NP and 27.9 for the NP + P arrangement. Again, the values for coupled columns represent the physical composition of the system but are not correlated with the effective separation behaviour.

Another and simpler method for the determination of relative polarity values of capillary columns was suggested previously [1] that compares the behaviour of polar columns with that of non-polar columns by measuring the difference between the intercept values of the straight lines obtained by plotting the ln t'_R values for compounds belonging to various homologous series as a function of the number of carbon atoms in the molecule, or by graphical determination of the horizontal distance between parallel lines for different homologous series, expressed as the difference in equivalent carbon atoms number (ΔC). Fig. 6 shows the linear behaviour of *n*-alkanes, 1-alkanols and 1-bromo- and 1-iodoalkanes on NP + P and P + NP coupled columns. Table III reports the values of the slope, m, intercept, p, correlation

TABLE II

I VALUES OF ROHRSCHNEIDER AND McREYNOLDS PROBES ON NON-POLAR SPB-1 (NP) AND POLAR SUPELCOWAX 10 (P) WIDE-BORE CAPILLARY COLUMNS; t'_R AND *I* VALUES ON P + NP AND NP + P COUPLED COLUMNS, AND DIFFERENCES (ΔI) CORRELATED WITH POLARITY (SEE TEXT)

t_M = Column dead time (min).

No.	Compound	$I^{(NP)}$	$I^{(P)}$	$I^{(P)} - I^{(NP)}$	P + NP (t_M = 13.93)			NP + P (t_M = 14.14)		
					t'_R	$I^{(P+PN)}$	$I^{(P+NP)} - I^{(NP)}$	t'_R	$I^{(NP+P)}$	$I^{(NP+P)} - I^{(NP)}$
1	Benzene	661.6	967.7	306.1	7.59	766.7	105.1	7.42	776.1	114.5
2	Ethanol	414.4	940.7	526.3	5.13	714.4	300.0	4.27	702.8	288.4
3	1-Butanol	658.7	1145.9	487.2	21.07	905.1	246.4	18.92	903.1	244.4
4	Methyl ethyl ketone	582.7	923.3	340.6	5.08	713.2	130.5	4.86	719.9	137.2
5	Methyl propyl ketone	664.6	997.6	332.8	8.94	788.6	124.0	8.72	797.6	133.0
6	Nitromethane	543.4	1160.9	617.3	20.89	904.0	360.6	18.87	902.8	359.4
7	Nitropropane	709.8	1219.3	509.5	32.12	960.7	250.9	29.90	963.1	253.3
8	Pyridine	731.5	1190.1	458.1	27.98	942.5	211.0	26.27	946.2	214.7
9	1-Iodobutane	806.2	1067.0	260.8	18.54	887.9	81.7	18.50	900.2	94.0
Sum ΔI (Rohrschneider) (1+2+4+6+8)				2248.6			1107.2			1114.2
Sum ΔI (McReynolds) (1+3+5+7+8)				2093.7			937.4			959.9

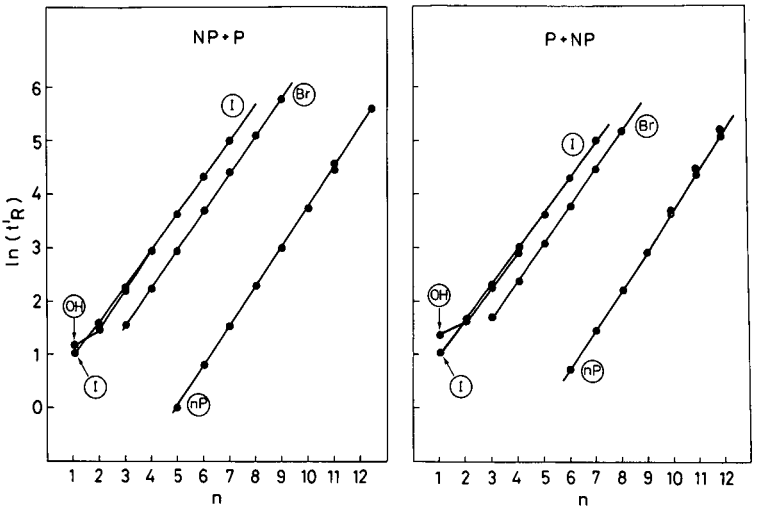

Fig. 6. Linear behaviour of the $\ln(t'_R)$ of terms of homologous series of linear alkanes (nP), 1-bromoalkanes (Br), 1-iodoalkanes (I) and n-alkanols (OH) as a function of the number of carbon atoms in the molecule (n) with series column arrangements.

coefficient, r, and ΔC measured from the horizontal distance between the line for n-alkanes and that for other homologous series.

As suggested previously [1], the ΔC value for 1-alkanols is probably the best way to identify rapidly the difference in polarity due to hydrogen-bond formation. These values for coupled columns are the average of the values for the non-polar and polar columns alone, and therefore agree with the values of average polarity listed in Table II and obtained by the sum of the ΔI values of Rohrschneider or McReynolds constants, and with the CP-index values reported above.

The determination of ΔC values for 1-alkanols is much easier than the calculation of ΔI or CP-index values, because it can be obtained by injecting

TABLE III

SLOPE, m, INTERCEPT, p, AND CORRELATION COEFFICIENT, r, OF STRAIGHT LINES OF $\ln t'_R$ AS A FUNCTION OF THE NUMBER OF CARBON ATOMS IN VARIOUS HOMOLOGOUS SERIES, AND HORIZONTAL DISTANCE BETWEEN PARALLEL LINES IN FIG. 6, Δc, USED AS A MEASURE OF THE COLUMN POLARITY

Column arrangement	Compounds	m	p	r	Δc
NP + P	n-Alkanes	0.755	−3.772	1.000	–
	1-Iodoalkanes	0.674	0.273	1.000	4.80
	1-Bromoalkanes	0.705	−0.559	1.000	3.90
	1-Alkanols	0.744	−0.036	1.000	4.40
P + NP	n-Alkanes	0.752	−3.832	1.000	–
	1-Iodoalkanes	0.660	0.315	0.999	5.10
	1-Bromoalkanes	0.699	−0.417	1.000	4.30
	1-Alkanols	0.707	0.218	1.000	5.00

only four compounds, *i.e.*, two *n*-alkanes and two 1-alkanols with a number of carbon atoms different enough to permit a precise calculation of the parameters of the straight lines in Fig. 6.

CONCLUSIONS

The use of a series arrangement of wide-bore capillary columns of different polarity permits the complete separation of many halogenated compounds that can occur in polluted environmental samples by application of the standard extraction and concentration procedures: headspace extraction, liquid–liquid partition, purge-and-trap method, etc. The high capacity of wide-bore columns compared with narrow-bore capillaries does not require injection splitting of the sample, which may be the source of uncertainty in quantitative analysis owing to different volatilities of the analyte compounds. The same columns, by increasing the temperature, can be used for the analysis of high-boiling samples such as chlorinated pesticides and PCBs, therefore requiring less frequent column changes and reconditioning of the column–detector system.

The overall polarity of the coupled column system changes when the order of connection is reversed, and this can be used to optimize the separation of closely eluting compounds, in conjunction with temperature programming. Twenty-six compounds were separated with this technique, compared with nineteen resolved on a non-polar wide-bore capillary, 20 on a polar wide-bore capillary and 24 with a series arrangement of non-polar and polar packed columns.

ACKNOWLEDGEMENT

This work was supported by the Ministero Pubblica Istruzione, Italy.

REFERENCES

1 G. Castello, A. Timossi and T. C. Gerbino, *J. Chromatogr.*, 454 (1990) 129.
2 G. Castello, T. C. Gerbino and S. Kanitz, *J. Chromatogr.*, 247 (1982) 263.
3 G. Castello and T. C. Gerbino, *J. Chromatogr.*, 366 (1986) 59.
4 L. D. Hinshaw, *J. Gas Chromatogr.*, 8 (1966) 300.
5 D. A. Solomons and J. S. Ratcliffe, *J. Chromatogr.*, 76 (1973) 101.
6 L. Zilka and H. Hatucha, *J. Chromatogr.*, 148 (1978) 229.
7 E. A. Dietz, Jr., and K. F. Singley, *Anal. Chem.*, 51 (1979) 1809.
8 G. Agazzotti and G. Predieri, *Water Res.*, 8 (1986) 959.
9 *The Analysis of Trihalomethanes in Finished Waters by the Purge and Trap Method, Method 501.1*, United States Environmental Agency, Environmental Monitoring and Support Laboratory, Cincinnati, OH, 1979.
10 *The Analysis of Trihalomethanes in Drinking Water by Liquid/Liquid Extraction Method, Method 501.2*, United States Environmental Agency, Environmental Monitoring and Support Laboratory, Cincinnati, OH, 1979.
11 K. Grob and F. French, *Int. Lab.*, 18 (1988) 18.
12 G. Castello, T. C. Gerbino and S. Kanitz, *J. Chromatogr.*, 351 (1986) 165.
13 P. Dawes and M. Cumbers, *Int. Lab.*, 19 (1984) 34.
14 G. Castello and G. D'Amato, *J. Chromatogr.*, 76 (1973) 293.
15 G. Castello and G. D'Amato, *J. Chromatogr.*, 79 (1973) 33.
16 R. J. Laub and J. H. Purnell, *J. Chromatogr.*, 112 (1975) 71.

17 J. H. Purnell, P. S. Williams and G. A. Zabierek, in R. E. Kaiser (Editor), *Proceedings of the 4th International Symposium on Capillary Chromatography*, Hüthig, Heidelberg, 1981, p. 573.
18 J. H. Purnell and P. S. Williams, *J. Chromatogr.*, 325 (1985) 1.
19 J. V. Hinshaw, Jr., and L. S. Ettre, *Chromatographia*, 21 (1986) 561.
20 J. V. Hinshaw, Jr., and L. S. Ettre, *Chromatographia*, 21 (1986) 669.
21 P. Sandra, F. David, M. Proot, G. Diricks, M. Verstappe and M. Verzale, *J. High Resolut. Chromatogr. Chromatogr. Commun.*, 8 (1985) 782.
22 L. Rohrschneider, *J. Chromatogr.*, 22 (1966) 6.
23 W. A. McReynolds, *J. Chromatogr. Sci.*, 8 (1970) 685.
24 *Chromatographic Supplies, International Catalog*, No. 26 Supelco, Bellefonte, PA, 1988, p. 100.
25 *General Catalog*, Chrompack International, Middelburg, 1986, p. 7.

Journal of Chromatography, 522 (1990) 344
Elsevier Science Publishers B.V., Amsterdam

CHROM. 22 818

Book Review

Chromatography/Fourier transform infrared spectroscopy and its applications, by R. White, Marcel Dekker, New York, Basle, 1990, VI + 328 pp., price US $ 99.75, ISBN 0-8247-8191-0.

The hyphenation of separation methods with a variety of modern spectroscopic identification techniques represents a major and continuing field of activity in chromatographic science. This clear and well produced book summarises methods for the combination of Fourier transform infrared spectroscopy (FT-IR) with gas chromatography (GC), high-performance liquid chromatography (HPLC) [and briefly supercritical fluid chromatography (SFC)] and thin-layer chromatography (TLC). The author eminently succeeds in his stated aim to provide both an introduction, and an up-to-date reference source for those experienced in FT-IR detection in chromatography.

There are six chapters. In the first, the general characteristics of all chromatography–FT-IR interfaces are discussed; particular attention is paid to the inevitable compromises imposed, on the one hand, on the chromatographic resolution by the requirements of the FT-IR method, and on the other on the enrichment factor and yield of solute which influence the quality of the FT-IR. The main features of the interfaces for GC, HPLC and TLC are described respectively in Chapters 2, 3 and 4; the pros and cons of each method are set out, with emphasis on practical aspects. Chapter 5 describes the methods for identification of separated components of mixtures, with emphasis on library searching, pattern recognition and expert systems. Each of these chapters has brief sections setting the current state of the art in historical context. Finally, Chapter 6, the longest chapter in the book, contains numerous applications of chromatography–FT-IR, including many drawn from environmental analysis, as well as others from fuel, natural product, pharmaceutical and industrial chemistry; here the reasons for the choice of a particular chromatographic method are well explained.

The references, collected at the end of each chapter, are taken from the literature up to the end of 1988. This means, inevitably, that the recent and rapid growth in the combination of SFC with FT-IR, *e.g.* in the use of xenon mobile phase in flow-cell SFC–FT-IR, could not be included in the HPLC–FT-IR chapter.

Overall, though, this book is to be strongly recommended to both beginner and experienced researcher alike as a source of both practical instrumental instructions and information on how chromatography–FT-IR may be applied.

Leeds (U.K.) KEITH D. BARTLE

Journal of Chromatography, 522 (1990) 345–346
Elsevier Science Publishers B.V., Amsterdam

CHROM. 22 817

Book Review

Modern thin-layer chromatography, edited by N. Grinberg, Marcel Dekker, New York, 1990, XII + 504 pp., price US $ 99.75, ISBN 0-8247-8138-4.

Modern thin-layer chromatography is a multi-authored text reviewing recent developments in thin-layer chromatography (TLC) and emphasizing solute–stationary phase–mobile phase interactions. The various chapters are mainly theoretical and one immediate disappointment with this text is the almost total lack of any supporting practical examples in the descriptive material or in the form of chromatograms. Also, although the title contains the word modern, there are few references to the literature after 1985, and in general, most of the cited work is to pre-1980s literature. These shortcomings have not resulted in a book which is of no value since TLC has been evolving slowly through the 1980s. However, there are some areas such as instrumentation, quantitative applications, chemically bonded phases, and methods development where the book is either already out of date or gives only a weak treatment of the subject.

The book contains three consecutive chapters by Simon Gocan entitled "Stationary phases in TLC", "Mobile phases in TLC" and "Theoretical aspects of TLC". These three chapters are the heart of the book representing about 50% of the text and more than 75% of the references cited. The chapter on stationary phases in TLC contains 810 reference citations alone. The emphasis is on conventional TLC materials and practices as well as an extensive discussion of general chromatographic materials that are more commonly used in column chromatography than TLC. Although most of this material is available elsewhere it has been carefully compiled and arranged and should be of interest to a more general audience than the TLC specialist. A general weakness is the treatment of solvent properties which are treated almost in the absence of any connection to how they would be selected for method development in TLC. The next two chapters are by Gabor Szepesi and deal with quantitation and instrumentation in TLC. These are perhaps the least useful in the book being superficial and already dated. Of course, the latter may not be the authors fault given the unusually long time span between the publication date for the book and the most recent cited references in the bibliography. However, more contemporary and thorough accounts are available for any one particularly interested in these topics. The following chapter is headed, "Special techniques" and is a collection of brief summaries of continuous TLC, forced-flow TLC, bidimensional TLC, gradients in TLC, chiral separations in TLC and preparative TLC. With the exception of preparative TLC, which is too short and contrite to be useful, the other sections portray the directions research in TLC has taken during the 1980s. Again, more dated than is

desirable in a new book, the sections are well constructed and will repay reading. The remaining three chapters deal with "Mobile phase and time optimization", "Relationship between thin-layer and column chromatography", and "Perspectives in TLC". The first two topics are treated theoretically and will be of interest to those workers looking for material on these topics. The optimization chapter could have provided more direction as far as methods development is concerned. The use of practical examples beyond those provided would have been useful in both chapters to demonstrate the use of the theory and the agreement obtained with experiment.

Overall, this is a reasonable book, bringing together some useful material. It is largely a theoretical text and will only be of cursory interest to the bench chemist. To those in academia the contents seem to be already out dated, seriously so in some sections. It can be cautiously recommended to university and industrial libraries for purchase.

Detroit, MI (U.S.A.) COLIN F. POOLE

Author Index

Erratum

J. Chromatogr., 511 (1990) 333–339.
Page 333, the title of the paper should read "Electric properties of photoaffinity-labelled pancreatic A-subtype cholecystokinin receptor".

Instructions to Authors

JOURNAL OF CHROMATOGRAPHY

JOURNAL OF CHROMATOGRAPHY, BIOMEDICAL APPLICATIONS

JOURNAL OF CHROMATOGRAPHY, SYMPOSIUM VOLUMES

Elsevier Science Publishers
Desk-Editorial Office Journal of Chromatography:
Sara Burgerhartstraat 25, 1055 KV Amsterdam, The Netherlands
P.O. Box 330, 1000 AH Amsterdam, The Netherlands
Tel. 31-20-5862793
FAX 31-20-5862304
Telex 10704 espom

ELSEVIER
AMSTERDAM – OXFORD – NEW YORK – TOKYO

General

The JOURNAL OF CHROMATOGRAPHY publishes papers on all aspects of **chromatography, electrophoresis** and related methods. Contributions consist mainly of research papers dealing with chromatographic theory, instrumental development and their applications.

BIOMEDICAL APPLICATIONS. This section, which is under separate editorship, deals with the following aspects: developments in and applications of chromatographic and electrophoretic techniques related to clinical diagnosis or alterations during medical treatment; screening and profiling of body fluids or tissues with special reference to metabolic disorders; results from basic medical research with direct consequences in clinical practice; drug level monitoring and pharmacokinetic studies; clinical toxicology; analytical studies in occupational medicine.

SYMPOSIUM VOLUMES. This publication, which is under separate editorship, publishes proceedings of symposia on chromatography, electrophoresis and related methods.

Types of contributions

The following types of papers are published in the JOURNAL OF CHROMATOGRAPHY and the section on BIOMEDICAL APPLICATIONS: Regular research papers (full-length papers), Review articles and Short Communications. Short Communications are usually descriptions of short investigations, or they can report minor technical improvements of previously published procedures; they reflect the same quality of research as full-length papers, but should preferably not exceed six printed pages. Review articles are invited or proposed in writing to the Editors. An outline of the proposed review should first be forwarded to the Editors for preliminary discussion prior to preparation.

Submission of an article is understood to imply that the article is original and unpublished and is not being considered for publication elsewhere.

Upon acceptance of an article by the journal, the author(s) will be asked to transfer the copyright of the article to the publisher. This transfer will ensure the widest possible dissemination of information.

Submission of papers

Manuscripts (***four*** copies are required), in English, should be submitted to:

for the JOURNAL OF CHROMATOGRAPHY:

Editorial office
JOURNAL OF CHROMATOGRAPHY
P.O. Box 681
1000 AR Amsterdam, The Netherlands

for the BIOMEDICAL APPLICATIONS section:

Dr. K. Macek
The Editor of
JOURNAL OF CHROMATOGRAPHY,
BIOMEDICAL APPLICATIONS
P.O. Box 681
1000 AR Amsterdam, The Netherlands

Manuscripts for the SYMPOSIUM VOLUMES section (*three* copies are required) should be submitted during the symposium concerned. After the symposium, correspondence should be sent by *regular airmail (NOT by registered, special delivery of private mail services)* to the Editor handling the corresponding proceedings, i.e., either:

Dr. E. Heftmann
Editor of
JOURNAL OF CHROMATOGRAPHY,
SYMPOSIUM VOLUMES
P.O. Box 928
ORINDA, CA 94563-0818, U.S.A.

or Dr. Z. Deyl
Editor of
JOURNAL OF CHROMATOGRAPHY,
SYMPOSIUM VOLUMES
Institute of Physiology
Czechoslovak Academy of Sciences
Videnská 1083
14220 PRAGUE 4-Krc
Czechoslovakia

Every paper must be accompanied by a letter from the senior author, stating that he/she is submitting the paper for publication in the *Journal of Chromatography*.

Manuscripts

Manuscripts should be typed in ***double spacing*** on consecutively numbered paper of uniform size. The manuscript should be preceded by a sheet of manuscript paper carrying the title of the paper and the name and full postal address of the person to whom the proofs are to be sent. As a rule, papers should be divided into sections, headed by a caption (*e.g.* Abstract, Introduction, Experimental, Results, Discussion). All illustrations, photographs, tables, etc. should be on separate sheets. **Four** copies of the complete manuscript should be submitted.

Title

The title of the paper should be concise and informative. Since titles ares widely used in information retrieval systems, care should be taken to include the key words. The title should be followed by the authors' full names, academic or professional affiliations, and the address of the laboratory where the work was carried out. If the present address of an author is different from that mentioned, it should be given in a footnote. Acknowledgements of financial support are not to be made in a footnote to the title or name of the author, but should be included in the Acknowledgements at the end of the paper.

Introduction

Every paper must have a concise introduction mentioning what has been done before on the topic described, and stating clearly what is new in the paper now submitted.

Abstract

All articles should have an abstract of 50–100 words which clearly and briefly indicates what is new, different and significant.

Illustrations

The figures should be submitted in a form suitable for reproduction, either drawn in Indian ink on drawing or tracing paper, or as sharp glossy prints. Axes of a graph should be clearly labelled. Please note that any lettering should also be in a form suitable for reproduction. Lettering (which should be kept to a minimum) and spacing on axes of graphs should be such that numbers, etc., remain legible after reduction. One original and three photocopies are required. The figures should preferably be of such a size that the same degree of reduction can be applied to all of them. The size of the figures should preferably not exceed the size of the text pages. Standard symbols should be used in line drawings, the following are available to the printers and can also be used in the legends:

○ ● □ ■ △ ▲ ◇ ◆

Photographs should have good contrast and intensity. Sharp, glossy photographs are required to obtain good halftones. References to the illustrations should be included in appropriate places in the text using Arabic numerals and the approximate position of the illustration should be indicated in the margin of the manuscript. Each illustration should have a legend, all the *legends* being typed (with double spacing) together on a *separate sheet*.

If structures are given in the text, the original drawings should be provided.

Coloured illustrations are reproduced at the author's expense, the cost being determined by the number of pages and by the number of colours needed.

The written permission of the author and publisher must be obtained for the use of any figure already published. Its source must be indicated in the legend.

Tables

The tables should be typed (in double spacing) on separate pages, and numbered in Roman numerals according to their sequence in the text. A brief descriptive heading should be given above each table. Below the heading the experimental conditions should be described. The layout of the tables should be given serious thought, so that the reader can grasp quickly the significance of the results.

Nomenclature, symbols and abbreviations

Widely accepted symbols, abbreviations and units (SI) should be used. If there is any doubt about a particular symbol or abbreviation, the full expression followed by the abbreviation should be given the first time it appears in the text. Abbreviations used in tables and figures should be explained in the legends. In general, the recommendations of the International Union of Pure and Applied Cemistry (I.U.P.A.C.) should be followed.

References

References should be numbered in the order in which they are cited in the text, and listed in numerical sequence on a separate sheet at the end of the article. The numbers should appear in the text at the appropriate places in square brackets. In the reference list, periodicals [1], books [2], multi-author books [3], and proceedings [4] should be cited in accordance with the following examples:

1 D. P. Ndiomu and C. F. Simpson, *Anal. Chim. Acta*, 213 (1988) 237.
2 T. Paryjczak, *Gas Chromatography in Adsorption and Catalysis*, Wiley, Chichester, 1986.
3 M. Saito, T. Hondo and Y. Yamauchi, in R. M. Smith (Editor), *Supercritical Fluid Chromatography*, Royal Society of Chemistry, London, 1988, Ch. 8, p. 203.
4 F. I. Onushka and K. A. Terry, in P. Sandra, G. Redant and F. David (Editors), *Proceedings of the 10th International Symposium on Capillary Chromatography, Riva del Garda, May 1989*, Hüthig, Heidelberg, 1989, p. 415.

Abbreviations for the titles of journals should follow the system used by *Chemical Abstracts*. Articles not yet published should be given as "in press" (journal should be specified), "submitted for publication" (journal should be specified), "in preparation" or "personal communication". The JOURNAL OF CHROMATOGRAPHY; JOURNAL OF CHROMATOGRAPHY, BIOMEDICAL APPLICATIONS and JOURNAL OF CHROMATOGRAPHY, SYMPOSIUM VOLUMES should be cited as *J. Chromatogr.*

Dispatch

Before dispatch of the manuscript please check that the envelope contains four copies of the paper complete with references, legends and figures. One of the sets of figures must be the originals suitable for direct reproduction. Please also ensure that permission to publish has been obtained from your institute.

Proofs

One set of proofs will be sent to the author to be carefully checked for printer's errors. Corrections must be restricted to instances in which the proof is at variance with the manuscript. We shall be obliged to make a charge for all "extra corrections" at a rate in accordance with their cost to us.

To ensure fastest possible publication, proofs are sent to authors by *airmail* and must be returned to the publisher also by *airmail*. If this is not done, the article will be passed for publication with house correction only. Proofs may also be returned by FAX; the FAX number of *Journal of Chromatography* is: 31 (The Netherlands) -20 (Amsterdam) -5862304.

Reprints

Fifty reprints of Full-length papers and Short Communications will be supplied free of charge. Additional reprints can be ordered by the authors. The order form containing price quotations will be sent to the authors together with the proofs of their article.

Subscription orders

Subscription orders should be sent to Elsevier Science Publishers B.V., P.O. Box 211, 1000 AE Amsterdam, The Netherlands. The JOURNAL OF CHROMATOGRAPHY and the BIOMEDICAL APPLICATIONS section can be subscribed to separately. Cumulative Author and Subject Indexes can also be ordered separately. Write to the Marketing Manager, Chemistry, at the above address for more details.

PUBLICATION SCHEDULE FOR 1990

Journal of Chromatography and Journal of Chromatography, Biomedical Applications

MONTH	J	F	M	A	M	J	J	A	S	O	N	D
Journal of Chromatography	498/1 498/2 499	500 502/1	502/2 503/1 503/2 504/1	504/2 505/1	505/2 506 507 508/1	508/2 509/1 509/2 510	511 512 513	514/1 514/2 515	516/1 516/2 517 518/1	518/2 519/1	519/2 520 521/1 521/2 522	523
Cumulative Indexes, Vols. 451–500		501										
Bibliography Section		524/1		524/2		524/3		524/4		524/5		524/6
Biomedical Applications	525/1	525/2	526/1	526/2 527/1	527/2	528/1 528/2	529/1	529/2 530/1	530/2	531 532/1	532/2 533	534

INFORMATION FOR AUTHORS

(Detailed *Instructions to Authors* were published in Vol. 522, pp. 351–354. A free reprint can be obtained by application to the publisher, Elsevier Science Publishers B.V., P.O. Box 330, 1000 AH Amsterdam, The Netherlands.)

Types of Contributions. The following types of papers are published in the *Journal of Chromatography* and the section on *Biomedical Applications:* Regular research papers (Full-length papers), Review articles and Short Communications. Short Communmications are usually descriptions of short investigations, or they can report minor technical improvements of previously published procedures; they reflect the same quality of research as Full-length papers, but should preferably not exceed six printed pages. For review articles, see inside front cover under Submission of Papers.

Submission. Every paper must be accompanied by a letter from the senior author, stating that he/she is submitting the paper for publication in the *Journal of Chromatography*.

Manuscripts. Manuscripts should be typed in double spacing on consecutively numbered pages of uniform size. The manuscript should be preceded by a sheet of manuscript paper carrying the title of the paper and the name and full postal address of the person to whom the proofs are to be sent. As a rule, papers should be divided into sections, headed by a caption (*e.g.*, Abstract, Introduction, Experimental, Results, Discussion, etc.). All illustrations, photographs, tables, etc., should be on separate sheets.

Introduction. Every paper must have a concise introduction mentioning what has been done before on the topic described, and stating clearly what is new in the paper now submitted.

Abstract. All articles should have an abstract of 50–100 words which clearly and briefly indicates what is new, different and significant.

Illustrations. The figures should be submitted in a form suitable for reproduction, drawn in Indian ink on drawing or tracing paper. Each illustration should have a legend, all the *legends* being typed (with double spacing) together on a *separate sheet*. If structures are given in the text, the original drawings should be supplied. Coloured illustrations are reproduced at the author's expense, the cost being determined by the number of pages and by the number of colours needed. The written permission of the author and publisher must be obtained for the use of any figure already published. Its source must be indicated in the legend.

References. References should be numbered in the order in which they are cited in the text, and listed in numerical sequence on a separate sheet at the end of the article. Please check a recent issue for the layout of the reference list. Abbreviations for the titles of journals should follow the system used by *Chemical Abstracts*. Articles not yet published should be given as "in press" (journal should be specified), "submitted for publication" (journal should be specified), "in preparation" or "personal communication".

Dispatch. Before sending the manuscript to the Editor please check that the envelope contains four copies of the paper complete with references, legends and figures. One of the sets of figures must be the originals suitable for direct reproduction. Please also ensure that permission to publish has been obtained from your institute.

Proofs. One set of proofs will be sent to the author to be carefully checked for printer's errors. Corrections must be restricted to instances in which the proof is at variance with the manuscript. "Extra corrections" will be inserted at the author's expense.

Reprints. Fifty reprints of Full-length papers and Short Communications will be supplied free of charge. Additional reprints can be ordered by the authors. An order form containing price quotations will be sent to the authors together with the proofs of their article.

Advertisements. Advertisement rates are available from the publisher on request. The Editors of the journal accept no responsibility for the contents of the advertisements.

15 th International

Symposium

on Column Liquid

Chromatography

Convention Center

Basel, Switzerland

June 3–7, 1991

HPLC '91 Basel

Chairman

Dr. Fritz Erni

Secretariat

Swiss Industries Fair

Congress Department

P. O. Box

CH-4021 Basel

Switzerland

Telephone

++41 61/686 28 28

Telefax

++41 61/691 80 49